FTD-MT-65-409

AD 663871

FOREIGN TECHNOLOGY DIVISION

INVESTIGATION AND CALCULATION OF AXIAL-TURBINE STAGES

By

M. Ye. Deych and B. M. Troyanovskiy

D D C
RECEIVED
JAN 22 1968
B

Distribution of this document is unlimited. It may be rele sed to the clearinghouse, Department of Commerce, for sale to the general public.

Reproduced by the
CLEARINGHOUSE
for Federal Scientific & Technical
Information Springfield Va. 22151

600

DISCLAIMER NOTICE

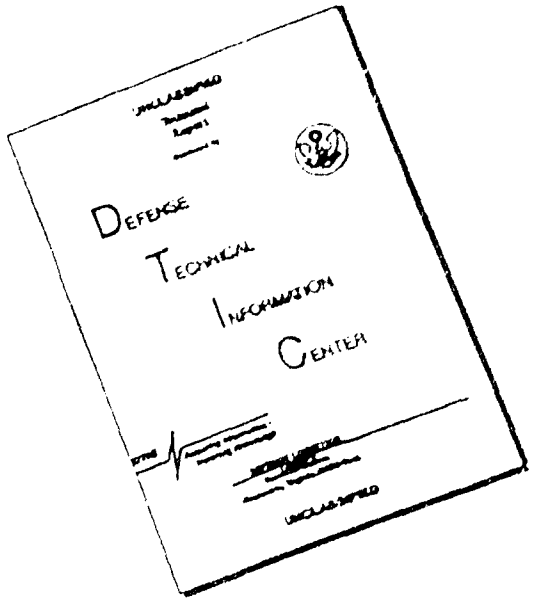

THIS DOCUMENT IS BEST QUALITY AVAILABLE. THE COPY FURNISHED TO DTIC CONTAINED A SIGNIFICANT NUMBER OF PAGES WHICH DO NOT REPRODUCE LEGIBLY.

ACCESSION for
CFSTI WHITE SECTION
DDC BUFF SECTION
UNANNOUNCED
JUSTIFICATION
BY
DISTRIBUTION/AVAILABILITY CODES
DIST. AVAIL. and/or SPECIAL
1

This document is a machine translation of Russian text which has been processed by the AN/GSQ-16(XW-2) Machine Translator, owned and operated by the United States Air Force. The machine output has been post-edited to correct for major ambiguities of meaning, words missing from the machine's dictionary, and words out of the context of meaning. The sentence word order has been partially rearranged for readability. The content of this translation does not indicate editorial accuracy, nor does it indicate USAF approval or disapproval of the material translated.

FTD-MT-65-409

EDITED MACHINE TRANSLATION

INVESTIGATION AND CALCULATION OF AXIAL-TURBINE STAGES

By: M. Ye. Deych and B. M. Troyanovskiy

English Pages: 589

TM/50/325

THIS TRANSLATION IS A RENDITION OF THE ORIGINAL FOREIGN TEXT WITHOUT ANY ANALYTICAL OR EDITORIAL COMMENT. STATEMENTS OR THEORIES ADVOCATED OR IMPLIED ARE THOSE OF THE SOURCE AND DO NOT NECESSARILY REFLECT THE POSITION OR OPINION OF THE FOREIGN TECHNOLOGY DIVISION.	PREPARED BY: TRANSLATION DIVISION FOREIGN TECHNOLOGY DIVISION WP-AFB, OHIO.

FTD-MT-[illegible]

Date [illegible] Apr. 19[illegible]

M. Ye. Deych i B. M. Troyanovskiy

ISSLEDOVANIYA I RASCHETY STUPENEY OSEVYKH TURBIN

Izdatel'stvo "Mashinostroyeniye"

Moskva - 1964

Page 1-627

CIRC ABSTRACT WORK SHEET 0897 0/37

(01) Acc Nr.	(65) SIS Acc Nr.	(40) Country of Info	(61) Translation Nr.
TM7500325		UR	MT6500409

(42) Author	Priority
DEYCH, M. YE.; TROYANOVSKIY, B. M.	1
	Distribution STD

(43) Source
ISSLEDOVANIYA I RASCHETY STUPENEY OSEVYKH TURBIN

(02) Ctry	(03) Ref	(04) Yr	(05) Vol	(06) Iss	(07) B. Pg	(08) E. Pg	(09) Date	(47) Subject Code
UR	0000	64	000	000	0001	0627	NONE	21, 10, 01

Language			
RUSS	N/A	MOSKVA	ISD-VO MASHINOSTROYENIYE

(39) Topic Tags axial flow turbine, gas turbine, steam turbine, turbine stage, turbine design

(66) Foreign Title
SEE SOURCE

(09) English Title
INVESTIGATION AND CALCULATION OF AXIAL-TURBINE STAGES

(97) Header Clas	(63) Clas	(64) Rel	(66) Release Expansion
0	00	0	

ABSTRACT: The book examines methods and results of experimental investigation of turbine lattices and stages, methods of thermal and aerodynamic calculation, and design of stages with axial gas (steam) flow. Great attention is given to regulation stages of various types and the intermediate and final stages of gas and steam turbines. The effect of moisture on the through stage is considered. The book contains the results of research conducted at MEI and other organizations in the Soviet Union and abroad. The book is intended for a wide circle of power engineers working with steam and gas turbines. For many problems it will also be of interest for researchers and engineers interested in transportation and aviation turbines. The book can be useful to advanced students of power engineering and polytechnic institutes. English Translation: 25 table, 351 figures, 375 formulas and 587 pages.

Partial Table of Contents

Chapter I. Turbine Cascades
Chapter II. Calculation of a Stage.
Chapter III. Methods of Investigating Turbine Stages.
Chapter IV. Results of the Investigation of Single-Wheel Stages with Full Input.
Chapter V. Velocity Stages.
Chapter VI. Stages with Partial Input and Supersonic Stages.
Chapter VII. Stages with Large Hare.
Chapter VIII. Last Stages of Condensing Steam Turbines.
Chapter IX. Generalized Economy Graphs and Calculation of Model Stages.

TABLE OF CONTENTS

U. S. Board on Geographic Names Transliteration System..... iv

Designations of the Trigonometric Functions..... v

Preface..... 1

Chapter I. Turbine Cascades..... 5

§ 1. Types of Cascades in Use..... 5

§ 2. Calculation of Cascades for Subsonic Velocities..... 10

§ 3. Blade Standards of Nozzle and Moving Cascades..... 21

§ 4. Aerodynamic Characteristics of Cascades for Subsonic Velocities..... 23

§ 5. Nozzle Cascades of Low Height..... 40

§ 6. Moving Cascades of Low Height..... 47

§ 7. Nozzle Cascades for Transonic and Supersonic Velocities..... 55

§ 8. Action Cascades for Transonic and Supersonic Velocities..... 78

§ 9. Flow Rate Coefficients of Turbine Cascades..... 87

Chapter II. Calculation of a Stage..... 93

§ 10. Selection of Cascades for the Stage Being Designed..... 93

§ 11. Calculation of a Stage According to Data of Static Investigations of Cascades..... 112

§ 12. Calculation of Additional Losses..... 130

Chapter III. Methods of Investigating Turbine Stages..... 145

§ 13. Similarity Conditions and Stage Modeling..... 145

§ 14. Experimental Turbines and Setup for Investigating Stage Cascades..... 155

§ 15. Measuring Devices of Experimental Turbines..... 168

§ 16. Methods of Testing and Measurement on Experimental Turbines..... 171

Chapter IV. Results of the Investigation of Single-Wheel Stages with Full Input..... 175

§ 17. Schematic Diagrams of Single Stages..... 175

§ 18. Influence of the Basic Performance Parameters on the Efficiency of a Stage..... 182

§ 19. Influence of Performance Parameters on Degree of Reaction..... 192

§ 20. Flow Rate Characteristics of a Stage..... 198

§ 21. Influence of Geometric Parameters on the Characteristics of a Stage 204

§ 22. The Influence of Certain Design Changes on the Characteristics of a Stage 216

§ 23. Basic Characteristics of Certain Single-Wheel Stages 230

§ 24. Stages Calculated for Low Velocity Ratios u/c_0 238

Chapter V. Velocity Stages 249

§ 25. Structural Diagrams of Double-Wheel Velocity Stages 249

§ 26. The Influence of the Basic Performance Parameters on the Efficiency, Reaction, and Relative Flow Rate of a Velocity Stage 258

§ 27. The Influence of Geometric Parameters on the Characteristics of a Stage 270

Chapter VI. Stages with Partial Input and Supersonic Stages 281

§ 28. The Influence of Partial Input on the Performance of a Single-Wheel Stage 281

§ 29. Performance of a Double-Wheel Velocity Stage with Partial Input 292

§ 30. Optimum Characteristics of a Partial Stage 298

§ 31. Supersonic Single-Wheel Stages 303

§ 32. Supersonic Double-Wheel Stages 314

§ 33. Comparison Single-Wheel Stages and Velocity Stages 322

§ 34. Adjustable Stages of Extracting Turbines 325

Chapter VII. Stages with Large Hare 332

§ 35. Structure of Flow in Annular Cascades with Large Flare at Subsonic Velocities 332

§ 36. The Influence of Certain Geometric and Performance Parameters on the Characteristics of Annular Cascades at Subsonic Velocities 339

§ 37. Approximate Method of Calculating the Flow in a Nozzle Cascade with Large Flare 349

§ 38. Calculation of the Flow Behind a Moving Cascade 362

§ 39. Methods for Twisting Blades and the Rational Organization of the Flow in a Stage 366

§ 40. Results of Investigations of the Effect of Individual Design Elements on the Effectiveness of Stages with Long Blades 375

§ 41. Some Special Problems of the Theory of Large-Flare Stages 399

Chapter VIII. Last Stages of Condensing Steam Turbines..... 408

§ 42. Designs of Last Stages..... 408

§ 43. Profiling and the Results of Static Investigation of Cascades of Last Stages..... 415

§ 44. Results of Investigation of Last Stage in Experimental Steam Turbines..... 432

§ 45. Method for Calculation of the Last Stages of Condensing Turbines..... 446

§ 46. Fundamentals of Designing the Last Stages of Condensing Turbines..... 481

Chapter IX. Generalized Economy Graphs and Calculation of Model Stages.... 495

§ 47. Single-Wheel Stages with Cylindrical Blading..... 495

§ 48. Double-Wheel Velocity Stages..... 506

§ 49. Model Stages with Variable Blading..... 513

Chapter X. Influence of Moisture on the Characteristics of Turbine Stages..... 526

§ 50. Some Properties of the Flow of Moist Steam in the Flow Area of a Stage..... 526

§ 51. Equations of One-Dimensional Motion of Moist Steam and the Slip Factor..... 538

§ 52. Condensing Shocks in a Flow of Moist Steam..... 543

§ 53. Flow Rate Characteristics of Nozzles Operating with Moist Steam..... 547

§ 54. Influence of Moisture on the Characteristics of a Turbine Stage..... 554

§ 55. Some Results of an Investigation of Blade Erosion..... 566

§ 56. Turbine Moisture Collectors..... 570

Appendix..... 577

Literature..... 580

U. S. BOARD ON GEOGRAPHIC NAMES TRANSLITERATION SYSTEM

Block	Italic	Transliteration	Block	Italic	Transliteration
А а	*А а*	A, a	Р р	*Р р*	R, r
Б б	*Б б*	B, b	С с	*С с*	S, s
В в	*В в*	V, v	Т т	*Т т*	T, t
Г г	*Г г*	G, g	У у	*У у*	U, u
Д д	*Д д*	D, d	Ф ф	*Ф ф*	F, f
Е е	*Е е*	Ye, ye; E, e*	Х х	*Х х*	Kh, kh
Ж ж	*Ж ж*	Zh, zh	Ц ц	*Ц ц*	Ts, ts
З з	*З з*	Z, z	Ч ч	*Ч ч*	Ch, ch
И и	*И и*	I, i	Ш ш	*Ш ш*	Sh, sh
Й й	*Й й*	Y, y	Щ щ	*Щ щ*	Shch, shch
К к	*К к*	K, k	Ъ ъ	*Ъ ъ*	"
Л л	*Л л*	L, l	Ы ы	*Ы ы*	Y, y
М м	*М м*	M, m	Ь ь	*Ь ь*	'
Н н	*Н н*	N, n	Э э	*Э э*	E, e
О о	*О о*	O, o	Ю ю	*Ю ю*	Yu, yu
П п	*П п*	P, p	Я я	*Я я*	Ya, ya

* ye initially, after vowels, and after ъ, ь; e elsewhere. When written as ё in Russian, transliterate as yё or ё. The use of diacritical marks is preferred, but such marks may be omitted when expediency dictates.

FOLLOWING ARE THE CORRESPONDING RUSSIAN AND ENGLISH

DESIGNATIONS OF THE TRIGONOMETRIC FUNCTIONS

Russian	English
sin	sin
cos	cos
tg	tan
ctg	cot
sec	sec
cosec	csc
sh	sinh
ch	cosh
th	tanh
cth	coth
sch	sech
csch	csch
arc sin	$\sin^{-1}$
arc cos	$\cos^{-1}$
arc tg	$\tan^{-1}$
arc ctg	$\cot^{-1}$
arc sec	$\sec^{-1}$
arc cosec	$\csc^{-1}$
arc sh	$\sinh^{-1}$
arc ch	$\cosh^{-1}$
arc th	$\tanh^{-1}$
arc cth	$\coth^{-1}$
arc sch	sech^{-1}
arc csch	csch^{-1}

---

rot	curl
lg	log

This book considers the methods and results of experimental investigation of turbine cascades and stages, means of thermal and aerodynamic calculation, and the practical designing of stages with axial gas (steam) flow. Considerable attention is allotted to regulating stages of various types, and to the intermediate and last stages of gas and condensing steam turbines. The influence of humidity on blading performance of a stage is considered. The book uses mainly the results of investigations conducted at the MEI; materials that were obtained at our other organizations and abroad are also presented.

This book is intended for power engineers engaged in the study of steam and gas turbines. It may be of interest in many respects also to scientists and engineers who are interested in vehicle and aircraft turbines. The book may be of use to students taking advanced courses at power engineering and polytechnical institutes.

ACRONYMS AND ABBREVIATIONS

BITM – Belorussian Institute of Turbomachinery

EVM – Electronic Computer

KAI – Kazan Aviation Institute

KhPI – Kharkov Polytechnic Institute

KhTGZ – Kharkov Turbogenerator Plant

KPI – Kiev Polytechnic Institute

KTZ – Kaluga Turbine Plant

LKZ – Leningrad Boiler Plant

LMZ – Leningrad Metallurgical Plant

LPI – Leningrad Polytechnic Institute

MEI – Moscow Power Engineering Institute

NZL – Neva Machinery Plant

ORGRES – State Trust for the Organization and Efficiency of Electric Power Plants

PGT – Steam and Gas Turbine (Department)

TMZ – Ural Turbine Plant

TsKTI – Central Scientific Research Institute for Boilers and Turbines

TsNII – Central Scientific Research Institute

UTMZ – Ural Turbomachinery Plant

VTI – All-Union Heat Engineering Institute

PREFACE

The creation of new, highly effective, steam and gas turbines, the increase of efficiency of operational turbine units — the most important task of power equipment construction and power engineering — was specially noted in the resolutions of the XXII Congress of the CPSU. Inasmuch as the economy of a turbine is determined mainly by the economy of the blading and its main element, i.e., the stage, during the last few years the efforts of many scientific and educational institutes, laboratories and design bureaus of turbine plants, and research organizations have been directed towards the study and improvement of turbine stages.

Experimental and theoretical studies in this field were conducted and are now being conducted at practically all turbine plants: the Leningrad Metallurgical Plant (named in honor of the XXII Congress of the CPSU), the Kaluga Turbine Plant, the V. I. Lenin Machine-Building Plant in Neva, the S. M. Kirov Plants in Leningrad, Kirov, and Kharkov, and the Ural Turbomotor Plant. Much has been done in this area in the scientific research institutes: the I. I. Polzunov TsKTI, F. E. Dzerzhinskiy VTI, the ORGRES, and at educational institutes: BITM, KhPI, LPI, KAI, and others. From our bibliographic sources we know of certain results of investigations made by foreign firms and laboratories.

Theoretical and experimental work on the gas dynamics of turbine blading is receiving considerable attention form the Department of Steam and Gas Turbines of the Moscow Power Engineering Institute. A characteristic of the activity of the MEI in this area is the close association of studies on turbine cascades and turbine stages, which is terminated by working out a combination of stage cascades, and methods of thermal and aerodynamic calculation, with specific practical recommendations to plants.

The experimental and theoretical results that have accumulated in various organizations require systematic analysis and generalization. Therefore, only in the last few years did there appear several special monographs dedicated to this problem (monographs written by I. I. Kirillov (BITM), M. Ye. Deych and G. S. Samoylovich (MEI), A. M. Zavadovskiy (TsKTI), G. A. Zal'fom and V. V. Zvyagintsev (NZL), and others).

However, as a rule, the generalizations in these books were confined to the experience of one laboratory and the results of investigations conducted in other organizations were not used; many problems in general were not studied or were considered only briefly; frequently there was no relation between the work conducted on stages and cascades, without which, of course, it is impossible to analyze the results of tests, and all the more so, it is impossible to create new combinations of turbine stages.

In the writing of this book the authors have attempted to avoid the above-noted shortcomings. Here we have widely used not only the works conducted at the MEI, but also, as much as possible, the results of investigations conducted in other organizations and abroad. One should note here the difficulties connected with the fact that a number of published articles and books did not always mention all the parameters for which one experiment or another was conducted.

In accordance with the problem on hand, the content of this book is arranged to consecutively consider the methods of experimental research, the results, theoretical research, and methods of thermal and aerodynamic calculation, and to point out some of the ways of practically designing the stages of steam and gas turbines.

This book discusses all types of axial-turbine stages: single stages and velocity stages, stages with low cascade heights and stages with large flare, and also stages with partial input. Considerable attention is allotted the last stages of condensing steam turbines, the practical design of which is apparently an extremely complicated task. This problem is the subject of not only a special chapter, i.e., Chapter VIII, but also Chapter VII, "Stages with Large Flare," special paragraphs in Chapter I (cascades for supersonic velocities), and finally, Chapter X, "The Influence of Humidity on the Characteristics of Turbine Stages." The last chapter, in particular, is of interest to atomic power engineering.

As it is known, turbine stages are designed not only from the point of view of economy, but also taking into account the requirements of reliability and the best manufacturing technology. However, the authors do not consider this entire complex

of interconnected problems in its logical relation and sequence here, since it would essentially complicate the book and, of course, would make it extremely long. At the same time, everywhere in the book we indicate how one solution or another can affect the reliability and productibility of the blading elements of turbines.

The very important and interesting problems of aerodynamics of a group of stages are not included in the book, since the experimental data collected at the present time are still insufficient. We also do not consider such blading elements as valves, labyrinth seals, and partially exhaust ducts. The inclusion of these sections would considerably increase the size of the book; furthermore, these problems have been sufficiently discussed in detail in other books written by members of the PGT Department of the MEI.

This monograph is an inseparable part of the entire work conducted by the Department on the given problem. It is a natural continuation of a series of books dedicated to the investigation and thermal calculation of steam and gas turbines: the textbook by A. V. Shcheglyayev, Steam Turbines, 3rd Edition, 1955; the book by G. S. Samoylovich and B. M. Troyanovskiy, Varying Duty of Steam Turbines, 1955; the monograph by M. Ye. Deych and G. S. Samoylovich, The Fundamentals of the Aerodynamics of Axial Turbomachines, 1959; the training aid by M. Ye. Deych, Technical Gas Dynamics, 2nd Edition, 1961.

The Appendix of this book, which is of independent value, is taken from the Mashgiz publication under the title of Atlas of Turbine Cascade Profiles (by M. Ye. Deych, G. A. Filippov, and L. Ya. Lazarev). Therefore, the detailed aerodynamic characteristics that are broadly covered in this atlas are omitted from the appendices of this book.

The experimental and theoretical materials presented in the book were obtained in the laboratory of the PGT Department of the MEI by members of the gas-dynamics group.

In addition to the authors, the following people took part in the principle investigations: Candidates of Technical Sciences, Docents V. A. Baranov, V. V. Frolov, and A. Ye. Zaryankin; senior scientific associates A. V. Gubarev and G. A. Filippov; senior engineers V. I. Abramov, M. F. Zatsepin, F. V. Kazintsev, L. Ye. Kiselev, L. Ya. Lazarev, Ye. V. Mayorskiy, Ye. V. Stekol'shchikov, and graduate student G. V. Tsiklauri.

A significant portion of the MEI investigations was conducted jointly with the Kaluga Turbine, Leningrad Metallurgical, and Ural Turbomotor Plants. The KTZ, in

addition to its active participation in the investigations, conducted their own verification of the MEI recommendations, and LMZ presented the authors with materials on the study of stage cascades which they conducted in their plant laboratory.

The Preface, Chapter I, and Chapter III with the exception of §§ 14 and 15, § 24 of Chapter IV, §§ 31, 32, 33, and 34 of Chapter VI, Chapters VII and X, and also the Appendix were written by M. Ye. Deych. Chapter II, Chapter IV except for § 24, Chapter V, §§ 28, 29, and 30 of Chapter VI, Chapter VIII and Chapter IX were written by B. M. Troyanovskiy. Sections 14 and 15 of Chapter III were written by Engineer F. V. Kazintsev. L. Ya. Lazarev took part in the selection and preparation of materials for Chapter I.

CHAPTER I

TURBINE CASCADES

§ 1. TYPES OF CASCADES IN USE

The selection and detailed calculation of cascades for a stage is carried out on the basis of data from preliminary thermal calculation. As a result of the thermal calculation, the tentative values of velocities c_1, w_1, w_2 (and correspondingly, numbers $M_{c_1} = \frac{c_1}{a_1}$, $M_{w_1} = \frac{w_1}{a_1}$, $M_{w_2} = \frac{w_2}{a_2}$, where a_1 and a_2 are the velocities of sound in the clearance and behind the stage), angles α_0, α_2, β_1, and β_2 in absolute and relative motion (Fig. 1), and also the reaction distribution along the radius are established.

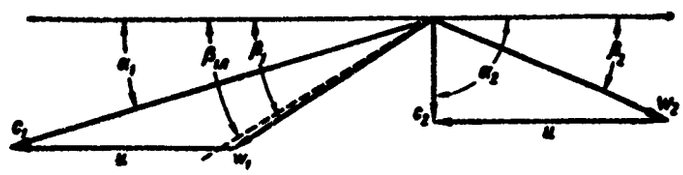

Fig. 1. Velocity triangles of a stage with axial gas flow: — — — direction of moving blade entrance.

In stages with small flare (with a large ratio of average diameter to blade height $\theta = d/l$) the variation of velocities along the radius is not great and for cascade selection it is sufficient to consider the velocity triangles for the average diameter.

In stages with large flare it is necessary to select the cascade profiles for several cross sections with respect to radius, thus designing the blades taking into account the characteristics of three-dimensional flow, strength, and technological considerations.

In the blading of a multistage turbine the specific volumes and the M and Re numbers in absolute and relative motion vary in very wide limits. Consequently, the heights, and also the optimum shapes of profiles of the nozzle and moving cascades for various stages will be different.

All types of profiles that are used in turbine construction may be divided into several groups and classified by various criteria.

By function, the turbine cascades are divided into:

I – reaction, nozzle (stationary) and moving (revolving);

II – action, moving and rotating.

Within the limits of each type (I and II), cascades also are divided into several groups by M numbers at the entrance and at the exit: A) subsonic ($M < M_*$), B) transonic ($M_* < M < 1.3$), and C) supersonic ($M > 1.2$) (here, M_* is the critical* Mach number M for the cascade).

For reaction cascades, a clearly expressed convergent flow in the vane channels is characteristic. In action cascades the mean static inlet and outlet pressures are close and usually differ only by the magnitude of pressure loss in the vane channels.

Cascades can also be classified by two of the most important geometric parameters, i.e., relative height and flare, whose influence should be considered jointly. The blading of steam turbines employs cascades of small relative height ($\bar{l} = l/b < 1.5$)** and small flare ($\theta > 20$); cascades of medium height ($\bar{l} = 1.5$ to 3.0) and medium flare ($\theta \geq 10$ to 20), and cascades of large height ($\bar{l} > 3.0$) and large flare ($\theta < 7$ to 10)***.

In cascades of the first type, the flow has a clearly expressed three-dimensional structure, in spite of the small flare in connection with the small height, which leads to the closing in of secondary flows. The small flare frequently makes it possible to use the results of tests made on foil cascades with high reliability.

In a simplified investigation of the second group, the cascade flow may be considered to be two-dimensional, with the exception of the root and peripheral sections, where the motion has a three-dimensional character due to the secondary

*The M_1 (M_2) number behind a cascade, at which the local velocity is equal to the velocity of sound at a certain point on the cascade, is said to be critical.

**Here, b is profile chord. The designations of the main geometric cascade parameters are given in Fig. 2.

***In certain gas turbines, cascades of small relative height and large flare are encountered.

currents, leakages, and several other causes [22].

The flow around long blades of large flare should be referred to the group of three-dimensional problems. The middle sections of these cascades in first approximation may be calculated according to the characteristics of two-dimensional cascades of corresponding profiles. It should be emphasized that blades of the third group frequently have varying profiles with respect to height.

At present, turbine construction plants are widely employing new turbine cascade profiles that have small profile and tip losses.* The nomenclature of profiles developed at the MEI** [26], [31], and the main geometric characteristics of cascades, are given in Table 1.

Table 1 includes groups of cascades*** that differ with respect to flow inlet and outlet angles, dimensionless M velocities, and relative heights $\bar{l}$. The profile number (0, 1, 2, etc.) indicates the range of accessible outlet angles for nozzle cascades and inlet and outlet angles for moving cascades. An increase of the profile number corresponds to the transition to profiles with larger inlet and outlet angles. Consequently, the profile number indicates the type of profile with respect to velocity triangle. The letters A, Б, and B indicate the type of profile depending upon M number (subsonic, transonic, and supersonic).

The shapes of the main types of profiles, with the designation of certain geometric parameters, in accordance Table 1, are shown in Fig. 2. A comparision shows that profiles of group "A" have contours of continuously varying curvature, whereby the entrances and exits are rounded. The vane channels are continuously converging toward the exit. Maximum convergence corresponds to channels of the nozzle and reaction moving cascades, and minimum convergence corresponds to channels of the action moving cascades.****

For small relative heights, action cascades are recommended to be made with divergent-convergent channels (see § 6) and nozzle cascades should have the

---

*See § 4.

**A large group of cascades for subsonic velocities (group "A") was developed by the TsKTI and standardized. Several of these nozzle cascades were proposed by the LMZ laboratory.

***The designations of cascades that are given in Table 1 are conditional and do not correspond to the designations adopted in the standards for profiles of guide and rotor blades.

****The geometric convergence of cascade channels is characterized by the ratio of cross sections at the entrance and exit a_1/a_2 (Fig. 2).

three-dimensional design discussed in §5.

Table 1. Principle Geometric Characteristics of MEI Turbine Cascades

Cascade group	Velocity range (M_{c1} and M_{c2} numbers)	Flow-inlet angle, α_0°; β_1°	Flow-outlet angle, α_1°; β_2°	MEI profile designation	Optimum pitch τ_{opt}	Optimum angle of incidence α_y°, β_y°	Remarks
Nozzle or moving action Group *A*	0,3—0,9	70—100	8—11	TC-0A	0,76—0,95	30—33	
			10—14	TC-1A	0,74—0,90	32—36	
			13—17	TC-2A	0,70—0,90	37—41	
			16—22	TC-3A	0,65—0,85	41—46	
			22—27	TC-4A	0,60—0,74	43—46	
			27—32	TC-5A	0,55—0,64	46—49	
			33—37	TC-6A	0,52—0,60	53—56	
			13—17	TC-1A-1	0,74—0,95	50—54	For intermediate stages, operating at small u/c_ϕ
		45—60	17—22	TC-2A-1	0,7—0,9	56—60	
		55—70	22—27	TC-3A-1	0,65—0,85	62—66	
		60—70	27—32	TC-4A-1	0,6—0,74	68—72	
		65—80	32—37	TC-5A-1	0,55—0,64	72—75	
Group *Б*	0,85—1,3	70—110	10—14	TC-1Б	0,74—0,95	32—36	
			13—17	TC-2Б	0,70—0,90	37—41	
			16—22	TC-3Б	0,65—0,85	41—46	
			22—27	TC-4Б	0,58—0,74	44—50	
			27—32	TC-5Б	0,55—0,64	48—54	
Group *B*	1,3—1,6	60—120	7—11	TC-1B	0,65—0,75	27—31	
			11—15	TC-2B	0,65—0,75	37—41	
			15—20	TC-3B	0,65—0,75	37—41	
			20—25	TC-4B	0,65—0,75	46—50	f = 1.05 to 1.3
	1,6—2,5	60—120	7—11	TC-1BP	0,55—0,65	27—31	
			11—15	TC-2BP	0,55—0,65	37—41	
			15—20	TC-3BP	0,52—0,65	37—41	
			20—25	TC-4BP	0,55—0,65	46—50	
Moving action Group *A*	0,3—0,9	14—25	13—15	TP-0A	0,6—0,75	76—79	
		18—33	16—19	TP-1A	0,5—0,7	76—79	
		25—40	19—22	TP-2A	0,58—0,65	76—79	
		28—45	24—28	TP-3A	0,56—0,61	77—80	
		35—50	28—32	TP-4A	0,55—0,64	74—78	
		40—55	32—36	TP-5A	0,52—0,60	76—79	
		45—65	36—39	TP-6A	0,52—0,58	77—81	
Group *Б*	0,85—1,25	18—28	17—20	TP-1Б TP-1Бк	0,59—0,7	77—82	
		22—33	19—22	TP-2Б TP-2Бк	0,58—0,65	81—85	
		26—38	24—28	TP-3Б	0,57—0,62	83—88	
		30—42	27—32	TP-4Б	0,55—0,60	84—88	
		35—48	32—35	TP-5Б	0,52—0,6	85—89	
Group *B*	1,25—1,9	18—24	18—20	TP-1B	0,57—0,65	87—89	
		20—26	20—23	TP-2B	0,58—0,63	87—89	
		23—30	22—26	TP-3B	0,55—0,60	87—90	
		26—32	25—28	TP-4B	0,54—0,58	88—90	

Profiles of nozzle cascades for transonic velocities (group "Б") are manufactured with rectilinear cross sections on the back in a slanting shear.

The action moving cascades of group "Б" have rectilinear contours also at the entrance of the back. The channels of cascades of this group are continuously convergent.

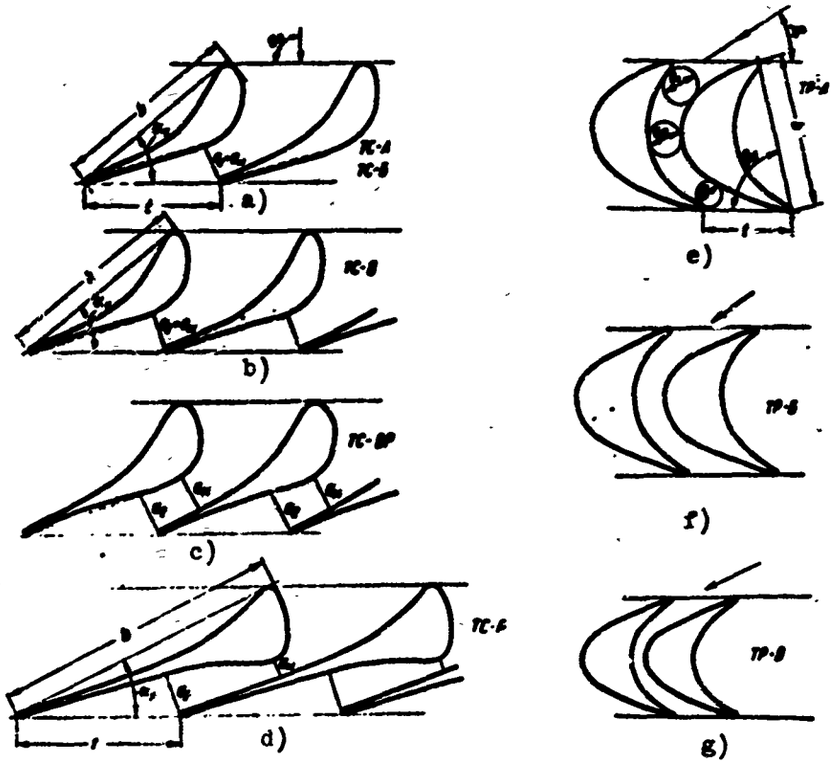

Fig. 2. Shapes of profiles and channels of reaction and action cascades for different M numbers. a) nozzle reaction cascade for subsonic (TC-A) and transonic (TC-B) velocities; b) nozzle cascade with convergent channels and concave back in slanting shear for supersonic velocities; c, d) nozzle cascades with convergent-divergent channels for supersonic velocities; e, f, g) action cascades for subsonic, transonic, and supersonic velocities.

The nozzle cascades for supersonic velocities* are made with a concave surface at the exit of the back in a slanting shear and with a slight expansion of the channel at the exit (see Fig. 2). For high supersonic velocities, the vane channels of the cascades are made in the form of convergent-divergent nozzles, i.e., they are manufactured with a large channel expansion $f = \frac{a_2}{a_M} > 1$ (see Fig. 2).

Action cascades for $M_1 > 1.5$ are also made with convergent-divergent channels. For smaller M_1 numbers, stagnation of supersonic flow in front of the cascade is carried out in normal shocks at the cascade entrance.

Thus, according to the preliminary thermal calculation of the blading, it is possible to select the profiles of nozzle and moving cascades and establish their geometric dimensions (pitch, angle of incidence), and perform a precise calculation,

*The design of nozzle and moving cascades for $M > 1$ is the subject of §§ 7 and 8.

using the experimental values of the loss factors, discharge coefficients, and flow angles which are given in the atlas or in the profile standards.

In certain cases the existing profiles cannot be used and it is necessary to design new cascades which correspond to the particular specifications of the stage being designed. For subsonic velocities, this problem is theoretically solved quite accurately. For transonic and supersonic velocities, and also for low relative heights, cascade profiles are constructed according to experimental data.

A method of calculating of two-dimensional cascades for subsonic velocities is given below. The following paragraphs consider methods of constructing cascades on the basis of experiments.

§ 2. CALCULATION OF CASCADES FOR SUBSONIC VELOCITIES

In those cases when it is necessary to design new cascades or calculate the velocity field in a designed cascade, it is possible to use a method of approximation that is based on the channel theory.

In the cascade theory there appear two main problems. One of them, which is called the prima problem, consists of determining the velocity field of potential flow through a given cascade, and in a subsequent estimate, the energy losses for various performance (inlet angle, Re and M numbers) and geometric (pitch, profile angle, cascade height, and others) parameters. Consequently, the primal problem is of much value for studying the varying performance of cascades and constructing their aerodynamic properties.

The inverse problem consists in constructing a cascade that corresponds to the selected or given cascade flow. In this setting, the problem of constructing a cascade with rational distribution of velocities (pressures) along the profile surface, which ensures minimum energy losses, is of practical importance.

At present, methods have been developed for calculating potential cascade flow, using complex-variable function apparatus.* However, these methods are awkward and are less convenient for programming the calculation on electronic computers (EVM), in the applied respect.

Other methods, which are based on the solution of integral equations [43, 90], are more convenient for programming, and therefore they can be recommended for machine computation of the potential flow around arbitrary cascades of blades.

---

*Methods for calculating potential flow and constructing cascades are presented in detail in [33], [43], and [90].

In the TsKTI, for programming on the EVM,* the method of solution proposed by M. I. Zhukovskiy [43] was adopted. This method is based on the solution of the following integral equation whose unknown function is the velocity potential Φ:

$$\Phi(x, y) = 2c_\infty (x\cos\beta_\infty + y\sin\beta_\infty) + \Gamma K_0 - \int_L \Phi(\sigma)\frac{dK}{d\sigma}d\sigma, \tag{1}$$

where $\Gamma = \Phi(L) - \Phi(0)$ is the circulation around a blade.

$$K = \frac{1}{\pi}\operatorname{arctg}\frac{\operatorname{th}\frac{\pi}{t}(y-\eta)}{\operatorname{tg}\frac{\pi}{t}(x_0-\xi)}$$

and

$$K_0 = \frac{1}{\pi}\operatorname{arctg}\frac{\operatorname{th}\frac{\pi}{t}(y_0-\eta)}{\operatorname{tg}\frac{\pi}{t}(x_0-\xi)},$$

here L is the length of the blade contour;

σ is the arc coordinate;

x, y, ξ, η are the blade coordinates;

x_0, y_0 are the coordinates of point B at the blade exit (Fig. 3);

c_∞, β_∞ are the velocity and angle of flow at infinity.

Equation (1) is a Fredholm integral equation of the 2nd kind with a continuous kernal $\frac{dK}{d\sigma}$.

The function $\theta = \pi K$ is continuous everywhere, with the exception of a straight line, where it has a discontinuity equal to

$$\theta(S, S-0) - \theta(S, S+0) = \pi. \tag{2}$$

Integral equation (1) has the following properties:

1) the kernel of the equation is continuous, and therefore it is calculated with an accuracy that is identical and sufficient for all points of the contour;

2) in the calculation of the kernel and the free term of equation (1) we use only the blade coordinates, and not their derivatives, as required for solving other types of integral equations;

3) the number $\lambda = 1$ is not the characteristic number of the equation, and consequently, its solution is unique;

---

*The description of the method presented below was given by M. I. Zhukovskiy, N. I. Durakov, and O. I. Novikova at the request of the authors.

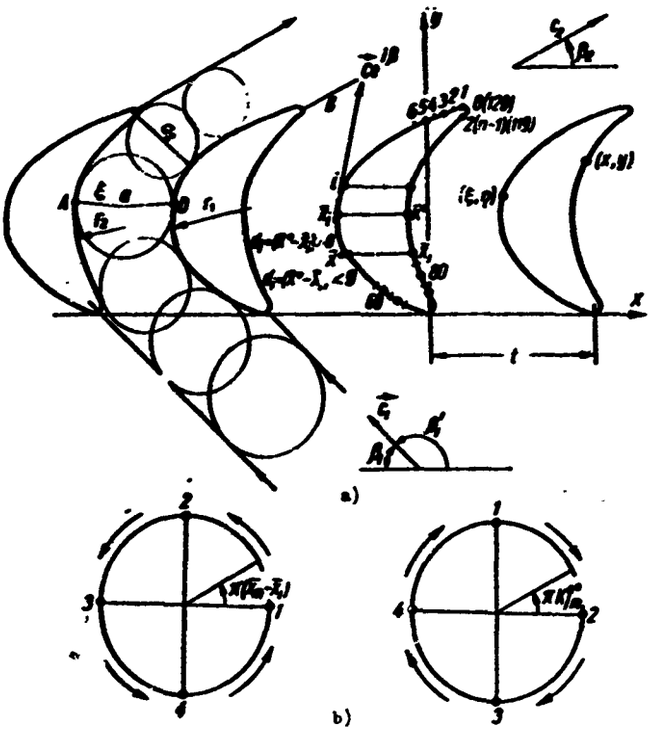

Fig. 3. Construction of a cascade for a given flow: a) diagram of cascade with division of blade contour reading of angles β_1 and β_2; b) change of function K_{im}^{0*} depending upon $(\overline{x}_m - \overline{x}_i)$.

4) to this equation we apply the method of successive approximations, since the kernels of equation (1) do not have characteristic numbers in the range of $R < 1$ [44];

5) in distinction from other types of equations, to integral equation (1) we apply a method of solution that makes it possible to replace this equation for 2n points of the contour by a system composed of n linear equations;

6) the free term of the equation contains β_1 and β_2 as parameters, in a form that allows us to modify them separately, which makes it possible to determine β_2 and construct a solution depending upon β_1;

7) we shall apply the method of calculation, based on the solution of equation (1) for all values of geometric and performance characteristics of cascades that are used in practice.

The construction of a solution with the help of equation (1) involves the numerical differentiation of the generalized potential Φ; however, numerical differentiation is produced at the end of the entire calculation; therefore, the errors

connected with differentiation do not affect the accuracy of the preceeding calculations.

As was shown above, the integral equation (1) can be solved by means of approximating it by a system composed of n linear equations with division of the blade contour into 2n intervals. We shall designate the calculation points by i = 1, 3, ..., 2n - 1, and the boundaries of the intervals by m = 0, 2, 4, ..., 2n (see Fig. 3a).

By introducing velocity potentials for the flow around the cascade axis, which are perpendicular to it and purely circulatory, we can write the corresponding systems of equations in the following form:

$$\left.\begin{aligned} &\Phi_i^{(x)} + \sum_{(i)} A_{i,j}\Phi_j^{(x)} = 2\bar{x}_i \\ &\Phi_i^{(y)} + \sum_{(i)} A_{i,j}\Phi_j^{(y)} = 2\bar{y}_i \\ &\Phi_i^{(\Gamma)} + \sum_{(i)} A_{i,j}\Phi_j^{(\Gamma)} = K_B \end{aligned}\right\}, \tag{3}$$

where

$$\begin{pmatrix} i = 1, 3, \ldots, 2n-1 \\ j = 1, 3, \ldots, 2n-1 \end{pmatrix} A_{i,j} = K_{i,j+1} - K_{i,j-1}, \quad \bar{x} = \frac{x}{t}, \quad \bar{y} = \frac{y}{t}.$$

The solution of these systems, which differ only by the right-hand sides of the equations, is in the following form:

$$\bar{\Phi}_i = \Phi_i^{(x)} \operatorname{ctg} \beta_\infty + \Phi_i^{(y)} + \Phi_i^{(\Gamma)}\bar{\Gamma}, \tag{4}$$

where

$$\bar{\Phi} = \frac{\Phi}{tc_\infty \sin\beta_\infty}, \quad \bar{\Gamma} = \frac{\Gamma}{tc_\infty \sin\beta_\infty} = \operatorname{ctg}\beta_1 - \operatorname{ctg}\beta_2. \tag{5}$$

We shall write an expression for the potential $\bar{\Phi}$ in proximity of the trailing edge at points i = 2n - 1 and i = 1, and shall subtract one from the other.

We obtain

$$\bar{\Gamma} = \frac{\Delta\Phi_x \operatorname{ctg}\beta_\infty + \Delta\Phi_y}{1 - \Delta\Phi_\Gamma + \frac{\Delta\Phi_x}{2}}, \tag{6}$$

where we designate

$$\bar{\Gamma} = \bar{\Phi}_{2n-1} - \bar{\Phi}_1, \quad \Delta\Phi_x = \Phi_{2n-1}^{(x)} - \Phi_1^{(x)}, \quad \Delta\Phi_y = \Phi_{2n-1}^{(y)} - \Phi_1^{(y)},$$
$$\Delta\Phi_\Gamma = \Phi_{2n-1}^{(\Gamma)} - \Phi_1^{(\Gamma)}.$$

With the help of formulas (5) and (6) for given β_1 we determine the approximate value of β_2'. By assigning one more value of β_2, for instance $\beta_2'' = \beta_2' + 1^\circ$, we shall calculate two velocity profiles in the proximity of the trailing edge. The outlet angle shall be defined by means of interpolation (or extrapolation), which in this case is precise,* from the condition of equality of velocities at characteristic points [43]. The calculation of velocities is then performed with the formula

$$c = (1 - x_2)c'' - x_2 c',$$

where

$$x_2 = \frac{\operatorname{ctg}\beta_2'' - \operatorname{ctg}\beta_2}{\operatorname{ctg}\beta_2'' - \operatorname{ctg}\beta_2'}.$$

In the case of a cascade of blades, function $K_{i,m}$ has the following form [43]:

$$K_{i,m} = \frac{1}{\pi}\operatorname{arctg}\frac{\operatorname{th}\pi(\bar{y}_m - \bar{y}_i)}{\operatorname{tg}\pi(\bar{x}_m - \bar{x}_i)}. \tag{7}$$

The numerator of formula (6) contains a single-valued function of $(\bar{y}_m - \bar{y}_i)$, which varies from -1 to +1, and the denominator contains the tg function, whose sign depends both on the sign of $(\bar{x}_m - \bar{x}_i)$, and also on the absolute value of this difference.

Therefore, normalization of the function $K_{i,m}$ depends not only on the signs of the differences $(\bar{x}_m - \bar{x}_i)$ and $(\bar{y}_m - \bar{y}_i)$, but also on the mutual location of points on the profile with the subscripts i and m, i.e., on the signs of the difference $d_i = \bar{x}^* - \bar{x}_i$ (see Fig. 3b) and on the magnitude of the modulus of $(\bar{x}_m - \bar{x}_i)$ ($\bar{x}^*$ is the abscissa of the point of intersection of the blade contour, horizontally passing through the point with the abscissa $\bar{x}_i$).

For all calculations of $K_{i,m}$ one should consider that the values of this function should vary continously, starting from the zero point B on the profile (S = 0), whereby in case of the transition from points for which m < i to points for which m > i, the jump in magnitude of $K_{i,m}$ must be removed by formula (2), which reduces to the transfer of the jump of function $K_{i,m}$ to the point S = 0.

If we consider the quantity $\pi K_{i,m}$ as the analog of an angle, then we may state that for a positive direction of reading the angle, the reading is counterclockwise.

---

*The possibility of a precise calculation of the velocity profile for any value of β_1, if it is known for any two values of β_1, was pointed out by G. Yu. Stepanov [90].

Normalization of the function $K_{i,m}$ is produced by the following formulas:

$$K_{i,m} = K^{0*}_{i,m}, \quad \text{if} \quad \begin{cases} \bar{x}_m - \bar{x}_i > 0 \\ \bar{y}_m - \bar{y}_i > 0, \end{cases}$$

$$K_{i,m} = 1 - K^{0*}_{i,m}, \quad \text{if} \quad \begin{cases} \bar{x}_m - \bar{x}_i < 0 \\ \bar{y}_m - \bar{y}_i > 0, \end{cases}$$

$$K_{i,m} = K^{0*}_{i,m} + \nu - 1, \quad \text{if} \quad \begin{cases} \bar{x}_m - \bar{x}_i < 0 \\ \bar{y}_m - \bar{y}_i < 0, \end{cases}$$

$$K_{i,m} = \nu - K^{0*}_{i,m}, \quad \text{if} \quad \begin{cases} \bar{x}_m - \bar{x}_i > 0 \\ \bar{y}_m - \bar{y}_i < 0, \end{cases}$$

where ν, depending upon the sign of the difference $d_i = \bar{x}^* - \bar{x}_i$ (see Fig. 3b), takes on the following values:

$$\nu = 0 \quad \text{when} \quad d_i > 0,$$
$$\nu = 2 \quad \text{when} \quad d_i < 0.$$

The quantity $K^{0*}_{i,m}$ is expressed by $K^{0}_{i,m}$, depending upon the magnitude of the modulus $(\bar{x}_m - \bar{x}_i)$:

$$K^{0*}_{i,m} = K^{0}_{i,m} \quad \text{when} \quad 0 < |\bar{x}_m - \bar{x}_i| < 0{,}5,$$
$$K^{0*}_{i,m} = -K^{0}_{i,m} \quad \text{when} \quad 0{,}5 < |\bar{x}_m - \bar{x}_i| < 1{,}0,$$
$$K^{0*}_{i,m} = -(1 - K^{0}_{i,m}) \quad \text{when} \quad 1{,}0 < |\bar{x}_m - \bar{x}_i| < 1{,}5,$$
$$K^{0*}_{i,m} = -(1 + K^{0}_{i,m}) \quad \text{when} \quad 1{,}5 < |\bar{x}_m - \bar{x}_i| < 2{,}0,$$

where

$$K_{i,m} = K_{i,m}(|\bar{x}_m - \bar{x}_i|, |\bar{y}_m - \bar{y}_i|) < 0{,}5 \quad \text{when} \quad 0 < |\bar{x}_m - \bar{x}_i| < 0{,}5.$$

The change of $K^{0*}_{i,m}$ and the conformity of points 1, 2, 3, and 4 is shown on Fig. 3b.

Furthermore, when $m > i$, a one is added to all values of $K_{i,m}$ in accordance with formula (2). The indicated method of normalization of the function $K_{i,m}$ was carried out in a program for performing calculations on a computer.

If the calculation is performed for profiles with very thick trailing edges, for instance for the profiles of gas turbines with cooled blades, then for determining Φ_r, the right sides of the system of equations must be recomputed for $|K_{i,0}| > 1$. In this case their new values, $K'_{i,0} = K_{i,0} - 2$, are calculated. The recalculation is forseen in the program.

In the program, the profile is divided into a given number 2n of intervals and the points of division are calculated. The points of division of the profile with

odd indices are taken as the calculation points, and the point with even indices are the boundaries of the sections. The consecutive numeration of points goes from the middle of the trailing along the convex side of the profile, but then along the concave side (Fig. 3a).

After finding the points of division, the function $K_{i,m}$ of the integral equation is calculated and they are normalized according to the rules stated above. Then the coefficients of the system (3) of linear algebraic equations are formulated:

$$A_{i,j} = K_{i,j+1} - K_{i,j-1} \quad (i, j = 1, 3, \ldots, 2n-1).$$

The right sides of the systems of equations will be the quantities $2x_i$, $2\bar{y}_i$, and K_{10}.

The systems of linear algebraic equations are solved by the method of sliding successive approximations. As the zero approximation we shall take the right sides of the equations. Calculations of the potentials Φ_x, Φ_y, and Φ_Γ are conducted with a specified degree of accuracy. As a result of the calculations we shall obtain the values of Φ_x, Φ_y, and Φ_Γ at the calculation points of the contour and shall calculate the generalized potential $\bar{\Phi}$ with formula (4).

For differentiation of the potential $\bar{\Phi}$ we use the interpolation formulas of Stirling and Newton, retaining the third order differences.

For calculation of cascades of blades that are given by the coordinates of the points, it is necessary that these coordinates be given with uniform pitch along axis x. The leading and trailing edges of the profiles should be rounded and the coordinates of the arc centers and the values of the radii should be indicated. In addition, the abscissas of the boundaries of these arcs are given. A check showed that the minimum permissible number of division intervals of a contour is 2n = 120.

As an example we shall present the calculation of a cascade of T-1 TsKTI turbine blades for a relative pitch of $\bar{t} = 0.646$. This cascade consists of greatly distorted thick blades and was calculated for small pitch.

A comparision of the velocity distribution $c(S) = \frac{d\bar{\Phi}}{d\bar{S}}\left(\bar{S} = \frac{S}{L}\right)$, which was obtained by numerical differentiation by the potential $\bar{\Phi}$ with the velocity distribution that was obtained earlier according to the method based on conformal mapping,* showed that differentiation should be carried out separately on the convex and concave sides of

*This method, as it is known, makes it possible to calculate the velocity distribution without numerical differentiation of the velocity potential.

the blades (Fig. 4).

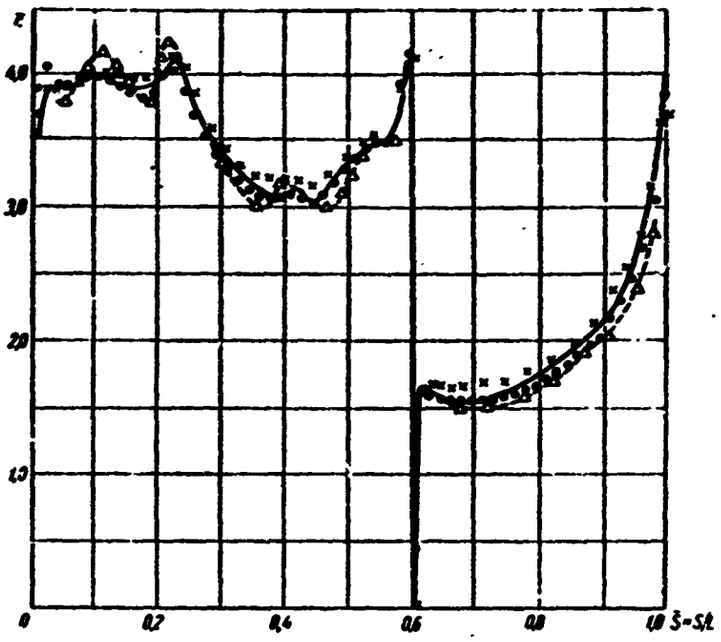

Fig. 4. Velocity distribution according to a TsKTI T-1 blade development for ($\bar{t}$ = 0.646; β_1' = 160°; β_2 = 16°):
—— calculation by the method of conformal mapping; o o o — calculation on electronic computer (EVM) for 2n = 120; -Δ -Δ -Δ — calculation according to the channel theory; × × × — TsKTI experiments.

In the calculation, for each value of β_1 we obtain two values of angles β_2, from which one value of β_2' is determined with the help of formula (6), and the second is given by $\beta_2'' = \beta_2' + 1^\circ$. For a T-1 cascade when $\beta_1' = 160^\circ$, the values of $\beta_2' = 14^\circ 42'$ are obtained.

In the given example the angle β_2, which was determined by means of extrapolation, is equal to 16°. The velocity profile is shown in Fig. 4. This figure also indicates the velocity values that were obtained experimentally [20]. The experimental value of the flow-outlet angle in this case is also equal to 16°. As can be seen from Fig. 4, the velocity profile obtained on the computer coincides well with the experimental profile.

Considerably simpler calculation methods, which make it possible to solve the direct and inverse problems with a satisfactory accuracy in certain cases, are based on the channel theory. These methods do not require the application of electronic computers. At this time we know of several methods for calculating cascades according to the channel theory [33].

Cascade calculation according to the channel theory is based on the use of a continuity equation and the condition of irrotational (potential) flow for a given or specially selected law of velocity distribution along the cross section of a channel.

The problem of the flow around cascades can be successfully reduced to the calculation of flow in the channel only for moderate values of relative pitch. Furthermore, the channel theory makes it possible to calculate the flow only in the vane channel; in the entrance area of the back and in the slanting shear on the exit it is necessary to use special methods, and the accuracy of calculation for these areas is lowered.

The channel theory was developed in the works of G. Flyugel', G. Yu. Stepanov, A. N. Sherstyuk, and G. S. Samoylovich. All known methods for calculating a cascade channel are based on the following assumptions: a) the shape of the isopotential lines and the points of their intersection with the channel walls are determined approximately; b) the law of velocity distribution along the cross section of the channel (along the isopotential lines) is selected.

In connection with the fact that the velocity distribution along the cross section of a channel has a hyperbolic character with respect to the radius of curvature, the appropriate equation can be selected in the form proposed by G. S. Samoylovich and A. N. Sherstyuk:

$$\frac{c}{c_1} = \frac{1}{1 + \bar{\xi} + k_1 \bar{\xi}^2}. \tag{8}$$

Here (see Fig. 3a) c_1 is the velocity on the convex surface of the channel (back of blade); $\bar{\xi} = \xi / r_1$ is a dimensionless ordinate; $\bar{a} = \frac{a}{r_1}$ is the dimensionless width of the channel; r_1 is the radius of curvature of the back of the blade;

$$k_1 = \frac{\varkappa - 1}{2\bar{r}_2 - \bar{a}}; \quad \varkappa = \frac{\bar{r}_2 - 1}{\bar{a}}; \quad \bar{r}_2 = \frac{r_2}{r_1},$$

where r_2 is the radius of curvature of the concave surface.

As the equipotential line we shall select a circular arc (see Fig. 3a) which is a smooth line that is normal at the intersection points to the walls of the channel. The velocity components along this equipotential are small as compared to the normal components.

Formula (8) is suitable for channels both with identical, and also with different (in sign) curvatures. The quantity $\bar{a}$ is positive, if the first wall is convex, and

negative, if it is concave. The dimensionless radius of curvature of the second wall $\bar{r}_2$ is considered to be positive when one wall is concave and the other convex, and negative when both walls are concave or convex.

We shall now find the gas flow through a cross section of the channel. For small numbers $M < 0.4$, when the influence of compressibility may be disregarded, we shall find the volume flow rate of fluid through the channel a with the following continuity equation:

$$Q = \int_0^a c\,da.$$

Replacing c here from (8) and integrating, we will obtain:

$$\delta = \frac{Q}{c_s a} = \frac{1}{\bar{a}} \frac{1}{\sqrt{1+4k_1}} \ln \frac{1-2k_1\bar{a}/(1-\sqrt{1+4k_1})}{1-2k_1\bar{a}/(1+\sqrt{1+4k_1})}. \tag{9}$$

For convenience of calculation, the Appendix gives graphs of the dependence of $\delta = f(\bar{a}, \varkappa)$ which is expressed by formula (9).

For a compressible fluid it is necessary to consider the change of density. The most simple way of calculating compressibility was indicated by A. N. Sherstyuk. By using the method of small disturbances, it is easy to show that in the case of a compressible fluid it is also possible to use formulas (8) and (9), if the volume flow rate of air (in the given "section") is determined for average density ρ_s:

$$Q = G/\rho_s,$$

where G is the mass flow rate of gas.

The density ρ_s is found by means of the given flow rate q_s and the tables of gas-dynamic functions [22], while q_s is determined by the formula

$$q_s = G/G_*$$

(G_* is the critical flow rate of gas through a given section of the channel).

But if

$$G = \rho_1 c_1 t \sin\beta_1 = \rho_2 c_2 t \sin\beta_2;$$
$$G_* = \gamma_* a_* a,$$

then

$$q_s = q_1 \frac{t\sin\beta_1}{a} = q_2 \frac{t\sin\beta_2}{a}, \tag{10}$$

where the given flow rate, q_1 or q_2, is determined correspondingly by the parameters of flow in front of the cascade or behind it.

The method of calculation of velocities reduces to the following. Circles are inscribed in the channel (see Fig. 3a). Equipotentials (circular arcs) are drawn through the points of tangency of these circles with the walls of the channel A and D. The length of the equipotentials and the radii of curvature of the boundary flow lines at points A and B (r_1 and r_2) are determined. Then the dimensionless parameters are found:

$$\bar{a} = \frac{a}{r_1};\ \bar{r}_2 = \frac{r_2}{r_1};\ \varkappa = \frac{\bar{r}_2 - 1}{\bar{a}}.$$

On the basis of the gas parameters in front of the cascade, the dimensionless velocity λ_1 is determined, and from the tables of gas-dynamic functions, the given flow rate q_1 is found.

Further, by formula (9) the average given flow rate for the constructed equipotentials is found, and from the tables of gas-dynamic functions and q_s, the corresponding ratio of ρ_s/ρ_0 is determined.

The volume flow rate through section a is determined by the formula

$$Q = Q_1 \frac{\varrho_1/\varrho_0}{\varrho_s/\varrho_0},$$

where Q_1 is the volume flow rate in front of the cascade;

$$Q_1 = tc_1 \sin \beta_1$$

(the ratio ρ_1/ρ_0 is determined by q_1).

Now, by means of formula (9) or the graph (see Appendix), we find the value of δ and then the velocity at point A:

$$c_A = Q/\delta_A.$$

The velocity at point D is determined by formula (8).

In the calculation of flow at the entrance and exit sections of the back in the slanting shear of a cascade, it is necessary to find the boundary flow line. In a simple case, the boundary flow lines in front of the cascade and behind it can be selected in the form of segments of straight lines (see Fig. 3a). The direction of these lines at the cascade entrance is given (angle β_1), and at the exit it can be determined by one of the known methods and, in particular, by the following formula (§ 4):

$$\beta_2 = \arcsin\left(m_0 \frac{a_2}{t}\right).$$

In reality, the separated boundary flow lines in front of and behind a cascade are distorted near the leading and trailing edges, whereby this distortion is more

considerable, the greater the relative pitch of the blades and the circulation.

The accuracy of velocity determination with the described method may be judged by Fig. 4, which gives a comparision of the calculated and experimental data for a cascade of T-1 TsKTI turbine blades. As follows from Fig. 4, an essential distinction between the calculated and experimental data is observed mainly near the leading and trailing edges, which is quite regular.

§ 3. BLADE STANDARDS OF NOZZLE AND MOVING CASCADES

The blades of nozzle and moving cascades developed by various organizations (TsKTI, MEI, TsNII, LMZ) are listed in blade atlas which is recommended for use by turbine-construction plants. The atlas includes blades with small design and tip losses, and ones with stable aerodynamic properties in a wide range of variation of geometric and performance parameters.

For the purpose of limiting the number of blades and their type and dimensions to the minimum practical, and for setting up the centralized production of blades in order to employ progressive technology methods and to decrease metal expenditures, some of the blades of nozzle and moving cascades given in the atlas are standardized. These standards include blades only for subsonic velocities (group "A"), developed by TsKTI, LMZ, and MEI.

Table 2 gives the main parameters of standardized cascades.* The standard includes four profiles of nozzle blades and nine profiles of moving blades of the action type.

The profiles of nozzle (guide) cascades, H-1, H-2, and H-4, have an approximately identical range of outlet angles of flow, i.e., $\alpha_1 = 9\text{-}15^\circ$, but different mechanical properties. Profile H-2 is designed for large outlet angles ($\alpha_1 = 12\text{-}20^\circ$).

As can be seen from Table 2, the standard designations of the profiles are modified (see Table 1). We shall consider the complete designations in an example of H-12-B and 4P-42-B profiles. Here the letters H and P, respectively, indicate the type of cascade (guide, i.e., nozzle and moving). The number after the letters H and P (1, 2, 3, 4, ...) indicates the organization that developed the profile.

For moving cascades, the numbers before the letter P indicate the fluid deflection, i.e., the type of profile with respect to velocity triangle. As the number increases, the inlet and outlet angles increase, and the fluid deflection

*All designations in Table 2 have been selected in accordance with the standard.

Table 2. Profiles of Nozzle and Moving Cascades (Included in the Standard)

Profile designations adopted in the standards	Range of outlet angles* α_1°, β_2°	Range of inlet angles,* α_0°, β_1°	Cross-sectional area f, cm²	Moments of resistance, cm³				Moments of inertia cross-sectional, cm⁴		Old profile designations	Organization that developed the profile
				W_x, кр	W_x, сп	$W_{y\,max}$, кр	$W_{y\,max}$, кр	J_x	J_y		
H-1	9—15	70—110	2,403	0,313	0,365	1,678	0,905	0,1976	2,127	C-1	Krylov TsNIIS
H-2	12—20	70—110	1,46	0,135	0,184	0,770	0,455	0,0916	1,069	TH-2	TsKTI, LMZ, MEIS
H-3	9—15	70—110	2,42	0,320	0,360	1,660	0,850	0,2185	2,401	2324	
H-4	10—17	70—110	2,168	0,232	0,288	1,525	0,760	0,1560	2,229	TC-1A	
1P-1	17 (19—22)	20 (14—25)	7,195	1,831	2,305	5,895	3,832	2,94	12,61	A-20	Krylov TsNIIS
3P-1	24 (24—28)	28 (28—45)	7,091	1,895	2,116	5,108	3,662	2,697	11,09	A-24	
4P-1	31 (28—32)	45 (40—55)	6,106	1,396	1,617	4,681	3,195	1,804	10,06	A-26	
1P-2	17 (16—19)	20 (18—30)	7,437	2,039	2,672	5,215	4,177	3,692	11,88	T-1	TsKTI
2P-2	20 (19—22)	25 (25—40)	7,131	1,827	2,312	5,087	3,749	3,063	11,08	T-2A	
3P-2	24 (24—28)	28 (28—45)	5,694	1,218	1,607	3,967	3,013	1,777	8,784	T-3	
2P-4	20 (19—22)	25 (25—40)	7,386	1,897	2,406	5,208	3,758	3,237	11,18	TP-2A	MEI
4P-4	31 (28—32)	45 (35—50)	4,853	0,896	1,125	3,397	2,495	1,069	7,340	TP-4A	MEI
5P-4	34 (32—36)	50 (40—55)	4,113	0,6607	0,8656	2,978	2,186	0,7214	6,450	TP-5A	

*For moving cascades, the standards indicate only one value of the inlet and outlet angle. In reality, every moving cascade can be used in a sufficiently wide range of β_1 and β_2 (see Table 1). This range is indicated here tentatively in parentheses.

**Given for nozzle cascades with a width of B = 25 mm and for moving cascades with a width of B = 50 mm; W_x and W_y are the moments of resistance of the profile with respect to axes x – x and y – y (see Fig. 3); I_x and I_y are the moments of inertia with respect to axes x – x and y – y; f is the cross-sectional area of the blade.

correspondingly decreases. Profile 1P corresponds to a deflection of $\Delta\beta = 180 - (\beta_1 + \beta_2) = 135\text{-}143^\circ$, and profile 5P indicates a deflection of $\Delta\beta = 86\text{-}96^\circ$.

The second digit in the designation for nozzle (guide) cascades and the third digit in the designation for moving cascades characterizes the thickness of the trailing edge. The letter B gives the width of the profile in mm.

The base line for the construction of profiles is the external chord. The adoption of this base line excludes the necessity of recalculating the principle dimensions of the profile contour for variation of the angles of incidence of the profiles.

All profiles of nozzle and moving cascades that are included in the standard (Table 2) are divided into groups, depending upon the relative thickness of the trailing edge $\Delta_{кр}$.

For the formation of geometrically similar cascades for the majority of profiles of rotor blades of steam turbines, a total of two thicknesses for trailing edges can be introduced for width intervals from 15 to 20 mm and from 25 mm and above.

In connection with the fact that the variation interval of edges for blades that are employed in stationary turbine construction is small, the introduction of a thicker edge for a width 15 to 20 mm is mainly stipulated by the technological considerations.

For nozzle cascades, for the purpose of decreasing the modifications of each type of profile in the development of the standard dimensions, the entire width scale from 25 to 100 mm is divided into three groups according to thickness of trailing edges: 1.0; 1.5, and 2.0 mm, with a variation in width by 25-35 mm, 40-65 mm, and 70-100 mm.

The standard contains profiles of different widths which are geometrically similar to the initial profiles, all their dimensions, including the trailing edge, vary within the limits of each group with complete geometric similarity. For a guarantee of complete geometric similarity of profiles, the standards include reference profiles whose dimensions are calculated with an accuracy of four places after the decimal point.

§ 4. AERODYNAMIC CHARACTERISTICS OF CASCADES FOR SUBSONIC VELOCITIES

Aerodynamic characteristics include the dependence of the coefficients of profile and tip losses of energy and inlet angles of flow on the basic geometric and performance parameters of a cascade.

The characteristics are obtained experimentally, e.g., by testing cascades in wind tunnels by the transverse method. Practically all experiments were conducted with a small degree of turbulence* of the incident flow, $E_0 = 0.5\text{-}1.5\%$*, and a uniform velocity field at the cascade entrance.

Consequently, the characteristics in the standard cannot be directly used for thermal calculation of a stage and a multistage turbine, since they do not consider a number of extremely important factors which determine cascade losses under real conditions: flare, discontinuity of velocity field with respect to height, and

*By degree of turbulence, we mean the quantity

$$E_0 = \frac{\overline{c'}}{c_m} = \frac{1}{c_m}\sqrt{\frac{1}{\Delta t}\int_0^{\Delta t} c'^2\,dt},$$

where c' and $\overline{c'}$ are the local and root-mean square values of the pulsating velocity component; c_m is the mean velocity of steady motion; Δt is the averaging-time interval.

turbulence of flow. It is natural that the first two factors are important only for estimating tip losses. Flow turbulence also influences profile losses.

Aerodynamic properties can be reliably used for selecting an optimum cascade variant for the stage being designed, and also for estimating the influence of the noted changes of geometric or performance parameters of a profile. Taking into account the correction for turbulence, the coefficients of profile losses can be used sometimes for calculating the cascades of stages with long blades of constant and variable profiles. In such stages with cylindrical outlines the tip losses are sometimes (with large relative height) small; therefore, it is possible to expect a satisfactory coincidence of the calculation with the experiment.

After selecting the cascades, it is necessary to use the appropriate aerodynamic properties which are given in the atlas of profiles. These characteristics are given in the Appendix for two types of cascades.

For reaction cascades, the profile characteristics, i.e., the coefficients of profile losses $\zeta_{пр}$ and the outlet angles of two-dimensional flow α_1, are given depending upon the relative pitch $\bar{t} = t/b$ and the angle of incidence of the profile α_y for Reynolds number* $Re_1 = \frac{c_{1t}b_1}{\nu_1} \geq 4 \cdot 10^5$ and number $M_{c_1} = \frac{c_{1t}}{a_1} = 0.3$. The influence of the inlet angle of flow α_0 is considered by the appropriate corrections for ζ and α_1. These corrections are given for the same initial values of Re_1 and M_1.

Experiments show that usually the influence of Re number at subsonic velocities must be considered up to $Re = 10^6$ (Fig. 5). For this purpose, the standard includes corrections which consider the influence of Re number on profile losses. Experiments conducted by different organizations distinctly showed that the influence of Re for various cascades is qualitatively similar. Therefore, the corresponding corrections are given in the form of $k_{Re} = \zeta_{пр}/\zeta_{пр\ 0} = f(Re)$, where $\zeta_{пр\ 0}$ is the coefficient of profile losses for $Re = 10^6$, which correspond to the minimum losses shown in Fig. 5.

The standard also contains the dependence of the coefficient of tip losses ζ_K on the quantity that is inverse to relative height $1/\bar{l} = b/l$ for different values of

$$K = 1 - \left(\frac{\sin\alpha_1}{\sin\alpha_0}\right)^2.$$

*The formulas for determining the Re and M numbers include the theoretical velocities c_{1t} and w_{2t}. The kinematic viscosity ν_1 and the velocity of sound a_1 for the theoretical process are selected according to the parameters behind the cascade.

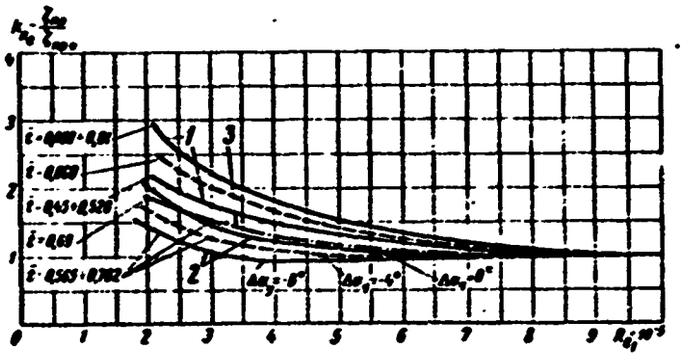

Fig. 5. Influence of Re number on profile losses in reaction cascades according to experiments at LMZ, MEI, and TsKTI. Curves: 1 – for profile H-31 (LMZ); 2 – profile H-26 (TsKTI); 3 – profile H-46 (MEI).

It should be emphasized that the influence of Re number on tip losses is also considerable. The other performance parameter, i.e., the inlet angle of flow α_0, has a more substantial effect on the tip losses than on the profile losses: the influence of these two parameters is especially great at small relative heights b/l. These results are confirmed by the data shown in Fig. 6, which were obtained at the MEI for low subsonic velocities.

However, in connection with the shortage of experimental data, the appropriate corrections are not included in the standard. For a tentative estimate of the influence of α_0 on profile and total losses in a reaction cascade of the type TC-A (MEI) and others, it is possible to use the graphs in Fig. 6.*

For action cascades, the influence of the inlet angle is illustrated by the graphs in Fig. 7.

The influence of compressibility (M number) on the characteristics of cascades of group "A" is different depending on the shape of the profile and the geometric parameters of the cascade, and in particular, the relative pitch and relative height. However, for the majority of cascades made out of profiles of group "A," there is noted a general tendency towards a sharp increase of profile losses with the increase of M_1 when $M_1 > M_{1*}$. In the subcritical region of $M_1 < M_{1*}$ the profile losses decrease

---

* $K_{\alpha 0} = \frac{\zeta}{\zeta_0}\left(R_{e0} = \frac{\zeta_{пр}}{\zeta_{пр.0}}\right)$ and $K_{\alpha 1} = \frac{\operatorname{tg}\alpha_1}{\operatorname{tg}\alpha_{10}}$.

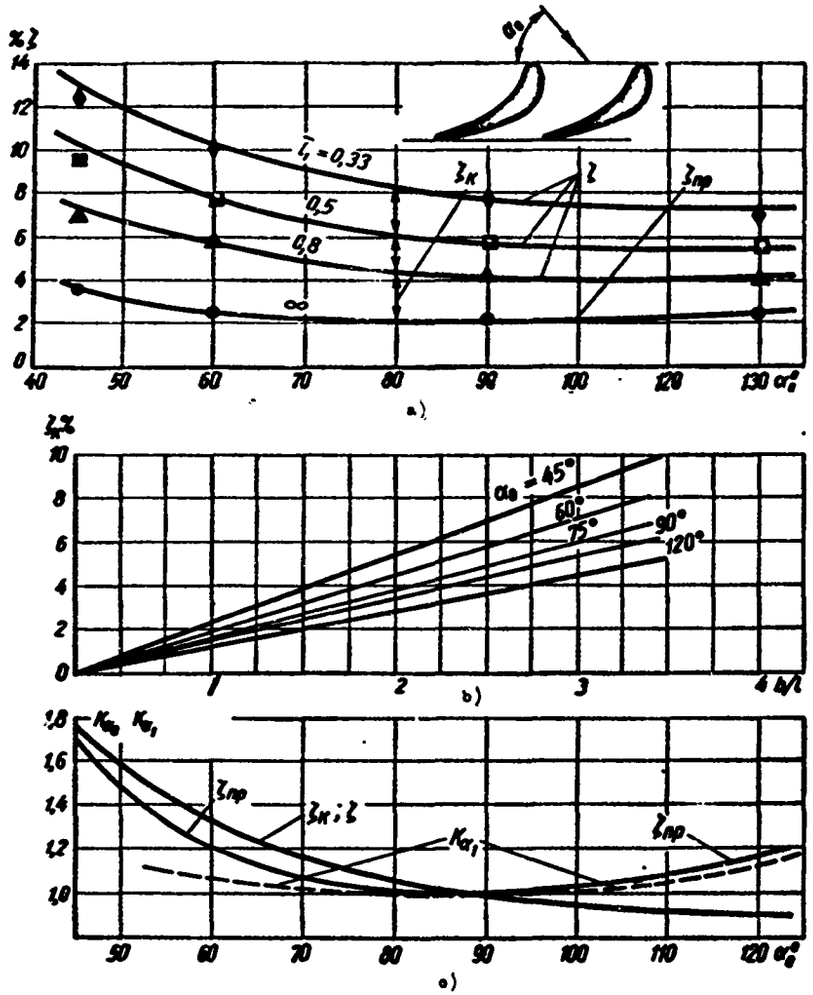

Fig. 6. Influence of inlet angle α_0 of reaction cascades at low subsonic velocities (profile TC-1A, M = 0.5 and Re = $4 \cdot 10^5$): a and b) total, profile, and tip losses ($\zeta_K = \zeta - \zeta_{пр}$); c) corrections that consider the influence of α_0 on the losses, and the outlet angle of flow.

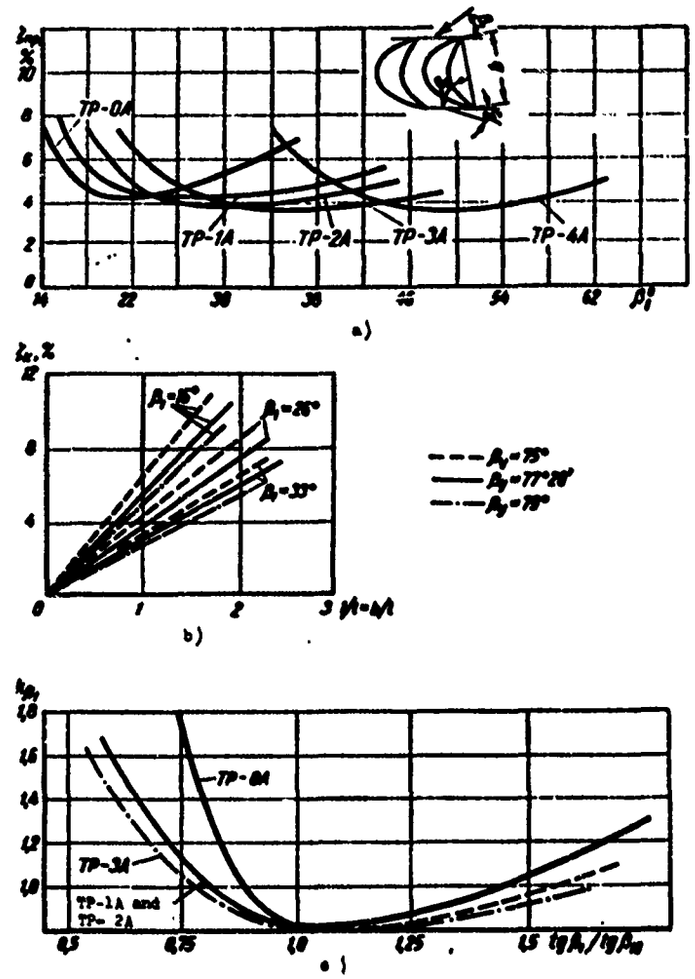

Fig. 7. Influence of inlet angle of flow β_1 of action cascades at low subsonic velocities (profiles of the type TP-A, M = 0.5 and Re = $3 \cdot 10^5$): a and b) profile and tip losses; c) corrections that consider the influence of β_1 on the losses. MEI experiments.

somewhat as M_1 increases. The intensity of the increase of $\zeta_{пр}$, depending upon M_1 in the transonic region, varies essentially as the relative pitch, inlet angle, and degree of flow turbulence vary.

The influence of pitch is explained by the displacement of the local supersonic zone and the closing shock waves on the back of the profile as $\bar{t}$ changes. As $\bar{t}$ increases the shocks move against the flow; therefore, the flow around the back becomes worse (Fig. 8a). The character of the change of profile losses, depending upon M_1, essentially depends on the conditions of flow in the boundary layer. The intensity of the increase of losses in the transonic region, during the interaction of local shocks with the laminar layer, is considerably higher than in those cases when the layer on the back of the profile in the slanting shear is turbulent. If in the shock zone there occurs turbulization of the layer on the back, the profile losses decrease somewhat at M_1 increases (see Fig. 8a).

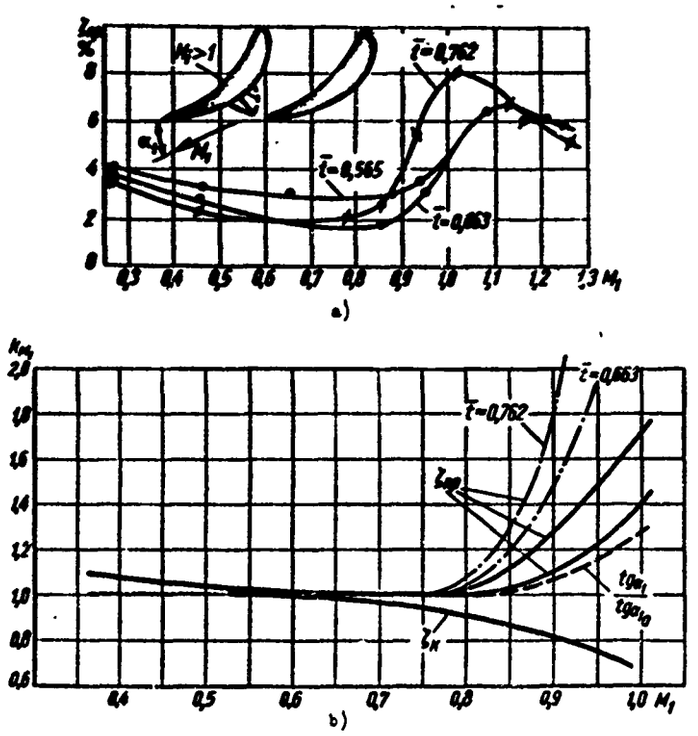

Fig. 8. Influence of compressibility (M_1 number) in reaction cascades for different relative pitch $\bar{t}$: a) profile losses, b) corrections for profile and tip losses and outlet angle of flow α_1. According to TsKTI — · — · —; according to MEI ———.

Tip losses in nozzle cascades decrease in the subsonic and transonic regions as M_1 increases (see Fig. 8b). Consequently, the total losses when $M_1 > 0.6$ increase less intensely as the relative height decreases. The corrections that consider the

influence of compressibility on profile and tip losses in nozzle cascades and the outlet angle of flow when $M_1 < 1$ can be taken from the curves in Fig. 8b.*

The aerodynamic properties of moving cascades of the action type are represented in the form of analogous dependences of profile and tip losses of energy and outlet angles of flow on the basic geometric and performance parameters (see Appendix).

The ranges of permissible values of relative pitch, angle of incidence, and inlet angles of flow are shown for each profile in the corresponding aerodynamic properties.

Let us note that the region of practical self-similarity with respect to Re number occurs in moving cascades for lower Re_2, which depend on the inlet angle of flow; this is connected with the earlier transition of the laminar layer to the turbulent layer on the profile contours; the transition region in weakly convergent flows is displaced against the flow.

For an estimate of the effect of M_1 number on profile and tip losses and on the outlet angles of flow for action moving cascades, we can use the graphs in Fig. 9, which were constructed on the basis of MEI experimental data. Qualitatively, these graphs coincide with the corresponding curves for nozzle cascades (see Fig. 8).

In action cascades, the transition through the velocity of sound is accompanied by a less intense increase of profile losses (Fig. 9), since in the zone of supersonic velocities on the back the boundary layer is turbulent. Tip losses decrease as the M_2 increase, especially intensely in the region of transonic velocities.

The aerodynamic properties of nozzle and moving cascades, which are given in the standards, do not contain corrections that consider the influence of initial turbulence on profile and tip losses and the outlet angle of flow.

At the same time, as indicated in the MEI experiments in Fig. 10, the profile losses essentially increase as the degree of turbulence increases, whereby the influence of E_0 is different, depending upon the type of cascade and the Re and M numbers. The outlet angle also increases as the degree of turbulence increases. Tip losses changes less significantly as E_0 increases. For moderate values of $Re < 5 \cdot 10^5$ and $M < 0.5$, the profile losses in nozzle and moving cascades decrease somewhat in the interval of $E_0 = 0.5$-2%, or remain constant.

---

*$K_{M_1} = \frac{\zeta_{пр}}{\zeta_{пр \cdot 0}}$, where $\zeta_{пр \cdot 0}$ is the minimum coefficient of profile losses.

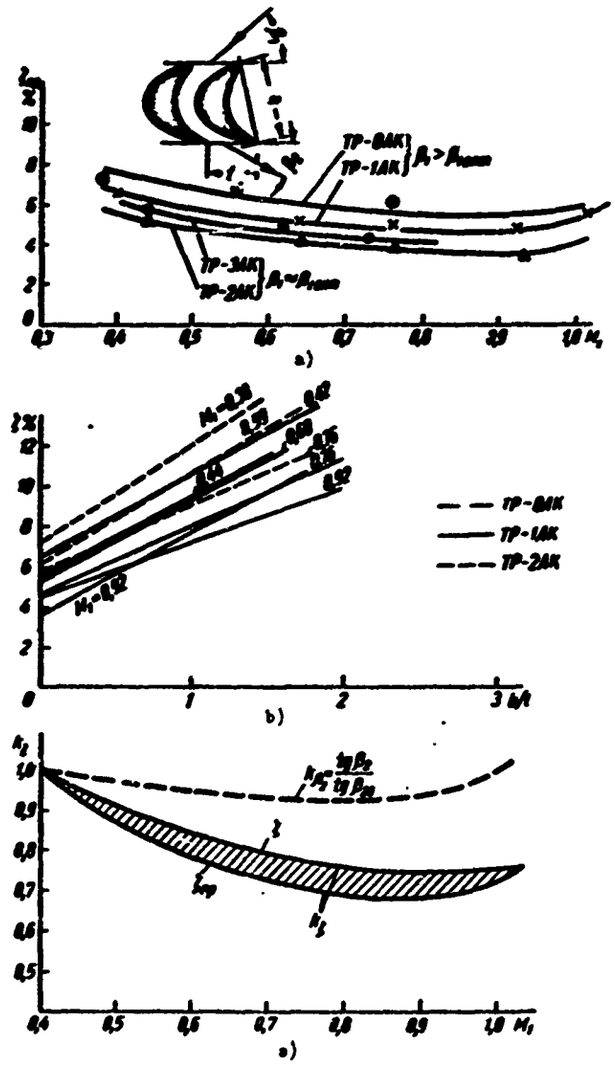

Fig. 9. Influence of compressibility in action cascades: a – on profile losses, b – the same, on total losses; c – corrections for profile and total losses according to MEI.

The certain lowering of losses $\zeta_{пр}$ in this interval of E_0 for action cascades is explained by the displacement of the separation line through the flow at the trailing edge, since an increase of turbulence of the layer increases its resistance to separation. For this reason, the losses in nozzle cascades in the same interval of E_0 are practically unchanged. However, in this case the influence of E_0 is less considerable because the rearrangement of the velocity profile in the boundary layer in a convergent flow is not so intense when E_0 changes.

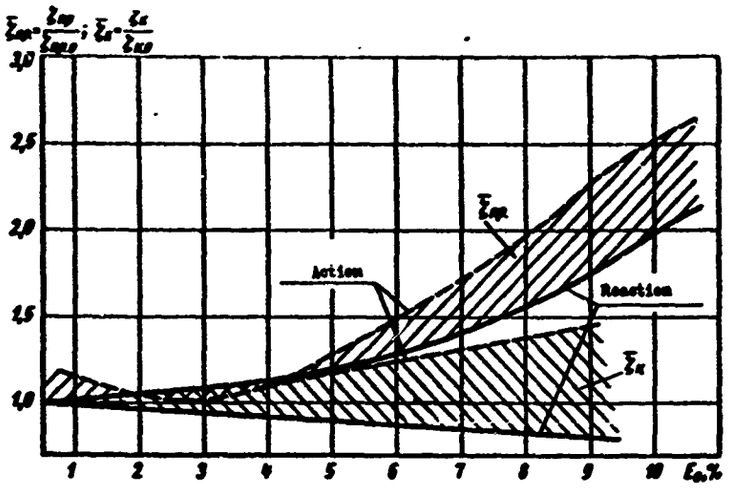

Fig. 10. Influence of degree of turbulence on profile and tip losses in reaction and action cascades for different M and Re numbers.

When $E_0 > 2\text{-}3\%$ the profile loses in the cascades increase, whereby the greatest increase occurs in action-type cascades, while the tip losses increase less intenselv.

A detailed analysis of the structure of flow in cascades for large E_0 shows that as the degree of turbulence increases, the frictional losses in the boundary layer usually increase. For an estimate of the increase of ζ, depending upon E_0, it is possible to use the curves in Fig. 10. Here it is necessary to know the tentative values of E_0 in the stage being designed. Minimum E_0 are detected in the first turbine stage, and maximum in the intermediate stages. Corresponding measurements, carried out at the MEI, showed that the degree of turbulence for various stages, depending upon Re and M numbers, varies in the range of $E_0 \approx 6\text{-}25\%$.

It should be emphasized that the influence of E_0 is less perceptible at large Re and M numbers, especially in the zone of transonic velocities, where a partial or complete degeneration of turbulence in the boundary layers is detected. For this reason, the influence of E_0 is different for stages that operate in various intervals of change of Re and M.

Experiments conducted at MEI showed that even with a high turbulence of flow at the entrance, at large M_1 numbers, in the cascade channels there is detected a reverse transition of the turbulent boundary layer to the laminar boundary layer. The reverse transition is accomplished gradually near the throat section and part of the back in the slanting shear is flowed around by the laminar layer.

Laminarization of the boundary layer is explained by the stabilizing influence

on layer rendered by the large negative pressure gradients that appear on a significant portion of the back contour. An intense convergent flow is especially characteristic for transonic and supersonic velocities. At these velocities on the back of the profile in the slanting shear, to the point of incidence of the shock on the back, the layer turns out to be laminarized.

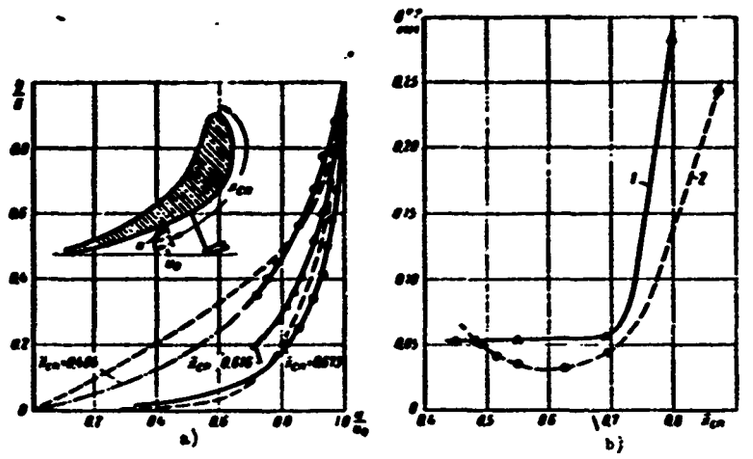

Fig. 11. Characteristics of reverse transition of turbulent to laminar boundary layer according to MEI experiments $M_1 = 1.27$: a — velocity profiles in boundary layer on back; b — change of thickness of inpulse loss along back; y — distance from back; δ — thickness of layer.

Experimental confirmation of the reverse transition at transonic and supersonic velocities is given in Fig. 11, which represents the velocity profiles and thickness variation of impulse losses along the back for small turbulence (curve 1) and for artificial flow turbulence in a channel (curve 2).

It is obvious that a reverse transition for a nonseparated flow leads to a lowering of profile losses in the cascade. However, if on the exit section of the back there forms a diffusion region, the cascade losses increase intensely, since the laminar layer is easily separated. At transonic and supersonic velocities, separation on the back of a profile is caused by shocks.

In those cases when the cascades of stages being designed cannot be taken from the standards or the atlas of profiles, the aerodynamic properties are calculated with empirical and semi-empirical formulas. We shall consider the method of calculating the individual components of energy losses which is used at MEI.

The frictional loss coefficient, taking compressibility into account, is generally calculated by the formula

$$\zeta_{\text{тр}} = \frac{\sum k_1 k_2 H^* \delta^{**}}{t \sin \alpha_1 - \sum k_1 k_2 H^* \delta^{**}}. \tag{11}$$

Here

$$k_1 = \left(\frac{1-\xi_1^2}{1-\xi_{1t}^2}\right)^{\frac{1}{k-1}}; \quad k_2 = \left(\frac{\xi_1}{\xi_{1t}}\right)^2; \quad k_3 = \frac{\xi_1}{\xi_{1t}};$$

$\xi_1 = \frac{c_1}{c_M}$ is the dimensionless flow rate at the trailing edges of the profile (the rate referred to the velocity of flow into a vacuum c_M);

ξ_{1t} is the same quantity for an isentropic process (without losses);

δ^{**} is the depth of the impulse loss;

H^* is the relation of the depth of energy and pulse losses, which is approximately constant and equal to $H^* = 1.8$;

t is cascade pitch;

α_1 is the outlet angle of flow.

In accordance with equation (11), summation is carried out along the concave and convex surfaces at the trailing edges.

The relative depth of the pulse losses on the back and the concave surface is determined by the following formulas:

a) for small longitudinal pressure gradients

$$\bar{\delta}^{**} = \frac{\delta^{**}}{L} = \frac{1}{f_1 \operatorname{Re}_*^{0.25}} \left(\bar{\delta}_0^{**} \operatorname{Re}^{0.25} f_3 + \int_{\bar{x}_0}^{\bar{x}} f_2 d\bar{x}\right)^{0.8}, \tag{12}$$

where L is the length of the back or the concave surface;

b) for large longitudinal pressure gradients

$$\bar{\delta}^{**} = \frac{1}{\varphi_1 \operatorname{Re}_*^{0.2}} \left(\bar{\delta}_0^{**} \operatorname{Re}^{0.25} \varphi_3 + \int_{\bar{x}_0}^{\bar{x}} \varphi_2 \, d\bar{x}\right)^{0.8}. \tag{13}$$

The functions f_1, f_2, f_3, φ_1, φ_2, and φ_3, which depend on ξ_1, are determined by means of graphs (or formulas) given in the Appendix; $\bar{\delta}_0^{**}$ is the value of $\bar{\delta}^{**}$ in the beginning of the turbulent section of the layer. For a completely turbulent flow around a profile, $\bar{\delta}_0^{**} = 0$. The Reynolds number is calculated with respect to stalling speed and the value of kinematic viscosity on the surface of the profile:

$$\operatorname{Re}_* = \frac{a_* x}{\nu_{ст}}.$$

Formulas (11), (12), and (13) are essentially simplified for an incompressible fluid, since the functions that consider compressibility (f_1, f_2, etc.) become equal to zero.

In the determination of frictional losses one may also consider the high turbulence of flow. The depth of the pulse losses in this case is determined by means of V. A. Vrublevskaya's approximate formula:

$$\bar{\delta}^{**}_{E_0} = A\bar{\delta}^{**}_1 e^{b\varphi(Re)\Delta E_0}, \tag{14}$$

where $\bar{\delta}^{**}_{E_0}$ is the value of $\bar{\delta}^{**}$ for large values of the degree of turbulence, $E_0 > 0.5\%$ and $\Delta E_0 = E_0 - 0.005$;

$\bar{\delta}^{**}_1$ is the relative depth of pulse losses when $E_0 \leq 0.5\%$;

A is an experimental coefficient that depends on the type of cascade (longitudinal pressure gradient).

For nozzle cascades at low velocities ($M_1 \leq 0.5$) it is possible to assume that

$$b = 6;\ A \approx 1{,}0 \div 1{,}2 \text{ and } \varphi(Re) = 2{,}3 - 1{,}1\,Re \cdot 10^{-6} + 0{,}86\,Re^2 \cdot 10^{-12}.$$

For an action cascade: b = 6 and A ≈ 1.2-1.4.

During the calculation of profile losses, when taking into account a raised degree of turbulence, one should consider the decrease of parameter H* in formula (11). According to MEI experiments, as E_0 increases to 10%, the parameter H* decreases by 12-15% and is equal to H* = 1.53-1.6.

The increase of profile losses is approximately estimated by means of the graphs in Fig. 10.

Edge losses for a small edge thickness can be determined by TsKTI formulas (M. I. Zhukovskiy and N. A. Sknar'):

$$\zeta_{кр} = 0{,}033\frac{\Delta_{кр}}{t\sin^2\alpha_1} = 0{,}033\frac{\Delta_{кр}t}{a_2^2} \tag{15}$$

for nozzle cascades, and

$$\zeta_{кр} = 0{,}046\frac{\Delta_{кр}}{t\sin^2\beta_2} = 0{,}046\frac{\Delta_{кр}t}{a_2^2} \tag{16}$$

for moving cascades of the action type. Here $\Delta_{кр}$ is the thickness of the trailing edge; a_2 is the width of the throat area.

Edge losses may be tentatively determined by Flyugel's formula:

$$\zeta_{кр} = K\frac{\Delta_{кр}}{a_2}, \tag{17}$$

where K is a coefficient that depends on the geometric and performance parameters of the cascade.

Experiments conducted at MEI indicated that in a known range of change of $\Delta_{кр}/a_2$, the dependence of $\zeta_{кр}(\Delta_{кр}/a_2)$ is also linear. Consequently, formula (17) obtained experimental confirmation. However, in accordance with the experimental data presented in Fig. 12a, coefficient K varies within the limits of K = 0.11-0.27, where the smaller values of K pertain to nozzle cascades. It should be emphasized that, depending upon the method of changing the relative thickness of the edge $\Delta_{кр}/a_2$, the linear character of the curves $\zeta_{кр}(\Delta_{кр}/a_2)$ is disturbed. This is confirmed by the location of experimental points on the curves in Fig. 12a, which were obtained for various pitch, profile angles, and trailing edge thicknesses.

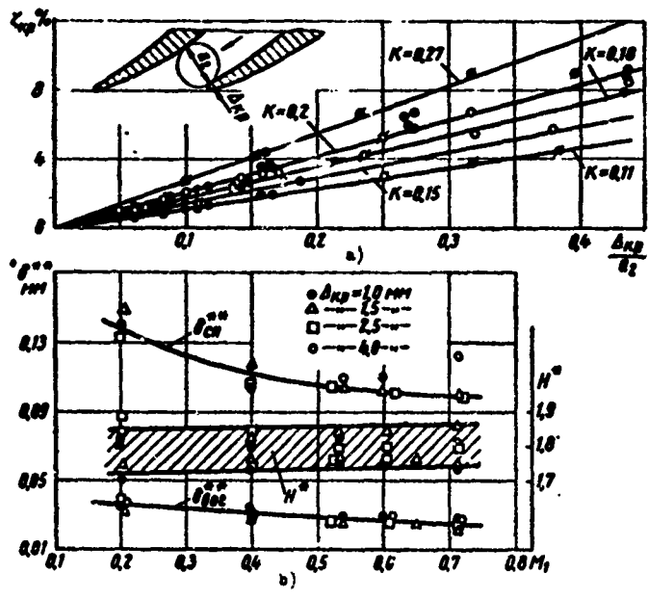

Fig. 12. Characteristics of edge losses depending upon edge thickness and conditions: a — edge losses; b — depth of pulse losses and parameter H* under different conditions. Profile TC-1A, MEI experiment.

The MEI experiments also showed that the depth of the pulse losses on the back and concave surface at the trailing edge and the parameter H* do not depend much on $\Delta_{кр}$ (see Fig. 12b); the ratio $\delta^{**}_{сп}/\delta^{**}_{вог}$, depending upon M_1, Re_1 and $\Delta_{кр}$, changes very little and varies from 3.8 to 4.0. The curves in Fig. 12 show that the edge losses at subsonic velocities depend very little on the M_1 and Re_1 numbers. Profile losses in the cascade are determined by the sum $\zeta_{пр} = \zeta_{тр} + \zeta_{кр}$.

At low subsonic velocities, for a tentative calculation of profile losses it is

possible to use the following formula [48]:

$$\zeta_{кр} = \frac{4\delta^{**}}{a_2},$$

where δ^{**} is the mean value of the depth of pulse losses determined by the formula

$$\delta^{**} = \frac{1}{2}(\delta^{**}_{сп} + \delta^{**}_{пол}).$$

Substituting $\delta^{**} = \xi b\ Re^{-m}$ and $a_2 = t \sin \alpha_{1\ эф} = b\bar{t} \sin \alpha_{1\ эф}$, where $\alpha_{1\ эфф} = \arcsin \frac{a_2}{t}$ is the effective cascade angle, we will obtain

$$\zeta_{кр} = \frac{4\xi}{Re^{m}\bar{t} \sin \alpha_{1\,эф}}. \tag{18}$$

Here m = 0.5 for laminar, and m = 0.25-0.3 for turbulent conditions; according to Zal'f, ξ = 0.05-0.17. For a recalculation of profile losses from one edge thickness to the other, it is possible to use formula (17):

$$\Delta\zeta_{кр} = K\frac{\Delta_{кр\,0} - \Delta_{кр\,2}}{a_2}, \tag{19}$$

where $\Delta_{кр\,0}$ is the edge thickness of the initial profile.

Tip losses are determined by the MEI formula:

$$\zeta_{к} = \frac{AK_1}{\bar{t}Re^{m}}\left\{1 + B\left[1 + \varphi(\lambda)\frac{ctg\,\beta_1}{ctg\,\beta_2}\right]^2 \bar{t}\cos^2\beta_2\right\}. \tag{20}$$

Coefficients A, B, m and K_1 are given in Table 3. The function $\varphi(\lambda) = \frac{\rho_2}{\rho_1}$ is the density ratio before and after the cascade and is expressed by the formula

$$\varphi(\lambda) = \left(\frac{1 - \xi_2^2}{1 - \xi_1^2}\right)^{\frac{1}{k-1}},$$

where ξ_1 and ξ_2 are the dimensionless velocities before and behind the cascade.

For calculation of tip losses it is possible to use certain approximate dependences and, in particular, the TsKTI formula:

$$\zeta_{к} = (0{,}02 \div 0{,}03)K\frac{b}{l}, \tag{21}$$

where, as already indicated, depending upon the parameter

$$K_c = 1 - \left(\frac{\sin \alpha_1}{\sin \alpha_2}\right)^2 \text{ for nozzle cascades,}$$

or

$$K_p = 1 - \left(\frac{\sin\beta_2}{\sin\beta_1}\right)^2$$

for moving cascades, the tip losses are represented in the standards.

Table 3. Values of Constant Coefficients in the Formula for Tip Losses

Action cascades :				Reaction cascades			
Laminar boundary layer		Turbulent boundary layer		Laminar boundary layer		Turbulent boundary layer	
A	B	A	B	A	B	A	B
0.045	5.5	0.13	1.99	0.045	2.0	0.13	0.7
m 0.5		0.25		0.5		0.25	
M_1	0.4	0.6		0.8		1.0	
K_1	0.984	0.957		0.92		0.865	

The outlet angles of flow from the cascade are calculated by means of the approximate formula

$$\alpha_1 = \arcsin m_0 \frac{a_1}{t}, \tag{22}$$

where m_0 is a coefficient that depends on the type of cascade and the conditions of flow (Re and M numbers), which vary within the limits of m_0 = 1-1.1. In many cases, at subsonic velocities it is possible to assume that

$m_0 = \frac{t}{t - \Delta_{кр}}$ ($\Delta_{кр}$ is the thickness of the trailing edge of the profile).

Calculation by means of the above-mentioned formulas permits us with sufficient accuracy to determine the profile characteristics and tip losses of normal cascades.

A comparison of calculated and experimental characteristics is shown in Fig. 13. The calculated and experimental values of the depth of pulse losses coincide satisfactorily for different degrees of turbulence (see Fig. 13a). Analogous conclusions may also be made by comparing the profile characteristics (see Fig. 13b). It should be noted that formula (22) does not consider the effect of Re number on the outlet angle of flow; therefore, in the zone of low Re numbers there is noted a considerable divergence of experimental and computed values of α_1.

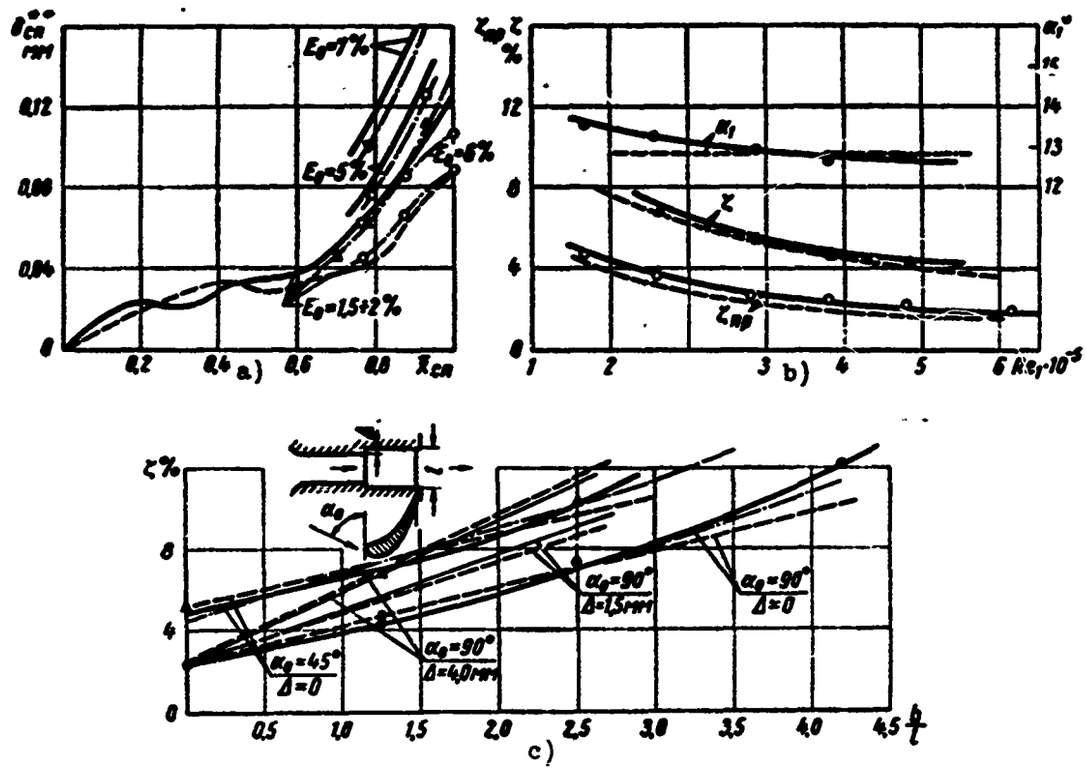

Fig. 13. Comparison of experimental and calculated cascade characteristics: a – depth distribution of pulse losses along the back of action and reaction cascades for different degrees of turbulence: — · — · — experiment; — — — calculation for TC-1A cascade; ——— calculation for TP-2A. b – profile and total (for l = 1.25) losses in TC-1A reaction cascade; —— experiment, — — — calculation by formulas (11), (16), and (20); – loss in TC-1A cascade, depending upon height, inlet angle of flow, and overlap: – experiment; — — — calculation by formulas (11), (16), and (21); — · — · calculation by formulas (11), (16), and (20).

Calculation of tip losses by formula (21) gives satisfactory results for large Re numbers and $\bar{l}_1 \geq 0.4$ for reaction cascades. For lower heights and arbitrary Re_1, formula (20) is more exact (see Fig. 13c).

The presented method of calculating cascade characteristics and the experimental data pertain to aerodynamically smooth blade surfaces. Investigations show that in actual use the surface roughness is essentially increased due to corrosion and erosion of blades, and also as a result of salt deposit. Tentative values of absolute blade roughness are given in Table 4.

For the characteristics of the state of blade surfaces we introduce relative roughness, $\bar{k}_{ш} = k_{ш}/b$ (or $1/\bar{k}_{ш} = b/k_{ш}$).

Profile and total losses in cascades depend on relative roughness, with the increase of which the losses increase and the Re number that corresponds to the beginning of the region of practical self-similarity decreases. In flow around

Table 4. Values of Absolute Blade Roughness

State of blade surface	Ground and polished blades	Milled and drawn blades	Corroded blade surfaces	Precision-cast blades	Rough cast blades	Stamped blades
Average height of rough projections $k_{ш}$ in mm.	0,001—0,002	0,015—0,025	0,01—0,03	0,015—0,03	0,05—0,25	0,1—0,4

aerodynamically smooth surfaces, the coefficient of profile losses decreases as the Reynolds number increases, and in a logarithmic grid this dependence is approximately depicted by a slanted straight line (Fig. 14). The position of the straight line $\lg \zeta_{пр} = f(\lg Re)$ depends on the type of cascade, the inlet angle of the flow, the degree of turbulence, and other parameters which affect $\zeta_{пр}$. Figure 14 shows corresponding straight lines that were constructed for a group of reaction and action cascades in a turbulent zone, depending upon certain parameters.

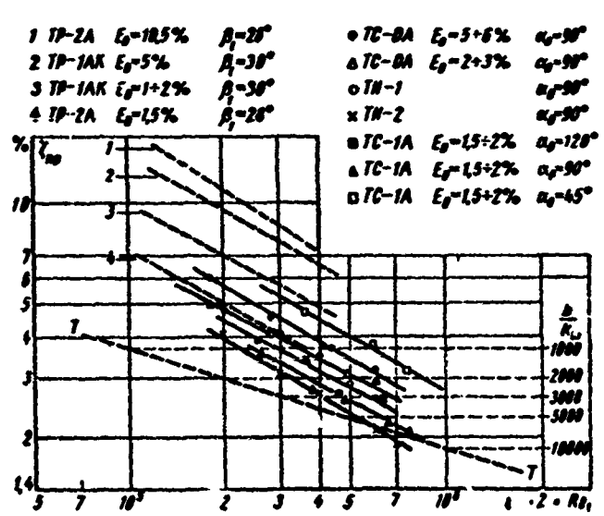

Fig. 14. Dependence of profile losses on Reynolds number for different cascades at various inlet angles and different initial degrees of turbulence. The thin dotted line shows the grid that corresponds to roughness according to G. A. Zal'f. The line T — T determines losses in the turbulent zone for a smooth surface. Experimental curves: — — — — action cascades; ——— reaction cascades.

For each cascade it is possible to note three characteristic regimes of flow. At low Re, when the thickness of the inner portion of the boundary layer with maximum

velocity gradients considerably exceeds the average size of the rough projections, roughness does not affect cascade losses, i.e., the blade surfaces may be considered as being aerodynamically smooth. As the Re number increases, the portion of the boundary layer that is near the wall, and also the whole layer, will be tapered and the rough projects will gradually protrude into the outer portion of the layer, where their flow occurs with separations of flow and eddy formations. There is then a sharp increase in the intensity of turbulence and frictional losses in the boundary layer; the profile losses increase as Re increases. Such conditions should consider as a transition to conditions of flow with raised roughness which are characterized by the independence of $\zeta_{пр}$ on Re ("self-similarity" conditions with respect to Re number).

A comparison of the lines in Fig. 14 shows that the beginning of the transition to the zone of raised roughness essentially depends on the longitudinal pressure gradient, the initial degree of flow turbulence, the inlet angle of the flow, and also the shape of the profile and the channel. These parameters also affect the extent of the transition regime. The grid of dotted lines plotted on Fig. 14, which was constructed according to G. A. Zal'f, is conditional; the experimental characteristics, depending on the enumerated factors, can essentially deviate from the dotted gird.

The influence of roughness on $\zeta_{пр}$ may be considered by means of the experimental data obtained for one roughness $b/k_ш$. After excluding the transition section, we can find the salient point at which the slanted line of losses passes into a horizontal line. For this point the transition Re number is equal to:

$$Re_{пер} = C\frac{b}{k_ш}, \tag{23}$$

where coefficient C is kept constant for the given cascade at fixed values of E_0, α_0, and M_1. A change of these quantities leads to a change of $Re_{пер}$, i.e., coefficient C.

The existing experimental data were insufficient for working out a reliable method of calculating $\zeta_{пр}$ when taking roughness into account. The works along this line do not consider the decisive influence of initial turbulence on the dependence of $\zeta_{пр}$ (Re). A rough estimate of the influence of roughness can be obtained by

calculating the depth of pulse losses at the trailing edges for various roughness.*

Another method, developed by G. A. Zal'f, involves the use of formula (23) for a zone of raised roughness. By substituting $Re_{пер} = Cb/k_{ш}$ into equation (15), we obtain:

$$\zeta_{пр.ш} = \frac{4\xi}{C^{2m} i \sin \alpha_{1эф}} \left(\frac{k_{ш}}{b}\right)^{m}, \tag{24}$$

where coefficient C is determined according to cascade tests for one roughness. Depending upon E_0 and α_0, the following values of coefficient C are obtained: C = 200-500.

In conclusion, let us note that for large negative pressure gradients, which cause a reverse transition of the turbulent regime into the laminar regime, the region of raised roughness (the region of independence of $\zeta_{пр}$ on Re_1) can gradually transfer into the laminar zone.

The calculations with the given formulas, and also the experimental cascade characteristics, which are included in the atlas and standards, do not consider the influence of nonuniformity of the velocity field with respect to height on tip losses.

Experiments have indicated that the influence of nonuniformity essentially depends on the character (structure) of the nonuniformity. The appropriate corrections can be made only after accumulating the necessary experimental data.

§ 5. NOZZLE CASCADES OF LOW HEIGHT

The new cascades that are listed in the atlas and in the standards, as shown above, have small profile losses (1.5 to 3.0% for reaction cascades, and 3.5 to 5% for action (impulse) moving cascades (with low flow turbulence and little roughness).

However, for low heights a decisive value is obtained by the tip losses, which reach large magnitudes in cascades that are made from well streamlined profiles. Further improvement of the profiles of nozzle cascades for decreasing tip losses does not lead to perceptible results. Considering that for low blade heights the flow in an annular cascade has a clearly expressed three-dimensional structure, for decreasing the tip losses one should resort three-dimensional designing of vane channels.

---

*The investigation of the influence of roughness on cascade losses was the subject of a paper by G. Yu. Stepanov, G. A. Zal'f, Shpeydel', and A. S. Laskin.

For decreasing the tip losses in convergent channels, it is necessary to lower the velocities on sections of maximum channel curvature, where secondary flows are intensely developed, and to ensure the most convergent motion in the slanting shear, which promotes thinning of the boundary layers on the back of the profile and also on the upper and lower walls of the channel.

This problem is solved by means of designing channels with respect to height (in the meridional plane). Various means of designing channels with respect to height are possible: a) symmetric contraction, which can be carried out with rectilinear [3] or curvilinear bevels; b) asymmetric contraction, which also is done with rectilinear or curvilinear generatrices [22]; c) designing that ensure motion on a hyperboloid of rotation for the purpose of equalizing the pressures in the peripheral and root areas (stage with constant reaction along radius). In the last case, the problem connected with decreasing the tip losses are unsolved.

Contraction that is symmetric with respect to height does not make it possible to decrease the difference in height reactions, and the decrease in tip losses is insufficient in this case, since in an annular nozzle cascade the distribution of losses with respect to height is asymmetric.

Asymmetric contraction makes it possible to solve both problems: decrease the tip losses and decrease the radial pressure gradient. The optimum form of contraction essentially depends on the basic geometric (θ, d/b, shape of profile, pitch and blade angle) and performance parameters of the stage.

Some results of an experimental investigation of regular and annular cascades with asymmetric contraction are examined below.

Figure 15a represents loss-distribution curves, with respect to height, of regular reaction cascades and annular ones having cylindrical contours with a MEI TC-2A profile. In the regular cascade (curve 1) the regions of increased losses are arranged symmetrically with respect to height and the local loss factors in the zone of secondary flows are identical for the two regions. In the annular cascade (curve 2) we find the asymmetric arrangement of eddy regions, whereby the losses in the root areas are essentially higher than in the peripheral areas. The total losses in the annular cascade are increased as compared to the regular cascade.

Figure 15b presents the distribution of losses with respect to the height of a regular cascade with different types of upper contours. A comparison of the loss coefficients indicates that the best results are obtained with the introduction of contraction in the zone of the slanting shear (variant 4), i.e., in the region

located behind the most curvilinear section of the channel.

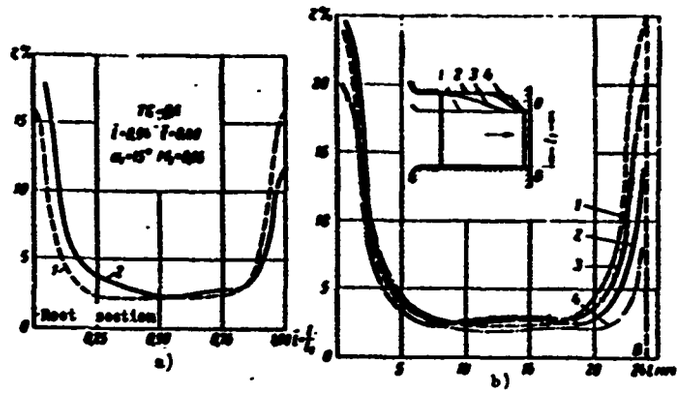

Fig. 15. Loss distribution in annular and regular reaction cascades: a — in regular cascade 1 and in annular cascade with cylindrical contours 2; b — the same, in regular cascade with various upper contours.

As compared to the cascade that has rectilinear contours (variant 1), the loss distribution in the cascade with contraction essentially changes: at the profiled wall, the losses are kept practically constant (or increase very insignificantly), and at the opposite straight wall, they sharply decrease. A certain lowering of loss factors is also noted in the mid-sections of the channel, which is a result of increasing the convergence of the slanting shear. The introduction of sharp contraction (variant 2) or, conversely, making the upper contour very sloping (variant 3), does not provide a very noticeable decrease in losses.

The obtained results — a considerable decrease of losses in a nozzle cascade of low height with asymmetric contraction at the exit area — are easily explained by the graphs of pressure distribution along the profile (Fig. 16a). With the introduction of contraction, the pressure coefficients in all points of the profile, except the regions adjacent to the trailing edge, increase, which indicates a decrease of velocities in the channel. Especially essential is the fact that the decrease of velocities occurs in the most curvilinear part of the channel, where the secondary flows are intensely developed. In accordance with this, there is a decrease in the difference of pressures between the concave and the convex surfaces. Thus, in the section $\bar{S} = 0.4$ and $\bar{S} = 0.7$ the pressure difference* is $\overline{\Delta p} = \bar{p}_{\text{вог}} - \bar{p}_{\text{сп}} = 1.1 - 0.5 = 0.60$ for a cascade with straight walls; after including contraction, this difference

*Here and subsequently the pressure coefficients $\bar{p}$ are determined by the following formula: $\bar{p} = [(p_i - p_1)/(\rho_1 c_1^2/2)]$: where p_i is the pressure at a point on the profile; p_1, ρ_1, and c_1 are the pressure, density, and velocity behind the cascade.

will decrease to $\overline{\Delta p}$ = 1.12 - 0.8 = 0.32, i.e., by two times.

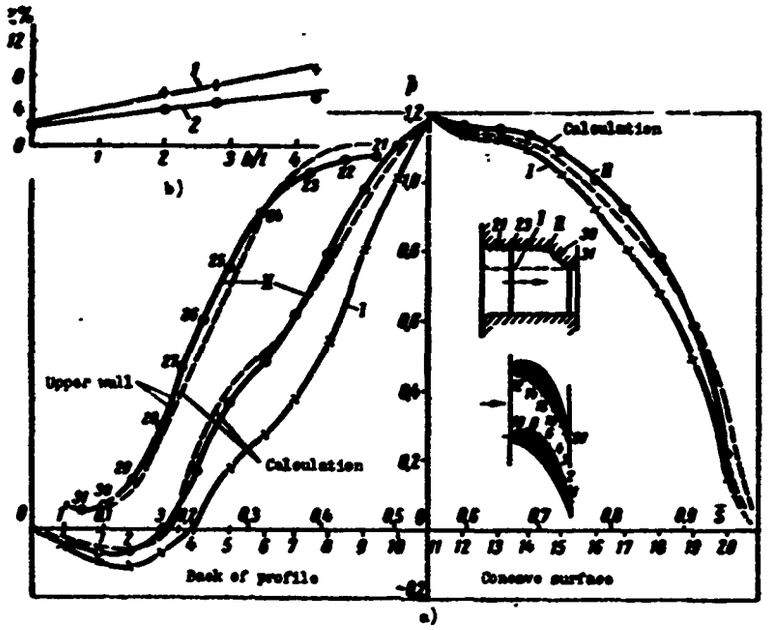

Fig. 16. Change of pressure distribution along a profile and losses for two kinds of upper contours of a reaction cascade: a) pressure curves along profile and upper profiled wall: I – straight upper wall, II – profiled upper wall: — — — calculation according to the channel method; b) dependence of losses on b/l for two kinds of contours; 1 – for a straight upper wall, 2 – for a profiled upper wall.

At the same time, if in the cascade without contraction we observe maximum longitudinal pressure gradients at the entrance sections of the back (points 8 and 9), and the pressure gradients then sharply decrease, in the cascade with contraction the greatest longitudinal pressure gradients are found at the exit section of the back (points 3-5) and the concave surface (points 17-20). In a sharply convergent flow, the thickness of the boundary layers on the profile contours and on the end walls of the channel is decreased, which leads to a lowering in the intensity of the secondary flows.

Let us also note one more feature of the pressure curves: in the cascade with contraction, the points of the pressure minimum are somewhat displaced along the flow, so that the extent of the diffuser section and the pressure gradients in it decrease somewhat for these reasons, in the cascade with contraction, not only are the tip losses reduced, but also the profile losses.

Thus, the introduction of contraction at the exit section of the channel increases the convergence of the flow in the slanting sheer, decreases the velocity

in the bend, shortens the length of the diffuser section, and consequently, the total cascade losses. The loss coefficient curves presented in Fig. 16b distinctly show that the advantage of cascades with contraction is especially great for low relative heights.

The effectiveness of contraction is increased in annular cascades. In this case the introduction of contraction not only lowers the losses, but also equalizes the velocity field in the exit section, since the losses in the root sections (where ζ in the usual annular cascades is higher) decrease more intensely. Equalization of the velocity field has a favorable effect on the flow around a moving cascade.

In returning to the question of the rational form of contraction, let us note that the effectiveness of a nozzle cascade is influenced not only by the form of the upper contour, but also by the relative contraction, which is characterized by the quantity $\Delta\bar{l}_0 = \frac{l_0 - l_1}{l_1}$. The results of corresponding experiments are given in Fig. 17b. Here it is distinctly shown that the optimum values of $\Delta\bar{l}_0$ depend on the cascade height, i.e., absolute contraction varies as cascade height varies.

It should be noted that the curves in Fig. 17b, which characterize the decrease of losses in a cascade with contraction as a function of $\Delta\bar{l}_0$, are flat. Consequently, depending upon the design parameters of the stage under construction and the technological factors, the value of $\Delta\bar{l}_0$ may be modified in sufficiently wide limits.

Let us note that the length of the upper profiled wall of the channel is increased as compared to an ordinary cascade that has cylindrical contours. For this reason, the loss factors at the profiled wall practically do not change, and in certain cases they even increase. Consequently, too much contraction leads to an enlarged surface of friction and corresponding losses.

The shape of the contraction curve can be selected on the basis of a calculation of potential flow in the channel.

For this purpose we used the channel method [38] and considered the curvature of the flow lines in the meridional plane, and also the curvature of the flow lines along the equipotential lines. By assigning the shape of the upper contour, it is simple to find the pressure distribution along the profile, along the upper and lower surfaces, and establish how close the pressure profiles are to optimum. The results of corresponding calculations for a straight TC-2A cascade for $\bar{l}_1 = 0.35$ are compared with the experimental data in Fig. 16a. It is possible to note a satisfactory convergence of the calculation with the experiment.

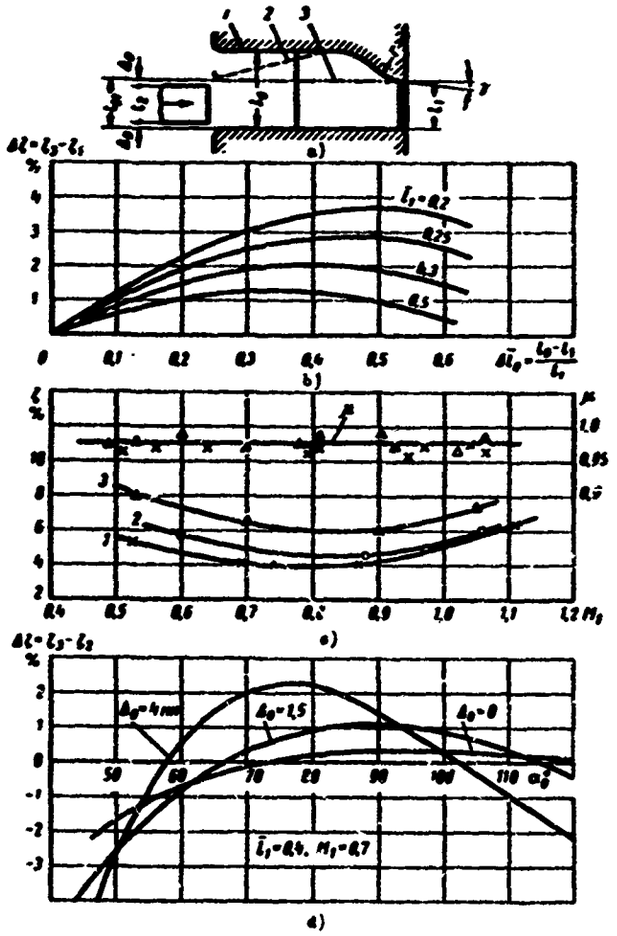

Fig. 17. Influence of asymmetric contraction on losses in a reaction cascade: a — diagram of channel with conditionally designated dimensions; b — decrease of losses in cascade with asymmetric contraction; c — influence of M_1 number on losses and discharge coefficient for different shapes of upper contour; d — corrections that consider the inlet angle of flow in a cascade with a diffuser entrance for various overlaps.

With the channel method it is also possible to obtain an approximate formula for calculating the radius of curvature of the upper contour:

$$r = \frac{l_1 \sin^2 \alpha_1}{2\left(\sqrt{\frac{\theta}{\theta - 2{,}5}} - 1\right)}.$$

Here r is the radius of curvature of the upper contour (Fig. 17a);

l_1 is the exit height of the cascade;

$\theta = \frac{d}{l}$ is the cascade flare;

α_1 is the outlet angle of the flow.

The main problem concerns the selection of rational pressure profiles along the blade contour, along the upper (profiled) and the lower walls. On the back it is necessary to provide a convergent flow with maximum negative pressure gradients in the exit portion (see Fig. 16). On the profiled walls and the lower walls the pressure distribution should be convergent with gradually decreasing pressure gradients toward the trailing edges in order to ensure a uniform field of static pressures at the cascade exit.

For providing a convergent flow along the upper profiled contour, it is necessary to bevel the shroud at an angle of $\gamma = 3\text{-}6^{\circ}$ (see Fig. 17a) at the channel exit, where the diffuser section is most probable (see Fig. 16). Smaller values of γ pertain to welded diaphragms, and larger ones refer to gang-milled diaphragms.

The shape of the channels in the meridional plane depends on the basic geometric parameters of the stage, in particular on the ratios θ, and d/b (or l/b), since the introduction of asymmetric contraction leads to a redistribution of static pressure around the radius behind the cascade, i.e., to a change in the distribution of the reaction.

Depending upon the indicated parameters, not only the shape of the upper contour changes, but also the lower one. In particular, at certain values of d/b and l/b it is necessary to profile the inner lower contour so that the reaction in the root section is not less than reaction at the vertex. Here it should be noted that with the application of contraction, the magnitude of optimum chord of the profile will be larger than for stages with cylindrical contours.

By increasing the chord and keeping the relative pitch $\bar{t} = t/b$ and absolute thickness of the trailing edge constant, it is possible to lower edge losses in the stage, and the tip losses will change less significantly with the corresponding change of the contraction profile.

The application of asymmetric contraction in intermediate stages can lead to a sharp increase of overlap at the entrance to a nozzle cascade, whose entrance height l_0 (see Fig. 17a) is essentially larger than its exit height l_1. In these cases the nozzle cascade should have a diffuser at its entrance, as shown in Fig. 17a by the dotted line. In this case the entrance height l_{01} is selected smaller than l_0, whereby the difference in heights l_{01} and l_2 – the exit height of the moving cascade of the preceding stage – should be within limits which ensure maximum utilization of kinetic energy at the exit.

Investigations of nozzle cascades of intermediate stages with a diffuser entrance

in static conditions showed that the introduction of a diffuser has little influence on the contraction effect in the slanting shear when calculating the inlet angles of flow. The results of corresponding experiments are shown in Fig. 17c.

The change of total losses, depending upon the M_1 number, for variants 1 and 2, remains practically identical. In a cascade with cylindrical generatrices (variant 3) the losses increase essentially.

The influence of an overlap at the entrance to the nozzle cascade $[\Delta_c = \Delta/(t_{01} - t_2)]$ is shown in Fig. 17d. The advantages of a cascade with a diffuser entrance and asymmetric contraction at its exit are retained in the interval of inlet angles $\alpha_0 = 65\text{-}110^\circ$.

Thus, with the use of nozzle cascades with a more complicated shape of the upper contour, the problem of increasing the efficiency of the intermediate stages may be solved with low blade heights.

For an estimate of the total losses $\zeta_м$ in MEI straight nozzle cascades with optimum contraction, depending upon height, the following formula may be used:

$$\zeta_м = \zeta_{пр} + 0.75 b/l_1, \tag{25}$$

which is valid for M_1 numbers ≤ 0.70 to 0.9 and Re_1 numbers $\geq 4 \cdot 10^5$.

Profile losses $\zeta_{пр}$ can be taken from the standards or the atlas of profiles.

By applying asymmetric contraction for stages with short blades, the optimum dimensions of the channel in the meridional plane should be selected in accordance with the data shown in Fig. 17b and d. Asymmetric contraction is applicable for any profile given in the standards, and also for obsolete profiles with rectilinear sections on the back. Nozzle cascades of group "Б" should also be manufactured with asymmetric contraction, since the advantage of cascades with such upper contours is also retained for low supersonic velocities ($M_1 \leq 1.2$).

In cascades with asymmetric contraction the area of the exit section is increased. This increase is considered in the thermal analysis (see Chapter IV).

The discharge coefficients, referred to the actual area F, coincide with the corresponding values of μ for a cascade with cylindrical contours (see Fig. 17c).

§ 6. MOVING CASCADES OF LOW HEIGHT

With low relative heights of moving blades, the continuously-convergent flow in

channels of action cascades does not insure minimum tip and total losses.

As shown by the experiments of Kh. Nippert [22], and later the experiments at VTI [3], the losses due to secondary flows in curvilinear channels and in cascades of low height do not attain their minimum in a continuously convergent flow if the deflection in the channel is great and the static pressures at entrance and exit are close (action cascades).

The results of these investigations show that the organization of a divergent-convergent flow in the vane channels of action cascades with large deflections $\Delta\beta = 180^{\circ} - (\beta_1 + \beta_2)$ leads to a reduction of tip losses.

It is possible to indicate various methods of constructing cascade profiles which satisfy the given requirement. In particular, it is possible to create special types of profiles for low relative heights.

Another method, which is considerably more economic, consists in that adapting the new profiles, which are designed for conditions of two-dimensional flow, for low heights by means of simple changes in profile shape. This method makes it possible to keep widely used profiles in production at turbine-construction plants by introducing modifications of the original profiles for low heights.

For a theoretical construction of action cascades of low height, after solving the inverse problem, it is necessary to correctly select the initial velocity profile on a blade, which would ensure minimum tip losses.

It is simple to theoretically prove that the initial velocity profile depends on the basic geometric parameters of the cascade and mainly on its relative height. Considering the complexity of the problem connected with a detailed calculation of tip losses and finding an optimum velocity profile, it is necessary to carry out an appropriate investigation.

Given below are certain results of an experimental study of the shapes of profiles of action cascades which provide minimum tip losses for different geometric parameters.

The initial profiles selected for the investigation were profiles of action cascades for subsonic velocities which were developed at MEI: TP-0A, TP-1A, TP-2A, and TP-3A. Their basic characteristics are given in Table 1.

New profiles, which were intended for low heights, were obtained by means of undercutting the concave surface in such a manner so that the vane channel was divergent in the beginning, and then convergent. The back of the profile was kept constant.

Figure 18a shows two profiles: an initial one (TP-2A) and one with a diffuser section at the entrance (TP-2Ak). The most characteristic dimensions of the channel are given there: width at the entrance (a_1), width of the mid-section of the channel (a_m), and width of the throat area at the exit (a_2).

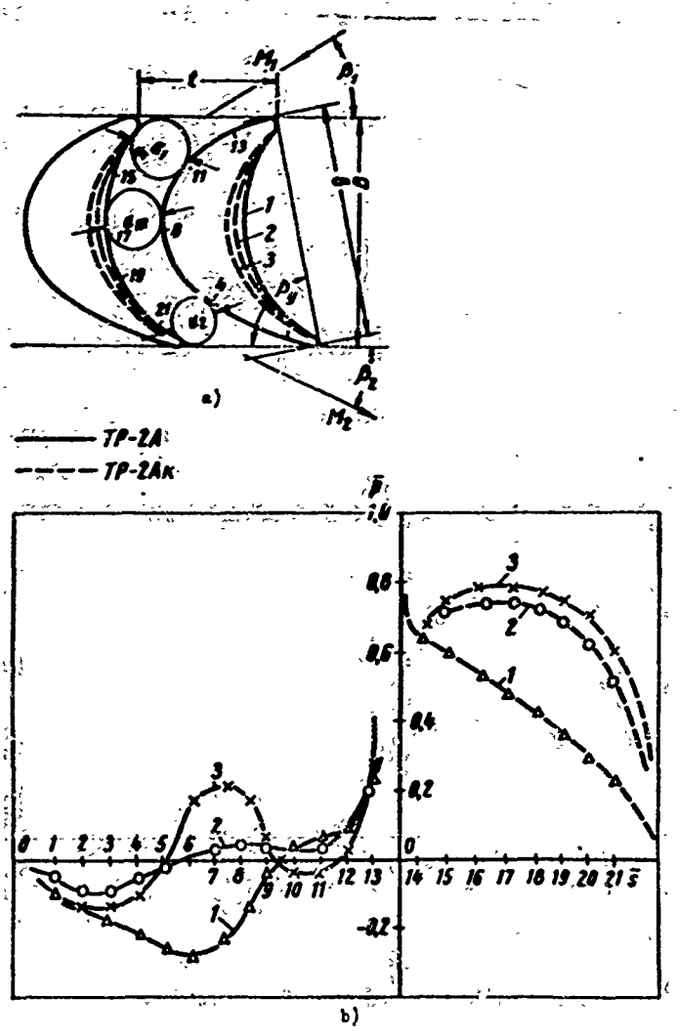

Fig. 18. Action cascade with diffuser section of channel at entrance: a – cascade profiles; b – pressure distribution along profile with various divergence at entrance; 1 – cascade with continuously converging channels ($\bar{a}_m = 0.92$); 2 – cascade with diverging-converging channel ($\bar{a}_m = 1.08$); 3 – the same, for $\bar{a}_m = 1.23$. MEI experiments with $\beta_1 = 25^\circ$; $M_2 = 0.6$; ——— TP-2A profile; — — — TP-2Ak.

Cascades of the initial profiles are characterized by the relations $\bar{a}_m = \frac{a_m}{a_1} < 1$ and $\bar{a}_1 = \frac{a_1}{a_2} > 1$. The new cascades (group "Ak") have diffuser channels at the entrance, i.e., they are characterized by the relations $\bar{a}_m > 1$ and $\bar{a}_1 > 1$.

It should be noted that a change in pitch and angle of incidence leads to a change in the characteristic sections of the channel and their relations $\bar{a}_m$ and $\bar{a}_1$.

For certain values of pitch $\bar{t}$ and angle of incidence β_γ, the initial profiles of group "A" (Table 1) also form divergent-convergent channels. However, as a rule, this does not ensure optimum convergence at the entrance, and in many cases it does not even ensure the necessary outlet angles of flow that are specified by the thermal calculation of pitch. Furthermore, with a deviation from optimum pitch, the cascade losses can increase.

Static tests were conducted on cascades for different heights and relations of $\bar{a}_m$ and $\bar{a}_1$, for varying pitch and angles of incidence, and for overlap ($\Delta = 3$ mm). The limits of variation of characteristics of cascades in group "Ак" are shown in Table 5.

Table 5. Basic Geometric Characteristics of Action Lattices of Group "Ак" for Low Relative Heights

Cascade	Range of variation				
	relative pitch	angles of incidence β_γ	ratios $\bar{a}_m = \frac{a_m}{a_1}$	ratios $\bar{a}_1 = \frac{a_1}{a_2}$	inlet angles of flow β_1°
TP-0Ак	0.65—0.8	76—80	1.00—1.23	1.15—1.50	17—28
TP-1Ак	0.58—0.72	75—79	1.00—1.18	1.15—1.50	22—32
TP-2Ак	0.56—0.68	74—79	1.00—1.15	1.25—1.50	26—37
TP-3Ак	0.52—0.62	74—79	1.00—1.08	1.15—1.50	29—40

The velocity field of the flow at the entrance to the cascade being investigated was nonuniform with respect to height, since the boundary layer was not drawn off from the flat walls of the delivery nozzle. The thickness of the layer at the entrance to the cascade varied depending upon the conditions and reached $\delta = 2$ to 3 mm, which corresponded to a nonuniformity* of $\bar{\delta} = \frac{\delta}{l} = 0.1$ to 0.12.

The advantages of divergent-convergent channels at small relative heights are confirmed by an experiment. Figure 18b gives pressure profiles for channels of TP-2A cascades of various shapes. An essential change of the pressure profile may be noted as the divergence at the entrance is increased. In a continuously convergent channel ($\bar{a}_m = 0.98$) the flow along the back is convergent to points (6-5); from point 5 to the trailing edge there is a region of divergent flow. On the entire

*It is possible to consider that the test conditions of cascades with a constant absolute overlap and variable nonuniformity of velocity field with respect to height at the entrance are most similar to the actual conditions of flow around a moving cascade in a stage. As a rule, the overlap in all high-pressure stages is practically identical, and the nonuniformity of the velocity field with respect to height varies with the height.

extent of the concave surface the motion is convergent.

In channels with a diverging entrance the flow along the entrance section of the back (points 12-10) is also convergent.

In the diverging section of a channel for the relation $\bar{a}_m = 1.08$, the pressure along the back (points 10-7) remains practically constant, and then, after point 7, it drops to point 3-2. As a result of this, the diffuser section in the slanting shear on the back of the profile is sharply reduced (the point of the pressure minimum is essentially displaced through the flow). For a blade height of $\bar{l}_2 = 1.17$ of a cascade of TP-2A profiles, the divergence $\bar{a}_m = 1.08$ close to optimum; the total cascade losses in this case will be minimum.

A further increase of divergence at the entrance ($\bar{a}_m = 1.23$) leads to the appearance of a diffuser section on the back of the profile (points 9-7) with a subsequent sharp acceleration of flow. The cascade losses increase.

Thus, it is possible to note that diffuser sections on the back of a profile (for calculation of inlet angles β_1) are undesirable both for profiles of group "A," and also for profiles of group "Ак." However, pressure distribution along the back for short cascades, when calculating angles β_1, should be more continuous and have smaller pressure gradients.

Analysis of the pressure distribution on the concave surface of a profile shows that for the case of minimum cascade losses ($\bar{a}_m = 1.08$) the pressure gradient varies very little up to the maximum section of the channel (points 14 to 18) and then sharply drops. Pressure distribution on the back and concave surface of a profile confirms that the velocities on the section of intense deflection of flow are decreased.

Thus, an analysis of the pressure profile makes it possible to point out the causes leading to a lowering of tip losses in cascades with divergent-convergent channels. There are three causes of this:

1) deflection of the flow in the vane channel takes place at a lower average velocity. Consequently, the transverse pressure gradient and the intensity of leakage from the concave to the convex surface along the end walls are decreased;

2) at the exit section of the back, where the secondary currents are intensified, the flow becomes more convergent, i.e., the longitudinal pressure gradients increase here;

3) the extent of the diffuser section on the back in the slanting shear is reduced since the point of the pressure minimum is displaced through the flow.

As can be seen from Fig. 19a the absolute values of the loss factors in cascades with divergent-convergent channels decrease, and, which is no less important, the distribution of losses with respect to height becomes more uniform.

Figure 19b represents the dependence of the coefficient of total losses in cascades of profiles TP-1A and TP-1Ak ($\bar{a}_m$ = 1.15)* on relative blade height $\bar{l}_2$.**

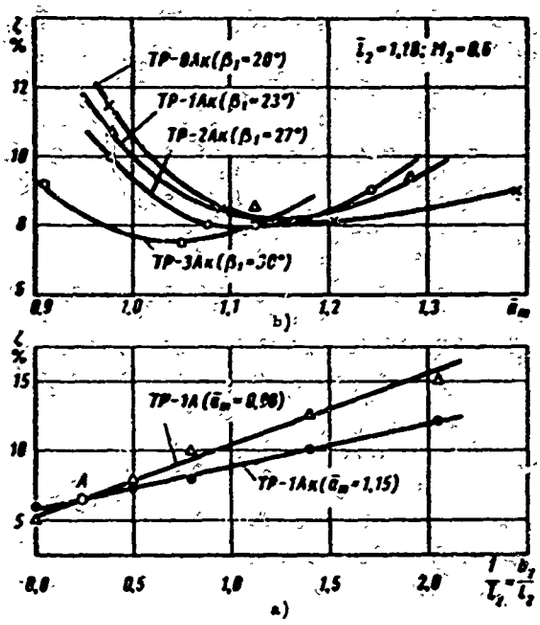

Fig. 19. Losses in action cascades with divergent-convergent channels: a – change of total losses depending on degree of divergence of entrance section; b – the same, depending upon height for two values of $\bar{a}_m$.

As can be seen from the graph, for blade heights $\bar{l}_2 < 2.86$ the losses in the TP-1Ak cascade are less than in the TP-1A one, whereby the difference of $\Delta\zeta$ increase with the blade height decreases.

Only when $\bar{l}_2 \geq 2.86$ (see point A on Fig. 19a) is the TP-1A cascade characterized by smaller losses, whereby the profile losses in the cascade with continuously converging channels is approximately 1% less.

By selecting an optimum relation of $\bar{a}_m$ for each blade height, for cascades of group "Ak" as compared to group "A," it is possible to obtain fewer losses in a wide range of $\bar{l}_2$.

It is necessary to consider that the limiting height that determines the region of use of cascades of group "Ak," which is shown in Fig. 19a for $\bar{a}_m$ = const, depends on the deflection of flow in the cascade $\Delta\beta$.

A decrease of the inlet angle of flow β_1 and a corresponding increase in the deflection of flow in the channel $\Delta\beta$ leads to a more significant lowering of losses in divergent-convergent channels as compared to convergent ones. The loss minimum, as the divergence of the channel at the entrance is increased, is displaced toward smaller β_1.

The data presented in Fig. 19b indicates the presence of optimum divergence for a cascade that is designed for specific operating conditions (M_2, $\Delta\beta$) and has specific

*The relation $\bar{a}_m$ = 1.5 is optimum for a relative height of $\bar{l} \approx 1$.

**Analogous dependences where also obtained for profiles TP-0Ak, TP-2Ak, and TP-3Ak.

geometric parameters. The quantity $\bar{a}_{m\,опт}$ mainly depends on the cascade height. The results of corresponding investigations are shown in Fig. 20a.

With the decrease of height, the optimum value of $\bar{a}_{m\,опт}$, which corresponds to minimum losses, increases and reaches maximum at $\bar{l}_2 = 0.6$. In cascades of lower height, optimum divergence decreases, and at very low heights ($\bar{l}_2 < 0.2$), obviously, the channels should be convergent.

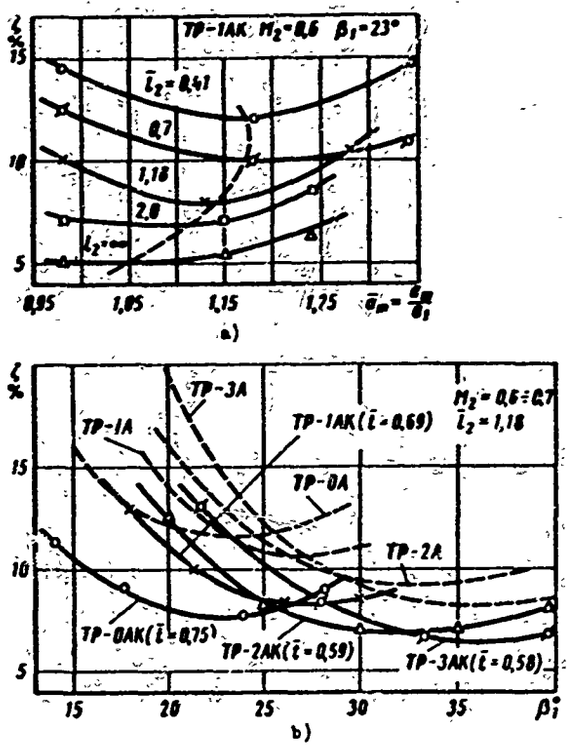

Fig. 20. Characteristics of action cascades with divergent-convergent channels. a — total losses in TP-1Ак, depending upon degree of divergence $\bar{a}_m$ and relative height $\bar{l}_2$ (— — — curve for optimum values of $\bar{a}_m$); b — effect of inlet angle β_1 on losses in convergent and divergent-convergent cascades.

It is possible to consider that at extremely low relative heights secondary flows do not develop in the channel and the effect of curvature is exhibited only in the formation of diffuser regions on the concave and convex surfaces, i.e., in a nonuniform velocity distribution. The organization of convergent flow in such a curvilinear channel promotes a lowering of losses.

For the biggest deflection, which is ensured by the TP-0Ак cascade, optimum divergence is about $\bar{a}_{m\,опт} \approx 1.22$, and for the TP-3Ак cascade, $\bar{a}_{m\,опт} \approx 1.06$ at a relative height of $\bar{l}_2 = 1.17$. TP-1Ак and TP-2Ак cascades correspondingly occupy an intermediate position.

Investigation of the influence of another important geometric parameter — relative pitch — on the effectiveness of cascades of group "Ак," showed that the dependence curve of $\zeta(\bar{t})$ for all cascades is sufficiently flat. The corresponding values of $\bar{t}_{опт}$ are shown in Table 5.

As already noted above, as pitch varies, the geometric divergence of the entrance section of the channel also varies. However, a small deviation of the relation $\bar{a}_m$ from the optimum value does not lead to an essential change of losses.

The influence of performance parameters on the effectiveness of cascades of group "Ак" may be estimated by means of the graphs in Fig. 20b, which gives the

curves of change of total losses in cascades of group "Ак" and "А," depending upon the inlet angle of flow β_1 and the M_2 number. Here we distinctly see two important peculiarities of the flow around these cascades at variable inlet angles; a) in a sufficiently wide range of variation of $\beta_1 \pm (10 \text{ to } 15^\circ)$ the cascade losses vary insignificantly; b) the optimum inlet angles for cascades of the new group, as compared to group "А," decrease, which is explained by the decrease of the inlet skeleton angle of the profile due to undercutting of the concave surface.

The influence of compressibility (M_2 number) on losses in cascades of the two groups being compared may be estimated by means of experimental data. As the M_2 number increases, the difference of losses in cascades of group "А" and "Ак" decreases somewhat. However, within the limits of the entire region of investigation, this difference remains significant. This served as a basis for checking the possibility of making of action cascades of group "Б" – for transonic velocities ($0.95 < M_2 < 1.$) – with divergent-convergent channels. A comparison of two types of cascades, "Б" and "Бк," shows that even at low supersonic velocities at the entrance, the diffuser entrance sections of the channels have a favorable effect on the losses.

An experimental check was also made for the outlet of flow for certain types of cascades of group "Ак." As shown by the experiment, the mean angles of outlet from two types of cascades are similar and satisfactorily coincide with the ones calculated by the formula

$$\beta_2 = \arcsin \frac{a_2}{t_2 - \Delta_{кр}}. \tag{26}$$

Of considerable interest is the possibility of a calculated determination of tip losses in cascades with divergent-convergent channels. A corresponding check showed that the coefficient of tip losses may be determined with sufficient accuracy by means of formula (20). However, in this case one should consider that the presence of a diffuser section at the entrance to the channel leads to an earlier transition of the laminar regime to the turbulent regime, in connection with which, for cascades of group "Ак" the coefficient A should be taken as equal to 0.13, which corresponds to a purely turbulent flow at the end walls.

For coefficient B, on the basis of the experiments conducted, a value is obtained that is close to unity ($B \approx 1$), while in action cascades of series "А" this value amounted to 1.9.

§ 7. NOZZLE CASCADES FOR TRANSONIC AND SUPERSONIC VELOCITIES

Optimum profile and channel shapes, as shown above, vary for transonic and especially for supersonic velocities. The nozzle-type reaction cascades for transonic velocities of group "Б" insignificantly differ from the cascades of group "A." In accordance with the experimental data, the main distinction consists in that the back of the profile in the slanting shear of these cascades is rectilinear. Consequently, the reaction cascades of group "Б" can be obtained by means of deformation of the exit section of a profile of group "A." As a result of this deformation, the curvature of the concave surface decreases, and the back in the slanting shear becomes rectilinear (see Fig. 2). Any profile of the reaction cascades of group "A" can be reconstructed in such a way, where the shape of the channel in the zone of narrow cross section, and consequently also the curvature of the concave surface, are determined by means of calculation according to the channel method (§ 2). The back is made rectilinear from the narrow cross section (the point of tangency of the curvilinear section with the rectilinear section is recessed somewhat into the depth of the channel). The pressure distribution along the back in the slanting shear is calculated by the method of characteristics for $M_1 > 1$. Corresponding methods of calculation are shown in [22, 30]. Nozzle cascades of group "Б" are used for velocities of $0.9 < M_1 < 1.25$.

The expediency of making rectilinear sections on the back in the slanting shear is necessitated by the fact that at high velocities the overexpansion of flow in the slanting shear will be smaller. In accordance with this, the intensity of the resulting shocks is lowered and the probability of boundary layer separation is decreased.

For an estimate of the losses and outlet angles of flow in nozzle cascades of group "Б," the curves presented in Fig. 21a and b may be used. Here for cascades of the type ТС-А and ТС-Б, generalized curves of corrections $\frac{\zeta_{прА}}{\zeta_{прБ}}$ and $\frac{tg\ \alpha_{1А}}{tg\ \alpha_{1Б}}$ are given as functions of M_1 number, which are suitable for all cascades of this group, the profiles of which are obtained by means of deforming the initial profiles of group "A."

Nozzle cascades for high supersonic velocities ($M_1 > 1.2$) are manufactured in three types: with converging channels and concave back in slanting shear (see Fig. 2b with slightly diverging channels and concave back in slanting shear (see Fig. 2c), and with diverging channels (see Fig. 2d).

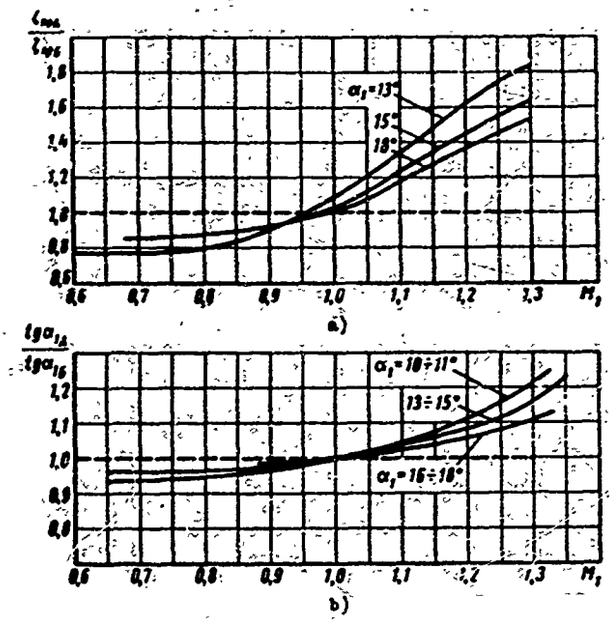

Fig. 21. Generalized corrections that consider the influence of compressibility (M_1 number) on profile losses and outlet angles of flow in cascades of groups "A" and "Б": a – relative increase of profile losses in cascades of group "A"; b – relative increase of outlet angle in cascades of group "A."

If the vane channel of a cascade is convergent before the narrow section, and the back in the slanting shear is calculated according to the method of characteristics in such a way so that along the back there is no overexpansion of flow, then in this cascade the energy losses at supersonic velocities will be small due to the smaller intensity of shocks, and also because the reflected shock does not lead to separation. Actually, the calculated M_1 number is reached in the slanting shear, whose cross sections are increased along the flow, owing to the concave shape of the back. Since the concave back annihilates reflected expansion waves, the overexpansion of flow in the slanting shear is small, and correspondingly, the intensity of the resulting shocks is small. At the same time, the function of the reverse concavity on the back; i.e., to decrease the angle between the velocity vector behind the shock and tangent to the back of the profile, is to decrease the danger of separation of flow. Theoretically, the most advantageous shape, from the point of view of the velocity distribution in the section behind the cascade, is the concave back that is constructed as a flow line in the flow around an angular point (the edge of the preceding blade). However, with this type of back, it is impossible to construct a one-dimensional cascade of profiles, since the angle of formation of the trailing edge is negative.

Consequently, an important problem when shaping the back of a blade in the slanting shear of a cascade with convergent channels is to provide a design angle of the trailing edge (1 to 2°). As experiments show, the region of intense growth of losses extends to higher M_1 numbers if the back of the profile in the slanting shear is convex-concave.

Figure 22 shows one of the variants of constructing the back in the slanting shear with help of a diagram of characteristics. The calculated M number for the cascade is $M_{1p} = 1.4$. The method of constructing the flow spectrum is the following: 1) the sonic line is straight in the narrow cross section a_M; 2) in an angular point there appears an expansion wave in which the flow is expanded from M = 1 to M_{1p}; 3) the back on the initial section is convex, and then some of the expansion waves are annihilated by turning the wall. The angle between the tangent to the back at the point of deflection and the tangent to the back on the trailing edge is 1 to 2° less than the angle between the tangent to back in the narrow cross section of the channel and the tangent to the back at the point of deflection. This attains a positive angle of edge formation. Figure 22b shows the consecutive change of dimensionless velocity* λ_1 in the transition through the characteristics in the diagram of characteristics.

However, the actual pattern of the flow in the slanting shear differs from that constructed by the method of characteristics. Overexpansion on the back does not reach the magnitudes which were obtained by calculation with the method of characteristics. Treatment of the results of the investigation of a large number of nozzle cascades made it possible to determine the maximum $M_{1\,max}$ number on the back in the slanting shear, depending on the calculated M_{1p} number (Fig. 23). The quantity $M_{1\,max}$ may be determined by the approximate formula

$$M_{1\,max} = 0{,}9M_{1p} + (0{,}25 - 0{,}35), \qquad (27)$$

which is suitable for the interval of numbers $1.0 < M_{1p} < 2$.

After reaching a velocity corresponding to $M_{1\,max}$, on the back there appears an oblique shock.

---

*Here and subsequently, $\lambda = \frac{c}{a_*}$ is the dimensionless velocity (velocity of flow referred to stalling velocity).

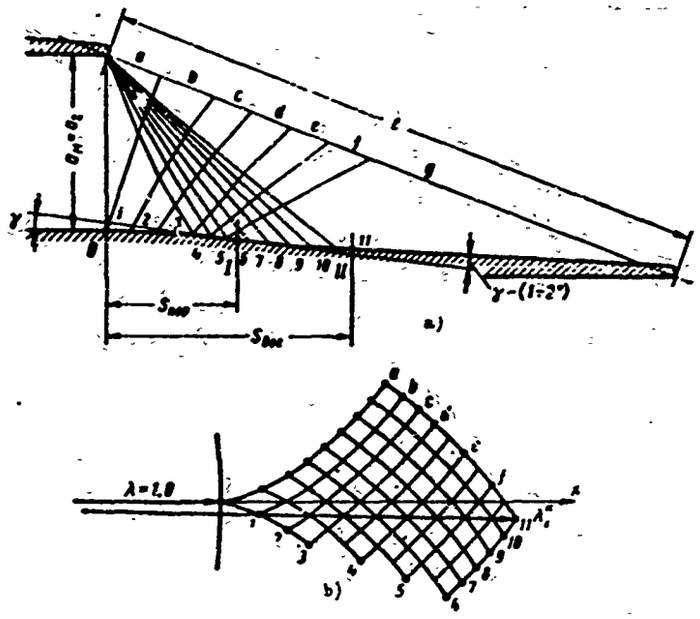

Fig. 22. Supersonic nozzle cascade, type TC-B (convergent channels): a – construction of back of profile in slanting shear; b – determination of velocity at different points of slanting shear according to diagram of characteristics.

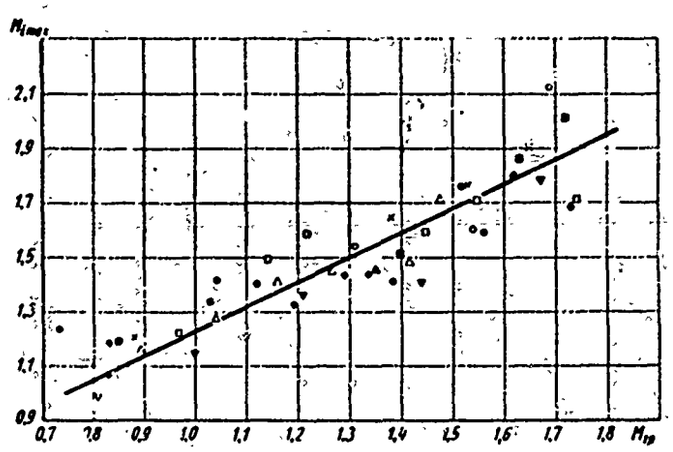

Fig. 23. Dependence of maximum velocities on back in slanting shear on calculated M_{1p} number according to MEI experiments. Experimental points of cascades (see Table 6):

✱✱✱ – № 3; ▼ ▼ – № 4; ○ ○ – № 8; × × – № 10; △ △ – № 14; ● ● – № 17; ■ ■ – № 21; □ □ – № 22.

For an approximate calculation of the back of the profile in the slanting shear of a cascade with convergent channels, it is possible to recommend the following

method. By assigning the size of the narrow section of the channel (a_2), the effective outlet angle of flow ($\alpha_{1\,эф} = \arcsin \frac{a_2}{t}$), and the calculated $M_{1\,p}$ number at the cascade exit, we find:

1. The maximum $M_{1\,max}$ number for the given $M_{1\,p}$ is determined by formula (27).
2. The position of deflection point I (Fig. 22a) is found by the equation

$$S_{вгр} = a_2 \left\{ \operatorname{tg} \left[\arcsin \frac{1}{M_{1\,max}} + \frac{\delta(M_{1p}) - \delta(M_{1\,max}) + (1 \div 2^\circ)}{2} \right] \right\}^{-1}. \tag{28}$$

where $\delta(M_{1\,p})$ is the deflection of flow during expansion from $M = 1$ to $M_{1\,p}$;

$\delta(M_{1\,max})$ is the deflection of flow during expansion from $M = 1$ to $M_{1\,max}$.

The obtained quantity is rounded off:

$$\gamma = \frac{1}{2} [\delta(M_{1p}) - \delta(M_{1\,max}) + (1 \div 2^\circ)].$$

From the narrow cross section to the deflection point we shall construct a straight broken line consisting of γ segments; the angle between these segments equals 1°. Through the salient points we shall draw a continuous convex line to deflection point I.

3. We determine the length of the concave part of the back:

$$S_{вог} = S_{вгр} + \frac{a_2}{q(M_{1p})} \left[\operatorname{tg} \left(\arcsin \frac{1}{M_{1p}} + \gamma \right) \right]^{-1}, \tag{29}$$

where $q(M_{1p})$ is the given flow rate, which corresponds to the calculated M_{1p} number.

4. We shall construct a concave, straight, broken line, starting from deflection point I and going to point II, which determines the length of the concave section $S_{вог}$. The number of segments of the broken line is equal to γ - (1 to 2°), and angle between segments is equal to 1°. Through the salient points we shall draw a continuous concave line that touches the convex line at the point of deflection.

5. At the end of the concave line we draw a tangent, and after determining the concave pitch t, by means of a_M and α_1, we construct the trailing edge of the profile.

It should be emphasized that the design of such a cascade for high supersonic velocities and small outlet angles of flow is difficult. When $M_1 > 1.4$ and $\alpha_1 < 13^\circ$ it is necessary to use combined cascades that have slight channel expansion to the exit section and a concave-shaped back. As the calculated $M_{1\,p}$ number increases, $M_{1\,p} > 1$, the minimum section and the concave portion of the back are displaced

into the depth of the channels. Thus, with the growth of $M_1 > 1$, the role of the divergent section of the channel increases, and that of the concave section of the back in the slanting shear decreases.

For cascades that have a calculated $M_{1\,p}$ number less than 2, the expansion ratio of the vane channel may be selected by the following MEI empirical formula:

$$f = 1 + (0.3 - 0.6)\left(\frac{1}{q(M_{1p})} - 1\right), \tag{30}$$

where $f = \frac{a_2}{a_M}$ is the ratio of the exit section of the channel to the minimum section.

A limiting case for nozzle cascades of group "B" is characterized by divergent channels and almost rectilinear sections of the back in the slanting shear. The back of the profile, which forms the divergent channel, is concave (this shape ensures the annihilation of expansion waves in the channel). Calculation of the concave wall is produced by the method of characteristics; ready-made profiles of two-dimensional convergent-divergent nozzles can also be used.

Figure 24a and b, shows an example of the construction of a divergent vane channel and profile back in a slanting shear with the help of a diagram of characteristics (for $M_{1\,p} = 1.7$). Behind the narrow section, the flow along the back is accelerated in an expansion wave obtained by deflection of the back, and then in a wave reflected from the concave surface of an adjacent profile. The position of the blade edge is determined by the quantity f, which is calculated by formula (30). Further, the flow is accelerated in an expansion wave that appears at the trailing edge, which is annihilated by an appropriate deflection of the back. Figure 24b shows the consecutive transition of vector λ_1 through the corresponding points in the diagram of characteristics. However, as already noted above, the $M_{1\,max}$ that is attained on the back is less than that calculated by the method of characteristics. At the point where the calculated $M_{1\,max}$ number is reached, which is calculated by formula (27), there appears an oblique shock. Behind this point, the back should be concave, which decreases the probability of separation of flow behind the shock.

Construction of the slanting shear and divergent part of a nozzle cascade is carried out in the following way:

1. According to the given values of $M_{1\,p}$ and a_M, and $\sin \alpha_1 = \frac{a_2}{t}$ (Fig. 24a) we determine the expansion ratio of the vane channel by formula (30) and find the size of the exit section of the channel $a_2 = a_M \cdot f$.

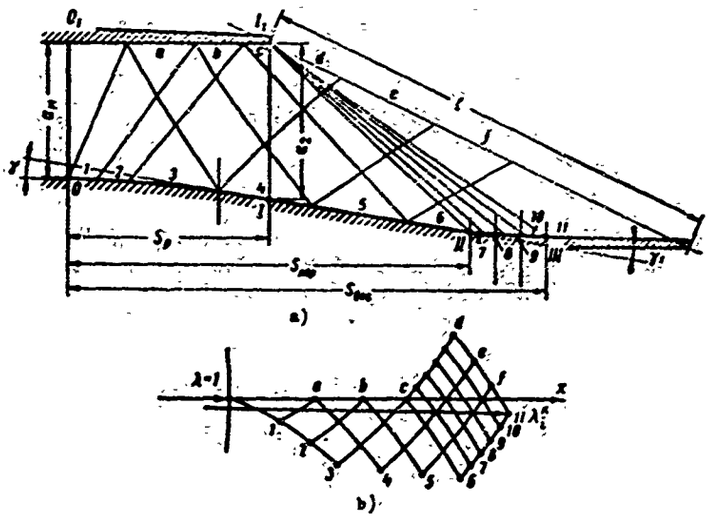

Fig. 24. Construction of divergent channel of TC-BP nozzle cascade: a – calculation of exit portion of channel and back of profile in slanting shear; b – determination of velocities at different points of the exit portion of the channel and in the slanting shear according to the diagram of characteristics.

2. From the tables of gas-dynamic functions we determine M_1 in the exit section of the divergent channel, which corresponds to $q(M_1) = \frac{1}{f}$. The "concave" surface of the profile, within the limits of the divergent portion, is rectilinear, and the angle between the tangents to the back in the exit section of the divergent channel and in the narrow section is

$$\delta(M_1)/2,$$

where $\delta(M_1)$ is the deflection of flow during expansion from $M = 1$ to M_1.

We shall designate the quantity $\delta(M_1)/2$, which is rounded off to an integer, by γ_0. Then the length of the divergent portion of the channel is

$$S_p = \frac{a_2 - a_H}{\operatorname{tg} \gamma_0}.$$

We shall connect points 0 and I (Fig. 24a) of the convex broken line that contains γ_0 segments; the angle between adjacent segments of the broken line is 1°. Then we connect the angular points by a continuous line.

3. We determine the maximum $M_{1\,max}$ number by formula (27) on the back and find the position of the deflection point of the back:

$$S_{H\,p} = S_p + a_2 f_1 \left[\operatorname{tg}\left(\arcsin \frac{1}{M_1} + \frac{\gamma}{2} \right) \right]^{-1}, \tag{31}$$

where

$$f_1 = \frac{1}{q(M_{1\,max})}.$$

We draw a tangent to the back of the profile at point I and extend it to deflection point II.

4. We determine the position of point III of the end of the concave portion:

$$S_{вых} = S_{кр} + a_2 f_1 \left[\operatorname{tg}\left(\arcsin \frac{1}{M_{1p}} + \frac{\gamma}{2} \right) \right]^{-1}. \qquad (32)$$

We connect points II and III of the concave broken line by a line that consists of γ_1 segments, where γ_1 is the deflection of flow during its expansion from M_1 to $M_{1\,p}$. The angle between adjacent segments of the broken line is selected as 1°.

5. At point III we draw a tangent to the back, and after determining cascade pitch t with respect to a_2 and α_1, we construct the trailing edge of the profile.

It should be emphasized that the divergent portion of the channel between sections a_M and a_2 may be profiled by expanding not only the back, but also the concave surface. This method decreases the danger of undercutting the leading edge in the direction of the back. Cascade losses are then held to a minimum (see Chapter VIII). The section of the "concave" surface O_1-I_1 (Fig. 24a) is rectilinear or convex, as shown for section O-I of the back. In the first case, at point O_1 it is possible to round off to an arbitrary radius. In the construction of the convex section O_1-I_1, the method described above in detail is used (for section O-I of the back).

It is known that at supersonic velocities nozzle cascades with divergent channels are sensitive to a change of conditions, and in particular, the change of the M_1 number.

The intensity of variation of cascade losses, depending on M_1, is determined by the geometric parameters of the cascade and mainly by the shape of the vane channel. Thus, for instance, if cascades with convergent channels are usually characterized by small losses at subsonic velocities, and at $M_1 > 1$ these losses sharply increase, then for cascades with divergent channels the losses will be small only in a narrow range of supersonic velocities, while for transonic velocities and at $M_1 \gg M_{1p}$ they attain large values.

The results of cascade tests with different expansion ratios of the vane

channels* are shown in Fig. 25 (MEI experiments). In these experiments, all cascades with an expansion ratio $f > 1.0$ had a height of $\bar{l} = 0.135$, and cascades with $f = 1.0$ were $\bar{l} = 0.28$ high. The lowering of losses in uncalculated conditions at $M_1 < M_{1p}$ with a decrease of parameter f should be considered as the most effective in the graphs under consideration.

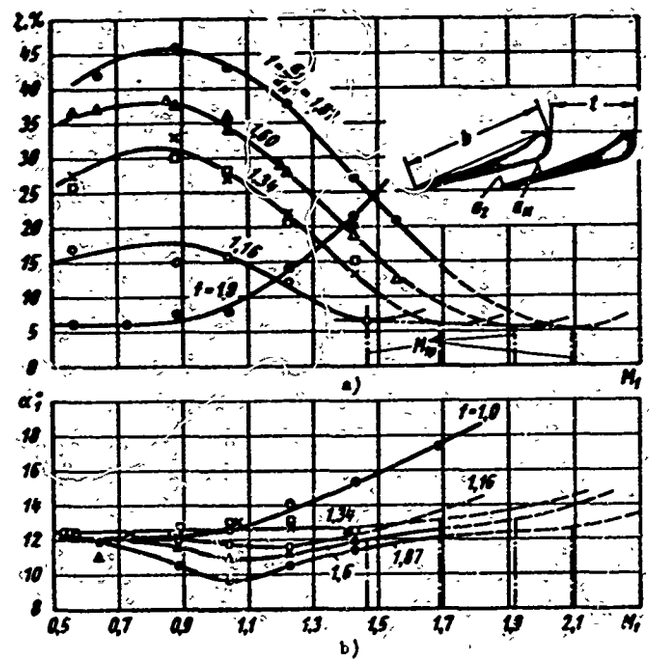

Fig. 25. Influence of M_1 number and degree of expansion f on characteristics of nozzle grids with divergent channels and straight back in slanting shear on: a – total losses ζ; b – outlet angles α_1. MEI experiments:

$$\left.\begin{matrix}\blacktriangledown - \bar{l} = 0.464 \\ \triangledown - \bar{l} = 0.487\end{matrix}\right\} f = 1.60; \quad \left.\begin{matrix}\times - \bar{l} = 0.544 \\ \square - \bar{l} = 0.464\end{matrix}\right\} f = 1.34;$$

The intense growth of losses in such cascades with a decrease of M_1 is explained by the displacement of shocks in the channel to the throat area and the corresponding expansion of the separation zone in the channel. With the decrease of f, the relative displacement of shocks to the throat area will be less intense. The lowering of losses at $M_1 < 0.8$ to 0.9 is explained by the fact that the wave losses in the cascade are decreased and the shocks near the throat area do not cause separation.

*The data presented in Fig. 25 pertain to obsolete supersonic cascades that were designed without taking into account the interference of expansion waves in the channel and with a rectilinear back in the slanting shear.

The curve of total losses in a cascade with convergent channels ($f = 1$) confirms the intensive increase of losses when $M_1 > 1$. The outlet angles of flow (see Fig. 25b) also change essentially, depending upon M_1 and f.

A detailed analysis of the curves ζ and α_1 for cascades at $M_1 > 1$, which were designed by the above-indicated methods, is given below. These cascades have moderate losses in a wide range of variation of M_1.

Let us consider some of the peculiarities of the flow of a gas in reaction cascades at supersonic velocities. For a solution to this problem, we shall write continuity and energy equations in two control sections: narrow (* — *), and to infinity (1 — 1), behind the cascade (Fig. 26a). We shall then consider that the parameters of flow in these sections are uniformly distributed. Then

$$\varrho_* a_* \sin \alpha_{1*} = \varrho_1 c_1 \sin \alpha_1; \tag{33}$$

$$\frac{p_*}{\varrho_*} + \frac{k-1}{k}\frac{a_*^2}{2} = \frac{p_1}{\varrho_1} + \frac{k-1}{k}\frac{c_1^2}{2}. \tag{34}$$

Here k is the index of the isentropic process;

p_1 and ρ_1 are the pressure and density behind the cascade;

p_* and ρ_* are the critical pressure and density;

$$\alpha_{1*} = \arcsin \frac{a_*}{t};$$

a_* is the critical velocity;

$$\alpha_1 = \alpha_{1*} + \delta;$$

δ is the deflection of the flow.

After substituting (33) and (34) and making the appropriate conversions, we obtain

$$\delta = \arcsin\left[\frac{p_*}{p_1}\frac{1}{\lambda_1}\frac{k+1}{2}\left(1 - \frac{k-1}{k+1}\lambda_1^2\right)\sin \alpha_{1*}\right] - \alpha_{1*}. \tag{35}$$

If during the flow of the gas between control section the losses are equal to zero, we will obtain an ordinary Beer formula:

$$\delta' = \arcsin\left(\frac{1}{q_{1t}}\sin \alpha_{1*}\right) - \alpha_{1*}. \tag{36}$$

Taking the losses into account, formula (36) can be written in the following form:

$$\delta = \arcsin\left[\frac{\sin \alpha_{1*}}{q_{1t} f(\lambda_1 \zeta)}\right] - \alpha_{1*}. \tag{37}$$

where

$$f(\lambda_{1t}, \zeta) = \frac{p_{01}}{p_0} \frac{q_1}{q_{1t}} < 1;$$

ζ is the loss factor;

q_1 and q_{1t} are the given flow rates for actual and isentropic processes;

λ_1 and λ_{1t} are the actual and theoretical dimensionless velocities in the section 1 – 1.

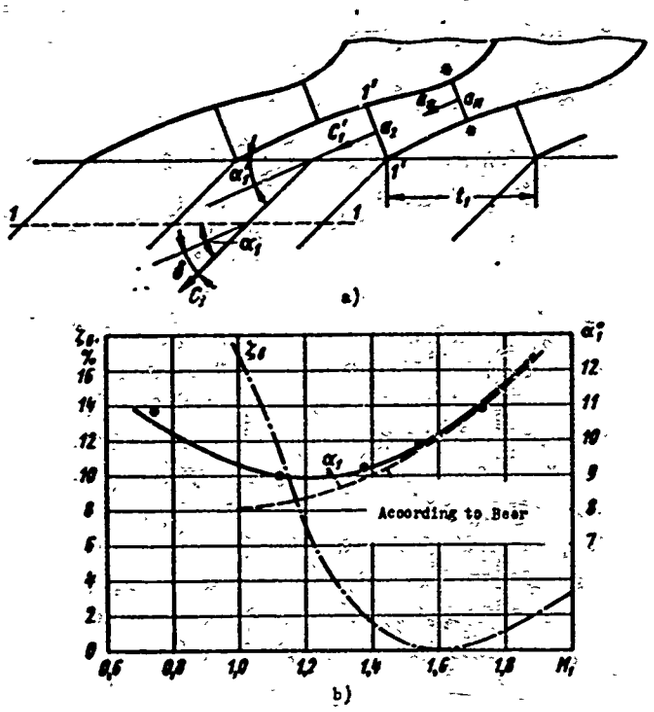

Fig. 26. Derivation of a formula for calculating the outlet angle of flow: a – flow diagram with designations; b – wave losses and outlet angles in cascade, depending upon M_1 for f = 1.28.

Hence it is clear that for the given value of λ_{1t} (M_{1t}) the displacement of flow is simply connected with energy losses during expansion of flow, i.e., the character of the change of energy losses in varying conditions for $M_1 > 1$ depends on the quantity

$$\Delta\delta = \delta - \delta'.$$

From Fig. 25b it is clear that in cascades with divergent channels of the usual type at $M_1 < M_{1p}$, the outlet angle of flow is $\alpha_1 \approx \alpha_{1p}$, while with formula (37) it should decrease. This constancy of angles is brought about by the presence of a slanting shear.

We shall write continuity, energy, and momentum equations for three control sections (* – *), (1' – 1'), and (1 – 1) (see Fig. 26a):

$$\varrho_* a_* \sin\alpha_{1*} = \varrho_1' c_1' \sin\alpha_1' = \varrho_1 c_1 \sin\alpha_1; \tag{38}$$

$$\frac{p_*}{\varrho_*} + \frac{k-1}{k}\frac{a_*^2}{2} = \frac{p_1'}{\varrho_1'} + \frac{k-1}{k}\frac{c_1'^2}{2} = \frac{p_1}{\varrho_1} + \frac{k-1}{k}\frac{c_1^2}{2}; \tag{39}$$

$$\varrho_* a_*^2 t \sin\alpha_{1*} + p_* t \sin\alpha_{1*} + \left(\frac{p_* + p_1'}{2}\right) t(\sin\alpha_1' - \sin\alpha_{1*}) =$$

$$= \varrho_1' c_1'^2 t \sin\alpha_1' + p_1' t \sin\alpha_1' = \varrho_1 c_1^2 t \sin\alpha_1 \cos(\alpha_1 - \alpha_1') + p_1 t \sin\alpha_1. \tag{40}$$

Here $\alpha_1' = \arcsin \frac{a_2}{t}$.

The solution of this system of equations makes it possible to determine the outlet angle of flow for a cascade with divergent channels:

$$\operatorname{tg}(\alpha_1 - \alpha_1') =$$

$$= \frac{\sqrt{\left(\frac{k}{k-1}\right)^2 \bar{p}^2 [\operatorname{ctg}^2\alpha_{1*} - (f^2-1)] + \frac{k+1}{k-1}\left[k^2 - \frac{(k-1)(K-\bar{p}f)^2 - 2\bar{p}fk(K-\bar{p}f)}{k+1}\right]}}{K - \bar{p}f}$$

$$- \frac{\frac{k}{k-1}\bar{p}\sqrt{\operatorname{ctg}^2\alpha_{1*} - (f^2-1)}}{K - \bar{p}f}, \tag{41}$$

and also wave losses:

$$\zeta_w = 1 - \frac{\left(K - \frac{\varepsilon_1}{\varepsilon_*} f\right)^2}{k^2\left(\frac{k+1}{k-1}\right)\left(1 - \varepsilon_1^{\frac{k-1}{k}}\right)\cos^2\delta}, \tag{42}$$

where

$$K = k + 1 + \frac{1}{2}\left(1 + \frac{p_1}{p_*}\right)(f - 1);$$

$$\bar{p} = \frac{p_1}{p_*}; \quad \varepsilon_1 = \frac{p_1}{p_0}; \quad \varepsilon_* = \frac{p_*}{p_0}.$$

When $f = 1.0$, these formulas will be converted into the well-known formulas of G. Yu. Stepanov.

Figure 26b gives a comparison of the calculation with an experiment for outlet angles of flow and a calculated curve of wave losses. As can be seen, the coincidence of calculations made with formula (37) with the experiment at $M_1 \geq M_{1p}$ is satisfactory. It should be noted also that at $M_1 < M_{1p}$ the wave losses will be

very great. Thus, a theoretical analysis shows that the outlet angle of flow from a cascade with divergent channels in transonic conditions is larger than the result obtained with formula (36). This result is connected with the sharp growth of losses in these cascades at $M_1 < M_{1\,p}$. Cascades with $f \gg 1$, in principle, cannot effectively operate at transonic velocities (see Fig. 25).

On the other hand, in cascades with convergent channels in supersonic conditions there is observed considerable overexpansion of flow on the back of the profile, and an edge shock,* as a rule, leads to separation of the boundary layer. Therefore, in cascades with convergent channels, which operate at transonic and low supersonic velocities, the back of the profile must be made rectilinear, and at $M_1 \geq 1.3$ the back should be concave. The greater the concavity of the back of the profile, the higher the economy possessed by a cascade with convergent channels at high M_1 numbers. However, as already indicated, such a method of designing a cascade is possible only to M_1 numbers less than 1.4, since as the concavity of the back is increased in the slanting shear, the solidity of the profile decrease, and there can occur undercutting of the edge.

Furthermore, experiments indicate that at $M_1 > 1.4$ to 1.5 the losses in cascades with convergent channels and concave back intensely increase in the slanting shear.

Therefore, for cascades designed for $M_1 > 1.4$, it is expedient to select a smaller expansion ratio of the vane channel than follows from the dependence $f = 1/q(M_{1\,p})$, and the back of the profile in the slanting shear should be made concave. This method of designing cascades makes it possible to lower the losses at transonic velocities, since their magnitude is determined, mainly, be parameter f. For a cascade, it is possible to determine two calculated values of M_1 number: one ($M'_{1\,p}$) is determined by taking according to the degree of channel expansion, and the other is determined by taking into account the concavity of the back in a slanting shear. The effectiveness of this cascade is sufficiently high in a wide range of M_1 numbers greater than 1.0

In accordance with what has been presented, the turbomachinery laboratory of the MEI developed three groups of profiles of nozzle cascades which are designated for operation at supersonic velocities:

a) for numbers $1.3 \leq M_1 \leq 1.4$ (TC-B cascade);

---

*Diagrams of flow spectra in cascades at high velocities and flow structure in a slanting shear behind a cascade are described in [14]. A diagram of shocks in the slanting shear of a cascade is shown in Fig. 28a. A photograph of the flow spectrum in a reaction cascade is presented in Fig. 40I.

b) for numbers $1.4 \leq M_1 \leq 3.5$ (TC-BP cascades);

c) for numbers $1.4 \leq M_1 \leq 5.0$ (TC-P cascades).

Cascades of the first type (TC-B) have convergent channels and concave backs in the slanting shear (see Fig. 2 and Fig. 27). TC-BP cascades are characterized by small expansion of the vane channel and concavity of the back in the slanting shear; acceleration of the flow in this cascade to the given M_1 number, in the divergent part of the channel and in the slanting shear, will be approximately identical. TC-P cascades have considerable expansion of the vane channel ($f > 1$), in which there also takes place a fundamental acceleration of flow to a M_1 number that is close to the calculated number $M_{1\,p}$ ($M_1 < M_{1\,p}$); expansion in the slanting shear is small.

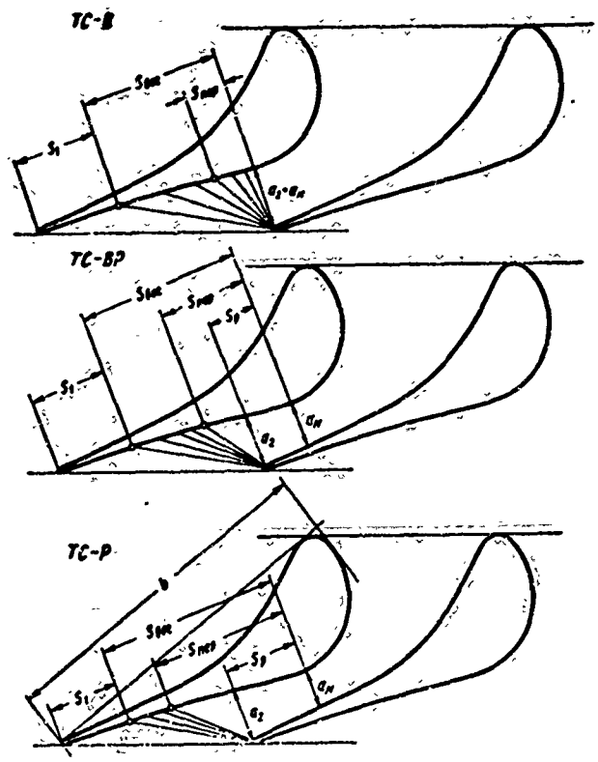

Fig. 27. Shapes of profiles and channels of supersonic reaction cascades tested at MEI. The following designations are used: S_p – length of divergent section of channel; $S_{пер}$ – length of transition section on back; $S_{вог}$ – length of concave section; S_1 – length of rectangular section.

Let us consider certain results of an experimental investigation of three groups of supersonic nozzle cascades under different conditions, carried out at MEI [30].

The shapes of the profiles and channels of the test cascades are shown in Fig. 27 and Fig. 28a.

Table 6 gives the basic geometric characteristics of TC-B and TC-BP cascades.* Here, $M'_{1\,p}$ is determined according to parameter f, and $M_{1\,p}$ is determined by taking into account the curvature of the back in the slanting shear.

Table 6. Geometric Characteristics of Supersonic Nozzle Cascades, Type TC-ПР and TC-BP

№	Type of profile in MKI designations	$\bar{t}$	α_y	α_{1e}	l	M'_{1p}	M_{1p}
1	TC-1BP-1	0,595	30° 00′	8° 30′	1,13	1,43	1,75
2	TC-1BP-2	0,703	29° 45′	9° 05′	1,0	1,00	1,3
3	TC-1BP-2	0,621	29° 45′	8° 20′	1,042	1,25	1,6
4	TC-1BP-2	0,550	29° 45′	8° 56′	1,10	1,48	1,6
5	TC-1BP-3	0,745	29° 36′	9° 30′	1,00	1,0	1,5
6	TC-1BP-3	0,655	29° 36′	10° 00′	1,06	1,28	1,6
7	TC-1BP-3	0,615	29° 36′	9° 15′	1,10	1,37	1,7
8	TC-1BP-3	0,550	29° 36′	8° 05′	1,28	1,63	1,75
9	TC-2ПР-4	0,675	40° 16′	12° 30′	1,00	1,0	1,0
10	TC-2ПР-4	0,611	40° 16′	12° 00′	1,10	1,37	1,37
11	TC-2BP-5	0,675	40° 16′	12° 30′	1,00	1,0	1,6
12	TC-2BP-5	0,611	40° 16′	12° 20′	1,09	1,35	1,45
13	TC-2BP-6	0,615	31° 30′	10° 50′	1,10	1,37	1,7
14	TC-2BP-7	0,620	35° 00′	13° 30′	1,06	1,28	1,6
15	TC-3BP-8	0,715	40° 00′	16° 20′	1,00	1,00	1,4
16	TC-3BP-8	0,660	40° 00′	16° 35′	1,055	1,25	1,55
17	TC-3BP-8	0,583	40° 00′	14° 10′	1,13	1,43	1,6
18	TC-3BP-8	0,520	40° 00′	13° 40′	1,24	1,59	1,7
19	TC-4BP-9	0,750	48° 00′	21° 50′	1,00	1,00	1,3
20	TC-4BP-9	0,698	48° 00′	21° 10′	1,02	1,15	1,5
21	TC-4BP-9	0,621	48° 00′	20° 00′	1,07	1,31	1,6
22	TC-4BP-9	0,565	48° 00′	19° 10′	1,20	1,53	1,65

Figure 28 gives the results of an investigation of the influence of the shape of the back of a profile on the characteristics of cascades. The profiles of these cascades differ only the curvature of the contours of the back on the exit section (see Fig. 28a). The pressure distribution along the profile in the cascades shows that with the growth of M_1, in cascade No. 9 with straight back, overexpansion of flow increases, and in cascade No. 11 with concave back in slanting shear, it decreases. The result of this is a change of the profile losses in these cascades. Actually, if for cascade No. 9 at $M_1 > 1.2$ the profile losses sharply increase, then for cascade No. 11 there is observed a maximum of losses in the range of M_1 numbers ≤ 1.2, and at $M_1 > 1.2$ the losses decrease, and their minimum is reached when $M_1 \approx 1.6$.

Also of great interest is the dependence of profile losses on M_1 number for cascades No. 10 and 12 with divergent channels. As can be seen, the losses for these

*Cascades No. 9 and No. 10, TC-2ПР-4, were manufactured with rectilinear back in slanting shear.

cascades are identical in the entire investigated range of M_1 numbers. Consequently, when $M_1 \approx 1.0$, the cascade losses practically do not depend on the shape of the channel, and are determined by parameter f. Here also, the influence of concavity of the back at $M_1 > 1.0$ is not detected. This specified by the fact that the reverse curvature in cascade No. 12 is concentrated mainly in the divergent part of the channel, and the back is straight in the slanting shear.

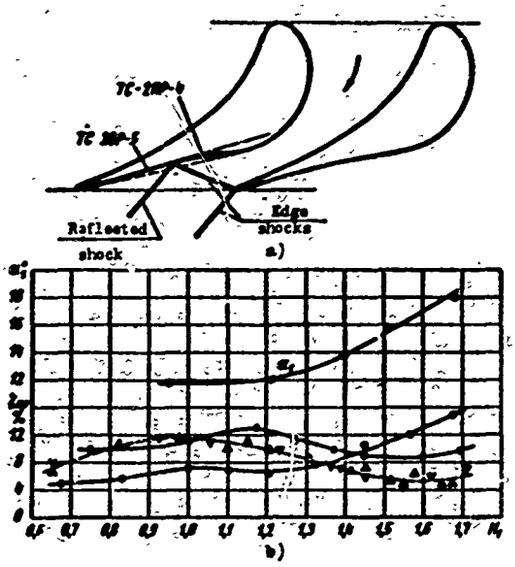

Fig. 28. Influence of shape of back of profile on characteristics of TC-2ПР-4 and TC-2BP-5 cascades (see Table 6): a – shape of back of profiles in slanting shear; b – dependence of losses $\zeta_{пр}$ and outlet angle α_1^o on M_1 number and parameter f:
○–○–○– cascade No. 9 (f = 1.0);
●–●–●– cascade No. 11 (f = 1.0);
▼–▼–▼– cascade No. 10 (f = 1.1);
△–△–△– cascade No. 12 (f = 1.09).

Figure 29 gives the curves of profile losses in cascades designed for small outlet angles of flow (cascades No. 1 through 8). For TC-1BP-1 profiles, which have concave backs (cascade No. 1), and TC-1BP-2 (cascades No. 5 through 8), the concavity of the back attains large magnitudes (1%), and in profile TC-1BP-2 (cascades No. 2 through 4) the concavity is not great. From the considered curves it is clear that for all cascades with divergent channels the profile losses at transonic velocities attain large magnitudes, and then decrease intensely. It should be noted that the level of losses at transonic velocities is determined mainly by parameter f. However, for cascade No. 1 (f = 1.13), at $M_1 > 1.0$ there are considerably smaller losses than in cascade No. 3 (when f = 1.042). The reason for this consists in that the length of the divergent part of the vane channel in cascade No. 1 is significantly less than in the other cascades. Of much interest is a comparison of the curves of the losses in cascades No. 2 and No. 5 when f = 1.0. Thus, if in cascade No. 2 (Fig. 29a), in the range of M_1 numbers from 0.8 to 1.5, the losses are practically constant ($\zeta_{пр}$ = 6%), and at $M_1 > 1.5$ they increase, then in cascade No. 5 the losses first increase and reach their maximum when $M_1 = 1.2$, and then decrease. A minimum of losses ($\zeta_{пр}$ = 6%) will be attained when $M_1 = 1.5$. This character of change of losses for cascade No. 5 is conditioned in the same way as for cascade No. 11, with respect to large concavity of the back of the profile in the slanting shear. It should be noted that the maximum of losses for cascade No. 5

is somewhat displaced towards higher M_1 numbers as compared to divergent-type cascades.

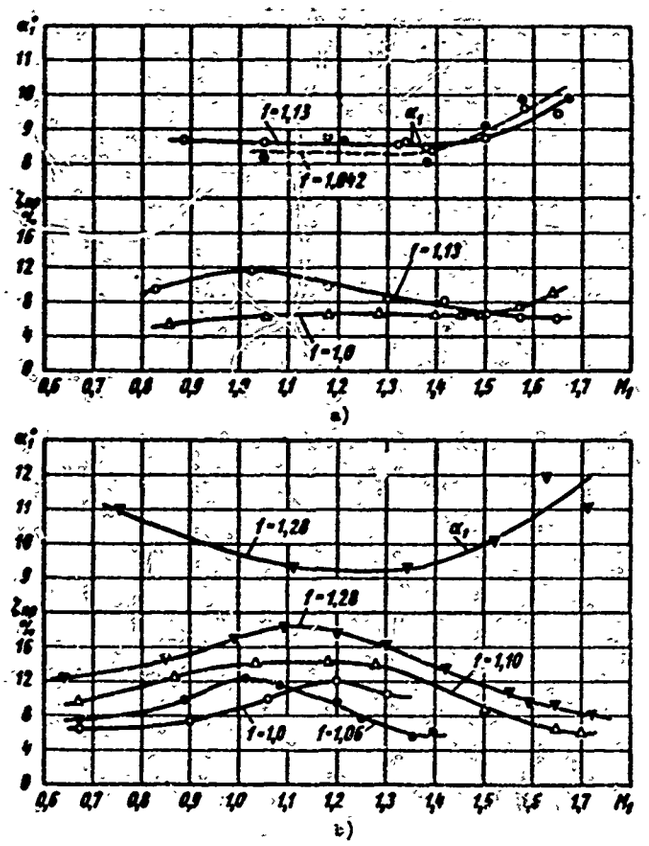

Fig. 29. Characteristics of supersonic nozzle cascades at small outlet angles of flow: a – –o–o– cascade No. 1; Δ–Δ–Δ– cascade No. 2; –●–●– cascade No. 3; b – o–o– cascade No. 5; ●–●– cascade No. 6; –Δ– cascade No. 7; ▼ – cascade No. 8.

Analysis of the curves shows that a minimum of cascade profile losses will be attained at $M_{1\,p}$, which is determined taking into account the concavity of the back of the profile in the slanting shear, and at $M'_{1\,p}$ the losses become somewhat greater. It should be noted that in the whole range of conditions the effectiveness of the developed cascades is significantly higher than those presently being used in turbine construction [30].

Figure 30a and b, gives the characteristics of cascades with large outlet angles of flow. The above-noted peculiarity of variation of profile losses also holds true for these cascades. It should be noted that the length of the divergent section of the vane channel for these cascades is considerably less than for the cascades whose characteristics are shown in Fig. 29. As a result, the level of losses for identical

f under transonic conditions is lower. Of much interest is a comparison of loss curves for cascades with f = 1.0 and f = 1.055, which are depicted in Fig. 30a.

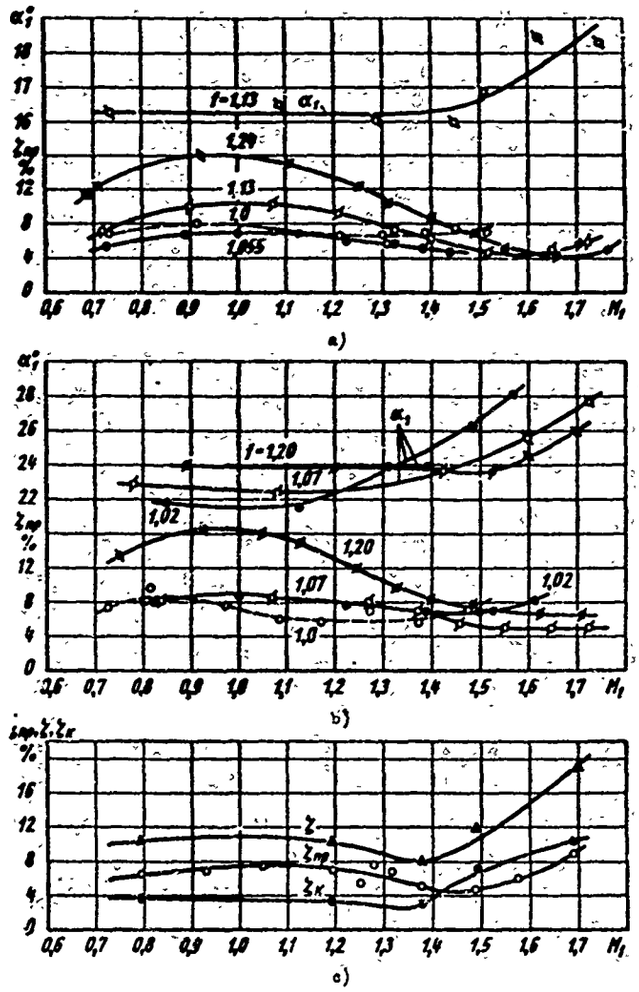

Fig. 30. Characteristics of supersonic nozzle cascades at large outlet angles of flow: a — cascade No. 15 (f = 1.0); cascade No. 16 (f = = 1.055); cascade No. 17 (f = 1.13); cascade No. 18 (f = 1.24); b — cascade No. 19 (f = 1.0); cascade No. 20 (f = 1.02); cascade No. 21 (f = 1.07); cascade No. 22 (f = 1.20); c — change of profile, tip and total losses in cascade with f = 1.01 depending upon M_1 number.

As can be seen, the losses in cascade No. 15 in the entire range of M_1 numbers are larger than in cascade No. 16. In cascade No. 15 the losses are practically constant and compose 7 to 8%. Of interest is a comparison of the loss curves for cascades No. 21 and No. 22 (Fig. 30b). A minimum of losses in these cascades, in spite of the considerable difference in parameters f, is attained at identical values of the M_1 number from 1.6 to 1.7.

Tip losses in cascades of type TC-B and TC-BP have not yet been studied sufficiently. Available experimental data show that with the increase of number $M_1 \leq 1.2$ to 1.3, tip losses decrease, and then at $M_1 > 1.3$ there is observed an intense growth of them.

The character of change of total losses in cascade TC-BP may be seen in Fig. 30c. Minimum values of ζ and ζ_K correspond to a lower M_1 number than $\zeta_{пр}$. Consequently, in short supersonic cascades the expansion ratio of the channel and the shape of the concave back, which correspond to rated conditions, should be selected with regard to the minimum of total losses, and not profile losses.

Figures 28-30 also give the curves of change of the outlet angles of flow from cascades. For cascade No. 9, at f = 1.0 (see Fig. 28b), the outlet angle of flow will start to increase when $M_1 > 1.0$, whereupon, if $\alpha_1 = 12^\circ$ when $M_1 = 1.0$, when $M_1 = 1.7$ the outlet angle of flow reaches 18°. Such a change of the outlet angle of flow can considerably worsen the work of a stage in varying conditions. For cascades with divergent channels, the outlet angles of flow at $M_1 < M'_{1p}$ are practically constant and start to increase only at $M_1 > M'_{1p}$. As a result of this, the change of the outlet angles of flow in the range of $M_1 = 1.0$ to 1.7 is considerably smaller.

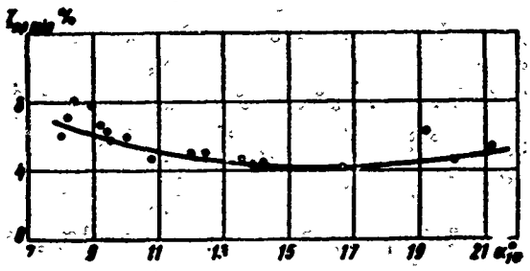

Fig. 31. Dependence of minimum profile losses $\zeta_{пр}$ in divergent cascades under rated conditions on angle $\alpha_{1*} = \arcsin \frac{a_M}{t}$.

Figure 31 shows the change of minimum profile losses in cascades at the computed value of M_{1p} depending upon angle $\alpha_{1*} = \arcsin \frac{a_M}{t}$. All experimental points are sufficiently well grouped on one curve. The losses at calculated M_{1p} number at $\alpha_{1*} = 8^\circ$ are 7%; as α_{1*} increases, the losses decrease, and at $\alpha_{1*} = 14$ to 16° they are 4 to 5%.

Analyzing the behavior of the characteristics of supersonic reaction cascades under varying conditions, it is necessary to establish the postion of the system of shocks in the channel and in the slanting shear, depending upon the M_1 number. Graphs of pressure distribution (Fig. 32a) make it possible to approximately estimate the place of location of the shocks under different conditions. The results of this treatment of graphs of pressure distribution are given in Fig. 32b and c. Shown there is the current position of a shock, $\bar{x}_{ск}$, depending upon the pressure ratio in the cascade, $\varepsilon_1 = p_1/p_0$, on parameter f, and on angle α_{1*}. The value of $\bar{x}_{ск} = 0$

corresponds to limiting conditions, when the shock disappears in the minimum throat area of the channel. The corresponding limiting pressure ratio is determined by the approximate formula

$$\varepsilon_{1пр} = \varepsilon_* + (1 - \varepsilon_*)\sqrt{1 - \frac{1}{\varepsilon_c f}}, \tag{43}$$

where ε_* is the critical pressure ratio;

$\varepsilon_c = \frac{p_{01}}{p_0}$ is the stagnation pressure ratio in the cascade.

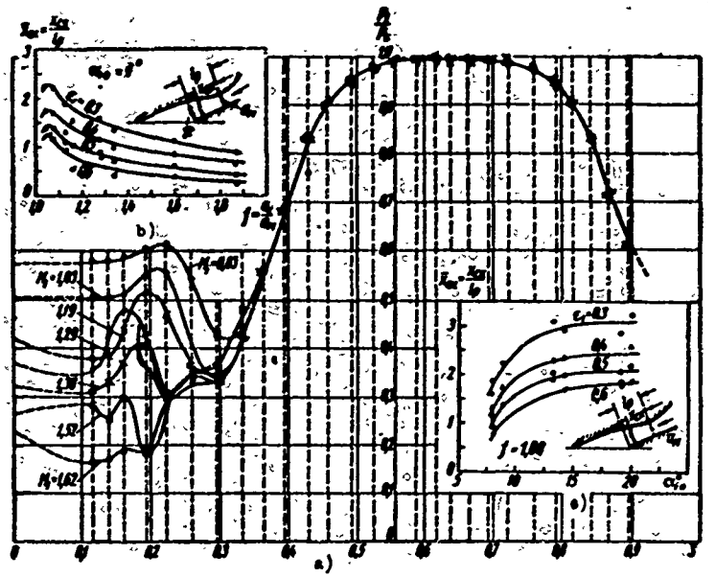

Fig. 32. Characteristics of supersonic reaction cascade TC-1BP under different conditions; f = 1.2; $\bar{t}$ =0.595; α_y = 30° and α_{1*} = 8°: a – pressure distribution along profile depending upon M_1 number; b – relative position of shock in divergent vane channels depending upon expansion ratio $f = \frac{a_2}{a_M^*}$; c – the same, depending upon angle $\alpha_{1*}(\varepsilon_1 \frac{p_1}{p_0})$.

From Fig. 32b it distinctly follows that with the decrease of f the shocks leave the channel more quickly and pass into the slanting shear, i.e., at the same pressure ratio ε_1 the shocks in the vane channel are closer to the exit section the smaller f is. In a limiting case of f = 1.0 (convergent channels) the line $\bar{x}_{ск}(\varepsilon$ is parallel to the vertical axis.

This result, from the physical point of view, explains the experimentally found varying dependence of losses and outlet angle of flow on the pressure ratio in off-design conditions. The smaller the geometric parameter f, the smaller the portion

of the back and concave surface of the profile under the influence of the shock system in off-design conditions. Consequently, the region of intense swelling of the boundary layer, and also in certain cases its separation under the influence of shocks, move through the flow, which leads to a sharp lowering of cascade losses. Since, in cascades with small f, as ε_1 decreases, the shocks leave the slanting shear more quickly, then the latter goes into operation more quickly and deflects the flow. Consequently, in cascades with small f, the outlet angle varies more intensely as the conditions vary.

The expansion angle of the divergent part of the vane channel also affects the relative position of the shock; as this angle increases, the shocks leave the channel more quickly.

A noticeable influence on the dependence $\bar{x}_{ск}(\varepsilon_1, f)$ is rendered by the characteristic cascade angle α_{1*} (Fig. 32c). As α_{1*} increases, $\bar{x}_{ск}$ increases, and losses in off-design conditions are lowered, since a smaller part of the back of the profile is under the influence of the shocks, which cause swelling of the layer and its separation.

An analysis of the structure of the boundary layer on the back of a profile with different contour shapes in the slanting shear at f = 1 and f > 1 confirms this conclusion. Figure 33a shows the distribution of δ^{**} along the back, and Fig. 33b indicates the change of $\delta^{**}_{сп}$ at the trailing edge, depending upon the conditions. Experiments showed that the minimum thickness δ^{**} corresponds to a concave back in the slanting shear. It is characteristic that in the zone of narrow cross section and behind it the thickness of the impulse loss is minimum and practically identical for three profiles at $x_{сп} \leq 0.5$. In cascades with convex and rectilinear backs, on a considerable section before the shock strikes the back, the boundary layer is laminar.

During artificial turbulization of the layer at the entrance to the cascade, in the zone of minimum cross section there also is detected a laminar layer, which proves the appearance of an inverse transition of the turbulent layer into a laminar layer also in this case. Under the influence of a shock, the laminar layer becomes turbulent, and is separated in most cases; here, there is a sharp increase in the thickness of the layer δ^{**} (see Fig. 33a). The occurring turbulization of the layer and its separation are observed at $\bar{x}_{сп} = 0.69$ to 0.74, i.e., at the point of incidence of the shock.

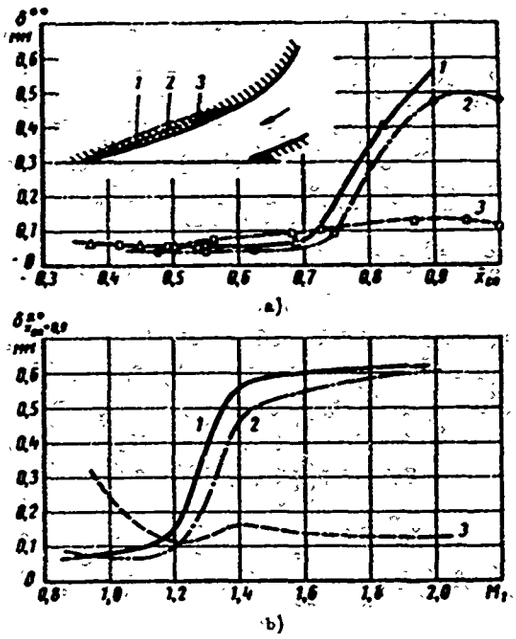

Fig. 33. Structure of boundary layer on back of profile of reaction cascade at supersonic velocities: a) distribution of thicknesses of impulse losses, at $M_1 = 1.6$, along the back; b) change of thickness δ^{**}, depending upon M_1 number, along section $\bar{x}_{сп} = 0.9$. Shape of back at slanting shear: 1 — convex; 2 — straight; 3 — concave.

In cascades with concave backs, at the deflection point of the back the laminar layer changes into a turbulent layer, whereupon the shock is already interacting with the turbulent section of the layer. In this case, separation of the layer in the shock zone, as a rule, does not occur.

Curve 3 on Fig. 33a shows that in a cascade with a concave back the transition of the laminar layer into a turbulent one is carried out in the section $\bar{x}_{сп} \doteq$ = 0.5 to 0.55.

The investigations conducted at MEI on reaction cascades at supersonic velocities confirm the above-stated recommendation for designing cascades.

In those cases when, because of the design and technological conditions, the calculated curvature cannot be carried out, deviations from the calculated profile are permissible, which, as shown by the MEI experiments, do not cause a noticeable change in the characteristics of the cascades.

Thus, the investigations confirmed the high effectiveness of cascades of type TC-BP in a wide range of conditions. In rated conditions the profile losses in these cascades only insignificantly exceed the profile losses in cascades that are designed for subsonic velocities.

Cascades of type TC-P, TC-BP, and TC-B, with divergent channels, can be used at different angles of incidence and relative pitch. It is obvious that as α_y and t change, there should also be a change in angle α_{1*}, which is determined by the formula

$$\alpha_{1*} = \arcsin \frac{a_м}{t},$$

where $a_м$ is the minimum cross section of the channel, and also the expansion ratio of the channel f. In accordance with formula (41), as α_{1*} and t vary, the outlet

angle α_1 also varies, and according to formula (42), the coefficient of wave losses also varies.

In Fig. 34, as an example there is shown the dependence of $\alpha_{1*}(\alpha_y, \bar{t})$ and $f(\alpha_y, \bar{t})$ for cascade TC-1BP. The use of the graph does not cause any difficulties. According to the thermal calculation, we know angle α_1. We also know the computed value of the $M_{1\,p}$ number at the cascade exit. After selecting the magnitude of the expansion ratio by means of formula (30), with the help of equation (33) we find the value of α_{1*}; knowing α_{1*} and f, on the graphs of Fig. 34 we determine the necessary α_y and $\bar{t}$ for one value.

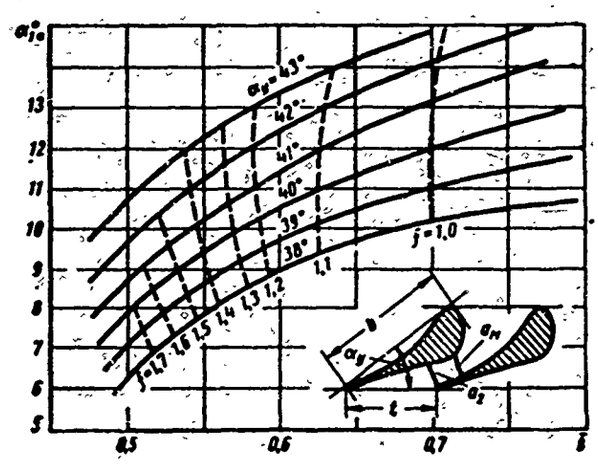

Fig. 34. Dependence of outlet angle of flow α_{1*} = arc sin a_M/t and ratio of areas $f = a_2/a_M$ on relative pitch $\bar{t} = \frac{t}{b}$ and angle of incidence of profile α_y.

The influence of the thickness of the trailing edge at supersonic velocities may be estimated by means of experimental data. Figure 35 gives the results of MEI experiments.

As M_1 increases, the profile losses in cascades with thick edges ($\Delta_{кр}$ = 2.5 to 4.0 mm) do not vary monotonically (Fig. 35). The first maximum of the curve $\zeta_{пр}(M_1)$ is explained by the displacement of the points of separation against the flow (laminar separation). The second maximum is connected with the formation of a supersonic region on the portion between sections AB (narrow section) and SD and the shocks that close off this region; the shocks displace the point of separation S against the flow. The transition to supersonic velocities is accompanied by an improvement of the flow around the edge. Section SD is then displaced along the flow, as a result of which

the channel cross section is increased ($\overline{SD} > \overline{AB}$) and the flow before the slanting shear becomes supersonic.

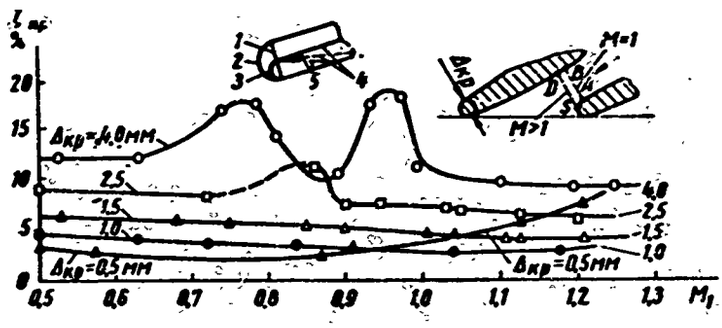

Fig. 35. Change of profile losses in reaction cascade depending upon M_1 number for various thicknesses of trailing edges. MEI experiments.

In this case the position of the separation point determines the quantity $f = \frac{\overline{SD}}{\overline{AB}}$, whereby f increases as M_1 increases.

Thus, a thick rounded edge will form a self-regulating divergent channel with a variable expansion ratio f.

For this reason, as the M_1 number increases, the losses in these cascades noticeably are lowered and at $M_1 > 1$ they become less than in a cascade with a thin edge ($\Delta_{кр}$ = 0.5 mm).

The influence of the form of the edge at $M_1 > 1$ may be estimated by means of the graphs in Fig. 35. The best results are given by the wedge-shaped sharp edge 5, and the biggest losses correspond to the normally cut edge 1 of maximum thickness. The rounded edge 3, whose thickness is twice as less than that of 1 and 2, gives satisfactory results.

§ 8. ACTION CASCADES FOR TRANSONIC AND SUPERSONIC VELOCITIES

As it is known [22], at transonic and supersonic velocities at entrances to action cascades there appear bow shocks that are connected with the flow around the entrance edges (Fig. 36). The shape of the bow shocks and their location with respect to the edges depend on the M_1 number at the entrance and on the shape of the edges and the vane channels.

During a supersonic flow in cascade channels there can appear shocks that are connected with the flow around the concave surface and back, and also due to the interference of bow shocks with the profile inside the channel (at high supersonic

velocities). In the slanting shear at the cascade exit and behind it there will form a well-known system of expansion shocks and waves which is induced by the trailing edges (see Fig. 36a and b).

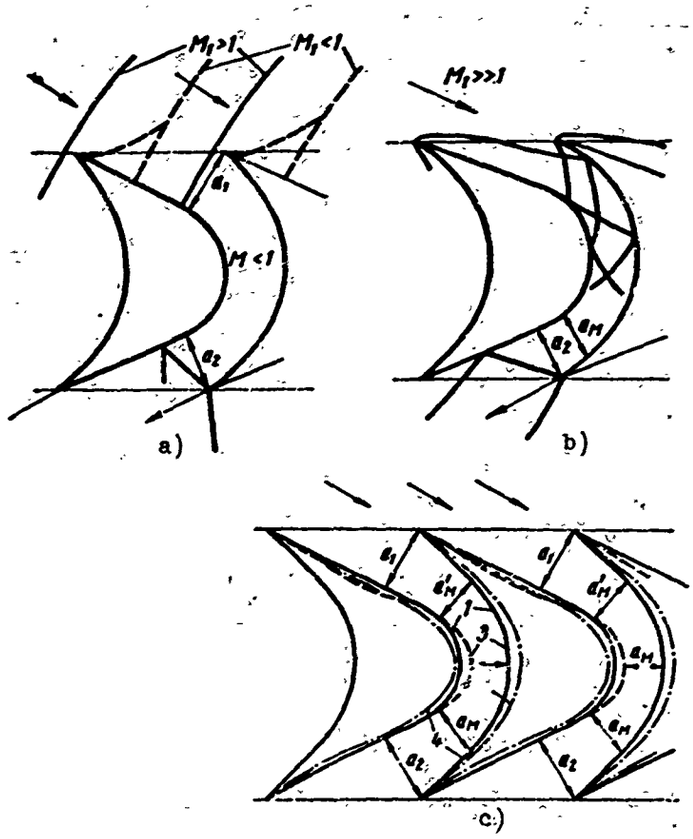

Fig. 36. Shapes of profiles and channels of action supersonic cascades: a — cascades for low supersonic velocities; b — cascades for high supersonic velocities; c — cascades with various-shaped channels.

It is obvious that the shape of the entrance and exit sections of the profile and the shape of the channel should ensure: a) minimum wave losses in bow and rear shocks and b) shock-free and continuous motion with minimum frictional losses in the vane channel.

These problems are solved differently for transonic and high supersonic velocities.

At transonic velocities ($M_* < M_1 < 1.3$) the shape of the bow shocks is similar to that of the normal shocks (see Fig. 36a). It is possible to consider that stagnation of flow at the entrance to the channel is carried out in a normal shock. At low supersonic velocities ($M_1 < 1.3$) the losses in normal shocks are small (1 to 1.5%);

therefore, cascades of group "Б" (see Table 1) are designed by the "normal shock" method. In cascades of this type the leading and trailing edges of the profile are pointed and rectilinear, and the vane channels are continuously convergent. The curvilinear portions of the back and concave surface have a varying curvature, whereby the shape of the curvilinear part of the channel is calculated according to the channel method (§ 2).

Action cascades for $M_1 > 1.3$ are designed by various methods which differ by the organization of the flow at the leading edges in the channel, and at exit of the slanting shear.

The entrance sections of the back of the profile of supersonic cascades (group "B," see Table 1) can ensure a constant velocity behind the bow shock (rectilinear entrance sections), a gradual stagnation of flow in the system of shocks (broken entrance section), or continuous stagnation along the concave wall (see Fig. 36c).

With any method of organization of the flow at the entrance, the middle curvilinear part of the channel can be made with a convergent (channels 1, 3, and 4 in Fig. 36c) or constant cross section (channel 2 in Fig. 36c). In the first case the flow is stagnated first, and then accelerated. The minimum cross section is disposed inside the channel ($a_M < a_2$). In a channel of constant cross section, flow stagnation occurs only due to friction. Acceleration of flow is carried out in the slanting shear at the exit. The minimum cross section then coincides with the exit section ($a_M = a_2$, Fig. 36c). Convergent-divergent channels may be shaped either with continuous convergence to the minimum cross section a_M and subsequent divergence to a_2 (channel 3), or with short convergent and divergent sections united by a curvilinear channel of constant cross section a'_M (channel 4).

The exit section of the back of the profile (in the slanting shear) may be calculated by the method of characteristics and made concave (as also for profiles of group TC-P or TC-BP) or rectilinear. In all design methods the leading and trailing edges are tapered and pointed.

The shape of the vane channel renders a decisive influence on the losses in an action supersonic cascade under calculated and variable conditions.

Of much practical interest is the selection of the curvature of the back and the concave surface for a supersonic flow in the vane channel. As shown by theoretical analysis, even in a channel of relatively great curvature it is possible to avoid the formation of shock waves on the concave surface. This conclusion is also confirmed by experimental data.

The design of action cascades with a continuous supersonic flow may be carried out by assuming that the flow lines in the channel are a set of concentric circles. The velocity distribution in such a channel obeys the equation

$$cR = a_* R_* = \text{const},$$

where c is the velocity of an arbitrary flow line; R is the radius of a flow line circle; a_* is the critical velocity reached on a flow line whose radius of curvature is R_*.

Consequently,

$$\lambda \bar{R} = 1;$$
$$\lambda = \frac{c}{a_*}; \quad \bar{R} = \frac{R}{R_*}.$$

We shall consider a theoretical case of infinitely thin leading and trailing edges of a profile (Fig. 37a). The flow at the entrance and behind the cascade may be considered as equal and uniform (direction of velocity at entrance M_1 coincides with direction of leading edges). Consequently, segments of the back and the concave surface in front of the portion of constant cross section of the channel and at its exit must ensure a shock-free transition to the flow line circles (at the entrance) and conversely, from the circles, from the circles to straight lines (at the exit).

The calculation of the transition sections, which are noted in Fig. 37a, may be carried out by the method of characteristics. With the given velocity at the entrance, the velocity behind the infinitely thin leading edges is $M_1' = M_1$, since in rated conditions the intensity of the shocks at the leading edges will be infinitesimal. At the transition section of the concave surface the flow should be slowed down to the given velocity M_B, and accelerated in the transition section of the back to M_C.

We shall designate by δ the deflections of the supersonic flow with its expansion from M = 1 to M_1' (angle δ_1'), from M = 1 to M_C (angle δ_C), and from M = 1 to M_B (angle δ_B).

In the zone of compression on the transition section of the concave surface, the deflection decreases by the quantity $\delta_C - \delta_B$; in the zone of expansion on the transition section of the back, the deflection increases by the quantity $\delta_1' - \delta_B$. Both transition sections should deflect the flow at an identical angle.

Consequently,

$$\delta_1' - \delta_a + \nu = \delta_c - \delta_1',$$

where ν is the angle of displacement of the transition sections of the back and the concave surface (see Fig. 37b).

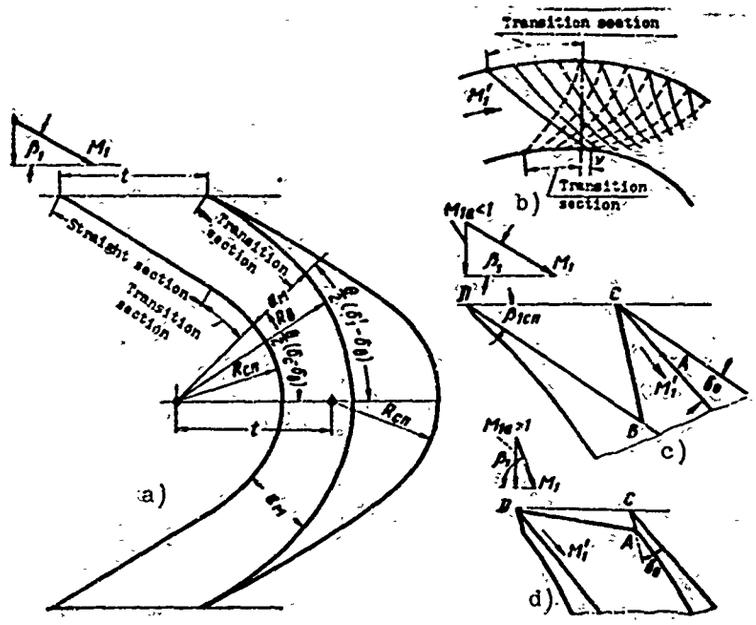

Fig. 37. Profiling of an action cascade with continuous supersonic flow: a — construction of symmetric profile of action lattice; b — profiling of channel; c and d — construction of leading edge.

The shape of the profile and the vane channel is determined by the M_1 and M_2 numbers at the entrance and exit, the angle of deflection of the flow in the cascade $\theta = \beta_1 + \beta_2$, and the selected values of M_B and M_C on the concave surface and the back. For a symmetric profile (see Fig. 37a) the angle of deflection is $\theta = 2\beta_1 = 2\beta_2$. In this case the concave surface and the back have a length that is determined by the following angles:

$$\theta - 2(\delta_1' - \delta_a) \text{ and } \theta - 2(\delta_c - \delta_1').$$

The transition sections on the back are connected to the edges by segments of straight lines which, together with the transition sections of the concave surface, form infinitely thin edges. It is not possible to make such edges.

The leading edges of the blades may be tapered (see Fig. 37c and d). The angle of taper δ_0 is selected in such a way so that the shock at point C is attached.

If the velocity of the incident flow is directed parallel to the back DB ($\beta_1 = \beta_{1cn}$) then there appears only one branch of the shock CB (Fig. 37c). The velocity behind the shock M_1' is easily determined by means of calculation. From points A and B begin the transition sections, whereby segment AC is selected with such a length, so that shock CB strikes at the beginning of the transition section of the back.

If angle $\beta_1 > \beta_{1cn}$, there appears shock DA (Fig. 37d). The edge (line AC) is undercut parallels to the velocity vector M_{1a}, whereby the shock is annihilated at point A, in the expansion wave that has formed there. The vane channel is calculated for velocity M_1', behind shock DA.

During the calculation of cascades by the indicated method it is necessary to be sure that for the selected M_B and M_C numbers there can exist a supersonic flow at the entrance to the vane channels. This probl: is solved with the help of the continuity equation presented in § 31.

Let us note here that the maximum M_C number is determined from the condition of maximum flow rate through the cascade in its minimum cross section with the calculation of losses and the curvature of the flow lines.

Figure 38 gives the curves of the dependence of maximum angles $\delta_{1\,max}'$ on δ_C for a certain range of values of δ_B. The curves in Fig. 38 give the boundary values of the $M_1'(\delta_1')$ numbers at the entrance, depending upon the $M_B(\delta_B)$ and $M_C(\delta_C)$ numbers, whereby the corresponding lines, δ_B = idem, divide the diagram into two regions; above the curves is the region in which supersonic velocities cannot appear at the entrance.

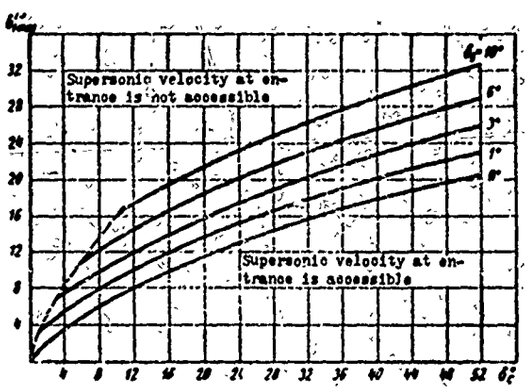

Fig. 38. Limiting values of angles $\delta_{1\,max}'$ depending upon δ_C (M_C) and δ_B (M_B), which determine the region of accessible supersonic velocities at the entrance.

As already indicated earlier, a decrease of wave losses in the bow shocks may be attained by introducing gradual deceleration in the system of shocks at the entrance. After appropriately constructing the back of the profile at the entrance (see Fig. 36a), this method may be applied for profiling the middle portion of the channel.

Let us consider some results of an experimental investigation of action cascades in a supersonic flow. Figure 39 presents the curves of pressure distribution along the profile of cascade TP-1B. The channels of the cascade are convergent-divergent and have no area of constant cross section. The minimum cross section is located near the entrance before the main deflection (points 8-7 and 13-14). Stagnation of flow on the back occurs in front of the entrance section of the channel (points 10 to 12). At $M_2 > 1$, in front of the channel there appears a normal shock which approaches the entrance section as the M_2 number increases. In conditions of $M_2 \gtrsim 1.5$, bow shocks enter the vane channel. The flow is accelerated in the channel behind the shocks, whereby a large expansion is detected near the minimum cross section on the back of the profile. As M_2 increases, the zone of the pressure minimum is displaced toward the flow and expansion decreases on the back.

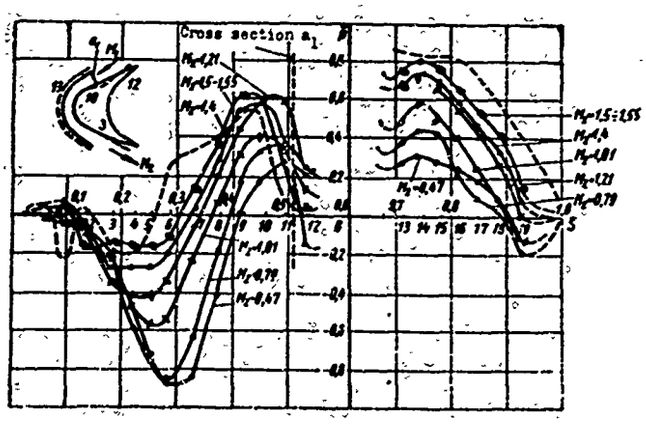

Fig. 39. Pressure distribution along profile of action cascade TP-1B (convergent-divergent channels) at $\bar{t} = 0.575$; $\beta_y = 89^\circ05$; $\beta_1 = 20^\circ$; — — — — cascade TP-1B with gradual stagnation at entrance when $\bar{t} = 0.625$; $\beta_y = 90^\circ$; $\beta_1 = 20^\circ$.

In conditions close to those calculated ($M_2 \approx 1.5$ to 1.6), the pressures distribution on the back and concave surface is favorable; the flow in the channel is supersonic. Figure 39 also contains a curve (dotted line) that corresponds to a cascade with channels of constant cross section and with gradual stagnation at the entrance. The stagnation in the system of shock here is less intense and in the middle portion of the channel the flow is less convergent. At the exit, the flow is accelerated more intensely.

The flow fields of supersonic reaction and action cascades are shown in Fig. 40. In the reaction cascade (Fig. 40, I) it is possible to see the characteristic spectrum of flow in a slanting shear with three shock waves (edge and reflected

shocks). The interaction of an edge shock with the boundary layer on the back leads to swelling of the layer and, in certain cases, to its separation.

GRAPHIC NOT REPRODUCIBLE

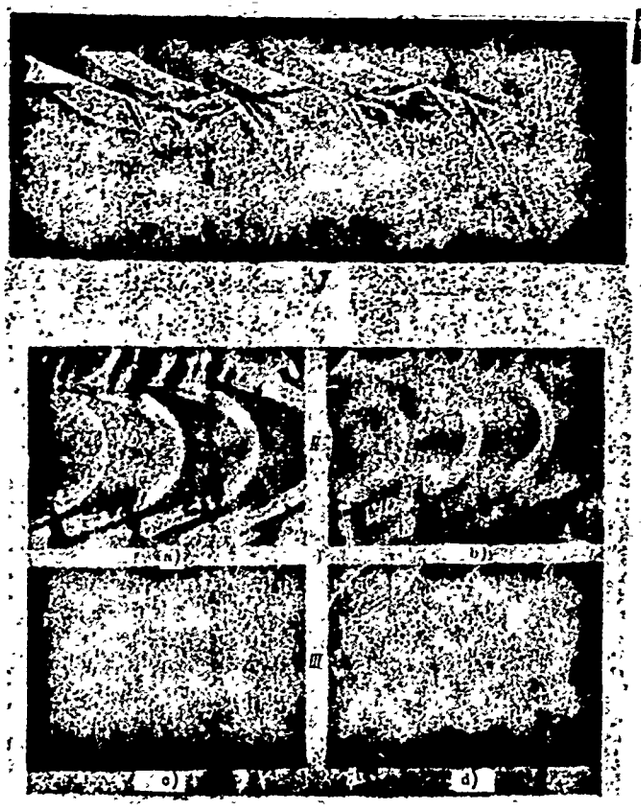

Fig. 40. Flow spectra in supersonic cascades: I – nozzle cascade TC-Б, $M_1 = 1.52$; II – action cascade with convergent-divergent channels (TP-1B); $\bar{t} = 0.575$, $\beta_y = 89°30'$, $\beta_1 = 18°$; a) $M_1 = 1.34$; b) $M_1 = 1.64$; III – cascade with gradual stagnation at entrance: $\bar{t}_1 = 0.625$, $\beta_y = 90°$; $\beta_1 = 22°30'$; c) $M_1 = 1.47$; d) $M_1 = 1.67$.

At the entrance sections of action profiles (Fig. 40, II and III), systems of shocks are formed in front of the edges. When the profiles are made according to the method of gradual stagnation (Fig. 40, III), at high supersonic velocities there are formed two shocks, one of which is located at the salient point. It is characteristic that at sufficiently high numbers $M_1 > 1$ the velocities are supersonic everywhere and there are no shock waves inside the channel.

At the cascade exit there will form a system of shocks that consists of, as also in the reaction cascade, two edge shocks and one reflected shock.

A comparison of the losses in supersonic cascades designed by different methods may be seen in Fig. 41. The characteristics of cascades of group "B" are given there with channels of different form, with gradual stagnation at the entrance, and without it. Gradual stagnation has noticeable advantages at $M_2 \geq 1.5$ to 1.6. In cascades with channels of constant cross section, the losses at transonic and subsonic velocities are essentially lower than in cascades with convergent-divergent channels. However, at $M_2 \geq 1.4$ to 1.5 the latter are characterized by minimum losses.

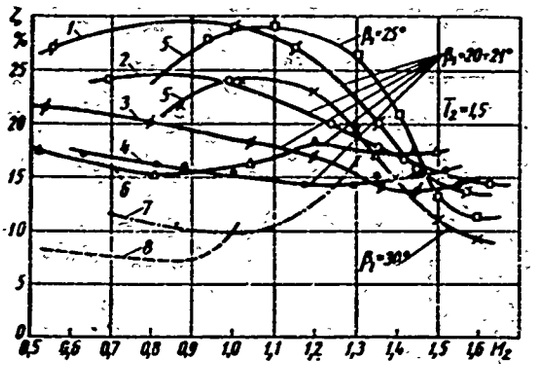

Fig. 41. Total losses in action supersonic cascades designed by different methods: 1, 3, 4 — cascades with convergent-divergent channels and rectilinear back at exit; 5 — cascade with channels of constant cross section and rectilinear back at entrance; 2, 6 — with broken back at entrance; 7 — TP-1Б; 8 — TP-1А.

At subsonic velocities, minimum losses correspond to cascade TP-1A. In conditions of $M_2 = 1.0$ to 1.25 the best characteristics are possessed by cascade TP-1Б, and at $M_2 > 1.25$ the total losses are minimum in cascades of group "B."

Thus, the experiments confirmed the correctness of the method of designing supersonic action cascades with gradual stagnation at the entrance and convergent-divergent channels. These cascades should be employed at $M_1 \geq 1.5$ to 1.6. The optimum contraction ratio of a channel at the entrance and the expansion ratio at the exit (the ratios a_1/a_M' and a_2/a_M', see Fig. 36c) depend on the M_1 (M_2) number and the deflection in the cascade. For the range of M_1 numbers from 1.5 to 2.0, these ratios lie within the following limits: $a_1/a_M = 1.1$ to 1.2 and $a_2/a_M = 1.15$ to 1.25.

At M_1 numbers from 1.25 to 1.5, satisfactory results are given by cascades with channels of constant cross section and pointed edges.

A check showed that the calculated* pressure distribution in the channels satisfactorily coincides with the experimental distribution in sections up to 40% of the chord on the back and up to 65% of the chord on the concave surface. Significant deviations from the calculation at the exit sections of the channel are explained by uncalculated influence of the boundary layer.

*According to the channel method that was presented above, which was first proposed by Guderley.

§ 9. FLOW RATE COEFFICIENTS OF TURBINE CASCADES

The calculation of flow areas of nozzle and moving cascades is produced with the help of an important characteristic, i.e., the flow rate coefficient, which is determined by the formula

$$\mu = \frac{G}{G_t},$$

where G and G_t are the actual and theoretical flow rates through the cascade.

The values of μ essentially depend on how the concept of the theoretical flow rate G_t is formulated. In accordance with the continuity equation, the actual mass flow rate of gas through a nozzle cascade may be calculated by different methods:

$$G = \mu G_t = \mu_1 \pi d l_1 \rho_{1t} c_{1t} \sin \alpha_{1,\varphi} = \mu^* \pi d l_1 \rho_{Mt} c_{Mt} \sin \alpha_{1,\varphi} = \mu_1' \pi d l_1 \rho_{1t} c_{1t} \sin \alpha_1. \tag{44}$$

Here d and l_1 are the mean diameter and height of the cascade; ρ_{1t} and c_{1t} are the density and velocity flow behind the cascade with isentropic expansion; ρ_{Mt} and c_{Mt} are the density and velocity in the throat area with isentropic expansion; α_1 is the mean actual (flow rate) angle of exit from the cascade.

The flow rate coefficients in equation (44) correspondingly refer to: the area of the throat sections and the theoretical parameters behind the cascade (μ_1), the area of the throat sections and the theoretical parameters in these sections (μ^*), the area of the exit section and the theoretical parameters in this section (μ_1').

Other methods of expressing the flow rate of gas through a cascade are also possible. Thus, for instance, equation (44) may be written in the following manner:

$$G = \mu_1^* \pi d l_1 \rho_M c_M \sin \alpha_1, \tag{45}$$

where ρ_M and c_M are the mean actual (taking losses into account) density and velocity in the throat sections.

The enumerated flow rate coefficients are interrelated:

$$\mu_1 = \mu^* \frac{\rho_{Mt} c_{Mt}}{\rho_{1t} c_{1t}} = \mu_1' \frac{\sin \alpha_1}{\sin \alpha_{1,\varphi}} = \mu_1^* \frac{\rho_M c_M}{\rho_{1t} c_{1t}} \tag{46}$$

and can be approximately expressed* through the velocity coefficient φ. Actually,

---

*In the determination of the velocity coefficient, the parameters are averaged with respect to the momentum equation, and the flow rate coefficient is averaged with respect to the continuity equation.

since

$$\varphi\varrho_1 c_{1t}\sin\alpha_1 \approx \mu_1\varrho_{1t}c_{1t}\sin\alpha_{1\text{эф}} = \mu^*\varrho_{nt}c_{nt}\sin\alpha_{1\text{эф}} =$$
$$= \mu_1'\varrho_{1t}c_{1t}\sin\alpha_1 = \mu_1^*\varrho_n c_n\sin\alpha_{1\text{эф}},$$

then

$$\varphi \approx \mu_1\frac{\varrho_{1t}}{\varrho_1}\frac{\sin\alpha_{1\text{эф}}}{\sin\alpha_1} = \mu_1'\cdot\frac{\varrho_{1t}}{\varrho_1} = \mu^*\frac{\varrho_{nt}}{\varrho_{1t}}\frac{c_{nt}}{c_{1t}}\frac{\sin\alpha_{1\text{эф}}}{\sin\alpha_1} =$$
$$= \mu_1^*\frac{\varrho_n}{\varrho_1}\frac{c_n}{c_{1t}}\frac{\sin\alpha_{1\text{эф}}}{\sin\alpha_1}. \qquad (47)$$

Formulas (46) and (47) distinctly show that the difference between the flow rate coefficients between μ and φ can be very significant, depending upon the geometric and performance parameters of the cascade.

Since the ratios of $\frac{\sin\alpha_{1\text{эф}}}{\sin\alpha_1}$ and the densities

$$\frac{\varrho_{1t}}{\varrho_1} = \left[\frac{1+\frac{k-1}{2}M_{1t}^2(1-\zeta_1)}{1+\frac{k-1}{2}M_{1t}^2}\right]^{\frac{1}{k-1}}$$

depend on the M_{1t} number and the loss coefficient ζ_1, it is obvious that these parameters determine the degree of difference of the indicated coefficients.

The selection of the flow rate characteristic of a cascade is determined first of all by the reliability of the experimental data with which it is calculated. In the experimental determination of the flow rate coefficients μ^*, μ_1^*, and μ_1', and also in the thermal calculation of a stage with these coefficients, it is necessary to know exactly the distribution of parameters in the throat section and the angles behind the cascade α_1. In many cases these data are absent, whereby even an insignificant error in estimating the outlet angles can lead to an appreciable error in the calculation of the area of flow sections of the cascade. Therefore, when performing thermal calculations, the factories mainly use the flow rate coefficient μ_1, which can be obtained from experiments with maximum accuracy.

The flow rate coefficients that refer to the throat sections of nozzle and moving cascades are calculated by the following formulas:

$$\mu_1 = \frac{G}{F_1\varrho_{1t}c_{1t}} \text{ and } \mu_2 = \frac{G}{F_2\varrho_{2t}w_{2t}}.$$

Here $F_1 = \pi dl_1 \sin\alpha_{1\text{эф}}$ is the area of the throat sections of a nozzle cascade and $F_2 = \pi dl_2 \sin\beta_{2\text{эф}}$ is the area of the throat sections of a moving cascade, since

$$\sin\alpha_{1\text{эф}} = \frac{a_1}{t_1} \text{ and } \sin\beta_{2\text{эф}} = \frac{a_2}{t_2};$$

ρ_{2t} and w_{2t} are the theoretical density and velocity in relative motion behind the moving cascade.

All geometric parameters that determine the areas F_1 and F_2 are easily measured by conducting the appropriate experiments. In the thermal calculation, these parameters are established by drawings.

The quantities μ_1 and μ_2 may also be expressed by gas-dynamic functions [22]:

$$\mu_1 = \frac{G\sqrt{T_{01}}}{KF_1 p_{01} q_{1t}} = \frac{G\sqrt{T_{01}}}{KF_1 p_1 \sigma_{1t}} \tag{48}$$

and

$$\mu_2 = \frac{G\sqrt{T_{02}}}{KF_2 p_{02} q_{2t}} = \frac{G\sqrt{T_{02}}}{KF_2 p_2 \sigma_{2t}}.$$

Here p_{01} and T_{01} are the pressure and stagnation temperature in absolute motion in front of a nozzle cascade; p_{02} and T_{02} are the pressure and stagnation temperature in relative motion in front of a moving cascade;

$$q_{1t} = \left(\frac{k+1}{2}\right)^{\frac{1}{k-1}} \lambda_{1t} \left(1 - \frac{k-1}{k+1}\lambda_{1t}^2\right)^{\frac{1}{k-1}}$$

is the given flow rate at the exit of a nozzle cascade in the theoretical process;

$$\sigma_{1t} = q_{1t}\frac{p_{01}}{p_1} = \left(\frac{k+1}{2}\right)^{\frac{1}{k-1}} \lambda_{1t} \left(1 - \frac{k-1}{k+1}\lambda_{1t}^2\right)^{-1}$$

is the flow rate function;* p_1 and p_2 are the static pressures behind nozzle and moving cascades;

$$K = \sqrt{\frac{k}{R}\left(\frac{2}{k+1}\right)^{\frac{k+1}{k-1}}}$$

is a constant (R is the gas constant).

---

*Functions q_{2t} and σ_{2t} are determined by $\lambda_{w2t} = \frac{w_{2t}}{a_{*w}}$ by means of an analogous formula (a_{*w} is the critical velocity in relative motion behind a moving cascade).

The flow rate coefficients μ^* and μ_1 also depend on profile shape, type of cascade, relative height, entrance angle of flow, and Re and M numbers, i.e., on the performance and geometric parameters which determine the outlet angle and losses in a cascade and must be given separately for each cascade.

However, up to now a large number of cascades being utilized in turbine construction do not have the indicated flow rate characteristics. At the same time, the experimental data accumulated at MEI can be generalized for certain groups of cascades.

Thus, for instance, Fig. 42 gives the flow rate coefficients, depending upon relative height and step pitch TC-1A and TC-3A cascades (see Table 1). In a sufficiently wide range of variation of the quantity $\frac{1}{\bar{t}} < 2.0$, the coefficient μ_1 weakly depends on cascade height. At lower heights, as $\bar{t}$ decreases, the flow rate coefficients decrease more intensely.

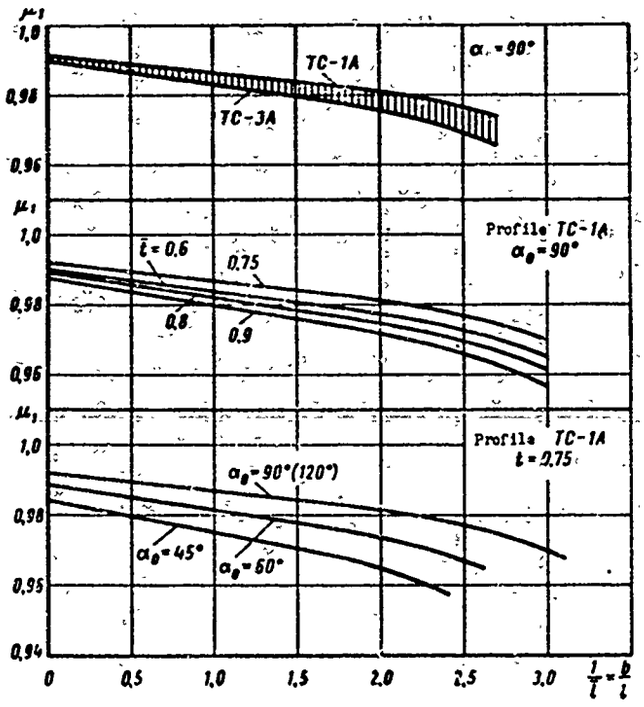

Fig. 42. Dependence of flow rate coefficients on relative height $\frac{1}{\bar{t}}$, for MEI nozzle cascades with various pitch $\bar{t}$ and entrance angles of flow α_0; Re_1 number equals $5 \cdot 10^5$; $M_1 = 0.63$.

A study of the influence of pitch $\bar{t}$ shows that the optimum (with respect to losses) range of $\bar{t}$ includes the maximum values of the flow rate coefficients.

The basic geometric parameters analogously (from the qualitative side) affect

the flow rate coefficient of action cascades. It is natural that the absolute values of μ_2 will be lower than those of μ_1.

The results of certain experiments for determining μ_2 are shown in Fig. 43.

A significant influence on the flow rate coefficients is also rendered by the Re number.

The graphs in Fig. 44 show that as the Re number increases, the flow rate coefficients μ_1 and μ_2 increase. At small Re, a growth of μ_2 with an increase of Re is more intense than μ_1. When Re $\geq$ $\geq 6 \cdot 10^5$, μ_1 and μ_2 practically do not depend on Re. The calculation of the flow rate through a cascade at supersonic velocities is produced with the help of the flow rate coefficient μ^*. In this case the density and velocity in the throat sections in a theoretical process are

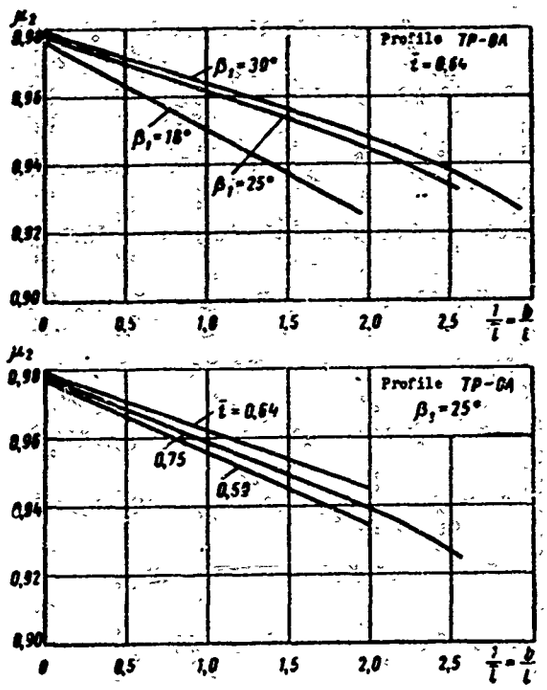

Fig. 43. Dependence of flow rate coefficient for moving cascade TP-0A MEI on relative height $\frac{l}{t}$ at different entrance angles β_1 and relative pitch $\bar{t}$.

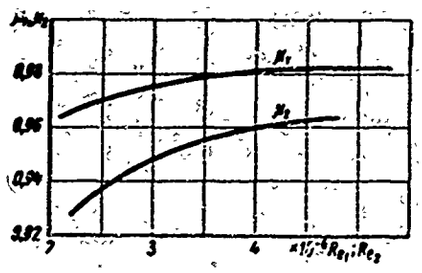

Fig. 44. Influence of Reynolds numbers Re_1 and Re_2 on flow rate coefficients of nozzle and moving action cascades μ_1 and μ_2.

equal to the critical values ($\rho_{мt} = \rho_*$; $c_{мt} = a_*$).

For these conditions ($M_1 \geq 1$) the coefficient μ^* weakly depends on the M_1 and Re_1 numbers (see Fig. 17c).

For an analytic determination it is also very convenient to use the flow rate coefficient μ^*. The calculation of the potential flow in a channel makes it possible to establish the velocity (pressure) distribution around the profile contour and find the displacement thickness δ^* in the throat section in any (including the throat) section of the channel.

The flow rate through one cascade channel is determined by the formula

$$G_z = G_{tz} - \sum(\varrho_{Mt} c_{Mt} \delta^*)_t, \tag{49}$$

where G_{tz} is the theoretical flow rate in one channel. The sign Σ indicates that the product in parentheses must be summed up for the concave surface, back, and two end walls.

Since, on the other hand,

$$G_z = \mu^* l_1 t_1 \varrho_{1t} c_{1t} \sin \alpha_{1\infty} = \mu^* G_{tz},$$

then

$$\mu^* = 1 - \frac{\sum(\varrho_{Mt} c_{Mt} \delta^*)_t}{l_1 t_1 \varrho_{1t} c_{1t} \sin \alpha_{1\infty}}. \tag{50}$$

In accordance with formula (50), for a determination of μ^* it is necessary to calculate the quantity $(\rho_{Mt}\ c_{Mt}\ \delta^*)$ for the back, concave surface, and end walls of the channel, and find their sum. This is easy to do after calculating the boundary layer on these surfaces. Calculation of the potential flow makes it possible to establish the values of ρ_{Mt} and c_{Mt} on the outer bound of the layer on these surfaces.

CHAPTER II

CALCULATION OF A STAGE

§ 10. SELECTION OF CASCADES FOR THE STAGE BEING DESIGNED

When designing a new turbine or reconstructing an existing turbine, which is conducted for the purpose of raising its economy, it is necessary to match cascades to the stages, select their dimensions, and determine the efficiency and degree of reaction, etc., i.e., calculate the stage.

The simplest and most reliable method is the selection of a stage that has undergone a check in an experimental turbine. As a result of testing the stages, the experimental turbine's basic characteristics are determined, e.g., efficiency, degree of reaction, and flow rate coefficient, depending upon u/c_{ϕ}, ε, and Re. If a combination of cascades is selected which has been tested, but, in the stage being designed, other, experimentally unchecked, geometric parameters (heights, diameter, clearances, and others) are proposed, then it is possible to use correction graphs that make it possible to consider the deviation of dimensions of the selected stage from the dimensions under investigation.

However, in a number of cases it becomes necessary to use cascades and their combinations that have not been checked in an experimental turbine, and investigated only in static conditions. In these cases it is necessary to select cascades which, after satisfying the basic requirements of thermal calculation of the turbine, will be optimum, i.e., the stage will have the highest efficiency accessible in these specific conditions. Furthermore, one should consider the requirements of reliability and unification.*

*Sometimes stages are used that are not calculated for the highest efficiency, which can be related to the problem of lowering turbine cost, simplifying the design, or stabilizing the economy under varying operating conditions.

This chapter considers only single stages with cylindrical blading and full gas supply.

The selection of cascades for a stage should be first conducted depending upon the type of conditions in which the stage will be operating, e.g., subcritical or supercritical.

This chapter considers stages with subcritical velocities.

Selection of Nozzle Cascade

The selection of cascades for a stage should begin from the nozzle cascade, since its dimensions determine the basic dimensions of the subsequent moving cascade. Furthermore, for action single stages, the effect of the nozzle cascade on economy is considerably greater than that of the moving cascade.

From the nozzle cascades that we have developed in recent years, it is possible to use many which have demonstrated good effectiveness and have been checked experimentally. Certainly, it is desirable to employ cascades which have been checked experimentally in annular cascades, in actual diaphragms with the usual plant technology of manufacture, and especially those investigated in experimental turbines. It is very important that the experimental check of cascades, both in static conditions, and also in turbines, be conducted under actual, or close to actual, test conditions (M and Re numbers, initial turbulence).

In this chapter the method of cascade selection is explained in reference to MEI cascades of group "A." As can be seen below from the text, this method is easily extended to other cascades, for which there are experimental aerodynamic characteristics. Some examples are the characteristics given in the atlas of profiles and in the standards (see Chapter I).

Usually during the calculation of a stage, we know the volume admission of gas passing through the stage and calculated according to the parameters in front of the nozzle cascade (or more exactly, in front of the parameters of stagnated flow) Gv_0; the average diameter of the stage d, which is determined from a preliminary calculation of the turbine, or selected from the conditions of design or unification; the turbine velocity n and the velocity ratio is

$$\frac{u^*}{c_\phi} = \frac{u}{\sqrt{2h_0 + c_0^2}}$$

(or the available stage heat drop h_0).

*Selection of the velocity ratio u/c_ϕ for the stage is considered later in Chapter IV.

With these known quantities it is easy to determine an approximate value:

$$l_1 \sin \alpha_{1эф} \approx 200 \frac{G v_0}{\sqrt{2h_0}} \, [мм] \tag{51}$$

or

$$l_1 \sin \alpha_{1эф} \approx 2{,}5 \frac{G v_0}{d^2} \left(\frac{3000}{n}\right) \frac{u}{c_ф}, \, [мм] \tag{52}$$

where G is the flow rate of gas per unit of time (kg/sec);

v_0 – (m^3/kg);

d – (m);

n – (rpm);

h_0 – (kj/kg).

This preliminary calculation is necessary in order to select the nozzle cascade and its basic geometric characteristics.

As we know, an increase of cascade height l_1, or more exactly, relative height $\bar{l}_1 = l_1/b$, leads to a lowering of tip losses, and consequently, to an increase of cascade efficiency. At the same time, it is not possible to select an arbitrary value of angle $\alpha_{1\ эф}$. Each cascade at a certain variation of the angle of incidence α_y and relative pitch $\bar{t} = t/b$ has a definite range of variation of angle $\alpha_{1\ эф}$ (see Chapter I).

$$\alpha_{1эф} = f(\bar{l}, \alpha_y).$$

Thus, the selection of angle $\alpha_{1\ эф}$ by itself signifies the selection of one cascade or another, or at least a limitation of the number of cascades available to the designer.

First, for simplicity, we shall consider that only one nozzle cascade can be used. From the range of possible angles $\alpha_{1\ эф}$ it is tempting to select the lowest value; this makes it possible to obtain a maximum height l_1, which means minimum tip losses. However, for a given cascade, a decrease of angle $\alpha_{1\ эф}$, as a rule, leads to an increase in losses (for the same $\bar{l}_1$). Actually, a decrease of angle $\alpha_{1\ эф}$ is a decrease of the mounting angle of the profile α_y and/or a decrease of the

relative pitch of the cascade. Both of these factors, as experiments show [22], usually leads to an increase of profile losses. The most intense increase is in the edge losses, which for the given profile (b and $\Delta_{кр}$) are essentially increased as the pitch $\bar{t}$ and angle α_y decrease.

In order to clearly present the relation between the angle

$$\alpha_{1\,эф} = f(\bar{t},\ \alpha_y) \text{ and the losses } \zeta'_c = f(\bar{t},\ \alpha_y)^*,$$

Fig. 45 shows graphs of the dependence of $\zeta'_c = (\alpha_{1\,эф},\ \alpha_y,\ \bar{t})$ for one MEI TC-2A cascade. The graphs were calculated for specific values of $\Delta_{кр}/b$; for other $\Delta_{кр}/b$, reconstruction of the curves presents no difficulties and does not result in any qualitative change of the dependence. The graphs in Fig. 45 were constructed according to the cascade characteristics given in the atlas of profiles. Analogous graphs can be constructed for all cascades that have sufficiently complete aerodynamic characteristics.

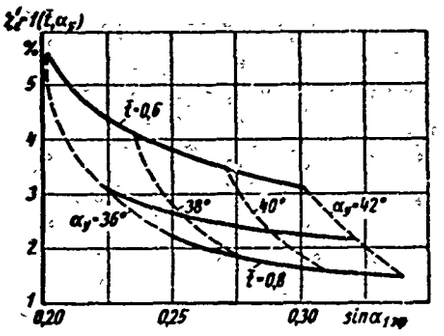

Fig. 45. Losses in nozzle cascade TC-2A depending on mounting angle of profile α_y and relative pitch $\bar{t}$.

By using diagrams of this type, it is possible for the given angle $\alpha_{1\,эф}$ to find the optimum values of relative pitch $\bar{t}$ and mounting angle of the profile α_y, and also to determine what additional losses will result from a deviation from the optimum characteristics that were adopted for unification purposes.

Thus, for a given grid with determined profile dimensions (b and $\Delta_{кр}$), selected with respect to conditions of technology, reliability, and unification** and at the obtained value of $\bar{t}_1 \sin\alpha_{1\,эф}$, i.e., for $\bar{t}_1 \sin\alpha_{1\,эф}$, one should determine the values of $\alpha_{1\,эф}$ and $\bar{t}_1$ which will give the least total cascade losses. It is natural that the designer will try to apply precisely these optimum dimensions. For a determination of the most advantageous dimensions of a specific cascade, a graph of $\zeta_c = f(\bar{t}_1 \sin\alpha_{1\,эф})$ is constructed. Since usually (except very short cascades) the tip losses are proportional $1/\bar{t}_1$, for a number of values of $\alpha_{1\,эф}$ it is possible

*ζ' implies that part of the losses in a nozzle cascade which depends only on $\bar{t}$ and α_y.

**The selection of quantity b from the point of view of economy is considered later.

to construct a series of straight lines, i.e., dependences of total cascade losses (by summarizing the tip losses and minimum losses for each $\alpha_{1\ эф}$ of losses from the diagram in Fig. 46) on $1/\bar{l}_1 \sin \alpha_{1\ эф}$. The lower envelope of the series of these straight lines gives the minimum value of losses in the given cascade, depending upon $1/\bar{l}_1 \sin \alpha_{1\ эф}$.

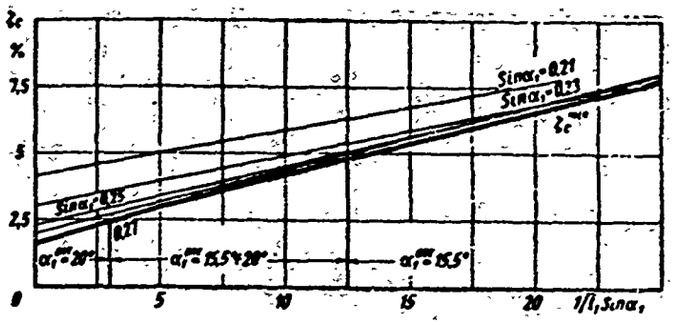

Fig. 46. Dependence of total losses in nozzle cascade TC-2A on $\bar{l}_1 \sin \alpha_{1\ эф}$ and $\sin \alpha_{1\ эф}$ for selection of optimum angle at $\Delta_{кр}/b = 0.012$.

Thus, knowing $\bar{l}_1 \sin \alpha_{1\ эф}$, we find the angle $\alpha_{1\ эф}$ at which the losses in the nozzle cascade are minimum, and according to it we select angle $\alpha_{1\ эф}$ and l_1.

Figure 46 shows the curves of $\zeta_c^{min} = f(\bar{l}_1 \sin \alpha_{1\ эф})$ for nozzle cascade MEI TC-2A.

It should be emphasized that the graphs in Figs. 45 and 46 were constructed for $M_1 \approx 0.6$-0.9 and for Re_1 numbers greater than $5 \cdot 10^6$.

During the calculation of a stage, with other values of M it is necessary to introduce corrections taken from the aerodynamic characteristics of cascades (see §§ 4 and 11); the influence of Re numbers is considered only in a certain zone (see §§ 4, 18, and 43).

The construction of graphs like those in Fig. 46 for other MEI TC-1A and TC-3A cascades and a comparison of the curves of ζ_c^{min} for these three very popular nozzle cascades, shows that:

a) for identical $\bar{l}_1 \sin \alpha_{1\ эф}$ the TC-2A and TC-3A cascades have approximately identical total losses;

b) cascade TC-1A for all $\bar{l}_1 \sin \alpha_{1\ эф}$ is less economic than TC-2A and TC-3A;*

*Taking into account the increased tip losses in actual annular cascades and also from the condition of blading continuity and the lowering of losses with the outlet velocity, it is sometimes of value to employ a cascade with angle α_1 smaller than optimum.

c) despite the wide-spread opinion concerning the necessity of using nozzle cascades with small angles $\alpha_{1\ эф}$ for stages that operate with small volume steam admissions, calculations of aerodynamic characteristics show that cascades with the same $\bar{t}_1 \sin \alpha_{1\ эф}$ and larger $\alpha_{1\ эф}$ frequently have less total losses.

Thus, for cascade TC-1A, angle $\alpha_{1\ эф} = 12.5^\circ$ gives minimum losses only when $\bar{t}_1 \sin \alpha_{1\ эф} < 0.055$; a smaller angle leads to an increase in losses at any $\bar{t}_1 \sin \alpha_{1\ эф}$. For cascade TC-2A, correspondingly, $\alpha_{1\ эф} = 15.5^\circ$ when $\bar{t}_1 \sin \alpha_{1\ эф} < 0.08$. For cascade TC-3A, correspondingly, $\alpha_{1\ эф} = 18.5^\circ$ when $\bar{t}_1 \sin \alpha_{1\ эф} < 0.085$.

It should be noted that the graphs presented above were constructed on the basis of the results of static tests of two-dimensional cascades. In actual annular cascades the losses will be different; moreover, in certain cases the optimum value of angle $\alpha_{1\ эф}$ may also change. Thus, for instance, in welded diaphragms with unprofiled shrouds, the tip losses in short cascades are essentially higher than in straight ones. In connection with this, it is possible that the optimum value of angle $\alpha_{1\ эф}$ at small $l_1 \sin \alpha_{1\ эф}$ will be somewhat lower than that obtained with the use of the results of static investigations of two-dimensional cascades. At the same time, tests of annular cascades in welded diaphragms indicated a significant increase of losses in the root sections of the cascades with small angles $\alpha_{1\ эф}$ and cylindrical shrouds.

In conclusion, we shall indicate that if an intermediate stage of multistage turbine is being designed, the selection of l_1, and consequently, also angle $\alpha_{1\ эф}$, should begin not only with the requirements of stage economy and unification, but also with the conditions of continuity of the turbine blading.

Selection of Moving Cascade

The selection of the moving cascade of a turbine stage is produced with respect to the outlet angle $\beta_{2\ эф}$, the inlet angle β_1, and the velocity flow M_{w_2}. For the cascade, the profile angle β_y and relative pitch $\bar{t}$, and consequently angle $\beta_{2\ эф}$, are selected with the overlap, shroud inclination, direction of absolute outlet velocity c_2 (i.e., angle α_2), and the degree of reaction taken into account.

The overlaps in intermediate single stages (Fig. 47) are recommended in the following limits.

It should be taken into account that the amount of overlap depends not only on the cascade height, but also on the axial and radial clearances, and on the technology of diaphragm manufacture. The table shown below gives recommendations for

Table 7. Overlaps of Intermediate Single Stages

Height of nozzle cascade l_1 in mm	Total overlap $\Delta_{ln} + \Delta_{lk}$ in mm	Height of nozzle cascade l_1 in mm	Total overlap $\Delta_{ln} + \Delta_{lk}$ in mm
15-25	2.5-3	50-75	3-4.5
25-50	2.5-3.5	75-150	3.5-5.5

stages with welded diaphragms, for the mean values of the axial dimensions of the stage and good stage sealing.

Usually intermediate stages with low moving-blade heights have cylindrical blade shrouds, i.e., constant inlet and outlet heights of the moving cascade. Then with respect to l_1, i.e., the height of the nozzle cascade and the overlap, the outlet height of the moving cascade l_2 is determined.

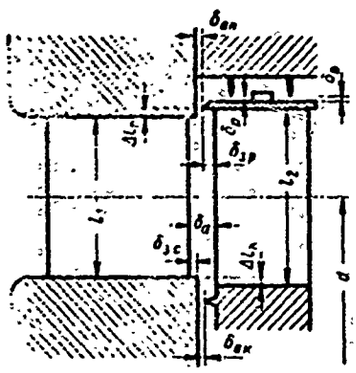

Fig. 47. Diagram of action type single stage.

In certain cases it is of value to incline the shroud of a moving blade. This should be done in stages of medium pressure, if it is not possible to create continuous blading by other means, i.e., the transition from one stage to another. Sometimes the requirements of unification also force the use of an inclined shroud. If the shroud is inclined (conical), the channel should be convergent, i.e., the channel area towards the flow should not be increased anywhere. Otherwise the cascade will have a divergent flow in certain sections, which, as a rule, increases the losses.

It is desirable that angle α_2 be close to a right angle ($75^\circ < \alpha_2 < 110^\circ$). If angle α_2 considerably deviates from 90°, then at the entrance to the following stage, where a standard conventional nozzle cascade is selected, both the profile and tip losses will be increased.

In certain turbines (usually turbines of low power and some ship machinery) the number of stages or their diameters are decreased by striving towards small nonoptimum velocity ratios u/c_ϕ. Then a considerable decrease of angle α_2 is inevitable. So that this decrease of α_2, and consequently, also the angle of entrance α_0 to the following cascade, does not cause an essential lowering of economy of the following stage, it is necessary to use specially designed nozzle cascades with small calculated angles (see § 24).

If the stage being calculated is the last one in the given section and its outlet velocity is not completely used, then it is desirable that α_2 be close to the quantity $\alpha_2 = 90^\circ + \beta_2$, and for a single stage, to $\alpha_2 = 90^\circ$. Very frequently it is considered that the minimum value of outlet velocity c_2 is attained when $\alpha_2 = 90^\circ$. If a stage with definite values of d and β_2 is being designed then for a fixed value of the peripheral velocity u it turns out that $(c_2)_{min}$ is attained when $\alpha_2 = 90^\circ + \beta_2$.

Actually, we shall use two equations:

$$\operatorname{tg} \alpha_2 = \frac{\sin \beta_2}{\cos \beta_2 - u/w_2}$$

and

$$w_2 \sin \beta_2 = c_2 \sin \alpha_2.$$

From these equations, after excluding velocity w_2, we obtain:

$$c_2 = \frac{u}{\sin \alpha_2 \operatorname{ctg} \beta_2 - \cos \alpha_2}.$$

It follows from this that the minimum value of c_2 is attained when $\alpha_2 = 90^\circ + \beta_2$. When $\alpha_2 = 90^\circ + \beta_2$, the efficiency of the given stage will naturally be lower than when $\alpha_2 = 90^\circ$, since a decrease of the outlet velocity is attained by means of decreasing h_0, i.e., the stage is calculated for $u/c_\Phi > (u/c_\Phi)_{опт}$. However, if in a given section each subsequent stage completely (or to a considerable extent) uses the outlet velocity of the preceding one, then the efficiency of the entire section, after redistribution of the heat drop between stages, will mainly depend on the $h_{вс} = \frac{c_2^2}{2}$ of the last stage. Consequently, the efficiency of the entire section will be the highest when $\alpha_2 = 90^\circ + \beta_2$ for the last stage.

The preliminary calculation of a stage and the selection of a cascade are governed by the magnitude of the mean reaction ρ_{cp}. The mean reaction of a stage (in the first approximation it is considered that this is the reaction on the mean diameter) is selected depending upon cascade flare (d/l) and the sealing of clearances in the stage. The less d/l, the bigger the change of the reaction with respect to height; and since it is desirable to have approximately a zero reaction in the root sections, ρ_{cp} increases as d/l decreases.

Selection of the reaction of a stage, taking into account the steam leakages, is considered in § 12. It is necessary also to consider that an increase of the reaction at the root can essentially increase the axial stresses.

For preliminary calculations it is possible to recommend, with a full steam supply and good sealing of clearances in a stage with cylindrical blading, the following values of the reaction on the mean diameter:*

$$\rho_{\varphi} \approx \frac{1.8}{1.8+\theta}, \tag{53}$$

where

$$\theta = \frac{d}{l}.$$

For more exact calculations it is possible to use the following formula [33]:

$$\rho_{\varphi} = \frac{2\varphi^2 \cos^2 \alpha_1}{2\varphi^2 \cos^2 \alpha_1 + \theta}, \tag{53a}$$

where $\varphi^2 = 1 - \zeta_c$ is the square of the velocity of the nozzle cascade.

Final selection of the moving cascade and its dimensions should be performed after a detailed calculation of the nozzle cascade and construction of velocity triangles of the stage.

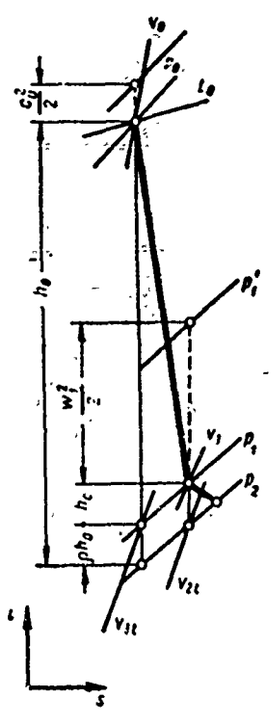

Fig. 48. Process of steam expansion in a stage in an is-diagram.

For a more precise determination of the dimensions of the nozzle cascade, on the basis of the selected reaction, with the help of an is-diagram we find the pressure p_1 (see Fig. 48) and specific volume v_{1t} behind the nozzle cascade during the isentropic process of expansion.

Then the height of the nozzle cascade is

$$l_1 = \frac{G v_{1t}}{\mu_1 \pi d c_{1t} \sin \alpha_{1эф}}, \tag{54}$$

where

$$c_{1t} = \sqrt{2h_{01} + c_0^2}.$$

The flow rate coefficient μ_1 is selected on the basis of an experiment; it is preferable to use the results of the experimental determination of the flow rate coefficient of an actual diaphragm. If there are no experimental data on μ_1, then for gases and superheated steam it is possible to take $\mu_1 \approx 0.97$ (see § 9).

*This question is considered in greater detail in Chapter VII.

Knowing the dimensions of the nozzle cascade and the conditions of flow, by means of the aerodynamic characteristics we find the losses in the nozzle cascade ζ_c and then h_c (kj/kg).

$$h_c = \left(h_{01} + \frac{c_0^2}{2}\right)\zeta_c = \frac{c_{1t}^2}{2}\zeta_c \tag{55}$$

Taking into account the selected overlap, height of the nozzle cascade, and inclination of the blade shroud, we obtain the height of the moving cascade l_2 and the angle $\beta_{2\,эф}$

$$\sin\beta_{2эф} = \frac{G v_{2t}}{\mu_2 \pi d l_2 w_{2t}}, \tag{56}$$

where $w_{2t} = \sqrt{2h_{02} + w_1^2}$; the relative inlet velocity w_1 is found with the help of the velocity triangles shown in Fig. 49.

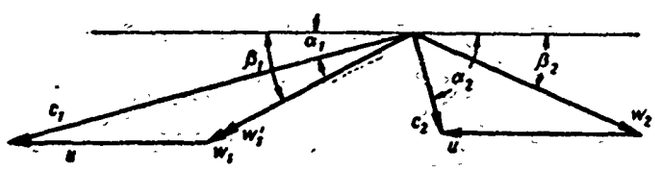

Fig. 49. Velocity triangles of a stage.

Formal use of formula (56) in a number of cases can lead to a noticeable error in the determination of $\beta_{2\,эф}$. Usually the flow rate coefficient μ_2 implies the coefficient that considers the losses also at the entrance to the moving cascade, and in the determination of velocity w_1, according to which the velocity w_{2t} is computed, these losses are not considered. It is more correct to perform the calculation in the following way.

We shall write a continuity equation for the entrance and exit sections of the moving cascade, whence we shall find the interdependence of angles $\beta_{2\,эф}$ and β_1:

$$\frac{\sin\beta_{2эф}}{\sin\beta_1} = \frac{w_1'}{w_{2t}} \frac{v_{2t}}{v_1} \frac{l_1}{l_2} \frac{1}{\mu_2'}.$$

We shall designate the velocity in the entrance section of the moving cascade by $w_1' = \psi' w_1$. Here w_1' is the relative velocity in the entrance section of the moving cascade; ψ' is a coefficient that considers the losses in the clearance between cascades and the losses at the entrance to the moving cascade. The flow rate

coefficient μ_2' considers the change of the flow rate as compared to the theoretical value with losses only in the convergent channel of the moving cascade.

It is obvious that $\psi' > \psi$ and $\mu_2' > \mu_2$. Usually it is possible to assume that they are equal (with the exception of a flow of moist steam). Then

$$\sin\beta_{2эф} = \frac{w_1}{w_{2t}} \frac{v_{2t}}{v_1} \frac{l_1}{l_2} \sin\beta_1. \tag{56a}$$

Here v_1 is the specific volume of steam (gas) at the entrance to the moving cascade.

If there are experimental values for angles α_1 and β_2, they should be used in the construction of velocity triangles.

On the basis of angles $\beta_{2\,эф}$ and β_1, the relative height of the moving cascade l_2/b_2 (chord b is usually selected on the basis of reliability and unification) and the M_{w_2} number, which is calculated with respect to relative outlet velocity w_{2t}, we shall select the moving cascade.

After determining the dimensions and total losses, for the selected moving cascade, we construct an outlet velocity triangle and find angle α_2.

If the value of angle α_2 goes beyond the recommended limits, then it is possible to somewhat change the reaction ρ or the value of the outlet height of the moving cascade l_2, i.e., the overlap. An increase of the reaction leads to a decrease of angle α_2; the same effect is caused by an increase of l_2 (angle $\beta_{2\,эф}$ correspondingly decreases).

It should be recalled that for the given initial parameters and heat drop of a stage, an increase of the degree of reaction leads to a small increase of the area of a nozzle cascade and to a considerable decrease of the outlet area of a moving cascade.

For the purposes of unification, frequently in the design of new turbines or the reconstruction of existing ones, it is expedient to employ cascades with predetermined dimensions. Then the stage, i.e., combination of nozzle and moving cascades, will have, under specific operating conditions ($u/c_ф$ and ε), a determined magnitude of reaction, which can be changed only by changing the dimensions of the cascades.

For rated operating conditions of a stage or with a small deviation, when we may practically disregard the influence of the change of the angle of entrance to the moving cascade (angle β_1), the mean reaction of the stage can be determined by

the following formula:*

$$\left(\frac{F_1}{F_2}\right)^2\left(\frac{\mu_1}{\mu_2}\right)^2=\frac{\varrho+\varphi^2(1-\varrho)+x_\phi^2-2\varphi\cos\alpha_1 x_\phi\sqrt{1-\varrho}}{(1-\varrho)\left[1+\varrho\left(\frac{1}{\varepsilon}-1\right)\right]^2}, \qquad (57)$$

where

$$x_\phi=\frac{u}{c_\phi},\ \varepsilon=p_2/p_0.$$

However, calculation of the reaction ρ by this formula is inconvenient and does not reveal the influence of different factors. Therefore, Fig. 50 illustrates a graph of the dependence of ρ on $\frac{l_1 \sin\alpha_{1\,эф}\mu_1}{l_2 \sin\beta_{2\,эф}\mu_2}$ and $x_ф = \frac{u}{c_ф}$. This graph was constructed for the particular case of $\alpha_1 = 13^\circ$, $\varphi = 0.96$ and $\varepsilon = 0.8$. For other values of φ, α_1, and ε, the correction curves shown in Fig. 51 should be used.

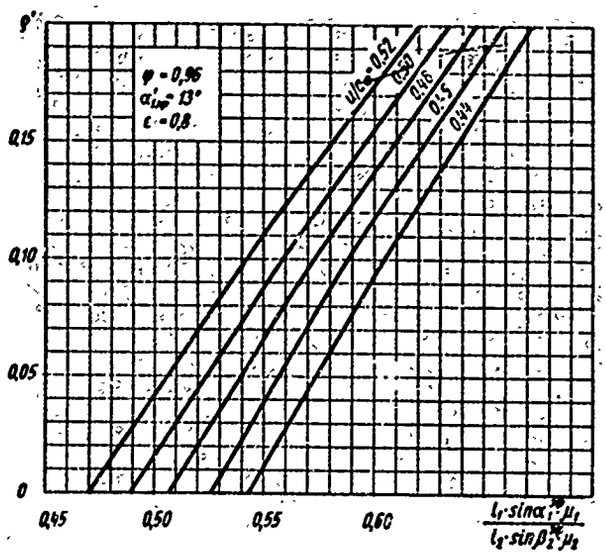

Fig. 50. Stage reaction ρ depending upon geometric characteristics of cascades.

In order to estimate what the moving cascade should be after selecting the nozzle cascade, without resorting to complicated calculations, the nomograph in Fig. 52 may be used. The nomograph contains the dependence $\beta_{2\,эф} = f(\alpha_{1\,эф}, \rho, x_ф, (l_2 - l_1)/l_1, \varepsilon, \mu_2/\mu_1)$.

After determining angle $\beta_{2\,эф}$ on the nomograph, using the aerodynamic characteristics, we shall select the moving cascade. The characteristics of moving cascades may be derived on the basis of the results of their tests (see Chapter I).

For instance, for group "A" of MEI moving cascades, the selection may be performed with the aid of Table 1.

If it is possible to select several cascades for the obtained angle $\beta_{2\,эф}$, the one that has the least losses under the specific conditions ($\beta_{2\,эф}$, β_1, $\bar{l}_2$, and M_{w_2})

*As already indicated earlier, this chapter, and in particular the given formula, pertains only to subcritical flow in stages with a full steam supply and cylindrical blading at large d/l.

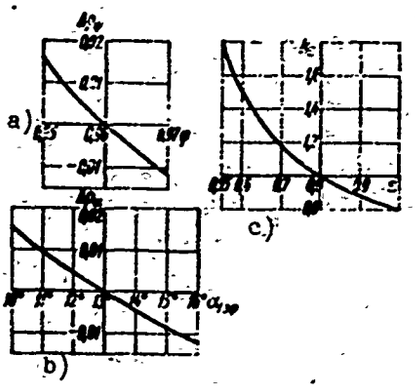

Fig. 51. Dependence of corrections for calculated degree of reaction on various values of parameters: a — φ; b — $\alpha_{1\ эф}$; c — ε; $\rho = k_\varepsilon \cdot \rho' + \Delta\rho_\varphi + \Delta\rho_\alpha$.

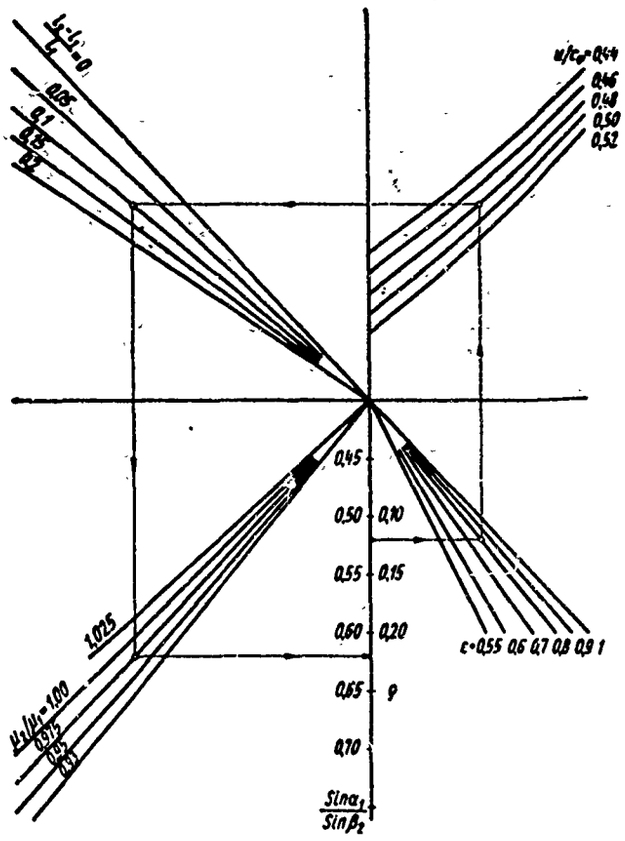

Fig. 52. Nomograph for determination of angle $\beta_{2\ эф}$.

should be used. Usually it is preferable to select a cascade with a smaller number, since the relative pitch of the cascade will then be higher, and consequently, the edge losses (certainly, in the zone of optimum $\bar{t}$) will be lower; the number of blades will also decrease.

In the selection of a moving cascade with respect to a given angle $\beta_{2\ эф}$ a large role is played by their unification and reliability.

Selection of Profile Chord

During the last few years the tendency to decrease the chord of the profile of a nozzle cascade appeared. A number of turbines here and abroad began to employ diaphragms with narrow blades. The purpose of decreasing the width, and consequently also the chord of the profile is to increase the relative height of the cascade in order to reduce tip losses.

However, it should be considered that for a given thickness of the trailing edge — it is doubtful whether its minimum value, a, which is determined by the conditions of technology and strength, can be decreased — a decrease in profile chord leads to an increase in the ratio $\Delta_{кр}/a_2$, i.e., the thickness of the edge to the throat of the channel, and consequently, to a growth of edge losses.

The Re number decreases proportionally and the relative roughness increases as chord decreases. Both factors in principle lead to an increase of losses (the Re number influences both the profile and the tip losses). However, for the first stages, where the blades are low and it is necessary to decrease the chord, the Re number is very large; therefore, their influence may be disregarded.

If the surface purity of the profile is poor, the influence of roughness must be considered. For this we shall use the materials of the preceding chapter.

Profile losses in the zone of raised roughness, according to (24) are equal to:

$$\zeta_{пр.ш} = \frac{4\xi}{C^{2m}\bar{t}\sin\alpha_{1\,эф}}\left(\frac{k_ш}{b}\right)^m.$$

Taking $\xi = 0.17$, $C \approx 400$, and $m = 0.25$, we will obtain:

$$\zeta_{пр.ш} = \frac{0{,}0344\,(k_ш)^{1/4}}{\bar{t}\sin\alpha_{1\,эф}}\,b^{-1/4}.$$

For a specific cascade for all, with the exception of chord b, constant geometric dimensions (l_1 = const, $\Delta_{кр}$ = const, $\bar{t}$ = const, $\alpha_{1\ эф}$ = const), the optimum value of profile chord can be found.

Numerous experiments of different organizations showed an approximately linear dependence of edge losses* on $\Delta_{кр}/a_2$ and a linear dependence of tip losses on $1/\bar{l}_1$ for not very short cascades. Then the total losses, which depend on the chord of the profile, will be equal to:

$$\zeta' = \zeta_{кр} + \zeta_{конц} + \zeta_{пр.ш} = K\frac{\Delta_{кр}}{b\bar{t}\sin\alpha_{1эф}} + \gamma\frac{b}{l_1} + \frac{0.0344\,(k_ш)^{1/4}}{\bar{t}\sin\alpha_{1эф}}\,b^{-1/4} = \\ = c_{кр}b^{-1} + \frac{\gamma}{l_1}b + c_ш b^{-1/4}. \qquad (58)$$

Here K is the tangent of the angle of incidence of the straight line $\zeta_{кр} = f\left(\frac{\Delta_{кр}}{a_2}\right)$;

γ is the same, for straight line $\zeta_{конц} = f(b/l_1)$.

Hence, the optimum value of profile chord, which gives minimum cascade losses, is

$$b_{опт} \approx \frac{mc_ш}{2\gamma}l_1 + \sqrt{\frac{c_{кр}}{\gamma}l_1 + \left(m\frac{c_ш}{2\gamma}l_1\right)^2}. \qquad (59)$$

Let us estimate the influence of roughness on the optimum value of chord in an example of a TC-2A cascade with the following given parameters: $\bar{t} = 0.6$; $\sin\alpha_{1\,эф} = 0.26$; $\Delta_{кр} = 0.6$ mm.

Let us assume that $k_ш = 0.002$ – for a polished surface (see Table 4).

Then $c_ш = 0.047$

$$b_{опт} = 0.29l_1 + \sqrt{90l_1 + 0.181l_1^2}.$$

When $l_1 = 20$ mm, $b_{опт} = 48.7$ mm (without taking into account the influence of roughness, $b_{опт} = 42.5$ mm).

If we assume that the surface of the profile is corroded and $k_ш = 0.02$, correspondingly, then $c_ш = 0.083$. Then at $l_1 = 20$ mm, $b_{опт} = 54.0$ mm.

Thus, the influence of roughness on $b_{опт}$ is perceptible when there is considerable roughness and in long blades, where tip losses are not great. It should be noted that the dependence of $\zeta = f(b)$ in the zone of $b_{опт}$ is continuous; therefore, the chord of the profile may be selected by inaccurately following formula (59).

For polished and ground blade surfaces, it is possible, disregarding the influence of roughness, to use the following formula:

$$b_{опт} = \sqrt{\frac{K}{\gamma}\frac{\Delta_{кр}l_1}{\bar{t}\sin\alpha_{1эф}}} = x\sqrt{l_1}. \qquad (59a)$$

*Edge losses practically do not depend on roughness (see § 4).

Here $b_{опт}$ and l_1 are given in mm.

From this formula it is clear that the optimum value of profile chord is proportional to the square root on the cascade height.

Figure 53 gives a graph, which may be used to determine the optimum value of chord $b_{опт}$ depending upon l_1 and $\bar{t}$ according to formula (59a). This graph was constructed for three MEI nozzle cascades of group "A," TC-1A, TC-2A, and TC-3A, for mean values of $\Delta_{кр}$ and $\sin \alpha_{1\ эф}$. A more precise determination of $b_{опт}$ for other values of $\Delta_{кр}$ and $\alpha_{1\ эф}$ is easily performed with formula (59a). These graphs are easily constructed for any cascade on the basis of the available aerodynamic characteristics.

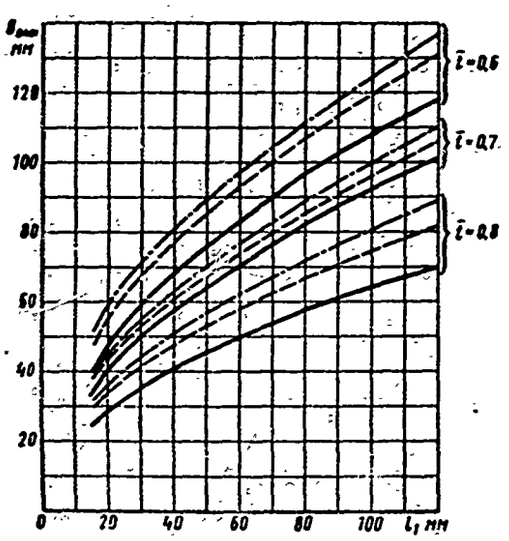

Fig. 53. Selection of optimum chord of MEI nozzle cascades (group "A") depending upon blade height l_1 and relative pitch $\bar{t}$: ——— profile TC-1A; $\sin \alpha_{1\ эф} = 0.22$; $\Delta_{кр} = 0.56$ mm; — — — profile TC-2A, $\sin \alpha_{1\ эф} = 0.26$; $\Delta_{кр} = 0.6$ mm; — · — profile TC-3A, $\sin \alpha_{1\ эф} = 0.31$; $\Delta_{кр} = 0.6$ mm.

The optimum values of chord for short cascades are higher than those adopted in certain steam-turbine designs; for cascades from 70 to 100 mm high, conversely, they are usually applied less often.

It should be taken into account that the graphs shown in Fig. 53 were constructed on the basis of results of static tests of two-dimensional cascades; in reality, especially in welded diaphragms, the effect of cascade height will be greater; secondly, turbine diaphragms, especially in the first stages of steam turbines with high and extra-high parameters, must be made wider than the optimum profile width requires with respect to conditions of reliability; therefore, in front of the cascade there is a significantly wide entrance section that is partially partitioned by posts, as a result of which there appear certain additional losses.

These factors undoubtedly affect the value of optimum chord of the profile; therefore, quantitative changes can be revealed only after special experiments with actual diaphragms. Independently of this, the existence of optimum profile chord is very important.

The selection of the width, and consequently, also the chord of the profile of a moving blade, is practically determined not by economy, but by reliability. Usually in the stage being designed, the width of the moving blade is selected on the basis of reliability and unification. It should be understood that a decrease of profile width leads to an increase of flexural stresses in the blade approximately to the third power.

Analogous considerations and calculations may also be conducted for a moving cascade. Thus, for MEI moving cascades of group "A," the approximate value of optimum chord, when $\Delta_{кр} = 0.4$ mm is*

$$b_{опт} = 4\sqrt{l_2}\ [мм]. \tag{59b}$$

where l_2 is given in mm.

Optimum chord can be found more exactly with the help of the aerodynamic characteristics of the cascade for specific values of $\Delta_{кр}$, $\bar{t}$, $\beta_{2\ эф}$, and β_1.

Example: Let us consider the use of the above-stated method for the selection of cascades.

Given: mass of steam per unit of time G = 90.0 kg/sec; steam parameters in front of stage: pressure p_0 = 50 bar; temperature $t_0 = 450^\circ C$; speed n = 3000 rpm; mean diameter d = 0.98; $u/c_ф = 0.48$.

The approximate value of

$$l_1 \sin\alpha_{1\,эф} = \frac{2{,}5Gv_0\frac{u}{c_ф}}{d^2} = 7{,}28\ мм.$$

We shall select nozzle cascade TC-2A with profile chord b = 52 mm and trailing edge $\Delta_{кр} = 0.6$ mm.

Then $\dfrac{1}{\bar{t}\ \sin\alpha_{1\ эф}} = 7.15.$

With respect to the optimum envelope in Fig. 46, angle $\alpha_{1\ эф} = 18^\circ$ ($\sin\alpha_{1\ эф} = 0.309$). This angle can be obtained when $\bar{t} = 0.8$ and $\alpha_y = 40^\circ$; height of the nozzle cascade is $l_1 = 23.6$ mm.

The optimum value of profile chord, according to formula (59a), is equal to

$$b_{опт} = 29\ мм.$$

*Without taking into account the influence of roughness. If necessary, this calculation can be performed with formulas that are analogous to (59).

A more precise determination of $\frac{1}{\bar{t}_1 \sin \alpha_{1\,эф}}$ does not result in an essential change of the optimum angle $\alpha_{1\,эф}$.

Assuming a straight shroud and an overlap of 3 mm we obtain the first approximation of the height of the moving cascade, $l_2 = 23.6 + 3 = 26.6$ mm.

For these dimensions ($d/l = 37$) we select the mean reaction

$$\varrho = 0{,}06.$$

According to the heat drop of the stage, $h_0 = 12.3(d/x_ф)^2 = 51.3$ kj/kg, we determine $\varepsilon = 0.84$.

Taking μ_2/μ_1 on the nomograph of Fig. 52, we find:

$$\frac{\sin \alpha_{1\,эф}}{\sin \beta_{2\,эф}} = 0{,}560 \text{ and } \beta_{2\,эф} = 33{,}5^\circ.$$

For this angle $\beta_{2\,эф}$ we select a TP-4A moving cascade.

Detailed calculation:

$$l_1 \sin \alpha_{1\,эф} = \frac{Gv_{1t}}{\mu_1 \pi d c_{1t}} = 7 \text{ мм}.$$

The exact value does not require a change of the optimum angle $\alpha_{1\,эф}$. Then the height of the nozzle cascade is $l_1 = 22.7$ mm. From the inlet velocity triangle we have: $\beta_1 = 35.3^\circ$ and $w_1 = 160$ m/sec. With the same overlap of 3 mm, the exit height of the moving cascade will be:

$$l_2 = 25{,}7 \text{ мм};$$

$$\sin \beta_{2\,эф} = \frac{w_1}{w_{2t}} \frac{v_{2t}}{v_1} \sin \beta_1 \frac{l_1}{l_2} = 0{,}467,$$

whence, $\beta_{2\,эф} = 27.8^\circ$. Thus, a more precise determination of angle $\beta_{2\,эф}$ does not require a change of the selected TP-4A cascade. The angle of direction of the absolute outlet velocity is $\alpha_2 = 99^\circ$, which is fully acceptable.

Thus, the geometric characteristics of the moving cascade are $\bar{t} = 0.59$ and $\beta_y = 77^\circ$. The profile chord is selected on the basis of unification and should be checked by means of a strength analysis of a moving blade. For the given case, the optimum chord is

$$b_{опт} = 4\sqrt{25{,}7} = 20 \text{ мм}.$$

Other Ways of Raising the Economy of a Stage with Low Heights

For low blade heights, if the technology of manufacture permits, meridional profiling of nozzle cascades should be employed (see § 5).

The application of special meridional profiling in an annular cascade gives a gain, i.e., a decrease in losses $\Delta\zeta_c$, which is approximately inversely proportional to $\bar{l}_1$ and can be roughly estimated by the following formula (Chapter I):

$$\Delta\zeta_c \approx 0{,}75\frac{b}{l}\,\%. \tag{60}$$

If the cascade is assembled from milled nozzles, the gain will be somewhat (by approximately 30%) less.

As shown in Chapter I, the application of meridional profiling not only decreases the losses in a nozzle cascade, but, in lowering the pressure gradient along the height in the clearance between cascades, lowers the leakage over the shroud of the moving blades.

If the cascade has a meridional contour, the optimum chord of the profile is increased. In this case $b_{опт}$, which is found by formula (59) or by means of the graphs in Fig. 53, should be increased approximately 1.5 times.

Using the results of experiments conducted on experimental turbines of MEI and KTZ, with full supply and welded diaphragms, it is possible to recommend (for subcritical flow) the application of meridional profiling for l_1b_1 < (1 to 1.2), and for nozzle cascades composed of separate milled blades, for l_1b_1 < (0.5 to 0.8).

Figure 54 shows the results of investigations conducted at MEI on a single stage with meridional profiling and without it. Dimensions of the stage: diameter d = 400 mm; l_1/b_1 = 0.28.

As can be seen from the experiments, the efficiency of the stage increased by $\Delta\eta_{0i}/\eta_{0i}$ = 4.7%, and the reaction drop, with respect to height, fell from 7.5 to 1% (at $u/c_ф$ = 0.5).

When designing stages with a unilateral meridional contour, one should consider that the calculated outlet area cannot be found with the usual formula for $\pi d l_1 \sin\alpha_{1\,эф}$, and will be somewhat larger than it. This area should be exactly determined on a drawing. We may preliminarily assume that

$$F_1 \approx 1{,}05\,\pi d l_1 \sin\alpha_{1\,эф}.$$

This increase in area should be considered either when selecting the dimensions of a nozzle cascade (for instance, with a decrease of angle $\alpha_{1\,эф}$) or when selecting

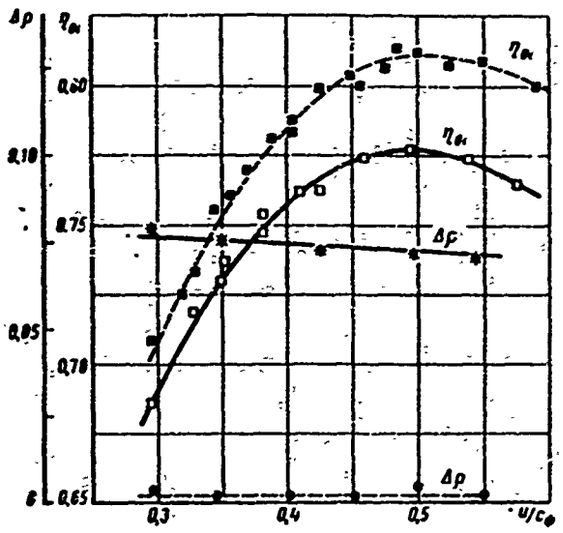

Fig. 54. Results of stage investigation according to MEI experiments with unilateral meridional profiling of nozzle cascade. Cascades TC-2A and TP-2A: d = = 400 mm, l_1 = 15 mm, l_2 = 18 mm, b_1 = = 51.5 mm, $\alpha_1 = 15^\circ$ ——— stage without contraction, F_2/F_1 = 1.73; — — — stage with 7 mm contraction, F_2/F_1 = 1.62; ε = = p_2/p_0 = 0.8 to 0.85, $Re_{c_1} \approx 4 \cdot 10^5$.

a moving cascade. If the area of a moving cascade is left equal to the F_2 of a stage without meridional profiling, and the nozzle area increases, the mean reaction will increase by approximately 3-4%.

In view of the great technological complexity of manufacturing a meridional contour, it is necessary to especially carefully control the quality of cascade manufacture, and all the more so for such small heights as l_1 = 10 to 12 mm.

For stages with low heights, it is also necessary to change the moving cascade, and namely, to employ moving cascades of group "K" (see § 6), which should be done at $l_2/b_2 < (1$ to $1.5)$. In this case, just as for nozzle cascades, the optimum chord of the profile increases somewhat, which can be estimated by the following formula for the TP-Ак series:

$$b_{опт} \approx 5\sqrt{l_2}, \qquad (59c)$$

where l_2 and $b_{опт}$ are in mm.

§ 11. CALCULATION OF A STAGE ACCORDING TO DATA OF STATIC INVESTIGATIONS OF CASCADES

As already indicated earlier, the determination of the basic characteristics of a stage, i.e., efficiency, reaction, and flow rate, is best performed on the basis of experiments in a test turbine. However, if these tests were not made, or if they do not include the required conditions, it is necessary to perform a preliminary calculation of the stage according to static investigations of cascades.

Data Required for Calculation of Stage

When carrying out such a calculation, it is necessary to have the following data:

1. Total geometric characteristic of stage, including cascade dimensions, relative position of cascades (clearances, overlaps, a diagram of the stage and seals,

and the technology of cascade manufacture.

2. Operating conditions of stage:

$$\frac{u}{c_\Phi} = \frac{u}{\sqrt{2h_0 + c_\Phi^2}} \text{ and } \varepsilon = p_2/p_0.$$

where p_0 is the pressure of the stagnated flow before the nozzle cascade.

The conditions of steam entry into the stage (nozzle cascade): angle of entrance α_0, initial turbulence, and irregularity of flow with respect to height.

If varying operating conditions of the stage are being considered, it is necessary to know whether the speed is constant or variable. For stages that operate in the region of low pressures, and consequently, low Re numbers, it is necessary to know the following tentative values: $Re_{c_\Phi} \approx b_1 c_\Phi / \nu$ for the nozzle cascade and $Re_{w_2} = \frac{b_2 w_{2t}}{\nu}$ for the moving cascade;

where c_Φ is a fictitious velocity, calculated for the entire heat drop of the stage;

b_1 is the chord of the nozzle cascade profile;

b_2 is the chord of the moving cascade profile;

w_{2t} is the relative velocity of outlet from the moving cascade, which is roughly approximate to $(w_{2t}/c_\Phi) \approx 0.7$;

ν is the kinematic viscosity, calculated on the basis of final (behind the stage) parameters.

More exact values of Re numbers can be obtained after determining the stage reaction. For determining the frictional losses of the disk it is necessary also to know $Re_u = \frac{du}{\nu}$.

3. Results of static tests of nozzle and moving cascades:

for a nozzle cascade*

$$\zeta_c = f(M_{c_1}, Re_{c_1});$$
$$\alpha_1 = f(M_{c_1}, Re_{c_1});$$
$$\mu_1 = f(M_{c_1}, Re_{c_1});$$

for a moving cascade

$$\zeta_1 = f(M_{w_1}, Re_{w_1}, \beta_1);$$
$$\beta_2 = f(M_{w_1}, Re_{w_1}, \beta_1);$$
$$\mu_2 = f(M_{w_1}, Re_{w_1}, \beta_1).$$

*In certain cases it is necessary to know the dependence of ζ_c, α_1, and μ_1 on the entrance conditions.

For a determination of relative blade efficiency of the stage $\eta_{0л}$ and its variation, a large role is played by the velocity coefficients φ and ψ. If an action-type single stage is being calculated, the influence of the velocity coefficient in a nozzle cascade is considerably greater than in a moving one.

Actually, if from the formula for $\eta_{0л}^{max}$ when $\rho = 0$

$$\eta_{0л}^{max} = \frac{\varphi^2}{2}\cos^2\alpha_1\left(1+\psi\frac{\cos\beta_2}{\cos\beta_1}\right) \tag{61}$$

we take the ratio of efficiency increments $(\Delta\eta_{0л})_\varphi$ and $(\Delta\eta_{0л})_\psi$, which are caused by corresponding changes of the velocity $\Delta\varphi$ and $\Delta\psi$, it will be equal to

$$\frac{(\Delta\eta_{0л})_\psi}{(\Delta\eta_{0л})_\varphi} = \frac{\Delta\psi}{\Delta\varphi}\,\frac{\varphi^2}{2\left(\psi+\frac{\cos\beta_2}{\cos\beta_1}\right)} \approx \frac{1}{4}\,\frac{\Delta\psi}{\Delta\varphi}. \tag{62}$$

For calculation of an action stage, it is especially important to have the dependence of the velocity coefficient in the nozzle cascade φ, which is obtained under conditions which are most similar to an actual stage. If there are no experimental data on the study of annular cascades, it is necessary to use the results of static investigations of straight cascades and introduce a number of corrections.

It is important to note that numerous experiments were conducted at MEI under various conditions: static investigations of two-dimensional nozzle cascades, a study of actual diaphragms, and tests in an experimental turbine. They constantly show that for all cascades investigated there is a clear dependence of losses on the M number. As a rule, most of the cascades* have minimum losses at high subsonic velocities. An example of this dependence of ζ_c on M_1 is the curve in Fig. 55, which gives the results of diaphragm tests with a TC-1A MEI cascade with $d = 534$ mm and $l_1 = 25$ mm.

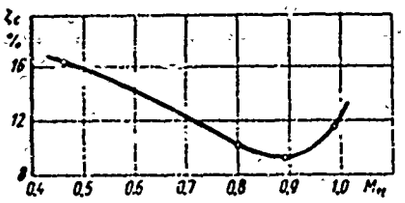

Fig. 55. Influence of M_1 number on losses in annular nozzle cascade with actual diaphragm (MEI experiments). Cascade TC-1A, $d = 534$ mm, $l_1 = 25$ mm, $l/b = 0.48$.

In the zone of M_1 numbers that were calculated with respect to velocity c_{1t}, from 0.7 to 0.9 the cascade losses are minimum and total 8%, while at low velocities ($M_1 = 0.6$) they increase to 11%.

The influence of the Re_{c_1} number on ζ_c was detected by many researchers; however, the transfer of the results of experiments conducted in static conditions

*Contemporary cascades created on the basis of aerodynamic research, considered in Chapter I. Cascades created specially for operation at $M > 1$ are considered in this chapter.

to the calculation of a stage is possible at this time only in certain cases. Usually the experiments in static facilities are conducted under a relatively small turbulence, less than that in a turbine stage.

Therefore, if there are no reliable data about the influence of Re on total cascade losses, it is necessary to consider the influence of the Re number directly on stage efficiency, using the results experiments in test turbines.

The losses in an annular nozzle cascade that are utilized during the calculation of a stage must be determined by the following formula:

$$\zeta_c = \zeta_c^{пл} k_{d/l} k_б k_{техн} k_{пр}, \tag{63}$$

where $\zeta_c^{пл}$ are the losses according to experiments with flat cascades;

$k_{d/l}$ is a coefficient that considers the influence of flare, which is determined experimentally or by the formula [115]

$$k_{d/l} = 1 + A(l/d)^2. \tag{64}$$

Here A is an experimental coefficient that depends on the configuration and the method of profiling the cascade; it varies from 5 to 10.

In nozzle cascades with constant profiles, at small d/l the pitch noticeably changes along the height and in certain sections $\bar{t}$ will not be optimum. For cascades having a sloping dependence $\zeta_c = f(\bar{t})$, in the optimum zone A = 5, for old cascades, A = 10.

$k_б$ is a coefficient that considers the influence of shroud configuration. Coefficient $k_б$ is especially great in cascades with small angles α_1, when in the zone of the root section the appearance of separation of flow is possible. It is natural that the influence of the shroud, which represents part of the tip losses in an annular cascade, will be even greater, the smaller the ratio l_1/b_1.

$k_{техн}$ is a coefficient which considers the influence of the technology of diaphragm manufacture, the quality of treatment, and the accuracy of manufacture. In ganged milled diaphragms it is possible to consider that $k_{техн} = 1$ when flat shrouds are used; it will be larger in welded diaphragms, and especially in cast ones. If welded diaphragms have a significantly larger thickness than the width of the nozzle cascade, and ribs are mounted in front of the cascade, then in such a diaphragm there will undoubtedly appear additional losses, which depend on the dimensions of the

diaphragm, the dimensions of the configuration, and the number and location of the ribs.

On the basis of the KhPI experiments [113], in a welded KhTGZ diaphragm (Fig. 56) the additional losses at the inlet section compose 0.3%. In other experiments they reach up to 0.7 to 1.0%. Experiments conducted in the LMZ laboratory for a diaphragm with ribs and without them did not indicate a noticeable change of economy. The influence of the technology of manufacture on cascade economy is very great. A characteristic experiment is that of the Kharkov Turbine Plant. In the modernization of the BP-25-1 turbine, diaphragms of type shown in Fig. 56 were first prepared with certain deviations from the drawings.

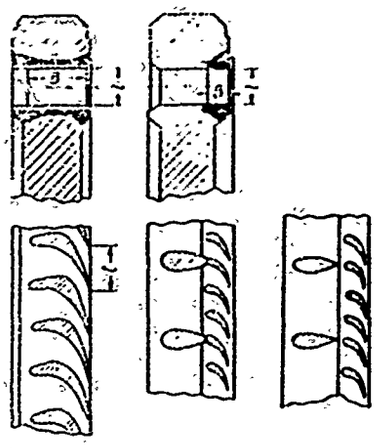

Fig. 56. Welded diaphragms of modernized KhTGZ turbine BP-25-1.

Thus, the edges of nozzle blades, for simplifying the milling of the back of the blades, were thickened to 2 mm. After welding to the body of the diaphragm, the blades were filed manually for bringing the edge thickness to the assigned dimension of 0.5 mm, as a result of which a thin profile of the back of the blade was not ensured. The blade warping detected during welding was corrected by straightening the edges of the blades, which also led to considerable distortions of the profile in the mounting sites of the blades. There were also other machining defects. The nozzle diaphragm and a second one, which was made without the indicated deviations, were tested at KhPI. The first one, as compared to the second, indicated a lowering of efficiency by 1.3% [88].

At certain plants, welded blade diaphragms have thickened trailing edges which must be set into the shroud. However, during assembly, due to the inaccuracy of machining and mounting, there sometimes remain projections of these thickenings in the channel or, conversely, they may fall into the body of the shroud, as a result of which there appear additional losses due to the disturbance of flow.

According to experiments conducted on straight cascades at KPI [17], total cascade losses increase, especially when the thickened edges fall into the body of the shroud. Thus, when this fall is equal to 3% of the blade height, the cascade losses increase by 2%.

Frequently in the manufacture of new turbines, modernization, and repair, and also after operation, many stages of steam turbines have considerable deviations

from the drawing; raised allowances, and considerable profile roughness; this is undoubtedly one of the main reasons why the efficiency of existing turbines frequently is lower than that which was calculated.

The influence of the technology of diaphragm manufacture, just as the influence of the shroud, will be more essential for cascades with small l_1/b_1.

If the cascades in a diaphragm are carried out with meridional profiling, it should be considered by the coefficient $k_{мер}$.

Figure 57 gives a graph of the coefficient $k_б$. Inasmuch as experiments with actual diaphragms of various types and dimensions are still very few, these graphs, which were constructed on the basis of separate experiments, are not universal, but only tentative, and will be substantial as more experimental material is collected.

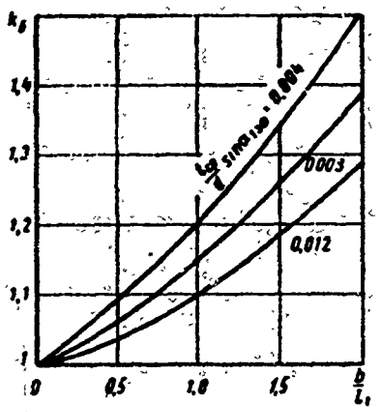

Fig. 57. Graph of the dependence of correction factor $k_б$ for annular cascades.

If there is the possibility of constructing a dependence of losses along the height of a nozzle cascade as was done, for example, in Fig. 263, the mean value of the loss factor for the entire cascade should be found by integration (certainly, approximately graphically), taking into account the change of the flow rate along the height. For this, the cascade is divided into streams of equal height Δr and ζ_i and $\varphi_i = \sqrt{1 - \zeta_i}$ is taken for each stream. Then the mean value of $\varphi_{cp} = \sqrt{1 - \zeta_{cp}}$ is found by the formula

$$\varphi_{cp} = \frac{2\pi \int_{r_k}^{r_a} \sin\alpha_{1\,эф} \cos\alpha_1 \varphi_i \frac{c_{1t}^2}{v_{1t}} r\,dr}{G(c_{1t}\cos\alpha_1)_{cp}}.$$

Here c_{1t} and v_{1t} are taken to be variable with respect to height in connection with the change of the reaction, while angle α_1 (and $\alpha_{1\,эф}$), with respect to the cascade characteristics depending upon $\bar{r}$. In zones of increased losses, angle α_1 is greater than according to the characteristics. In most cases, ζ_{cp} can be determined by the formula

$$\zeta_{cp} = \frac{\sum \zeta_i F_i}{\sum F_i}.$$

The angle of exit from the nozzle cascade, α_1 as shown earlier, varies both with respect to the height, and also with respect to the pitch of the cascade.

The change of the outlet angle with respect to height is determined in particular by the tip phenomena. This question was investigated in detail at MEI, TsKTI, and other organizations. The Japanese scientist Comi [141] derived a dependence of the deviation of the outlet angle $\alpha_1 - \alpha_1^{\infty}$ (here α_1^{∞} is the outlet angle at a distance from the end walls where their influence does not show up). Figure 58 shows the results of a calculation with Comi's formula. For a nozzle cascade with pitch t = 44 mm, angle α_1 increases in a zone of 10 to 25 mm from the wall, whereby its greatest increase is attained when $l/t = 0.3$ and equals $\Delta\alpha_1 = 1.4^{\circ}$. For moving cascades, the deviation of angle $\beta_2 - \beta_{2t}$ reaches up to 8° (at an inlet angle of $\beta_1 = 30^{\circ}$). Figure 58 shows the biggest deviation of outlet angle $\alpha_1 - \alpha_{1t}$, depending upon the inlet and outlet angles. The theoretical research is well substantiated by experiments.

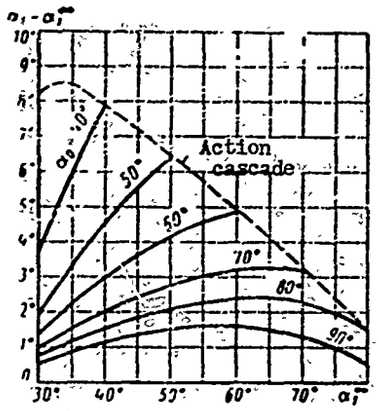

Fig. 58. Determination of deflection of flow due to tip losses at a distance of $y/t = 0.5$ from a restricting wall depending upon α_0 and α_1^{∞}.

During the calculation of a stage, the mean-integral value of the angle α_1 is introduced; it is determined by cascade investigations in static conditions. It should be pointed out that the determination of the cross-sectional area of nozzle cascades in a turbine cannot be performed for angle α_1, which is obtained on the basis of preliminary investigations. The area of the outlet (throat) section of a nozzle cascade should be taken from a drawing or from measurements as the sum of the minimum (throat) cross sections of the cascade channels. If, however, in the determination of the steam flow rate, the area is calculated through $\sin \alpha_1$, then even a small error in the magnitude of the angle may cause a change of the operating conditions of the whole turbine.

Thus, during tests of turbine BP-25-1, the 1° error in the determination of angle α_1 led to a lowering (at the same steam flow rate) of vapor pressure in the chamber of the regulating stage from 63.5 to 57.2 atm (abs), a corresponding increase of the heat drop in the regulating stage, large throttling in the regulating valve, and finally, to a lowering of turbine efficiency as compared to that expected.

Everything stated above pertains to conditions of subcritical flow, when the direction of flow, i.e., angle α_1, may be approximately considered to be constant.

If there are no experimental data, angle α_1 should be determined with the formula for the so-called effective angle (see Chapter I).

$$\alpha_1 \approx \alpha_{1\,эф} = \arcsin \frac{a_2}{t}.$$

For annular cascades a_2 and t are taken on the mean diameter.

With the use of this formula it is possible to calculate the cross section of a cascade with respect to $\alpha_{1\,эф}$. If it appears that the actual angle α_1 may differ somewhat from the effective one, it will not lead to a significant error and will affect the magnitude of stage efficiency to a small extent, and the effect on the magnitude of the reaction will be very insignificant. An error of 1° in the determination of angle α_1 gives an error in computing the reaction by approximately $\Delta\rho = 0.005$ (see Fig. 51). The influence of a slight inaccuracy in the determination of angle α_1 on the conditions of the flow around moving cascades also is small. For stages of the action type, an error of $\Delta\alpha_1 = 1^\circ$ leads to an error in the determination of the angle of entrance to the moving cascade of approximately $\Delta\beta_1 = 2$ to 3° which, especially for contemporary aerodynamically developed cascades, will not lead to a noticeable change in the losses.

However, one should not forget that a noticeable error in angle α_1, especially in the root sections of the diaphragm, and an error in the determination of the reaction, can lead to a perceptible deviation of the actual angle β_1 from that calculated; therefore, a moving cascade should operate sufficiently stably in a certain zone of variation of the entrance angle. With a supercritical flow in a nozzle cascade there takes place a deviation of flow in the slanting shear of the cascade channel.

The values of the flow rate coefficient μ_1 for a nozzle cascade strongly affect the determination of the cascade's dimensions (or with given dimensions, the flow rate), and also the degree of reaction. For a number of turbine cascades, the flow rate coefficient can be taken on the basis of the aerodynamic characteristics or, even better, on the basis of tests of actual annular cascades.

An investigation of an actual diaphragm, which was conducted at MEI in superheated steam, showed an approximate coincidence with the results of investigations of this diaphragm in air. Of much interest was the clear dependence of the flow rate coefficient on the Re number, which was obtained in this experiment.

In a welded diaphragm with a TC-2A nozzle cascade having the following dimensions – mean diameter 400 mm, nozzle height 48 mm, profile chord 52 mm, with a

variation of Re number, calculated with respect to velocity c_{1t}, from $2.9 \cdot 10^5$ to $4.7 \cdot 10^5$, the flow rate coefficient continuously increases, practically linearly from $\mu_1 = 0.955$ to $\mu_1 = 0.97$, i.e., by 1.5%.

For the calculation of a stage, besides the characteristics of the nozzle cascade, the characteristics of the moving cascade are necessary.

The influence of two additional factors, which are usually immaterial for nozzle cascades, is specific in the characteristics of moving cascades. These factors are the angle of entrance to the working cascade, angle β_1, and the overlap.

A change of angle β_1 undoubtedly has an influence on the reaction of the stage. However, as will be shown later, different views on the character of the direction and the use of the velocity of entrance to a moving cascade do not give an essential difference in the determination of the change of reaction under varying operating conditions of a stage.

The necessity of calculating the influence of all side factors with the help of a correction factor is obvious. This correction factor must also include the influence of periodic instability on the entrance to a moving cascade.

Thus, in calculating a stage, one should introduce the magnitude of losses in the moving cascade with the following formula:

$$\zeta_л = \zeta_л^{пл} k_л, \tag{65}$$

where $\zeta_л^{пл}$ are losses obtained as a result of testing flat moving cascades;

$k_л$ is a coefficient that considers the influence of flare, overlap, and the technology and accuracy of manufacture.

$$k_л = 1.1 \text{ to } 1.4.$$

For calculating a stage, one should know the angle of exit from the moving cascade, β_2. Everything stated above with respect to angle α_1 can also be referred to angle β_2. Both for the nozzle cascade, and also for the moving one, the determination of the cascade area or flow rate should be performed not with respect to angle β_2', but according to measurements of the minimum cross section of the cascade or with drawings.

If there are no experimental data, the calculation may include the so-called effective angle (see Chapter I)

$$\beta_2 \simeq \beta_{2,\phi} = \arcsin \frac{a_2}{t}.$$

Under supercritical flow conditions and with a subsonic entrance to the cascade,* one should consider the deflection of flow in the slanting shear of the channels of the moving cascade.

For the moving cascade, it is necessary to consider the influence of velocity, i.e., the M_{w_2} number, which is given in the aerodynamic characteristics of the cascades.

Unfortunately, the materials on flow rate coefficients in moving cascades μ_2, specially for actual conditions (in annular cascades and high inlet turbulence), are still very limited (see § 9). At the same time, the influence of the flow rate coefficient μ_2 on the stage's reaction is very great, and its influence on the area of the moving and nozzle cascades is very great throughout the reaction. The influence of μ_2 on stage efficiency is insignificant and shows up only indirectly on the steam leakage, which is determined by the reaction of the stage. The influence of the reaction on steam leakage is discussed in the following paragraph.

In the absence of experimental data, the stage calculation should include the value of the flow rate coefficient $\mu_2 = 0.95$ (for gases and superheated steam).

The Order of Calculation of a Stage

After the selection of cascades and calculation of their dimensions, the stage is calculated, which includes the determination of the reaction and efficiency.

1. Reaction of stage ρ. For calculated stage conditions or conditions that insignificantly deviate from calculated conditions, i.e., at the angle of entrance to the moving cascade β_1 and especially with the velocity ratio u/c_ϕ, which are in the optimum zone, the stage reaction can be determined with the formulas and graphs of the preceding paragraph. For steam leakages in a stage, which vary the magnitude of ρ, the stage reaction should be accurately found by using the materials of the following paragraph. If the flow in any of the cascades is supercritical, the stage reaction is determined only by means of a detailed calculation of the stage from its final state. An example of such a calculation is given in [82].

For determining the reaction of a stage, it is necessary to know the calculated areas of the cascades, F_1 and F_2. The outlet areas of the cascades, if they were not determined beforehand, may be found with the following formulas:

$$F_1 = \pi d l_1 \sin \alpha_{1\,эф}$$

and

$$F_2 = \pi d l_2 \sin \beta_{2\,эф}. \qquad (66)$$

*Supersonic velocities of entry into a cascade are considered in § 8.

Furthermore, it is necessary to know the pressure ratio in the nozzle cascade, $\varepsilon_1 = p_1/p_0$. In the first approximation it is $\varepsilon_1 \approx \varepsilon \approx p_2/p_0$, and after determining ρ the value of ε_1 is accurately determined, and then (the second approximation) the reaction ρ is found again.

For small stage reactions it is possible to use the approximate formula

$$\varepsilon_1 = \frac{p_1}{p_0} \approx \varepsilon + \rho(1-\varepsilon). \tag{67}$$

For a calculation of the reaction it is necessary also to know the magnitude of the velocity coefficient in the nozzle cascade, φ, which should be determined depending upon ε_1.

2. Relative blade efficiency. The relative blade efficiency $\eta_{ол}$ or, as it is frequently called, the rim efficiency $\eta_{и}$, considers the cascade losses, including the losses at the entrance to the cascades, losses connected with overlaps, the axial clearance between cascades and the interference of the cascades, and losses with outlet velocity.

The efficiency $\eta_{ол}$ can be determined with the help of velocity triangles and analytically, with formulas. The determination of $\eta_{ол}$ by means of integral curves obtained as a result of investigating stages in experimental turbines is considered in Chapters IV and IX.

In connection with the fact the literature references contain different concepts of stage efficiency, or to be more exact, available energy, it is necessary to indicate which efficiencies our discussion will include. Following A. V. Shcheglyayev [126], by the available energy of a stage we shall imply the following quantity:

$$E_0 = \frac{c_0^2}{2} + h_0 - \xi_{вс} h_{вс},$$

where $0 \leq \xi_{вс} \leq 1$ is the utilization factor of the kinetic energy of the outlet velocity, $h_{вс} = c_2^2/2$.

Below, based on the results of an investigation of stages in an experimental turbine, we shall consider two extreme cases:

$$1.\ \xi_{вс} = 0,\quad E_0 = \frac{c_0^2}{2} + h_0.$$

Then the stage efficiency is designated as $\eta_{ол}$.

$$2.\ \xi_{вс} = 1,\ E_0 = \frac{c_0^2}{2} + h_0 - h_{вс}.$$

Then the stage efficiency is designated as $\eta^*_{ОЛ}$.

The interconnection of $\eta^*_{ОЛ}$ and $\eta_{ОЛ}$ is given by the formula

$$\eta^*_{ОЛ} = \eta_{ОЛ} \frac{1}{1 - (c_2/c_\Phi)^2}. \tag{68}$$

We calculate the stage efficiency $\eta_{ОЛ}$ with respect to the balance of losses

$$\eta_{ОЛ} = 1 - \frac{h_c + h_л + h_{вс}}{h_0 + c_0^2/2}. \tag{69}$$

and for a control of the stage efficiency, with respect to the circular components of velocities

$$\eta_{ОЛ} = \frac{u(c_1 \cos\alpha_1 + c_2 \cos\alpha_2)}{1000\left(h_0 + c_0^2/2\right)}. \tag{70}$$

In the use of the outlet velocity, we determine $\eta^*_{ОЛ}$ with formula (68).

It is possible, without detailed calculations and construction of velocity triangles, to estimate the efficiency of an action-type stage, $\eta_{ОЛ}$, in design conditions on the basis of the known basic characteristics. In the first place, it is necessary to know the velocity ratio u/c_Φ and the velocity coefficient of the nozzle cascade φ. For this estimate it is possible to use the calculated graph in Fig. 59. It gives the dependence of stage efficiency $\eta_{ОЛ}$ on the velocity ratio u/c_Φ and the calculated reaction on the mean diameter $\rho_{ср}$. The graph was constructed for velocity coefficients of $\varphi = 0.96$, $\psi = 0.90$, $\cos\alpha_1 = 0.97$ and $\cos\beta_2 = 0.90$.

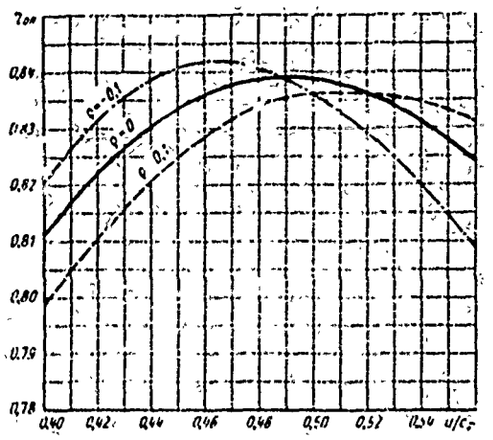

Fig. 59. Dependence of the efficiency $\eta_{ОЛ}$ of a single stage on the velocity ratio u/c_Φ and the mean reaction ρ when: $\varphi = 0.97$, $\psi = 0.90$, $\cos\alpha_1 = 0.97$, $\cos\beta_2 = 0.90$.

It is interesting to note that on the three curves of this graph, which were calculated for different values of the mean reactions, i.e., $\rho_{ср} = +0.1$, $\rho_{ср} = 0$, and $\rho_{ср} = -0.1$, the maximum value of efficiency turns out to be the biggest during a negative reaction. This is connected with the fact that the velocity coefficients were assumed to be independent of the reaction and the velocity coefficient of the

nozzle cascade was assumed to be greater than that in the moving one, $\varphi > \psi$. Thus, as the reaction decreases, an increase of the drop to a more economic cascade leads to an increase in efficiency. If φ and ψ are identical or close, the influence of ρ on $\eta_{0л}$ is practically imperceptible in the calculations.

For other values of φ, ψ, α_1, and β_2, in addition to the graph in Fig. 59, the following formula, which accurately determines the value of $\eta_{0л}$, should be used.

$$\eta_{0л} = (\eta_{0л})\left(1 + \frac{2\Delta\varphi}{\varphi} + \frac{0{,}5\Delta\psi}{\psi} + \frac{0{,}5\Delta\cos\beta_2}{\cos\beta_2} + \frac{0{,}2\Delta\cos\alpha_1}{\cos\alpha_1}\right). \tag{71}$$

Varying Performance of a Stage

Variation in the performance of a stage can be reduced to the variation of three characteristics: $u/c_ф$, ε, and Re.

The influence of Re number is considered in § 18. In the calculation of a stage, the change of the Re number may be considered if we know the characteristics of the cascades investigated under conditions close to actual. In most cases it is first necessary to assume that the stage operates in a self-similar region, i.e., that the Re number practically does not affect the characteristics of the stage.

In turbines with constant speed, the quantities ε and $u/c_ф$ are interconnected: if ε changes, there is a simultaneous change of $u/c_ф$. Since usually during varying performance of a turbine the temperature of the gas before the stage varies insignificantly, the change of $x_ф = u/c_ф$ may be expressed through the change of ε:

$$\frac{x_ф}{x_{ф_0}} = \sqrt{\frac{1-\varepsilon_0^{\frac{k-1}{k}}}{1-\varepsilon^{\frac{k-1}{k}}}}, \tag{72}$$

where the subscript 0 corresponds to design performance. At variable temperature, formula (63) has a somewhat different form:

$$\frac{x_ф}{x_{ф_0}} = \sqrt{\frac{1-\varepsilon_0^{\frac{k-1}{k}}}{1-\varepsilon^{\frac{k-1}{k}}}}\sqrt{\frac{T_{0л}}{T_0}}.$$

For stages with constant speed and constant initial temperature, graphs must be constructed to illustrate the efficiency of the reaction and the relative flow rate, depending upon $u/c_ф$ or depending upon ε. However, such a graph will not be

universal, since various stages at the same ε can have different ratios u/c_{Φ}. Consequently, this graph will correspond to a stage not only with specific geometric characteristics, but also with specific physical parameters.

Hence, it is clear that it is preferable to construct a dependence of the basic characteristics of a stage for ε = const and u/c_{Φ} = var and have a series of curves for different ε. In most cases, stages are investigated in experimental turbines in the same manner.

Having such a universal graph, for a specific stage in accordance with its computed values of u/c_{Φ} and ε, it is easy to reconstruct the series of curves into one, where $\eta_{оп}$ and ρ are functions of only one quantity (u/c_{Φ} or ε). Figure 60 illustrates the primary and final graphs of efficiency for one stage. The thin lines correspond to various experiments that were conducted with ε = const and n = var in a range from ε = 0.8 to ε = 0.6. The heavy curve denotes the recalculation of these experiments for n = 3000 rpm = const, u = 204 m/sec, and initial parameters p_0v_0 = 300 kj/kg.

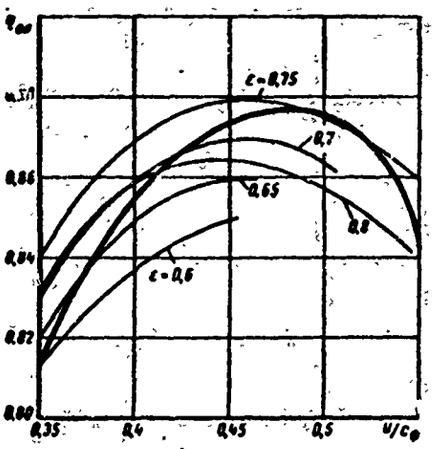

Fig. 60. Dependence of stage efficiency on velocity ratio u/c_{Φ} according to results of experiments in a test turbine for: n = var and ε = const — (thin lines); n = const (t — heavy line).

It is interesting to note that the resultant curve when n = const is essentially steeper than when any ε = const, and the optimum ratio u/c_{Φ} increased from $(x_{\Phi})_{опт}$ = 0.45-0.47 to $(x_{\Phi})_{опт}$ = 0.5 when n = const.

The same series of graphs of $\eta_{оп}$, depending upon ε and x_{Φ}, is also constructed for a turbine with a variable speed, where n and h_0 are interrelated.

If the efficiency of a stage during varying performance is determined not by the results of investigations in an experimental turbine, but by means of calculation, it is necessary to know the dependence $\rho = f(u/c_{\Phi}, \varepsilon)$.

Let us find a dependence that would allow us to estimate the variation of a stage's reaction (a formula is derived for the case of subcritical flow in the cascades of a stage).

From the continuity equations for the outlet sections of nozzle and moving cascades during calculated and varying performance, we will obtain:

$$\left(\frac{w_{2t}}{c_{1t}}\frac{v_{1t}}{v_{2t}}\frac{\mu_1}{\mu_2}\right)_0 = \frac{w_{2t}}{c_{1t}}\frac{v_{1t}}{v_{2t}}\frac{\mu_2}{\mu_1}.$$

Assuming that $(\mu_2/\mu_1) = (\mu_2/\mu_1)_0$, and allowing at first that $(v_{2t}/v_{1t} = (v_{2t}/v_{1t})_0)$, we shall conduct further transformations, proceeding from the formula

$$\frac{w_{2t}}{c_{1t}} = \left(\frac{w_{2t}}{c_{1t}}\right)_0.$$

Considering that the relative entrance velocity $\overline{w}_1 = \overline{c}_1 - \overline{u}$, is completely used in the moving cascade, and applying the basic formulas for a stage

$$c_{1t}^2 = (1-\varrho)c_\phi^2$$

and

$$w_1^2 = c_1^2 + u^2 - 2uc_1\cos\alpha_1 = \varphi^2(1-\varrho)c_\phi^2 + u^2 - 2u\varphi\cos\alpha_1 \times \\ \times c_\phi\sqrt{1-\varrho},$$

we will obtain

$$\left(\frac{c_{1t}}{w_{2t}}\right)^2 = \frac{1-\varrho}{\varphi^2(1-\varrho) + x_\phi^2 - 2\varphi\cos\alpha_1 x_\phi\sqrt{1-\varrho} + \varrho}$$

and

$$\frac{1-\varrho}{1-\varrho_0} = \frac{\varphi^2(1-\varrho) + x_\phi^2 + \varrho - 2\varphi\cos\alpha_1 x_\phi\sqrt{1-\varrho}}{\varphi^2(1-\varrho_0) + x_{\phi_0}^2 + \varrho_0 - 2\varphi\cos\alpha_1 x_{\phi_0}\sqrt{1-\varrho_0}}.$$

We shall designate

$$\varrho = \varrho_0 + \Delta\varrho,\ x_\phi = x_{\phi_0} + \Delta x_\phi$$

and assume that

$$\varphi = \text{const and } \cos\alpha_1 = \text{const}.$$

Then disregarding the terms containing $(\Delta\rho)^2$ and $\Delta\rho\Delta x_\phi$, after a number of transformations we will obtain a square dependence of $\Delta\rho = f(\Delta x_\phi/x_{\phi_0})$:

$$\frac{\Delta\varrho}{1-\varrho_0} = A\frac{\Delta x_\phi}{x_{\phi_0}} - B\left(\frac{\Delta x_\phi}{x_{\phi_0}}\right)^2, \tag{73}$$

where

$$A = \frac{2}{\dfrac{1}{\varphi x_{\phi_0}\cos\alpha_1\sqrt{1-\varrho_0}} - 1};\quad B = \frac{x_{\phi_0}^2}{1-(\varphi\cos\alpha_1 x_{\phi_0}\sqrt{1-\varrho_0} - x_{\phi_0}^2)}.$$

The dependence of A and B on x_{Φ_0} and $\varphi \cos \alpha_1 \sqrt{1 - \rho_0}$ is given in Fig. 61.

For a rougher estimate of the reaction variation, the following formula may be used:

$$\frac{\Delta\rho}{1-\rho_0} = 0{,}5\frac{\Delta x_\Phi}{x_{\Phi_0}} - 0{,}3\left(\frac{\Delta x_\Phi}{x_{\Phi_0}}\right)^2, \tag{74}$$

and for small changes of Δx_Φ the formula may be further simplified:

$$\frac{\Delta\rho}{1-\rho_0} \approx 0{,}4\frac{\Delta x_\Phi}{x_{\Phi_0}}. \tag{75}$$

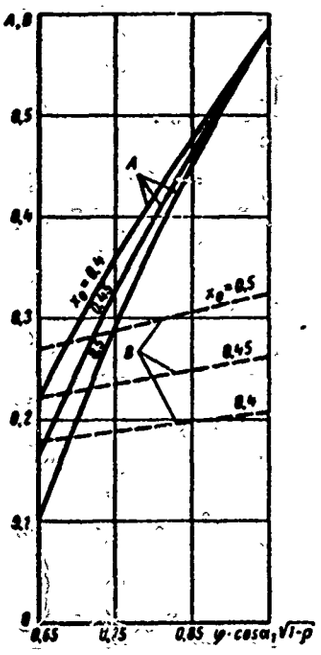

Fig. 61. Graph of the dependence of A and B on x_0 and $\varphi \cos \alpha_1 \sqrt{1-\rho_0}$ (for computing the variation of the reaction of a stage.

It is interesting to note that an analogous derivation of the formula for the reaction variation, which was performed earlier [83] on the assumption of using not the velocity w_1 in a moving cascade, but only its component directed at the design angle of entrance $\beta_{1л}$ gave practically the same result.

Let us derive a formula for the reaction variation when u/c_Φ = const and ε = const, and the variation of the area ratio $f = F_1/F_2$ from the rated value of $f_0 = (F_1/F_2)_0$.

The continuity equation will be written in the following form:

$$\frac{c_{1l}}{w_{1l}} f = \left(\frac{c_{1l}}{w_{1l}}\right)_0 f_0.$$

We shall designate $\rho = \rho_0 + \Delta\rho_f$, $f = f_0 + \Delta f$, and we shall assume that $f^2 = f_0^2 + 2f_0\Delta f$. Then, by analogy with the derivation of formula (73), we will obtain:

$$\frac{\Delta\rho_f}{1-\rho_0} = K_f\frac{\Delta f}{f_0}, \tag{76}$$

where

$$K_f = \frac{2}{1 + \dfrac{\varphi^2 - 1 + \dfrac{x_\Phi \varphi \cos\alpha_1}{\sqrt{1-\rho_0}}}{\varphi^2(1-\rho_0) + \lambda_\Phi^2 - 2\varphi\cos\alpha_1\sqrt{1-\rho_0}\,\lambda_\Phi + \rho_0}}.$$

The coefficient K_f = 0.55 to 1.0 and depends mainly on the value of x_Φ, and decreases as it increases.

At a constant velocity ratio, a decrease of ε, i.e., an increase of the heat drop in the stage, leads to an increase of the stage's reaction. This important

conclusion, which was noted in [83] in 1955 and repeatedly confirmed by experiments on a test turbine at MEI, is almost never used during the calculation and design of stages, especially regulating ones. When applying one cascade combination or another, and in particular, standard combinations of double velocity stages, that fact is not taken into account that the stage's reaction under other conditions may be essentially different. It should be added that a change of the pressure ratio in the stage leads to a change of the stage's reaction also due to the influence of the M numbers on the coefficients of velocity and flow rate. For a quantitative calculation of the influence of ε, it is necessary to perform a detailed calculation of the stage with the use of the complete aerodynamic characteristics of the cascades.

Figure 62 shows the calculated dependence of the reaction variation and experimental data obtained in an investigation of stage КД-2-3-А for mean diameter d = 400 mm and nozzle height l_1 = 48 mm. Tests of this stage were conducted in an experimental steam turbine at MEI. The reaction was measured at the vertex and at the root of the cascade. As can be seen from a consideration of Fig. 62, the calculation with formula (74) gives sufficiently good coincidence with the experiment for different pressure ratios and Re numbers in the stage.

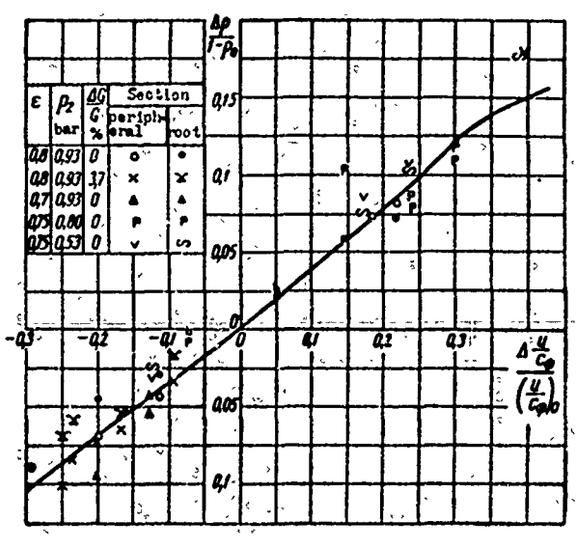

Fig. 62. Variation of stage reaction $\frac{\Delta\rho}{1-\rho_0}$ depending upon $\Delta x/x_0$ in the root and peripheral sections of stage MEI КД-2-3А: line — calculation according to formula (74); points of MEI experiments for different ε, Re (p_2 = const), and ΔG.

It should be indicated that in this case there were no steam leakages into the open clearance on the root diameter of the stage (or they were no more than 3.7%), and over the blade shroud, owing to good sealing, the leakages were small. Many other experiments confirmed an approximately linear dependence of $\rho = f(u/c_\Phi)$.

Example of stage calculation:

Before the beginning of the investigation stage КД-2-2-А in an experimental turbine having MEI ТС-2А and ТР-2А cascades, mean stage diameter 534 mm, height of nozzle cascade 25 mm, and height of moving cascade 28 mm, a calculation of the stage was performed.

The reaction of the stage was determined by means of the formulas and graphs of this and preceding paragraphs. Since the relative magnitude of the clearance in the seal of the blade shroud was not so small that we could disregard steam leakage and its influence on the reaction, the latter was considered specially, by a method considered in the following paragraph.

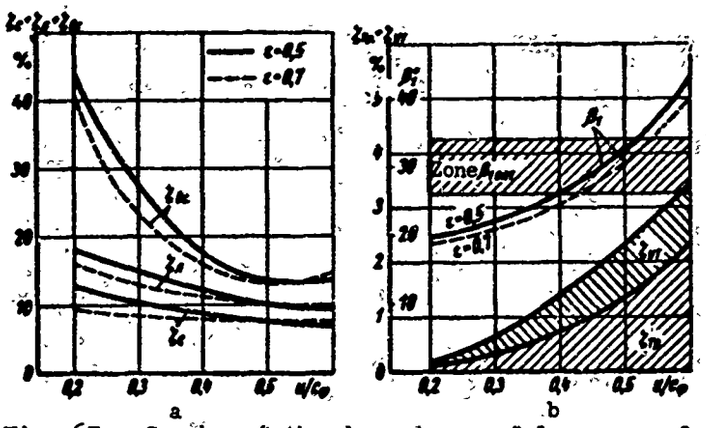

Fig. 63. Graphs of the dependence of losses ρ of angle β_1 on the velocity ratio $u/c_ф$ and the pressure ratio ε by means of calculation of stage КД-2-2А: a — main losses ζ_c, $\zeta_л$, $\zeta_{вс}$; b — angle β_1 when $\varepsilon = 0.5$ and 0.7, and also additional losses when $\varepsilon = 0.5$.

Figure 63 shows the losses in the nozzle and moving cascades and the losses with the outlet velocity with respect to the available heat drop of the stage. These graphs were constructed by the above-described method, whereby the losses in the nozzle cascade we found directly from the results of tests of an actual diaphragm, while the losses in the moving cascade were obtained from the aerodynamic characteristics, taking into account the correction factor $k_л = 1.1$.

These graphs were constructed for various pressure ratios $\varepsilon = 0.7$ and $\varepsilon = 0.5$, where it is distinctly seen how the losses vary, depending upon $u/c_ф$ and ε. The graphs of efficiency $\eta_{ол} = f(u/c_ф)$ for two pressure ratios turned out to be different. If the maximum efficiency $\eta_{ол}^{max}$ in the range from $\varepsilon = 0.7$ to $\varepsilon = 0.5$ was almost unchanged, then the magnitude of optimum $u/c_ф$ was somewhat decreased.

For $\varepsilon = 0.7$, $x_{ф\,опт} = 0.5$, and for $\varepsilon = 0.5$, $x_{ф\,опт} = 0.54$. The losses in the nozzle cascade when $\varepsilon = 0.7$, depending upon $u/c_ф$ vary in the range of $0.2 \leq u/c_ф \leq 0.6$; h_c/h_0 varied only from 9 to 7.4%. The pressure ratio in the nozzle cascade varied from $\varepsilon_1 = 0.65$ to $\varepsilon_1 = 0.73$, i.e., it was in the zone of insignificant

influence on the cascade losses, where the velocity coefficient φ decreased from 0.961 to 0.958.

When $\varepsilon = 0.5$, a variation of u/c_{Φ} from 0.2 to 0.6 corresponds to a variation of ε_1 from 0.45 to 0.59; due to this, there took place an increase of the velocity coefficient φ from 0.941 to 0.959. Taking into account the fact that at small u/c_{Φ} the drop in the nozzle cascade is larger (less than ρ), the relative magnitude of these losses h_c/h_0 decreases from 12.4 to 6.6%, i.e., almost twice.

The velocity coefficient in the moving cascade ψ varied very little, since the M_{w_2} number for the moving cascade was almost constant, and thus, ψ is influenced mainly by the inlet angle β_1. The graph in Fig. 63b shows the change of the angle β_1 depending upon u/c_{Φ} and ε. It depicts the zone of optimum angles β_1 for the given cascade, and consequently, the zone of the highest coefficients ψ.

A comparison of the results of the calculation of this stage with the experiment is shown in Fig. 64. Inasmuch as the experimental efficiency of a stage includes, besides the above-mentioned losses, also losses due to friction of the disk and shroud against the steam and the losses due to steam leakage over the shroud, such a comparision could be performed only after calculating these additional losses* (see Fig. 63b).

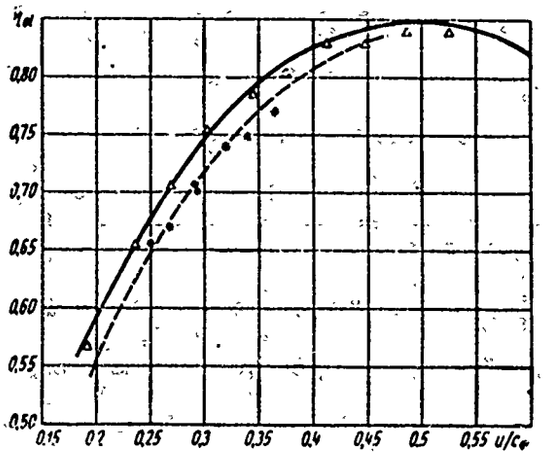

Fig. 64. Graph of the dependence of efficiency η_{oi} on the velocity ratio u/c_{Φ} according to experiments in an MEI test turbine for stage КД-2-2А, d = 534 mm, l_1 = 25 mm; l_2 = 28 mm; calculated data — lines: —— solid for $\varepsilon = 0.7$; — — — broken for $\varepsilon = 0.5$; experimental data — points: Δ — for $\varepsilon = 0.7$, * — for $\varepsilon = 0.5$.

The graph in Fig. 64 showed a good coincidence of the calculation and the experiment that was conducted in the experimental steam turbine, not only with respect to maximum efficiency, but also depending upon u/c_{φ} and ε, which is very important.

§ 12. CALCULATION OF ADDITIONAL LOSSES

The above-considered relative blade efficiency η_{oil} does not cover all the losses in a stage. In a stage there appear additional losses; taking into account these losses, the economy of the stage is estimated according to the relative internal efficiency

*The method of determining the frictional and leakage losses is given in the following section.

$$\eta_{ol} = \eta_{os} - \sum \zeta_{don}. \tag{77}$$

In a stage with complete gas supply, the additional losses are connected with the following phenomena:

a) friction of disk against gas $\zeta_{тр}$;

b) friction of shroud of moving blades against gas $\zeta_{тр.б}$;

c) leakage past nozzle cascade (leakage through diaphragm sealing) ζ_{y1};

d) leakage or suction through peripheral clearance ζ_{y2};

e) leakage or suction through root clearance of stage ζ_{y3}.

Disk Friction

In the literature [119, 126, and 134] there are many materials that theoretically and experimentally consider the frictional losses of a revolving disk.

A problem concerning disk rotation is considered theoretically. A disk with diameter d revolves with angular velocity ω in a closed chamber. The distance from the lateral surface of the disk to the chamber wall is s.

During rotation of the disk, particles of fluid that adhere to the disk are attracted by it, and then ejected to the periphery. In the closed chamber there occurs a meridional flow of steam.

The moment of friction of both lateral surfaces of the disk is equal to

$$M = C_{тр} \cdot 157 \frac{\omega^2 d^5}{v} [\text{n.m}]. \tag{78}$$

Considering the density of the fluid on both sides of disk to be identical, we obtain the determination of M, which means that the frictional losses depend only on the magnitude of the coefficient $C_{тр}$.

Theoretical and experimental investigations showed that the coefficient $C_{тр}$ depends mainly on two characteristics: the Reynolds number $Re_u = ud/\nu$, where $u = \pi dn/60$, and the relative clearance s/d.*

For Conditions I, i.e., completely laminar flow in the clearance [134],

*In the zone of raised roughness — also on the relative roughness of the disk surface.

$$C_{mp} = \frac{2\pi}{s/d} \mathrm{Re}_u^{-1}.$$

For Conditions II, i.e., laminar flow on walls of disk and stator, but with constant velocity between these two layers [134] with an infinitely large gap $s \to \infty$,

$$C_{mp} = 3{,}68\, \mathrm{Re}_u^{-1/2}.$$

For Conditions III, i.e., turbulent flow [154],

$$C_{mp} = 0{,}0622\, (s/d)^{-1/5}\, \mathrm{Re}_u^{-1/5}.$$

For Conditions IV, i.e., turbulent flow with separation of boundary layer, encountered at large Re_u numbers:

$$C_{mp} = 0{,}096\, \mathrm{Re}_u^{-1/5}.$$

The use of these theoretical formulas requires an experimental check and a determination of the bounds of the conditions.

Experiments [134] showed that bounds of the conditions depend on Re_u and s/d.

At the Re_u numbers and s/d that are practically encountered in steam and gas turbines, we are concerned only with Conditions III and IV, and taking into account the actual flow in turbine stages, when there takes place leakage through the diaphragm seal, only Conditions IV.

For Conditions IV, Daily [134] gives the following empirical formula:

$$C_{mp} = 0{,}0102\, (s/d)^{1/10}\, \mathrm{Re}_u^{-1/5}. \tag{79}$$

Converting the formula for the moment M, we will obtain an expression for the power expended due to friction:

$$N_{mp} = B \frac{u^3 \cdot d_K^2}{v_1} \text{ kw}, \tag{80}$$

where $u = \frac{\pi d_K n}{60}$ m/sec, d_K is given in m, and v_1 is in m^3/kg,

$$B = 0{,}2\, (s/d_K)^{1/10}\, \mathrm{Re}_u^{-1/5}. \tag{81}$$

The relative magnitude of frictional losses $\zeta_{тр}$ will be found in the following way:

$$\zeta_{mp} = \frac{N_{mp}}{Gh_0} = \frac{Au^3 d_K^2}{Gh_0 v_1}. \tag{82}$$

After approximately replacing $Gv_1 \approx F_1 c_\Phi$, and considering that $d_K = d - l_2$, we will obtain:

$$\zeta_{mp} = B\frac{d_K^2}{F_1}\left(\frac{u}{c_\Phi}\right)^3 = B\frac{(d-l_2)^2}{F_1}\left(\frac{u}{c_\Phi}\right)^3, \tag{83}$$

where F_1 is the outlet area of the nozzle cascade.

Figure 65 presents a graph for $B = f(s/d_K, Re_u)$. In the zone actual Re_u numbers and s/d_K for steam turbines, the coefficient B varies from $0.3 \cdot 10^{-2}$ to $1.5 \cdot 10^{-2}$.

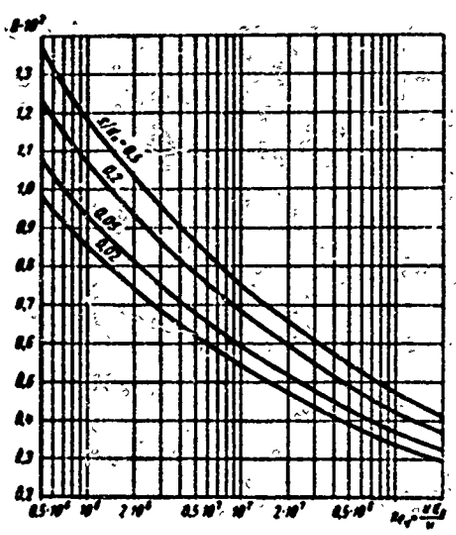

Fig. 65. Dependence of coefficient B on Re_u and s/d_K for computing the losses of disk friction against steam.

It is obvious that in reality the friction of turbine disks will also be influenced by the surface roughness of the disk. Therefore, the proposed formula is approximate, but it is better to use this substantiated formula than purely empirical dependences, or more complicated, but not more exact, formulas [48, 117, 157].

Disk friction does not occur over the entire surface $\pi d_K^2/4$, but over the surface $\frac{\pi}{4}(d_K^2 - d_{BT}^2)$, where d_{BT} is the boss diameter. If into the formula for disk-friction losses we introduce an accurate determination, the coefficient ζ_{Tp} must be multiplied by the quantity $[1 - (d_{BT}/d_K)^5]$; this factor differs little from unity (when $d_{BT}/d_K = 0.5$ it is equal to 0.97) and it may be disregarded.

More important is the presence of free cylindrical and conical surfaces on the disk crown, which increase the frictional losses. With the formula proposed by G. Flugel and converted by analogy with (71), we obtain an additional frictional loss:

$$N'_{mp} = 0.22\left(\frac{n}{3000}\right)^3 d_K^4 \sum b \frac{1}{v_1} \text{ kw} \tag{84}$$

and

$$\zeta'_{mp} = 3 \cdot 10^{-3}\frac{d_K \sum b}{F_1}\left(\frac{u}{c_\Phi}\right)^3, \tag{85}$$

where Σb is the total length of the free cylindrical surfaces of the disk.

Frictional Losses of the Outer Shroud Surface

These losses can be determined with the same formula which was used for frictional losses of the cylindrical surface of a disk. However, in distinction

from the disk, the surface of the shroud cannot be hydraulically smooth; therefore, the numerical coefficient in the formula for $\zeta_{тр.б}$ should be increased. We shall assume that it is equal to $6 \cdot 10^3$. Then

$$\zeta_{тр.б} = 6 \cdot 10^{-3} \frac{d_б \Sigma b_б}{F_1} \left(\frac{u}{c_ф}\right)^2. \tag{86}$$

Here $d_б = d + l_2$ is the shroud diameter and $b_б$ is the axial width of the shroud (for a double-rim disk, the width of the shrouds of two moving cascades is summarized).

In order to illustrate the values of the total frictional losses in a stage (friction of disk and shrouds), Fig. 66 shows a graph of the calculated losses $\zeta_{тр} + \zeta'_{тр} + \zeta_{тр.б}$ for a ВК-50 turbine (for turbine calculation, see [126]).

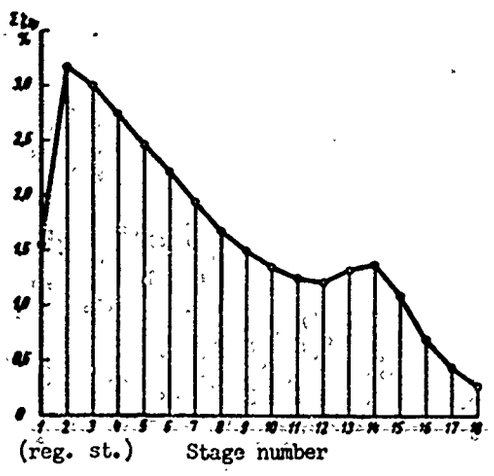

Fig. 66. Frictional losses of a disk and shroud against steam for ВК-50 turbine stages.

Leakage Through Diaphragm Seal

In a turbine stage a certain quantity of the working medium $G_{y\,1}$ inevitably flows past the nozzle cascade. Not considering the possibility of gas suction into the moving cascade and the influence of this suction on the economy of the stage, we shall consider that $G_{y\,1}$ is lost and does not participate in the creation of net output. Then the losses connected with this leakage will be equal to

$$\zeta_{y1} = \frac{G_{y1}}{G - G_{y1}} \eta_{oi} \approx \frac{G_{y1}}{G} \bar{\eta}_{oi}. \tag{87}$$

Taking into account the relatively small magnitude of $\frac{G_{y\,1}}{G}$, we shall find approximately $\zeta_{y\,1}$ [126]:

$$\zeta_{y1} = \frac{\mu_y}{\mu_1} \cdot \frac{F_y \eta_{oi}}{F_1 \cdot \sqrt{z_y}} k_y. \tag{88}$$

Here $F_y = \pi d_y \delta_y$ is the annular area of the clearance, F_1 is the area of the nozzle cascade, z_y is the number of clearances (strips) of the seal, $\mu_1 \approx 0.97$ is the flow rate coefficient in the nozzle cascade, and μ_y is the flow rate coefficient in the seal clearance. It may be taken from the MEI experiments [97]. The dependence of μ_y on the shape and dimensions of the clearance is represented in Fig. 67a. If

the seal completely decreases the speed after every clearance (stepped or branched seal), then $k_y = 1$. For a direct-flow seal it is possible to use the formula of G. S. Samoylovich [82] or Fig. 67b.

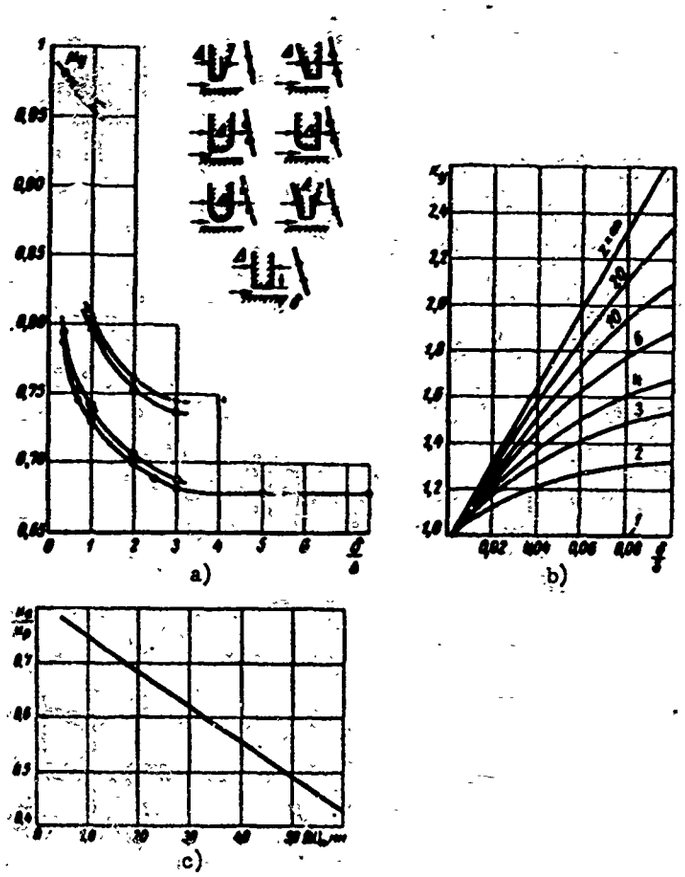

Fig. 67. Coefficients for calculation of stage leakage: a — flow rate coefficient μ_y through labyrinth seal clearance depending upon shape and dimensions of clearance (MEI experiments); b — correction factor k_y for direct-flow labyrinth seal depending upon the ratio δ/s (where s is the seal spacing); c — dependence of the ratio of flow rate coefficients μ_a/μ_p, during leakage through axial and peripheral clearances, on the overlap Δl_π when $\alpha_1 = 11^\circ 30'$ (experimental data of TsKTI).

The detailed investigations of labyrinth seals that have appeared recently [144] for calculating stage efficiency are of no use in view of the smallness of the losses $\zeta_{y\,1}$, and also a rough estimate of it is useless due to the inaccuracy determining the clearance δ_y during operation.

Leakage or Suction Through Peripheral Clearance

The influence of leakage through the periphral clearance near moving blades on stage economy was noted very long ago. Even in the well-known KhTGZ graphs [117] for determining the efficiency of stages there were corrections for the magnitude of the banding clearances; in 1941, Hartmann's experiments [143] on an experimental turbine obtained a change in stage efficiency that depended upon the clearance.

During leakage of steam past moving blades there is a change in the reaction of the stage. The effect of leakages on the reaction was discussed in detail in the book by G. S. Samoylovich and B. M. Troyanovskiy "Varying Performance of Steam Turbines" [83] and was later confirmed by experiments at MEI [29, 35, 100], TsKTI [47], BITM [5], NZL [48], and others.

For stages with nonbanded blades, which are encountered in reaction turbines, the influence of peripheral leakage was studied by many researchers [47, 49, 96, and others].

In principle, in a peripheral clearance there can appear both leakage, and also suction. However, suction will occur only in a negative and a zero reaction on the periphery, which is possible either during varying performance (with small u/c_{Φ}), or with poor stage designing (very large F_2/F_1). The usual case is that of leakage.

Let us consider the factors that influence the magnitude of this leakage. One of them is the reaction on the periphery (calculated, i.e., without leakage), which depends mainly on the geometric characteristics of the stage: F_2/F_1 and d/l, and the design parameters $\varepsilon = p_2/p_0$ and u/c_{Φ} (the influence of the Re number, which takes place only in the last stages of condensing turbines, is not considered here).

For cylindrical blading, we shall find ρ_{Π} by the formula

$$\varrho_{\Pi} = \varrho_{cp} + 1{,}8(1 - \varrho_{cp})\frac{l}{d}, \tag{89}$$

where ρ_{cp} is found according to the data in the preceding paragraph (see Fig. 50).

Further, leakage depends on the dimensions of the clearances shown in Fig. 7[illegible], i.e., the so-called open clearance δ_a, the radial clearances δ_p above the band and also the flow rate coefficients through these clearances. These clearances may be reduced to an equivalent clearance:

$$\delta_{экв} = \frac{1}{\sqrt{\frac{1}{\mu_a^2 \delta_a^2} + \frac{z_p}{\mu_p^2 k_y^2 \delta_p^2}}}. \tag{90}$$

Here μ_p is the flow rate coefficient in the radial clearance according to Fig. 67a;

k_y is for a direct-flow seal, taken from Fig. 67b;

z_p is the number of radial clearances;

μ_a is the flow rate coefficient in the axial clearance, which depends on the the shape and magnitude of the clearance, the overlap, and angle α_1.

Unfortunately, the various experiments conducted on experimental turbines, do not give clear and corresponding recommendations on the quantity μ_a. Until more reliable experimental material is collected, it is possible to use the graph in Fig. 67c [6], where μ_p is taken from Fig. 67a, and $\Delta l_п$ is the external overlap (see Fig. 47).

In the first approximation it is possible to assume that $\mu_p = 0.8$ and $\mu_a = 0.5$. Then

$$\delta_{экв} = \frac{1}{\sqrt{\frac{u}{\delta_a^2} + \frac{1{,}5 z_p}{\delta_p^2}}}. \tag{90a}$$

Losses due to leakage over the band of a moving blade will be found by the approximate formula

$$\zeta_{уг} = \frac{\pi d_n \delta_{экв}}{F_1} \sqrt{\frac{\rho_п}{1-\rho_{ср}}}\, \eta_{ол} \left[1 - \rho_{ср} \frac{1-\varepsilon}{\varepsilon}\right]. \tag{91}$$

Here $\rho_п$ is the actual reaction on the blade periphery which is determined with leakage taken into account. It may be found on the graph in Fig. 68 [83], depending upon the theoretical reaction ρ_t, which is calculated by formula (89), and the relationship

$$\Phi = \frac{\delta_{экв}}{l_1 \sin \alpha_{1эф}} \left(1 + \frac{l}{d}\right). \tag{92}$$

However, it is more convenient to use the formula

$$\zeta_{уг} = \frac{\delta_{экв}}{l_1 \sin \alpha_{1эф}} \eta_{ол} \chi_{ут}. \tag{93}$$

where $\chi_y = f(d/l, \rho_{cp})$ is represented in Fig. 69a.

During suction through the peripheral clearance there occurs an increase of the reaction, some stagnation of the main flow of steam passing through the moving cascade, and a disturbance of the structure of the flow.

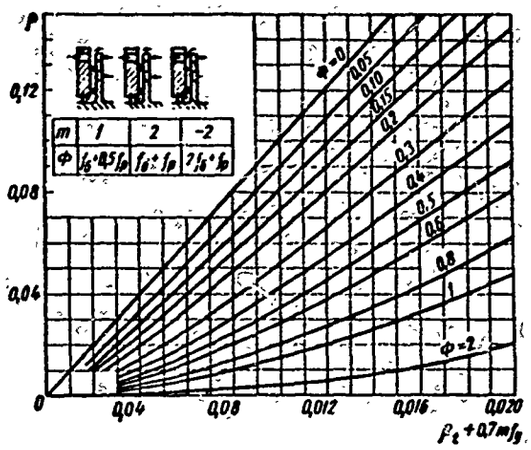

Fig. 68. Determination of stage ρ reaction for different values of Φ taking into account the steam leakage in clearances.

If we consider only the stagnation losses, we can obtain calculated formulas.

Let us assume that after suction of quantity $G_{y\,2}$ the absolute velocity at the entrance to the moving cascade will be c_1'. Then, with the momentum equation,

$$c_1' = c_1 \frac{G}{G + G_{y2}}; \quad \frac{c_1'}{c_1} = \frac{1}{1 + G_{y2}/G};$$

$$\frac{G_{y2}}{G} = \frac{\pi d_n \delta_{экв} \sqrt{-\varrho_n}}{\pi d l_1 \sin \alpha_{1эф} \sqrt{1 - \varrho_{cp}}};$$

$$\frac{c_1'}{c_1} = 1 - \frac{\delta_{экв}}{l_1 \sin \alpha_{1эф}} \left(1 + \frac{l}{d}\right) \sqrt{\frac{-\varrho_n}{1 - \varrho_{cp}}}.$$

If, by Banka's formula,

$$\eta_{oa} = 2\left(1 + \psi \frac{\cos \beta_2}{\cos \beta_1}\right)(\varphi \cos \alpha_1 - x_\Phi) x_\Phi,$$

then

$$\zeta_{y2}' = \eta_{oa}' - \eta_{oa} \approx 2\left(1 + \psi \frac{\cos \beta_2}{\cos \beta_1}\right) \varphi \cos \alpha_1 \frac{\delta_{экв}}{l_1 \sin \alpha_{1эф}} \times$$
$$\times \left(1 + \frac{l}{d}\right) \sqrt{\frac{-\varrho_n}{1 - \varrho_{cp}}}$$

or

$$\zeta_{y2}' \approx \frac{4\delta_{экв}}{l_1 \sin \alpha_{1эф}} \left(1 + \frac{l}{d}\right) \sqrt{\frac{-\varrho_n}{1 - \varrho_{cp}}}. \qquad (94)$$

Here $\delta_{экв}$ is found by formula (90), but with another value of μ_a ($\mu_a \approx 0.8$). $\rho_п$, just as for the case of leakage, will be determined as an actual quantity in Fig. 68.

Formula (94) does not consider the disturbance of the structure of the flow during suction; furthermore, it also does not consider the effect of ejection, due to which suction will also occur and when $\rho_п \approx 0$. However, taking into account that suction is rarely encountered over a band, it is possible to limit ourselves to a calculation by formula (94).

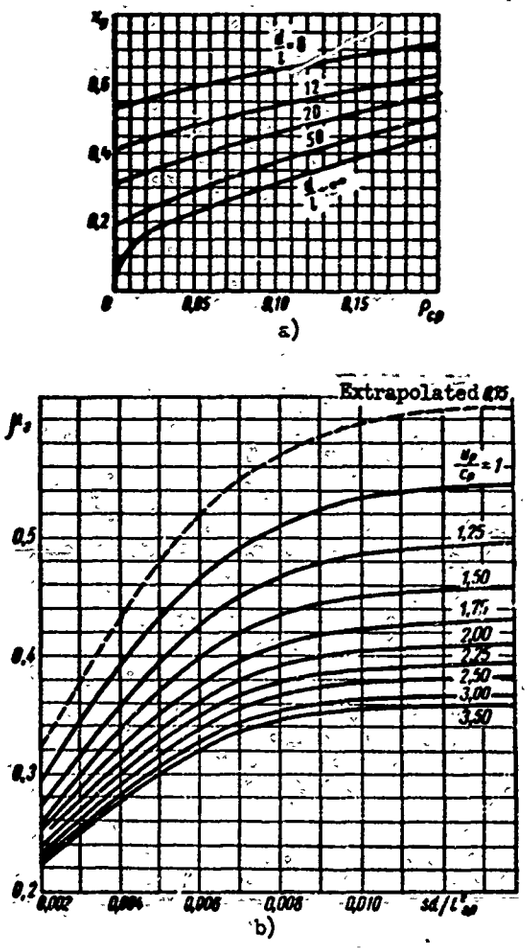

Fig. 69. Coefficients for calculating leakage losses: a – auxiliary loss coefficient χ_y of steam leakage in peripheral clearance; b – coefficient of flow rate μ_p through relief holes of disks depending upon sd/t^2_{op}.

Leakage or Suction Through Root Clearance

It is first necessary to determine whether leakage or suction is taking place. For this it is necessary to set up a leakage balance in the stage, depending upon the dimensions of the stage and the root reaction.

The root reaction is determined by the geometric characteristics of the stage: mainly, F_2/F_1 and d/l, and the design parameters u/c_ϕ and ε.

If the mean reaction ρ_{cp} is determined, which can be done from Fig. 50, the root reaction is found by the formula

$$\varrho_{\kappa} \approx \varrho_{cp} - \frac{2\varphi^2 \cos^2 \alpha_{1\kappa\phi}}{2\varphi^2 \cos^2 \alpha_{1\kappa\phi} + d/l} \approx \varrho_{cp} - \frac{1.8}{1.8 + d/l}. \qquad (95)$$

After that, we compose equations of flow rates, which are common in the determination of axial stress. Depending upon the leakage balance and ρ_K, we determine the direction and and magnitude of leakage through the root clearance. This calculation involves several difficulties. The first one is connected with the insufficiency of experimental data on the flow rate coefficients in a root clearance and the relief holes of disks, and also with the complexity of calculating the pump effect of a disk and the ejection of the main flow. This difficulty, undoubtedly, is temporary. Already now there are several of experimental projects at LMZ, MEI [81], and TsKTI [6], which provide the necessary data for calculating the leakage balance.

The second, practically insuperable, difficulty is the uncertainty of the clearance dimensions, e.g., the root and diaphragm seals. Even following the plant instructions [105], in certain stages the root clearance can vary by $1\frac{1}{2}$ to 2 times; in diaphragm seals usually it also varies by 1.5 to 2 times. Practically, during assembly and operation this variation can be even greater.

It should also be taken into account that an inaccuracy (even within the limits of the plant allowances) in the manufacture of stage cascades, which leads to change of the ratio of areas F_2/F_1 by ±4%, will cause a change of the reaction (including the root reaction) by ±3% [83].

It follows from this that when calculating the losses (just as axial stress) due to leakages, for calculated dimensions of a stage, the probable deviations in dimensions, and consequently also the economy of the stage should not be forgotten. In connection with this, the certain difference in the flow rate coefficients, obtained by various researchers, is secondary.

We shall use empirical formulas for computing the averaged value of the reaction of a stage in the clearance between the diaphragm and the disk.

Case I: the disk does not have relief holes; consequently, through the root clearance there always occurs suction, which is equal to the leakage through the diaphragm seal. Inasmuch as the area of the root clearance usually is a few times larger than the equivalent area of the diaphragm seal clearances,

$$F_{\text{[illegible]}} = \frac{\mu_{\text{[illegible]}} \pi d_{\text{[illegible]}} \delta_{\text{[illegible]}}}{\sqrt{\tau_{\text{[illegible]}}}},$$

the influence of the root clearance on suction, and consequently also on the change of efficiency, may be disregarded (however, when calculating axial stress it must not be disregarded!).

Then

$$\frac{\Delta G_{\text{[illegible]}}}{G} \approx \frac{F_{\text{[illegible]}}}{F_1} \sqrt{1 - \frac{1{,}5}{(1{,}5 + d_{\text{[illegible]}} l)(1 - \varrho_{\text{[illegible]}})}} \approx \frac{F_{\text{[illegible]}}}{F_1}.$$

<u>Case II:</u> the disk has relief holes with total area F_p.

The leakage balance has the following form:

$$a\sqrt{r} = b \pm \sqrt{\pm 1 \mp r}, \qquad (96)$$

where

$$r = \frac{\varrho_{\text{д}}}{\varrho_{\text{к}}} \approx \frac{p_{\text{д}} - p_2}{p_{1\text{к}} - p_2}; \quad a = \frac{\mu_p F_p}{\mu_{\text{к}} F_{\text{к}}}; \quad b = \frac{F_{\text{[illegible]}}}{\mu_{\text{[illegible]}} F_{\text{к}}} \sqrt{\frac{1 - \varrho_{\text{к}}}{|\varrho_{\text{к}}|}};$$

$p_{\text{д}}$ is the vapor pressure in the clearance between the diaphragm and the disk;

$p_{1\text{к}}$ is pressure behind the nozzle cascade on the root diameter;

$F_{\text{к}} = \pi d_{\text{к}} \delta_{\text{к}}$ is the area of the root clearance (if the design has several strips in this clearance, then $F_{\text{к}}$ denotes the equivalent area);

μ_p and $\mu_{\text{к}}$ are the flow rate coefficients for the flow in the relief holes and the root clearance.

The coefficient of the flow rate through a relief hole μ_p is found on a graph which generalized the experimental data of different organizations, depending upon the velocity ratio u_p/c_p,

where u_p is the peripheral velocity on the diameter of a disk with holes;

c_p is the rate of flow through these holes, $c_p = \sqrt{2\rho_{\text{д}} h_0}$, and it depends on the dimensionless parameter

$$s d_p / l^2_{\text{[illegible]}},$$

here s is the clearance between the diaphragm and the disk (if the clearances on both sides of the disk are unequal, then the formula contains the value of the smaller clearance);

d_p is the diameter of a hole;

$t_{отв}$ is the pitch of the holes.

A generalized graph is presented in Fig. 69b [6]. On the basis of the materials of Kh. L. Babenko, the coefficient of the flow rate through the root clearance μ_K is found, depending on the direction of flow, the size of the clearance and, the Reynolds number

$$Re_K = \frac{2c_K\delta_K}{\nu},$$

where

$$c_K = \sqrt{2h_0(\varrho_0 - \varrho_{1K})}.$$

Graphs for μ_K are constructed in Fig. 70.

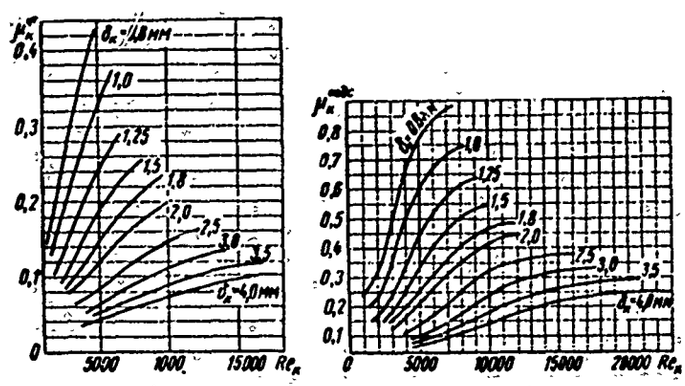

a) b)

Fig. 70. Coefficient of flow rate μ_K through root clearance: a – for leakage; b – for suction (according to experiments of LMZ, MEI, and TsKTI).

In formula (96) the upper sign corresponds to leakage in the root clearance, and the lower sign refers to suction.

For convenience of calculation, V. V. Zvyagintsev [48] constructed graphs for $r = f(a, b)$.

The solution of the problem concerning the direction of flow (and consequently, the selection of the signs in the flow rate equation) is determined by the following inequality:

$$a \gtrless b,$$

where the upper sign corresponds to leakage, and the lower one refers to suction.

If $\rho_{1K} = 0$, then the equation contains an indeterminant. After expanding the indeterminant, we obtain:

$$\varrho_\partial = \left(\frac{b_0}{1+a}\right)^2, \text{ where } b_0 = \frac{F_\partial^{max}}{F_к}.$$

Calculation by the above-mentioned formulas must be conducted by trial and error, since u_p/c_p and $Re_к$ depend on $\rho_д$.

After determining $\rho_д$, we calculate the relative magnitude of leakage through the root clearance

$$\frac{\Delta G_к}{G} = \frac{\mu_к F_к}{F_1}\sqrt{\frac{|\varrho_\partial - \varrho_к|}{1-\varrho_{cp}}}. \tag{97}$$

Leakage through the root clearance decreases the quantity of steam (gas) which is usefully operating in a stage. Furthermore, this leakage somewhat disturbs the flow entering a moving cascade in the root sections of the stage. On the other hand, there occurs suction of the boundary layer, which decreases the losses in the rotor. The insufficiency of experiments for determining the influence of leakage through the root clearance on the economy of a stage permits us to make only a rough estimate at this time:

$$\zeta'_{уз} \approx 0{,}7\frac{\Delta G_к}{G}\eta_{ол} \approx 0{,}7\frac{\mu_к F_к}{F_1}\sqrt{\frac{|\varrho_\partial - \varrho_к|}{1-\varrho_{cp}}}\eta_{ол}.$$

During suction, there occurs stagnation and disturbance of the normal structure of flow in the root sections. Especially sensitive is this disturbance in negative reactions at the root.

Experiments at MEI [29, 103], TsKTI [47], and other organizations showed that losses due to suction are approximately proportional to the amount of fluid taken in and increase as the negative reaction increases. Steam suction in a positive reaction at the root in MEI experiments did not cause a noticeable change in losses depending upon the reaction. According to TsKTI, an increase in the zone of positive $\rho_к$ decreases the losses due to suction. Thus, if at $\rho_к = 0$, $\frac{\zeta'_{уз}}{G_у/G} = 1\%$, then at $\rho_к = 20\%$, $\frac{\zeta'_{уз}}{G_у/G} = 0.25\%$. The results of the MEI experiments are more logical, since losses due to stagnation, conversely, should increase as the reaction increases (as it is known, with the increase of ρ there is an increase in the significance of losses in the moving cascade), and the change in the structure of the flow during suction does not depend much on the reaction in the zone of $\rho > 0$.

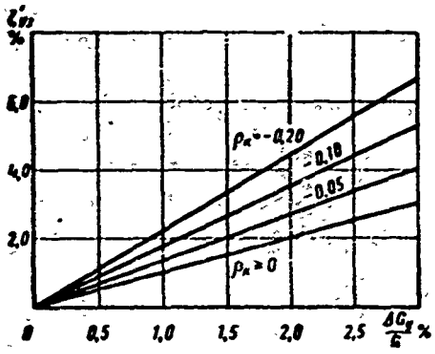

Fig. 71. Losses $\zeta'_{уТ1}$ during suction through root clearance (according to MEI experiments).

For an estimate of the losses during suction through a root clearance $\zeta'_{уз}$, it is possible to use the graph in Fig. 71, according to [103].

Let us consider an example of the calculation of leakage $\zeta'_{уз}$.

The following stage dimensions are known: $F_1 = 400\ cm^2$; $\delta_к = 1.5$ mm; $d_к = 100$ cm; $F_{у_{экв}} = 4\ cm^2$; $F_p = 67\ cm^2$; $u_p = 115$ m/sec; $\rho_{ср} = 0.42$; $\rho_к = 0.03$.

We shall determine the quantities a and b from formula (96), assuming in first approximation that $\mu_p = 0.2$ and $\mu_к = 0.6$:

$$a = 0.477;\ b = 0.812.$$

Since b > a, there takes place steam suction in the root clearance. Then $0.477\sqrt{r} = 0.812 - \sqrt{r - 1}$, whence r = 1.1 and $\rho_д = 0.033$.

Hence, when $h_0 = 50.3$ kJ/kg, $c_p = \sqrt{2\rho_д h_0} = 59$ m/sec; $\frac{u_p}{c_p} = 2.0$ and, according to Fig. 69b, when $\frac{sd_p}{t^2_{отв}} = 0.02$, $\mu_p = 0.25$, $c_к = \sqrt{2(\rho_д - \rho_к)h_0} = 18$ m/sec, and when $\nu = 3.2\cdot10^{-6}\ m^2/sec$ and $Re_к = \frac{2\cdot18\cdot0.0015}{3.2\cdot10^{-6}} = 1.7\cdot10^4$, $\mu_к = 0.6$.

We shall find the accurate value of a and b: a = 0.596; b = 0.812.

Then r = 1.04 and $\rho_д = 0.0312$.

The magnitude of suction is calculated by formula (97):

$$\frac{\Delta G_к}{G} = 0{,}071\sqrt{\frac{0{,}0012}{0{,}88}} = 0{,}0026 = 0{,}26\%,$$

and by the graph in Fig. 71, $\zeta'_{уз} = 0.26\%$.

It is interesting to note that when $\rho_к = 0.05$ and with other constant data, $\zeta'_{уз} = 0$, and when $\delta_к = 2.0$ mm and $\rho_к = 0.03$, there will be steam leakage and losses $\zeta_{уз} = 0.15\%$.

C H A P T E R III

METHODS OF INVESTIGATING TURBINE STAGES

§ 13. SIMILARITY CONDITIONS AND STAGE MODELING

Experimental investigations of turbine stages are based on the methods of the similarity theory, which establishes the totality of conditions that are necessary and sufficient for creating models which reproduce all the physical properties of actual stages.

The similarity theory considers objects that are geometrically similar in all elements. Consequently, the condition of absolute geometric similarity of a model with an actual object is necessary in the practice of modeling. At the same time, for similarity of physical processes it is necessary to ensure the identity of all parameters in the model and in the actual object which determine the operating conditions of a stage.

The number of determining parameters is dictated by a system of equations that describes the process of the flow of gas through the flow passages and by the appropriate boundary conditions. However, of decisive value in the selection of these parameters are the physical characteristics of the process under consideration.

Considering the flow of gas into a stage in the absence of heat exchange, but in the presence of heat conduction and friction, it is simple to establish a set of dimensional parameters that determine the operating conditions of a turbine stage. These parameters include:

a) initial pressure and temperature of gas p_0 and T_0;

b) final pressure p_2 (or temperature T_2);

c) speed of stage n;

d) a geometric parameter, e.g., diameter d (or any other);

e) characteristics of the physical properties of the gas, which includes:

R [$m^2/sec^2\ {}^oK$] – the gas constant;

c_v [$m^2/sec^2\ {}^oK$] – heat capacity at constant volume;

λ [$kgm/msec\ {}^oK$] – heat conductivity factor;

μ [$kg/sec/m^2$] – viscosity coefficient.

A dimensional analysis shows that the enumerated parameters can be reduced to five dimensionless determining sets, i.e., similarity criteria, which are written in the following form:

1) index of isentropic process:

$$k = \frac{c_v + R}{c_v} = \frac{c_p}{c_v};$$

2) Prandtl number

$$Pr = \frac{\mu c_p}{\lambda};$$

3) Reynolds number

$$Re_c = \frac{cb_1}{\nu_1} \text{ — for an absolute flow}$$

and

$$Re_w = \frac{wb_2}{\nu_2} \text{ — for a relative flow.}$$

4) dimensionless velocity

$$M_c = \frac{c}{a} \text{ — for absolute motion}$$

and

$$M_w = \frac{w}{a} \text{ — for relative motion}$$

or, correspondingly:* $\lambda_c = \frac{c}{a_{*c}}$ and $\lambda_w = \frac{w}{a_{*w}}$;

5) velocity ratio

$$x_\phi = \frac{u}{c_\phi}.$$

The system of characteristic criteria for a simplified formulation of the problem can be written in somewhat different form.

Thus, in particular, there arises a question about the selection of the determining geometric parameter which enters into the Re number and u/c_ϕ.

---

*a_{*c} and a_{*w} are the critical velocities for absolute and relative flows.

In accordance with the rules of modeling, the selection of the geometric dimensions can be arbitrary. Thus, for instance, in the case of a turbine stage, as the characteristic geometric dimensions the following can be selected: mean diameter , hydraulic radius of cascade (height l), chord b, or width of profile B. In the determination of similarity criteria it is permissible to use various, but identical for the model and the actual object, geometric dimensions. When computing the criterion x_Φ, it is naturally possible to use the mean diameter. However, in reference to blading, the calculation of the Re number with respect to profile chord has a known advantage. Here it is possible to compare the established losses with the losses that appear in the flow around cascades in static conditions.

Furthermore, the M and Re numbers may be determined with respect to peripheral velocity u in the following form:

$$M_u = \frac{u}{a} = \frac{1}{60}\frac{\pi d n}{\sqrt{kRT}},$$

where a and T are the velocity of sound and temperature of gas in a clearance or behind a stage;

$$Re_u = \frac{u d \varrho}{\mu} = \frac{u d p}{\mu R T}.$$

It is easy to note that the transition from M_c and M_w to M_u is carried out by the following formulas:

$$M_u = M_c \frac{u}{c} \text{ and } M_u = M_w \frac{u}{w}.$$

Analogously,

$$Re_u = Re_c \frac{u}{c}\frac{d}{b} \text{ and } Re_u = Re_w \frac{u}{w}\frac{d}{b}.$$

Consequently, the equality of Re_u and M_u numbers is a result of the equality of the criteria $Re_c(Re_w)$ and $M_c(M_w)$ for a model and the actual object.

Between the Re and M numbers of absolute and relative flows it is also easy to establish a relationship:

$$Re_c = Re_w \frac{c}{w}\frac{b_1}{b_2}\frac{\nu_w}{\nu_c}$$

and

$$M_c = M_w \frac{c}{w},$$

where b_1 and b_2 are the chords of the nozzle and moving cascades.

The problem is solved in this setup, since the process of flow of gas into the flow passage is considered to be steady.

In reality, this process is periodically nonstationary and is characterized by high degrees of turbulence. Consequently, the set of similarity criteria should

be augmented by the Strouhal number

$$Sh = \frac{l}{c\Delta t},$$

where Δt is a characteristic time interval and l is a geometric dimension, and also the degree of turbulence

$$E_0 = \frac{\bar{c}'}{c_m}$$

which appears here as an independent characteristic similarity criterion. The formula for E_0 includes the mean pulsating component of velocity $\bar{c}'$, which is determined by the following equation:

$$\bar{c}' = \sqrt{\frac{1}{\Delta t}\int_0^{\Delta t} c'^2 d\Delta t},$$

and mean velocity of steady motion c_m.

The Sh number for a turbine stage with absolute geometric similarity takes on a specific form.

As shown by analysis, identical Sh numbers for a turbine stage in the actual object and in a model with absolute geometric similarity are ensured by the equality of the ratio u/c_Φ.

The condition of u/c_Φ = idem is a condition of kinematic similarity of the operating conditions of turbine stages and can be obtained directly from a consideration of velocity triangles.

The Re_c, Re_w, M_c, M_w, Sh, and E_0 numbers contain the velocities of absolute and relative motion. Theoretically, these velocities can be selected at arbitrary, but certainly similar, points of the actual object and the model. However, considering the establishment of a clear relationship between the results of static cascade tests and dynamic stage tests, the indicated criteria are expediently calculated with respect to velocity c_1 and w_1 or w_2, respectively. Consequently, the density ρ and viscosity μ must be calculated with respect to the gas parameters in the clearance and behind the stage, respectively.

The modeling problem may be considerably simplified in the case when all five (or seven, correspondingly) criteria in the formulation of the problem of investigating a determined direction do not have an equal value. For a solution of the question of the possibility of disregarding the influence of one criterion or another, it is necessary to estimate this influence on the basis of theoretical considerations or by means of an experiment.

Let us first of all turn to the role of the Reynolds number. Later, in special

sections of the book, this question is examined in detail on the basis of a considerable number of experimental results. Here it should be noted that the influence of the Re number on the characteristics of a stage (efficiency, degree of reaction) is considerable when $Re_{c1} < (3 \text{ to } 6)\cdot 10^5$, depending upon the geometric, design, and performance parameters of the stage. Thus, experiments show that the boundary of self-similarity with respect to Reynolds number can vary in sufficiently wide limits. Thus, as also in the flow of a gas in cylindrical pipes, the boundary of the region of self-similarity depends on the relative roughness, whereupon Re_{aBT} decreases as the latter increases. It follows from this that in the process of machine operation the influence of Re on the machine's characteristics is lowered.

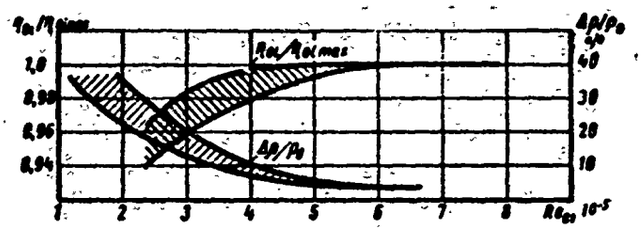

Fig. 72. Influence of Reynolds number on stage characteristics: relative internal efficiency $\eta_{oi}/\eta_{oi\,max}$ and change of degree of reaction $\Delta\rho/\rho_0$.

An example of the dependence of efficiency and reaction on the Re number for certain stages may be seen in Fig. 72.

Considering such a significant influence of Re on the characteristics of a stage, we shall examine the method of changing this number in experimental turbines. For this purpose we shall present this criterion in the following form:

$$Re_{c1} = \frac{c_1 b_1 \rho_1}{\mu_1} = \frac{c_1 b_1 p_1}{\mu_1 R T_1}.$$

Taking an approximate dependence for the viscosity coefficient

$$\frac{\mu_1}{\mu_1'} = \left(\frac{T_1}{T_1'}\right)^n,$$

where μ_1' is the initial value of μ_1 at temperature T_1', and using the evident relationships

$$RT_1 = \frac{a_1^2}{k};\ \frac{T_1}{T_0} = \left(1 + \frac{k-1}{2}M_{c1}^2\right)^{-1};\ \frac{p_1}{p_0} = \left(1 + \frac{k-1}{2}M_{c1}^2\right)^{-\frac{k}{k-1}},$$

after simple transformations, it is simple to obtain:

$$Re_{c1} = AM_{c1}\left(1 + \frac{k-1}{2}M_{c1}^2\right)^{n - \frac{k}{2(k-1)}} \frac{p_0}{T_0^n T^{1/2}}, \tag{98}$$

where

$$A = \sqrt{\frac{k}{R}}\,\frac{T_1'^n b_1}{\mu_1'}.$$

Formula (98), which connects the Re_{c1} and M_1 numbers in the stage clearance, makes it possible to establish that at constant M_1 the Re_c number can be changed by changing the initial parameters before the stage, p_0 and T_0. An increase of the Re_c number is attained by increasing the initial pressure and by lowering the initial temperature.

In formula (98) it is possible to proceed to the parameters behind the nozzle cascade. Then

$$Re_{c1} = A \frac{M_1 p_1}{T_1^{a+1/2}}. \tag{99}$$

The obtained formulas (98) and (99) permit us to conclude that a change of p_0 (or p_1) at constant $\varepsilon_1 = \frac{p_1}{p_0}$ (M_1 = const) may result in a larger change of the Reynolds number of the nozzle and moving cascades, respectively.

Let us now examine the second criterion, i.e., the M_{c1} number, which considers the influence of compressibility. According to experimental data, the M_{c1} number can essentially affect the losses in isolated cascades (see Chapter I), and the efficiency and degree of reaction of a stage. Numerous results of tests of stages with cascades having convergent channels show that the influence of M becomes perceptible when $M_{c1} \geq 0.6$ to 0.7, whereby for a considerable number of stages the maximum efficiencies correspond to $M_{c1} \approx 0.9$ to 1.0. The influence of M, which was detected in certain experiments at smaller M, should be referred to taking into account $Re < Re_{aBT}$. Therefore, in estimating the role of the M number, it is necessary to check if the stage is in the zone of Reynolds self-similarity.

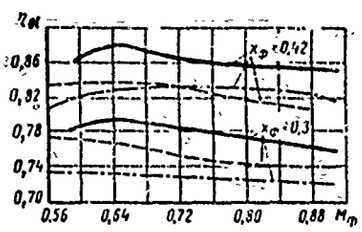

Fig. 73. Dependence of stage efficiency on M_0 number. According to MEI experiments for the following stages: КД-1-2А — (solid curve); КД-2-2А – – – – (dashes); КД-1-3А —·—·— (dots and dashes).

Typical dependences of stage efficiency on M_0 number are shown in Fig. 73. It is characteristic that with the growth of M, when M > 1, there occurs a noticeable lowering of efficiency, and the reaction of the stage then increases.

It should be noted that the influence of Re is also apparent at considerable M_0 numbers,* especially in the zone of transonic velocities. Hence it may be concluded that for a group of the last stages of a low-pressure cylinder of condensing turbines it is necessary to carry out separate modeling for M and Re

*The M_0 number is determined for the total drop on the stage.

numbers in a wide range of numbers $0.5 < M \leq 1.8$. Let us emphasize that for certain groups of stages the required region of separate M and Re modeling has not yet been established. This problem should be solved for groups of stages that operate in specific conditions (regulating stages and the last stages of turbine sections).

Of special interest is an experimental estimate of the influence of two criteria which characterize the physical properties of the working substance (k) and the phenomena of internal friction and heat conductivity (Pr number).

At moderate M numbers, the influence of the physical properties given by the index of the isentropic process k, in a narrow range of its variation, is weak.

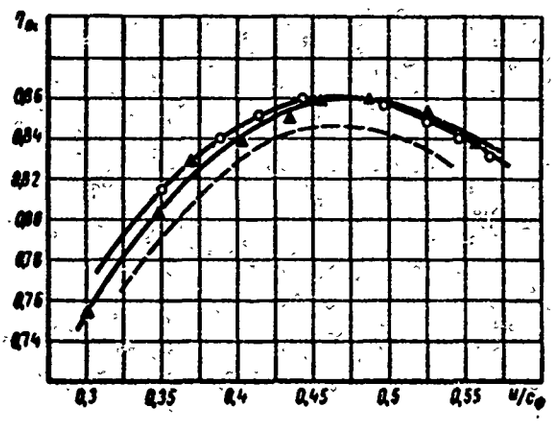

Fig. 74. Dependence of efficiency of a single stage MEI КД-2÷2А on the velocity ratio u/c_ϕ, at $M_0 \doteq 0.6$ and $Re_{c1} = 4.2 \cdot 10^5$. MEI experiments: air -Δ-Δ-Δ; superheated steam -0-0-0; saturated steam — — — — (dashed line).

Thus, Fig. 74 gives the efficiency curves for the same stage, tested in air ($k = 1.4$) and superheated steam ($k = 1.3$). It is not difficult to note that for all values of u/c_ϕ the divergence of the efficiency curves lies within the limits of the accuracy of the experiment. Considering a wider range of variation of k, it should be noted that the efficiency and reaction of the stage will vary more, the lower the value of index k and the larger the M number (utilized heat drop). Thus, for instance, the test of the stage of a steam turbine whose heat process occurs near the upper boundary curve with a mean value of $k = 1.14$ to 1.2 showed a noticeable divergence of efficiency curves as compared to experiments in air (see Fig. 74). The data given here, and also other experimental data [86] show that at moderate M numbers practical self-similarity with respect to k is kept in the interval of $k = 1.3$ to 1.5. At high velocities ($M > 0.8$) the similarity of the processes is retained if the equality of the kM^2 sets (or $\frac{k}{k-1}M^2$) is ensured, which completely corresponds to the conclusions of the theory of similarity.

Investigations of stages operating with moist gases, and in particular, with moist steam, show an essential change in efficiency, depending on the moisture (see Chapter X). Since the index k varies as the moisture varies, it is possible

to assume that the lowering in efficiency is explained by the combined influence of two of these factors, whereby a larger role is played by moisture. It follows from this that when modeling stages that operate in the zone of moist steam, the moisture should enter as a characteristic criterion.

It should be emphasized that the problem of modeling stages in the region of moist steam is more complicated, since even with observance of all conditions of similarity the structure of the moist steam in a model can essentially differ. The most important condition is the circumstance that the separating ability of model stage that operates, as a rule, at a high speed, will differ. The distribution of moisture (moisture field) in characteristic sections of the flow passage, and consequently also the efficiency of the stage, will be different. At the same time, the possibility of modeling stages that operate in a region of moist steam is not excluded. Along with the theoretical development of the problem, it is necessary to carry out methodical tests which make it possible to judge the changes in structure of the moisture and the conditions of separation in geometrically similar stages. The solution of this problem is possible only with help of instruments which measure the local values of moisture.

In considering the influence of the physical properties of the working substance, the role of the Prandtl number should be mentioned. For air, this criterion is practically constant, Pr = 0.72, under laminar conditions. For turbulent conditions, its analog is introduced, which, under constant turbulence, may also be considered as constant. For steam, the Pr number depends on pressure and temperature and can vary in wide limits, whereby in the zone of moderate temperatures and pressures the Prandtl number for steam and air essentially differs. The influence of the difference in Pr numbers for actual and model working substances can noticeably show up at high velocities in the flow passage, i.e., at high M numbers and large stage flare. In this case the nonobservance of the condition of Pr = idem leads to an unequal distribution of the stagnation temperature in characteristic sections of the stage, and consequently, to a divergence of the stage characteristics. It is possible to consider that the change of the physical properties of the working substance in the transition to model tests in cold air proceeds namely in this direction.*

---

*The question concerning the influence of the Pr number is considered in detail in Chapter VII.

The influence of instability of flow in the flow passage and high turbulence has not yet been subjected to a detailed theoretical and experimental investigation. It is possible to allow that with the observance of absolute geometric similarity and identical values of the basic performance parameter of a stage, u/c_Φ, the Strouhal number in the actual object and in the model will be identical, i.e., instability of the process will also appear to an equal extent. However, this assumption should be checked.

The considerable influence of turbulence on the characteristics of isolated cascades was established by appropriate experiments (see Chapter I). This criterion obtains an especially important value for the investigation of isolated intermediate stages when at the entrance to the stage being tested it is necessary to reproduce the corresponding initial conditions. The results of experiments of isolated stages should be corrected in the appropriate way, under the condition that the influence of the degree of turbulence E_0 on stage efficiency is known.

In a simplified formulation of the problem concerning modeling of a turbine stage (approximate modeling) the necessary conditions of similarity may be:

1) geometric similarity;

2) Re = idem;

3) M = idem;

4) $x_\Phi = u/c_\Phi$ = idem.

The last three criteria are simultaneously the basic performance parameters of the stage.

Equality of the basic criteria of similarity for the actual object and a model

$$\mathrm{Re}_н = \mathrm{Re}_м;\ \mathrm{M}_н = \mathrm{M}_м;\ \left(\frac{u}{c_\Phi}\right)_н = \left(\frac{u}{c_\Phi}\right)_м$$

leads to the following evident dependences which make it possible to select the basic parameters of the model stage:

$$\frac{c_{1н}b_{1н}\varrho_{1н}}{\mu_{1н}} = \frac{c_{1м}b_{1м}\varrho_{1м}}{\mu_{1м}}, \tag{100}$$

$$\frac{c_{1н}}{a_{1н}} = \frac{c_{1м}}{a_{1м}},$$

$$\frac{d_{1н}n_н}{c_{1н}} = \frac{d_{1м}n_м}{c_{1м}}.$$

Assuming as we did earlier, an approximate dependence of viscosity on temperature

$$\mu = \mu' \left(\frac{T}{273}\right)^n,$$

there can be obtained a relationship between the parameters in the following form:

$$\frac{c_{1H} b_{1H} \varrho_{1H}}{T_{1H}^n} = \frac{c_{1M} b_{1M} \varrho_{1M}}{T_{1M}^n}; \quad \frac{c_{1H}}{\sqrt{T_{1H}}} = \frac{c_{1M}}{\sqrt{T_{1M}}}. \tag{101}$$

Formulas (100) and (101) serve for establishing a relationship between the dimensions and parameters of an actual stage and a model. This relationship is expressed by a system of conversion factors.

We shall consider that the geometric scale of the model, $K_l = d_{1H}/d_{1M} = l_{1H}/l_{1M} = b_{1H}/b_{1M}$, and the temperature scale, $K_t = T_H/T_M$, are given. Selection of these scales is determined by the productivity and the parameters of the power source (compressor or boiler), the conditions of simplicity and reliability of the experiment, and also the necessity of providing a definite range of accessible conditions.

Depending upon the conditions of the problem, any two other factors can be assumed to be known. The remaining factors are determined by two selected ones, and in particular, by K_l and K_t.

Thus, for instance, from the first condition of (101) we find the following relationship between conversion factors:

$$\frac{c_{1H}}{c_{1M}} \frac{b_{1H}}{b_{1M}} = \left(\frac{T_{1H}}{T_{1M}}\right)^n \frac{\varrho_{1H}}{\varrho_{1M}} \quad \text{or} \quad K_c K_l = \frac{K_\varrho}{K_t},$$

where K_c and K_ρ are the conversion factors of velocities and densities.

From the second equation of (101) we find

$$K_c = \sqrt{K_t}.$$

After making a comparison, we find the density conversion factor

$$K_\varrho = K_l K_t^{n+1/2}.$$

Using the well-known equations that connect the basic characteristics of a stage, it is simple to obtain the following conversion factors:

a) pressure $K_p = \frac{K_t}{K_l}$;

b) speed $K_n = \frac{\sqrt{K_t}}{K_l}$;

c) volumetric flow rate $K_Q = K_l^2 \sqrt{K_t}$;

d) power of stage $K_N = K_l \sqrt{K_t^3}$.

§ 14. EXPERIMENTAL TURBINES AND SETUP FOR INVESTIGATING STAGE CASCADES

Investigations of single turbine stages, the results of which are presented in this book, were conducted in three experimental MEI turbines connected to a steam-air rig.* The experiments were conducted both in steam, and also in air. Most of the experiments were conducted in steam.

The advantages of the steam tests are evident and include:

1) tests in steam which ensure a wide range of independent variation of M and Re numbers (separate modeling for M and Re numbers);

2) easily conducted investigations of stages with long blades, including ones in moist steam;

3) investigations conducted under conditions as close as possible to real conditions; this automatically satisfies the equality of the criteria of similarity, k and Pr.

The disadvantages of steam tests include the more complicated design of the experimental facilities, the difficulties connected with measuring the parameters of steam flow, and consequently, the complication of the method of investigation.

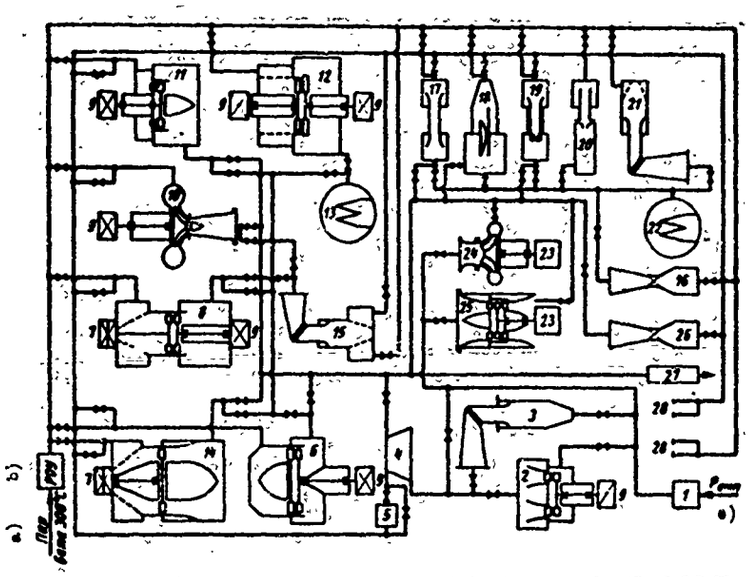

Fig. 75. Schematic diagram of MEI steam-air facility: 1 — filter; 2 — "inverted model" of turbine; 3 — vacuum wind tunnel; 4 — air compressor; 5 — air heater; 6, 8, 10, 11, 12 — experimental turbines; 7 — weighing device; 9 — loading device; 13 and 22 — condensers; 14, 15, 21 — wind tunnels; 16 and 26 — steam and air calibration loops; 17, 18, 19, 20 — devices for studying the processes of flow of moist steam; 23 — drive turbines; 24 — experimental centrifugal compressor; 25 — experimental axial-flow compressor; 27 — silencer; 28 — reserve facilities.
KEY: (a) steam; 6 atm(abs.) 300°C; (b) manual pump; (c) atm.

*The results of investigations conducted with experimental turbines of other laboratories are also used, the laboratory of the Kaluga Turbine Plant, in particular. Descriptions of the majority of these turbines are known from literature [5], [22], [33], [62], and [135].

A schematic diagram of the MEI aerodynamic steam-air laboratory is shown in Fig. 75.

Air is supplied to the laboratory from a centrifugal compressor 4 with a delivery of 220 m^3/min at an initial pressure of p_0 = 3.5 bar.

The suction line of the compressor 4 includes an "inverted model"* 2 and a wind tunnel 3, which operate with atmospheric inlet pressure and with a vacuum at the outlet.

The remaining devices of the laboratory can operate both with steam, and also with air supply. The steam parameters include p_0 = 6 bar, t_0 = 300°C, and consumption to 25 tons/hour.

In addition to the indicated units, the laboratory contains four experimental steam-air turbines of different design and function (6, 8, 10, 11); one double-shaft steam turbine 12 for investigating the last stages of steam turbines, annular 14 and flat 15 steam-air tunnels, and centrifugal 24 and axial 25 experimental compressors.

An important complex of the laboratory is a group of units for studying the processes of the flow of moist steam. It includes the following: unit 17 — for investigating the velocity of propagation of small disturbances in moist steam; unit 18 — for investigating condensation shocks and the boundary layer; 19 — a device for weighing reaction stresses during the flow of moist steam; 20 — a device for investigating the flow rate characteristics; 21 — a steam-type high-speed wind tunnel.

The testing laboratory is serviced by two condensation units 13 and 22 which include, besides the usual equipment, measuring tanks for the basic and drain condensed steam and high-pressure pumps that service the steam-moistening system. The heat systems of the units are characterized by the presence of two- and three-stage moistening systems.

Intermediate single stages of small diameter ($d \leq 550$ mm; $l \leq 60$ mm) are tested in experimental turbine ЭТ-11 (see position 6 in Fig. 75), which was designed and manufactured by the Leningrad Kirov Plant. A sectional drawing of this turbine is shown in Fig. 76.

---

*A turbine with stationary rotor and revolving nozzle cascades.

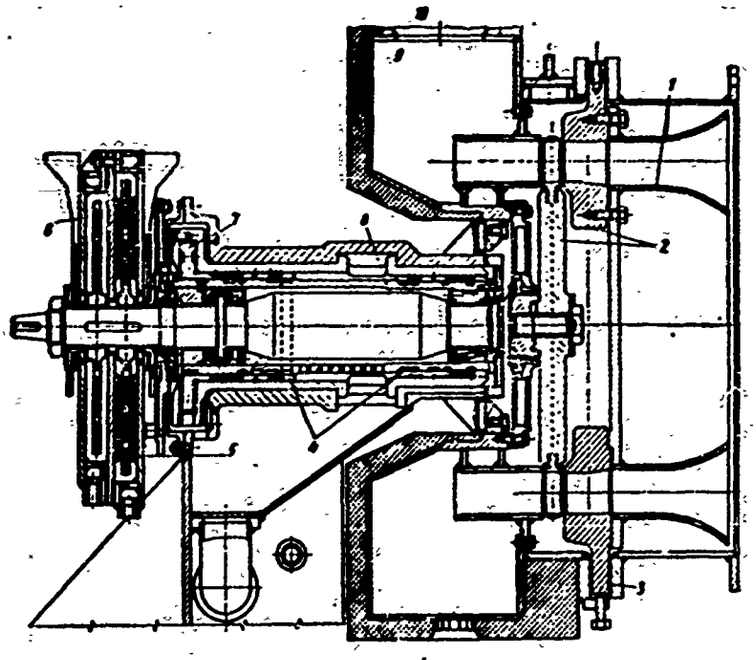

Fig. 76. Experimental turbine ЭТ-11 of the Leningrad Kirov Plant: 1 – entrance section; 2 – flow passage; 3 – diaphragm attachment; 4 – hydraulic bushings; 3 – insertable blades of water brake; 6 – water brake; 7 – hydraulic pivot; 8 – floating journal; 9 – exhaust chamber; 10 – exhaust duct.

The operational experience of the experimental turbines shows that an insufficiently exact determination of the moment of friction in the bearings leads to appreciable errors in the determination of efficiency. In machines whose design does not exclude the necessity of calibrating the bearings, it is difficult to study the influence of such factors as the Re and M numbers, the change in the number of nozzle groups during partial feed, clearances, etc. A sufficiently exact determination of the total power of friction at variable oil temperature, various steam densities, various axial stress, and various vibration is a complicated problem. Therefore, the turbine ЭТ-11 is manufactured with floating journals. This machine employs ordinary sliding bearings with an oil lubricant. The loading device is a disk-type two-stage water brake 6 with separate independent water supply and regulation. Furthermore, the brake makes it possible to change the range of absorbed power by means of mounting radial rectilinear insertable blades 5 on the casing.

The casing of the water brake is rigidly joined to floating carrier journal 8 in which the bearing casing is also attached. During operation, the floating journal 8, together with the casing of the water brake and the bearings, emerges on two hydraulic bushings 4 which operate from the common oil system of the turbine.

The axial stress of the entire design is perceived by the hydraulic pivot 7. Careful manufacture and proper adjustment of the hydraulic bushings completely eliminates dry friction between the suspended unit and the stationary housing of the machine. The moment obtained from the fluid friction in the hydraulic bushings has an insignificantly small magnitude. As a result, we obtain a moment that is measured on the casing of the water brake (including the braking moment of the disks and the moment friction in the bearings) with a high degree of accuracy, which corresponds to the moment developed on the turbine shaft.

The turbine ЭТ-11 has an annular symmetric exhaust chamber 9. Outlet of steam into a condenser or air into the atmosphere is carried out through five symmetrically located exhaust ducts 10 which have chokes for regulating the counterpressure.

The ЭТ-11 turbine was modernized while it was in use. Replacement of the turbine housing made it possible to increase the maximum diameter of the stages under investigation to 550 to 600 mm. The rotor design was simultaneously modified: the power of the water brake was increased and the limiting speed of the machine was increased, which made it possible to expand the range of accessible M and Re numbers.

Investigations of double regulating stages and large-flare stages were carried out with experimental turbine No. 3. This machine was produced in several models.

The first model, which is intended for the investigation of double regulating stages with relatively low blade heights, made it possible to test stages with a maximum diameter less than 800 mm, but due to the small dimensions of the exhaust chamber it was not possible to test stages with $\theta = d/l < 5$.

Turbine No. 3 was modernized during operation. Replacement of the housing and the exhaust duct made it possible to increase the diameter of the stages being investigated to 1000 mm and to test stages with long blades at $\theta \geq 2.6$.

Further improvement of the machine, to ensure a more detailed investigation of the last stages, had as its goal the creation of a unit with two independent coaxial shafts and two loading devices (twin-shaft version).

This design makes it possible to test a stage operating with moist steam and having superheated steam at the entrance to the turbine. This design feature avoids the undesirable initial moistening of steam and the tedious and unreliable determination of moisture with respect to heat balance, and it also creates a normal moisture field at the entrance to the investigated stage. A sectional drawing of the second twin-shaft version of turbine ЭТ-3 is shown in Fig. 77.

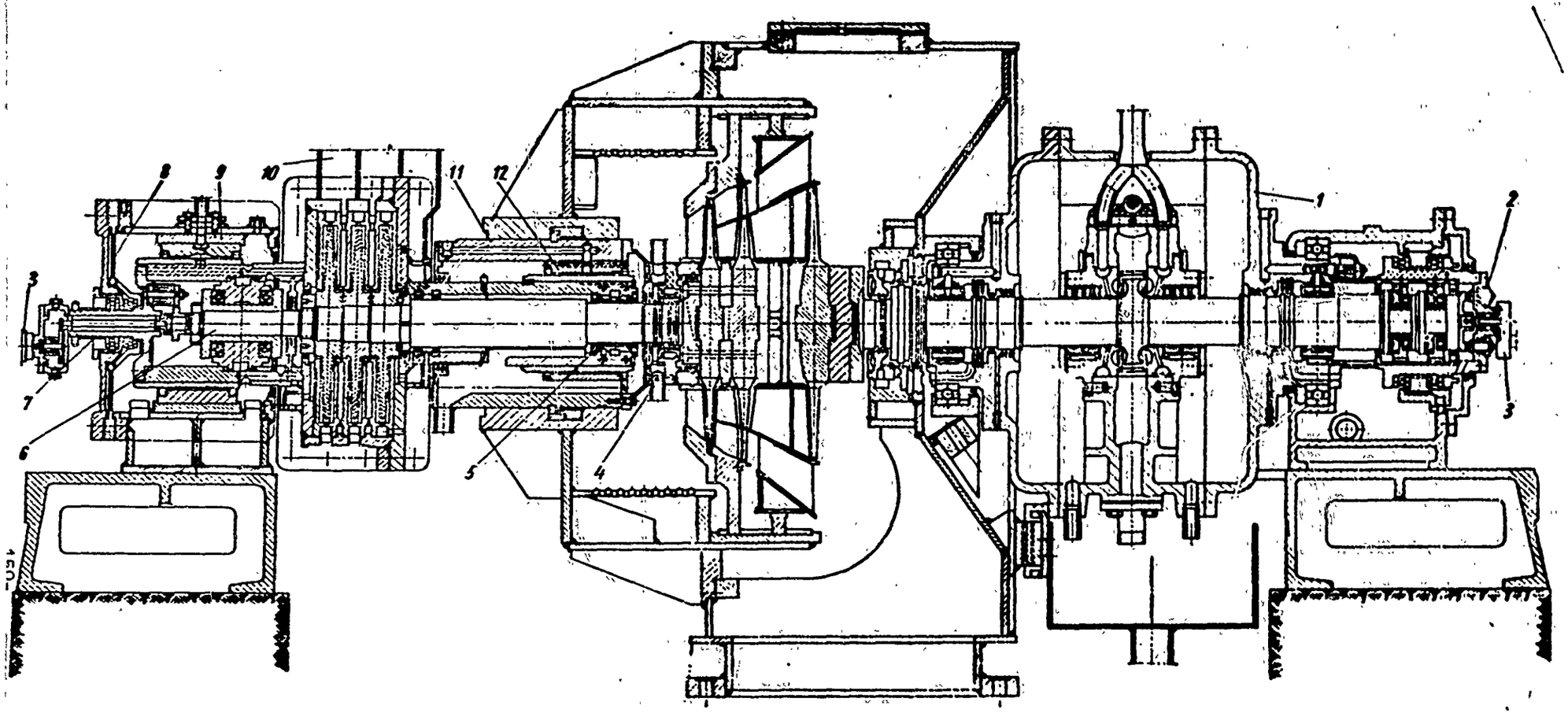

Fig. 77. Twin-shaft version of experimental turbine ЭТ-3 MEI: 1 — water brake of right shaft; 2 — induction pickup of an impulse system of speed counter, tachometer, and protection; 3 — pickup of magnetic-induction tachometer and sinusoidal protection system; 4 — right sealing block; 5 — radial bearing; 6 — radial-thrust bearing; 7 — adjusting sleeves of calibration device; 8 — axial-stress weighing device; 9 and 12 — floating sleeves; 10 — water brake of shaft; 11 — race.

The machine ЭТ-3 can have two to four stages. The water brake of the right shaft 1, i.e., the blade shaft and the suspension of the housing, is mounted on ball bearings. This design ensures total weighing of the moment on the brake wheel and the moments of friction in the radial and thrust bearings.

The water brake of left shaft 10 is disk-type, sectional, and has an open water supply.

Suspension of the housing is carried out in oil-type four-chamber floating bushings 9 and 12 and ensures weighing of the moments of friction in the radial 5 and radial-thrust 6 bearings of conventional design.

For prevention of the possibility of oil falling into the steam box under vacuum conditions, the right sealing block 4 is carried out with steam supply and air supercharging.

The design under consideration includes independent weighing of torque and axial stress on the rotor. Axial stress is transmitted to the casing of the water brake through KTZ thrust bearings which make it possible to perceive the considerable specific loads that are perceived by the weighing device 8 with an elastic element that makes it possible to calibrate the loads on the running machine. Torque is weighed on the casing of the water brake by an ordinary weight head.

For setting up the conditions and observing the speed of shaft rotation, the machine has a magnetic-induction tachometer 3. The speed counter and an additional tachometer operate from an induction pickup 2.

The protection of the machine is electrical, duplicate, and uses the impulse from the induction pickup 2 and the generator of tachometer 3.

The turbine housing is welded, with horizontal and vertical joints. The steam-inlet portion is of an annular design and has a stabilizing lattice; a steam-cooler is mounted at the entrance to the machine.

The main advantage of the twin-shaft design under consideration consists in that the stages of the left shaft create a corresponding velocity, pressure, and moisture field at the entrance to the stage of the right shaft; the characteristics of the two stages are determined separately.

For installing different groups of stages, the possibility is foreseen to move the entire block of the left shaft in an axial direction by 90 mm. Axial movement is carried out by means of transposing the casing 11 and replacing the adjusting bushings of the calibration device 7.

Of great interest in the development of turbine stages is the static testing of nozzle cascades under actual conditions of their operation. The turbine ЭТ-3 permits

a similar experiment. For this, the whole block of the right shaft, together with the rotor, is removed, and the diaphragm of the investigated (single-stage) stage and the block of the left shaft remain in the machine. The machine (left shaft) is started in the usual order, and the diaphragm to be tested is traversed by a special gear that is mounted at the position of the right shaft.

At the entrance to the investigated diaphragm there are created natural fields of angles, pressures, velocities, and moisture, and also the periodic instability that is peculiar to the given stage. In addition to this, these fields can be regulated to a considerable extent by means of varying the operating conditions of the left shaft.

Similar conditions for testing an annular nozzle cascade, even in a special steam-type annular wind tunnel, are practically unattainable.

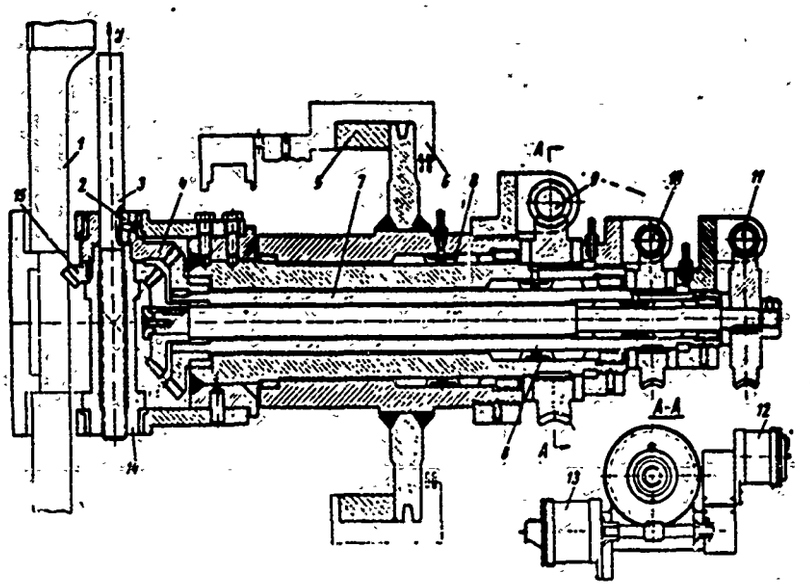

Fig. 78. Traverse gear of experimental turbine ЭТ-3: 1 – diaphragm to be investigated; 2 – sliding key; 3 – rod; 4 – transmission gear pair; 5 – adjusting ring of axial position; 6 – turbine housing; 7 – bushing for movement of angle α_1; 8 – seal; 9 – worm gear of pitch drive x; 10 – worm gear of angle of rotation α_1; 11 – worm gear for radial movement y; 12 – indicator selsyn; 13 – electric-drive motor; 14 – drive bushing for movement y; 15 – gear pair for movement y.

For ensuring the possibility of tests, it is necessary to apply the traverse gear shown in Fig. 78. It is mounted at the required axial distance from the investigated diaphragm 1 along the axis of the turbine housing 6 with the help of an adjusting ring 5. A head is mounted on rod 3 and has the following movements, which are controlled during the test:

1) linear radial (along blade edge) y;

2) rotary around turbine axis (pitch movement) x;

3) rotary around axis y (angle α_1).

All these movements are independent and accomplished with the help of a remote electric drive and indication system. The electric motors of the pitch drive 13 and the indicator selsyn 12 are connected with the shaft of worm gear 9, the axis of which is fixed with respect to the turbine housing. The axes of the worm gears of the drives, α_1 and y (10 and 11), revolve with respect to the turbine housing.

The rotation of worm gear 11 revolves bushing 14, in which rod 3 sits on the thread; the rod is connected through sliding key 2, gear pair 4, and bushing 7 with worm-gear pair 10. Consequently, when worm gear 10 is stationary, rod 3 is not able to revolve, and rotation of worm gear 11 will cause it to move along axis y. During rotation of worm gear 10, gear pairs 4 and 15 revolve synchronously, since the axis of worm gear 11 remains fixed with respect to bushing 7; therefore, it revolves together with it. The synchronous rotation of pairs 4 and 15, which is caused by the rotation of worm gear 10, will lead to the rotation of rod 3 around axis y without it moving along the axis.

Finally, rotation of worm gear 9 leads to rotation of the entire unit around the turbine axis. The head then moves along the circumference (lattice pitch x). The traverse gear is sealed by means of glands with water supply 15.*

A graphic illustration of the possible operating ranges of the turbine ЭТ-3 is given in Fig. 79 by means of a diagram of the conditions of the left shaft. The diagram was constructed for one of the single-stage groups.

This diagram determines the region of the possible combined operating conditions of the turbine stages and the loading device of the left shaft.

The diagram was constructed in the coordinates N kw – n rpm and was obtained as a result of plotting the characteristics of the stages being investigated on the external loading characteristic of the water brake.

The external loading characteristic of the water brake is bounded by the lines 1 – 3 – 4 – 2.

Line 1 – the lower bound of stable operation of the brake – corresponds to the absorbed power as a function of speed during the operation of one disk; ϕ450 mm, with minimum filling.

*A description of the electrical circuit of the traverse gear is not given due to the limited size of the book.

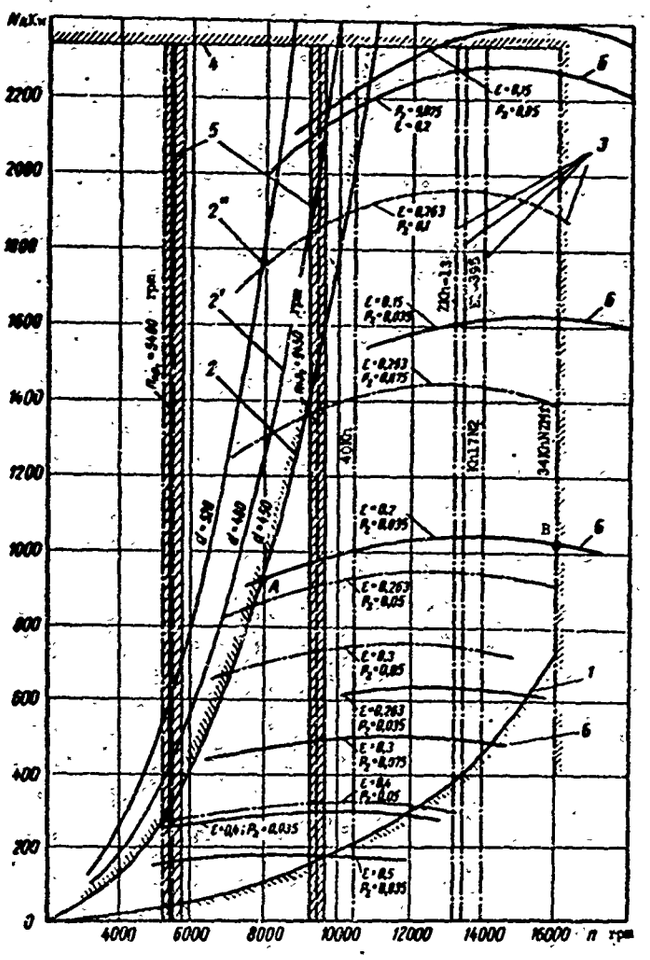

Fig. 79. Diagram of the behavior of the left shaft of experimental turbine ЭТ-3: 1 — lower characteristic of water brake; 2 — upper characteristics for various disk diameters; 3 — range of n_{max} for disks made from different types of steel; 4 — level of N_{max} for cooling; 5 — $n_{кр}$ zones; 6 — external characteristics of two stages of left shaft, p_2 and $\varepsilon = p_2/p_0$, of last stage during combined conditions (speed of rotation of rotors is identical).

Line 3 — the maximum permissible rotor speed — with respect to the strength conditions of brake disks with ϕ450 mm, manufactured from different types of steel with a safety factor of n = 1.5.

Line 4 refers to the maximum power of the brake with regard to heat removal, i.e., with regard to the maximum possible heating of the water coolant at its maximum flow rate.

Lines 2, 2' and 2" denote the possible upper bounds of the external characteristic, which determine the dependence of N = f(n) during combined operation with

complete filling of three disks with diameters of 450, 480, and 520 mm, respectively.

Curves 6 represent the characteristics of two turbine stages of the left shaft at different ε and p_2.

The values of ε and p_2 in Fig. 79 pertain to the last investigated stage of the right shaft, under the condition of synchronous rotation of the rotors.

For instance, with a 450 mm diameter of the brake disks, made of steel 34KhNZMF, and under the given test conditions of the investigated (last) stage, which sits on the right shaft, with the values of $\varepsilon = 0.2$ and $p_2 = 0.035$ bar, the left shaft will provide an experiment with a speed that varies from 8000 to 16,000 rpm (from point A to point Б). This machine is manufactured with a flexible rotor having a first critical speed of $n_{кр1} = 5400$ rpm and a second critical speed of $n_{кр2} = 9450$ rpm. The zones of critical speeds $n_{кр} \pm 250$ rpm are indicated in the diagram.

A very wide possibility of variation is ensured by the steam parameters and the heat drop of the investigated stage.

At a counterpressure of $p_2 = 0.035$ bar, the minimum pressure ratio on the stage amounts to $\varepsilon_{min} = 0.13$; at $p_2 = 0.05$ bar, $\varepsilon_{min} = 0.15$; at $p_2 = 0.075$ bar, $\varepsilon_{min} = 0.2$, and at $p_2 = 0.1$ bar, $\varepsilon_{min} = 0.25$.

All the last stages of condensing turbines practically operate in this range of p_2 and ε, and consequently, their models can be tested in the ЭТ-3 turbine at actual counterpressures, velocities, heat drops, and moistures.

Detailed investigations of the structure of flow in annular cascades, and also in stages with long blades, tested in air, were carried out in experimental turbine ЭТ-7 (see position 8 in Fig. 75), which is the combined unit shown in Fig. 80. In this unit, air from the pressure chamber goes through the inlet duct 2 and the equalizing grid 18 and enters the turbine housing 1 and then proceeds through the shroud 20 to the investigated nozzle cascade 22.

The nozzle cascade 22 is mounted in cantilever fashion on the shaft of diaphragm 17, which is mounted on two ball bearings. The left end of this shaft is connected to a turning device and a two-component tensometeric balance.

The turning device with a stationary probe makes it possible to measure the pitch behind the nozzle cascade. The two-component balance serves for measurement of the tangential and axial forces acting on the nozzle cascade. These measurements are also made in the stage; they make it possible to obtain averaged values of the coefficients of velocity φ and the exit angle α_1 for the nozzle cascade, and thereby separate the mean values of the losses in two cascades.

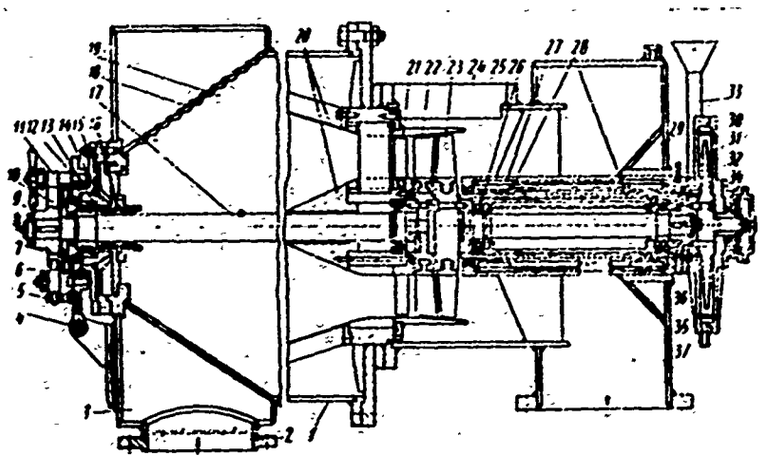

Fig. 80. MEI high-speed experimental air-type turbine with weighing of $M_{кр}$ and P_a on diaphragm and rotor: 1 and 25 – turbine housing; 2 – inlet duct; 3 – annular chamber; 4 – drive for turning nozzle cascade; 5 – needle bearing; 6 – elastic balance beam for $M_{кр}$; 7 – cogwheel; 8 – key; 9 – measuring coupling; 10 – rigid beam of measuring coupling for $M_{кр}$; 11 – cam; 12 – ring; 13 – bearing; 14 – spherical insert; 15 – elastic balance element; 16 – seal; 17 – diaphragm shaft; 18 – grid; 19 – pressure chamber; 20 – shrouds; 21 – guide row of plates; 22 – nozzle cascade; 23 – rotor; 24 – hatch of upper part of housing; 26 – floating bushing; 27 – bushing; 28 and 36 – chambers; 29 – annular chamber; 30 – brake disk; 31 and 32 – brake casing; 33 – supply duct; 34 – induction pickup; 35 – drain; 37 – exhaust duct.

The rotor 23 and the disk of the water brake 30 are located in cantilever fashion on the shaft. The shaft is mounted in anti-friction bearings that are placed in a floating bushing 26.

The rotor, together with exhaust duct 37, is easily dismantled. The exhaust portion is easily replaced by a device that ensures the necessary conditions for testing annular cascades. The group of bearings is then replaced by a cylindrical bushing, while the casing of the exhaust portion serves as the peripheral boundary.

In the investigation of stages, and also isolated annular cascades, in the upper part of the housing 24, on the flange of the housing 25, there is mounted a traverse gear which provides a preliminary three-dimensional zone.

The unit under consideration was used to investigate cascades, and also several stages with small θ. A detailed description of this unit is presented in [22].

For testing stages that are designed for higher supersonic heat drops for small diameters, it is very convenient to use the experimental turbine ЭТ-500, which was developed and built at the Kaluga Turbine Plant (Fig. 81).

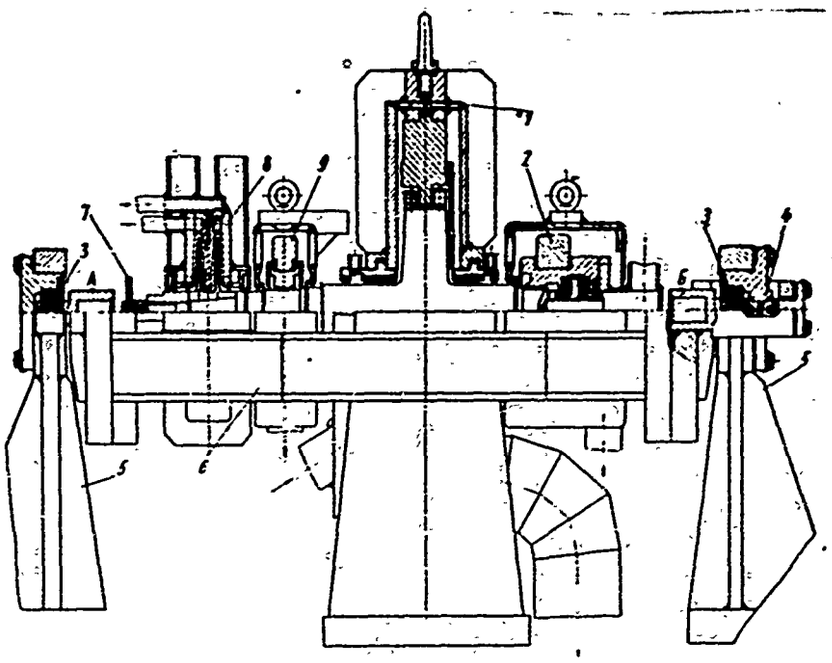

Fig. 81. Experimental high-speed turbine with frame suspension, Kaluga Turbine Plant: 1 – stationary turbine housing; 2 – radial-thrust bearing; 3 – bearings of frame suspension; 4 – axial retainer; 5 – stationary struts; 6 – frame; 7 – magneto of tachometer and protection system; 8 – water brake casing; 9 – radial bearing.

The turbine housing and the struts 5 are secured to the foundation. Radial bearing 9, radial-thrust bearing 2, and the casing of the water brake 8 are mounted on a rigid frame 6 that envelopes the turbine housing. Frame 6 on ball bearings 3 is suspended in struts 5 and secured in an axial direction by a ball-type device 4.

During operation of the brake, the moment and the moment of friction in bearings 2 and 9 are transmitted to the frame and are balanced by a conventional balance head.

For decreasing parasitic moments of friction in the suspension bearings 3, the frame is suspended on springs at points A and Б. The tensions of the springs are correspondingly equal to the reactions on the bearings 3.

Water is fed to the brake in an open stream. After an insignificant change in design, oil is also fed to the bearings without flexible hoses.

This design, in addition to simplicity and reliability, ensures operation with a rigid rotor practically under any conditions, and also gives a very high accuracy of torque measurement, which is especially important for tests of small high-speed stages.

Investigations of cascades in static conditions are conducted in various wind

tunnels set up at the MEI laboratory. One of latest versions – the large MEI wind tunnel (see position 15 in Fig. 75) – serves for investigating straight cascade-packs of the turbine and compressor type. The peculiarity of this installation is the possibility of using both air and steam as the working medium.

The packs to be tested are placed in the working part of the wind tunnel (Fig. 82). The packs are up to 100 mm high and up to 350 mm in length along the front of the cascade. The entrance angle of flow to the cascade varies from 15 to 165°. The exit angle varies from 10 to 60°. A convergent channel 1 is placed at the entrance to the working portion. The pressure chamber of the working portion ensures a uniform field of flow at the entrance to the guide nozzle 2, which is located in front of the cascade. In the pressure chamber there exists a drain system for determining static pressures and impact pressures. The design of the working portion makes it possible to perform precise measurements of the direction of flow at the entrance to the cascade.

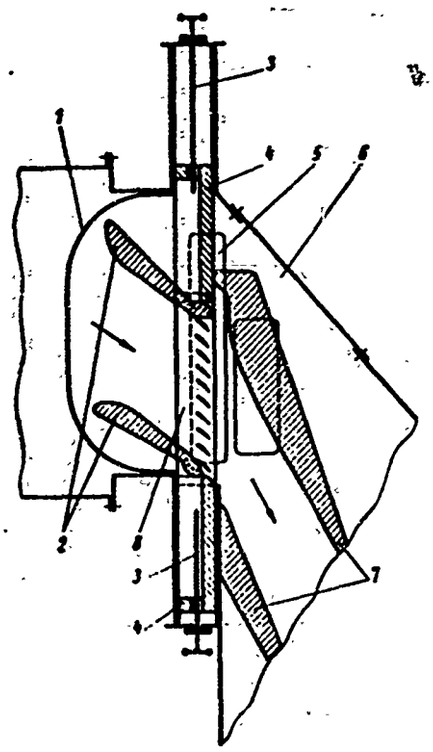

Fig. 82. Diagram of large MEI steam wind tunnel: 1 – convergent channel; 2 – guide nozzle; 3 – slider drives; 4 – slider; 5 – traverse gear port; 6 – exhaust chamber; 7 – divergent channel; 8 – shroud plates of pack.

The entrance angle of flow to the cascade is by the guide nozzle 2, which should be specially designed for the range of entrance angles and M_1 numbers. The walls of the nozzle are securely attached to the shroud plates 8 of the cascade pack and placed together with it in the working portion. In the working part, the pack is held in place by sliders 4 which have screw drives 3. The exhaust chamber 6 is made with a recessed pack and has a clearance of 140 mm. At the cascade exit there is a divergent channel 7 which makes it possible to increase the M number at the cascade exit.

The exhaust chamber has a system of drains for measuring static pressures. In addition, it contains a combined probe [22] for investigating the field of flow directly behind the cascade. The probe moves in a special port of the tranverse gear 5, where it is mounted on the specially sealed rod of the tranverse gear, which has four degrees of freedom.

Control of the traverse gear, which is mounted in the working portion, is fully automated and accomplished from a special panel at some distance from the installation. There are several protection systems that duplicate one another and eliminate the possibility of the probe breaking during the experiment. It should be emphasized that for wind tunnels in general, including the steam-type, which operate with deep vacuums in the exhaust chamber, expecially, the questions concerning the sealing play a paramount role. However, a detailed description of the design of the turbine, the traverse gear, and the electrical circuit is not within the scope of this book.

§ 15. MEASURING DEVICES OF EXPERIMENTAL TURBINES

Experimental turbines have two independent measuring systems: an operational one and an experimental one. The operational measuring system practically does not differ at all from the conventional type used in turbine units. It can be put together by the usual operational instruments of class 1.5 to 2.5 and it is used to control the operation of a machine on the whole and for a rough approximation of the necessary parameters for an experiment.

The experimental system provides exact measurement of the various parameters that are necessary for the specific investigation. It should be sufficiently flexible, reliable, and simple to assemble, since in various investigations the number of measurement points of various parameters can vary from 15-20 to 80-100 and more.

Let us consider in greater detail the measuring devices and instruments of the experimental system.

Measurement of temperatures is possible by various methods. In the PGT laboratory at MEI, with experimental steam turbines, they measure the stagnation temperature T_0 in front of the nozzle cascade. Considering this to be the base temperature, the temperature fields in the clearance and behind the rotor are measured by the differential method, which gives maximum accuracy.

In principle, the base temperature can be the temperature at any point of the flow passage; however, maximum accuracy of measurements is attained in the region of minimum velocities. In the steam box the velocities of the working medium are minimum; therefore, it is the place that houses the base-temperature collectors. The MEI measures the base temperature with platinum resistance thermometers whose cases contain junctions of control and differential thermocouples. The steam boxes of various machines contain 3 to 8 of these heat collectors.

The meters used in various experiments are high-precision laboratory-type and standard automatic electronic bridges and potentiometers. They are checked with the help of normal elements and standard resistance coils of the first class. A schematic diagram of the arrangement of heat collectors and pressure measurement on the ЭТ-3 turbine is shown in Fig. 83.

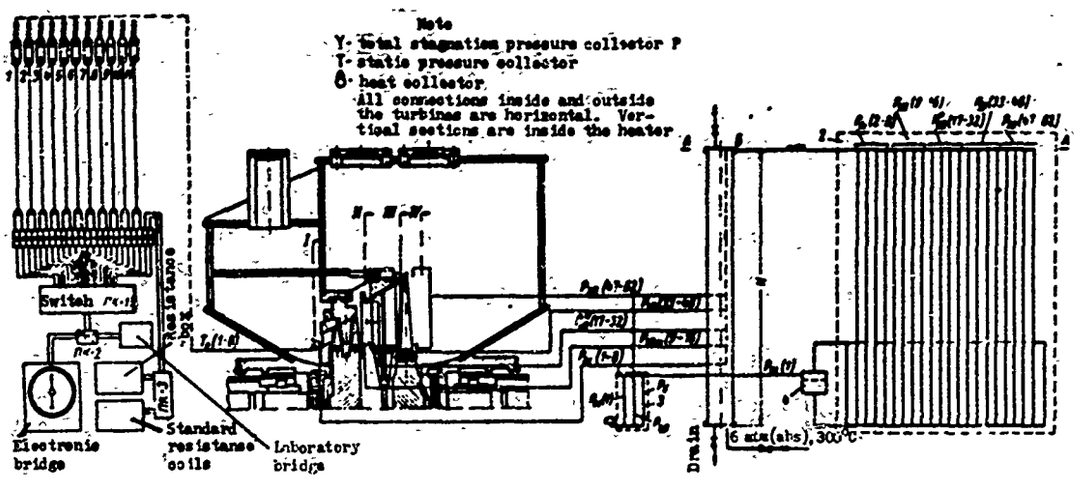

Fig. 83. Schematic diagram for measuring pressures and temperatures in the experimental turbine ЭТ-3 MEI: 1 — heater column; 2 — liquid-column battery manometer; 3 — liquid-column base-pressure manometer; 4 — tank for battery manometer.

The measurement of pressure, due to the large quantity of measurement points, is the most tedious. Since the requirements for the accuracy of pressure measurement are very strict, in most cases it is necessary to use battery-type liquid-column manometers, filled with water or tetrabromoethane, and only at pressures of the order of 2 bar is the use of standard manometers of class 0.2 or 0.35 possible.

In principle, the systems of pressure measurement for air and steam are identical. Their distinction consists only in the way the connections are arranged, which is caused by the condensation of steam in the pulse lines.

Figure 83 gives the schematic diagram for measuring pressures in the ЭТ-3 turbine. In this turbine it is necessary to measure the pressure in four sections:

1. Section I-I. Total stagnation pressure p_{0I} is measured at eight equidistant points on the mid-diameter of the nozzle cascade 40 mm from the leading edges of the blades ($T_{0I}(1\text{-}8)$ in Fig. 83).

In the entire system of pressure measurement the connections inside and outside the machine from the sampling points to the heater column 1 are strictly horizontal. Further, tubes from various points are introduced into the heater column at different levels and lifted inside the column to a common level of H = 2 m

(horizontal plane A-A).

The connections from the column outlet (point Б) to the entrance to the measuring tubes of the battery manometer 2 are arranged in the plane AA. Since the condensed steam, which builds up in the horizontal sections of the measuring connections, does not introduce an error into the measurements, and the vertical sections, which pass inside column 1, are heated up by live steam and therefore are free from the accumulation of condensed steam, possible condensation in the connecting lines does not distort the value of the measured pressures.

One of the points, p_{01I}, is selected as the base, and the absolute value of p_{01I} is measured by the liquid-column manometer 3 with as much accuracy as possible. Further, the pressure p_{01I} of the horizontal pipe is fed into the tank 4 of the liquid-column battery manometer 2.

Consequently, all measurements of p_{0I}, p_{0II}, p_{1II}, and p_{2II} in the flow passages are conducted by the differential method with respect to the base pressure p_{01I}.

2. Section II-II. Static pressure $p_{0II\ ст}$ (9-16) is measured at eight points (4 in the root and 4 in the upper cylindrical sections at 90°) and the total stagnation pressure p^*_{0II} (17-32) is measured at 16 points (8 on the mid-diameter, 4 on the root, and 4 on the upper section at equal distances).

3. Section III-III. Static pressure with respect to nozzle cascade pitch p_{1II} (33-46) is measured by means of draining the cylindrical bypasses of one channel in seven points of the root and seven points of the upper section.

4. Section IV-IV. Static pressure $p_{2II\ ст}$ (47-62) is measured at eight points of the upper and eight points of the root sections of the last stage.

Besides the described system, systematic investigations and the solution of certain special problems employ moving probes for p^* and $p_{ст}$, which give the distribution of the indicated parameters along the height of the blade under investigation.

For measurement of the speed of rotor rotation, experimental turbines are equipped with indicating tachometers and integrating speedometers.

The tachometer is used to monitor the operating conditions of the turbine, but for the accuracy of even the best operational tachometers is insufficient; therefore, domestic machines widely employ various types of meters to integrate the speed in a defined interval of time.

The most convenient to use are electrical teletachometers and decimal electronic counters which are fed from an induction transmitter.

The simplest transmitter of a meter is a magnetic system with field coils and measuring coils. The clearance in the magnetic system is periodically changed by a cam that rests on the shaft. This leads to a change of the magnetic flux in the magnetic circuit of the transmitter and the appearance of a peak-like emf in the measuring coil.

Peaks of defined polarity are fixed by an electronic counter during the time of the experiment.

For measurement of the flow rate during experiments with steam, the greatest accuracy ($\Delta\overline{G} \approx 0.1\%$) and reliability can be obtained by using condensed steam measuring tanks. Venturis may be recommended when chokes are employed in the air-supply system. During operating in a supercritical regime, the venturis ensure sufficient accuracy, especially for calibration of superheated steam with the use of measuring tanks.

Measurement of torque with high accuracy is a rather complicated problem. It may be solved by using torsion dynamometers of various designs or loading devices with a "weighted" stator. The second method at present ensures the greater accuracy; however, it leads to considerable complication of the machine design.

With the correct designing of the machine, the use of floating hydraulic bushings and special weight heads with damping devices, torque can be measured with an error of 0.1 to 0.15% in the zone of optimum moments for the selected type of loading device.

§ 16. METHODS OF TESTING AND MEASUREMENT ON EXPERIMENTAL TURBINES

The procedure for setting up the main problems to be solved on experimental turbines is given below. This procedure has been used at the MEI laboratory for a number of years. The testing of a stage includes a series of experiments, each of which is given a constant value of $\varepsilon = p_2/p_0$. An experiment is conducted with a variation of rotor speed from n_{min} to n_{max}. In this case, n_{min} is determined by the least required value of u/c_Φ; n_{max} is determined either by the maximum required value of u/c_Φ, or in certain cases, by the strength of the stage being tested. Fixation of parameters during the experiment is produced in 6 to 10 points, each of which is assigned a specific speed.

At each point the values of the measured parameters are recorded 5 to 10 times. After making the recordings, the speed is changed by adjusting the loading moment of the water brake, and after a pause which is necessary for stabilizing the regime, the following cycle of measurements begins. The measurement cycle is

produced in a strictly defined period of time, during which the measuring tank of condensed steam and the integrating tachometer is turned on.

The values p_{0i}, T_{0i}, and p_{2i} that are obtained for each point i are averaged according to the known formula $A = \frac{\sum_{i=1}^{i=a} A_i}{a}$, where a is the number of measurements in the selected time interval.

Further calculations of stage parameters are conducted on the basis of the averaged results. The flow rate and velocity of rotation are measured in the form of total quantities G_σ and n_σ during the time of the experiment Δt, whereby $G_\sigma = G\Delta t$ and $n_\sigma = n\Delta t$.

On the basis of the averaged values of p_0, T_0, and p_2 the available heat drop of the stage, h_0, is calculated.

One of the main results of stage tests is the obtainment of the dependence

$$\eta_{ol} = f(u/c_\phi)\Big|_{\substack{M=const \\ p_2=const}}.$$

The internal relative efficiency η_{0i} and u/c_ϕ are calculated by the following formulas:

$$\eta_{ol} = \frac{M_{кр}n}{1000Gh_0} \text{ and } u/c_\phi = \frac{\pi dn}{60\sqrt{h_0}},$$

where $M_{кр}$ is the torque in m(NTP);

n is the speed of rotation in rps;

G is the flow rate in kg/sec;

h_0 is the heat drop in kj/kg.

When conducting the experiment it is more convenient to use the following formula:

$$\eta_{ol} = \frac{M_{кр}n_\sigma}{1000\,G_\sigma h_0},$$

which somewhat simplifies the calculation and makes it more exact. In this case the results of the investigation are presented in the form of tables or graphs which are similar to those shown in Figs. 84 and 85.

For investigation of the reaction distribution in a stage, it is necessary to know the static pressure behind the nozzle cascade, p_1.

This pressure in the simplest case is measured by means of draining along the pitch of the nozzle cascade in the upper and root sections. The pressure field at

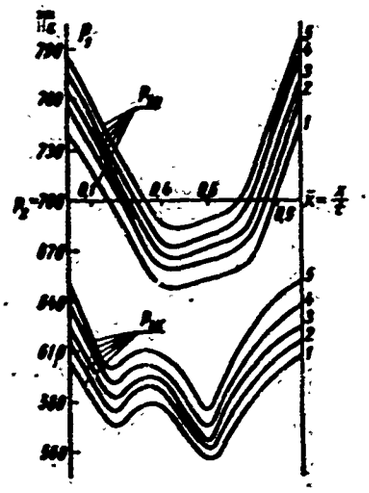

Fig. 84. Graphs of the variation of static pressure in the root $p_{1к}$ and peripheral $p_{1п}$ sections of a nozzle cascade with respect to pitch $\bar{x}$ and the velocity ratio $u/c_ф$: 1) $u/c_ф$ = = 0.254; 2) 0.304; 3) 0.329; 4) 0.376; 5) 0.42 (according to MEI experiments at ε = = 0.65).

the cascade exit, which is shown in Fig. 84, is distinguished by considerable irregularity with respect to pitch; therefore, to avoid errors in the measurement of the degree of reaction, drainage must not be replaced by one point for sampling pressure.

For determination of the mean values of pressure $p_{1п}$ and $p_{1к}$ in the upper and root sections, it is possible to use the following known formula:

$$p_{cp} = \frac{1}{z-1}\left(\sum_{i=1}^{i=z} p_i - \frac{p_1 + p_z}{2}\right),$$

where z is the number of drainage points, which ranges from 5 to 10.

In the investigation of stages, of considerable interest is the study of the change of the flow rate coefficient from $u/c_ф$ and ε (or M).

On the basis of experimental data, it is easy to determine

$$\mu q = \frac{G}{BF_1\sqrt{p_0/v_0}},$$

where q is the given flow rate of gas; B = 0.661 for k = 1.3, and B = 0.674 for k = 1.4.

When $\varepsilon \leq \varepsilon_*$ and q = 1, this formula gives the value of μ for μ_q.

According to the results of an experimental investigation conducted by MEI, when ε = const, $\mu_q = f(u/c_ф)$. The investigations established that when $\varepsilon_1 > \varepsilon_*$, μ_q decreases as $x_ф$ increases. These changes can be explained by the growth of the reaction, which leads to a decrease of the pressure drop in the nozzle cascade (an increase of $\varepsilon_1 = p_1/p_0$), and consequently, also to a decrease of q.

For the characteristics of a stage, considerable interest is stimulated by an investigation of the influence of leakages through the diaphragm seals. When setting up this experiment, the chamber between the rotor and the diaphragm (with a cantilever-type shaft design) is fed a certain amount of steam, $\overline{\Delta G} = \Delta G/G_0$ (G_0 is the flow rate of steam through the nozzle cascade), with an initial temperature T_0.

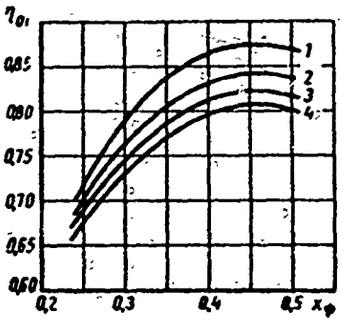

Fig. 85. Dependence of internal efficiency η_{0i} on velocity ratio x_ϕ and diaphragm leakages $\overline{\Delta G} = \frac{\Delta G}{G_0}$: 1 – $\overline{\Delta G}$ = 0%; 2 – 1.2%; 3 – 2.4%; 4 – 3.6% (MEI experiments).

The results of this investigation are shown in Fig. 85. This graph distinctly illustrates how the efficiency of a stage drops as the diaphragm leakage increases.

The graphs in Fig. 85 were constructed according to MEI experiments conducted at $M_0 = 0.58$ and $\varepsilon = 0.8$.

In an experimental investigation of turbine stages, as already noted above, of great interest is the study of the influence of the Re number on the stage characteristics. This is especially important in the investigation of the last stages of steam turbines, which can operate outside the region of self-similarity.

On the other hand, in any investigation of stages, the manifestation of the region of Reynolds self-similarity answers the question of the possibility of extending the experimental data of a model to actual stages, and therefore it is absolutely necessary. Since the characteristics of a stage depend on Re and M, in the investigation of the influence of Re it is necessary to maintain $\varepsilon(M_0)$ = const.

This condition is comparatively easy to fulfill during operation with an experimental steam turbine that has a condensing unit.

The results of corresponding experiments, conducted with one of the experimental steam turbines of MEI, were shown earlier in Fig. 72. It was established for a group of stages that the region of self-similarity corresponds to the following numbers: $Re_c > (3.0 \text{ to } 6.0)\cdot 10^5$ and $Re_w > (1.2 \text{ to } 1.5)\cdot 10^5$ [see § 13].

These data coincide well with the known magnitudes of Re_{aBTM} that were obtained during static investigations of cascades (see Chapter I), with the observance of similarity for all the basic criteria (M, Re, and E_0).

However, they cannot be extended to the last stage of condensing turbines, in which the steam flow is characterized by large M numbers and low values of Re. The influence of Re numbers at high (including supersonic) velocities has not yet been sufficiently studied.

The reliability of the obtained data, which estimates the influence of Re, is determined to a considerable extent by the design of the experimental turbine, the procedure employed, and the measurement systems. The MEI uses machines in which bearing losses have been eliminated for conducting their systematic investigations.

CHAPTER IV

RESULTS OF THE INVESTIGATION OF SINGLE-WHEEL STAGES WITH FULL INPUT

§ 17. SCHEMATIC DIAGRAMS OF SINGLE STAGES

Single-wheel turbine stages can be of the impulse and reaction type. Stages of the impulse type are formed by the nozzle cascade, which is mounted in the diaphragm (or in the form of special assembly sections), and the moving cascade. The impulse stages used in steam turbines are unregulated and are called chamber stages because of their design; they are frequently called pressure stages, also. The nozzle and moving cascades in the stages of impulse steam turbines are of various types. They differ in profile shape and width, the entrance conditions (usually the entrance angles of flow), the technology of manufacture, and the methods of connecting the profiles to the cascade, etc.

The reaction in an impulse stage can be positive (equal to zero) and negative (when the pressure behind the stage is higher than the pressure behind the nozzle cascade). When speaking of the reaction of a stage, usually the mean reaction is implied.* Impulse stages can have a considerable reaction. Especially great are the reactions in the last stages of condensing turbines with small d/l ratios. As a rule, these stages are not manufactured with cylindrical blading, but with specially profiled blading. These stages are considered in Chapters VII and VIII.

Reaction stages are designed with a mean reaction that is equal or close to 0.5. The profiles of the stationary and moving blades of these stages usually have identical chords and are congruent. Stationary cascades are mounted directly in

*The mean reaction is discussed in detail on p. 194.

the housing or its casing (Fig. 86a).*

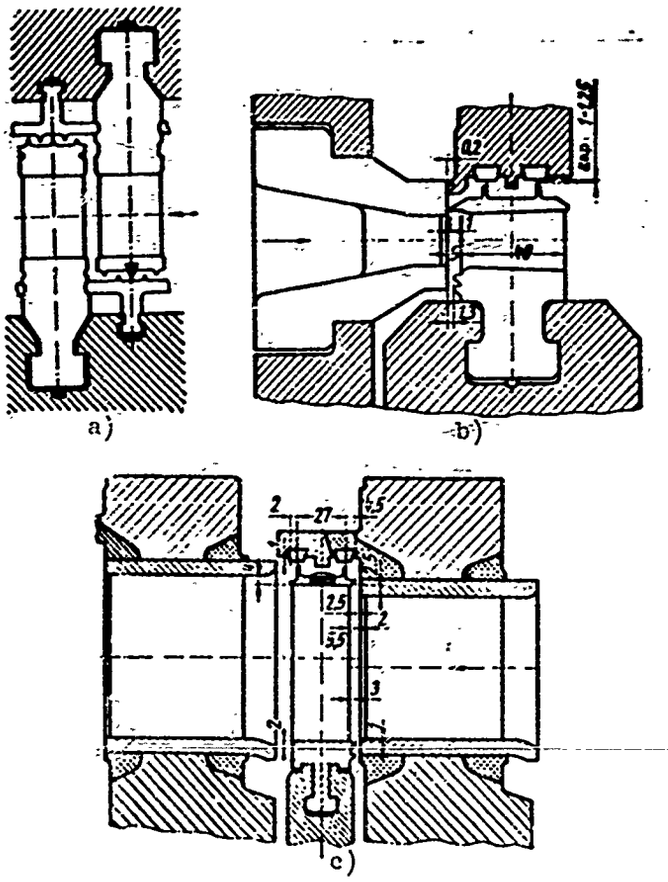

Fig. 86. Typical diagrams of turbine stages: a) reaction stage of KhTGZ turbine; b) regulating stage of LMZ turbine; c) intermediate impulse stage of TM-Z turbine.

The last stages of reaction condensing turbines, from the point of view of aerodynamics of flow and calculation, do not differ from the analogous stages of impulse turbines.

Inasmuch as most stationary turbines that are manufactured at domestic plants are of the impulse type, this book is concerned mainly with stages of this sort. At the same time, many of the questions considered in the book can also be referred to the reaction stages of steam and gas turbines with equal sucess.

Single-wheel stages can be both regulating and unregulated as well.

---

*Figure 86a, does not show the holes for passage of the cooling steam which are foreseen in the turbine design [122].

Many combinations of single-wheel stages were investigated in experimental turbines. These investigations, which were conducted at MEI, KTZ, LMZ, TsKTI, LKZ, NZL, BITM, and others, showed the advantages of new cascades and combinations, and made it possible to find best geometric parameters of the stages. Tests of regular turbines installed at electric power plants also confirmed an increase of economy after replacing the old blading with the new type.

The design of the passage area of an impulse-type single-wheel stage is determined by:

1) the cascades;

2) the combination of cascades;

3) the relationship between the geometric characteristics of the cascades; the relationship of the areas, angles, and heights;

4) the axial clearances (open and closed), the stage sealing, the presence and size of discharge holes;

5) the admission of the stage;*

6) the design of the stage elements (diaphragm, blade shroud, and others) and the manufacturing technology of the cascades.

Figure 86b, and c, shows typical geometric diagrams of impulse-type regulating and intermediate stages of a high-pressure turbine. Some other types of stages are represented in Figs. 56, 119, 132, 134, 136, and 138.

The selection of a geometric diagram for a stage depends on many factors, the main ones of which include:

1) the function of the stage, e.g., regulating or unregulated;

2) the approximate value of d/l, which is determined in the first place by the volume flow rate of the working medium and the rotor speed;

3) the absolute height of the cascades;

4) the operating conditions of the stage, i.e., the pressure ratio $\varepsilon = p_2/p_0$, the velocity ratio $u/c_\Phi = \frac{u}{\sqrt{2h_0 + c_0^2}}$, and for stages that operate in a range of low pressures, the Re number, moisture content of the steam and, in certain cases, the conditions of steam entrance to the stage (angle α_0 and the irregularity of flow along the height);

---

*Stages with partial steam input are considered separately in Chapter VI.

5) the possibility of further using the kinetic energy of the outlet velocity;

6) the possibility of changing the operating conditions of the stage;

7) the admission of the stages and the quantity of nozzle arcs (including the gap between nozzle sets);

8) the possibilities of the stage sealing;

9) the strength conditions of the stage elements (blades, disk, diaphragm);

10) the technology of manufacture of the blading and, in particular, the design of the diaphragm.

Let us consider the influence of these factors.

1. The regulating stages has its own distinctive features; namely: a) partial steam input through several nozzle arcs; b) variable heat drop, and consequently, variation of ε and u/c_ϕ; c) steam leakage through the front end seal; d) connection of nozzles to separate sections; e) increased chords of rotor blades (in the majority of cases).

2. The magnitude of $\theta = \frac{d}{l}$ renders a large influence on stage design. For small d/l, usually when $d/l < 6$ to 12, the moving blades, and sometimes the nozzle blades also, have a varying profile height. Even at large θ, when there is no need for twisting the stage, θ determines the selection of the mean reaction of the stage, i.e., the ratio of cascade areas. The smaller d/l is, the higher the reaction at the periphery, the more important the sealing of the outer open clearance and the installation of the seals of the blade shroud.

3. In the first stages of turbines it is necessary to make the stages with low absolute cascade heights. This creates additional requirements for the stage design: a) a decrease in the chord of the nozzle and moving cascades, taking reliability into account. This decrease of chord should be accomplished to definite limits, when it gives an increase in stage economy (see §§ 10 and 22). The narrow nozzle blades in high-pressure stages frequently require diaphragms of special design; b) for nozzle and moving cascades with low relative heights, special profiling methods should be employed, in particular, meridional profiling, modified profiles of rotor blades, and others; c) for low heights, an essential influence on economy (and also reliability) is rendered by the accuracy and technology of manufacture; d) for low cascade heights, there is an increase in the relative size of the clearances in the stage. Therefore, such a stage should be thoroughly sealed. Inasmuch as steam leakages over the shroud depend on the reaction, small reactions should be selected for these stages.

4. The operating conditions of the stage mainly determine the selection of cascades. At supersonic and transonic velocities, cascades designed for high economy under such conditions should be selected. Various stages have different values of the optimum velocity ratio u/c_{Φ}. This also should be considered. In particular, an increase of the reaction increases the optimum ratio u/c_{Φ}. On the other hand, considerable additional losses (due to friction, steam leakage and, with partial input, losses connected with partial admission) lower the optimum value of u/c_{Φ}. If the stage preceding the one under consideration operates with a small u/c_{Φ} ratio, angle α_0, the angle of entrance of steam into the stage, will be considerably lower than 90°. In this case the nozzle cascades should be designed for conditions of work at a small α_0 angle. The irregularity of the parameters of velocity and its direction with respect to height also must be considered during the designing of a nozzle cascade.

5. If a stage whose kinetic energy cannot be further utilized (a regulating stage, e.g., the last stage of a turbine or cylinder, a stage before a sudden change in diameter, and so forth) is being designed, it is desirable that the output loss be reduced to a minimum. In particular, the angle of direction of the outlet velocity from the last stage of a set should be close to $(90^{\circ} + \beta_2)$ and 90° for some stages. For these stages, angle α_1 should be the smallest of those which provide a sufficiently high economy. In the first approximation one may assume that the relative loss with the outlet velocity is equal to

$$\zeta_{\omega.c} = (c_2/c_{\phi})^2 \approx \sin^2 \alpha_1.$$

6. If it is known for certain that a given stage will be operating with a change of conditions (turbine stages with variable speeds, regulating stages, and the last stages of all turbines), it should be selected in such a way (and in particular, its cascades) as to ensure economic stability in the entire considered range of conditions. Proceeding from varying conditions, such stage characteristics as u/c_{Φ} and ρ, for design conditions, sometimes are expediently selected as nonoptimum.

7. The admission of steam requires a special calculation of the ratio of cascade areas, a moderate reaction, a lowering of the velocity ratios u/c_{Φ} and, for decreasing the losses, special protection.

8. Clearance seals are useful in any stages, since they reduce parasitic steam leakages and increase the economy of the stage. However, in a number of cases the seals of a stage, especially the seals of the open axial clearances and the radial

clearance over the shroud, complicate the turbine design, assembly, and operation. In connection with this, stringent requirements should be placed on the clearances only where it is actually necessary. At the same time, if it is not possible to seal a stage very well, it is necessary to work out its design in such a way so as not to considerably lower the stage efficiency. It should be recalled that stage seals influence not only economy, but also the magnitude of axial stress.

Diaphragm seals, which are installed in all chamber-type stages, on the one hand, reduce parasitic steam leakage past the nozzle cascade, and on the other hand, they decrease the suction of steam into the moving cascade through the open root clearance. An increase in leakage through a diaphragm seal increases the axial stress in the stage. BITM experiments [5] also showed that leakage through this seal increases the disk friction losses. The relative magnitude of this leakage depends on the ratio of equivalent area of the seal

$$F_{y.экв} = \mu_y \pi d_y \delta_y \frac{1}{\sqrt{z_y}} \tag{102}$$

to the area of the nozzle cascade F_1.

The ratio $F_{y.экв}/F_1$ is especially great in the first stages of turbines, where the volume flow rate of gas, and consequently also F_1, are small. In these stages it is necessary to increase the number of strips of the diaphragm seal with minimum clearances on the sharp edges [97], [126].

The discharge holes in disks make it possible to essentially lower the negative influence of this steam leakage on the process in the moving cascade. It is necessary, however, to consider that a very large area of discharge holes will lead to suction from the chamber behind the disk into the moving cascade. Unfortunately, it is impossible to exactly calculate the optimum area of the discharge holes practically, since this requires a knowledge of all the clearances in the stage and its reaction with a high accuracy. The limiting area of discharge holes is found by the formula

$$F_p = \frac{\mu_y}{\mu_1} \frac{F_y}{\sqrt{z_y}} \sqrt{\frac{1-\varrho_\kappa}{\varrho_\kappa}}. \tag{103}$$

The designations adopted in this formula and the computation of the necessary magnitudes are found in § 12.

Sealing on the periphery of a stage is especially necessary in stages with small cascade flow areas and with a large reaction on the periphery. If it is not

possible to seal a stage on the periphery very well, a small stage reaction must be employed, although this can sometimes lower the efficiency, which is calculated without leakages. It should be indicated that radial shroud seals are of value only if the clearance in them is less than the upper open clearance or, at least, of the same order (for greater detail, see §§ 12 and 22).

9. The stringent requirements of reliability determine many dimensions of a stage. First, the width of the rotor blades, as a rule, is determined by strength. Secondly, the thickness of the diaphragm and its design also depends on strength. Thirdly, the conditions of reliability frequently determine the full axial clearances in a stage (the distance between the trailing edges of the nozzles and the leading edges of the blades). As shown by experiments, full clearances within known limits do not render a noticeable influence on economy (and sometimes it is even favorable to increase then); at the same time, large axial clearances increases the vibrational reliability of the rotor blades. Fourth, the requirements of vibrational reliability force the application of lacing or damping wire, and sometimes in the places where these wires are installed it is necessary to thicken the profile. These circumstances lower the economy of the stage.

It is especially unfavorable to install a wire shroud in short blades, which is applied sometimes for removing type "B" vibrations. In this case the flow over the entire cascade is essentially disturbed.

The installation of stellite cover plates for protection from blade erosion in stages that operate in a moist steam region frequently disturbes the shape of the profile, which naturally lowers the conditions of flow in the cascade. Therefore, stellite cover plates as much as possible should be placed flush with the profile or, at least, without abrupt transitions which cause separation of flow.

10. The technology of blading manufacture renders a large influence on the effectiveness of a stage. Although there are still no sufficient experimental materials, an increase in the quality and accuracy of manufacture of profiles and internal surfaces of end walls, all the same, is undoubtedly important. Stage economy is lowered by the following deviations in the manufacture of blading: a) deviations in dimensions of separate channels (height, pitch, angle); b) non-observance of the diameters of nozzle and moving cascades, which leads to a change of the internal and external overlaps; c) thickened trailing edges; d) raised roughness; e) an essential change of cascade pitch in the disassembly points of the diaphragm and in the locked rotor blade; f) looseness between shrouds of the assembled nozzle cascade and gaps between the shrouds of the rotor blades; g) loose

adhesion of blade shroud to profile, and others.

All this can essentially lower the efficiency of a stage. The technology of manufacture of welded diaphragms frequently does not make it possible to obtain a sufficient accuracy for all channels of the nozzle cascade, especially with low heights. The cast-iron diaphragms with lined nozzle blades, which are employed in stages with low steam temperature, also have their peculiarities: high roughness of the bounding surfaces and low accuracy in channel dimensions.

It should be indicated that a deviation in blading dimensions leads not only to increased cascade losses, but also causes a change of the reaction and, in connection with this, a change of the leakages and the axial stress. Both welded and cast diaphragms have channels with restriction on the root and peripheral radii along the circumference; milled nozzle cascades usually are bounded by straight lines.

§ 18. INFLUENCE OF THE BASIC PERFORMANCE PARAMETERS ON THE EFFICIENCY OF A STAGE

The basic characteristic of a stage is the efficiency which considers all the losses, e.g., relative internal efficiency, η_{0i}. Relative internal efficiency is usually defined as the difference of the relative blade efficiency, $\eta_{0л}$, and the sum of all additional losses:

$$\eta_{0i} = \eta_{0л} - \Sigma \zeta_{доп}. \tag{104}$$

Relative blade efficiency can be expressed analytically by the following formula:

$$\eta_{0л} = 2x_\phi\left[\varphi\cos\varphi_1\sqrt{1-\varrho} + \psi\cos\beta_2\sqrt{\varrho + \left(\frac{w_1}{c_\phi}\right)^2} - x_\phi\right], \tag{105}$$

where

$$x_\phi = \frac{u}{c_\phi} \text{ and } \left(\frac{w_1}{c_\phi}\right)^2 = \varphi^2(1-\varrho) + x_\phi^2 - 2\varphi x_\phi\cos\alpha_1\sqrt{1-\varrho}.$$

Direct use of the results of static investigations, especially the results of static tests of two-dimensional cascades, in a number of cases can lead not only to errors, but also to incorrect qualitative conclusions. It is especially difficult to directly use the results of static investigations of cascades during variable operating conditions of the stage, when it is necessary to know the velocity coefficients, depending upon the M numbers, and in certain cases also on the Re number. It is also necessary to consider the change in conditions of entrance to the cascade. A change of the reaction of the stage influences not only the redistribution of heat drops between the cascades and losses with the outlet

velocity, but also the losses due to steam leakages, which formula (105) does not consider.

The following example shows how unreliable it is sometimes to use these kinds of formulas and the results of static wind tests of two-dimensionsl cascades [66].

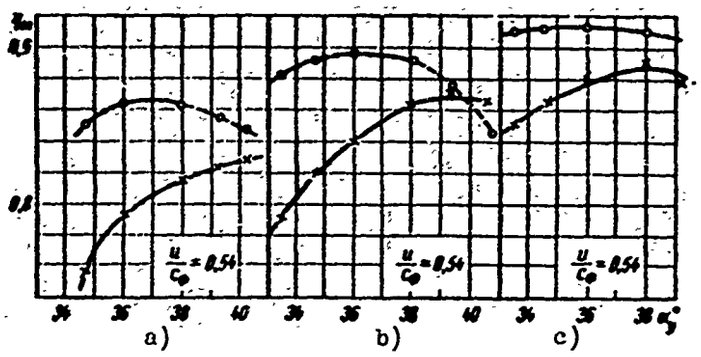

Fig. 87. Comparison of experimental data with calculation according to the results of investigations of two-dimensional cascades in an experimental turbine for different heights: a) l_1 = 16.9 mm; b) l_1 = 29.4 mm; c) l_1 = 47.1 mm (LMZ experiments). x-x-x- experimental data, 0-0-0- computed values.

Figure 87 presents a comparison of experimental data from experimental turbine tests with a calculation based on the results of investigations of two-dimensional cascades. A comparison is made for a typical LMZ stage when $u/c_\Phi = 0.54$ and $M_{c_1} \approx 0.5$ for three heights, depending upon the angle of incidence of the nozzle blades, α_y. From Fig. 87 it follows that the curves which were constructed directly according to tests of two-dimensional cascades in static conditions* do not give proper coincidence with the results of experiments in a turbine even with respect to its character (see § 11).

In connection with this, the best and the most reliable means of determining the efficiency of a stage and the influence of performance parameters on efficiency are tests in experimental turbines that are conducted according to the requirements of the similarity theory (see § 13).

Let us consider how the basic performance parameters influence the efficiency of a stage. The performance parameters include: the velocity ratio u/c_Φ, the pressure ratio $\varepsilon = p_2/p_0$ (or M_0 number), and the Reynolds number, Re. The efficiency of a stage is normally calculated depending upon the utilization of the outlet velocity in the following stage, i.e., η_{0i} and η^*_{0i}.

---

*The values of efficiency that are calculated according to static test data, starting from $\alpha_y = 37^\circ 58'$, are insufficiently reliable, since there are no exact data on the losses in a moving cascade at large leakage angles. In this zone, the indicated efficiency curves are represented by a dotted line (note from LMZ engineer A. O. Lopatitskiy).

In this paragraph we shall consider the dependence

$$\eta_{oi} = f\left(\frac{u}{c_\Phi}, \varepsilon, Re\right).$$

1. Influence of Velocity Ratios u/c_Φ on the Efficiency of a Stage

A change in the velocity ratio u/c_Φ (when ε = const) shows up in the efficiency of a stage due to:

a) a change in the outlet velocity c_2, and consequently, the magnitude of losses with the outlet velocity

$$\zeta_{o.c} = (c_2/c_\Phi)^2;$$

b) a change in the outlet velocity from the nozzle cascade, c_1, in connection with a change in the reaction, and sometimes the heat drop in addition; the cascade losses also change, since the M_{c_1} and Re_{c_1} numbers change;

c) a change in the flow entrance angle β_1 and the velocity w_1;

d) redistribution of heat drops between cascades, inasmuch as the effectiveness of the nozzle and moving cascades is various;

e) a change in the losses due to leakages, which directly (or indirectly through the reaction) depend on u/c_Φ;

f) a change in the losses due to disk friction.

For a specific stage with its conditions (ε and Re) and geometric parameters known, the following dependence may be found

$$\eta_{oi} = f\left(\frac{u}{c_\Phi}\right).$$

Such a typical dependence is the curve that was shown earlier in Fig. 64. The experimental points were obtained in an MEI experimental steam turbine for a КД-2-2А stage at ε = 0.7 and ε = 0.5. The diameter of the stage is d = 534 mm, l_1 = 25 mm (two) radial shroud seals, δ_p = 1 to 1.2 mm, and open axial clearance δ_a = 1.8 mm. The efficiency, η_{oi}, takes into account all losses, including the losses with the outlet velocity, disk friction, and leakage through the peripheral clearance. The specific gravity of various losses in the common balance can vary for different stages and different conditions. Earlier, in Fig. 63, for the same step we showed the calculated distribution of losses in this stage. From the graphs it is clear that the efficiency (in the considered range of u/c_Φ) is determined mainly by the losses with the outlet velocity.

It is obvious that the optimum value of the velocity ratio, $x_{\Phi_{опт}}$, is of

much importance to a stage. For impulse stages with cylindrical blading, $x_{\Phi_{опт}}$ varies from 0.45 to 0.55 and depends mainly on ρ_{cp} (or on F_2/F_1 and ε), d/l, the relative size of the clearances, and the disk friction losses. Inasmuch as usually ρ_{cp} also depends on d/l (for the selection of $\rho_{cp} = f(d/l)$, see Fig. 112), the absolute values of the clearances in a group of stages change very little, and the losses due to disk friction are functions of the area of the nozzle cascade, which in turn are proportional to the height l_1, therefore, in the determination of $x_{\Phi_{опт}}$ it is possible to be governed mainly by the dependence

$$x_{\Phi_{опт}} = f(\rho, l_1).$$

This dependence, for a stage with good sealing (without meridional profiling) is represented in Fig. 88.

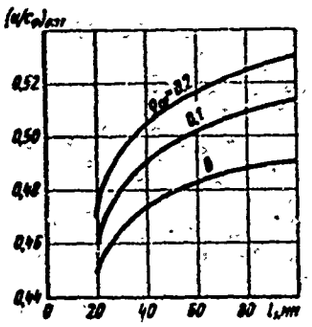

Fig. 88. Selection of optimum ratio $u/c_{\Phi_{опт}}$, depending on height of nozzle cascade l_1 and mean reaction ρ_{cp}.

It should be considered that with the use of the outlet velocity the optimum velocity ratio, $x_{\Phi_{опт}}$, increases somewhat, and the curve for $\eta^*_{0i} = f(u/c_\Phi)$ is more sloping than the one for $\eta_{0i} = f(u/c_\Phi)$.

No less important is the stability of stage efficiency, depending upon u/c_Φ, inasmuch as with a deviation of the conditions from the calculated ones, this ratio also changes. But also under rated conditions it is frequently necessary to design the stage with $u/c_\Phi \neq (u/c_\Phi)_{опт}$, especially when the u/c_Φ ratio is low.

A lowering of x_Φ makes it possible to develop a large heat drop with the same stage diameter (actually, the cascade height will decrease somewhat in this instance, but this decrease usually is very small), which reduces the number of stages:

$$\frac{z_1}{z} = \frac{x^2_{\Phi_1}}{x^2_\Phi}. \qquad (106)$$

If the number of stages, and consequently also the heat drop of each stage remain the same, then a decrease of the calculated velocity ratio x_Φ makes it possible to lower the diameter of the stage and to correspondingly increase the length of the cascades. Since the effect of cascade height on the efficiency of a stage is greater than the effect of the diameter, then for a sloping curve of the dependence $\eta_{0i} = f(x_\Phi)$, a certain lowering of x_Φ may even be profitable. This it should be added that with a constant heat drop, the disk friction losses are

approximately proportional to x_{Φ}^{5}.

A lowering of u/c_{Φ} may be especially necessary. For the acceptable values of blade heights, this lowering would make it possible to reject partial steam input. This would lead not only to an increase in stage efficiency, but would make it possible to use the outlet velocity in the following stage. Generally, in the case of the use of the outlet velocity c_2 or even its axial component c_{2a} only, the stage efficiency has a more sloping dependence on u/c_{Φ}, which makes it possible to lower u/c_{Φ} with a greater benefit. It is necessary, however, to consider that a significant decrease of u/c_{Φ} causes an essential change of the angle α_2. This angle becomes considerably less than 90° and, in this case, if we apply the usual profiles for the nozzle cascade of the following stage, the losses in it will increase (for greater detail, see § 24).

Certainly, in stages with a sufficiently high cascade height, a lowering of the computed value of u/c_{Φ} will not give an increase in economy, since the effect of height drops as l increases. Here, a decrease of u/c_{Φ} can be justified only by simplifying the design.*

In MEI stages, as compared to old and certain new combinations, the stage efficiency with deviation of u/c_{Φ} from the computed value changes in a much smaller degree. Thus, for instance, the efficiency without the use of the outlet velocity $\eta_{ол}$ for a КД-2-2А stage whose nozzle cascade height is 25 mm and with a variation from $x_{\Phi_{опт}}$ to $x_{\Phi} = 0.3$, drops a total of $\Delta\eta_{ол}/\eta_{ол} = 11.7\%$, and $\Delta\eta_{ол}/\eta_{ол} = 2.4\%$ with an increase to $x_{\Phi} = 0.6$. According to old company graphs (see Fig. 129) for efficiency with the use of the outlet velocity $\eta^{*}_{ол}$, this change amounts to 16.1 and 5.1%, respectively, and on the basis of NZL curves (Fig. 130), it is equal to 13.3 and 7.0%. The higher stability of the efficiency of MEI stage is explained by the following reasons:

a) resistance of nozzle and moving cascades to variation of velocity and entrance angle;

b) selection of a favorable reaction;

c) correct selection of combinations.

The sealing is of much value for stable stage operation. If at optimum values of u/c_{Φ} the reaction of the stage is selected in such a way so as not to allow

*The technical and economic foundation for the selection of $u/c_{\Phi} < (u/c_{\Phi})_{опт}$ was given in the NZL reports.

considerable losses due to steam leakages through the clearances, then as u/c_Φ changes, there is a corresponding change of the reaction, and additional losses due to parasitic leakages can increase essentially.

2. Influence of Pressure Ratio ε on Stage Efficiency

Until recently, the influence of the pressure ratio, $\varepsilon = p_2/p_0$, on the efficiency of a single-wheel stage was not noted at all in literature and was not considered in calculations. Certain organizations that conducted investigations of stages in experimental turbines did not detect the influence of ε. This apparently may be explained by the fact that there are still very few experimental steam turbines and many laboratories are limited to tests in air-driven turbines, where usually the influence of compressibility is not investigated. In the MEI experimental steam turbine, in the majority of experiments the pressure ratio ε varied form 0.9 to 0.5, which not only made it possible to detect the influence of ε, but also to use the results of these investigations for a wide range of turbine stages, including regulating stages, and also for calculation of variable stage performance.

The influence of ε on stage efficiency due to the following causes:

a) change of cascade losses, depending upon the M number; especially perceptible is the change of losses depending upon the M_{c_1} number in the nozzle cascade; a graph for $\zeta_c = f(M_{c_1})$ was illustrated earlier in Fig. 55; it is this dependence that mainly determines the influence of ε on stage efficiency;

b) change of the reaction of the stage and, due to this, redistribution of heat drops between cascades, and a change in the steam leakages.

In various stages the influence of ε is expressed differently. The function $\eta_{0i} = f(\varepsilon)$ depends on the cascades of the stage, the ratio of areas, F_2/F_1 and d/l, and u/c_Φ in a number of cases. In certain stages the optimum velocity ratio $(u/c_\Phi)_{ОПТ}$ is kept for various ε, while in others it depends on ε.

In MEI stages of group "A," which are recommended for the first stages of power turbines, the first and middle (and sometimes the last) stages of turbines of low and medium power, and for regulating stages calculated for a large heat drop, the optimum pressure ratio ε varies from 0.65 to 0.8. An increase in the heat drop (decrease of ε) leads to a lowering in efficiency due to the less favorable conditions of flow in the nozzle cascade and the raised reaction, which causes increased steam leakage. Small heat drops (large ε) also lower efficiency, but to a smaller degree. In this case, the lowering of efficiency is connected with the raised losses in the nozzle cascade, the optimum conditions of which usually amount to $\varepsilon_1 = 0.6$ to 0.7,

and also in certain stages it is connected with the appearance of a negative reaction in the root sections.

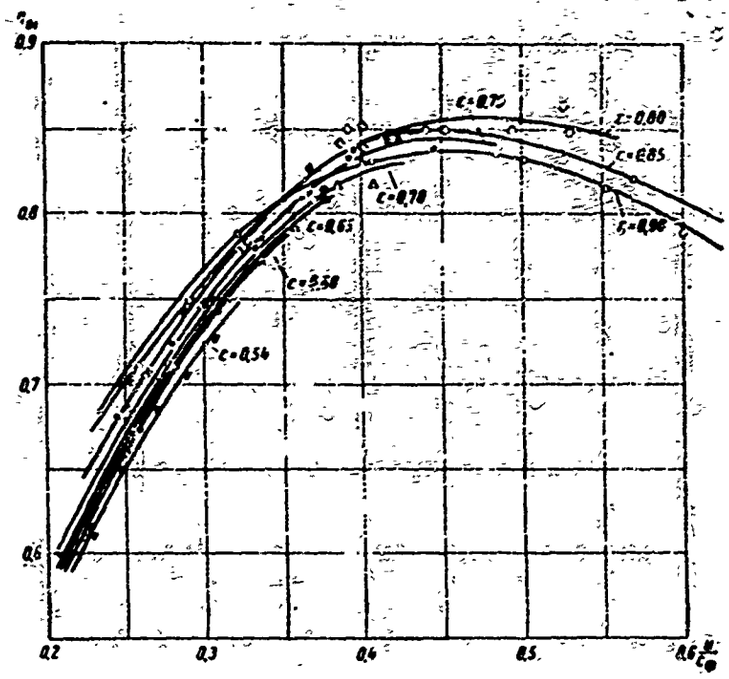

Fig. 89. Dependence of efficiency η_{0i} on velocity ratio u/c_ϕ for various values of pressure ratio $\varepsilon = p_2/p_0$ (MEI experiments):

▲ — ε = 0.54; × — ε = 0.60; ● — ε = 0.65; △ — ε = 0.70; ✳ — ε = 0.75; ◇ — ε = 0.80; ▽ — ε = 0.85; C — ε = 0.90.

Figure 89 illustrates experimental (from MEI experiments) graphs for the dependence $\eta_{0i} = f(\varepsilon, u/c_\phi)$, obtained from tests of an MEI КД-2-3А stage for $l_1 = 48$ mm, $d = 400$ mm, $(Re_1)_{max} \approx 5.8 \cdot 10^5$, and $F_2/F_1 = 1.55$. For the value of $u/c_\phi > 0.35$, the maximum efficiency corresponds to conditions of $\varepsilon = 0.8$. If $u/c_\phi = 0.45$ and ε is increased to $\varepsilon = 0.9$, the efficiency η_{0i} is lowered by 1.5%, and with a large heat drop ($\varepsilon = 0.75$), only by 0.5%. The intersection of the efficiency curves is not random, but is confirmed by a detailed calculation of the stage. An analogous dependence was obtained during the calculation of a stage with respect to the aerodynamic characteristics of the cascades (including an actual diaphragm).

For another stage, КД-2-2А ($l_1 = 25$ mm and $d = 534$ mm), Fig. 90 shows the dependence of efficiency η_{0i} on ε for several values of u/c_ϕ. A graph of the square of the velocity coefficient φ^2 and the welded diaphragm of this stage is plotted there. Both graphs for η_{0i} and φ^2 are qualitatively similar and are combined into one; it should be considered here that due to the reaction of $p_1/p_0 > p_2/p_0$, the

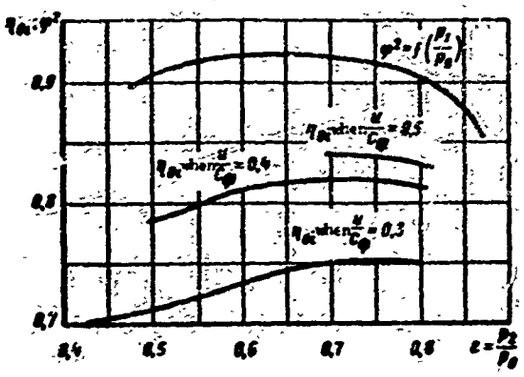

Fig. 90. Dependence of relative internal efficiency η_{0i} of a КД-2-2А stage (d = 534 mm and l_1 = 25 mm) and the square of the velocity coefficient φ^2 of the welded diaphragm of this stage on the pressure ratio ε (MEI experiments).

curves for η_{0i} and φ^2 for the same conditions should move along the axis ε.

Inasmuch as in a turbine (especially when n = const) both u/c_Φ and ε change simultaneously, for specific conditions (initial steam parameters and peripheral velocity) it is necessary to reconstruct the graphs and obtain a simple dependence of efficiency on the change of conditions. An example of such reconstruction was shown in Fig. 60. Another example of reconstructing the efficiency according to the results of tests at MEI, depending upon heat drop h_0 and peripheral velocity u (for given initial parameters), is shown in Fig. 91.

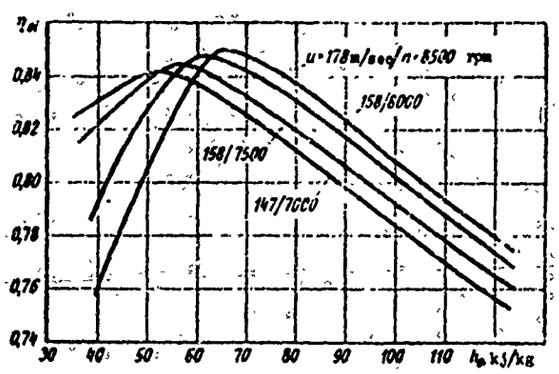

Fig. 91. Reconstruction of curves for $\eta_{0i} = f(u/c_\Phi, \varepsilon)$ depending upon the heat drop h_0 and peripheral velocity u with constant parameters (MEI experiments).

From a consideration of these two graphs, it is clear that for the same stage, depending upon the selected constant speed, the character of the dependence $\eta_{0i} = f(h_0)$ (or $\eta_{0i} = f(u/c_\Phi)$), the optimum ratio $(u/c_\Phi)_{опт}$, and even the magnitude of maximum efficiency η_{0i}^{max}, all change to some extent.

The influence of ε on efficiency was also noted in experiments at KTZ, LKZ, and others.

It is possible to design a stage in advance which has the highest efficiency for the given pressure ratio ε. For this, as indicated in Chapters I and II, it is necessary to select cascades that have minimum losses, namely at M_{c_1} and M_{w_2} numbers which correspond to the ε ratio; for given ε and x_Φ, a ratio of areas should be selected at which the losses due to leakages will be minimum (usually in practice, with a root reaction of ρ_K = 0.03 to 0.05).

3. Influence of Re Number on Stage Efficiency

The influence of the Re number is evident in the conditions of flow in the

nozzle and moving cascades, and consequently, in the velocity and flow-rate coefficients.

At LMZ, tests were conducted in an experimental turbine with a typical stage for ε = const and Re = var. In this case, $Re_{c_1} = \frac{b_1 c_{1t}}{\nu}$ varied from $2 \cdot 10^5$ to $16 \cdot 10^5$. In this case, a decrease of the Re number by 3 to 3.5 times did not result in a perceptible change of efficiency [66].

The effect of this criterion was noticeable in MEI experiments with an experimental steam turbine at large values of Re, and it was even considerable in a particular zone (see Fig. 72).

For stages with a small reaction, on the one hand, the influence of losses in the nozzle cascade on stage efficiency is much greater than the effect of losses in the moving cascade. On the other hand, the influence of Re in the moving cascades is greater than in the nozzle cascades, and $Re_{c_1} = b_1 c_{1t}/\nu_1$ usually exceeds $Re_{w_2} = b_2 w_{2t}/\nu_2$ a few times. In general, therefore, it is difficult to decide which one plays predominant role in this influence, the nozzle cascade or the moving one. This may be done only for a specific stage and known conditions of its operation. It should be indicated that it is impossible to analyze the influence of the Reynolds number on stage performance without keeping the other criteria constant; the pressure ratio ε, in particular. A disregard of this can lead to incorrect conclusions.

The influence of the Reynolds number on the efficiency of a stage is not only exhibited in a change of cascade losses, but also a change in the reaction, which is connected with this. Losses due to steam leakages with a change in the reaction, in turn, also change. Furthermore, the Re number also renders an influence on the losses due to disk friction.

If a stage is being calculated, it is possible to compute the Re number separately for the nozzle and moving cascades. If the magnitude of the reaction is unknown in the calculation of test stage, it is more convenient to use the generalized criterion

$$Re_{\phi} = \frac{b_1 c_{\phi}}{\nu_2},$$

where c_{ϕ} is a fictitious velocity that is calculated for the entire heat drop of the stage from the stagnation parameters; b_1 is the chord of the nozzle cascade; ν_2 is the kinematic viscosity with respect to theoretical parameters behind the stage.

In experiments with various stages in MEI experimental turbines, the influence of the Re number on stage efficiency was detected at approximately Re ≈ 3 to $6 \cdot 10^5$. The boundary of Reynolds self-similarity, and also the quantitative influence of Re on efficiency, depends on the cascades of the stage, ε (or M number), the reaction, and other factors.

Figure 92 shows the change of the maximum efficiency of MEI stages, η_{01}^{max}, depending upon Re_{c_1} for three MEI stages having d = 400 mm and l_1 = 48 mm. Experiments were conducted at MEI with an experimental steam turbine, whereby the Re_{c_1} number was changed at ε = const (with a simultaneous change of p_0 and p_2). For stage КД-2-2А, the influence of Re is considered at three values of ε (ε = 0.65, 0.75, and 0.8).

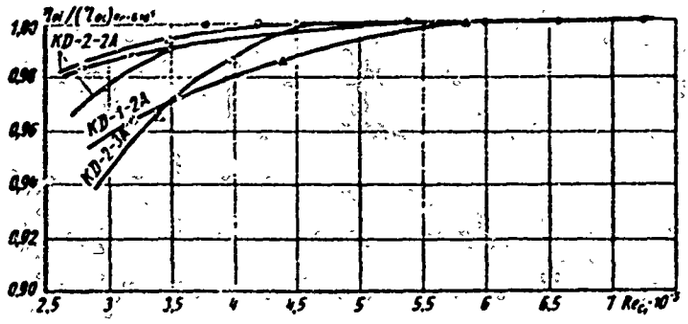

Fig. 92. Dependence of maximum efficiency η_{01}^{max} on Re_{c_1} numbers and various pressure ratios ε for three MEI stages:

КЛ-2А (F_2/F_1 = 1.41), ● — ● — ε = 0.65; × — × — ε = 0.70; ▲ — ▲ — ε = 0.75; ○ — ○ — ε = 0.8; КД — 1 — 2А (F_2/F_1 = 1.73); ◇ — ◇ — ε = 0.75; КД — 2 — 3А (F_2/F_1 = 1.65); △ — △ — ε = 0.75.

For the investigated stages the region of self-similarity starts from $Re_{автом}$ = = 4 to $6 \cdot 10^5$, which approximately corresponds to $Re_{автом}$ for the cascades of these stages ($Re_{w_2} \approx 1/3\ Re_{c_1}$). The influence of Re at identical $u/c_ф$ and ε for the three stages is different. The larger the ratio F_2/F_1, the lower the mean reaction, and in stage КД-1-2А there even appears a negative reaction in the root sections. The negative reaction results in a separation of flow, the appearance of which makes the influence of Re more perceptible. Therefore the greater the ratio F_2/F_1 (under the given conditions), the higher $Re_{автом}$ is. Furthermore, in the КД-2-3А and КД-1-2А stages under the given conditions, the angles of entrance to the moving cascade are less than the optimum ones, which results in the possible appearance of separation on the back of the profile of the moving cascades.

As ε increases (as the M number decreases), the influence of Re is greater, which coincides with the data of static cascade investigations; furthermore, at larger ε,

the reaction of the stage is less.

W. Traupel [96], after generalizing a number of experimental materials (mainly on the basis of results of static cascade tests, taking initial turbulence into account), gives a generalized correction for the influence of the Re number (Fig. 93) which also depends on the axial width of the stage. Quantitatively, the influence of Re on efficiency, according to Traupel, approximately coincides with the MEI experiments.

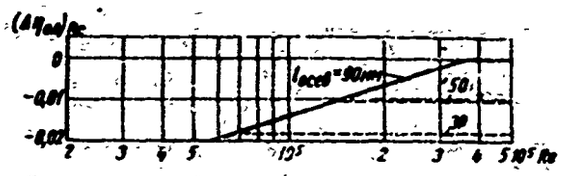

Fig. 93. Correction of efficiency, $\Delta\eta_{оп}$ depending upon Re number (according to W. Traupel).

The influence of the Re number on stage efficiency is also confirmed by certain other experiments, in particular the experiments of N. M. Markov [69], Slepik [132], and others. It should be noted, however, that certain research on the influence of Re on the efficiency of a stage was conducted incorrectly in principle (ε also changed simultaneously); therefore, the treatment of their results was erroneous.

In steam turbines, the influence of Re on efficiency, $\eta_{оп}$, practically shows up in low-pressure stages at approximately $p < 1$ bar. Inasmuch as these stages, as a rule, are equipped with twisted blading, this question is additionally discussed in Chapter VIII.

§ 19. INFLUENCE OF PERFORMANCE PARAMETERS ON DEGREE OF REACTION

The reaction of a stage with given geometric characteristics is influenced by all three performance parameters: velocity ratio $u/c_ф$, pressure ratio ε, and Reynolds number Re.

The influence of $u/c_ф$ on ρ was considered above theoretically in § 11, where it was indicated that within limits of the change of $u/c_ф$ (which is encountered for all turbine stages except regulating and last stages) the dependence $\rho = f(u/c_ф)$ is practically linear. Deviation from the linear law is possible only with very large changes of $u/c_ф$ and with an essential influence of steam leakages into open clearances, which decrease the absolute value of the reaction. This deviation is especially noticeable in a considerable negative reaction.

Although formulas (74)-(76) were derived on the assumption of a subcritical flow, they are applicable practically also for a flow with supersonic velocities in the nozzle cascade. At outlet velocities from the moving cascade which exceed the critical value, the dependence $\rho = f(u/c_ф)$ changes even qualitatively, namely,

when ε is constant, the reaction also remains constant, and when u = const, the reaction increases as u/c_{Φ} decreases. This occurs due to choking of the moving cascade.

The dependence $\rho = f(u/c_{\Phi})$ is explained by the following factors:

a) change of the relative magnitude of velocity w_1 and flow entrance angle β_1 into the moving cascade; an increase of u/c_{Φ} in this instance leads to a relative decrease of velocity w_1, which is usefully utilized in the moving cascade, as compared to velocity c_1 and the additional acceleration of flow in channels of the moving cascade, respectively; a change in the conditions of flow in the moving cascade also changes the magnitude of the flow rate coefficient μ_2, which shows up in the reaction of the stage:

b) change in the steam leakages, which are influenced by the velocity ratio u/c_{Φ}.

A determining factor is the change of magnitude and direction of velocity w_1; therefore, the theoretical formulas, derived on the basis of only one change of w_1 in most cases give a good coincidence with the experiment.

Figure 94 shows the dependence of the reaction of an MEI КД-2-2А stage (l_1 = = 48 mm, d/l_2 = 7.7; F_2/F_1 = 1.44) on u/c_{Φ} with a small heat drop (ε = 0.7). As can be seen from the experimental graph, even at a considerable magnitude of negative reaction, the dependence $\rho = f(u/c_{\Phi})$ remains practically linear, which is determined by the small influence of leakages (for large cascade heights).

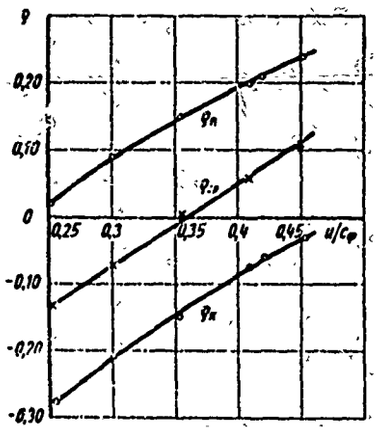

Fig. 94. Dependence of the reaction of a stage, ρ, on the velocity ratio, u/c_{Φ}, according to MEI experiments conducted for ε = 0.7.

The reaction of a stage sometimes implies the ratio of the available heat drop of the moving cascade h_{02} to the total heat drop of the stage h_0, which is calculated on the basis of the static parameters before the stage (and not the parameters of stagnant flow). Let us designate this reaction by

$$\rho^* = \frac{h_{02}}{h_0}. \qquad (107)$$

In experiments on <u>single-stage</u> experimental turbines, the stagnation parameters are measured before the stage; therefore the reaction is determined by these parameters:

$$\rho = \frac{h_{02}}{h_0 + c_0^2/2}. \qquad (108)$$

The given values of ρ in this book and in other literature are presented on the basis of the results of tests made with experimental single-wheel turbines. If necessary, they may be recalculated by means of the following formula:

$$\rho^* = \rho\left[\frac{1}{1-(c_a/c_\phi)^2}\right] \approx$$
$$\approx \rho(1+\sin^2\alpha_1). \qquad (109)$$

In certain cases, for instance in experiments with single-stage turbines, the static pressure between the stages is determined, and consequently, the reaction ρ^*. For reaction turbines and, in general, for stages with large angle α_1, the recalculation ρ should be performed more carefully.

The mean reaction of a stage, ρ_{cp}, may be found experimentally by the following three methods:

1. It is assumed that the mean reaction is the reaction on the mid-diameter, which is determined a direct measurement of the static pressure in the clearance between cascades on the mid-diameter. However, this procedure is complicated and is rarely applied because of the difficulties in the measurements, especially in steam turbines. Since the reaction varies with respect to pitch (see § 14), there are probable errors in the determination of the mean (with respect to pitch) static pressure in a clearance in a similar measurement.

2. The reaction is changed by averaging with respect to pitch on the root and peripheral diameters, and then it is arithmetically averaged

$$\rho_{cp} = \frac{\rho_\text{п} + \rho_\text{к}}{2}. \qquad (110)$$

In an overwhelming majority of cases this method is applied. As shown by numerous experiments with moderate l_1 (large d/l) and the absence of leakages, the reaction along the blade height varies approximately linearly (see curve 2 in Fig. 123) and the same method is employed to calculate the reaction on the mid-diameter. However, this method has the following deficiencies:

a) the reaction on the mid-diameter in general is not equal to the mean reaction, since the flow rate of steam through the elementary steams is various. Thus, the steam flow through the stage is not equal to the steam flow determined according to the mean parameters.

$$G \neq G_{cp},$$

where

$$G = 2\pi \int_{r_\text{к}}^{r_\text{п}} \mu_1 \frac{c_{1t}}{v_{1t}} \sin\alpha_1 \, r\,dr, \qquad (111)$$

$$G_{cp} = 2\,\mu_{1cp}\frac{c_{u\,cp}}{v_{1cp}}r_{cp}l_1; \tag{112}$$

the difference of $\frac{G - G_{cp}}{G}$ will be greater, the smaller d/l is and the larger ε is; for a critical flow, this difference will be insignificantly small (see § 45);

b) for flow into a clearance (suction or leakage) the linearity of the law of $\rho = f(r)$ is disturbed;

c) for small d/l the dependence $\rho = f(r)$ also is not linear (see below, Chapters VII and VIII).

3. The reaction on the mid-diameter of a wheel is determined by the integral characteristics of the stage. For this it is necessary to know the relative blade efficiency $\eta_{0л}$, the available heat drop of the stage h_0 (with respect to stagnation parameters), the flow rate through the moving cascade G_2, the areas of the cascades, F_2 and F_1, the flow angles on the mid-diameter, α_1 and β_2 (usually for subcritical flow, the effective angles $\alpha_{1\ эф}$ and $\beta_{2\ эф}$), the peripheral velocity on the mid-diameter u_{cp}, and the specific volume at the moving cascade exit, v_2.

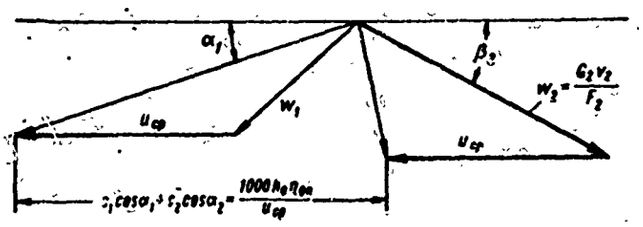

Fig. 95. Velocity triangles for the determination of the mean reaction of a stage according to integral characteristics.

The specific volume v_2 is computed according to the pressure behind the stage, p_2, and the efficiency, $\eta^{x}_{0л}$. Using a simplified continuity equation, we find $w_2 = G_2 v_2/F_2$; for β_2, w_2 and u_{cp} we construct an outlet velocity triangle (Fig. 95); we plot the quantity

$$c_1\cos\alpha_1 + c_2\cos\alpha_2 = \frac{1000 h_0 \eta_{0л}}{u_{cp}}$$

and construct the outlet velocity triangle. Then

$$1 - \rho = \frac{1}{1 + \left(\frac{\varphi}{\psi}\right)^2\left(\frac{w_2}{c_1}\right)^2 - \frac{1}{\psi^2}\left(\frac{w_1}{c_1}\right)^2}, \tag{113}$$

where w_2/c_1 and w_1/c_1 are taken from the velocity triangles. The velocity coefficients in the first approximation are selected arbitrarily. After computing ρ, the efficiency is found.

$$\eta_{0л} = 1 - (1-\varphi^2)(1-\rho) - \left(\frac{w_2}{c_ф}\right)^2\left(\frac{1}{\psi^2}-1\right) - \left(\frac{c_2}{c_ф}\right)^2. \qquad (114)$$

If $\eta_{0л}$ in formula (114) noticeably differs from the measured $\eta_{0л}$ efficiency, other values of φ and ψ should be given. Even a gross error in the velocity coefficients, especially in ψ, very insignificantly changes the reaction that was calculated in this manner.

The reaction must be determined in this way when clearance measurements, a check of these measurements, and especially the calculation of the flow rate coefficients for nozzle cascades according to stage tests are not available.

If the mean reaction of a stage gives the general characteristic of the stage's performance and is required for its averaged calculation, then for an analysis of the stage's performance and its exact calculation it is very important to know the magnitude of the reaction in the root and peripheral sections. The change of the peripheral $\rho_п$ and root reaction $\rho_к$ from $u/c_ф$ (in the absence of leakages) is governed by the same law as the change of the mean reaction, i.e., it will be practically linear. This is illustrated by the graph in Fig. 94 for a stage with $d/l_2 = 7.7$ and $F_2/F_1 = 1.44$.

It is interesting to note that in the entire zone of change of $u/c_ф$ from 0.25 to 0.45 the reaction at the periphery remained positive and the reaction at the root remained negative, attaining the value of $\rho_к = -0.28$ when $u/c_ф = 0.25$. There were no steam leakages in the root clearances in the experiments.

The pressure drop, i.e., $\Delta\rho = \rho_п - \rho_к$, along the height depends very little on $u/c_ф$ and ε. If the stage is designed with a large reaction at the vertex (with small F_2/F_1), an increase of $u/c_ф$ leads to a small increase of gas leakage in the peripheral clearance; the difference of $\Delta\rho$ will then drop somewhat. Figure 96 shows the dependence of $\Delta\rho$ for stages КД-2-3А and КД-1-3А, which have the same $d/l_2 = 7.7$, but different area ratios, and consequently, different ρ. In the first stage ρ is greater; therefore, $\Delta\rho$ drops; and in the second stage, $\Delta\rho \approx$ const.

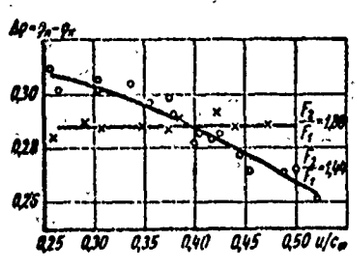

Fig. 96. Dependence of the difference in the reaction along the blade height, $\Delta\rho = \rho_п - \rho_к$, on the velocity ratio $u/c_ф$ for stage КД-2-3А ($F_2/F_1 = 1.44$) and КД-1-3А ($F_2/F_1 = 1.88$) (MEI experiments).

The influence of the pressure ratio in the stage, $\varepsilon = p_2/p_0$, on the reaction is connected with the influence of the M number on the velocity and flow

rate coefficients and the influence of the specific volume ratio v_2/v_1 behind the cascades. Figure 97 contains a graph that illustrates the influence of ε on ρ for different velocity ratios u/c_Φ. It is clear from the graph that the smaller ε is, the greater the reaction, which definitely must be considered in turbine calculations. For a sufficiently accurate calculation of the change of $\rho = f(\varepsilon)$, it is necessary to know the aerodynamic characteristics of the stage, including the change of the flow rate coefficients of the cascades, the clearances in the stage, and so forth.

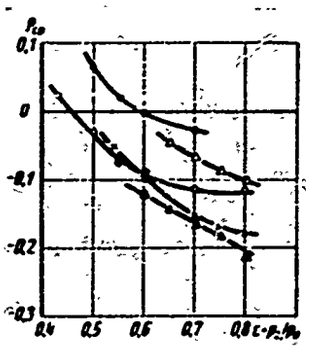

Fig. 97. Dependence of mean reaction on ε according to MEI experiments for the following stages:

КД-1-2А, $l_1 = 48$ мм, $u/c_\Phi = 0,3$ — Δ — Δ — Δ & $u/c_\Phi = 0,4$ — □ — □ — □; КД-2-2А, $l_1 = 25$ мм, $u/c_\Phi = 0,3$ ○ — ○ — ○ and $u/c_\Phi = 0,4$ — ● — ●: КД-2-3А, $l_1 = 48$ мм, $u/c_\Phi = 0,3$ — × — × — ×.

For a rough estimate of the influence of ε on the reaction it is possible to use the following formula:

$$\Delta\rho_\varepsilon = \rho - (\rho)_{\varepsilon=0,75} = \left[1 - \left(\frac{\varepsilon}{0,75}\right)^{\frac{k-1}{k}}\right]\left(\frac{l_1}{25}\right)^{1/2}, \qquad (115)$$

where l_1 is the height of the nozzle cascade in mm. The influence of l_1 is evident in the leakages, which decrease the growth of the reaction upon transition to larger heat drops. Figure 98 shows a comparison of the experiments and calculation by formula (115) for $l_1 = 25$ and 48 mm.

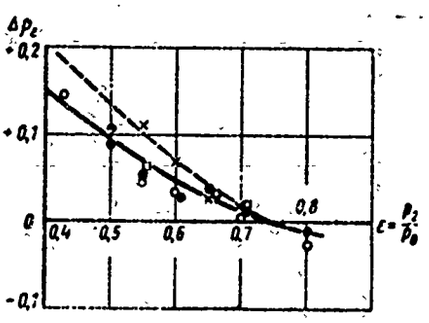

Fig. 98. Change of mean reaction of stage, $\Delta\rho_\varepsilon$, depending upon ε for various blade heights l_1: calculated data according to formula (115) —— solid line for $l_1 = 25$ mm; – – – – dotted line $l_1 = 48$ mm; experimental data: points ●, ○, ◐ — $l_1 = 25$ мм and ×, ◇ — $l_1 = 48$ мм.

The influence of Reynolds number on the reaction is caused by a change of the velocity and flow rate coefficients of the cascades of the stage. In many experiments with stages, a change of the reaction at constant ε and u/c_Φ and variable pressure was found, i.e., at variable Re number. Usually the influence of Re is detected at $Re < 5 \cdot 10^5$ and low M numbers. Both $Re_{\text{автом}}$ and the quantitative change of the reaction depend on a number of factors, including the separation of flow in the cascades to a considerable extent. Experiments show that the reaction increases as the Re number decreases. This is explained by the fact that the Re number for a moving cascade is usually less than that for a nozzle cascade, and separation of flow is also possibly faster in a moving cascade. Thus, the flow rate coefficient of the moving cascade varies more than for the

nozzle cascade. The influence of the Re number on the flow rate characteristics is examined in greater detail in § 20.

The influence of Re number on the reaction, ρ, may be seen from the graph in Fig. 99 for a КД-2-3А stage at $\varepsilon = 0.75 = \text{const}$. At velocity ratio $u/c_\Phi = 0.45$, a decrease of Re_{c_1} from $4.5 \cdot 10^5$ to $2.5 \cdot 10^5$ (which corresponds to a change of Re_{w_2} from $1.3 \cdot 10^5$ to $0.7 \cdot 10^5$) leads to a growth of the stage reaction from -0.01 to +0.05. At the same ε, but other u/c_Φ and with the same decrease of the Re number, the change of the reaction amounts to $\Delta_\rho = 0.05$ to 0.08%.

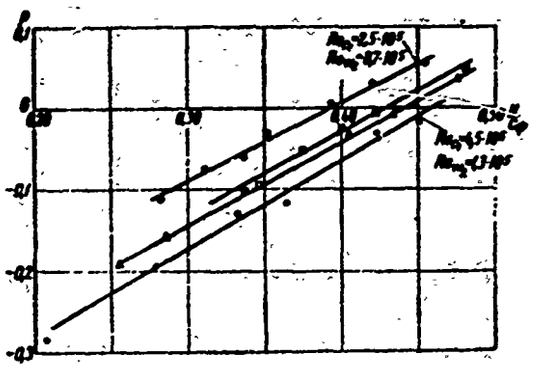

Fig. 99. Influence of Re number on reaction of КД-2-3А stage ($d/l_2 = 7.7$, $F_2/F_1 = 1.55$), $\varepsilon = 0.75 = \text{const}$ (MEI experiments).

§ 20. FLOW RATE CHARACTERISTICS OF A STAGE

During the calculation of a turbine that has just been designed, or when checking the calculation of an existing one, it is important to exactly determine the flow rate of the working medium through a stage. An error in computing the flow rate of the working medium through a stage can lead to the incorrect selection of stage dimensions and a redistribution of pressures along the stages. For the first (regulating) stage, an incorrect calculation of the flow rate can even affect the rated power of a turbine.

As an example, we shall illustrate the case dealing with the modernization of the ВР-25-1 turbine [88]. An error in the determination of the flow areas of the nozzle cascades of unregulated stages led to the fact that the pressure in the changer of the regulating stage, instead of the calculated value of 61.3 bar, was equal to 56.1 bar. This caused an increase in the heat drop to a less economic regulating stage and additional losses due to throttling. Analogous errors were allowed during the designing of certain gas turbines.

In practice, scientific organizations and plants employ various flow rate characteristics for stages. LMZ, NZL, and several TsKTI laboratories determine the flow rate coefficient of a stage during stage tests

$$\mu_{cm} = \frac{G}{F_1 c_\Phi / v_2}, \tag{116}$$

i.e., the actual flow rate through a stage with respect to the theoretical flow rate through the nozzle cascade, calculated according to the total heat drop of the stage ($c_{\Phi} = \sqrt{2h_0 + c_0^2}$, v_2 – behind the moving cascade). Within the limits of the accuracy of the assumption that ρ_{cp} is equal to the reaction averaged with respect to the flow rate (see § 19) when $\rho_{cp} = 0$, the flow rate coefficients of the stage and nozzle cascade coincide.

The MEI processed the results of experiments with an experimental turbine, depending on $\mu q = f(x_{\Phi}, \varepsilon$, and other physical and geometrical parameters). Here μq is the ratio of the actual flow rate through the stage to the theoretical critical flow rate through the nozzle cascade

$$\mu q = \frac{G}{G_{кр}} = \frac{G}{B \cdot F_1 \sqrt{p_0/v_0}} \qquad (117)$$

(B is a coefficient that depends on the isentropic exponent k; for superheated steam, B = 0.661; for air, B = 0.674; for dry saturated steam, B = 0.63, p_0[N/m^2], v_0[m^3/kg], G[kg/sec], and F_1[m^2].

An advantage of the characteristic μq is its independence from the accuracy of measurement of pressure behind the stage. Very convenient for monitoring also is the fact that, independently of the stage's reaction, q = 1 for a critical flow and $\mu q = \mu_1$ is the flow rate coefficient of the nozzle cascade. The quantities $\mu_{ст}$ and μq are recomputed by the following formula:

$$\mu_{ст} = \frac{\mu q}{q},$$

where $q = f(\varepsilon)$ is determined by tables.

In a number of cases for aircraft gas turbines, and also at TsKTI, A. M. Zavadovskiy selected c_{2a}/u as the flow rate characteristic, which is given depending upon u/c_{Φ} (shown in Fig. 100). The characteristic is of no use to us, especially for impulse stages, since it first requires the determination of the dimensions of the moving cascade, and then the nozzle cascade. As it is known, in impulse stages the influence of the area of the moving cascade on the steam flow through a stage (or at a given flow rate for pressure before a stage) is much less than the influence of the area of the nozzle cascade. Actually, a change of the area F_1 causes a change of the reaction. When $\varepsilon_1 = p_1/p_0 < \varepsilon_*$, a change of the reaction does not affect the flow of steam through the stage; consequently, the change in the flow rate of steam will be proportional to the change of the area F_1. For a subcritical flow, due to a change of the reaction, the steam flow rate will change somewhat less than under critical conditions.

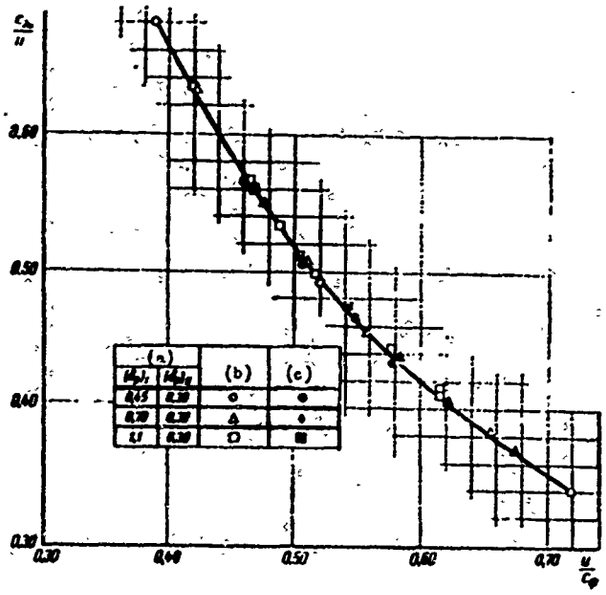

Fig. 100. Flow rate characteristic $c_{2a}/u = f(u/c_\Phi)$ (TsKTI experiments).
KEY: (a) clearances in mm; (b) single stage; (c) stage operating in a set.

Thus, for instance, if in a stage with $\varepsilon = 0.8$ and $\rho = 0.05$, the area F_1 is decreased by 3%, the reaction will decrease to 0.03. Consequently, $\varepsilon_1 = p_1/p_0$, instead of 0.810, will decrease to 0.806. Then the flow rate of the working medium will decrease not by 3%, but only by 2.4%.

If, however, the area F_2 is decreased by 3%, the reaction will increase to 0.07, and the flow rate of the working medium through the stage will decrease by a total of 0.5%. The given figures show how important it is to exactly determine the area of the nozzle cascade, in particular.

During tests in turbines the quantity c_{2a} should be calculated according to the flow rate of the working medium through the moving cascade, which requires a special estimate or determination of the leakages in the clearances. This naturally lowers the accuracy of the calculation of c_{2a}/u. We do not know of any experiments on the influence of the pressure ratio ε on c_{2a}/u, and also a number of other factors. Proceeding from this, it is impossible to say that the calculation of the dimensions of a stage with respect to c_{2a}/u is convenient.

Let us return to the flow rate characteristic μq. The value of μq depends on:

a) the pressure ratio in the stage, ε;

b) the reaction of the stage, ρ;

c) the flow rate coefficient of the particular nozzle cascade, μ_1.

For stages with large d/l ratios it is possible to select a mean reaction for the calculation, and for small d/l it is necessary to consider the change of the reaction and the flow rate along the height. In the last case, regardless of whether the stage has cylindrical blading or is twisted according to some law, the nozzle cascade should be divided into several sections along the height and the total flow rate G should be found, taking into account the change of the flow area of each section and the reaction through the sections [see formula (111)]. If there are data on the change of the flow rate coefficient of a cascade with respect to height, various values of μ_1 should be considered.

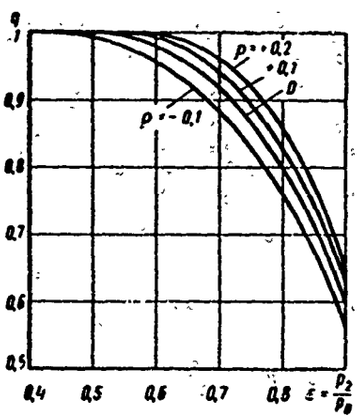

Fig. 101. Dependence of relative steam flow q through a stage on $\varepsilon = p_2/p_0$ and the reaction ρ.

If we consider that $\mu_1 = 1 = \text{const}$, then $q = f(\varepsilon, \rho)$. Figure 101 shows a graph of $q = f(\varepsilon)$ for four values of the reaction ρ_{cp}.

For a critical flow, and also when $\rho = 0$ (with the reliable determination of the reaction), the flow rate coefficient of the stage and the flow rate coefficient of the nozzle cascade coincide. In this way, also for μ_{cT} or μq, knowing ε and ρ, we can find μ_1, i.e., the necessary quantity for the determination of the steam flow rate of the dimensions of the cascade.

Investigations show a dependence of the flow rate coefficient μ_1 on three basic quantities: the cascade dimensions (mainly on l_1/b_1), the mean pressure ratio $\varepsilon_1 = p_1/p_0$ (or M_{c_1}), and the Reynolds number $Re_{c_1} = b_1 c_{1t}/\nu_1$.

The influence of the cascade dimensions on μ_1 is discussed in §§ 9 and 21. According to tests of stages with contemporary cascades, usually in the transition from low velocities to critical ones, the flow rate coefficient μ_1 increases by approximately 0.5 to 1.5%, which is connected with the improvement of the flow around the cascades at large pressure gradients. Although in a supersonic flow the losses in ordinary cascades are increased, the flow rate coefficient does not change or it even increases somewhat [11]. The cause of this is the fact that this coefficient has practically no effect on the structure of the flow and the losses in the slanting shear and behind the cascade, and in the convergent part of the channel the conditional thickness of displacement of the boundary layer, which also determines the value of μ, decreases somewhat.

The influence of the Reynolds number was investigated at MEI in the process of static steam tests of an actual diaphragm. The results of these tests are shown in Fig. 102 for a welded diaphragm with a TC-2A cascade (l_1 = 48 mm, d = 400 mm). The experiments were conducted at ε = 0.75 to 0.8 = const. As should have been expected, outside of the self-similar zone, a lowering of Re, which leads to an increase in the thickness of the displacement, decreases the flow rate coefficient μ_1.

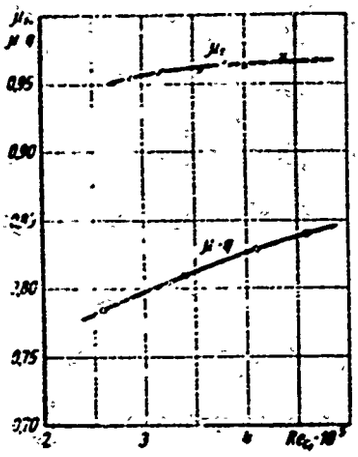

Fig. 102. Influence of $Re_{c_1} = \frac{b_1 c_{1t}}{\nu_1}$ on the flow rate coefficient μ_1 of the nozzle cascade of an actual welded diaphragm and on the relative flow rate of steam through the stage μq.

Inasmuch as the reaction of the stage depends on ε_1, u/c_Φ, and Re, and $\mu_1 = f(\varepsilon, Re)$, the magnitude of the relative flow rate through the stage, μq, comprises the following function:

$$\mu q = f\left(\varepsilon, \frac{u}{c_\Phi}, Re\right).$$

The smaller ε is, the greater the flow rate of gas through the stage; however, if $\varepsilon_1 = p_1/p_0$ in the nozzle cascade is below critical, a further lowering of ε practically will not lead to a change of the flow rate.

An increase of u/c_Φ simultaneously signifies a growth of the reaction of the stage, and consequently, a reduction of the flow rate. Figure 103 illustrates the dependence $\mu q = f(x_\Phi, \varepsilon)$, for stage КД-1-1А ($l_1$ = 25 mm, F_2/F_1 = 1.66). Figure 104 shows the influence of ε on the flow rate through the stage. The curve of the dependence of the flow rate through the stage on $\varepsilon_1 = p_1/p_0$ (at x_Φ = const) and the curve of the theoretical flow rate, q_t, multiplied by μ_1 = 0.98 = const, are plotted on this graph. The difference in the flow of these curves is determined by the reaction and the influence of ε on μ_1.

For a КД-2-3А stage (l_1 = 48 mm, d = 400 mm), when ε = 0.75 and x_Φ = 0.4, Fig. 102 shows how μq changes depending on Re_{c_1}. The influence of the Re number on the reaction for the same stage is represented in Fig. 99.

The change of the flow rate coefficient of the stage, μ_{CT}, from $x_\Phi = u/c_\Phi$ and ε depends on the change of the reaction. An example of such a graph of $\mu_{CT} = f(u/c_\Phi)$ is shown in Fig. 105 for two LMZ stages with the ratio d/l_1 = 14.7 and 9.5; it is constructed according to the results of tests in an LMZ experimental air turbine with $M_1 \approx 0.47$.

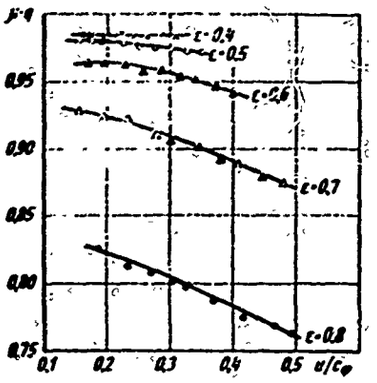

Fig. 103. Dependence of relative steam flow rate through a stage on μq from $u/c_{ф}$ and ε (MEI experiments).

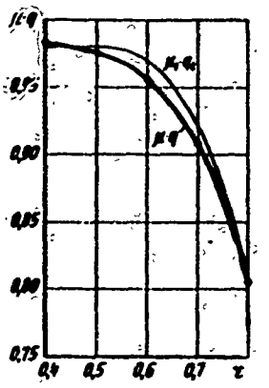

Fig. 104. Change of μq and $\mu_1 q_t$ depending upon ε for $u/c_{ф}$ = = 0.4, μ_1 = 0.98 = = const (MEI experiments).

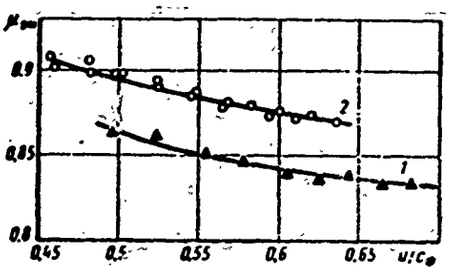

Fig. 105. Flow rate coefficient of a stage, $\mu_{ст}$, depending upon $u/c_{ф}$ for a typical LMZ stage: 1 – d/l_1 = 9.5; F_2/F_1 = 1.42 –▲–▲–▲; 2 – d/l_1 = = 14.7; F_2/F_1 = 1.75 –O–O–O.

The change of the flow rate through the stage depending upon ε and $u/c_{ф}$ may be analyzed by formula [83] for constant initial parameters without taking leakages into account

$$\frac{G'}{G} = \frac{\mu_1'}{\mu_1}\sqrt{\frac{(1-\varepsilon'^a)-a(1-\varepsilon')^2}{(1-\varepsilon^a)-a(1-\varepsilon)^2}}\sqrt{1-0{,}4\frac{\Delta x_{ф}}{x_{ф}}}, \tag{118}$$

where $a = \frac{\varepsilon_*}{1-\varepsilon_*}$ for superheated steam a ≈ 1.2, for air a ≈ 1.12. This formula can be used only for a subcritical flow.

When the pressure ratio ε is constant, i.e., when ε' = ε, and consequently, when $h_0' = h_0$, disregarding the change of the flow rate coefficient of the nozzle cascade and considering a small influence of leakages,

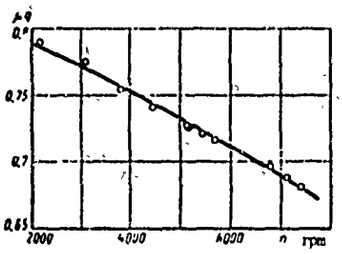

Fig. 106. Change of relative steam flow rate, μq, through stage КД-2-1А from speed n: according to MEI experiments. Calculated data according to formula (119) — solid curve, experimental data O – O – O.

$$\frac{G'}{G} \approx \sqrt{1-0{,}4\frac{\Delta x_{ф}}{x_{ф}}} = \sqrt{1-0{,}4\frac{\Delta n}{n}}. \tag{119}$$

Figure 106 shows the change of μq for a КД-2-1А stage (l_1 = 25 mm, d = 534 mm) at ε = 0.8 = const, on the basis of experiments in an MEI experimental steam turbine and by calculation with formula (119) (at $n_{расч}$ = 6500 rpm). As can be seen from the graph, the coincidence of the experimental and calculated data is satisfactory. It should be noted, however, that

for considerable steam leakages and, in particular, for large heat drops, when these leakages grow, formula (119) indicates a larger change of the flow rate than is actually the case.

§ 21. INFLUENCE OF GEOMETRIC PARAMETERS ON THE CHARACTERISTICS OF A STAGE

In the designing of a new turbine, and also for reconstruction, assembly, repair, and operation, it is necessary to know the influence of the basic geometric parameters of the stage on the efficiency, reaction, and flow rate coefficient.

The influence of cascades and their dimensions, such as $\bar{t}$, α_1, β_2, $\Delta_{кр}$, and others, on losses was considered in Chapter I. This paragraph discusses the influence of three basic geometric parameters on the performance of a stage: blade height l, diameter d, and ratio of areas F_2/F_1.

An increase of the absolute blade height, the other parameters being constant, including b = const and d = const, has a favorable effect on the economy of a stage within wide limits. The end losses in the nozzle and moving cascades and certain additional stage losses (losses due to steam leakage, losses connected with overlaps, and due to inaccuracies in manufacture) decrease. With a constant diameter d, an increase of l simultaneously signifies a decrease of d/l. As long as d/l is sufficiently great (with cylindrical blading, to $d/l > 6$ to 10) and the loss due to flare are insignificant, a growth of l leads to an increase in stage efficiency. However, with very large l, when an increase in height practically does not affect the end losses and other losses, a lowering of d/l can be especially unfavorable (see Chapters VII and IX).

The phenomena connected with flare, and especially the additional losses due to an off-design entrance angle in the upper and root sections of a moving cascade, lower the effectiveness of a stage. Although the difference of the reaction along the height increases as d/l decreases, the losses due to leakage decrease somewhat with constant diameter and clearances.

The influence of l on the efficiency of a stage to a significant extent is determined by the design and the manufacturing technology of the cascades and the cascades themselves. As it is known (see §§ 5 and 6), it is possible to specially create cascades having decreased end losses with low heights. In the first approximation for not very low heights, one may assume that the stage efficiency is inversely proportional to $1/l$.

Figure 107 shows the influence of the effect of blade height on efficiency for various stages. As already noted above, inasmuch as this influence depends on a

number of other geometric characteristics, we shall give a detailed description of the stages that were investigated.

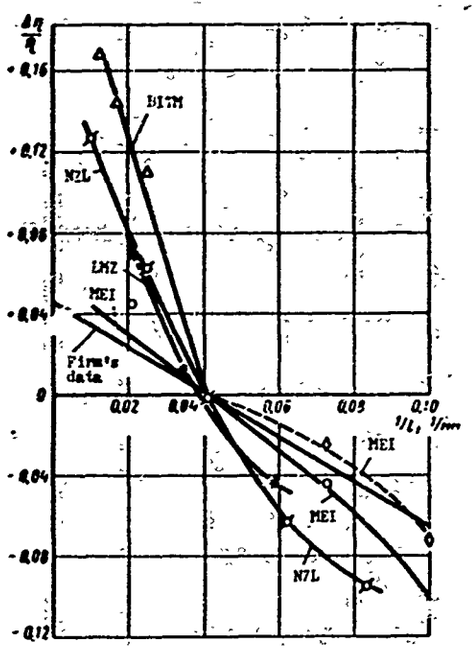

Fig. 107. The effect of blade height l_1 on the maximum efficiency of a stage: Δ — Δ — BITM experiments; ϕ — ϕ — NZL data; ** — LMZ experiments; O — O — MEI experiments; ◇ — ◇ — ◇ — MEI experiments (meridional profiling).

At BITM, during tests in an experimental air turbine with laboratory manufacture of cascades and nozzle chord $b_1 = 44.1$ mm, the efficiency for various heights was measured. Angle $\alpha_1 = 11^\circ 20'$ to $11^\circ 40'$ and $M_{c_1} = 0.3$. $Re_{c_1} = 2$ to $8 \cdot 10^5$. The stage diameter was 825 to 880 mm. The NZL data [48] were taken from a series of graphs for $\eta_{ол} = f(l_1, x_ф)$. The LMZ experiments were conducted with a typical stage at $b_1 = 58.9$ mm and diameter 420 to 450 mm; the stage efficiency was recalculated for "zero" leakages. The MEI experiments were conducted with actual welded diaphragms manufactured by KTZ for КД-2-2А stages with $b_1 = 51.5$ mm and diameter 400 mm. The MEI experiments were conducted with diaphragms of two types: with a cylindrical contour and meridional contraction around the periphery. Figure 107 also shows curves constructed with the firm's data. The strict straight line, upon reaching a height of 10 mm, indicates that calculated data were used here. It should be pointed out that a check of these stages in various experimental turbines, especially with low heights, did not confirm the firm's values of efficiency. From a consideration of the curves in Fig. 107 it is clear that the MEI stages have the least height effect (especially with meridional profiling). This is connected with the special selection of cascades having smaller end losses, and also a somewhat larger angle α_1.

The various effects of height on the efficiency of a stage, depending upon the technology and special profiling of the cascades when designing a turbine, can lead to a completely different machine design, i.e., they affect the selection of the stage diameter, the selection of admission, and even the selection of the initial parameters and the speed for turbines of low and medium power.

For instance, with a very large influence of l on efficiency, for turbines with low volume passage it is necessary to design the stages with small diameters, select

high speeds, increase the number of stages, and sometimes reject high initial steam parameters, thereby lowering the economy of the entire unit. It is known that in turbine-construction practice the minimum heights of nozzle cascades in turbines from 4 thousand kilowatts and more until recently amount to 14-15 mm, then, for instance, in DZhII turbine with a power of 125 thousand kilowatts at the Filo station, the nozzle blades of the first stage are 9.5 mm high. At the same time, turbines are encountered, when first unregulated stages have partial steam input even at considerable heights, l_1 = 25 to 35 mm.

MEI projects for meridional profiling of nozzle cascades and a certain change of the configuration of the moving cascade channels with low l/b ratios made it possible to essentially increase the effectiveness of the cascades and the stage efficiency. Figure 108 gives the dependence of the gain in efficiency, $\Delta\eta_{01}/\eta_{01}$, with meridional profiling for stages КД-2-2А, at F_2/F_1 = 1.6 to 1.7, $\alpha_{1\ эф}$ = 15°, and d = 400 mm, depending upon the height of the nozzle blades l_1. The nozzle chord amounted to 51.5 mm. Experiments were conducted at ε = 0.7 to 0.85. As can be seen from the graph, the gain from meridional profiling for a height of l_1 = 10 mm (l_1/b_1 = = 0.18) amounts to $\Delta\eta_{01}/\eta_{01}$ = 5.2%. At large heat drops, especially under supercritical operating conditions, the advantages of meridional profiling are exhibited to an even larger degree.

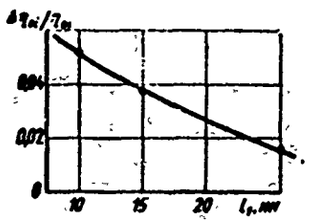

Fig. 108. Dependence of the gain in efficiency of a stage with meridional profiling on the height of the nozzle blade l_1.

For meridional profiling of a nozzle cascade it is important to correctly select the contraction configuration. Figure 109 gives efficiency graphs, η_{01}, for a КД-2-2А stage at d = 400 mm with various external meridional contours.

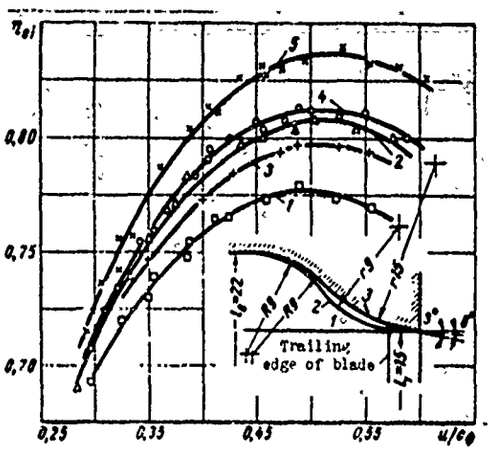

Fig. 109. Influence of meridional profiling (contraction configuration) on stage efficiency for various velocity ratios $u/c_ф$ (MEI experiments). Curves: 1, 2, and 3: l_1 = 15 mm; 4 and 5: l_1 = 25 mm; 1 and 4: cylindrical cascade contour; ε = 0.8-0.85; Re_1 ≈ ≈ $4\cdot10^5$.

As already noted earlier, meridional profiling not only increases the economy of a nozzle cascade, but also decreases the pressure drop (the difference in reactions) along the height of a stage. A decrease of $\Delta\rho = \rho_п - \rho_к$ makes it possible to essentially lower the reaction on the periphery

and thereby lower the losses due to leakage of steam over the blade shroud, i.e., a loss which is very great namely in stages with short blades.

Figure 110, for a КД-2-2А stage with nozzle heights l_1 = 15 and 25 mm (d = = 400 mm), shows the dependence of the reaction on the periphery $\rho_п$, the root reaction $\rho_к$, and the difference in the reactions $\Delta\rho = \rho_п - \rho_к$, on $x_ф$. Stage tests were conducted with nozzle cascades having the usual cylindrical contour with contraction.

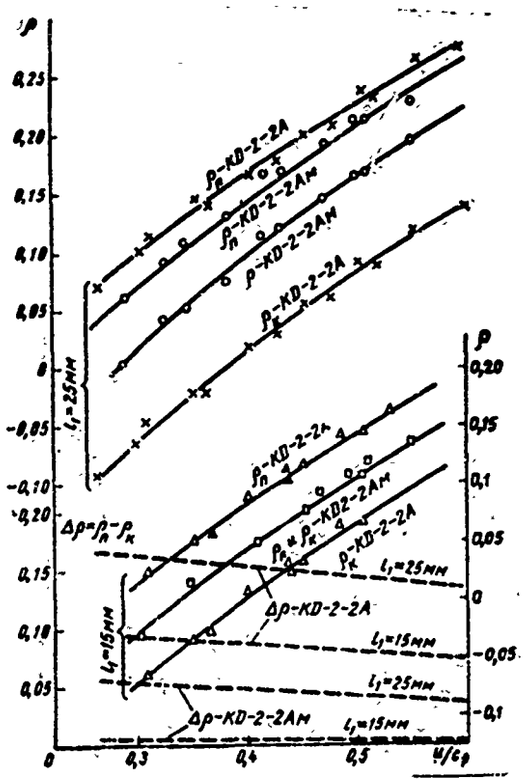

Fig. 110. Dependence of reactions on periphery $\rho_п$, at the root $\rho_к$, and the difference $\Delta\rho = \rho_п - \rho_к$, on the velocity ratio $x_ф = u/c_ф$ for a КД-2-2А stage (without meridional profiling) and a КД-2-2АМ stage (with meridional profiling (MEI experiments).

For a stage with a height of 25 mm the difference in the reactions upon transition to meridional profiling at $x_ф$ = 0.45 was lowered from 0.15 to 0.095, and for l_1 = 15 mm, from 0.08 to 0.005, respectively. Cascades that are specially profiled for low heights make it possible to employ very low heights of up to 10 to 8 mm with sufficiently high quality and high accuracy of manufacture in turbine constructions; in a number of cases this makes it possible to profitably reject partial steam input. Based on MEI recommendations that were confirmed by its own experiments, the Kaluga Turbine Plant is sucessfully employing stages with low heights.

Blade height influences not only the economy of a stage, but also the magnitude of the optimum velocity ratio $u/c_ф$. This circumstance is connected mainly with the large leakages in stages with low blade height. Approximate generalized data on the influence of l_1 on $x_{ф опт}$ are shown in Fig. 88.

Of the geometric parameters, only the cascade height practically influences the flow rate coefficient. The experiments of G. A. Filippov, conducted at MEI with stage of different height l_1/b_1, are shown in Fig. 111. The experiments were set up in an MEI experimental steam turbine with a КД-2-2А stage at ε = 0.8. Stages

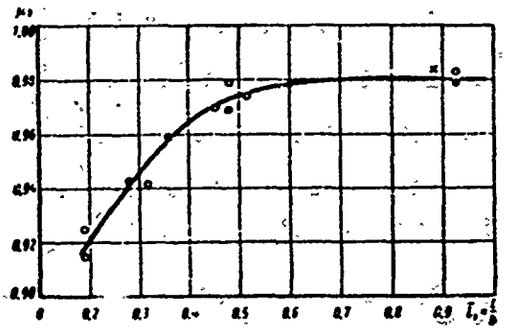

Fig. 111. Change of flow rate coefficient of nozzle cascade, μ_1, depending on l/b ratio under various conditions of tests conducted at MEI: x – x – static tests; experiments in turbine; O – O – at b = 51.5 mm; ● – ● – at b = 41.5 mm.

were investigated with d = 400 mm and b_1 = 51.5 mm, with welded diaphragms without special meridional profiling (one experimental point refers to b_1 = 41.5 mm). The decrease of the flow rate coefficient in diaphragms with low cascade height is explained by the large boundary layer effect on the bounding walls. The experiments of M. F. Fedorov at KhPI with a weighing installation [114] give approximately the same quantitative picture of the effect of height on μ_1.

The influence of diameter on the economy of a stage at present has not been investigated sufficiently. Attempts are being made to create formulas that consider this influence. According to a firm's data, the change of efficiency with a deviation of the diameter from d = 1 m is calculated by the following formula:

$$\Delta\eta/\eta = 0{,}075\,(1{,}0 - d), \tag{120}$$

where d is the stage diameter in m. This formula is applicable for d = 0.6 to 1.0 m.

G. A. Zal'f and V. V. Zvyagintsev [48] propose an analogous formula:

$$\Delta\eta = 0{,}05\,\frac{u}{c_\phi}\,(1 - d), \tag{120a}$$

where d is the stage diameter in m.

Other parameters being constant, including l = const and b = const, the influence of diameter on the economy of a stage is exhibited through the flare, i.e., through the ratio of the diameter to the blade height, d/l, and, due to the double curvature of the channel, especially in the root portion of the cascade.

The ratio of stage diameters to blade height, d/l, is one of the most important characteristics of a stage. In comtemporary turbines, d/l varies in very wide limits from 100 to 2.4. The influence of d/l on stage performance is determined by the change of cascade characteristics, the reaction, and the peripheral velocity along the height.

For a stage with cylindrical blading, without taking leakages into account, the reaction of the stage can be calculated by an approximate formula [33]:

$$\varrho = \varrho_{cp} + 2\,(1 - \varrho_{cp})\,\varphi^2 \cos^2\alpha_1 \left(\frac{r}{r_{cp}} - 1\right). \tag{121}$$

The change of the reaction, depending upon height, will be found by the following formula:

$$\frac{\rho_п - \rho_к}{1-\rho_{ср}} = 4\varphi_{ср}^2 \cos^2\alpha_1 \frac{l}{d}, \tag{122}$$

where $\rho_п$ is the reaction on the periphery and $\rho_к$ is the root reaction.

Although formula (121) was derived for design conditions of stage performance, as shown by experiment, it is valid in a sufficiently wide range of variation of $u/c_ф$.

If we assume in first approximation that the angle α_1 does not change along the height, then at $(\varphi_{ср} \cos \alpha_1)^2 = 0.9$ we will obtain:

$$\frac{\rho_п - \rho_к}{1-\rho_{ср}} = 3{,}6 \cdot l/d. \tag{123}$$

Inasmuch as the mean reaction of the stage is usually selected in such a way so that $\rho_к \approx 0$ under design conditions, the formula for the reaction at the periphery will take on the following form (for design conditions)

$$\rho_п \approx \frac{3{,}6}{1{,}8 + d/l}. \tag{124}$$

Formulas (123) and (124) are graphically represented in Fig. 112.

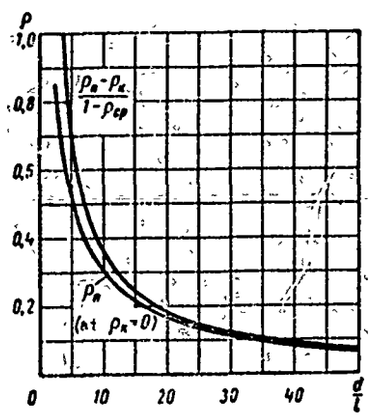

Fig. 112. Change of reaction depending upon d/l.

An essential change of the reaction along the height unfavorably shows up in cylindrical blading, since when designing a stage for a mean cross section, sufficiently large zones at the root and at the periphery are in off-design conditions, while nonoptimum velocities (M_{c_1} and M_{w_2}) and nonoptimum angles of entrance to the moving cascade β_1 are obtained. With cylindrical blading, along the cascade height there is a change in the relative pitch $\bar{t}$. The sections that are the farthest from the mean section – the root and the peripheral – at low d/l ratios can have nonoptimum values of relative pitch, which lowers the effectiveness of the cascades. A decrease of d/l, if the reaction of the stage is correctly selected and there is a small positive reaction in the root section leads to a growth of the reaction on the periphery (see Fig. 112) and a corresponding increase of leakages through the peripheral clearances. The loss due to this leakage, according to formula (91), is proportional to the following quantity (at l = const)

$$\sqrt{\frac{\varrho_a}{1-\varrho_{cp}}} = \sqrt{3{,}6\frac{l}{d}}$$

and consequently, upon transition from $d/l = 30$ to $d/l = 10$, it will increase by 1.7 times.

Ways of decreasing the negative influence of small d/l:

1. Twisting of profiles or, at least, twisting of the rotor blades.

2. Application of cascades that work stably in a wide range of variation of relative pitch, M numbers, and entrance angles for moving cascades.

3. Special methods of meridional profiling, which lower the pressure drop along the height and increase the effectiveness of the root sections of the nozzle cascade.

4. Correct selection of mean reaction of stage, which ensures the smallest sum of losses due to leakages in the root and peripheral clearances.

5. Good stage sealing.

6. Change of blade inclination.

The work done at plants and scientific organizations on the creation of new, aerodynamically improved, profile cascades made it possible at present not only to decrease the losses, but also to essentially increase the stability to changes in the conditions of flow. The graph of Fig. 113 show the results of LMZ experiments for moving cascades of the old and new types. From a consideration of the graph it is clear that profile losses not only decreased from 7.5 to 3%, but for a new cascade, in a wide range of deviation of the entrance angle, they are almost constant (with a change by 25°).

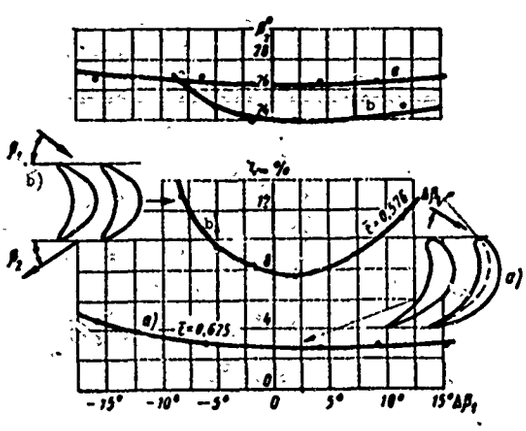

Fig. 113. Profile losses $\zeta_{пр}$ in a moving cascade: old b) and new a) type, depending upon change of entrance angle $\Delta\beta_1$ (LMZ experiments).

A formula that considers the losses due to flare was proposed by G. Flyugel' [115] in the following form:

$$\zeta_{d/l} = A\left(\frac{l}{d}\right)^2 \eta_{o.л}. \qquad (125)$$

G. Flyugel' and, after him, I. Amboz and others [130], propose to take coefficient A = 0.5 to 1. On the basis of MEI experiments conducted with stages

having contemporary blading (in particular, MEI blading), under subcritical conditions, it is possible to take $A = 0.25$.

V. Traupel [96], in considering the change of efficiency along the height for a square parabola with maximum efficiency in the middle section, arrives at the same formula as did Flyugel', but with the coefficient $A = 1/3$; for profiles of favorable shape, he proposes to decrease the losses due to flare by one third, i.e., he obtains the coefficient $A = 0.22$.

The influence of diameter, which is connected with an increase of end losses in a nozzle cascade due to double curvature, unfortunately, was not investigated; therefore, its estimate can be only very rough.

Thus, for instance, for a complete estimate of the influence of diameter, it is possible to assume the following estimate formula:

$$\zeta_d = \frac{0.25}{(d/l)^2} + K\frac{b_1/d}{(d/l)^2}, \tag{126}$$

where the coefficient K is taken from the results of experiments.

The third basic geometric parameter that determines the economy of a stage is the ratio of the discharge areas of the moving and nozzle cascades, F_2/F_1. The effect of F_2/F_1 on efficiency went almost unnoticed until not too long ago.*

Actually, the ratio of areas F_2/F_1 renders an essential influence on the performance of a stage, also on its reliability and, in particular, on the axial stress. For the given basic dimensions of a stage (d, l_1, α_1) the ratio F_2/F_1 determines the reaction of the stage, and consequently, the cascade losses, losses with the outlet velocity, and losses due to leakages.

The influence of the ratio of areas F_2/F_1 was investigated in experimental turbines by a number of scientific organizations. These investigations were conducted by two principally different methods. In air-driven turbines in particular, at BITM and LMZ, the angle of incidence α_y of the nozzle cascade was varied; the flow area F_1 of the nozzle cascade and, consequently, F_2/F_1 was then varied. Analogous tests can also be conducted with moving rotor blades or with a slight change of the pitch of the rotor blades.

---

*A number of authors still disregard this important stage characteristic. Thus, in certain special books devoted to the designing of steps of steam and gas turbines, the ratio F_2/F_1 is not considered as a determining stage parameter.

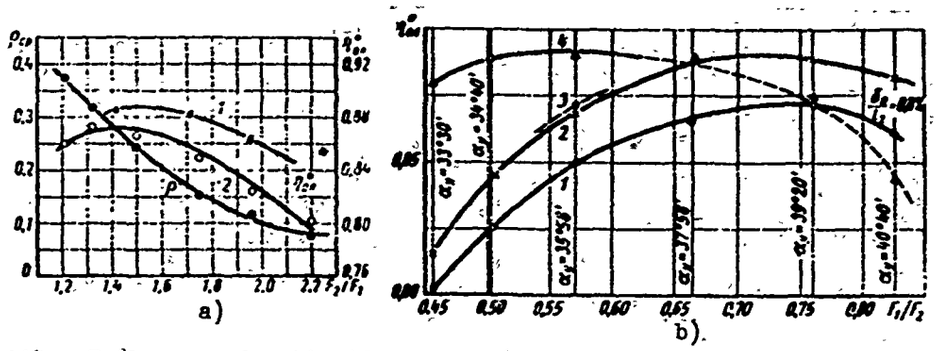

Fig. 114. Influence of ratio of areas F_2/F_1 on characteristics of typical stages of steam turbines according to LMZ experiments. a) dependence of $\eta_{0л}$ and $\rho_{ср}$ of typical LMZ stage on F_2/F_1 for various heights l_1 and ratios d/l_2; curves: 1 – l_1 = 47.1 mm and d/l_2 = 9; 2 – l_1 = 29.4 mm, d/l_2 = 13.3, and δ/l_2 = 0.8%; b) dependence of $\eta_{0л}$ for various values of α_y on ratio of areas F_1/F_2; curves: 1 – experiments with experimental air turbine; 2 – recalculation of curve 1 for "zero leakages"; 3 – calculation according to results of static tests of an annular nozzle cascade (for traverse in clearance) and a two-dimensional moving cascade. 4 – calculation according to results of static tests of two-dimensional cascades.

Figure 114a, represents an LMZ experimental graph of the influence of the ratio of areas F_2/F_1 for a typical LMZ stage at l_1 = 29.4 mm and l_1 = 47.1 mm. The area of the nozzle cascade was determined by the angle of incidence ($\alpha_y = 33^\circ30'$ to $40^\circ40'$). In this case naturally, the characteristics were varied, including the losses in the nozzle cascade, the entrance angle, and consequently, the losses in the moving cascade. The graph was constructed for the conditions of $u/c_ф$ = 0.54 and $M_1 \approx 0.45$. For this stage, at l_1 = 29.4 mm, there is a change of the mean stage reaction. It is absolutely obvious that such a method of investigating the influence on efficiency cannot be exhaustive. It is of interest only in two cases. First, if during design, for purposes of unification or reconstruction of a turbine, it is necessary to apply nonoptimal design ratios of cascades. Secondly, for checking the use of the results of static cascade tests during calculation and design of a stage. The latter was accomplished by A. O. Lopatitskiy and is illustrated for an LMZ stage with l_1 = 29.4 mm in Fig. 114b. Here, under the same experimental conditions, curve 1 represents the obtained experimental dependences of efficiency with the use of the outlet velocity $\eta^*_{0л}$; curve 2 shows the recalculation of this efficiency for "zero leakages"; curve 3 gives the results of the calculation of a stage according to data obtained from static tests of two-dimensional cascades. For F_2/F_1 = 1.5, efficiency was calculated according to the results of tests of an annular cascade (with traverse of flow in clearance). If for this ratio, F_2/F_1, the efficiency calculated according to the results of investigations of straight

cascades exceeds the experimental value by 2.3%, then with the use of the data of investigations of an annular cascade, the efficiency is 0.3% higher than according experiments in a turbine. This confirms the earlier point of view (see § 11) concerning the validity of extending the results of static investigations of annular cascades to the calculation of a stage (if losses in an annular moving cascade are considered, the efficiency by calculation and experiment practically coincides).

For one stage (l_1 = 47.1 mm) the LMZ conducted a series of tests in which the angles of incidence of the nozzle cascade and the pitch in the moving cascade were varied.

The degree of the reaction of the stage within the limits of each series of experiments with a constant angle of nozzle incidence α_y was varied by varying the pitch of the rotor blades in the limits in which it does not yet render a perceptible influence on losses (according to static investigations of two-dimensional cascades). The area of the moving cascade, F_2, was also varied. The results of these tests are shown in Fig. 115, where the efficiency of the stage is given depending upon the angle of nozzle incidence, α_y. As can be seen from a consideration of the graph, a change of the ratio of areas for given α_y practically did not influence efficiency, although the reaction of the stage, including the root reaction ρ_K, varied. Figure 115a shows that when α_y = const, a change of the root reaction ρ_K by 6 to 8% did not change the efficiency. However, the results of the LMZ experiments still cannot lead to the conclusion that the ratio of areas, including the reaction of the stage, does not affect economy. First, the change of the reaction within the limits of each series of experiments was not so large as to cause a noticeable redistribution of the heat drops through the cascades. Secondly, the investigations were conducted at low velocities; therefore, a change of the

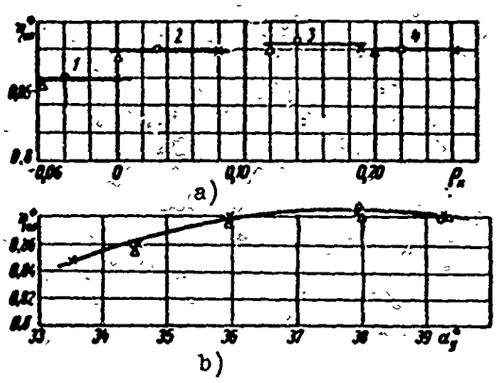

Fig. 115. Dependence of efficiency, $\eta^*_{0л}$, of a typical LMZ stage (l_1 = 47.1 mm, d/l_2 = 9) on: a) reaction ρ_K at blade root for various pitch of moving cascade, t_2; b) on angle of incidence of nozzles, α^o_y. Curves: 1 – $\alpha_y = 34^o30'$; 2 – $\alpha_y = 35^o58'$; 3 – $\alpha_y = 37^o58'$; 4 – $\alpha_y = 39^o20'$; Δ – t_2 = 0.816; O – t_2 = 0.757; * – $\bar{t}$ = 0.663 (LMZ experiments).

velocities M_{c_1} and M_{w_2} practically did not affect the cascade losses. Third, there were no leakages in the root clearance, and those in the peripheral clearance were insignificant; consequently, a change of the reaction in the given experiments did not affect the losses due to parasitic leakages in the stage. Finally, Fig. 115b gives the efficiency of a stage with the use of the outlet velocity $\eta^*_{0л}$. A change of the area of the moving cascade, which causes a corresponding change of the outlet velocity, did not change the efficiency $\eta^*_{0л}$.

It is interesting to note that a slight negative reaction of a stage in the absence of leakages does not give a perceptible lowering of efficiency of the stage; this coincides with the MEI experiments.

An investigation of the ratio of areas was conducted at MEI by another method. Several cascade combinations were tested in an experimental turbine. The cascade heights and chords, the diameter, and all clearances were kept constant. The cascades used for these combinations possessed approximately equal economy and each one had optimum relative pitch and angles of incidence. Therefore the difference in effectiveness of stages was mainly determined by the ratio of areas, F_2/F_1, which was changed for each combination. Thus, six combinations were investigated with l_1 = = 25 mm and d = 534 mm and four combinations with l_1 = 48 mm and d = 400 mm. The ratio of areas in these experiments varied in the range of $1.36 \leq F_2/F_1 \leq 2.01$. Stages with different F_2/F_1, as should have been expected, had various reactions. Figure 116 shows the dependence of mean reaction ρ_{cp} of a stage on the ratio of areas at $\varepsilon = 0.7$ and $x_ф = 0.45$. In spite of the difference in d/l and α_1, and the cascades themselves, the functional dependence $\rho_ф = f(F_2/F_1)$ was single-valued and almost linear. Even before a consideration of the graphs of the dependence of efficiency on F_2/F_1, it is clear from this curve, $\rho_{cp} = f(F_2/F_1)$, that very small F_2/F_1 ratios lead to considerable reactions, and consequently also to large losses due to leakage; conversely, very large F_2/F_1 ratio can cause a profound negative reaction which lowers efficiency with practically inevitable suction. For the given

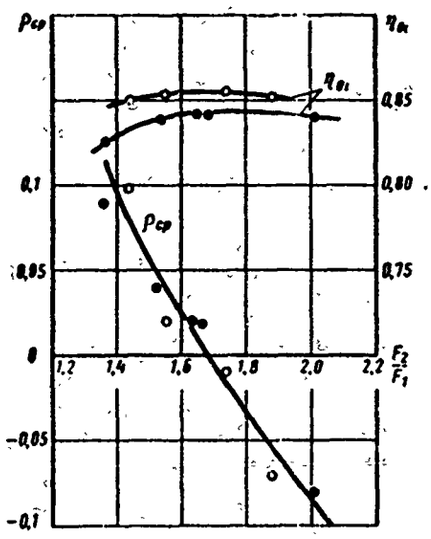

Fig. 116. Influence of ratio of areas F_2/F_1 on characteristics of stages, according to MEI experiments.
O–O–O–l_1 = 48 мм, d/l_1 = 7,7; ●–●–●–l = = 26 мм, d/l_1 = 19.

operating conditions, $\varepsilon = 0.7$, $x_{\Phi} = 0.45 \approx x_{\Phi опт}$, an analysis of the curve for $\rho_{cp} = f(F_2/F_1)$ can preliminarily predict the optimum ratios of areas, $F_2/F_1 = 1.5$ to 1.8. The relative internal efficiency of stages without the use of the outlet velocity, η_{01}, depending upon F_2/F_1, is shown in Fig. 116. Here the zone of optimum ratios of areas was expanded to $F_2/F_1 = 1.9$. It should be borne in mind that these experiments were conducted in the absence of leakage in the root clearance, when a slight negative reaction did not affect the economy of the stage. Actually, these leakages always take place in a turbine; therefore, the optimum ratio of areas, $F_2/F_1 = 1.4$ to 1.7, should be recommended, depending upon the relative size of the clearances through which leakage is possible. Figure 117a gives the value of efficiency, η_{01}, depending upon the mean reaction. This graph was reconstructed from the preceding one. Figure 117b, for the same stages, gives the dependence of efficiency on the root reaction. It is interesting to note that in the zone of the negative root reaction to $\rho_K \approx 0.1$, the efficiency of the stage is not lowered (there were no leakages in the root clearance) and, as compared to the positive reaction at the root, it is even increased somewhat. Thus, as in the LMZ experiments, a small negative reaction at the root does not lead to a lowering of economy. It is necessary, indeed, to stipulate that, first of all, this pertains not to all stages, and secondly, in the absence of suction in the root clearance. The high efficiency of the MEI stages with a negative reaction is not accidental. A calculation of the stages according to static tests of annular cascades sufficiently well confirmed the dependence $\eta_{01} = f \cdot (F_2/F_1) = f'(\rho)$ which was obtained in experiments with an experimental turbine. Indeed, with the same heat drop of the stage, the drop in the nozzle cascade, whose velocity coefficient φ is high, increases, and decreases in the moving cascade. At the same time, a certain lowering of the conditions of flow past the moving cascade with a negative reaction, in

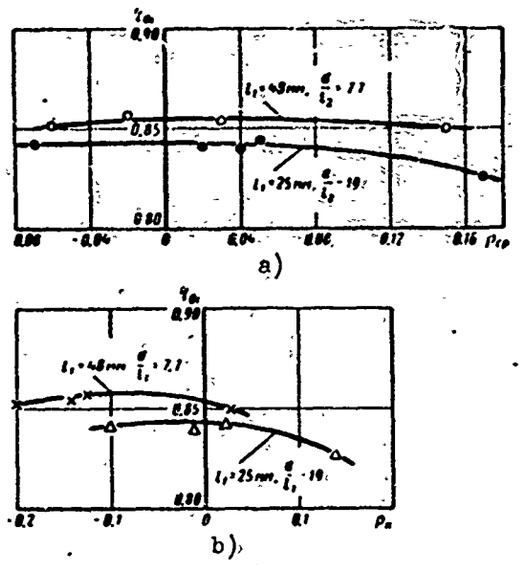

Fig. 117. Dependence of the efficiency η_{01} of a stage on the reaction, with $\varepsilon = 0.7$ and $u/c_{\Phi} = 0.45$ (according to MEI experiments): a) change of η_{01} from mean reaction ρ_{cp}; b) change of η_{01} from root reaction ρ_K (in the absence of leakages in root clearance).

connection with the insignificant influence of the velocity coefficient ψ on the efficiency of an impluse stage, does not play a large role. Furthermore, a decrease in the reaction at the root for the given d/l corresponded to a decrease in the reaction on the periphery and a reduction in steam leakage over the blade shroud. For moderate values of u/c_Φ, while angle α_2 is less than 90°, a lowering of the reaction, caused by the growth of F_2/F_1, leads to a certain decrease in losses with the outlet velocity.

Experiments at KhPI [112], conducted with stages having the ratio $d/l = 19$, showed that a negative reaction did not lead to the appearance of reverse leakages or separation of flow at the blade root, but rendered an influence only on the velocity coefficient in the moving cascade. The latter, depending upon the geometric characteristics of the stage, was decreased by 2 to 5%.

The change of F_2/F_1, and consequently, the reaction ρ_{cp}, changes the optimum velocity ratio. This is confirmed by experiments and calculations and is considered in a graph (see Fig. 88), where recommendations are given for the selection of an optimum velocity ratio, $x_{\Phi_{опт}}$.

§ 22. THE INFLUENCE OF CERTAIN DESIGN CHANGES ON THE CHARACTERISTICS OF A STAGE

Besides the basic geometric parameters considered in the preceding paragraph, the performance of a stage is also influenced by other changes in the design and dimensions of the stage. In the first place, they include a change in the dimensions of the cascades themselves (besides the height and diameter which were considered earlier), the clearances, and the overlaps.

When designing a stage, for purposes of unification and increasing the reliability, it may be necessary to change such geometric parameters of the cascades as relative pitch, trailing edge, and chord. By changing the relative pitch, the behavior of the change of the cascade losses and the velocity coefficients can be determined according to the cascade characteristics. The flow rate coefficient of a cascade depends very little on relative pitch. The change of the cascade losses from the thickness of the trailing edge can be found analogously. The thickness of the trailing edges has a weak effect on the flow rate coefficient, since the flow rate coefficient of a cascade depends on the flow inside the convergent part of the channel, and not on the process behind the cascade or even in the slanting shear. After the change of the cascade losses is determined with respect to the cascade characteristics, it is necessary to estimate how this will affect the efficiency of the entire stage.

For a determination of the efficiency of a stage without using the outlet velocity, we shall write the expression for efficiency in a known form [126]:

$$\eta_{oi} = 2x_\phi\left(\varphi\cos\alpha_1\sqrt{1-\varrho} + \psi\cos\beta_2 x_\phi\frac{w_u}{c_\phi} - x_\phi\right)$$

or

$$\eta_{oi} = 2x_\phi\sqrt{1-\varrho}\left(\varphi\cos\alpha_1 + \psi\cos\beta_2 x_\phi\frac{w_u}{c_u} - \frac{u}{c_u}\right). \tag{127}$$

Replacing

$$\frac{w_u}{c_u} \approx \frac{F_1}{F_2}\left(1+\varrho\frac{1-\varepsilon}{\varepsilon}\right), \tag{128}$$

we obtain

$$\eta_{oi} = 2x_\phi\sqrt{1-\varrho}\left[\varphi\cos\alpha_1 + \psi\cos\beta_2\frac{F_1}{F_2}\left(1+\varrho\frac{1-\varepsilon}{\varepsilon}\right) - \frac{x_\phi}{\sqrt{1-\varrho}}\right]. \tag{129}$$

If the velocity coefficient φ varied by the quantity $\Delta\varphi$, the efficiency of the stage will vary correspondingly by the quantity

$$(\Delta\eta_{oi})_\varphi = 2x_\phi\sqrt{1-\varrho}\cos\alpha_1\Delta\varphi; \tag{130}$$

analogously with a change of the velocity coefficient of the moving cascade ψ

$$(\Delta\eta_{oi})_\psi = 2x_\phi\sqrt{1-\varrho}\frac{F_1}{F_2}\cos\beta_2\left(1+\varrho\frac{1-\varepsilon}{\varepsilon}\right)\Delta\psi. \tag{131}$$

If the cascade chord is changed, the end losses, edge losses (with the same thickness of the trailing edge), and also the profile losses are also changed. For a two-dimensional cascade the influence of chord and the question of its optimum value is considered in § 10. It should be borne in mind that profile losses (without edge losses) will not vary only at Reynolds numbers exceeding Re_{ABTOM} and for a hydraulically smooth blade surface. Otherwise a decrease of chord will lead to an increase of profile losses.

The conclusions in § 10 can be used quantitatively only for two-dimensional cascades, and they can be applied qualitatively and approximately quantitatively to stages only with large diameters. For stages with small diameters, the cascade losses to a considerable extent will be determined by the losses due to the double curvature of the channel, and the transfer of the results of static tests of two-dimensional cascades can lead to incorrect conclusions for such a stage. Thus, in experiments [66] with a typical LMZ stage for three dimensions of blade heights and two values of chord of the nozzle cascade, results were obtained which contradict the experiments with two-dimensional cascades and coincide with the experiments with an annular cascade. These qualitative contradictions are explained, in the first place, by the small diameter of the stage: the root diameter is 400 mm for chords

that correspond to $d \approx 1$ m. A large coincidence with the results of static tests of two-dimensional cascades was obtained at BITM during tests of a series of stages with a root diameter of 800 mm.

Four heights and four chords of a nozzle cascade were investigated (maintaining absolute similarity), i.e., 16 variants; angle $\alpha_{1\,\text{ф}} \approx 11.5^{\circ}$; $M_1 \approx 0.3$; $Re_1 = (2 \text{ to } 8) \times 10^5$, and for small chords Re is lower than $Re_{\text{автом}}$. In spite of this, in all experiments with heights of 25 and 40 mm a decrease of chord had a favorable effect on efficiency. The results of these experiments are shown in Fig. 118. Unfortunately, there are still few experiments in experimental turbines and with annular cascades for studying the influence of chord. Moreover, the experiments at LMZ and BITM were not conducted with actual welded diaphragms, but with blades of special, more careful manufacture, where, naturally, the end losses are lower than in turbine diaphragms. The MEI [35] tested a КД-2-1А stage with $l_1 = 20$ mm and $d = 534$ mm with two diaphragms that differed only by the blade chord. The blade height did not vary; the remaining cascade dimensions varied in proportion to the chord in such a way that the profiles and the channels were similar. The narrow diaphragm, which was 45 mm wide with a blade width of 30.6 mm, had $l_1/b_1 = 0.39$; the wide diaphragm was 68 mm, 60 mm, and $l_1/b_1 = 0.20$, respectively. Investigations of these stages in an experimental turbine with $\varepsilon = 0.6$ and $Re = 6 \cdot 10^5$ showed that the maximum difference in efficiency reaches 2.5%; this corresponds to a calculation on the basis of static tests of the investigated diaphragms.

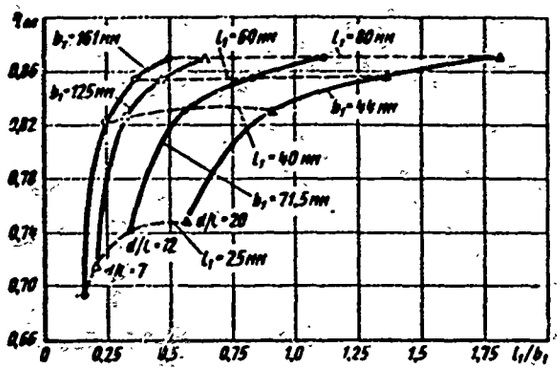

Fig. 118. Effect of chord of nozzle blades b_1 on economy of a stage, according to BITM experiments with similar profiles and channels [at $d_K = 800$ mm, $M_{c\,1} = 0.3$, $Re_{c\,1} = (2 \text{ to } 8) \cdot 10^5$].

The influence of the chord of nozzle cascades on the pressure variation behind the diaphragm was noted by A. V. Garkusha at KhPI. The complete equation of radial equilibrium (see § 37) shows that with the decrease of chord, the influence of the term $c_a = \frac{\partial c_r}{\partial z}$ increases. Thus, a change of blade chord affects the reaction of a stage and the leakage.

From the KhPI experiments [112], the dependence of losses in an annular cascade

on chord was established for constant d and l (l/b = 1.22, 0.61, and 0.305 were investigated), which is determined by the axial clearance between the nozzle and rotor blades. For small values of these clearances, absolute similarity of profiles, and t = const, there is an optimum value of blade chord.

Thus, for instance, when $\delta_{з.с}/b$ = 0.05, the least cascade losses are attained at l/b = 0.6. An increase of chord lowers φ twice by 1.5%. As $\delta_{з.с}/b$ increase, the minimum of losses is displaced in the direction of smaller chords.

The application of small chords for nozzle cascades, the so-called narrow blades, is usually required for increasing the rigidity of mounting the strips, for example, as shown for a KhTGZ turbine in Fig. 86a, and an LMZ turbine in Fig. 119. The experiments of various organizations, including the LMZ experiments with a turbine, showed that these strips have little effect on efficiency, under the condition that they do not block the flow, of course.

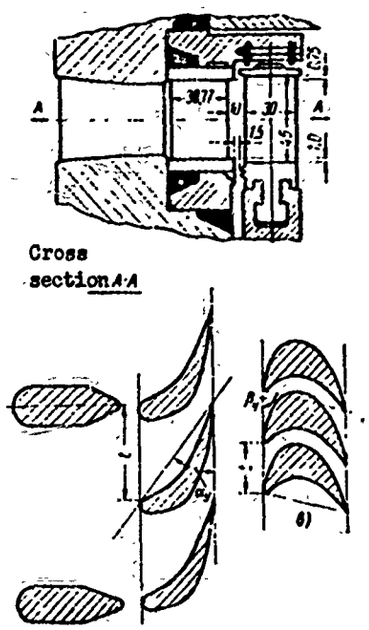

Fig. 119. Diagram of a stage with narrow nozzle blades and stiffeners (LMZ experimental turbine).

When designing a stage, the designer can, in rather wide limits, vary the distance between the trailing edges of the nozzle cascade and the leading edges of the moving cascade. This distance — the so-called complete axial clearance δ_a — is composed of $\delta_{з.с}$ — the closed clearance of the nozzle grid, δ_{an} — the open clearance, and $\delta_{з.р}$ — the closed clearance of the moving cascade (see Fig. 47). The open clearance is limited by the accuracy of assembly and the thermal expansions under nonsteady conditions. Its minimum value depends on a number of design and performance factors. The smaller this clearance, is the less the leakage of the blade shroud, and the higher the efficiency. The closed clearance of the moving blades, $\delta_{з.р}$, can vary practically in a narrow range. It is inconvenient to increase it constructively. At the same time, the closed axial clearance of the nozzle cascade can vary in a wide range, from minimum, which is determined by the technology of manufacture of the diaphragm, to practically any value.

Let us consider how a change of the complete clearance, by means of changing the closed axial clearance of the nozzle grid $\delta_{з.с}$, will affect stage performance.

As $\delta_{з.с}$ increases, the frictional losses on the end walls of the nozzle cascade increase along the length of $\delta_{з.с}$. I. M. Vol'fson proposed a formula for determining these losses [12], which is well confirmed by experiments at LMZ and KhPI

$$\zeta_{з.с} = 2 \cdot \frac{A}{Re_{c_1}^{0.14}} \cdot \frac{\delta_{з.с}}{l_1 \sin \alpha_1}, \tag{132}$$

where

$$Re_{c_1} = \frac{b_1 c_{1t}}{\nu_1}, \quad A = f\left(\frac{\delta_{з.с}}{l_1 \sin \alpha_1}\right).$$

These losses may be calculated approximately by the following formula:

$$\zeta_{з.с} = \frac{0.45 \cdot 10^{-5}}{Re^{0.14}} \cdot \frac{\delta_{з.с}}{l_1 \sin \alpha_1}. \tag{133}$$

It should be borne in mind that formula (132) was derived for two-dimensional cascades.

As it is known, at the exit of a nozzle cascade the flow is nonuniform; for contemporary cascades, working under design conditions of flow, this nonuniformity depends mainly on the thickness of the trailing edge $\Delta_{кр}$, or to be more exact, on $\Delta_{кр}/t$ and on the distance behind the trailing edges, δ_a. The further behind the cascade the measurement is conducted, the larger the losses, since balancing and mixing of flow requires additional energy. Furthermore, along the cascade pitch there is some nonuniformity connected with the various static pressure. This was noted by us earlier (see Fig. 84) and is confirmed by many other experiments. For instance, Fig. 120, according to the experiments of I. I. Kirillov and R. M. Yablonik [5], gives graphs of the change of the field of static and total pressure in the clearance between the nozzle and moving cascades in various sections along the pitch. The field and angles of flow, α_1, also vary along the pitch. The larger the complete axial clearance is, the greater the mixing

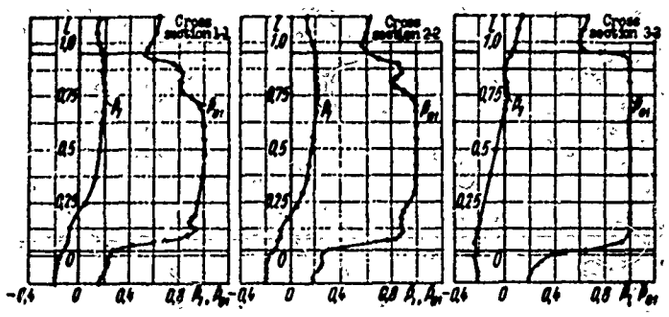

Fig. 120. Change of field of static pressure, $\bar{p}_1 = p_1/p_0$, and stagnation pressure, $\bar{p}_{01} = \bar{p}_{01}/p_0$, with respect to pitch and height behind the nozzle cascade of a stage (l_2 = 80.5 mm, d/l = 7) with cylindrical blading and stamped nozzle blades: $\rho_{ср} = 0$ ($u/c_{ф\,опт}$, BITM experiments).

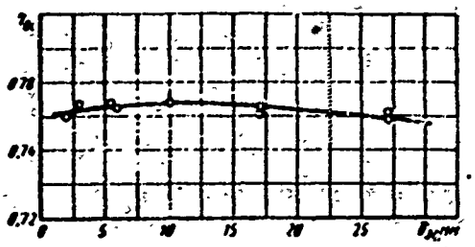

Fig. 121. Dependence of the efficiency of a stage η_{0i} on the closed axial clearance of a nozzle cascade $\delta_{з.с}$ (BITM experiments).

of flow and the greater the losses due to mixing. Usually at a distance of $\delta \approx 1.5t$ from the trailing edges of the nozzles there occurs a sufficiently complete balancing of the flow. On the other hand, the losses in the moving cascade to a considerable extent are determined by the entrance conditions. Nonuniformity of flow at the entrance to the moving cascade and deviation of angle β_1 from the calculated value increase the losses in the moving cascade, and consequently, also in the stage. An analytic calculation of the change of efficiency of a stage, depending upon the complete clearance, is difficult. As shown by experiments in experimental turbines at BITM, TsKTI, LMZ, and MEI, these losses are of approximately one order; therefore, it is natural to expect the optimum value of the complete clearance. It is assumed here that the losses due to leakage do not change or at least their change is immaterial. Experiments at BITM, where the influence of closed clearances was investigated in detail, showed that there actually exists a value of such an optimum clearance. The results of this investigation are shown in Fig. 121 [5] for a stage with cylindrical blading (l_1 = 66 mm, d = 549 mm, $x_ф$ = 0.53, $\delta_{зп}$ = 1 mm = const).

The reaction in the stage changes along the height; the difference of the reaction at the periphery and at the root depends mainly on d/l. With an increase of the closed clearance and, in general, the complete axial clearance (with constant open clearance) the difference of the reaction, $\Delta\rho = \rho_п - \rho_к$, increases: the pressure at the periphery increases and decreases at the root. This change of the reaction at the ends of the blades occurs up to a definite value of the clearance.

The mean reaction of the stage $\rho_{ср}$ practically does not change in this instance. Both statements expressed above are confirmed by numerous experiments, for instance the experiments of W. Hartmann [143] (see Fig. 122a) and BITM experiments (see Fig. 122b). A certain increase of the difference of the reaction along the height will have little effect on the conditions of entrance to the moving cascade; however, the losses due to leakage can change. Therefore, the optimum value of the closed clearance depends on d/l, which determines $\Delta\rho = \rho_п - \rho_к$, and on the clearance sealing. With a large d/l and good sealing, the optimum value of the complete axial clearance, other things being equal, will be higher than for a relatively large

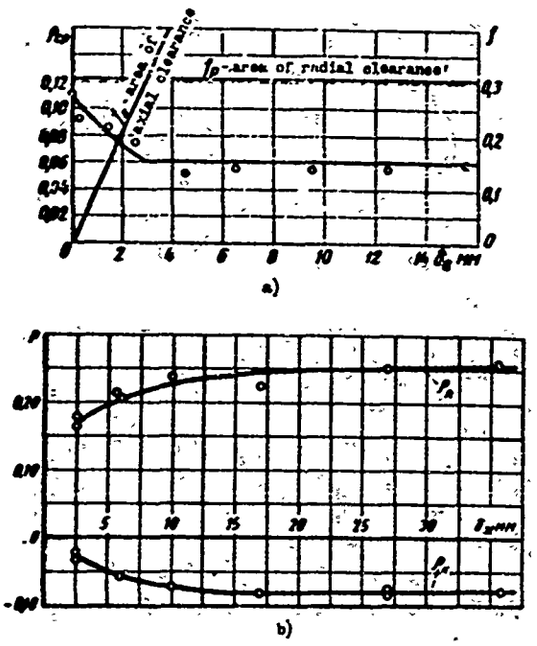

Fig. 122. Reaction of a stage depending upon axial clearance: a) mean reaction of stage; when $\delta_a > 3$ mm the leakage over the shroud is limited by the constant radial clearance δ_p; $b_2 = 50$ mm, $d/l_2 = 9.1$, $u/c_ф = 0.55$ (experiments at the Dresden Institute); b) reaction on the periphery $\rho_п$ and at the root $\rho_к$ for a stage with cylindrical blading, $l_1 = 66$ mm, $d/l_1 = 8.3$, $u/c_ф = 0.53$ (BITM experiments).

magnitude of leakage. Furthermore, the magnitude of the optimum clearance $(\delta_a)_{опт}$ is influenced by the thickness of the trailing edge of the nozzle blades (the greater $\Delta_{кр}$ is, the greater $(\delta_a)_{опт}$) and the shape of the moving cascade. If the moving cascade is not very sensitive to a change of the entrance conditions, the closed clearance should be small.

For want of reliable data on the influence of periodic instability on the flow in moving cascades of various shape, it is necessary to limit ourselves to a rough estimate of the optimum value of the total closed axial clearance.

$$\delta_a = (0{,}05 - 0{,}10)\, l_1; \qquad (134)$$

the smaller value of the coefficient pertains to small d/l and the worst sealing; the large value refers to large d/l and good stage sealing.*

Inasmuch as independently of cascade height there occurs practically full balancing of the flow at a distance of $\delta \approx (1.2$ to $1.5)t$ from the trailing edges of the nozzle cascade, the full axial clearance should not be larger than this magnitude, independently of the calculation by formula (134). An increase of the full axial clearance is favorable from the point of view of vibrational reliability of the rotor blades. However, even here it is important only within the limits of the quantity $\delta < (1 - 1.5)t$.

The open axial clearances in a stage i.e., at the periphery $\delta_{aп}$ and at the root $\delta_{aк}$, and also the radial seal above the shroud of the rotor blade, δ_p,

*The optimum value of the total axial clearance also depends on the conditions of entrance to the moving cascade. Thus, according to LMZ experiments, it turned out that at an off-design angle of entrance to the moving cascade the magnitude of the optimum clearance noticeably decreases.

determine the losses due to parasitic leakages and also render a noticeable influence on the reaction of the stage. The method of calculating the losses due to leakages in these clearances was discussed in § 12. The results of an experimental investigation are considered here.

Leakage or suction in clearance changes the reaction of the entire stage, but mostly the reaction in that part of the stage where leakage occurs. Leakage decreases the reaction, while suction increases it. This is clearly illustrated by the graph in Fig. 123, where experiments on a traverse of flow in a clearance are shown for a typical LMZ stage with l_1 = 47.1 mm, d/l_2 = 9.0, and $x_ф$ = 0.54. Curve 2 corresponds to an experiment in the absence of leakages. The reactions along the height change linearly, and the mean reaction ρ_{cp} = 0.16. Curve 1, for suction $\frac{\Delta G}{G}$ = 2.42% in the root clearance, illustrates a mean reaction of ρ_{cp} = 0.24; in the lower sections the change of the reaction deviated from the linear law. In the case of leakage $\Delta G/G$ = 1.7% in the same root clearance (see curve 3), the mean reaction decreased to ρ_{cp} = 0.09, whereby in the lower part of the blade, from the root section to a height equal to 0.2l, the reaction remained constant and practically equal to zero. This is explained by the fact that during leakage, independently of the sign, the absolute value of the reaction decreases. Analogous results of measurement of the reaction due to leakages were observed by all researchers.

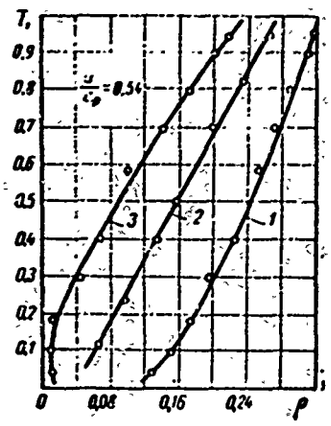

Fig. 123. Results of traverse of flow in a clearance of an LMZ stage; l_1 = 47.1 mm, d/l_2 = 9.0; $u/c_ф$ = 0.54 (LMZ experiments): 1 – suction in root clearance $\Delta G/G$ = 2.42%; 2 – no leakages; 3 – leakage in root clearance $\Delta G/G$ = 1.7%.

It is important to note that when there is steam leakage in a clearance, just as in the absence of this leakage, the reaction on the ends of the blades and the mean reaction change linearly depending upon the velocity ratio $u/c_ф$. This may be seen from an illustration (Fig. 124), where for a КД-2-2А stage, l_1 = 48 mm, d/l_2 = 7.7, and F_2/F_1 = 1.44, a graph for $\rho_п = f(u/c_ф)$ and $\rho_к = f(u/c_ф)$ at ε = 0.7 is presented for four values of steam suction in a root clearance from $\frac{\Delta G}{G}$ = 0 to $\frac{\Delta G}{G}$ = 3%. The root reaction in this case increased to a larger degree than the peripheral reaction.

We shall consider the change of the reaction, analogous to [83], for steam leakage.

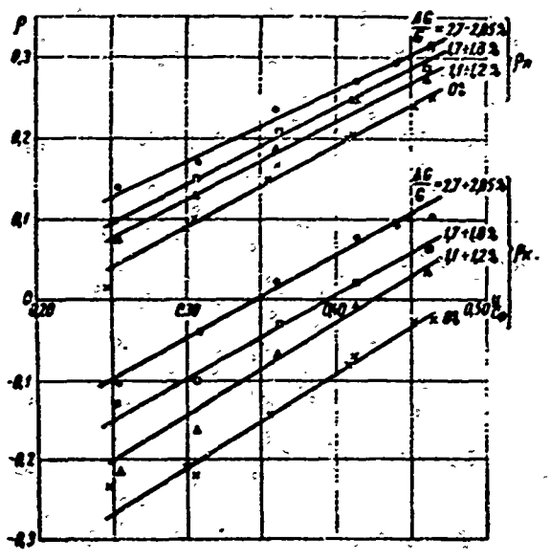

Fig. 124. Dependence of root ρ_K and peripheral reaction $\rho_П$ on $u/c_Ф$ and steam suction in root clearance (MEI experiments).

1. Leakage over the shroud (the reaction at the periphery is positive).

The steam flow through the nozzle cascade is equal to the sum of the flow rates through the moving cascade and the leakage over the shroud

$$G_1 = G_2 + G_y;$$

$$\frac{\mu_1 F_1 c_{1t}}{v_{1t}} = \frac{\mu_2 F_2 w_{2t}}{v_{2t}} + \frac{F^п_{экв} c_{6t}}{v_6}$$

or

$$\frac{\mu_1 F'_1 c_{1t}}{v_{1t}} = \frac{\mu_2 F_2 w_{2t}}{v_{2t}},$$

where

$$F'_1 = F_1\left(1 - \frac{F^п_{экв} c_{6t} v_{1t}}{\mu_1 F_1 c_{1t} v_5}\right), \quad F^п_{экв} = \pi d_п \delta_{экв}.$$

Then, approximately,

$$F'_1 = F_1\left(1 - f^п_{экв}\sqrt{\frac{\varrho_п}{1-\varrho_{ср}}}\right),$$

where

$$f^п_{экв} = \frac{F^п_{экв}}{\mu_1 F_1}.$$

Let us assume that the change of the reaction due to leakage is analogous to the change of the reaction that is caused by a reduction in the area of the nozzle cascade from F_1 to F'_1. Then

$$\Delta\varrho_y = \varrho_t - \varrho = k f^п_{экв}\sqrt{\frac{\varrho_п}{1-\varrho_{ср}}}. \tag{135}$$

where k is found from formula (76)

$$\frac{\Delta\varrho_f}{1-\varrho_0} = k\,\frac{(F_1/F_2) - (F_1/F_2)_0}{(F_1/F_2)_0}. \tag{136}$$

k = 0.55 to 1.00, whereby the greater $x_Ф$ is, the smaller k is.

2. Suction over the shroud (the reaction at the periphery is negative).

In this case the flow rate balance will be written in the following manner:

$$G_2 = G_1 + G_y.$$

If at the entrance to the moving cascade we write a continuity equation for the flow after mixing

$$\frac{F'_1 c'_1}{v_1} = G_2 = \frac{\mu_2 F_2 w_{2t}}{v_{2t}}.$$

where

$$c_1' = \varphi c_{1t} \frac{G_1}{G_1 + G_y} \approx \mu_1 c_{1t} \frac{1}{1 + f_{\text{экв}}^{n} \frac{c_{0t}}{c_{1t}}}.$$

Since

$$\frac{F_1' c_1'}{v_1} = \frac{\mu_1 F_1 c_{1t}}{v_{1t}} + \frac{F_{\text{экв}}^{n} c_{0t}}{v_1},$$

then

$$F_1' = F_1 \left(1 + f_{\text{экв}}^{n} \frac{c_{0t}}{c_{1t}}\right)^2 \approx F_1 \left(1 + 2 f_{\text{экв}}^{n} \frac{c_{0t}}{c_{1t}}\right),$$

and in final form we will obtain:

$$\Delta \varrho_y = \varrho_t - \varrho = -2k f_{\text{экв}}^{n} \sqrt{\frac{-\varrho_n}{1 - \varrho_{cp}}}. \tag{137}$$

3. Steam leakage in the root clearance:

$$\Delta \varrho_y = \varrho_t - \varrho = k \frac{\Delta G}{G}. \tag{137a}$$

4. Steam suction in the root clearance

$$\Delta \varrho_y = \varrho_t - \varrho = -2k \frac{\Delta G}{G}. \tag{137b}$$

In formulas (136) and (137) it is necessary to place not the theoretical values of the reaction, but the actual ones, taking into account the leakages. Thus, a calculation may be performed by the formulas, either by the method of successive approximations or by using the graph in Fig. 68, where for the case of leakage

$$\Phi = \frac{\delta_{\text{экв}}}{l_1 \sin \alpha_1} \left(1 + \frac{l}{d}\right)$$

and for the case of suction

$$\Phi = -\frac{2\delta_{\text{экв}}}{l_1 \sin \alpha_1} \left(1 + \frac{l}{d}\right).$$

Graph 68 is constructed for k = 0.7.

Figure 125 shows the concluding graphs of the influence of leakages in the root clearance on the mean reaction of a stage according to LMZ and MEI experiments. Here, for these stages, the lines $\rho_{cp} = f(\Delta G/G)$ are drawn (constructed according to the calculation formulas of this paragraph). The coincidence of the calculation and the experiments in all cases is not good. In our opinion, this is explained mainly by the difficulties in the accurate measurement of the reaction of stages in experimental turbines. The accuracy of reaction measurement may be seen in §§ 16 and 19. The change of economy of a stage due to leakages in open clearances was discussed in § 12. Let us consider here the results of an experimental investigation. Numerous experiments give the following qualitative picture: any increase of the

peripheral clearances, which leads to an increase of steam leakage, lowers the economy of a stage. Thus, in all cases the efficiency of a stage decreases when there is suction in the root clearance. Here the influence of suction to a considerable extent is determined by the root reaction of the stage. In this clearance, when there is very little leakage, the efficiency of the stage almost does not change, and sometimes it even increases somewhat. These statements are connected with the favorable influence of suction of the boundary layer and the best conditions of entrance to the moving cascade in its lower part. A further increase of leakage inevitably lowers the economy of the stage. The difference in the change of efficiency during steam leakage in the peripheral and root clearances is explained by the considerable losses in the root portion of the annular nozzle cascade.

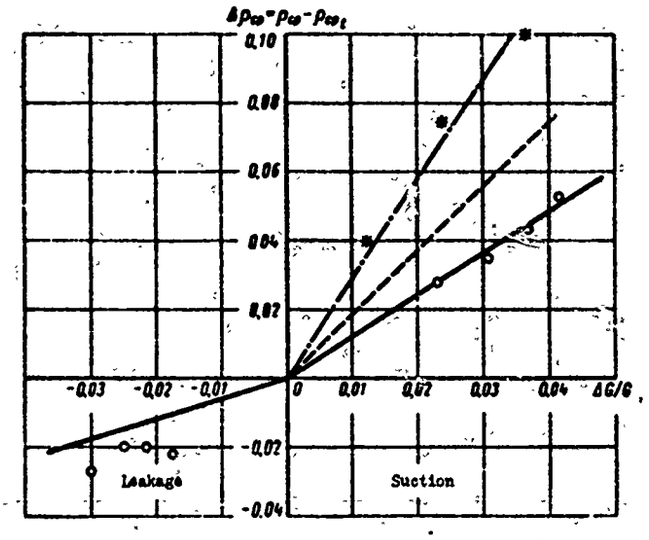

Fig. 125. Influence of steam leakages on the reaction of a stage: LMZ experiments with $u/c_\phi = 0.54$, O – O – O; MEI experiments with $u/c_\phi = 0.45$, x – x – x; calculated data – – – – (dotted line).

Figure 126a gives experimental graphs from LMZ which consider the influence of leakages in the root clearance. The experimental points on the graph confirm the statements made above. In a stage with a low height, especially in a stage with a small diameter, in the lower part of the nozzle cascade the losses are so much greater that the certain decrease in efficiency due to suction is insignificant for the entire stage. With leakage up to 1-2% the efficiency practically does not change. The effect of leakage on the economy of a stage is noticeably less than the influence of suction. It should be noted that in all the LMZ experiments considered

here the root reaction was positive.

Figure 126b illustrates the influence of steam suction on the economy of a КД-2-2А stage: l_1 = 48 mm, d/l_2 = 7.7, F_2/F_1 = 1.44, and ε = 0.7. At $x_ф$ = 0.43 to 0.47, when the root reaction is positive, each percent of suction corresponds to a percent of lowering of efficiency. At smaller $x_ф$, with the appearance of a negative reaction at the root, the relative influence of suction increases.

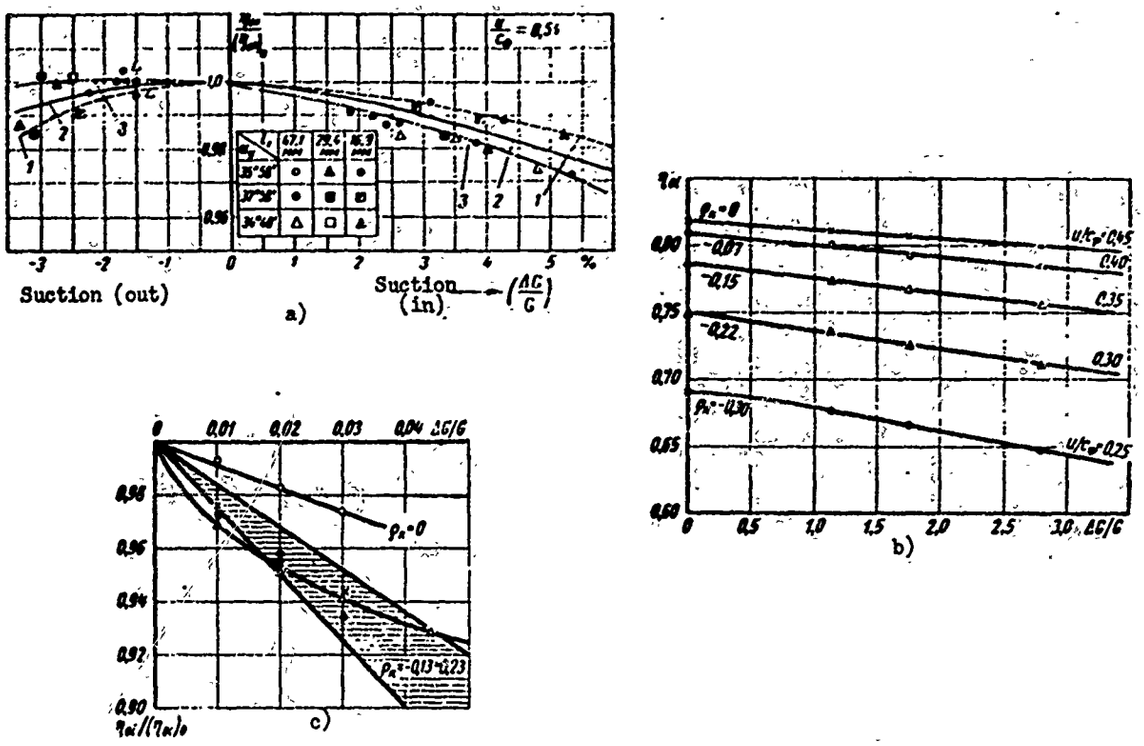

Fig. 126. The economy of turbine stages depending upon: a) leakages in the root clearance of a typical LMZ stage $(\eta_{oл})_0$ – efficiency at $\Delta G/G$ = 0, $u/c_ф$ = = 0.54, d_K = 400 mm (LMZ experiments); b) velocity ratio and reaction with suction in the root clearance of a КД-2-2А stage (l_1 = 48 mm, d/l_2 = 7.7; ε = 0.7) according to MEI experiments; c) suction and root reaction of stages of MEI series: O – O – O КД-2-2А; F_2/F_1 = 1.44; ρ_K = 0; * – * – * – КД-2-3А; F_2/F_1 = 1.55; ρ_K = -0.13; Δ – Δ – Δ КД-1-2А; F_2/F_1 = 1.73, ρ_K = -0.20; ◇ – ◇ – ◇ КД-1-3А. F_2/F_1 = 1.88, ρ_K = -0.23.

The influence of suction through the root clearance, according to MEI experiments for four stages that differ by their ratio of areas, and consequently, also by the root reaction ρ_K, is shown in Fig. 126c. For a КД-2-2А stage with F_2/F_1 = 1.44 and ρ_K = 0 at l_1 = 48 mm, d = 400 mm, and given conditions ($x_ф$ = 0.45, ε = 0.7), the obtained dependence of efficiency on suction is approximately linear, whereby 1% of suction also lowers the efficiency by 1%. In stages with a large negative root reaction, with 1% suction the efficiency is lowered by 2-2.5%. TsKTI experiments

[47] also confirm the large influence of suction with a negative reaction. The averaged values of the quantities for calculating the losses due to suction in the root clearance are given in Fig. 71.

The investigation of the influence of leakage through the peripheral clearance is more complicated, since the change in the amount by this leakage, due to the change of the flow rate coefficient in this clearance, does not remain proportional to the area of the clearance. There is also a change in the total axial clearance, which affects economy. An example of the dependence of the economy of a stage on the size of the peripheral open clearance, according to BITM experiments, is the graph in Fig. 127a. It is important to note that an increase of the open peripheral clearance above the blades not only lowers the effectiveness of the stage, but also noticeably lowers the optimum ratio $u/c_{ф}$. Thus, for the investigated stage (l_1 = 35 mm, d = 567 mm) with an increase of $\delta_{ап}$ (no radial seal for blade shroud) from 1 to 4.5 mm, the maximum efficiency is lowered from 0.78 to 0.685, and $x_{ф_{опт}}$ decreases from 0.48 to 0.44. For the same stage, the installation of a radial seal (Fig. 127b) essentially increased the efficiency of the stage, especially with large $\delta_{ап}$. With this, $x_{ф_{опт}}$ also increased. The higher $x_{ф}$ is, the greater the reaction on the periphery, and the better the sealing of the stage.

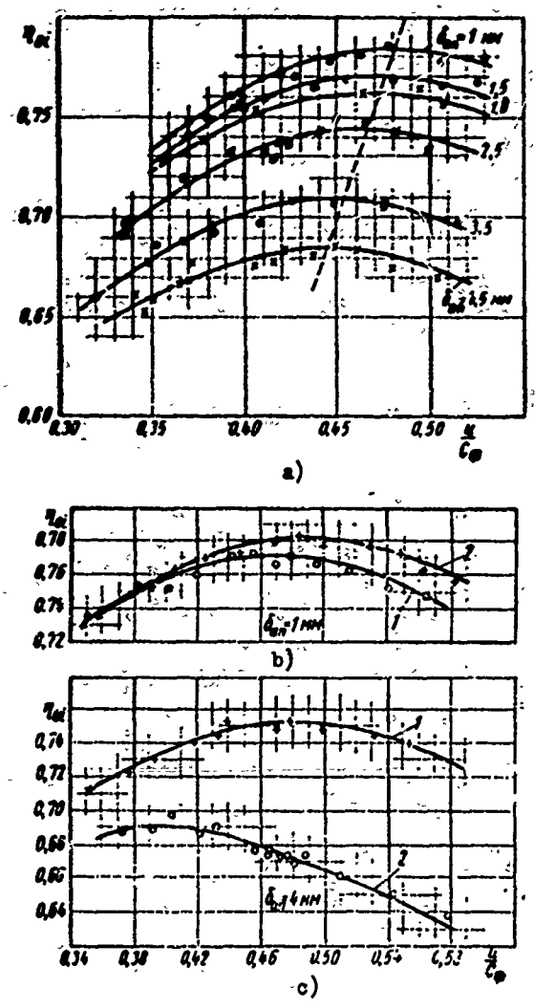

Fig. 127. Change of the efficiency of a stage (d = 567 mm, l_1 = 35 mm) depending upon the leakage over the rotor blades and the ratio $u/c_{ф}$ (BITM experiments) a) stage without radial sealing; b) curve; 1 – without radial seals; 2 – with radial seals; c) curve; 1 – with radial seals; 2 – without radial seals.

The influence of the external overlap, $\Delta l_{п}$, is determined mainly by two factors: the leakage over the blade shroud and the change of the conditions of entrance to the moving cascade. It is obvious that the leakage will depend on the relative

clearances in the stage and the sealing of the radial clearance. In general, an increase of $\Delta l_п$ leads to a decrease of the flow rate coefficient through the peripheral open axial clearance. However, with good stage sealing, this factor is insignificant. In a limiting case, when this leakage is negligible, it is inexpedient to increase the value of $\Delta l_п$. On the other hand, an increase of the external overlap leads to an increase of the nonuniformity of flow at the entrance to the moving cascade. Here, a large influence is rendered by the size of the closed axial clearance. The smaller the size of this clearance, the less should the value of $\Delta l_п$ be.

The influence of overlap was theoretically investigated for the first time by V. V. Zvyagintsev. The influence of $\Delta l_п$ on stage efficiency was recently investigated experimentally and theoretically at the BITM, MEI, TsKTI, NZL, TMZ, and KhPI. As a result of the experiments of A. G. Sheykman, which were conducted in an experimental air turbine with an actual stage from a TMZ BP-6-3 turbine with l_2 = 41.1 mm and d/l_2 = 15, a graph was constructed which characterizes the influence of $\Delta l_п$ and

$$\bar{\delta}_{экв} = \frac{\delta_{ап}}{l_1} \frac{1}{\sqrt{1 + z_0 \delta_{ап}^2/\delta_z^2}}.$$

This graph is shown in Fig. 128. It should be borne in mind that the TMZ experiments were conducted with a constant total axial clearance, which was relatively small. An increase of this clearance increases the magnitude of the optimum overlap. In [39] is proposed a formula for selecting the most advantageous value of $\Delta l_п$, which is obtained on the basis of TMZ and BITM experiments.

$$(\Delta l_п)_{опт} = 0{,}7 \frac{\sqrt{\varrho_п}}{1 - \varrho_п} \frac{\delta_{экв}}{\sin \alpha_1}. \qquad (138)$$

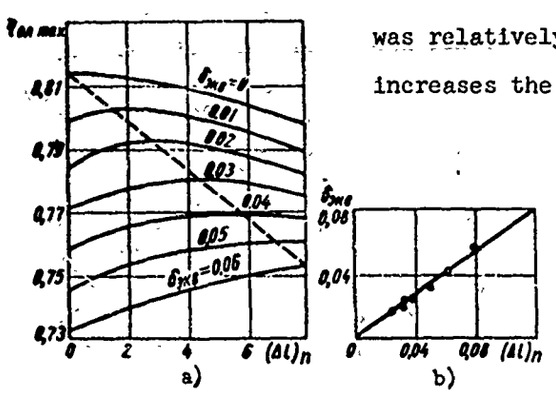

Fig. 128. The influence of overlap on the efficiency of a stage: a) dependence of the stage efficiency on the magnitude of upper overlap $\Delta l_п / l_1$ and equivalent clearance $\delta_{экв}$. Dimensions of the stage: d_2 = 615 mm, l_2 = 41.1 mm, $u/c_ф$ = 0.5; M_1 = 0.3; $Re_{c_1} = 4 \cdot 10^5$ (TMZ experiments); b) dependence of equivalent clearance $\bar{\delta}_{экв}$ on $\Delta l_п / l_1$.

When designing a turbine, it is not recommended to select $\Delta_п$ less than 1.5 mm, since an inaccuracy in manufacture can lead to a negative overlap, which essentially lowers the

economy of the stage.

In distinction from the experiments when the overlap was changed by means of changing the height of one cascade, interesting investigations were conducted at KhPI [16]. In these experiments the overlap was changed by simultaneously turning the blades in such a way that the ratio F_2/F_1, i.e., the calculated reaction of the stage, remained constant. As compared to experiments at β_2 = const, the optimum overlap was smaller; this is caused by the influence of leakages through the peripheral clearance, which depend both on $\Delta l_п$ and F_2/F_1.

§ 23. BASIC CHARACTERISTICS OF CERTAIN SINGLE-WHEEL STAGES

Old-Type Stages

Many turbines installed at electric power stations are equipped with old-type profiles and stages which, at best, underwent purely empirical checks in experimental turbines. The cascade profiles of these stages are given in literature and, according to the investigations of many organizations (LMZ, TsKTI, MEI), they have large losses, are sensitive to changes of the angle of leakage, and are especially poor at low heights. Figure 129 presents a firm's curves ($\eta_{0л}$) for the efficiency of old-type stages, depending upon the velocity ratio $u/c_ф$ and the height of the nozzle cascade l_1. The ratios of the dimensions of the cascades and the clearances of these stages are given in [117]. These curves anticipate a very high quality of stage manufacture and give values of efficiency with the full use of the outlet velocity of the preceding stage. The experiments of a number of organizations, especially for low heights, did not confirm values of efficiency that are given in Fig. 129. Actually, the efficiency of these stages was considerably lower.

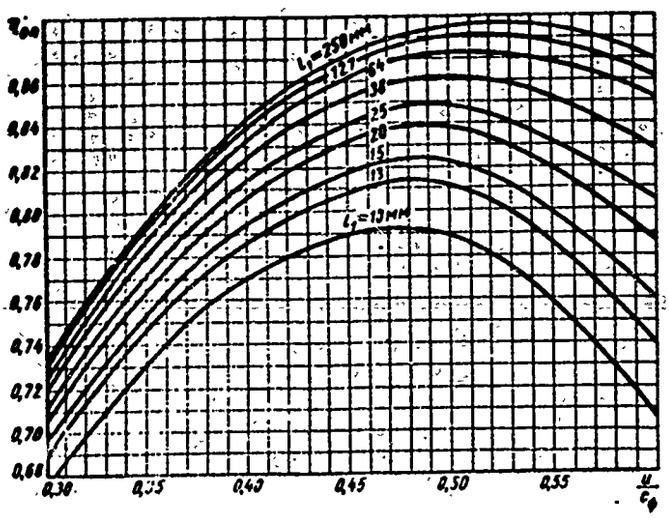

Fig. 129. Efficiency $\eta_{0л}$ (with the use of the outlet velocity of the preceding stage) for old-type stages (firm's data).

The Lenin Factory in Leningrad conducted a test on a series of old-type stages, the results of which are shown in Fig. 130. The tests were conducted by L. A. Dorfman

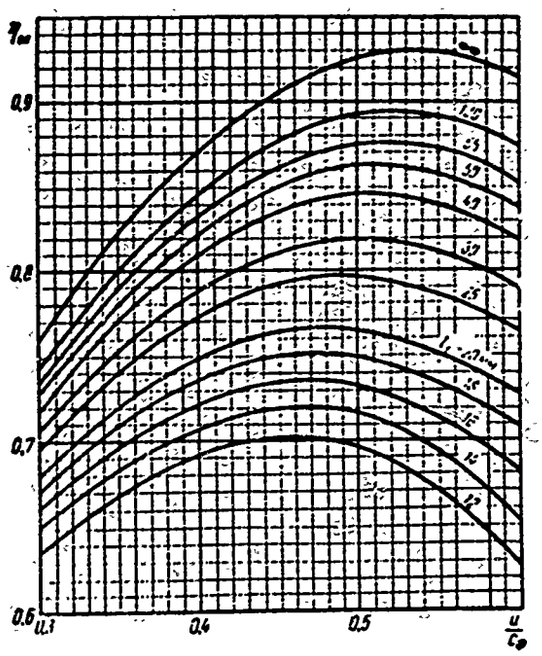

Fig. 130. Efficiency $\eta_{оп}$ for old-type stages (according to NZL data).

under the following conditions: Re number from $3 \cdot 10^5$ to $8 \cdot 10^5$, $M_ф = c_ф/a_2 = 0.35$ to 0.5, blade height to $l_1 = 36$ to 43.5 mm and, only in certain cases, to $l_1 = 50$ mm. The remaining curves were constructed by extrapolation. The stages had no radial shroud sealing. The experiments were conducted in an air-driven experimental turbine. The bearing and disk friction losses were determined by means of run-out curves.

Stages of the V. I. Lenin Neva Factory

A series of stages with improved profiles was tested under the same conditions. An efficiency graph for this test is shown in Fig. 131.* G. A. Zal'f and V. V. Zvyagintsev [48] recommend for these stages the angles $\alpha_{1эф} = 13^\circ 25'$ and $\beta_{2эф} = 22^\circ$, overlaps $\Delta l_к = 1.5$ mm and $\Delta l_п = 2.5$ to 3 mm, and an axial clearance of 1.5 mm.

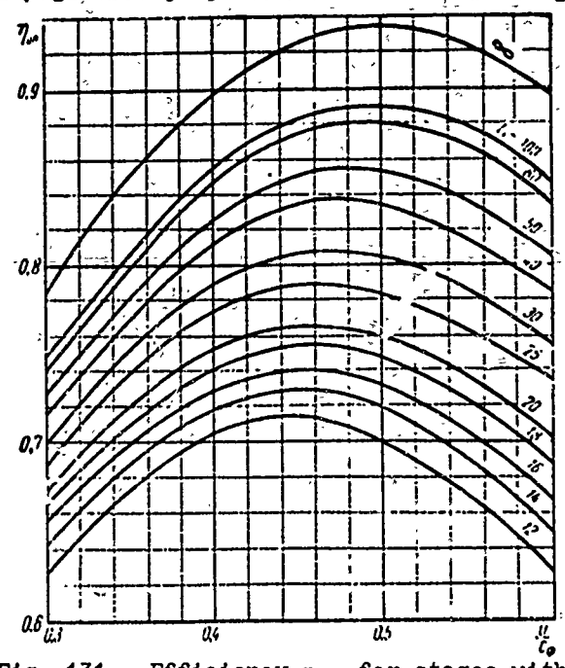

Fig. 131. Efficiency $\eta_{оп}$ for stages with improved blade profiles (according to NZL data).

Stages of the XXII Congress CPSU Leningrad Metallurgical Plant

The LMZ, and also certain other plants, for unregulated high-pressure stages, employ a typical stage that was developed and studied in the LMZ laboratory under the supervision of A. S. Zil'berman. The nozzle cascade of this stage was designed and thoroughly investigated by I. M. Vol'fson [50]. The dimensions, configuration, and

*Here and subsequently in the entire book, the experimental graphs for the efficiency of stages are presented. These graphs cannot be used for a comparison of the economy of stages designed by different organizations. Such a comparison can be made only as a result of tests of different stages with identical or similar geometric characteristics and an identical technology of manufacture. It is desirable that these tests be conducted in the same experimental turbine. Unfortunately, there are very few of these experiments with single-wheel stages.

characteristics of this cascade are in the profile standards. The plant replaced the old cascade, and only the end losses then decreased by 1.5 times. The exit angle of the cascade is $\alpha_1 = 11^\circ$. As the profile of the moving cascade they have adopted the TsKTI profile T-1.

The flow area of a typical LMZ stage is shown in Figs. 119 and 132. This stage was investigated in detail by Z. A. Lapteva and A. O. Lopatitskiy in an experimental air turbine [62]. Tests on a typical stage were also conducted in other laboratories.

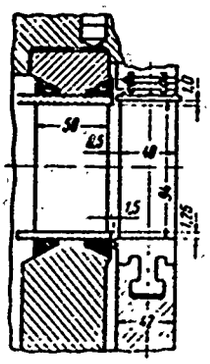

Fig. 132. Flow area of typical LMZ stage.

The cascades and the stage itself were investigated at large pressure ratios ε($M_{c_1} \approx 0.435$ to 0.515), when the effect of compressibility is insignificant, and at $Re_{c_1} > 5.8 \cdot 10^5$, i.e., the self-similar region of investigation. Experiments were conducted at l_1 = 16.9, 29.4, and 47.1 mm (six relative heights of nozzle cascades within the limits of $0.238 \leq l_1/b_1 \leq 1.63$), three relative heights of moving cascades with d/l_2 = 21, 13.3, and 9, and l_2/b_2 from 0.9 to 2.25. The overlaps in the stage remained practically constant; $l_2 - l_1$ = 2.9 to 3.1 mm; the effective entrance angles at mid-diameter were changed by means of turning the cascade and changing the pitch within the following limits:

$$\alpha_{1\,эф} = 8^\circ 56' \div 15^\circ 58'; \quad \beta_{2\,эф} = 17^\circ 45' \div 19^\circ 58'.$$

The ratio of areas is F_2/F_1 = 1.18 to 2.19.

Thus, there are stage characteristics with various dimensions which are sufficient for application in a wide range of stages, high-pressure ones in particular.

The graphs include the characteristics of the stage.

1. The efficiency of the stage $\eta_{0л}$ (Fig. 133a), depending upon $u/c_ф$ and l_1,

$$\eta'_{0л} = f\left(\frac{u}{c_ф}, l_1\right)$$

for F_2/F_1 = 1.7 and $\alpha_{1\,эф} \approx 11$ to 12° with zero leakages.

Cascade chords b_1 = 58.9 mm, l_2 = 22.2 mm, and thickness of trailing edge of nozzle blades $\Delta^c_{кр}$ = 0.3 - 0.33 mm.

2. The influence of the angle of incidence of the nozzle cascade, α_y, on the angle α_1. the efficiency of the stage $\eta'_{0л}$ (Fig. 133b), and the reaction ρ (at $u/c_ф$ = 0.54) (Fig. 133c). In these experiments the efficiency was calculated according to the static parameters in front of the stage.

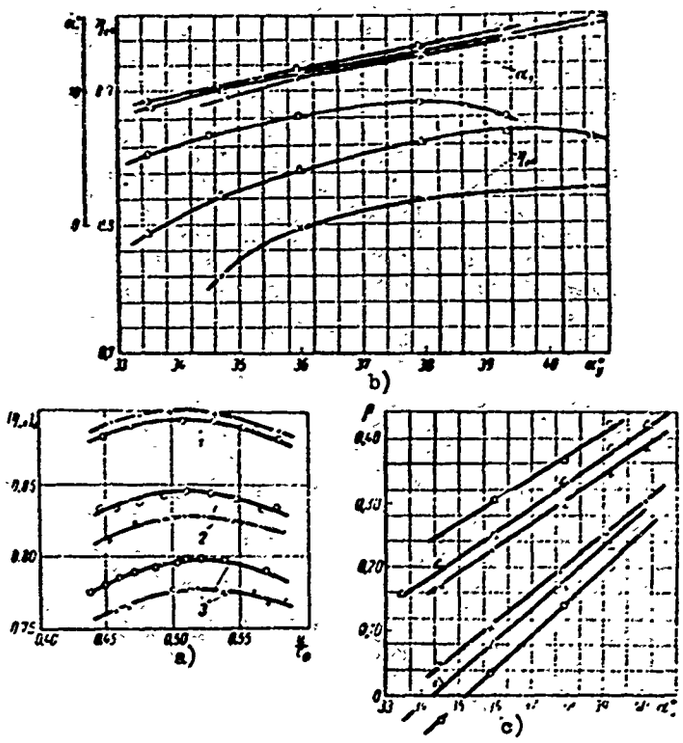

Fig. 133. Characteristics of a typical LMZ stage: a) efficiency $(\eta_{оп})'_0$ with zero leakages. Curves: 1 – l_1 = 47.1 mm; 2 – l_1 = 29.4 mm; 3 – l_1 = 16.9 mm; XXX – nozzle cascade from Fig. 119; O O O – nozzle cascade from Fig. 132; b) dependence of angle α_1 and efficiency $\eta'_{оп}$ on angle of incidence of nozzle blades α_y with $u/c_ф$ = 0.54; c) dependence of reaction of stage ρ on angle of incidence of nozzle blades α_y with $u/c_ф$ = 0.54 (X – X – X – l_1 = 16.9 mm; Δ – Δ – Δ – l_1 = 29.4 mm; O – O – O – l_1 = 47.1 mm).

The characteristics of the stage do not include graphs of the reaction as a function of $x_ф$ and l_1 and the flow rate coefficient, which makes the calculation of the stage dimensions and the additional losses difficult. If necessary, these data can be replaced by appropriate graphs and formulas which refer to other stages.

Stages of the Moscow Power Engineering Institute

The MEI stages were developed and investigated by the development of steam and gas turbines;* they are employed by the majority of plants as regulating stages; many plants and organizations use them as unregulated stages for various turbines.

---

*The investigations of stages were conducted engineer V. I. Abramov, F. V. Kazintsev, L. Ye. Kiselev, and G. A. Filippov.

For single-wheel stages that operate with subcritical and transonic velocities, MEI recommends the use of the following cascades (and their modifications):

nozzle cascades TC-0A, TC-1A, and TC-2A;

moving cascades TP-1A, TP-2A, and TP-3A.

From the enumerated cascades it is possible to make up several combinations. These combinations were tested in an experimental turbine cna can be recommended depending upon the specific operating conditions of the designed stage. The cylindrical blading (with profiles of constant height) of MEI stage can be quite effectively applied even at relatively low values of d/l, to d/l = 10-8, and in some cases to d/l = 6-4.

Three shapes are proposed for the flow area of the stage; they are shown in Fig. 134.

1. Cylindrical flow area: the clearances and overlaps conform to Fig. 134a, and the recommendations in Chapters II and IV.

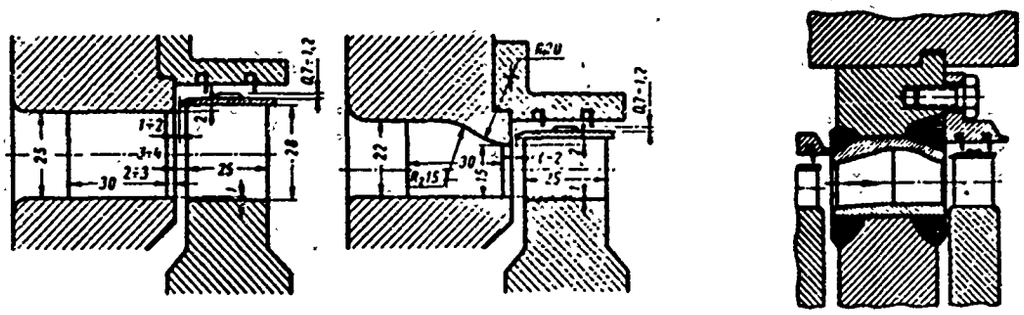

a) b) c)

Fig. 134. Typical MEI stages: a) cylindrical flow area; b) flow area of stage with meridional profiling for first stage of section; c) flow area of intermediate stage with meridional profiling.

2. Conical flow area. In this type of flow area it may be necessary to employ blading with constant profiles in the low-pressure stages of turbines with low steam rates (low-power condensing turbines, the low-pressure parts of selected machines) and to reconstruct the old turbines.

3. If the cascade heights are low, the technology of manufacture permitting:

a) the first stage of a section (regulating stage, first unregulated stage, first stage after intermediate steam reheating, and others) should have meridional profiling of the nozzle cascade, as in Fig. 134b;

b) the intermediate stage should have meridional profiling, in accordance with 134c.

For short blades, somewhat modified profiles for the moving cascades also are

recommended; these are the so-called type "K" cascades, which have smaller end losses.

For single-wheel stages with full steam input, the following combinations of MEI cascades, shown in Table 8, are recommended.

Table 8. MEI Single-Wheel Stages

l_1, мм	d/l	Nozzle cascade	Moving cascade	Stage designation	Ratio of areas
10—20	>20	TC-1Aм	TP-2Aк	КЛ-1-2Аик	1.6—1.65
		TC-2Aм	TP-2Aк	КЛ-2-2Аик	1.4—1.5
		TC-1Aм	TP-2Aк	КЛ-1-2Аик	1.55—1.65
		TC-1A	TP-2Aк	КЛ-1-2Ак	1.45—1.65
		TC-1A	TP-2A	КЛ-1-2A	1.45—1.65
		TC-2A	TP-2A	КЛ-2-2Аик	1.4—1.5
		TC-2Aм	TP-2Aк	КЛ-2-2A	1.5—1.6
		TC-2A	TP-3A	КЛ-2-3A	1.6—1.7
30—50	>10	TC-1A	TP-2A	КЛ-1-2A	1.62—1.75
		TC-2A	TP-2A	КЛ-2-2A	1.45—1.55
		TC-2A	TP-3A	КЛ-2-3A	1.55—1.65
50—100	>8	TC-2A	TP-2A	КЛ-2-2A	1.4—1.55
	(6)	TC-2A	TP-3A	КЛ-2-3A	1.5—1.6

The cascades and their angles of incidence are selected according to the recommendations in § 10.

The MEI stages presented in Table 8 were investigated in MEI experimental steam turbines, and also during operation in air [23, 29, 35, and 103] with heights of 10, 15, 25, and 48 mm, and $d/l \geq 8$. The MEI stages underwent an experimental check in KTZ experimental steam turbines, including a multistage experimental turbine. Furthermore, the MEI cascades, and also their proposals for increasing the economy of stages with short blades, were investigated in experimental turbines at LKZ, LMZ, and NZL. All investigations of MEI stages were conducted with the plant's technology of manufacture, sometimes even with the quality of manufacture being worst than for the permanent machines. Tests of MEI stages were conducted in a wide range of M numbers, and sometimes with M numbers > 1; in certain cases also with different Re numbers (with a separate change of M and Re). Many cascades of MEI stages underwent an experimental check in static rigs in annular packs, and sometimes in actual diaphragms also.

With the exception of the tests conducted in the LKZ turbine, all MEI stages had welded diaphragms.

Characteristics of MEI stages. Generalized characteristics should be used for calculating the economy of MEI stages and for determinating their parameters, and also for finding the influence of various performance and geometric parameters (see § 47). Furthermore, a basic characteristic is given below for these stages, i.e., efficiency

curves η_{01} (without the use of the outlet velocity) for КД-2-2А stages, depending upon height l_1 and the velocity ratio $u/c_ф$. The curves are constructed according to the results of experiments in an experimental steam turbine with the following dimensions: cascade chords $b_1 = 51.5$ mm and $b_2 = 25.0$ mm; mid-diameter of stage 400 mm; overlaps $\Delta l_к + \Delta l_п = 2.5$ to 3.5 mm; ratio of areas $F_2/F_1 = 1.6$ to 1.7; angles $\alpha_{1\ эф} = 15^o$, $\beta_{2\ эф} = 20$ to 21°; stage sealing: no leakage in root clearance, open axial clearance on periphery of stage $\delta_a = 1$ mm, and two radial clearances, $\delta_p = 1$ mm, above the shroud.

The efficiency curves are constructed for КД-2-2А stages at $\varepsilon = 0.8$ to 0.85 and $Re_{c_1} \approx (3.5$ to $4)\cdot 10^5$ (Fig. 135). Here the dotted lines indicate the curves for a stage with meridional profiling.

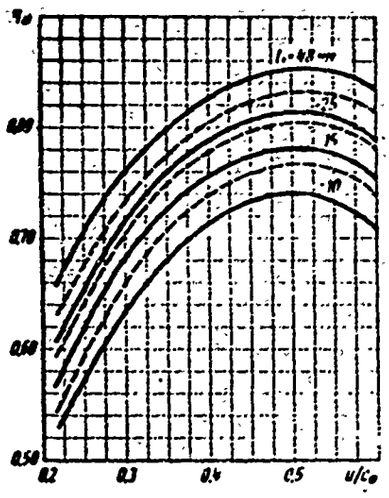

Fig. 135. The efficiency of MEI stages КД-2-2А and КД-2-2Ам, depending on the velocity ratio and cascade height (MEI experiments): —— solid lines – КД-2-2А stage; – – – – dotted lines – КД-2-2Ам stage with meridional bend according to Fig. 134b.

For a determination of the stage dimensions, it is possible to use curves for the flow rate coefficient μ_1 of the nozzle cascade, which are obtained from stage tests (Fig. 111).

Stages of the Polzumov Central Scientific Institute for Boilers and Turbines

In the laboratory of turbine aerodynamics of TsKTI, A. M. Zavadovskiy developed and investigated an impluse stage. The stage was made up of a nozzle cascade ТН-2 and a moving cascade Т-2. The cascades and their characteristics are given in the profile standards. The basic dimensions of the stage are $l_1 = 30$ mm, $l_2 = 34.5$ mm, $d/l = 29$, $l_1/b_1 = 0.59$, $l_2/b_2 = 1.7$, $\Delta_{1\ кр} = 0.22$ mm. The flow area of the stage is shown in Fig. 136. This stage was investigated in an experimental air turbine without special sealing above the shrouding (open axial clearance on periphery, $\delta_{a\,п} = 1.6$ mm), without taking into account the influence of compressibility of flow, and it is intended for $M_{c_1} < 0.5$. The results of the investigations are given in the form of curves of relative blade efficiency $\eta_{оп}$ at various angles of incidence of nozzles α_y and relative pitch $\bar{t}$. Graphs are given for determined values of $u/c_ф$. Reconstruction of these graphs for the best conditions gives the curve that is represented in Fig. 137 ($\alpha_y = 42^o$, $\bar{t}_1 = 0.76$). The reaction of the stage at $u/c_ф = 0.5$ amounts to $\rho = 0.10$. Under optimum conditions sin $\alpha_{1\ эф} = 0.212$. The given stage, just as the other stages investigated in experimental

air turbines, usually are manufactured more carefully in the laboratory than plant stages and, in particular, than the stages investigated in the experimental steam turbines of KTZ, MEI, LMZ, and NZL. The flow rate characteristic of the stage, i.e., the ratio of the axial component of the outlet velocity to the peripheral velocity, c_{2a}/u_{cp}, depending upon $u/c_{ф}$, was constructed by us in Fig. 137. (The difficulties involved in the practical use of this characteristic for calculating the area of a stage are discussed on page 132).

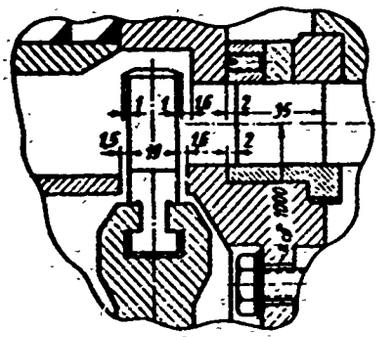

Fig. 136. Flow area of TsKTI impulse stage.

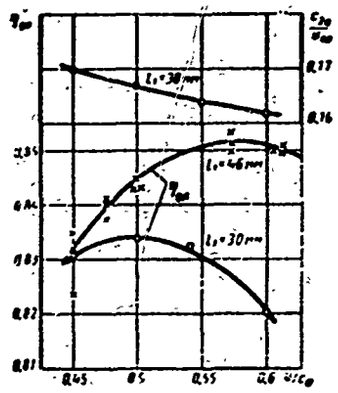

Fig. 137. Characteristic curve of a TsKTI stage with various heights, l_1 = 30 mm and l_1 = 46 mm (according to experiments of A. M. Zavadovskiy).

N. M. Markov presented data from TsKTI tests performed on a stage with the same cascades, TH-2 and T-2, with d = 580 mm, l_1 = = 46 mm, l_1/b = 0.75, l_2 = 50 mm, δ_a = 1.6 mm, and $Re_1 = 7.6 \cdot 10^5$ [70].

Another series of TsKTI stages has an C-1 nozzle cascade developed by the Krylov TsNII and two versions of TsKTI moving cascades, T-1 and T-2. The characteristics of the cascades and their profiles are given in the profile standards. A stage was tested in an experimental air turbine developed at TsKTI by N. M. Markov. The flow area of this stage is shown in Fig. 138. The geometric characteristics of the experimental stage: l_1 = 20 mm, l_1/b_1 = 0.37, $\bar{t}_1$ = 0.76, $\alpha_y = 39^\circ$, $\alpha_{1\,эф} = 12^\circ 55'$, l_2 = 23 mm, l_2/b_2 = = 23 mm, l_2/b_2 = 1.15, $\bar{t}_2$ = 0.675, and d/l_2 = 26.1. The experiments were conducted at M_1 = 0.65 to 0.75, and Re = 7.4 to $8.0 \cdot 10^5$. Four versions of the stage were investigated:

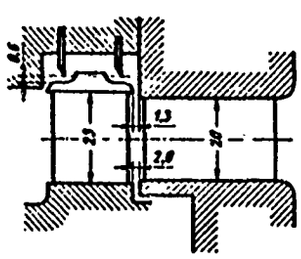

Fig. 138. Flow area of TsKTI stage with radial sealing.

1 – cascade T-1, angle $\beta = 77^\circ 30'$; 2 – cascade T-11, $\beta_y = 77^\circ 33'$; 3 – cascade T-1, angle $\beta_y = 80^\circ 30'$; 4 – cascade T-11, $\beta_y = 78^\circ 45'$ (for curves 1, 2, 3, and 4, see the graphs in Fig. 139).

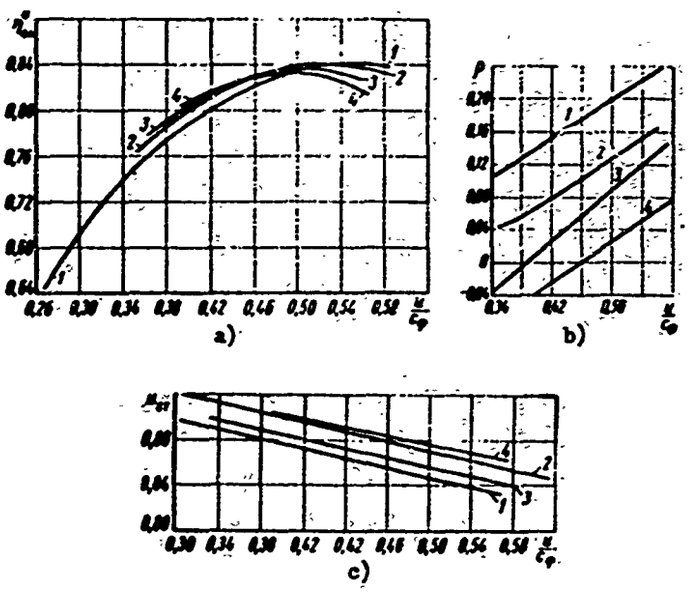

Fig. 139. Characteristic curves of a series of stages (see Fig. 138): a) efficiency; b) mean reaction; c) flow-rate coefficient.

The usual characteristics are given for this series of stages: relative blade efficiency $\eta_{ОЛ} = f(u/c_{ф})$ in Fig. 139a, reaction $\rho = f(u/c_{ф})$ in Fig. 139b, and flow rate coefficient of stage $\mu_{СТ} = f(u/c_{ф})$ in Fig. 139c.

By comparing the results of the experiments with the various combinations in Fig. 139, we see that the optimum $x_{ф_{ОПТ}} = 0.5$ to 0.54. The highest efficiency is given by stages 1 and 2. However, these stages (especially stage 1) have a very large reaction which, with an increase of the sealing clearances, will lead to considerable losses due to steam leakages. Stage 4, conversely, when $x_{ф} < 0.5$, will have a negative root reaction which, as we know (see § 22), has an unfavorable effect on economy, and will cause additional losses in an actual stage. From these positions, the best one seems to be the stage of curve 3; however, in the investigated conditions, it has an efficiency that is 0.5% lower.

The flow rate coefficient of a stage was defined as the ratio of the actual flow rate to the flow rate calculated according to the area of the nozzle cascade and the entire drop of the stage. The coefficient $\mu_{СТ}$ depends mainly on the reaction of stage and at $\rho = 0$ it should coincide with the flow rate coefficient of the nozzle cascade, μ_1, (especially at very low M numbers). In these experiments they obtained $\mu_1 \approx 0.89$, which is extremely small and does not correspond to the experiments conducted by other organizations (MEI, NZL, and LMZ), and also the results of static investigations.

§ 24. STAGES CALCULATED FOR LOW VELOCITY RATIOS $u/c_{ф}$

An important practical problem is the transfer of groups of stages of certain machines to operation with low velocity ratios, $x_{ф} = u/c_{ф}$. It is well known that in this way, by retaining the power and the speed, it is possible to considerably lower the weight and dimensions of a turbine, since the number of steps in the flow

area and their dimensions are then decreased.

With the help of a formula that determines the available heat drop in a turbine,

$$H_0 = (1+\nu) h_{ac,p} z = (1+\nu) \frac{u_{cp}^2 z}{2x_{\phi cp}^2}, \tag{139}$$

where ν is the reheat factor, it is easy to establish that, with the preservation of the peripheral velocities, the number of stages in the flow area varies in inverse proportion to $x_{\Phi cp}^2$, i.e.,

$$\frac{z_2}{z_1} = \left(\frac{x_{\phi 1}}{x_{\phi 2}}\right)^2.$$

It follows from this, for instance, that with a transition from $x_\Phi = 0.5$ to $x_\Phi = 0.34$-0.35, the number of stages decreases by 2 times.

By keeping the peripheral velocity constant, the diameters of stages also do not change. This means that front and rear parts of a machine in two comparable cases have identical dimensions and weight characteristics. A decrease of the dimensions and weight of a machine occurs only after reducing the number of stages.

Let us consider another extreme case, assuming that the number of stages, upon transition to small u/c_Φ, remains constant. Then from formula (139) we obtain:

$$\frac{u_1}{u_2} = \frac{x_{\phi 1}}{x_{\phi 2}} \text{ or } \frac{d_1}{d_2} = \frac{x_{\phi 1}}{x_{\phi 2}},$$

i.e., the diameters of the stages decrease in proportion to the x_Φ ratio. In accordance with this, the diameters and the thickness of the diaphragms and the machine casing decrease, and the dimensions and weight of the inlet and outlet parts of the machine are reduced.

An intermediate solution of the problem is also possible, when the peripheral velocities and the number of stages of the flow area are changed. From formula (139) there can be obtained a simple relationship:

$$\frac{z_1}{z_2}\left(\frac{u_1}{u_2}\right)^2 = \left(\frac{x_{\phi 1}}{x_{\phi 2}}\right)^2 \text{ or } \frac{d_1}{d_2} = \frac{x_{\phi 1}}{x_{\phi 2}}\sqrt{\frac{z_2}{z_1}}.$$

Comparison of the considered variants is performed on the basis of formulas that express the stress in the diaphragms, disks, blades, and turbine casing. If we assume that the stresses in the indicated elements remain constant, then the corresponding formulas make it possible to establish a decrease in the weight and dimensions of the turbine upon transition to lowered u/c_Φ ratios.

Calculations show that the transition to smaller diameters, while retaining the former stresses in the components, lowers the weight of the diaphragms in proportion to x_Φ^3, while the weight of the casing and the weight of the disks is $\sim x_\Phi^2$.

It is obvious that a transition to small $x_{ф}$ is expedient only in the case when the economy of installation is kept practically on the level which corresponds to optimum values of $x_{ф}$. In solving the aerodynamic part of the problem, it is necessary to consider ways of increasing the effectiveness of the regulating, intermediate, and last stages upon transition to small $x_{ф}$ ratios.

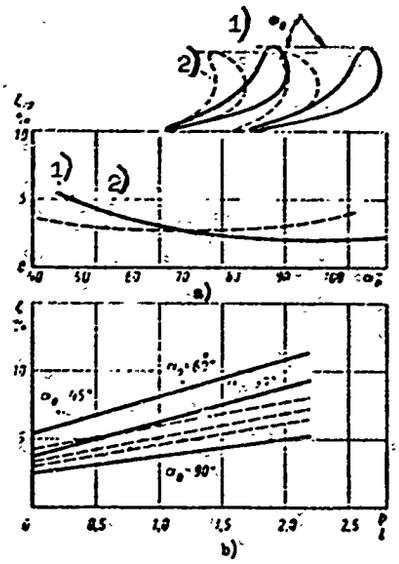

Fig. 140. Characteristics of nozzle cascades: a) profile losses in nozzle cascades for optimum (TC-1A) and lowered (TC-1A-1) $x_{ф}$ ratios; b) total losses in nozzle cascades: —— solid line TC-1A; – – – – dotted line TC-1A-1. 1) TC-1A; 2) TC-1A-1.

We shall first mention the methods of profiling intermediate stages. The transition to small x leads to a decrease of the entrance angle of flow α_0 into the nozzle cascades of intermediate stages, which causes an increase of both profile losses, and also end losses in the nozzle cascades. Corresponding data on the influence of α_0 are given in Chapter I. Figure 140a represents the dependence of profile losses in a TC-1A cascade on the entrance angle α_0. With a change of angle α_0 from 90 to 45°, the profile losses increase from 2 to 5.5%.

The end losses vary depending upon the entrance angle to a larger degree and especially at low relative heights. With the decrease of α_0 for usual profiles, not only a growth of total losses is noted, but also an increase of the angle of inclination of the straight lines in the coordinates ζ and b/l (see Fig. 140b).

It should be emphasized that with the transfer to smaller stages diameters, the blade heights increase; therefore, the actual growth of the end losses, and consequently, also the total losses for small $x_{ф}$ will be less considerable. At the same time, the given experimental data distinctly show the necessity for special profiling of nozzle cascades for special profiling of nozzle cascades for small entrance angles of flow.

The MEI laboratory developed a group of nozzle cascade profiles for small angles α_0. The corresponding results of tests are shown in Fig. 140, where the profile and total losses are given depending upon the entrance angle of flow α_0 and for a cascade of TC-1A-1 profiles.

The advantages of new profiles are especially noticeable for low relative heights ($b/l > 1.0$).

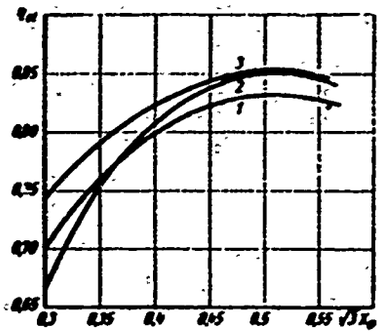

Fig. 141. Relative internal efficiency of stages, depending upon $\sqrt{3}x_{\Phi}$ with d = = 860 mm, l_{cp} = 23 mm). Curves: 1 — one average stage; 2 — group of three stages with TC-1A nozzle cascades; 3 — group of three stages with TC-1A-1 nozzle cascades (experiments of Kaluga Turbine Plant).

Experimental turbine investigations of cascades with profiles of this type showed that they had considerable advantages for operation in a group of stages with small x_{Φ}. Figure 141 illustrates the efficiency curves for a group of three stages; the curves were obtained in the laboratory of the Kaluga Turbine Plant.

From a consideration of the graph, it is distinctly clear that the application of new nozzle cascades made it possible to raise the efficiency by 3 to 7% in a range of x_{Φ} = 0.3 to 0.4. The curves in Fig. 141 also show that for small x_{Φ} the effectiveness of a group of stage with the usual nozzle cascades is lowered more intensely than that of one stage, and when $\sqrt{3}\cdot x_{\Phi} \leq 0.37$ the efficiency of a single stage is higher.

This indicates that nozzle cascades with the usual leading edge of the profile, with a geometric angle of ~90°, operate at low heights with a sharp growth in losses when $\alpha_0 < 90°$. Consequently, in this case the use of the kinetic energy of the preceding stage noticeably decreases.

For stages that operate at small x_{Φ}, it is necessary also to apply special profiles for the moving cascades, considering that in the conditions of $x_{\Phi} < x_{\Phi_{опт}}$ a usual stage works with a negative reaction and angle $\beta_1 < \beta_2$. Consequently, in these conditions it is necessary to lower the losses in the moving cascade as much as possible; this is attained by decreasing the ratio F_2/F_1, by applying special profiles and, to a lesser degree, by meridional profiling of the moving cascades.

In the first case it is necessary to construct a cascade with diffuser channels or channels of constant cross section, depending upon the selected relationship of angles β_1 and β_2. It should be noted here that for small x_{Φ} it is expedient to use increased angles α_1 and β_2, if this does not lead to a sharp decrease in height, and correspondingly, to a lowering of efficiency, greater than the gain obtained as a result of the transition to more rational velocity triangles.

Let us note that the application of expansion for moving cascades (tapered shrouds), which is shown in Fig. 142a, leads to a considerable growth in losses.

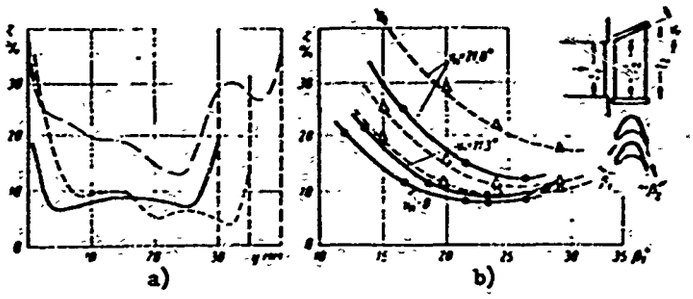

Fig. 142. The influence of the taper of shrouds on losses in a moving cascade: a) influence of the taper of shrouds on the distribution of losses along the height of a TP-1Ак cascade: — · — · — $\nu_п = 21.8^o$; — — — $\nu_п = 11.3^o$; —— $\nu_п = 0$; b) total losses in cascades with various fluid deflections: —— for TP-0Ак; — — — TP-1Ак at $M_2 = 0.6$ to 0.7; $Re_2 = 3.1 \cdot 10^5$.

With the increase of the fluid deflection in the cascade, the influence of the taper of the shrouds weakens (Fig. 142b).

An essential increase in the effectiveness of regulating stages and last stages at small $x_ф$ may be attained by installing diffusers. Diffusers behind a stage can be of two types: the vaned type, in the form of compressor cascades, and the vaneless type.

A diagram of the flow area of a single-wheel regulating КД-1-2Д stage with a vaned diffuser is shown in Fig. 143a.

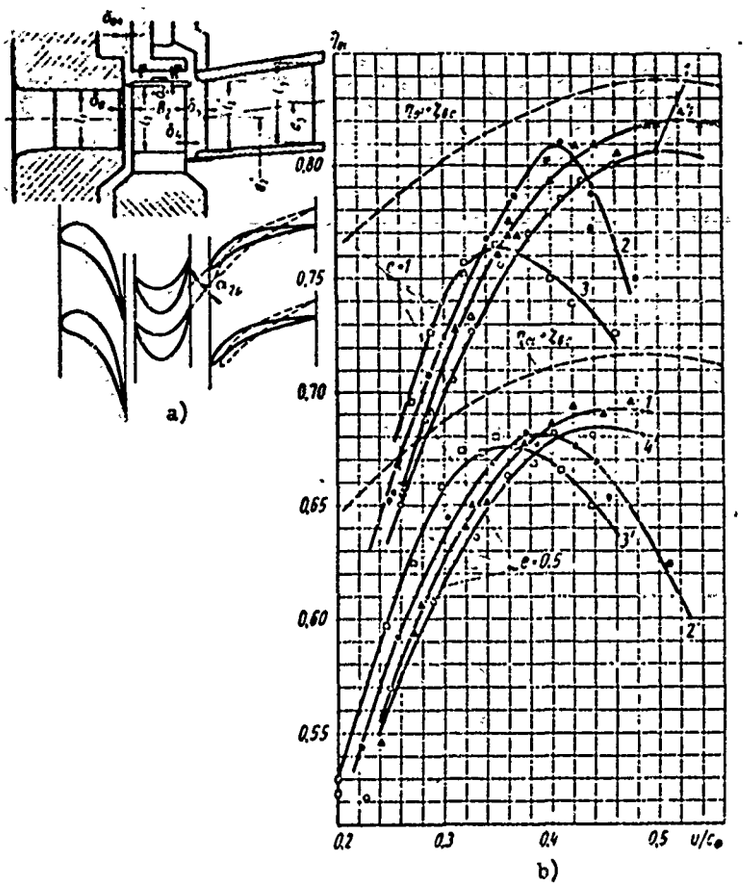

Fig. 143. Characteristics of a single-wheel regulating stage with a diffuser: a) flow area of КД-1-2Д regulating stage; b) dependence of relative internal efficiency of single-wheel stage with diffuser for various admission. Curves: 1 — without diffuser at full input (e = 1); 2 — with vaned diffuser (α_{2p} = = 50°); 3 — with vaned diffuser ($\alpha_{2p} = 40^o$); 4 — for vaneless diffuser (e = = 1); 1' — vaneless diffuser (e = 0.5); 2' — with vaned diffuser; $\alpha_{2p} = 50^o$; 3' — with vaned diffuser (α_{2p} = = 40°); 4' — without diffuser (d_{cp} = 400 mm; l_1 = 25 mm, ε = 0.8 - 0.75; F_3/F_2 = = 1.49, $Re_{c_1} = 5.4 \cdot 10^5$) (MEI experiments). — — — — dotted curve without taking into account the losses with the outlet velocity.

An important geometric parameter of the vaned diffuser is the ratio of the outlet and inlet flow areas (F_3/F_2). The inlet area is determined by the exit angle of flow from the moving cascade during absoulte motion, α_2; the geometric entrance angle of the profile, α_{2p}, should be close to α_2. The height of the diffuser at the entrance should exceed the exit height of the moving cascade of the stage by 2 to 3 mm; the entrance to the diffuser should be rounded in this case. By turning the profiles in the diffuser, it is possible to adapt the diffuser to other angles α_2. The necessary area of the outlet section may be ensured not only by expanding the vane channels, but also by increasing the height of the diffuser.

The vaneless diffuser is formed by two tapered shrouds which increase the cross-sectional areas by increasing the diameter and height of the channel.

The results of an investigation of the influence of diffusers (vaned and vaneless) on the effectiveness of a single-wheel with full and partial input are shown in Fig. 143b).

As can be seen from the curves, diffusers give a noticeable increase in efficiency in a wide range of conditions both with full, and also with partial input. The vaneless diffuser leads to an increase in efficiency under all conditions and especially at optimum x_Φ and values close to it. In the zone of small x_Φ, the increase in the efficiency of a stage with a vaneless diffuser is insignificant. Consequently, the vaneless diffuser does not make it possible to noticeably lower x_Φ while preserving the effectiveness of the stage and its use is recommended in those cases when the designed partial stage must operate in a wide range of conditions.

Vaned diffusers, which are made up of compressor vanes, lead to an essential increase in efficiency at small x_Φ for full partial input. In conditions of $x_\Phi \geq$ ≥ 0.4, the efficiency of a stage with a vaned diffuser sharply drops; under these conditions the compressor cascade is streamlined with negative angles of attack, which leads to separation of flow. In this case the diffuser is an additional large resistance.

By changing the angle of incidence of the vanes, the maximum efficiency can be displaced with respect to x_Φ (see Fig. 143b) in one direction or another. The same result can be obtained by the appropriate profiling of the diffuser vanes.

Figure 143b illustrates curves for efficiency without taking into account the losses with the outlet velocity (dotted line). A comparison of it with the curves of efficiency η_{01} for a vaned diffuser ($\alpha_{2p} = 50^\circ$) shows that with this diffuser, at the points of maximum efficiency (curve 2; $x_\Phi = 0.4$), more than 50% of the losses with the outlet velocity is restored in the diffuser. By changing the

entrance angle of the profile, α_{2p}, and increasing the divergence of the channels, it is possible to displace the efficiency curve to the left without essentially lowering the efficiency at the point of maximum.

By deforming the profile of the vaned diffuser somewhat, it is not difficult to obtain an efficiency maximum at $x_{\Phi} = 0.3$ to 0.35.

The curves in Fig. 143b distinctly show that the effectiveness of a vaned diffuser is especially great when the input is partial, whereby the efficiency maxima for all versions are essentially close.

The relative increase of the internal of a stage with a diffuser, depending upon x_{Φ}, is shown in Fig. 144. When $\alpha_{2p} = 40$, the biggest increase in efficiency is obtained, and with partial input ($e = 0.5$) when $x_{\Phi} \geq 0.3$, it reaches 6 to 7%. For $\alpha_{2p} = 50^{\circ}$, the maximum $\Delta\eta_{0i}$ is reached at $x_{\Phi} \leq 0.4$ and amounts to 3.8% (when $x_{\Phi} = 0.38$). The vaneless diffuser shows an increase in efficiency of ~2% with full inputs, whereby $\Delta\eta_{0i} > 0$ in the entire range of the velocity ratio.

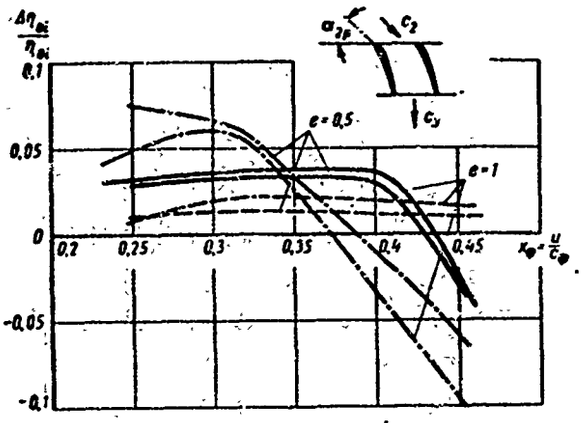

Fig. 144. Increase of the efficiency of a stage, created by diffusers, with full and partial inputs, depending upon x_{Φ}; — solid curve for vaned diffuser with angle of vane incidence $\alpha_{2p} = 50^{\circ}$; — · — · — the same for $\alpha_{2p} = 40$; — — — dotted line indicates vaneless diffuser.

Let us consider the methods of estimating the increase in the efficiency of a stage with the use of diffusers. The most simple method of performing this estimate is in case when the diffuser, which is mounted behind the stage, decreases the available heat drop in it.

In this case the pressure behind the stage increases from the value of p_2 to p_3, and the heat drop decreases from h_0 to h_0' (Fig. 145a).

The stagnation process in a diffuser is depicted in an i-s diagram in section 2-3. At the exit from the diffuser the velocity will be c_3 and point 0_2 gives the state of the isentropically stagnated flow behind the diffuser. The actual process of stagnation may be assumed as isobaric (section 3-4 on isobar p_3). The available kinetic energy before the diffuser is equal to $c_2^2/2$, where c_2 is the absolute outlet velocity from the moving cascade. Line 2-4' depicts the process of isobaric annihilation of the kinetic energy behind a stage without a diffuser. It is obvious that in the considered case the points 0_2, 4, and 4' lie on one line,

i_{oc_2} = const, and the heat drop h_i used in the stage remains constant.

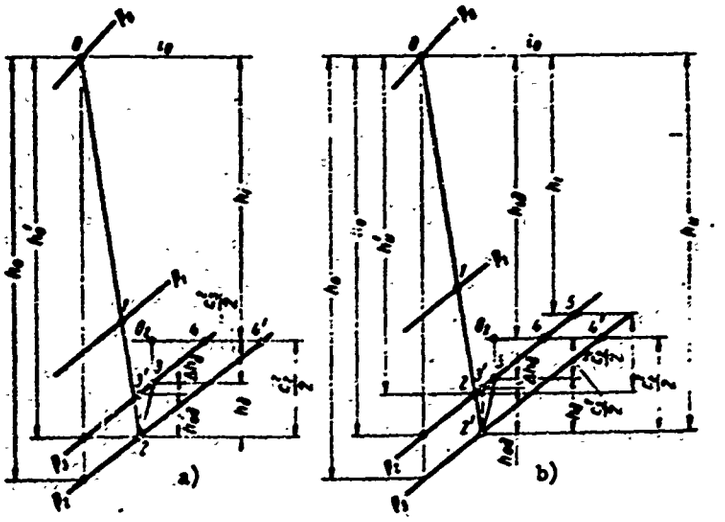

Fig. 145. I-s diagram of the thermal process of a stage with a diffuser: a) increase of pressure behind stage, caused by diffuser; b) lowering of pressure behind stage.

The efficiency of a stage without a diffuser will be:

$$\eta_{oi} = \frac{h_i}{h_0},$$

and with the installation of a diffuser

$$\eta_{oi\,д} = \frac{h_i}{h_0'}.$$

By comparing these expressions, we obtain:

$$\eta_{oi\,д} = \eta_{oi}\frac{h_0}{h_0'} = \eta_{oi}\frac{h_0' + h_{oд}}{h_0'} = \eta_{oi}(1 + \bar{h}_{oд}). \qquad (140)$$

Here $h'_{oд}$ is the work of compression in the diffuser for an isentropic flow (without losses), which is determined by segment 2-3' in Fig. 145a.

The quantity $h_{oд}$ is determined by the following formula:

$$h_{oд} = \frac{1}{2}(c_2^2 - c_3^2) - \Delta h_д = \frac{c_2^2}{2}\left(1 - \frac{c_3^2}{c_2^2}\right) - \Delta h_д.$$

Here $\Delta h_д$ are the losses of kinetic energy in the diffuser (see Fig. 145a).

Let us introduce the efficiency of the diffuser, and determine this quantity as the following ratio

$$\eta_д = \frac{\frac{c_3^2}{2} + h'_{oд}}{\frac{c_2^2}{2}} = \frac{\frac{c_2^2}{2} - \Delta h_д}{\frac{c_2^2}{2}} = 1 - 2\,\frac{\Delta h}{c_2^2} \qquad (141)$$

or

$\eta_Д = 1 - \zeta_Д$, where $\zeta_Д = 2\frac{\Delta h_Д}{c_2^2}$ is the loss coefficient in the diffuser. Consequently:

$$\Delta h_д = (1 - \eta_д)\frac{c_2^2}{2} = \zeta_д \frac{c_2^2}{2}.$$

The relative work of compression for an isentropic flow is determined:

$$\bar{h}_{od} = \frac{h_{od}}{h_0'} = \xi_{вс}'\left(1 - \frac{c_3^2}{c_2^2}\right) - \xi_{вс}'(1 - \eta_д) = \xi_{вс}'\left(\eta_д - \frac{c_3^2}{c_2^2}\right), \tag{142}$$

where $\xi_{вс}' = \frac{c_2^2}{2h_0'}$ is the loss coefficient with the outlet velocity (losses refer to a new heat drop on the stage).

Substituting $\bar{h}_{oД}$ in formula (140), we finally find:

$$\eta_{oid} = \eta_{oi}\left[1 + \xi_{вс}'\left(\eta_д - \frac{c_3^2}{c_2^2}\right)\right]. \tag{143}$$

The velocity ratio here, by means of a continuity equation, may be replaced by the cross-sectional ratio of the diffuser.

At a given pressure behind the stage, p_2, and a fixed heat drop, h_0', the installation of a diffuser lowers the pressure behind the moving cascade. The heat process that corresponds to this case is shown in Fig. 145b. In this case the pressure behind the moving cascade without a diffuser is accepted as equal to p_2 and with the installation of a diffuser the same pressure is established in the chamber of the stage.

Without a diffuser, the process in the stage proceeds along the line 0-2-5, whereby the losses with the outlet velocity are measured by the segment 2-5, which is equal to $c_2'^2/2$ (c_2' is the absolute outlet velocity from a stage during operation without a diffuser). In the presence of a diffuser, the expansion in the stage corresponds to the line 0-2-2'-3-4. The kinetic energy at the moving cascade exit will be $c_2^2/2$, and $c_3^2/2$ behind the diffuser. Point 4 determines the stage of the gas behind the stage. As a result, the used heat drops will be various (h_i and $h_{iД}$), and the efficiency in the presence of a diffuser may be expressed by the following formula:

$$\eta_{oid} = \eta_{oi}\frac{h_{id}}{h_i}, \tag{144}$$

since

$$\eta_{oid} = \frac{h_{id}}{h_0} \text{ and } \eta_{oi} = \frac{h_i}{h_0}.$$

The values of h_i and $h_{iД}$ are determined by the following formulas (see Fig. 145b):

$$h_i = h'_u - \frac{c'^2_2}{2} \text{ and } h_{iд} = h_u - \frac{c_2^2}{2}.$$

After substituting h_i and $h_{iД}$ in formula (144), and making simple transformations, we will obtain:

$$\eta_{oid} = \eta_{oi} \frac{\eta_u - \xi_{вс}}{\eta'_u - \xi'_{вс}} (1 + \bar{h}_{od}). \tag{145}$$

Here

$$\eta_u = \frac{h_u}{h_0}; \quad \eta'_u = \frac{h'_u}{h'_0}; \quad \xi_{вс} = \frac{c_2^2}{2h_0}; \quad \xi'_{вс} = \frac{c'^2_2}{2h'_0}.$$

The relative isentropic heat drop in a diffuser is determined by a formula (142) that is well-known to us.

We shall use expression (145) and, after substituting $\bar{h}_{oД}$ in it, we will obtain:

$$\eta_{oid} = \eta_{oi} \frac{\eta_u - \xi_{вс}}{\eta'_u - \xi'_{вс}} \left[1 + \xi'_{вс} \left(\eta_д - \frac{c_3^2}{c_2^2} \right) \right]. \tag{146}$$

Formula (146) changes into (143), if

$$\eta_u - \xi_{вс} = \eta'_u - \xi'_{вс}.$$

How formulas (143) and (146) show, an increase in the efficiency of a stage with the installation of a diffuser very significantly depends on the loss coefficient with the outlet velocity $\xi_{вс}$, the efficiency of the diffuser $\eta_Д$, and the velocity ratio c_3/c_2, which may be replaced approximately by the ratio of areas (disregarding the change of density in the diffuser):

$$\frac{c_3}{c_2} \simeq \frac{F_2}{F_3},$$

and in the case of a vaned diffuser

$$\frac{c_3}{c_2} \simeq \frac{d_2}{d_3} \frac{l_2}{l_3} \frac{\sin \alpha_2}{\sin \alpha_3},$$

where the subscripts 2 and 3 designate the corresponding parameters at the entrance to the diffuser and at the exit.

In comparing the two considered methods for determining the effect of a diffuser behind a stage, it should be noted that in the first case the influence of the diffuser is estimated for an increase of $x_ф$, which is created by the diffuser, and in the second case, for constant $x_ф$.

It should be emphasized that the physical influence of a diffuser remains identical in both cases, and differs only by the formulation of the problem and the calculation formulas, correspondingly.

For the calculation of a stage with a diffuser, it is necessary to know the magnitude of the power efficiency of the diffuser, which is determined by experimental means.

Figure 146a gives the curves of the change of $\eta_д$ depending upon the entrance angle α_2 for several types of diffusers, and Fig. 146b shows the influence of the basic geometric parameters on $\eta_д$.

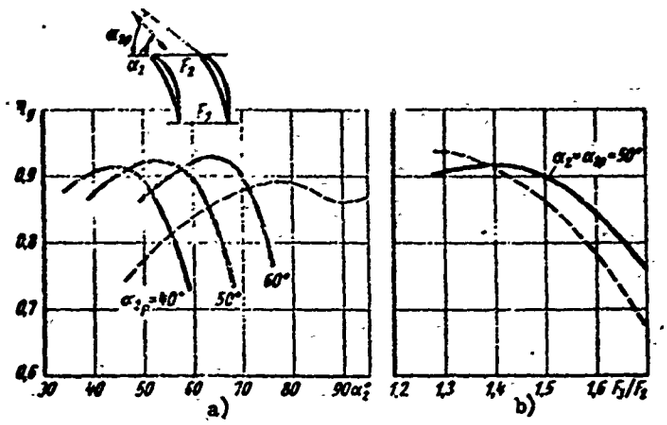

Fig. 146. The influence of certain geometric and performance parameters on the efficiency of diffusers: a) entrance angle of flow α_2^o; b) ratio of areas F_3/F_2. Curves: —— with vaned diffuser; – – – – vaneless. M_2 = 0.4 to 0.5; $Re_2 = 4.2 \cdot 10^5$.

As should have been expected, the vaned diffuser is more sensitive to changes in the entrance angle of flow, and the vaneless diffuser is more sensitive to changes in the ratio of areas. At small entrance angles, the vaned diffuser has an indisputable advantage, which gives us a basis to recommend it for regulating stages that operate at lowered values of $x_ф$. The vaneless diffuser may be used for increasing the efficiency of a stage in the zone of optimum values of $x_ф$.

The vaned diffuser should also be recommeded for the last stages in a group (cylinder), if the flare of the stage is not too great ($\theta \geq 7$ to 10). For the last stages of condensing steam turbines of limited dimensions, the question of an optimum diffuser setup remains open. The transition in such stage to lowered $x_ф$ sometimes is expedient; however, the possibility of providing sufficiently high efficiency at small $x_ф$ should be established experimentally. A set of problems arises here in connection with the selection of the reaction, the determination of a rational method of twisting, the establishment of the most rational design for the outlet duct, etc.

CHAPTER V

VELOCITY STAGES

§ 25. STRUCTURAL DIAGRAMS OF DOUBLE-WHEEL VELOCITY STAGES

Velocity stages, which are frequently called Curtis stages (disks), are widely used in various types of steam turbines.* The possibility of sufficiently effectively producing a large heat drop, thereby simplyfying the design and reducing the construction costs of a turbine, on the one hand, and essentially lowering the steam temperature inside a turbine, on the other hand, led to the fact that velocity stages are being applied in turbines of various power from several kilowatts to several hundred thousand kilowatts. These stages are being applied everywhere in turbines of low and medium power, in marine turbines, and drive turbines. The use of velocity stages in these machines is prompted by the large range of load variation, when it is expedient to increase the heat drop of the regulating stage. The same should also be extended to turbines with steam bleed. Velocity stages are also widely used in power machinery. An example of this is the LMZ series of high-pressure turbines, the LMZ turbine CBK-150, turbine No. 1 at the Addistown Station (USA), the Westinghouse 325 thousand-kilowatt turbine, the Siemens-Schuckert 150 thousand-kilowatt turbine for the Fortuna Station (FRG), and others. Velocity stages are used everywhere in the form of regulating stages or first stages (for throttled steam distribution), in marine turbines, and for astern stages.

It should be noted that the economy of velocity disks was determined recently only on the basis of the results of tests of steam turbines with old-type velocity wheels. Thorough investigations of velocity wheels, including comparative analyses,

---

*Recently, velocity stages have also been employed in gas turbines.

and also attempts to create new, highly economical stage, began only recently.

In the steam turbines that were manufactured earlier by our turbine-construction plants, several combinations of double-rim* velocity wheels were employed. These wheels were developed lately by certain foreign firms (mainly by GE in the United States), and were modified to some extent by our plants. In 1955, the Department of Steam and Gas Turbines of the MEI created several combinations of velocity stages, checked them in experimental turbines, and had them manufactured by the turbine-construction plants (KTZ, LMZ, LKZ, UTMZ, the Pilsen plants in Czechoslovakia, and others). Following the MEI, the VTI and TsKTI began developing new velocity stages.

The double-wheel velocity stage, as compared to the single-wheel model, is a more complicated cascade combination. The design of the flow area of a velocity wheel is determined by:

a) the cascades;

b) the relationships between the geometric characteristics of the cascades (areas, heights, and angles);

c) the axial clearances (open and closed) and the stage sealing.

Selection of the geometric design of a velocity stage depends on many factors, the basic ones of which are:

1) the operating conditions of the stage, i.e., the pressure ratio $\varepsilon = p_2/p_0$ and the velocity ratio u/c_ϕ, where $c_\phi = \sqrt{2h_0}$ is the fictitious velocity, which is calculated for the entire heat drop of the stage;

2) the change of the operating conditions of the stage;

3) the admission of the stage and the quantity of nozzle arcs (including the clearances between arcs), and the possibility of installing special protection;

4) the possibilities of the stage sealing;

5) the conditions of strength and vibrational reliability of the blading;

6) the technology and quality of manufacture.

Let us discuss the influence of these factors (the influence of admission is considered in the following chapter). Stages that are calculated for operation with supersonic velocities at very large drops ($\varepsilon < 0.4$ to 0.3) can have nozzle cascades with expanded channels (see § 32). However, even at velocities exceeding critical, to $\varepsilon > 0.4$, convergent nozzles are usually applied.

---

*This book does not consider the triple-wheel velocity stages which are rarely encountered and only under specific conditions.

In the last case it is necessary to consider the effectiveness of these cascades under supersonic conditions of flow, and also the change of the direction of the exit angle (taking into account the deflection of flow in the slanting shear of the cascade).

As the experiments show, the optimum values of $x_{\Phi} = u/c_{\Phi}$ depend on the cascade combination, $\varepsilon = \frac{p_2}{p_0}$, and on certain additional geometric factors (absolute values of areas, clearance sealing, and others). For known quantities of the computed values of x_{Φ} and ε, the combination that provides the highest efficiency should usually be selected.

Besides the computed values of x_{Φ} and ε, it is necessary to know within what limits these quantities vary. In most cases we try to attain a sufficiently high stability of efficiency in a wide range of variation of x_{Φ} and ε, sometimes being satisfied with a lower efficiency under design conditions.

The possibilities of the stage sealing to a considerable extent determine the selection of the calculated reactions, i.e., the ratio of the cascade areas. If for some reason it is not possible to ensure sufficient sealing of the clearances, and also for partial steam input, then it is not recommended to apply considerable positive, and all the more so, negative degrees of reaction. It should be recalled that when the conditions are changed (ε, and mainly x_{Φ}), the reaction of the stage and of its separate wheels changes. Increase of x_{Φ} causes a growth of the reaction, and with poor sealing, it brings about an increase in steam leakages. This is the tendency with the decrease of ε. One should not forget that an increase of the reaction leads to the large influence of losses in the moving and rotating cascades on the efficiency of the stage. The losses in these cascades are considerably higher than those in a nozzle cascade, mainly due to the considerable end effects.

In a regulating stage with a low steam rate, the velocities of the flow become so high that there occurs choking of the channels of the moving cascade and, in spite of the lowering of x_{Φ}, the reaction increases.

In turbines with high parameters with respect to conditions of strength and vibrational reliability, it is necessary to make the rotor blades wider than is usually done. Consequently, the relative height of the cascades decreases, and their effectiveness is lowered. For design simplification in low-power turbines, the blades frequently are made with straight shrouds, which creates additional conditions for the ratio of areas and heights.

The geometric characteristics of a number of velocity stages with convergent nozzle channels are presented below.

Old Cascade Combinations for Low-Power Turbines

This combination was employed earlier in several modifications by the KTZ and NZL.

Let us consider a stage according to the data of NZL (AK-6 stage). The geometric characteristics of the velocity stage are given in Table 9.

Table 9. Geometric Characteristics of NZL Velocity Stages

Parameters of stage	Type of stage	
	AK-6	AKB-14
Height of nozzle cascade	18 мм	15.2 мм
Sine of effective angle:		
nozzle cascade	0.171	0.245
1st moving cascade	0.22	0.285
rotating cascade	0.31	0.398
2nd moving cascade	0.50	0.527
Ratio of areas:		
F_{1p}/F_1	1.57	1.53
F_n/F_1	2.52	2.56
F_{2p}/F_1	4.71	4.25
Ratio of heights:		
l_{1p}/l_1	1.23	1.32
l_n/l_1	1.39	1.58
l_{2p}/l_1	1.61	1.98

A consideration of the cascades of this stage and investigations of certain ones, conducted by a number of organizations, showed that they have unsatisfactory profile shapes, are sensitive to changes in the conditions of flow (velocities and exit angles). At the same time, the successful selection of ratios of heights and areas, performed on experimental installations, made it possible, in spite of the poor quality of the cascades themselves, to attain satisfactory economy under design conditions. This selection made it possible, under these circumstances and with full steam input, to obtain an optimum distribution of the wheel reaction.

Old Combination of Velocity Stage Cascades for High-Power Turbines

This cascade combination differs by the large exit angle of the nozzle cascade, and the tapered shrouds of the rotating and second moving cascades. Its basic relationships are given in Table 10.

Table 10. Basic Characteristic Old Type of Velocity Stage Intended for Power Turbines

Designation	Symbol	Quantities
Cascade angles:		
nozzle	α_1	16°—18°
1st moving	β_2/β_1	25°/20°
rotating	α_{1R}/α_2	30°/26° or 27°/24°
2nd moving	β_2/β_1	50°/35° or 50°/40°
Ratio of cascade areas	F_{1R}/F_1	1.5
	F_R/F_1	2.5
	F_{2R}/F_1	4.2
Ratio of cascade heights	l_{1R}/l_1	1.1—1.2
	l_R/l_1	1.2—1.4
	l_{2R}/l_1	1.15—1.3

Plants, in applying this cascade combination, for different reasons frequently deviated from the relationships in Table 10, and they sometimes replaced certain cascades.

Thus, as also in the preceding stage, the moving cascades of this combination are unsatisfactory; at the same time, the losses in the nozzle cascade, with high heights, are not much higher than those in contemporary profiles. It should be borne in mind, however, that for velocity stages, in distinction from impulse single-wheel stages, the specific gravity of losses in the first moving cascade is very great and therefore a decrease of losses in it essentially improves the economy of the whole stage.

MEI Velocity Stages

The velocity stages created and developed by the Department of Steam and Gas Turbines at MEI are calculated for various heat drops and are recommended for steam turbines of various power and different purpose.

The investigations conducted at MEI, LKZ, KTZ, LMZ, and NZL by V. A. Abramov, F. V. Kazintsev, Yu. Ya. Kachuriner, V. D. Pshenichny, L. P. Sokolovskiy, and A. V. Shchekoldiny showed the advantages of these stages as compared to the others. The stages are composed of MEI cascades that were tested in static test rigs.

Inasmuch as velocity stages, as a rule, have low blade heights, and in a number of cases for guarantee of reliability it is necessary to have large chords, in the creation of the MEI velocity stages special attention was allotted to lowering the end losses. For this, in particular, the special measures listed above were applied, i.e., meridional profiling in the nozzle cascade with one-sided contraction, and type "K" profiles for the moving and rotating cascades.

The cascade combinations and the area ratios are selected in such a way as to ensure, first, high efficiency with partial steam admission and, secondly, low sensitivity to changes in conditions (ε and x_{ϕ}), which is very important practically for all velocity stages.

Depending upon the calculated pressure ratio ε and the volume flow rate Gv_0, various combinations of MEI velocity stages are recommended. Although the MEI developed a large number of combinations, this paragraph considers only those stages which were tested in the experimental turbines of various plants, those being used in new turbines, and modernized versions of old ones installed at electric power stations.

Three stages underwent this development:

1) stage KC-0A – intended for low volume flow rates of steam and low heat drops (for $0.7 > \varepsilon > 0.45$);

2) stage KC-1A – for high volume flow rates of steam and low heat drops ($0.75 > \varepsilon > 0.45$);

3) stage KC-1Б – for medium and high volume flow rates of steam and high heat drops ($0.7 > \varepsilon > 0.35$).

All of these stages can be recommended both in their original form, and also in an improved form (with meridional profiling and with type K moving cascades). The velocity stages were tested both with ganged milled nozzles, and also with welded nozzle cascades. The flow areas of MEI velocity stages are shown in Fig. 147. The cascades used for the blading of these stages, and their characteristics, are considered in Chapter I and are given in the atlas of profiles.

The geometric characteristisc of MEI velocity stages are given in Table 11.

The MEI velocity stages were investigated for various geometric parameters and they can be applied for any diameters and various heights, starting from l_1 = 14 mm and l_1/b_1 = 0.3 with a cylindrical contour and from l_1 = 10 mm and l_1/b_1 = 0.2 for meridional profiling with a high quality of manufacture.

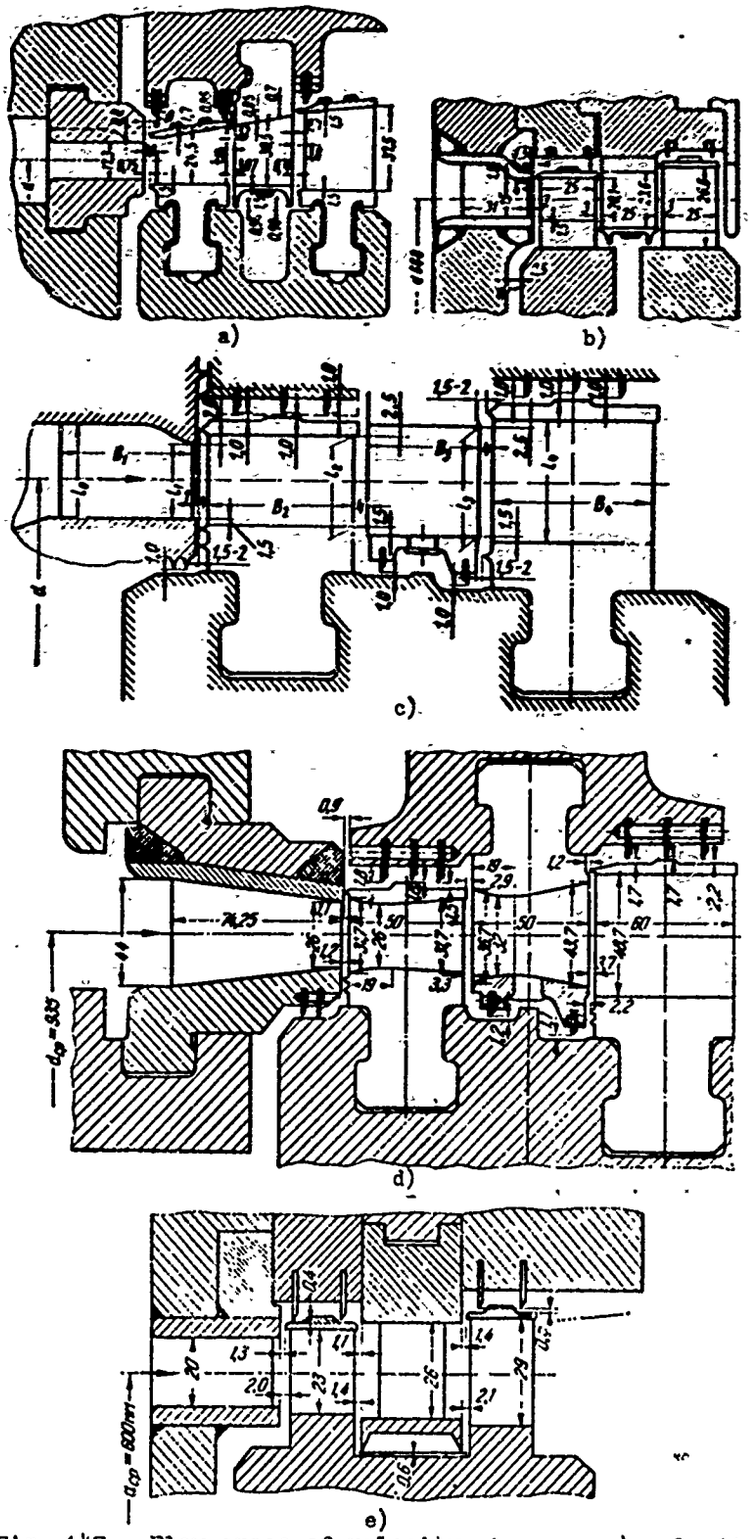

Fig. 147. Flow areas of velocity stages: a) velocity stage MEI KC-1Б with milled nozzles (LKZ design); b) velocity stages MEI KC-0A and KC-1Б with meridional profiling (KTZ design); c) MEI velocity stage for high-power turbines; d) VTI velocity stage; e) TsKTI velocity stage.

Table 11. Geometric Characteristics of MEI Velocity Stages

Designation		Type of stages		
		KC-0A	KC-1A	KC-1Б
Nozzle cascade.....		TC-1A	TC-2A or TC-2Aк	TC-2Б or TC-2Бк
1st moving cascade..		TP-0A	TP-1 or TP-1Aк	TP-1Б or TP-1Бк
Rotating cascade....		TP-2Aк	TP-3Aк	TP-3Aк
2nd moving cascade..		TP-4A	TP-4A	TP-5A
Cascade exit angles	1st nozzle	11—13°	14—16°	15—17°
	1st moving	14—16°	17—19°	17—20°
	rotating	20—22°	23—25°	23—25°
	2nd moving	28—30°	29—32°	31—33°
Ratio of cascade areas F/F_1	1st moving	1.52—1.56	1.48—1.54	1.5—1.56
	rotating	2.4—2.5	2.40—2.50	2.45—2.55
	2nd moving	3.5—3.6	3.4—3.6	3.5—3.8

VTI Velocity Stage

The VTI is using its own velocity stage for modernizing old-type turbines. The flow area of the VTI stage is shown in Fig. 147d. The geometric ratios of the VTI stage are given in Table 12. VTI velocity stages were investigated in experimental turbines at LMZ, LKZ, and NZL.

Table 12. Geometric Characteristics of VTI Velocity Stage for Modernization of LMZ Turbines BK-100-2

Designation	Cascade No.	Angles	F_2/F_1
Nozzle cascade.....	LM-2222	15°	1
1st moving cascade....	VTI-28	20°/16° 24′	1.23
Rotating cascade.....	VTI-34	25°/20° 37′	2.28
2nd moving cascade....	VTI-42	35°/32° 13′	4.16

In spite of meridional profiling and new moving and rotating cascades which, of course, should increase the economy of a stage, the VTI cascade combination has, in our opinion, essential deficiencies. First, the nozzle cascade is not the best under these circumstances, which was proven by static tests of LMZ]50]. Secondly, as may be seen from Table 12, the first moving cascade has a very small relative area as compared to the other combinations, and consequently, with full steam input it has a high reaction, which was confirmed by experiments in a turbine. With partial steam input, this high reaction will cause increased losses due to leakages, which considerably lower the economy.

TsKTI Velocity Stage

For subsonic velocities, the TsKTI developed and investigated [70] a velocity

stage. The stage was tested with one cascade combination and one height, l_1 = = 20 mm (l_1/b_1 = 0.87). The dimensions of the stage are shown in Fig. 147e. The axial, and especially the radial clearances are small. The stage was equipped with an C-1 nozzle cascade and T-1, T-2, and T-3 cascades. Angles $\alpha_{1\ эф} = 12^\circ.55'$. The stage was tested in two modifications; in the second, the angle of incidence of the profile of the first moving cascade was decreased by 1°, and increased by 2° for the rotating cascade.

The efficiency of the stage with full input is shown in Fig. 148. At optimum $x_ф$ the experiments were conducted with M_{c_1} = 0.9 and $Re_{c_1} = 11 \cdot 10^5$. The total reaction of the stage in the optimum zone amounts to Σ_ρ = 0.22 to 0.24 (curve 2).

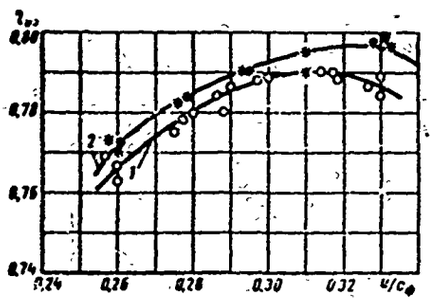

Fig. 148. Efficiency of TsKTI velocity stage with full input (TsKTI experiments): l_1 = 20 mm; ε = 0.5; $Re_{c_1} = 11 \cdot 10^5$.

The stage of the second modification, in experiments with radial seals removed (curve 1), showed a decrease in economy by $\frac{\Delta\eta_{oл}}{\eta_{oл}} = 0.05$ (at ε = 0.48 to 0.57). This stage was also investigated with partial input. In this case, in the inactive part of the rotating cascade the channels were closed and the bounds of the impulse arc were somewhat displaced. The efficiency of the stage with partial admission e = 0.5 amounted to $(\eta_{0i})_{max}$ = = 0.74.

Comparisons of Velocity Stage Economy

Plant laboratories conducted comparative investigations of various combinations of velocity stages, which are considered in this paragraph, in experimental steam turbines.

Similar tests are the most correct for a comparison of the economy of different combinations. An obligatory condition must be identical technology and quality of manufacture. In a number of cases these requirements were not observed, which should be borne in mind during the analysis of the results of the experiments.

KTZ experiments. The KTZ laboratory conducted a comparison of the economy of an old combination and MEI stages KC-1A in the original version. The stage tested had a diameter of 800 mm, nozzle height 15 mm, and partial admission e = = 0.41. Under transonic conditions (ε = 0.48 to 0.59) the efficiency η_{0i} was increased from 56.7% to 72%. The technology of manufacture of the stage was

practically identical and corresponded to standard plant technology [74].

LMZ experiments. With an identical diameter of $d = 935$ mm, nozzle height $l_1 = 19.7$, and full steam input, three full-scale velocity stages were tested; an old LMZ stage similar to the stage considered above in Table 10; an MEI KC-1A stage in original form, i.e., without meridional profiling; a VTI stage with meridional profiling. All three stages were manufactured with large design deviations. The experiments were conducted at a constant speed, $n = 3000$ rpm. The highest efficiency of the MEI stage, as compared to the old stage, gave a gain of $\frac{\Delta\eta}{\eta} = 14\%$. The curve of efficiency of the VTI stage lies between these two curves. With partial steam input, the advantages of the MEI stage should be exhibited to an even greater degree (see Chapter VI).

NZL experiments. The economy of an AK-6 NZL and an MEI KC-1B velocity stage was compared. The MEI stage was tested in original form with a welded diaphragm manufactured by KTZ. The NZL stage had milled nozzles; therefore, a comparison of the results of the experiments is difficult. Furthermore, it should be noted that the AK-6 NZL stage must be compared with an MEI KC-0A stage, which is also calculated for low volume flow rates of steam. According to the results of NZL experiments with full steam input, both stages that were investigated have approximately identical economy. With partial steam input, the MEI stage has an advantage of 0.3 to 0.8% [52, 53]. Even without the latest improvements, the MEI stage with identical technology will show a noticeable gain in economy in a comparison for identical area $F_1 = \pi d l_1 e \sin \alpha_{1эф}$ (see below, Fig. 178).

LKZ experiments. The LKZ tested, in particular, an old stage, the so-called combination No. 113, an MEI KC-1B stage, and a VTI stage. The technology of manufacture of the stages (milled nozzles) and the basic dimensions were identical. With full steam input, the experiments showed a lower economy for stage No. 113 than for the new stages; the MEI stages have a somewhat higher efficiency than the other stages (this advantage shows up essentially at small $u/c_{ф}$).

With partial input, the MEI stage should have a better economy than the remaining combinations, especially with high heat drops. Recently a version of the MEI stage was investigated [78].

§ 26. THE INFLUENCE OF THE BASIC PERFORMANCE PARAMETERS ON THE EFFICIENCY, REACTION, AND RELATIVE FLOW RATE OF A VELOCITY STAGE

For the calculation and selection of a velocity stage, and a comparison of it with a single-wheel stage, it is necessary to know the efficiency of the stage η_{01}, the reaction ρ, and the flow rate characteristic, i.e., the relative flow rate

μq or the flow rate coefficient of the stage $\mu_{ст}$. Knowing these quantities and all the geometric characteristics of the stage, one can determine the steam flow through the stage and its power, and perform a strength analysis on the stage elements.

All three of these quantities, η_{01}, ρ, and μq (or $\mu_{ст}$), depend on the geometric and performance parameters. The latter imply, as usual, $x_{\Phi} = \frac{u}{\sqrt{2h_0}}$, $\varepsilon = p_2/p_0$, and the Reynolds number.

Since static investigations and experiments with stages in experimental turbines showed that the influence of the Re number on the efficiency and the other characteristics starts to show up only at $Re_{c_1} < (3 \text{ to } 6)\cdot 10^5$, i.e., at Re numbers which are not encounted in the velocity stages of stationary steam turbines, then, in distinction from Chapter IV, the effect of Reynolds number is not considered here.* Thus, only three dependences remain.

$$\eta_{0i} = f(x_{\phi}, \varepsilon);$$
$$\rho = f'(x_{\phi}, \varepsilon);$$
$$\mu q = f''(x_{\phi}, \varepsilon) \text{ and } \mu_{cm} = f''(x_{\phi}, \varepsilon).$$

In analyzing the change of the reaction, we shall not limit ourselves to the total reaction, $\Sigma\rho$, which is the ratio of the available heat drop of both moving and rotating cascades to the available heat drop of the stage, and we shall investigate the reaction around the wheels, i.e., for separate cascades, ρ_1, $\rho_п$, and ρ_2, inasmuch as only a detailed analysis of the reaction around the wheels makes it possible to correctly select the dimensions and calculate the stage.

The Influence of x_{Φ} on Stage Efficiency

A change in x_{Φ} (when ε = const) affects the efficiency of a velocity stage due to:

a) the change of the magnitude and direction of the outlet velocity c_2, and consequently, the magnitude of the losses with the outlet velocity $\zeta_{в.с}$;

b) the change of the exhaust velocity from the nozzle cascade in connection with the change of the reaction and the losses in this cascade ζ_c, inasmuch as they depend on the M_{c_1} number;

c) the change of the magnitude and direction of the inlet velocities to the moving and rotating cascades, and consequently, the conditions of the flow around

---

*If the stages are tested in experimental turbines at $Re < Re_{автом}$, it is necessary to introduce a correction for the Re number.

these cascades with the losses in them;

d) the redistribution of heat drops between cascades, taking into account the various effectiveness of all four cascades, leads to a change in the stage efficiency;

e) the change of losses due to steam leakages, directly or indirectly (through the reaction), depending on $x_ф$;

f) the change of disk friction losses, which depend on $x_ф^3$.

The dependence $\eta_{oi} = f(x_ф)$ for a specific stage, with its geometric characteristics determined and given ε, can be determined experimentally. Such a typical dependence is the curve shown in Fig. 149. The points were obtained by experiments in an MEI experimental steam turbine for a KC-1A stage with the area ratio 1:1.63:2.48:3.60, diameter d = 668 mm, and nozzle height l_1 = 25 mm, $l_1/b_1 \approx 0.5$. The characteristic curve was obtained for constant ε. When $\varepsilon = 0.60$ the highest efficiency η_{oi}, considering all losses in the stage, including the losses due to disk friction, is attained at $x_ф = 0.31$. At the value of $x_ф = 0.23$, the efficiency is lowered by $\Delta\eta_{oi}/\eta_{oi} = 2.8\%$, and at $x_ф = 0.42$, by $\frac{\Delta\eta_{oi}}{\eta_{oi}} = 9.1\%$. This sharp lowering in efficiency with the growth of $x_ф$ to a considerable extent is explained by the increase of losses due to disk friction which, as compared to $x_ф = 0.31$, increase by 2.5 times.

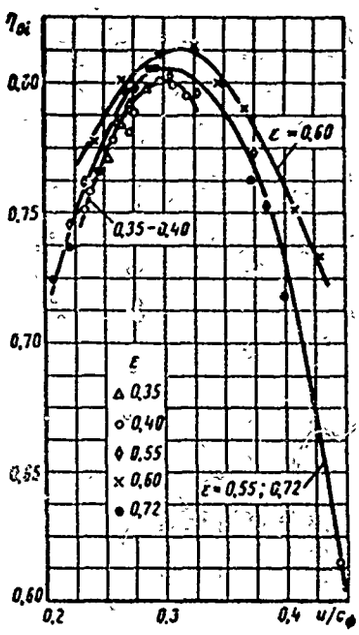

Fig. 149. Relative internal efficiency of an MEI velocity stage KC-1A, depending upon $u/c_ф$ and various ε (MEI experiments).

It is considerably more difficult to calculate the dependence $\eta_{oi} = f(x_ф)$ for a double-wheel stage than for a single-wheel stage, since it is necessary to know the change of the conditions of flow around the four cascades, the characteristics of which are usually known only on the basis of the results of investigations of two-dimensional cascades, and the flow rate coefficients are inaccurate.

If, for a determined efficiency of a single-wheel stage, the main condition of correctness of the calculation according to the results of static test was an exact knowledge of the losses in the nozzle cascade under conditions most approximating actual, then for a velocity stage this requirement is also extended to the moving cascade of the first wheel.

For a double-wheel velocity stage, the change in efficiency, depending upon

the change in cascade losses (at optimum $x_ф$), may be expressed by the approximate formula

$$-\Delta\eta_{oi} = 0{,}9\Delta\zeta_c + 0{,}5\Delta\zeta_{1p} + 0{,}2\Delta\zeta_{\text{п}} + 0{,}05\Delta\zeta_{\text{вс}}. \qquad (147)$$

Thus, an error in the determination of ζ_{1p} by 1% will lead to an error in the determination of efficiency $\Delta\eta_{oi}$ by 0.5%, and at the same time, for an impulse single-wheel stage, this will give an error in efficiency by only 0.25%. However, the calculation of a velocity stage, although it does not give full coincidence with the experiments in a turbine, nevertheless makes it possible to perform an analysis of the influence of various factors on the economy of the stage.

Figure 150a gives the dependence of cascade losses and loss with the outlet velocity for a КС-ОА double-wheel velocity stage with $\varepsilon = 0.55$, which was calculated according to static cascade tests, including tests of a nozzle cascade in a full-scale diaphragm. One would think that the main influence on the change of efficiency $\eta_{ол}$ would be rendered by the losses with the outlet velocity, while the losses in the nozzle cascade would not change essentially. In reality, for a given stage and given ε, upon transition from $x_ф = 0.34$ to $x_ф = 0.20$, the losses in the nozzle cascade increase from 8 to 15.5%, i.e., they increase almost twice; the losses in the first moving cascade increase from 5.5 to 8.5%; in the rotating cascade they increase from 2 to 3.5%; in the second moving cascade the losses almost do not change. The losses with the outlet velocity, after reaching a minimum of 2.5% at $x_ф = 0.3$, increase at $x_1 = 0.35$ and $x_ф = 0.2$ to 3%. Thus, from a consideration of the graph it is clear that the main change in efficiency is connected with the losses in the nozzle cascade. This is explained by the increase of the heat drop in front of this cascade in connection with the decrease of the total reaction

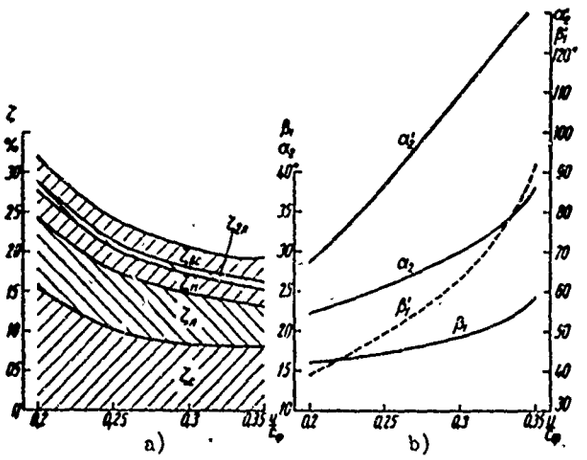

Fig. 150. Calculation of КС-ОА velocity stage at $\varepsilon = 0.55$; a) change of cascade losses and losses with outlet velocity depending upon $u/c_ф$; b) change of entrance angles and angle of direction of outlet velocity from $u/c_ф$.

and the transition from subsonic to supersonic velocity, when the losses noticeably increase in the given cascade.

For another ε, the picture of the change of losses from $x_{ф}$ can be completely different.

Thus, for instance, for the same HC-CA stage, but at $\varepsilon = 0.7$, in the same range of variation of $x_{ф}$, the losses in the nozzle cascade change from 9.3% to 12.7%. For an analysis of the performance of each cascade it is necessary also to know the changes of their angles at $\varepsilon = 0.55$, which are shown in Fig. 150b.

The optimum* value of the velocity ratio $x_{ф_{опт}}$ is very important for a velocity stage. For velocity stage with full steam input, this value varies from 0.26 to 0.33 and depends mainly on the total reaction of the stage $\Sigma\rho$ (or the area ratios and ε). The greater $\Sigma\rho$ is, the higher the value of $x_{ф_{опт}}$. A large influence on $x_{ф_{опт}}$ is rendered the stage sealing and the dimensions of the nozzle cascade. In the absence of sealing, $x_{ф_{опт}}$ decreases and, other things being equal, $x_{ф_{опт}}$ increases as the area F_1 increases.

Inasmuch as a decrease of the optimum value of $x_{ф_{опт}}$ is very important, since it leads to the development of a large heat drop, i.e., the solution of the main problem of a velocity stage, it would be of interest to create special stages with low $x_{ф_{опт}}$. However, a lowering of optimum $x_{ф_{опт}}$ is possible only at small $\Sigma\rho$ and large additional losses. Other ways of lowering $x_{ф_{опт}}$, which is applied in a number of cases, is the installation of a diffuser behind the stage (see § 24). A very small $\Sigma\rho$ leads to a certain decrease in economy and, most of all, it gives a steeper, descending character of the dependence of efficiency on $x_{ф}$ with the decrease of $x_{ф}$. Thus, an increase in the efficiency of a velocity stage is inseparably connected with an increase of $x_{ф_{опт}}$.

It should be noted that in the practice of a number of turbine plants and in training literature for design conditions of a regulating double-wheel velocity stage, even with low additional losses, decreased values of $x_{ф_{опт}}$ were selected. Quite often this was encountered in unified turbines.

For powerful steam turbines, where economy is a decisive factor when designing the flow area, sufficiently high optimum values of $x_{ф}$ must be selected. According

---

*Here and below, the optimum velocity ratio $x_{ф}$ implies the quantity that ensures the highest stage efficiency, and not the maximum economy of the whole turbine. In technical-economic calculations, the heat drop of a regulating stage does not correspond to the optimum value of $x_{ф}$. These questions pertain to the designing of an entire turbine on the whole and are not considered in this book.

to available data on foreign turbines, the practice of the GE Company should be noted; GE designs their double-wheel regulating stages for $x_{ф} = 0.31$ [142].

Of large value for a velocity stage is the stability of the efficiency, which is especially important from the point of view of varying operating conditions, in which there is a wide change of the characteristics of $x_{ф}$ and ε in velocity stages. This position pertains practically to all cases of the application of velocity stage: in the form of a regulating stage, the astern stages in marine turbines, and the stages of a drive turbine. The stability of a stage's economy is attained by: first, the selection of cascades with low losses in a wide range of variation of M number and angle of leakage; secondly, the correct selection of the area ratios, especially for the first wheel, which ensures moderate positive reactions; thirdly, good stage sealing, which lowers the losses due to steam leakages.

If the stage has an insignificant drop in efficiency when $x_{ф}$ is decreased, it would be of value in a number of cases to design the velocity stage with a velocity ratio below optimum for turbines with low volume steam admission.

We shall discuss two cases.

1. The heat drop of the stage remains the same, but the calculated $x_{ф}$ is lowered. This leads to a decrease of the diameter and to a corresponding increase of either the blade height or the partial admission. If partial admission is disregarded, and a stage with full steam input is considered (for instance, throttled steam distribution with the first stage – a Curtis disk – of the Westinghouse turbine, USA, with a power of 325 thousand kilowatts, an increase of the cascade height undoubtedly will increase the stage efficiency to a larger degree than it can lower the decrease of diameter. Thus, for instance, for a stage with a welded nozzle cascade without meridional profiling, with d = 1000 mm and height $l_1 = 20$ mm, $x_{ф\,опт} = 0.32$ and $\eta_{оп} = 76.5\%$. A decrease of $x_{ф}$ to 0.28 will lower the efficiency by 1.2%. For the same heat drop, the diameter of the stage will be 875 mm, which will decrease the efficiency by 0.4%. An increase of the height of the nozzle grid to 22.9 mm will increase the efficiency by 1.5%. As a result, the relative blade efficiency will almost be unchanged, and the relative internal efficiency will even increase somewhat because of the decrease of losses due to disk friction. The calculation of this example was performed on the basis of materials of an investigation of a MEI stage with a very sloping characteristic curve, $\eta_{оп} = f(x_{ф})$. If the stage has milled ganged nozzles, the effect of height will be smaller. Therefore, $x_{ф}$ should be selected in conformance with the

specific characteristics of the stage, including the technology of its manufacture.

2. The diameter of the stage is the same, but the calculated velocity ratio x_{ϕ} is decreased. In this case the efficiency of the stage will drop, the cascade area will decrease somewhat (for a subcritical flow), the efficiency of the whole turbine will be lowered, and the design of the entire turbine will be considerably simplified, i.e., the number of stages will decrease, the steam temperature after the regulating stage will be lowered, and steam leakage through the front end seal will simultaneously decrease. Therefore, the computed value of x_{ϕ} and the diameter d of the regulating stage (or the first stage) should be selected with consideration for the design and the economy of the turbine on the whole. If it is a question of a turbine with steam reheating, then the selection of the characteristics of the regulating stage should be conducted by taking into account the economy of the entire unit, bearing in mind the decrease of the heat input in the reheat for lowering the efficiency of the high-pressure portion.

The Influence of the Pressure Ratio ε on Stage Efficiency

In distinction from a single-wheel stage, the influence of ε on the efficiency of a velocity stage was known long ago and has been noted by all researchers, although there is no fundamental difference here, of course.

The influence of ε on the efficiency of a velocity stage is caused by:

a) a change in the cascade losses, depending upon the M number; for a double-wheel stage, as already noted earlier, a decisive role in economy is played by the losses in the nozzle cascade and the first moving cascade; the dependence of these losses on the M number also determines mainly the influence of ε on stage efficiency;

b) a change in the reaction of the stage and, due to this, the redistribution of heat drops between cascades and the change in steam leakages.

Thus, it is obvious that the change in efficiency, depending upon ε, will be determined by: first, the selected cascades; secondly, the area ratios of the cascades, i.e., the reactions; thirdly, the relative clearances. For a KC-1A stage with dimensions d = 668 mm and l_1 = 25 mm, Fig. 151 illustrates the results of experiments with x_{ϕ} = 0.3. In general, the dependence $\eta_{oi} = f(\varepsilon)$ for different u/c_{ϕ} can have an absolutely diverse character. Illustrations of this are given in Fig. 149, where, according to MEI experiments, graphs for $\eta_{oi} = f(x_{\phi}, \varepsilon)$ are given for a KC-1A MEI stage, while Fig. 151b refers to an LKZ stage No. 113. In the KC-1A stage, for the entire range of investigation of x_{ϕ}, the highest efficiency

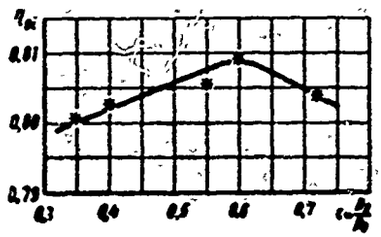

a)

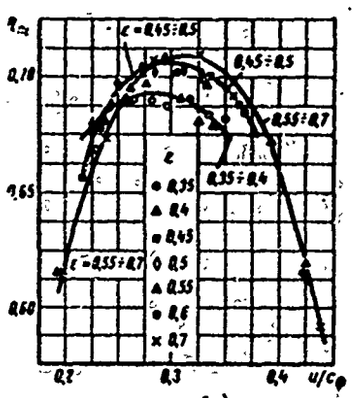

b)

Fig. 151. Relative internal efficiency, η_{oi}, depending upon the pressure ratio $\varepsilon = p_2/p_0$ (MEI experiments): a) for velocity stage KC-1A with $u/c_\phi = 0.3$; b) for LKZ velocity stage No. 113, $d = 653$ mm, $l_1 = 15$ mm, nozzles are ganged and milled.

corresponds to $\varepsilon = 0.6$; both a decrease of it, and also an increase lead to a decrease in economy. This dependence is explained by the fact that, taking into account the reaction for a pressure ratio in the stage $\varepsilon = 0.6$, the condition of flow past the nozzle cascade and the first moving cascade remains optimum for all values of x_ϕ. Supersonic velocities in the nozzle cascade, just as low M numbers increase the losses in it.

In stage No. 113 the characteristics of the cascades are different, and the reaction is also different. The nozzle cascade of this stage, in distinction from the TC-2A cascade of the KC-1A stage, which has its minimum of losses in the zone of $M = 0.9$, is the most economic at $M = 0.7$. Therefore, when $x_\phi > 0.29$, the highest stage efficiency is attained in subsonic conditions of flow ($\varepsilon = 0.55$ to 0.7). A lowering of ε, especially in the zone of supersonic velocities, leads to a decrease in economy. With small x_ϕ and large ε in the stage and, in particular, in the first wheel, there appears a negative reaction. Since this stage is equipped with old profiles that are sensitive to changes in conditions, the negative reaction essentially lowers the economy and the efficiency curve has a steeply descending character. At the same time, with small ε, the reaction will be greater, and positive for the investigated x_ϕ. Therefore, the efficiency curve for small ε has a sloping character. This leads to the fact that when $x_\phi > 0.29$ the highest efficiency corresponds to the value of $\varepsilon = 0.55$ to 0.7; when $0.23 < x_\phi < 0.29$, it corresponds to $\varepsilon = 0.45$ to 0.5, and when $x_\phi < 0.23$, the pressure ratio is $\varepsilon = 0.35$ to 0.4.

An analysis of the influence of ε on the economy of a velocity stage can be performed with the help of the aerodynamic characteristics of the cascades and the known reaction. As the calculations show, in spite of the indicated difficulties, for a velocity stage, just as for a single-wheel stage, it is possible to calculate efficiency not only depending upon x_ϕ, but also for various ε. Such a calculated

graph for the KC-0A stage is shown in Fig. 152. As can be seen from the graph, for the given stage, just as according to the experiments, the curves for $\eta_{0л} = f(x_ф)$ intersect when ε = const.

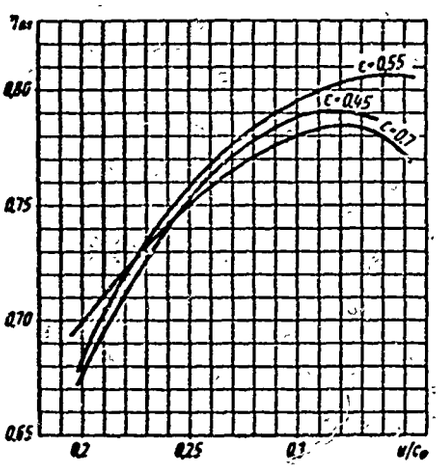

Fig. 152. Calculated graph of the dependence of relative blade efficiency, $\eta_{0л}$, of a KC-0A velocity stage, on $u/c_ф$ and ε.

The Efficiency of a Double-Wheel Regulating Stage with Constant Speed

For the calculation of a regulating state it is necessary to know its characteristics for a constant speed, when the change of $x_ф$ is connected with the change of ε. Inasmuch as, depending upon the steam parameters (practically on the initial temperature), the computed value of $x_ф$ can correspond to different ε, this stage characteristic will correspond not only to definite geometric parameters of the stage, but also to definite steam parameters and a definite speed. This dependence can be obtained by two methods: by testing the stage in an experimental turbine with a constant speed, and by means of recalculating the stage characteristics obtained in the experimental turbine for a variable speed and constant ε. It is natural that the first method usually is not applied for investigation, since it is not universal. It is sometimes used in plant laboratories, when it is necessary to obtain the characteristics of a specific full-scale stage.

Figure 153 shows two curves, i.e., the efficiency of an LMZ old-type double-wheel stage according to the results of test with n = 3000 rpm = const in an LMZ experimental turbine [50], and the efficiency of a KC-1A stage, obtained by recalculation from MEI experimental curves.

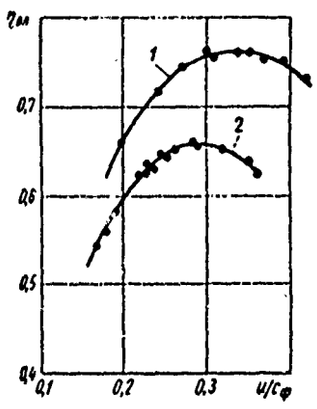

Fig. 153. Value of the efficiency of a double-wheel velocity stage: 1 — curve of stage MEI KC-1A, obtained by recalculating the experimental curves for ε = const, and n = var (MEI experiments); 2 — LMZ experimental curve for an old stage combination with n = 3000 rpm = = const.

When using the experimental curves obtained for n = var and ε = const, it should be recalled that the optimum value of x_{Φ}, and also the highest possible efficiency, can vary after recalculation for n = const.

The Influence of u/c_{Φ} and ε on the Reaction of a Stage

The reaction of a velocity stage is composed of the reactions around the wheels, $\Sigma\rho = \rho_1 + \rho_{II} + \rho_2$. For the given operating conditions of a stage, the ratio of the reactions around the wheel depends mainly on the cascade area ratios.

When x_{Φ} changes, the reaction around all the wheels changes, and consequently, the total reaction also changes. As demonstrated by numerous experiments with various combinations of velocity stages, and also calculations, the reaction in the second row of a moving cascade almost does not depend on x_{Φ}. The reaction in the rotating cascade and in the first moving cascade depends on x_{Φ} approximately linearly.

These facts are illustrated by graphs for three different combinations. Figure 154a shows experimental graphs for an NZL AK-6 stage at $\varepsilon > \varepsilon_*$ (NZL experiments); Figure 154b illustrates the results of MEI experiments with an LKZ stage No. 113 at ε = 0.35 (dot-dash lines) and a calculated graph 2 (dotted line) for an MEI KC-OA stage at ε = 0.45. In the last case the solid lines indicate the curves of the reaction without taking leakages into account, and the dotted lines represent with reaction curves with leakages taken into account.

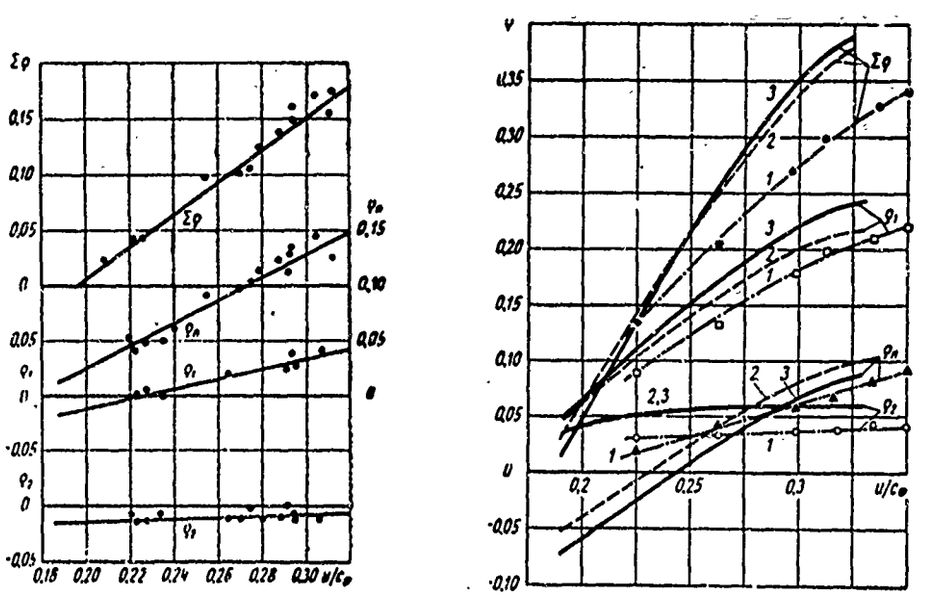

a) b)

Fig. 154. Curves of total reaction and wheel reaction for a velocity stage with full steam input: a) $\varepsilon > \varepsilon_*$, NZL stage AK-6 (NZL experiments); b) 1 —·—·— ε = = 0.35, LKZ stage No. 113 (MEI experiments); 2 — — — taking into account leakages in clearances (calculation), ε = 0.45, MEI stage KC-OA; 3 —— the same. without taking into account leakages in clearances (calculation).

The total reaction also varies approximately linearly, depending upon the pressure ratio ε, whereby the greater the pressure ratio ε, the smaller the reaction, which is clear from the graph in Fig. 155, where curves Σρ are given for an LKZ stage No. 113 at $x_{ф}$ = 0.35 and $x_{ф}$ = 0.45.

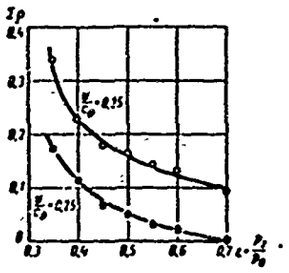

Fig. 155. Total reaction of No. 113 LKZ velocity stage with full steam input, depending upon pressure ratio ε (MEI experiments).

By analogy with formula (75), for a single-wheel stage it is possible to derive a formula for calculating the change of the total reaction of a velocity stage (with full input), depending upon $x_{ф}$. In simplified form, this formula is written as

$$\Delta(\Sigma\rho) = 0{,}45\,\frac{x_{ф} - 0{,}3}{0{,}3}. \qquad (148)$$

The graph in Fig. 156 illustrates MEI experiments with five stages for various ε, which indicate that formula (148) is satisfactorily confirmed by the experiments.

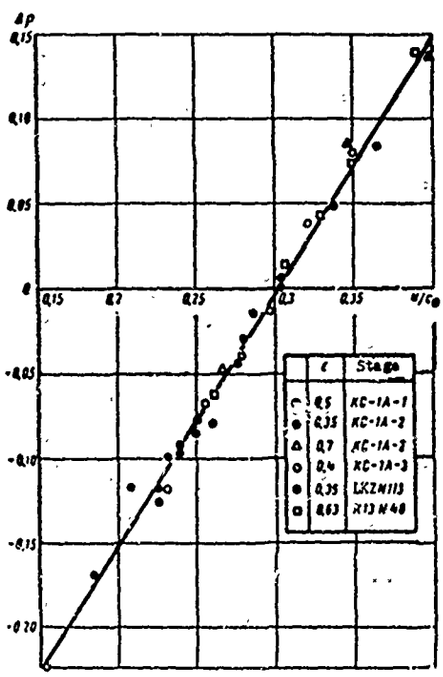

Fig. 156. Comparison of formula $\Delta(\Sigma\rho) = 0.45[(u/c_{ф})/0.3 - 1]$ with MEI experiments.

A simple and universal formula for calculating the influence of ε on ρ cannot be created, since this influence in many respects is determined by the aerodynamic characteristic of the cascades. However, for a preliminary estimate it is possible to use the following empirical dependence:

$$\Delta(\Sigma\rho)_{\varepsilon} = 0{,}8\left[1 - \left(\frac{\varepsilon}{0{,}6}\right)^{\frac{k-1}{k}}\right]\sqrt{\frac{l_1}{20}}, \qquad (149)$$

where l_1 – [mm],

k – the isentropic exponent.

Flow Rate Characteristics of a Velocity Stage

For the calculation of a stage, in particular in varying conditions of its performance, it is necessary to know the steam flow rate. Of particular importance is to know exactly the discharge capacity of the regulating stage. If for an intermediate stage an error in the determination of the flow rate leads to a certain redistribution of pressures and heat drops through the stages and, in the final result because of this, to a change of economy, then an error in the determination of the steam flow rate through the first stage leads to the same

(for a critical flow) or almost the same power error of the turbine, if the flow rate is less than the maximum calculated value.

For the calculation of the regulation system in general, it is impossible to avoid using curves for the change of the steam flow rate through the regulating stage, depending upon the operating conditions of the entire turbine.

As also for a single-wheel stage, for the determination of the discharge capacity of a velocity stage it is possible to use two characteristics: the flow rate coefficient of the stage

$$\mu_{ст} = \frac{G}{G_{1*}}$$

and the relative flow rate

$$\mu q = \frac{G}{G_{1*}},$$

where G_{1*} is the critical flow rate through the nozzle cascade.

The flow rate coefficient of a stage μ_{CT} depends on the total reaction of the stage and the flow rate coefficient of its nozzle cascade μ_1. The relative flow rate, furthermore, depends on the pressure ratio of the stage ε.

For a small range of variation of the dimensions (heights) of the nozzle cascade of a velocity stage, the flow rate coefficient of the nozzles μ_1 changes insignificantly, from 0.96 to 0.98. The reaction of the stage $\Sigma\rho$ depends on the area ratio, the clearances in the stage, and two performance parameters, i.e., the velocity ratio $x_{ф}$ and the pressure ratio ε. Inasmuch as μ_1 also depends on ε, the relative flow rate is

$$\mu q = f(\varepsilon, x_{ф}).$$

Figure 157 gives a typical graph for $\mu q = f(\varepsilon, x_{ф})$, which was obtained from tests of an LKZ velocity stage in an MEI experimental steam turbine. Measurement of the steam flow rate was accomplished by weighing the condensed steam.

While the pressure ratio in nozzle cascade amounts to $\varepsilon_1 = p_1/p_0 < \varepsilon_*$, the steam flow rate remains practically constant, an increase of ε leads to a lowering of the flow rate, and an increase of $x_{ф}$, with given ε, leads to an increase of the reaction and, consequently, to a growth of ε_1, which means a lowering of the steam flow rate.

For the calculation of a specific stage analogously to the method employed above for efficiency, it is necessary to reconstruct the graph for $\mu q = f(\varepsilon, x_{ф})$ into such a dependence $\mu q = f'(x_{ф})$ with n = const, when $\varepsilon = f''(x_{ф})$. An example of such reconstruction for this stage is shown in the same Figure 157.

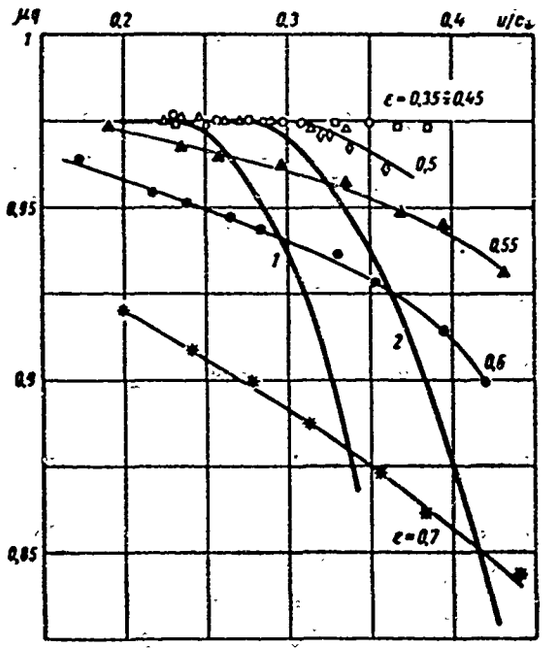

Fig. 157. Relative steam flow rate μq of a velocity stage in an MEI experimental turbine (with full steam input and n = var) and recalculation of experimental results for n = 3000 rpm = = const. Curves: 1 — for ε = 0.5, $u/c_{ф}$ = 0.24; 2 — ε = 0.5; $u/c_{ф}$ = = 0.306.

Curves are reconstructed for n = 3000 rpm = = const; each curve for given ε corresponds to its own $x_{ф}$, i.e., to a different stage diameter. The graph shows that the use of the results of experiments with a model stage for each specific case gives its own dependence $\mu q = f'(x_{ф})$.

According to NZL experiments conducted with an MEI KC-15 stage, the values of the flow rate coefficient of the nozzle cascade are $\mu_1 \approx 0.975$.

§ 27. THE INFLUENCE OF GEOMETRIC PARAMETERS ON THE CHARACTERISTICS OF A STAGE

Velocity stages, as already indicated in § 25, can differ by the types of cascades, the ratios of their dimensions, the absolute dimensions of the cascades, in the first place the nozzle cascade, and also the axial and radial clearances. Of large value is the shape of the flow area in the meridional plane and the technology of cascade manufacture, mainly for the nozzle cascade.

The selection of cascades for a velocity stage has certain peculiarities.

1. Inasmuch as velocity stages are applied in the overwhelming majority of cases for low volume steam admissions, the absolute values of the blade heights are low and the end losses in them usually are considerable. In the moving and rotating cascades very frequently, for the sake of reliability it is necessary to increase the chords, which decreases the relative heights and increases the end losses. Therefore, the cascades of a velocity stage must be selected in such a way as to lower the end losses. This requires special profiling of the cascades, in particular meridional profiling of the nozzle cascade. Since the influence of the technology and quality of cascade manufacture increases as the height decrease, high requirements should be set up for the manufacture of velocity stages. In particular, it is desirable to manufacture not welded, but gang-milled nozzle cascades with straight shrouds, with the observance of density between separate

nozzle segments. Special attention should be given to the joints between rotor blades, where there are frequently rough spots, the attachment of the shroud to the blade casing along the entire length, and the proper design of both the trailing and leading edges. Even hand finishing of a low-quality velocity stage can noticeably increase its economy.

2. The application of blades of low height and large diameters of velocity stages (i.e., with high ratio d/l) excludes the necessity of special blade twisting.*

3. Usually velocity stages operate in a wide range of variation of conditions, whereby both the velocity ratio and the pressure ratio change. In connection with this, the discharge velocities change in the nozzle cascade, the first moving cascade and, to a smaller degree, in the rotating cascade due to the change of ε, the ratio also changes. Therefore, the cascades of velocity stages must be able to resist changes of the M number. Both the moving and the rotating cascades are streamlined by steam with considerable deviations of the entrance angle from the calculated value. This naturally requires the selection of cascades that are not very sensitive to changes of the entrance angle. Thus, for instance, in the KC-0A velocity stage, with a change of $x_{\text{ф}}$ from 0.2 to 0.35 (comparatively small change of $x_{\text{ф}}$) and ε from 0.7 to 0.45, the angle of entrance to the first moving cascade β_1 changes from 15.7° to 24.4°, the angle of entrance to the rotating cascade α_2 varies from 22.5° to 39°, and the angle of entrance to the second moving cascade β_1' varies from 38° to 92°. Figure 150b shows a calculated graph of the change angles for this stage, depending upon $x_{\text{ф}}$ (at $\varepsilon = 0.55 = \text{const}$).

4. Many velocity stages are designed on large heat drops which correspond to near-critical and even supercritical velocities. An even greater number of velocity stages, which operate in design conditions with relatively low velocities, attain supersonic drops when the conditions are changed. In certain stages, even relative velocities of steam entrance to the first moving cascade, w_1, can exceed critical values.

As it is known, many old turbine cascades, including those applied earlier in velocity stages, do not correspond to the above-indicated requirements. This was one of the main causes of low efficiency of the old velocity stages.

---

*With the exception of certain special cases in gas-turbine construction.

The LMZ laboratory investigated an old-type LMZ double-wheel velocity stage, which was employed earlier in a series of high-pressure turbines, and an MEI КС-1А stage with the same basic dimensions. The efficiency gain obtained in this case upon transition to a new stage is explained by many reasons. However, the main factor that ensures an increase in efficiency is the application of aerodynamically improved cascades that are adapted to the specific operating conditions of a double-wheel stage.

Of interest from this point of view are the experiments that were conducted by V. D. Pshenichny at the LKZ laboratory with a КС-1Б MEI stage having a diameter of 700 mm and nozzle height 17.3 mm. When the MEI ТС-2Б nozzle cascade was replaced by an С-1 TsNII cascade, which is also specially profiled and has approximately the same profile losses under design conditions as the ТС-2Б, then, in spite of a certain increase in relative height (l_1/b_1 = 0.32, instead of 0.30), the stage efficiency was lowered by $\Delta\eta/\eta$ = 1.5 to 2.3%. Actually, the С-1 cascade has an effective angle 1.3° less than that of the ТС-2Б, but such a small difference in angles, of course, cannot play any essential role in the change of the angle of leakage in the first moving cascade which, moreover, was specially profiled for stable performance at various angles β_1.

The basic causes of the difference in efficiency of these two stages are:

1) the end losses; the ТС-2Б cascade, which is profiled for low heights, has an increased relative pitch; for the investigated cascade dimensions, the end losses amount to 2.8%, whereas for the С-1 cascade they are equal to 4.4%;

2) the ТС-2Б cascade is intended for operation with transonic velocities.

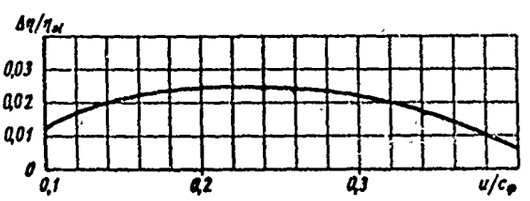

Fig. 158. Increase of economy of a С1-1Б stage with an MEI ТС-2Б cascade as compared to a stage with an С-1 cascade: nozzle cascades are ganged and milled, d = 700 mm, l_1 = 17.3 mm, ε = 0.465 - 0.48, full steam input (LKZ experiments).

Figure 158 shows the difference in economy, $\Delta\eta_{oi}/\eta_{oi}$, of these two stages according to LKZ experiments. In the entire investigated range of u/c_ϕ for a stage with a ТС-2Б nozzle cascade, the MEI КС-1Б combination was more economical.

If we consider that the main difference in the economy of cascades is explained by the end losses, i.e.,

$$\Delta\zeta_c = 4{,}4 - 2{,}8 = 1{,}6\ \%,$$

then for velocity stages with optimum $x_{ф}$

$$\Delta\eta_{ol} = -0{,}9\Delta\zeta_c = -1{,}45\ \% \text{ and } \frac{\Delta\eta_{ol}}{\eta_{ol}} \approx 2\ \%.$$

After an analysis of the graph of comparison of the econony of these stages (Fig. 158), it is clear that for all investigated values of $x_{ф}$ the cascade combination of stage КС-1Б has a higher efficiency. As $x_{ф}$ increases, the difference in efficiency decreases. This is explained by the fact that in the КС-1Б stage, because of the large area of the nozzle cascade, the reaction of the stage is somewhat higher. As $x_{ф}$ increases, the reaction of the stage increases, and the losses due to steam leakages become noticeable. At small $x_{ф}$, a decisive influence on the economy of the stage is rendered by the losses with the outlet velocity.

The Effect of Cascade Height

An increase of the absolute height of a cascade, all other quantities being constant, has a favorable effect on the economy of a stage. An increase of l_1, leads to a decrease of the end losses in the cascades and to a lowering of parasitic steam leakages, and also to a lowering of the losses connected with overlaps, inaccuracy of manufacture, and so forth.

For low cascade heights, special measures for decreasing the end losses should be applied, e.g.:

1. A decrease of profile chord and a corresponding increase of relative cascade height. The influence of a number of factors, which were discussed above in § 22, should be considered here. A decrease of profile chord lowers the Reynolds number. For velocity stages, as a rule, the Re numbers lie in a self-similar region; therefore, the influence of this factor can usually be disregarded. As the profile chord decreases, the relative surface roughness increases. Independently of the profile chord, the conditions of technology and strength necessitate the manufacture of profiles with a definite magnitude of the trailing edge. A decrease of chord in this instance leads to an increase of edge losses. Hence there appears the concept of optimum cascade chord, which was considered in Chapter II, where the losses connected with double curvature have a defined, but almost uninvestigated value.

2. Meridional profiling of the nozzle cascade.

3. Moving cascades specially profiled for lowering the end losses, in particular the К-type cascades.

4. Good sealing of stage clearances.

The effect of cascade height on the efficiency of a double-wheel stage essentially depends on the technology of manufacture; in particular, with the use of welded nozzle cascades, the influence of l_1 is considerably larger than with ganged and milled nozzles. This is explained by the rougher manufacture of the end walls, the additional losses in the welding spots, and the losses in the root section due to double curvature. Below, Fig. 308 gives the dependences of the efficiency of MEI velocity stages for various heights of nozzle cascades with a welded diaphragm. It should be pointed out that with a large height, the optimum value of the velocity ratio $x_{ф}$ is somewhat larger, especially if curves of the relative internal efficiency η_{oi} are being compared.

If a stage has meridional profiling of the nozzle cascade with one-way contraction, as shown in Fig. 147b, the efficiency of the stage increases.

The LKZ laboratory conducted comparative experiments with a KC-1B stage for two variants: one of usual design and one with meridional profiling of the nozzles and the moving cascade of the first row of type K. The flow area of the stage was represented in Fig. 147a. Both stages had ganged and milled nozzles.

The results of the experiments are shown in Fig. 159. As can be seen from the graph, in transonic conditions the second stage variant gave a gain of 1.2%. With larger, supercritical drops, this gain increased (this is mainly connected with the fact that meridional profiling in the first place improves the flow process in the slanting shear of the cascade, where, at supersonic velocities, a large part of losses is concentrated) to 1.6%. Inasmuch as upon transition to meridional profiling the outlet area of the nozzle cascade was increased, a recalculation should be made for an identical area F_1. This recalculation, naturally, will somewhat lower the gain, reducing it to approximately 0.8 and 1.2%. It should be indicated that when welded nozzles are employed, where the influence of end losses is greater, the application of these special measures for increasing efficiency will give a considerably larger gain.

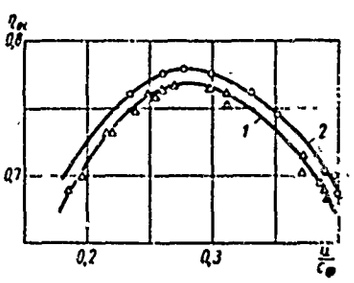

Fig. 159. The efficiency of a velocity stage, η_{oi}, for a KC-1B stage, d = 700 mm, l_1 = 17.3 mm, nozzles are ganged and milled (with full steam input and pressure ratio in stage ε = 0.5): 1 — usual stage design; 2 — stage with meridional profiling of nozzle cascade and moving cascade of first wheel, type K.

Figure 160 gives a graph of the dependence of the difference in relative internal efficiency of an MEI velocity stage (type KC-0A, KC-1A, and KC-1Б) upon transition to meridional profiling and type K moving cascades of the first wheel. A comparison is performed for full steam input at $x_{\Phi_{опт}}$ $\varepsilon = 0.6$, and identical d and F_1; $b_1 \approx 45$ mm.

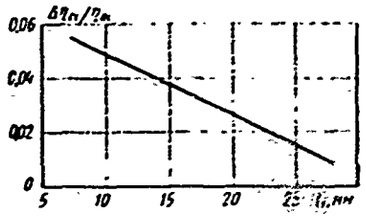

Fig. 160. Gain in economy for velocity stage upon transition to meridional profiling and moving cascades of first wheel, type K (for welded diaphragm).

The influence of the technology of manufacture for stages with short blades is extraordinarily great. This is clearly illustrated by the graph in Fig. 161. Illustrated there are the experimental curves of η_{oi} for a KC-1Б stage with a diameter of 705 mm, height of nozzle cascade 15 mm, and with a welded diaphragm, according to tests in an NZL experimental steam turbine, and for the same stage with a diameter of 700 mm, nozzle height 17.3 mm, and with ganged and milled nozzles, according to tests in an LKZ experimental steam turbine. The LKZ data are recalculated here for a nozzle height of $l_1 = 15$ mm. Although, of course, the experiments conducted in different turbines and with somewhat different experimental methods do not make it possible to perform an exact comparison, a rough estimate can be made, however. It shows that the influence of the technology and quality of manufacture also essentially gives a difference in efficiency of approximately 1.5-2% in this case.

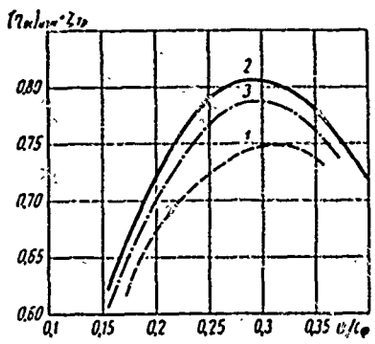

Fig. 161. Investigation of KC-1Б velocity stage with full steam input. d = 700 mm: 1 – stage with welded diaphragm, l_1 = 15 mm (NZL experiments); 2 – stage with ganged and milled nozzle, l_1 = = 17.3 mm (LKZ experiments); 3 – recalculation of LKZ experiments for height l_1 = = 15 mm.

The Influence of Stage Diameter

The influence of the diameter of a stage should be considered for constant height and other geometric parameters. The diameter influences the economy of a velocity stage for the following reasons:

1. A change of d/l with an increase of the diameter leads to a lowering of losses due to flare. Inasmuch as the cascade heights are low in velocity stages, the change of d/l has a very insignificant effect.

2. A change of stage clearances and the overlaps. An increase of the diameter of a stage correspondingly requires an increase of the clearances and overlaps which,

with constant l_1, increases the losses. This factor is usually considered separately, independently of diameter.

3. A decrease of diameter brings about a greater influence of double curvature, which is especially noticeable for low blade heights. This is the main cause of the dependence of stage efficiency on diameter.

The influence of diameter on stage efficiency has been noted by many researchers. However, it is very difficult to set up experiments with stages that differ only by one diameter. For old cascade combinations we have a firm's curve which is shown in Fig. 162; this curve makes it possible to estimate the influence of diameter. The influence of diameter is inseparably connected with cascade height. The lower the height, the greater the influence of the diameter. This circumstance is not considered by the graph in Fig. 162. Below, in § 48, where generalized curves are given for calculation of velocity stages, a graph is presented; this graph permits us to estimate the dependence of efficiency on diameter at various heights for contemporary velocity stages.

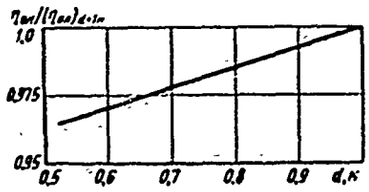

Fig. 162. Correction of efficiency depending on diameter for an old cascade combination of a velocity stage intended for high-power turbines (firm's data).

The Influence of Area Ratio

The area ratio of the cascades of a velocity stage renders an influence on the total reaction of the stage, the reaction on the wheel, and consequently, on the distribution of heat drops between cascades, the entrance and exit velocities, the entrance angles, and losses due to steam leakages. Table 13 gives the results of an investigation of four KC-1A velocity stages having the same cascades and different area ratio. The table characterizes the reaction on the wheels with full steam input, and under the same conditions, $x_{ф} = 0.30$ and $\varepsilon = 0.6$.

Table 13. Results of Investigations of Four Stages with Identical Cascades and Different Area Ratio

Stage	F_{1p}/F_1	F_n/F_1	F_{2p}/F_1	ϱ_1	ϱ_n	ϱ_2	$\Sigma\varrho$
KC-1A-1	1,46	2,30	3,18	0,07	0,08	0,06	0,21
KC-1A-2	1,52	2,39	3,40	0,03	0,08	0,05	0,16
KC-1A-3	1,63	2,48	3,60	−0,06	0,08	0,03	0,05
KC-1A-4	1,56	2,73	4,17	0,02	0,06	0,02	0,10

As should have been expected, an increase of the opening in the moving and rotating cascades led to a decrease of the reaction. Besides the change of the conditions of flow in all four cascades, the increase of the flow area of the second moving cascade in stage KC-1A-3 caused a corresponding decrease of the outlet velocity. Thus, in stage No. 3, as compared to stage No. 1 the relative area of the rotor blades of the second wheel increased by 13%, and the losses with the outlet velocity decreased by 28%. During operation of a stage with optimum u/c_{Φ} ratios, such a decrease of losses with the outlet velocity hardly affects efficiency. However, in certain conditions it can be sensitive.

Investigations of the optimum characteristics of a velocity stage were conducted at MEI by an interesting method developed by V. I. Abramov in which a double-wheel velocity stage and its first wheel (nozzle and first moving cascade) were tested separately. As a result of this investigation, the obtained data on type A velocity stages, which are presented in Table 13, are the most expedient in model KC-1A-2. Usually the optimum area ratio is $F_{1p}/F_1 \approx 1.48$ to 1.56.

In stages with identical cascades, but with different area ratios, not only the reactions will be different, but also the efficiencies, the optimum conditions (x_{Φ} and ε), and the stability of efficiency upon deviation of the investigated conditions from the calculated conditions. Consequently, it is possible to affirm that there exist optimum area ratios. Moreover, for the same cascade combination there can be different optimum area ratios depending on the calculated conditions, the size of the clearances, and the requirements from the point of view of variable conditions.

For a stage with full steam input, when selecting cascades to operate stably in a wide range of variation of velocities and entrance angles, with good stage sealing, when the losses due to leakages are small, small deviations in the values of optimum relative areas do not lead to a noticeable lowering in efficiency of a velocity stage. The recommended area ratios are given in Table 12. If the operating conditions of a velocity stage are essentially different than the recommended optimum ones, it is possible to calculate the change of efficiency, basing it on the method used in § 11 and, if necessary, the stage should be redesigned for these conditions.

For the case of partial steam input, the influence of the area ratio is considered in the following chapter.

The Influence of Clearances on the Performance of a Velocity Stage

In principle, the influence of clearances on the performance of a velocity stage does not differ from that of single-wheel stages. A new and essentially complicated investigation and calculation is that of steam suction over the blade shroud of the first wheel in a rotating cascade, and the steam suction, in addition to this cascade, in the second moving cascade.

For negative reactions, the picture of steam leakages is also complicated.

However, in spite of the indicated difference, the general conclusions concerning the influence of clearances on the efficiency and stability of operation of a stage remain the same:

1. Selection of closed axial clearances, just as for a single-wheel stage, is produced with the cascade height, overlap, and other factors taken into account (see § 22).

2. In all cases, a decrease of the radial clearances has a favorable effect on the magnitude and stability of efficiency.

3. The open axial clearances should be minimum. With sealing above the shroud, the open clearances should be decreased if they can be made of one order, of less than the radial shroud clearances of this cascade.

4. An especially great influence of clearances takes place when the reaction is high (calculated according to the absolute value of F/F_1, i.e., without taking leakage into account).

5. When all cascades are sealed, special attention should be given to decreasing the clearances and steam leakages in the first wheel. The least influence on the economy of a velocity stage is rendered by the steam leakage over the shroud of the moving cascade of the second wheel. The unloading of the casing of a rotating cascade without special seals, which is employed in some designs, can noticeably lower the efficiency of the stage.

The calculation of the change of efficiency of a double-wheel velocity stage, depending upon the sealing and the size of the clearances, is quite difficult and not universal. Certain data on the influence of clearances on the performance of a double-wheel stage are presented below.

According to one firm's data, for old cascade combinations of double-wheel stages with an average area ratio (see Table 10) the stage efficiency, depending upon the radial seal and the size of the open axial clearance, is shown in Fig. 163. As can be seen from the graph, the difference in the economy of the stage with an

axial clearance of 1 mm and a radial seal with a clearance of 0.5 mm, and in the case of a stage without radial sealing rings with an axial clearance of 2 mm, amounts to more than 3.5%. The influence of clearances is different, depending upon the conditions, i.e., the velocity ratio $u/c_{ф}$ and the pressure ratio ε. For a normal velocity ratio, the difference in the efficiency of a stage with sealing and without it is usually greater than for low values of $u/c_{ф}$.

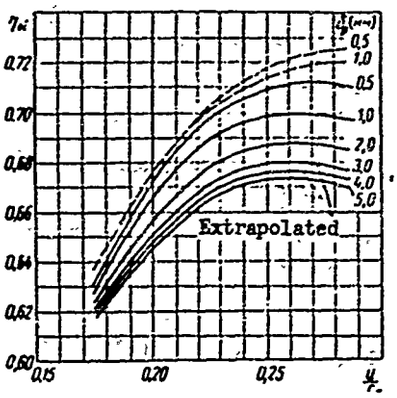

Fig. 163. Influence of radial sealing and open axial clearance on the efficiency of a double-wheel velocity stage: ——— without radial sealing rings; — — — with radial shroud seals and radial clearance 1 mm.

For another velocity stage, experiments were conducted with variation of an open axial clearance (no radial seals) from 0.5 to 1.65 mm with the same velocity ratio $x_{ф} = 0.26$, and different pressure ratios, $\varepsilon = 0.61$ and $\varepsilon = 0.32$. In first case, an increase of the clearance caused a lowering in efficiency by 1%; in the second case a 1.7% decrease. These data once again emphasize that the influence of clearances depends on the reaction on the wheels under the considered conditions.

Experiments were conducted in an MEI experimental turbine for studying the influence of a clearance between the nozzle and moving cascade of the first wheel. In this case there was a simultaneous change of both the full axial clearance, and also the open peripheral one. The remaining clearances, both axial and radial, remained constant. There was no steam leakage in the root axial clearance of the first wheel. A test was performed with an LKZ velocity stage No. 113 with milled and ganged nozzles. The results of this investigation, $\varepsilon = 0.6$, are shown in Fig. 164 and 165. With a change of the full axial clearance (the clearance between the trailing edges of the nozzle blades and the trailing edges of the first moving cascade) from 3.0 to 6.0 mm, the stage efficiency essentially changes. Since the minimum size of the open

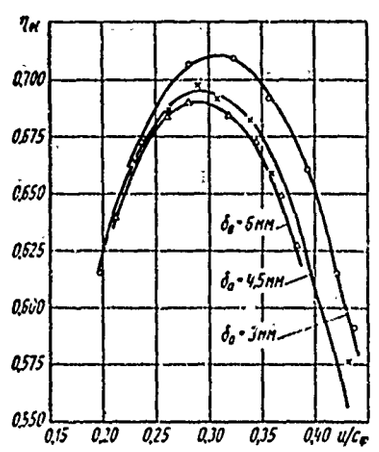

Fig. 164. Influence of the full axial clearance of the first wheel of a velocity stage with full steam input on efficiency η_{oi} ($d = 0.653$ m, $l_1 = 15$ mm, $\varepsilon = 0.6$ MEI experiments): — O — O — O — with radial sealing rings; — Δ — Δ — Δ — without radial sealing rings.

peripheral clearance, 0.6 mm, is commensurable with the size of the radial clearances, an increase of the axial clearance caused additional steam leakage, which may be noted during the analysis of curves of the relative flow rate (Fig. 165). Therefore, the first increase of the clearance led to a noticeable lowering of economy (when x_{Φ} = = 0.28, the stage efficiency dropped by 1.9%), and a decrease of the reaction due to the large leakage, which means an increase of the flow rate; a further increase of the axial clearance, when the open clearance was a little larger the radial one and practically did not affect leakage, the reaction did not change, and consequently, the steam flow rate also remained the same. The change of efficiency, with the same increase of the clearance by 1.5 mm, amounts to 0.6%, which is connected with the additional mixing of flow behind the nozzles, and also with the greater influence of the overlap.

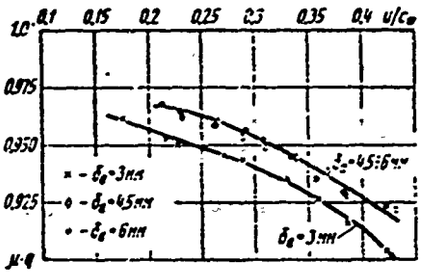

Fig. 165. Influence of the full axial clearance of the first wheel of a stage on the relative steam flow rate (MEI experiments).

C H A P T E R VI

STAGES WITH PARTIAL INPUT AND SUPERSONIC STAGES

§ 28. THE INFLUENCE OF PARTIAL INPUT ON THE PERFORMANCE OF A SINGLE-WHEEL STAGE

In steam turbines, and sometimes also in low-power gas turbines, there are stages with such small cross sections that it is impossible to avoid partial input. The regulating stages of steam turbines are always constructed with partial steam input.

The introduction of partial admission to a considerable extent disturbs the above-considered procedure for the calculation and design of stages. Problems arise in the selection of the area ratio of nozzle and moving cascades. This area ratio, F_2/F_1, under given conditions, determines such an important stage characteristic as the degree of reaction. F_2/F_1 is usually calculated as for full input:

$$\frac{F_2}{F_1} = \frac{d_2 l_2 \sin \beta_{2,\phi}}{d_1 l_1 \sin \alpha_{1,\phi}}, \tag{150}$$

i.e., assuming that in the moving cascade the steam passes along the same arc as in nozzle cascade. However, calculation and experiments point out the increase of the arc of the moving cascade, e_2, as compared to the input arc in the nozzle cascade, e_1:

$$e_2 > e_1.$$

Therefore, the calculation of a stage with partial input must include a conditional quantity

$$\left(\frac{F_2}{F_1}\right)_e = \frac{d_2 l_2 \sin \beta_{2,\phi} e_2}{d_1 l_1 \sin \alpha_{1,\phi} e_1}. \tag{151}$$

However, when determining the reaction of a stage, it is insufficient to use this quantity $(F_2/F_1)_e$; it is necessary to also consider the increase of leakages which is inevitable with partial input, and consequently, also the decrease of the absolute value of the reaction.

Thus, when selecting the cascade dimensions of a stage with partial input, the ratio F_2/F_1 should be used; this is the ratio recommended in Chapter IV. It is also necessary to substitute the values of $(F_2/F_1)_e$.

The ratio e_2/e_1 can be found by the following, rough estimating, formula:

$$\frac{e_2}{e_1} = 1 + \frac{0{,}01}{e_1}. \qquad (152)$$

Taking into account the increase of leakages in a partial stage, the calculated reaction of the stage, which is calculated with respect to $(F_2/F_1)_e$ without taking into account all leakages, should be selected on the mid-diameter: approximately, $\rho_{cp} \doteq 3\text{-}8\%$. A higher value of the calculated ρ_{cp} will lead to a noticeable increase of leakage, and thereby to a lowering of economy; a lower value of ρ_{cp} may cause steam suction, and thereby cause a further decrease in efficiency. The selection of the calculated value of ρ_{cp} depends on the stage's design. For an intermediate stage, where there almost always takes place suction in the moving cascade through the root clearance, a smaller value of ρ_{cp} (and consequently, ρ_K) should be selected than for a regulating stage, where through this same clearance there occurs steam leakage.

When there are large full axial clearances, it is necessary to select smaller reactions, since an increase of ρ with partial steam input increases the leakage.

It should be emphasized that for a stage with partial steam input, the selection of the area ratio, and consequently also the determination of the calculated reaction, has a larger value than for a stage with full input. This has been confirmed by many experimenters. Furthermore, F_2/F_1 must be selected with the change of the reaction and the efficiency in the whole range of operating conditions taken into account.

The second problem that arises with partial input is the determination of the stage's economy. Upon transition from full to partial steam input, the following additional losses appear:

a) windage losses, i.e., due to pumping of unused steam from one chamber into another;*

*Reference [48] proposes that this loss occurs due to increased friction of the "rough" edges of the end surfaces of the rotor blades.

b) run-outs (end) connected with the so-called run-out of stagnant steam (possessing low kinetic energy) from the extreme channels of a moving cascade.

c) connected with a noticeable increase of parasitic steam leakages in a partial stage; additional steam leakage occurs through the meridional clearances between cascades; a large role is performed in these losses by steam suction through this clearance into the extreme channel of a moving cascade, which essentially lowers effectiveness of the flow in this channel;

d) due to wash-out of the stream proceeding from a nozzle cascade with partial steam input, and because of additional leakages, the reaction of the stage noticeably drops; in this case, naturally, the effectiveness of the stage also changes; a change of the stage's reaction itself can lead to a change of efficiency;

e) in the steam flow proceeding from the extreme channels of a nozzle cascade, independently of run-out and leakages, it is less effective than the steam flow proceeding from the middle channels;

f) with partial input, the stage's reaction along the input arc will be different, which lowers the economy of the stage.

This by far is not a full list of the changes occurring in the process of steam flow in a stage with the introduction of partial input.

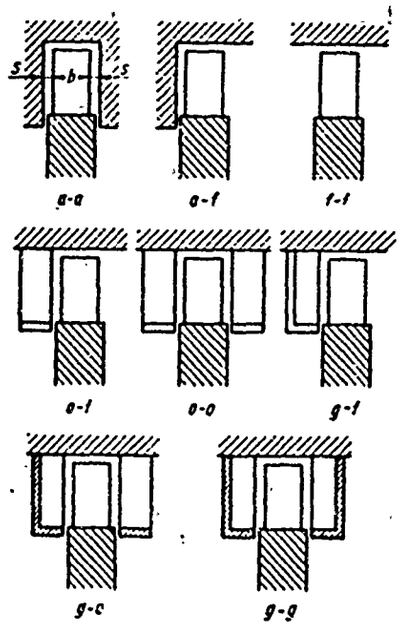

Fig. 166. Stage designs (for determining windage losses).

It is obvious that the classification of all the above-mentioned losses is practically impossible not only because it requires

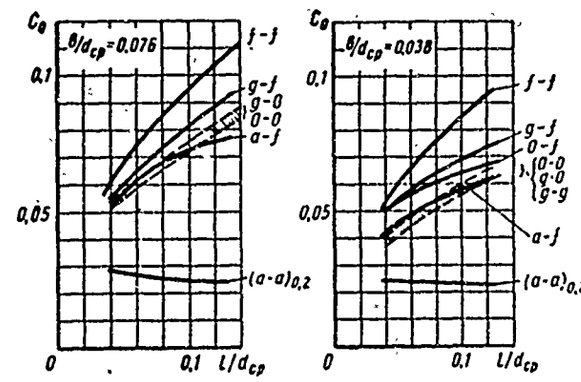

Fig. 167. The determination of windage losses and the coefficient C_0 (case a - a was investigated for $s/l = 0.02$).

complicated, detailed and tedious experimenting on static and revolving installations, but also because the above-mentioned factors are interconnected.

First we shall discuss a simpler case, when all nozzle channels are united into one group. For computing the losses in this case, the majority of researchers limit themselves to the first component of these losses, i.e., the so-called windage losses. This method is tempting since it permits us quite easily to conduct investigations with rotation of disk blading. However, as confirmed by experiments, windage losses do not exhaust all the losses appearing in the transition from full to partial input. Inasmuch as a knowledge of purely windage losses is necessary for finding ways of increasing the economy of a stage, and also for the calculation of the astern stages of marine machinery, we shall consider these experiments.

They were most fully conducted at the Institute of Thermal Turbomachines in Zürich by P. Suter and W. Traupel [156]. On the basis of a large series of carefully planned experiments, they propose the following formula:

$$\zeta_{вент} = C\,\frac{1-e}{e}\cdot\frac{1}{\sin\alpha_1}\,x_\phi^3, \tag{153}$$

where

$$C = C_0\left(\frac{Re_u}{2{,}8\cdot 10^6}\right)^{-1/16}, \tag{154}$$

where $Re_u = \frac{d_{cp}\,u_{cp}}{\nu}$, and C_0 is determined depending upon the design and geometric characteristics of the stage which are shown in Fig. 166:

$$C_0 = f\left(\frac{l}{d_{cp}}, \frac{b}{d_{cp}}\right).$$

C_0 is represented in Fig. 167.

For shrouded blading (design a - a, Fig. 166), when the influence of the clearance s is great, the coefficient C_0 is found by the following formulas:

for normal rotation of rotor

$$C_0 = \left(0{,}017 + \frac{s}{l}\,k_s k_l\right); \tag{155}$$

for reverse rotation of rotor

$$C_0 = \left(0{,}018 + \frac{s}{l}\,k_s k_l\right), \tag{156}$$

where

$$k_s = f(s/l)$$

is determined by Fig. 168a, and

$$k_l = f\left(\frac{l}{d_{cp}}, \frac{b}{d_{cp}}\right)$$

is found according to Fig. 168b.

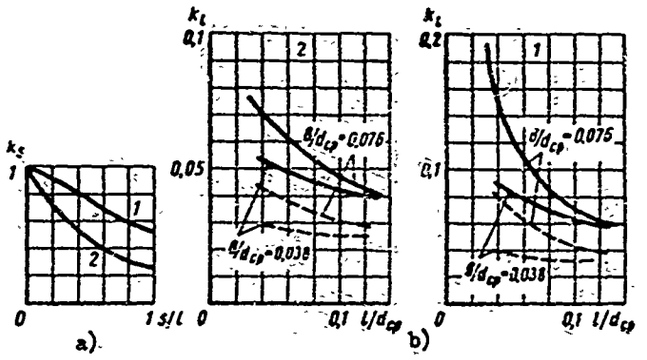

Fig. 168. The determination of windage losses: a) coefficient k_s; b) coefficient k_l: 1 — normal rotation of rotor; 2 — reverse rotation: —— unimpeded, — — — — impeded flow.

As can be seen from Fig. 167, the influence of the geometric factors (design dimensions) on windage losses is extraordinarily great: the coefficient C_0 changes from 0.11 to 0.023, i.e., almost by 5 times. Usually the reference literature for an unprotected wheel (f - f in Fig. 166) assumes that this loss does not depend on dimensions, and it is considered that designs a - f and o - f must have the same magnitude of losses. In the design with a casing (shape a - a) the losses decrease twice.

According to NZL, for the usual design of a stage, C = 0.0385; this value of coefficient C, as compared to the experiments of Suter and Traupel, decreases the windage loss by three times.

The experiments of I. K. Terent'yev (TsKTI) [94], for the case of a - f in Fig. 166, give $C_0 = 0.0141\ (1 + 20s/d_{cp})$, i.e., for $s/d_{cp} = 0.005$ to 0.045, the coefficient $C_0 = 0.016$ to 0.027, which is a few times less than in Fig. 167. For the case f - f the values of the windage losses according to formula (153) and Fig. 167 give a close coincidence with the experiments of Stodola [157] and Buckingham [156].

Figure 169 [156] shows a conditional diagram of the flow of gas in freely revolving blading. Some of the gas accomplishes circular flow in the meridional plane, not passing through the whole cascade channel (arrow K), and the remaining part (arrow F) passing through the cascade.

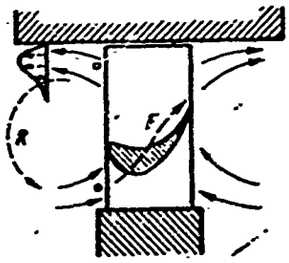

Fig. 169. Structure of gas flow with freely revolving blading.

The second important component of losses for the case partial input is the so-called run-out, which totally characterizes the losses on the edges of the input arc. The magnitude of this loss can be found experimental by an experimental turbine with the same degree of partial admission, only changing the number of input arc sectors.

Such experiments were performed by the GE, Asher-Wiess, and Skoda firms, and at MEI, BITM, LKZ, and NZL.

Let us consider some of the formulas recommended for computing these losses:*

GE formula [117]

$$\zeta_{конц.\ дуги} = 0{,}11\,\frac{bl_2}{F_1}\,\frac{u}{c_\phi}\,\eta_{ол}; \tag{157}$$

NZL formula [48]

$$\zeta_{конц.\ дуги} = 0{,}42\,\frac{bl_2}{F_1}\,\frac{u}{c_\phi}; \tag{158}$$

BITM-NZL formula [48]

$$\zeta_{конц.\ дуги} = 0{,}0085 + \frac{0{,}0137}{d}\,\frac{1}{e}\,\frac{u}{c_\phi}. \tag{159}$$

TsKTI formula [94]

$$\zeta_{конц.\ дуги} = 0{,}33\,\frac{bl_2}{F_1}\,\frac{u}{c_\phi}; \tag{160}$$

Olson's formula [156]

$$\zeta_{конц.\ дуги} = 0{,}27\,\frac{b}{d}\,\frac{1}{e}\,\frac{u}{c_\phi}. \tag{161}$$

The TsKTI formula was obtained from turbine experiments with the subtraction of windage losses which, as noted above, are too low; the BITM-NZL formula has a nonphysical structure. The most logical one is the GE formula; however, the numerical coefficient in it, as many experiments indicate, is too low. This coefficient should depend on the stage's reaction, the clearance between cascades, and also on the partial admission of one sector. There still are no experimental data, however, which would make it possible to give the numerical dependence of this coefficient on the mentioned factors. Therefore, it is necessary to limit ourselves to a rougher estimate of this coefficient. Using experiments of MEI [36], LKZ, and

*NZL uses formulas (158) and (159) for selecting the optimum characteristics of a stage, and the stage's efficiency is determined directly on the basis of the results of experiments.

Asher-Wiess [96], it is possible to recommend the following formula

$$\zeta_{\text{вкл.}\,\text{дуги}} = 0{,}25\,\frac{bl_2}{F_1}\,\frac{u}{c_\phi}\,\eta_{\text{ол}}. \qquad (162)$$

Finally, the third problem is the selection of the optimum dimensions of a partial stage. For a given volume admission and the basic performance parameters (x_ϕ and ε) it is possible to modify the stage's dimensions, in the first place by changing the cascade height and the degree of partial admission.

It is then possible to select the stage dimensions which will ensure the highest efficiency. This selection is the subject of § 30.

We shall consider the results of an experimental investigation of a single-wheel stage with partial input.

Figure 170 shows the dependence of the efficiency of a stage of an experimental air-driven turbine with full air input (e = 1) and with partial input (e = 0.76; 0.5; 0.26) according to the experiments of N. M. Markov (TsKTI).

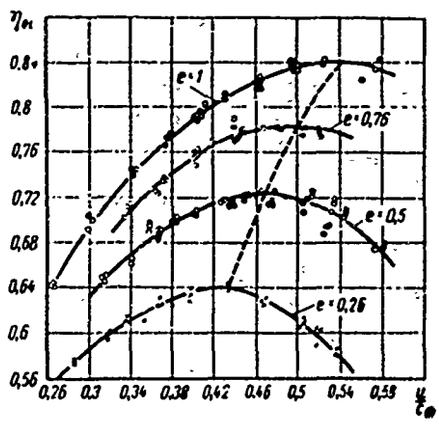

Fig. 170. Dependence of stage efficiency on x_ϕ and e for one input arc; d = 600 mm, l_1 = = 20 mm, l_2 = 23 mm, C-1 and T-1 profiles with shroud seals (two strips), δ = 0.6 mm, M_{c_1} = = 0.75, Re_{c_1} = $8\cdot10^5$ (TsKTI experiments).

Experiments with partial input were conducted at MEI in an experimental steam turbine at various cascade heights, including very low heights, where the question concerning the economy of a partial stage and the selection of optimum dimensions is especially critical.

Figure 171 gives a graph of the full relative internal efficiency of a КД-2-2Ак stage with TC-2A and TP-2Ак cacades at l_1 = 25 mm. Experiments were conducted with the pressure ratio $\varepsilon = p_2/p_0$ = = 0.7-0.85 in the stage with full and partial steam input.

Of interest in these experiments is the considerable decrease of economy upon transition to e = 0.9, when the influence of natural windage is small. Stage tests were conducted with the inactive nozzle arc shut off from the steam input side. The stage had a plant technology of manufacture that was somewhat poorer than in permanent machines; its diaphragm was welded. With full steam input, leakage can occur only over the blade shroud, where two strips are mounted for sealing with a decrease of $\delta_2 \approx 0.8$ mm.

Analogous stage tests were conducted at heights of 6, 10, 15, 20, 25 and 48 mm.

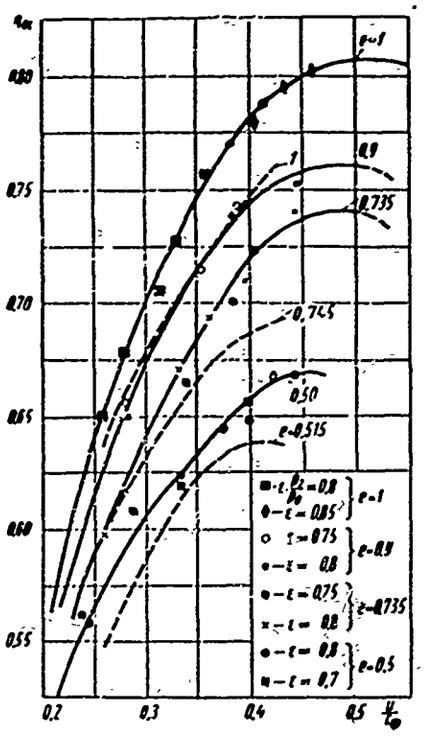

Fig. 171. Dependence of efficiency on $x_{ф}$ and e for one input arc (MEI experiments): — — stage КД-2-2Ак, d = 400 mm, l_1 = 25 mm, l_2 = 28 mm, α_1 = = 12°40'; – – – – stage КД-2-2Ак, d = 400 mm, l_1 = 10 mm, α_1 = 15°30', F_2/F_1 = 1.41, ε = 0.7.

The character of the dependence of efficiency on $x_{ф}$ and e remains approximately identical. Figure 171 gives curves of the dependence of efficiency for stages КД-2-2-Амк (with one-sided meridional profiling) on $x_{ф}$ and e at a height of l_1 = 10 mm.

It should be noted that a comparison of the economy of partial stages with the usual cylindrical contour and special meridional profiling showed that the relative losses upon transition to partial input practically do not depend on the meridional shape of the nozzle cascade.

As noted earlier [126, 157], the transition to partial input and a further decrease of the degree of partial admission lead to a decrease of the optimum velocity ratio $x_{ф}$. Thus, according to Fig. 170 with full input, $x_{ф_{опт}}$ = 0.54, and when e = 0.26 it decreases to $x_{ф_{опт}}$ = 0.43. Taking into account the large disk friction loss upon transition to a smaller area F_1, i.e., to a smaller e, this lowering of $x_{ф_{опт}}$ will be even more considerable.

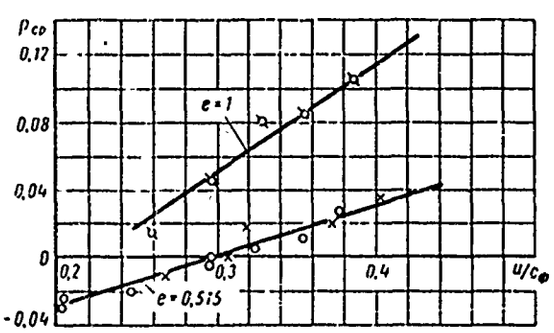

Fig. 172. Change of mean reaction of stage, $\rho_{ср}$, on $u/c_{ф}$ at full, e = 1, and partial, e = 0.515, steam input (MEI experiments).

The change of the reaction, depending upon $u/c_{ф}$ and e for a partial stage, is governed by the same laws as for full input. The dependence of the mean reaction, i.e., the reaction in a mean portion of the input arc (with averaging of the reaction on the periphery and at the root) on $x_{ф}$ for e = 0.515 and e = 1, is shown in Fig. 172.

With the decrease of the partial admission of a stage, its reaction drops.

This is explained by wash-out of the stream at the nozzle cascade exit and the large amount of leakage. Figure 173 shows the dependence of the mean reaction on the degree of partial admission for various stages which differ by cascade height and meridional profiling of nozzle cascade. The test stages had seals above the blade shroud with two strips and a radial clearance of $\delta_2 = 0.8$ mm. The higher the cascade height, the less the influence of the above-noted factors, and as the input arc decreases, the curve of the reaction drop will be more sloping.

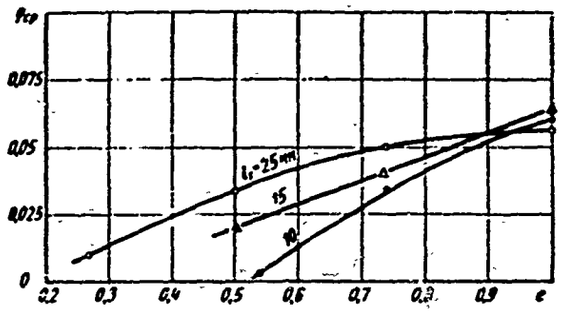

Fig. 173. Influence of partial steam input on mean reaction of КД-2-2А stage, d = = 400 mm, with various heights: l_1 = 25, 15, and 10 mm; $u/c_ф$ = 0.4; ε = 0.75 (MEI experiments).

Attempts to use the formulas recommended in the reference literature for computing losses upon transition from full to partial input were not successful. In an overwhelming majority of cases, especially at low blade heights, the actual losses are considerably larger than according to the formulas of Stodola, TsKTI, the Zurich School, and others.

A semi-empirical formula [104] is proposed below for computing the losses with partial input (one arc) without protection. In order to avoid confusion, this formula does not consider such factors as the ratio of cascade areas, the pressure ratio, axial clearance, stage sealing, suction (or leakage) through the root clearance, and others. Therefore, the formula cannot be universal and exact. However, even in such a form, it gives satisfactory coincidence of the calculated data with experiments at e > 0.25. A smaller degree of partial admission was weakly investigated, and the value of the geometric stage characteristics, which were indicated above and not considered by the formula, was extremely great for it.

It is assumed that the ratio of cascade areas, and consequently, also the reaction of the stage for the given conditions (e, $u/c_ф$, ε) are selected as optimum and the clearances are small. In another case the losses, which are calculated by the recommended formula, will be too low:

$$\zeta_e = 0{,}35\left(\frac{0{,}3x_ф}{d\sin\alpha_1} + \frac{1-e}{e}\right)x_ф^2\eta_{oi}, \qquad (163)$$

where d is given in meters.

3

Figure 174 gives the results of MEI experiments with six stages with different cascade heights. Here for $x_{ф} = 0.4$, a graphic dependence of $\zeta_e/\eta_{ол} = f(\frac{1-e}{e})$ is shown. The graph indicates the large scatter of experimental points, which confirms the influence of many factors on stage economy with partial input. However, even with this scatter of points, formula (163) seems to us to be closer to the majority of experimental data than the other known formulas that are based on computing losses of pure windage.

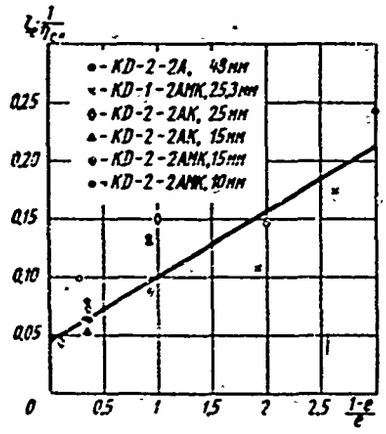

Fig. 174. Dependence of losses with partial input, ζ_e, on the degree of partial admission with one input arc, d = 400 mm; ε = 0.75-0.85; $u/c_{fic} = 0.4$ (MEI experiments).

An investigation of the influence of the number of input arcs of feed, i (to be more exact, pairs of ends, since nozzle arcs can be located close to one another), was conducted at BITM, MEI, LKZ, Asher-Wiess, and others.

According to the experiments of I. G. Gogolev [5], the change of the highest efficiency for a stage with e = 0.5, depending upon i, is shown in Fig. 175. Here, the results of the Asher-Wiess experiments are given [96].

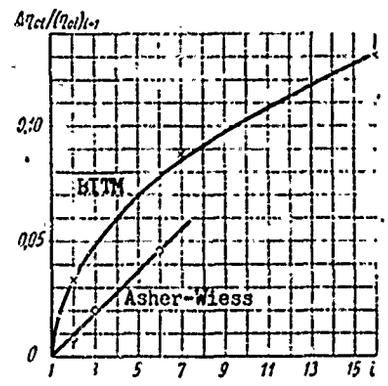

Fig. 175. Influence of the number of input arcs, i, on the economy of a partial stage with e = 0.5 (experiments of BITM and Asher-Wiess).

The experiments of the Asher-Wiess firm, just as the experiments of Olson, MEI, and GE, confirm the linear dependence of losses on the number of input arcs, i. BITM experiments were conducted with a small air-driven turbine with characteristics of flow and dimensions that are not encountered in the partial stages of steam turbines ($M_{c1} = 0.15$, $Re_{c1} = 1.05 \cdot 10^5$, $l_1 \geq 51$ mm). Therefore the use of them for the calculation of turbine stages is difficult. However, even with these tests at a small number of i, it is possible to take the losses to be proportional to the number of input arcs. Numerous experiments confirm the approximate proportionality of the losses that appear upon transition to $i > 1$ from $x_{ф}$. Therefore, as the number of input arcs increase (pairs of ends), the additional losses will be taken by the following formula

$$\zeta_i = 0.25 \frac{bl_2}{F_1} x_{ф} \eta_{ол} (i - 1). \qquad (164)$$

Decrease of Losses with Partial Input

For decreasing losses with partial input, the following measures should be applied:

1) Selection of an area ratio which, taking expansion into account, would give a minimum positive reaction. It should be considered that the selection of F_2/F_1 depends on the stage's x_{ϕ} and ε.

2) Decrease of the full axial clearance. For a partial stage, in distinction from a stage with full input (see § 24), practically the most advantageous clearance size is its minimum, constructively possible, magnitude.

However, the reliability of stage operation also should not be forgotten. A decrease of the full axial clearance lowers the vibration reliability of the blades, which is especially important when partial input is employed.

3) Decrease of open clearances and installation of radial shroud seals. For partial stages, however, the influence of this sealing is somewhat less than for a stage with full input. This peculiarity is explained by the fact that in a partial stage a considerable part of the parasitic leakages passes through the meridional clearances.

4) With steam input to the regulating stage, the adjacent nozzle arcs should be as close as possible. If the nozzle box is common, this condition usually is observed. For certain nozzle boxes which, in particular, are applied in turbines with high parameters, the clearance between adjacent boxes should be the minimum necessary for heat expansion.

5) For decreasing the windage component of losses, a housing should be installed. With Fig. 167 one can determine the increase of stage economy by means of installing this housing. The gain in efficiency, $\zeta_{\text{кож}}$, is calculated by the following formula

$$\zeta_{\text{кож}} = (C_1 - C_2)\frac{1 - e_{\text{кож}}}{e} \cdot \frac{1}{\sin \alpha_1} x_{\phi}^3. \qquad (165)$$

Here $e_{\text{кож}}$ is the part of the contour occupied by the housing; the coefficients C_1 and C_2 are found on the graph of Fig. 167 for a stage without a housing and with a housing, respectively.

With the installation of a housing behind the moving cascade, the site of the housing and its size must be determined with the movement of the steam flow around the circumference and the wash-out taken into account. This calculation is performed with known values of angles, blade width, and clearances, and for a

specific $x_{\text{ф}}$ ratio. It should be borne in mind that with a change of the conditions, i.e., a change of $x_{\text{ф}}$, the optimum site of the housing also changes. Therefore the housing, whose site was determined only for one condition, with a change of the conditions, can shut off the flow proceeding from the rotor blades, and thereby will even lower the efficiency of the stage.

In the direction of rotation, the edge of the housing should be no closer than the edge of the extreme nozzle by the quantity

$$s_1 = 1{,}2(\delta_{\text{п}} \operatorname{ctg} \alpha_1 + 1{,}05 b x_{\text{ф}}). \tag{166}$$

Here $\delta_{\text{п}}$ is the full axial clearance; b is the width of a rotor blade.

On the other side of the nozzle segment, the housing should be placed so that it may rotate, but no more than by the quantity

$$s_2 = 0{,}6(\delta_{\text{п}} \operatorname{ctg} \alpha_1 + 1{,}05 b x_{\text{ф}} - \delta_{\text{к}} \operatorname{ctg} \beta_2). \tag{167}$$

Here $\delta_{\text{к}}$ is the axial clearance between the moving cascade and the housing (Fig. 176).

6) It is necessary to seal the casing of the rotating cascade, where, sometimes for decreasing the axial stress, relief holes are made.

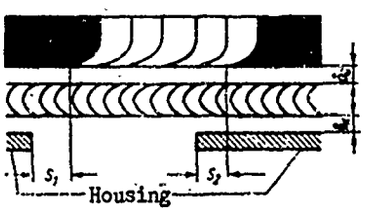

Fig. 176. Location of protective housing in partial stage.

7) For decreasing the losses connected with the irregularity along the input arc, it is logical to decrease this irregularity, whereupon the reaction in the extreme channels at the exit of the nozzle segment is increased somewhat. This apparently, may be attained by a certain increase of the angle α_1 in one or two extreme channels.

§ 29. PERFORMANCE OF A DOUBLE-WHEEL VELOCITY STAGE WITH PARTIAL INPUT

There is no fundamental distinction in the performance of a partial velocity stage and a single-wheel stage. If it is a question of purely windage losses, then, according to experiments of the Zurich School, these losses are increased by $\sqrt{2}$ times as compared to the date obtained for single-wheel stages which was given in the preceding paragraph.

Double-wheel stages with partial steam input were investigated by very many individuals. The investigation of double-wheel stages developed at MEI was especially detailed; these stages were tested in MEI, NZL, and LKZ experimental turbines [32, 34, 36, 53, 74, 78]. Let us present some of these results. Thus,

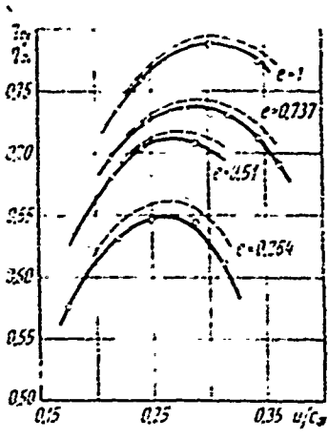

Fig. 177. Dependence of the efficiency of an MEI velocity stage KC-1A-5 on $u/c_{ф}$ and the degree of partial admission e (one input arc), d = 668 mm, l_1 = 25 mm: F/F_1 = = 1:1.53:2.23:3.38, ε = = 0.5, welded diaphragm (MEI experiments): —— η_{oi} measured relative internal efficiency of stage, considering all losses; — — — — $\eta'_{oi} = \eta_{oi} + \zeta_{тр}$.

Fig. 177 shows the dependence of the efficiency the MEI stage KC-1A-5, with a different degree of partial admission, e (MEI experiments). Figure 178 gives a graph of the measured efficiency of the MEI stage KC-1Б, according to the experiments of Yu. Ya. Kachuriner (NZL). This figure gives the curves of efficiency for various pressure ratios p_2/p_0 from 0.70 to 0.35, i.e., both in the subcritical, and also in the supercritical zone.*

As also in the case of a single-wheel stage, velocity stages have a characteristic lowering of the optimum velocity ratio, $x_{ф_{опт}}$, with a decrease of partial admission. This may be seen from Fig. 178. Thus, in the investigated stage the transition from e = 1 to e = 0.264 decreases $x_{ф_{опт}}$ from 0.305 to 0.26, i.e., for the same diameter the optimum heat drop of the stage was increased by 40%. Upon transition to partial input and $x_{ф}$ ratios which exceed the optimum values, there occurs a large lowering of economy. If at $x_{ф_{опт}}$ the efficiency η_{oi} decreases by $\Delta\eta/\eta$ = = 17%, then at $x_{ф}$ = 0.35 this decrease of efficiency already amounts to 30%. These figures once again emphasize how important, especially in conditions of partial input, it is to correctly to select $x_{ф}$ taking into account both the calculated, so also varying operating conditions of the turbine.

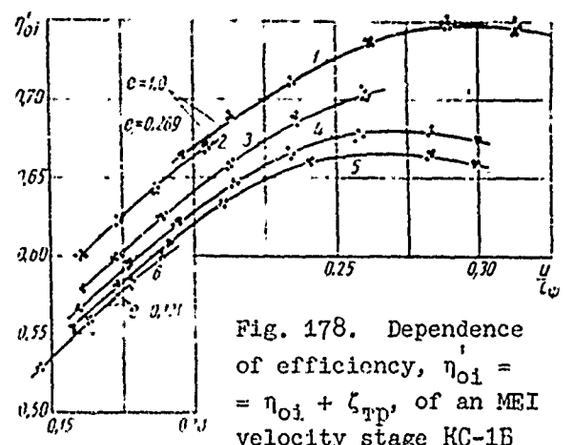

Fig. 178. Dependence of efficiency, η'_{oi} = = $\eta_{oi} + \zeta_{тр}$, of an MEI velocity stage KC-1Б on $u/c_{ф}$ and the pressure ratio, ε, for different degree of partial admission, e, (one input arc), d = 709 mm, l_1 = 15 mm, F/F_1 = 1:1.54:2.48:3.64, welded diaphragm; curves: 1 and 4 - ε = = 0.7; 2 and 5 - ε = 0.55; 3 — ε = 0.60; 6 — ε = 0.35 (NZL experiments).

For a velocity stage, to a larger extent than for a single-wheel stage, the selection of the area ratio, and consequently, the reaction of the stage, is of importance. This is illustrated

*The NZL experiments with old combinations of velocity stages (see Chapter V), the experiments of V. D. Pshenichnyy (LKZ) with various stages, and the MEI experiments with the GE combination No. 113 were [FOOTNOTE CONT'D ON FOLLOWING PAGE]

by the following examples.

The same experimental MEI turbine was employed for testing two MEI stages, KC-1A-2 and KC-1A-4. These stages has identical cascades, diameter, and height of nozzle cascade. The system of clearances and seals, just as the technology of their manufacture, was also approximately identical (welded diaphragm). The main difference in the stages consisted in the area ratios:

	F_3/F_1	F_N/F_1	F_2/F_1
KC-1A-2	1.52	2.39	3.49
KC-1A-4	1.56	2.73	4.17

As can be seen from the graph in Fig. 179, the smaller (more optimum under the given circumstances) area ratios, and consequently, the larger reaction of the KC-1A-2 stage, led to smaller losses with partial steam input. This is explained by the fact that due to wash-out during partial input to the KC-1A-2 stage, the reaction was moderate, while in the KC-1A-4, when $\varepsilon = 0.5$, the reaction became very small, and on the first wheel it was even negative, which led to considerable losses due to suction and losses along the edges of the input arc.

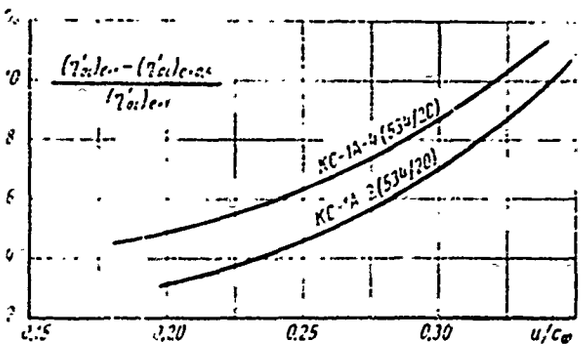

Fig. 179. Dependence of losses on partial steam input for KC-1A-2 and KC-1A-4 stages with different area ratio, according to MEI experiments, with e = 0.5 (one input arc), $\varepsilon = 0.6$, d = 534 mm, l_1 = 20 mm.

However, a very large calculated reaction even in a well sealed step will cause large losses due to steam leakages and because of the essential irregularity ρ along the input arc.

It should be noted that many organizations, in attempting to increase the economy of a stage, select area ratios at which there appear large reactions around the wheels; as a result of this, the efficiency with full input increases somewhat (under the condition of good sealing, which is not always obtainable in operating conditions), and upon transition to partial input, η_{oi} is essentially lowered.

Thus, in the comparison of the MEI stage KC-1Б and the NZL stage, which have approximately identical geometric dimensions, the experiments of Yu. Ya. Kachuriner

[FOOTNOTE CONT'D FROM PRECEDING PAGE]

conducted with a much better technology of maufacture, i.e., milled nozzles [34, 52, 78]. Therefore, the comparison of old and new velocity stages, which is partially performed without taking into account the technology and quality of manufacture, is inadmissible.

[53] showed that with full steam input the NZL stage's efficiency is 0.5% higher than that of the MEI stage. This is explained by the considerably better technology of manufacture of the NZL stage (milled nozzles as compared to the MEI welded diaphragm) and the raised reaction. However, with a partial admission of e = 0.15, which typical for small turbines, the additional losses (at $x_{ф}$ = 0.2) in the KC-1Б stage amounted to 5.4%, and in the NZL stage they were 6.9%, which is explained by the nonoptimum selection of areas of the NZL stage and the more effective (aerodynamically developed) cascades of the MEI KC-1Б stage.

Of large value for the analysis of a velocity stage's performance is the reaction, and for a double-wheel stage, the reaction on the wheels. It is interesting to note (this is confirmed theoretically) that in a velocity stage the reaction in the second wheel practically does not change depending upon $x_{ф}$ both with full, and also with partial input.

Figure 180 presents a graph of the dependence of the reaction on the wheels for a KC-1A-5 stage with full (e = 1) and partial steam input (e = 0.51).

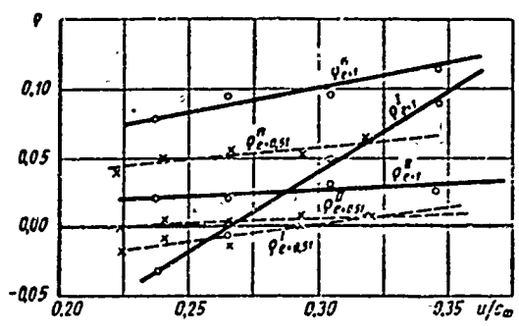

Fig. 180. Dependence of the reaction on the wheels of a KC-1A-5 velocity stage on the degree of partial admission, e (MEI experiments), for ε = 0.5, d = 688 mm, l_1 = 20 mm, F/F_1 = 1:1.53:2.23:3.38 (one input arc): ρ^{I} – reaction in moving cascade of first wheel; ρ^{II} – reaction in rotating cascade; ρ^{II} – reaction in moving cascade of second wheel.

For the second wheel, upon transition from $x_{ф}$ = 0.22 to $x_{ф}$ = 0.36 when e = = 1, the reaction increases from ρ^{II} = = 2% to ρ^{II} = 3%, and it increases just as insignificantly when e = 0.51, where ρ^{II} = 0 and 1%, respectively.

The change of the reaction is small also in the rotating (guide) cascade. However, in the first wheel the influence of partial admission on the dependence of the reaction on $x_{ф}$ is very noticeable and decisive for the performance of the entire stage. This is well illustrated in Fig. 180.

The influence of $\varepsilon = p_2/p_0$, i.e., the influence of compressibility on the reaction of a partial stage, is the same as with full input. As ε decreases, the reaction increases. For instance, for the KC-1A-4 when ($x_{ф}$ = 0.25), upon transition from ε = 0.6 to ε = 0.5, the total mean reaction of the stage was increased by 0.035 for full steam input, and by 0.025 for partial input (e = 0.5). The

dependence of the reaction on $x_ф$, including the total reaction of the stage, remains linear in rather wide limits of variation of $x_ф$. However, the slope of the straight line is determined by the partial admission for a given stage: the smaller e is, the less the influence of $x_ф$. This is explained by the large influence of wash-out of the flow proceeding from the cascade, and the leakages. Figure 181, for a HC-1A-5 stage, presents a graph of $\Sigma\rho_{cp} = f(x_ф, e)$. It is distinctly clear from it that with the decrease of partial admission, the reaction decreases. Thus, when e = 1, a change of $x_ф$ from 0.24 to 0.37 leads to an increase of the reaction from 6 to 24%, and when e = 0.264, from 2 to 10%, correspondingly.

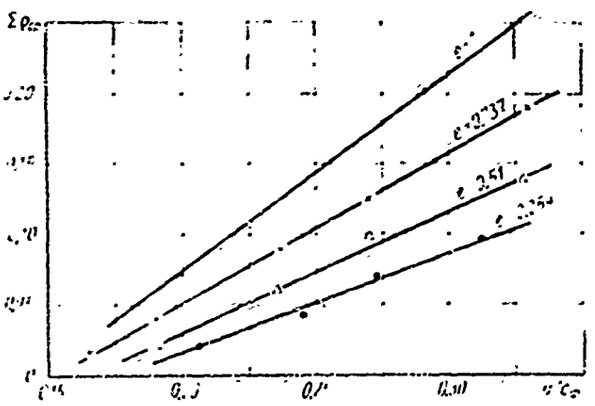

Fig. 181. Total mean reaction $\Sigma\rho_{cp}$ of a HC-1A-5 velocity stage, depending upon $x_ф$ and partial admission e, with one input arc and ε = 0.6 (MEI experiments).

It should be noted (and this may be seen in Fig. 180) that for small $x_ф$ the reaction with partial input can be higher than that with full input. This is explained by the fact that the considerable influence of leakage in a partial stage leads to a decrease of the absolute value of ρ. Generally, in a partial stage, in distinction from a stage with full input, an extreme negative reaction is impossible.

It is absolutely obvious that the formula for calculating the losses upon transition from full to partial input for a single-wheel stage and a velocity stage should be identical in structure. This formula has other numerical coefficients:

$$\zeta_e = 0{,}65\left(\frac{0{,}3x_ф}{d\sin\alpha_1} + 1{,}1\frac{1-e}{e}\right)x_ф^2\eta_{o.i}. \qquad (168)$$

A comparison of the calculation performed by this formula, with the results of different experiments, is presented in Fig. 182. In connection with the larger (than for a single-wheel stage) influence of the area ratio on economy, a large scatter of the experimental points is observed here. As also in the case of a single-wheel stage, formula (168) is useful only for stages in which the area ratio is correctly selected for the given conditions (e, $u/c_ф$, ε).

Experiments for determining the influence of the number of input arcs (pairs of ends), i, on the economy of a double-wheel velocity stage, were conducted at MEI, LKZ, and several other organizations. These experiments showed that the qualitative

picture of the dependence of $\eta_{oi} = f(i)$ is the same as for a single-wheel stage (Fig. 183). The increase losses upon transition to a larger number of input arcs is calculated by a formula which is analogous to (164)

$$\zeta_i = 0{,}25 \frac{\Sigma bl}{F_1} x_\phi \eta_{oi} (i - 1). \tag{169}$$

Here Σbl is the sum of the products of the chord divided by the height of three cascades: first moving, rotating, and second moving.

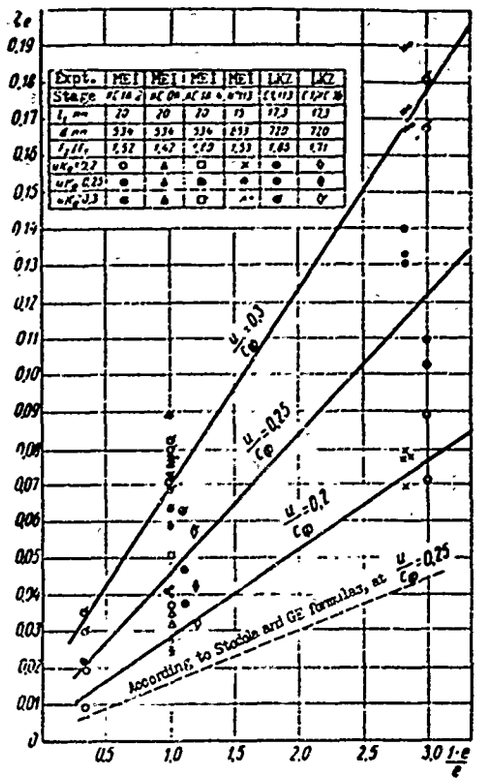

Fig. 182. Losses due to partial input, ζ_e, depending upon the degree of partial admission, according to experiments and calculations.

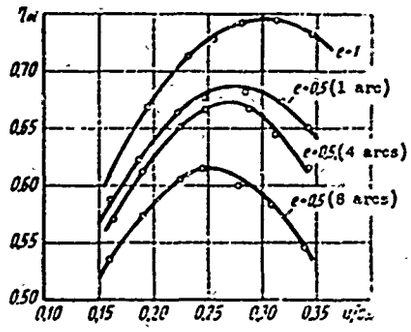

Fig. 183. Dependence of relative internal efficiency of a KC-1A-4 velocity stage on the number of input arcs with a partial admission of $e = 0.5$; $d = 534$ mm; $l_1 = 20$ mm; $\varepsilon = 0.6$.

For determining the dimensions of the nozzle cascade, it is necessary to know the flow rate characteristic of the stage. The steam flow rate, if it is not critical, for constant initial parameters and constant counterpressure, depends on the characteristic of u/c_ϕ. This dependence is determined by the quantity $\varepsilon = p_2/p_0$ and the total reaction of the stage. The same thing may also be said about the partial stage. However, the dependence of $\Sigma\rho = f(x_\phi, \varepsilon)$ in this case will be other than that for full input.

Since, as a rule, the reaction with partial input decreases at large x_ϕ and somewhat increases at small x_ϕ (Fig. 181), the relative flow rate in a stage with partial input at identical pressure ratios will be equal to the flow rate with full input (with critical flow from the nozzles), or larger at larger x_ϕ and smaller

at smaller x_{Φ}. On the whole, the character of the graphs becomes more sloping, since the dependence of $\Sigma\rho = f(x_{\Phi})$ will also be more sloping.

The methods of decreasing losses due to partial input for velocity stages are the same as for single-wheel stages. In particular, one of the methods of increasing economy is the installation of protective housings. The protective housings should be mounted before the moving cascade of the first wheel, behind the entire stage, and instead of the rotating blades. The location and dimensions of the protective housings should be selected with the movement of the steam flow around the circumference and the wash-out taken into account.

The size and place of location of the protective housing must be determined with varying operating conditions of the stage taken into account, for which it is possible to use formulas that are analogous to (166) and (167).

§ 30. OPTIMUM CHARACTERISTICS OF A PARTIAL STAGE

When designing a stage with partial input and, in general, a stage with a low cascade height, it is necessary to make a rational selection of the optimum dimensions. Actually, a decrease of the partial admission and, all the more so, a transition from full to partial input, on the one hand, brings about an increase of losses ζ_e; on the other hand, high cascade heights lead to a lowering of end losses, and consequently, to an increase of the relative blade efficiency $\eta_{oл}$. It is obvious that for each specific case there can be found optimum stage dimensions at which the full relative internal efficiency η_{oi} will be maximum. Selection of the optimum dimensions of a partial stage was studied many researchers. Usually the solution of this problem is performed with the help of variant calculations. An example of such a calculation is given in the textbook by A. V. Shcheglyayev. This procedure is inconvenient due to its tediousness and the impossibility of making a quick estimate of the influence of various factors. Attempts at the analytic calculation of the most advantageous dimensions of a partial stage were made in the NZL method [48] and in the work of Czech scientists [130]. For derivations of dependences which make it possible to find the optimum dimensions of a stage, we shall use the above-mentioned experimental material.

We shall also consider the features of meridional profiling of the nozzle cascade, which is now being employed everywhere in stages with low blades heights, i.e., almost in all stages with partial input. Furthermore, for velocity stages these methods are oriented on old cascade combinations which are presently being replaced by new stages.

The efficiency of the stage is found in the form of

$$\eta_{oi} = \eta_{oл} - \zeta_e - \zeta_{тр} - \zeta_l + \zeta_{кож}. \tag{170}$$

Here η_{oi} is the full relative internal efficiency of the stage without considering only the losses due to leakage through the diaphragm seals. The influence of these losses on the performance of a partial stage almost has not been investigated, and for a determination of the optimum characteristics of a stage it is doubtful whether it can be essential. $\eta_{oл}$ is the efficiency of a stage with full input, after subtracting the losses due to disk friction and shrouds. For stages with the usual nozzle cascade (welded diaphragm), generalized characteristics of MEI stages (see Chapter IX) are mainly used; of the many factors that determine the quantity $\eta_{oл}$, the main ones remain here

$$\eta_{oл} = f(i_1, x_\phi, d).$$

It is assumed that the optimum area ratios and other geometric parameters have been selected. Here and subsequently, we shall not consider the influence of the M number, which is necessary for simplification of the calculations. As usual, single-wheel stages are calculated for operation in a zone of subcritical flow, while double-wheel stages operate in a wider range, up to low supersonic velocities.

For stage with one-sided meridional profiling of the nozzle cascade, the results presented in Chapters IV and V are used.

Losses ζ_e are calculated by formulas (163) and (168), and losses ζ_l, by formulas (164) and (169). If a protective housing is installed, the efficiency of the stage is increased by the quantity $\zeta_{кож}$, which is determined by formula (165). It was assumed here that the housing occupies a portion which is free from the steam input of the arc, i.e., $e_{кож} = 0.8 - e$. In order to make the formulas and graphs more universal, the terms depending on the Reynolds number, the clearances, and the ratio d/l are assumed to be constant. As will be shown later, this does not introduce a considerable error into the final calculation:

$$\zeta_{кож} = \frac{2}{3} C \frac{x_\phi^3}{\sin \alpha_1} \frac{0{,}2 - e}{e}, \tag{171}$$

where C depends on the type of housing.

The losses due to disk friction and blade shrouds, $\zeta_{тр}$, are determined by the formulas in § 12. Here also for simplicity, the Re number and the clearances are assumed to be constant.

After a number of transformations, the efficiency η_{oi} turns out to be a function of three main parameters, el_1, e, and x_ϕ, and a number of secondary

parameters, d, α_1, i, $e_{кож}$, b, and b_c. After differentiating this function, we find that the maximum efficiency η_{oi}^{max} is attained at the optimum degree of partial admission, $e_{опт}$, which is calculated by the following formula

$$e_{опт} = k\sqrt{el_1}. \tag{172}$$

where l_1 is given in millimeters.

Here the coefficient k depends mainly on the type or stage and the velocity ratio $x_ф$, and also on the above-mentioned secondary geometric parameters.

The curves labeled 1 in Fig. 184 represent the graphic dependence of $k = f(x_ф)$ for a single-wheel stage fixed values of the remaining parameters [2]. As follows from the graph, in the real range of variation of $x_ф$, the coefficient k for a usual stage changes approximately one and a half times from 0.16 when $x_ф$ = 0.30 to 0.25 when $x_ф$ = 0.50. With one-sided meridional profiling of the nozzle cascade, a decrease of blade height has a smaller effect on the efficiency $\eta_{оп}$, the losses due to partial input almost do not change. Therefore, the value of optimum partial admission, and consequently also the value of coefficient k, increases in the same zone of $x_ф$ and amounts to 0.19 and 0.28, respectively. Thus, for a stage with a diameter of 1 m, when $\alpha_1 = 15^\circ$ and $x_ф$ = 0.5 (in the usual model, but with a good quality of manufacture), partial input becomes impractical for cascade heights of 14-15 mm, and for a stage with meridional profiling, at l_1 = 11-12 mm. These values coincide with the results of stage tests conducted at the MEI laboratory.

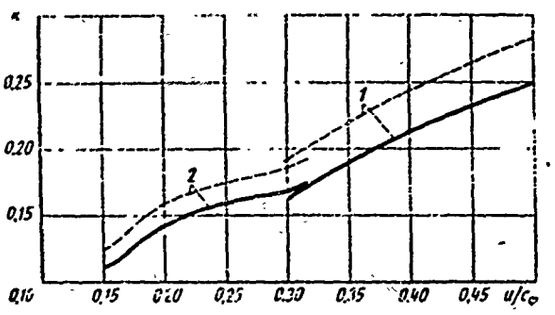

Fig. 184. Dependence of coefficient k in the formula for $e_{опт} = k\sqrt{el_1}$ on the velocity ratio $u/c_ф$; d = 1 m; number of nozzle groups i = 3, no protective housing. Curves: 1 – for single-wheel stage; 2 – double-wheel velocity stage. —— (solid line) – nozzle cascade of usual type; – – – – (dotted line) – nozzle cascade with one-sided meridional profiling.

With the change of the angle α_1, the optimum partial admission changes insignificantly. Thus, for instance, upon transition from $\sin\alpha_1 = 0.2$ to $\sin\alpha_1 = 0.25$, it decreases a total of several percents. A much more complicated question is that concerning the influence of the diameter. As it is known, on the stage diameter depend the efficiency $\eta_{оп}$, the losses on the ends of the active arc,

frictional losses, and others. Calculations show that for a given velocity ratio, x_{ϕ}, the optimum partial admission increases somewhat as the diameter decreases. It is necessary, however, to indicate that not only the quantitative, but also the qualitative estimate of the influence of diameter on the efficiency of a partial stage requires an additional check, since reliable experiments have not yet been conducted with partial stages of different diameter.

As the number of input arcs increases, the optimum partial admission increase perceptibly. Upon transition from $i = 3$ to $i = 6$, $e_{опт}$ increases by 10-15%.

The influence of the protective housing on $e_{опт}$ (but not on efficiency !) is noticeable only when the flow areas are small: $el_1 < 10$ mm. At larger el_1, in practical calculations it may be disregarded. This is explained by the fact that a protective housing, at least according to the experiments of Suter and Traupel, on the basis of which formula (171) was created, decreases only the purely windage losses, which usually make up only a portion of the ζ_e losses.

Besides the selection of the most advantageous stage dimensions for the selected value of the ratio u/c_{ϕ}, another problem can also be set up: to simultaneously select two optimum stage characteristics, i.e., partial admission $e_{опт}$ and velocity ratio $x_{\phi_{опт}}$, at which the highest stage efficiency is attained η_{oi}^{max} for the given area of a cascade and its diameter.* The solution of this problem is possible with the help of the following system of equations [2]

$$\frac{\partial \eta_{oi}}{de} = 0 \quad \text{and} \quad \frac{\partial \eta_{oi}}{\partial x_{\phi}} = 0.$$

By graphically solving this system for every value of el_1, the other secondary geometric parameters being constant, we find the optimum values of the velocity ratio and the optimum (for this velocity ratio) degree of partial admission. These optimum characteristics are given for a single-wheel stage in the form of graphs (curves 1) in Fig. 185. In the construction of the graphs we assumed $d = 1$ m and $i = 3$; the stage does not have a protective housing.

Frequently when designing a turbine it is not practical to maintain an exact value of optimum partial admission. Therefore, it is necessary to know how the relative internal efficiency of the stage changes with a certain deviation of partial admission from $e_{опт}$. This is illustrated by the dotted curves of the graph

*Here we do not consider the selection of an optimum velocity ratio, x_{ϕ}, from the point of view of technical and economic indices of the entire assembly.

in Fig. 186. It should be noted that this graph may be used only for estimating the decrease of efficiency with the change of the degree of partial admission, and by no means for finding the value of efficiency, which depends on very many factors, which deviate in reality from those adopted in the given calculation. The graph in Fig. 186 was constructed for d = 1 m and i = 3, and for values of x_{Φ} that are optimum for the given el_1. However, even for other x_{Φ}, it is fully permissible to use the curves in Fig. 186. As can be seen from the graph (with the exception of those stages where maximum efficiency is attained with full input), the deviation of partial admission from the most advantageous magnitude, within to limits of 20%, has a very slight effect on stage economy especially with an increase of e. This property of a partial stage facilitates the design of turbines and , in particular, the unification of blading.

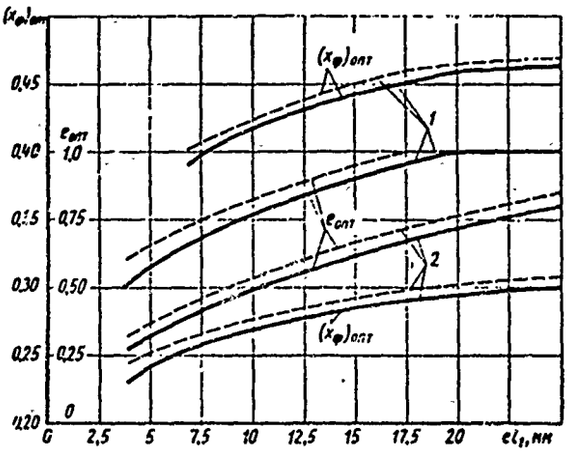

Fig. 185. Dependence of optimum stage characteristics on el_1. Curves: 1 – for a single-wheel stage; 2 – for a double-wheel velocity stage: —— (solid lines) – welded nozzle cascade of usual type; – – – – (dotted) – nozzle cascade with one-sided meridional profiling.

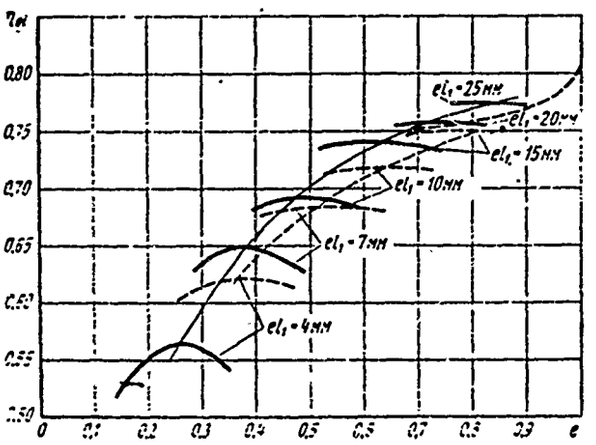

Fig. 186. Influence of deviation of partial admission of a stage from the optimum value of efficiency η_{oi}: Curves —— (solid) – for a double-wheel velocity stage: – – – – (dotted) – for a single-wheel stage.

Analogous graphs were also constructed for double-wheel velocity stages. Although the results of experiments conducted with MEI stages of the type KC-1A and KC-1Б were used for this, the data of these graphs can also be used for other new double-wheel velocity stages. The main criterion that permits the use of these data for other cascade combinations is the area ratio, which should approximately correspond to the value adopted for MEI stages. A change of the area ratio, and consequently, also the calculated reaction, leads to a considerable increase in losses with partial input.

Curves 2, which are represented in Fig. 184, show that partial steam input for double-wheel velocity stages is practical to values of $el_1 < 30$ mm, i.e., with blades almost twice as long as for single-wheel stages. This is explained by the essentially smaller optimum velocity ratios. At small values of u/c_Φ the effect of cascade height on efficiency $\eta_{oл}$ is somewhat larger, and the additional losses, which are inherent to a partial stage, are noticeably lowered.

The solid curves in Fig. 185 show the dependence of the optimum velocity ratios and optimum degree of partial admission for double-wheel stages. Figure 186 illustrates the influence of the deviation of e from $e_{опт}$ on stage efficiency η_{oi}.

The presented graphs for determining the optimum characteristics of single-wheel stages and velocity stages with partial steam input should be of assistance to the designer when planning turbines. Additional research on the influence of stage diameter on the effectiveness of a partial stage, and also further work on the creation and investigation of various safety devices, undoubtedly, will substantiate the most advantageous characteristics which are recommemded here. However, one may assume that it is doubtful whether these substantiations will essentially change the value of the optimum parameters of a partial stage.

§ 31. SUPERSONIC SINGLE-WHEEL STAGES

These stages are used in multistage turbines, and also in the form of small single-stage turbines applied as the drive mechanisms of various assemblies.

In the last case, supersonic stages have relatively small flare and the whole flow of steam or gas at the nozzle cascade exit, which sometimes depends upon the expended heat drop at the entrance and exit out of the moving cascade, is supersonic.

The flow area of these stages should be composed of group B profiles or should depend upon the heat drop of B and Б. Various profile combinations are possible depending upon the specific operating conditions of the machine.

Selection of the aerodynamic and design parameters of a supersonic stage essentially depends on the pressure ratio p_2/p_0 (or M_0), the flow rate of the working medium, and the given (or selected) limiting speed.

The nozzle cascades of supersonic stages can be of three types: a) with divergent channels of rectangular cross section, with an expansion ratio of $f_1 = F_1/F_*$, which ensures the achievement of the design M_{c1} number, TC-P profiles for instance (see § 7); b) with axially symmetric channels, having the same expansion ratios; c) with divergent channels and concave back in slanting shear (TC-BP profiles), which ensure stably small losses in off-design conditions; the

expansion ratio of the channels is considerably smaller the value determined by the given design M_{c1} number (see Chapter I) or convergent channels and concave back (TC-B). Impulse-type moving cascades, depending upon $M_{w1} > 1$, are of type Б or type B (§ 8).

When profiling the flow area of a supersonic stage, it is necessary to consider the possibility of the phenomenon of "choking" of the moving cascade at supersonic velocities in relative motion. At the same time, in accordance with the condition of inseparability, not all conditions at $M_{w1} > 1$ are accessible in the moving cascade. An important part of the problem is also the determination of the angle of exit from the cascade at $M_{w2} > 1$. The enumerated problems can be approximately solved with the help of the hodograph of dimensionless velocity λ_w (or M_w), which was proposed in [25]. Let us consider briefly the method of constructing and using the velocity hodograph.

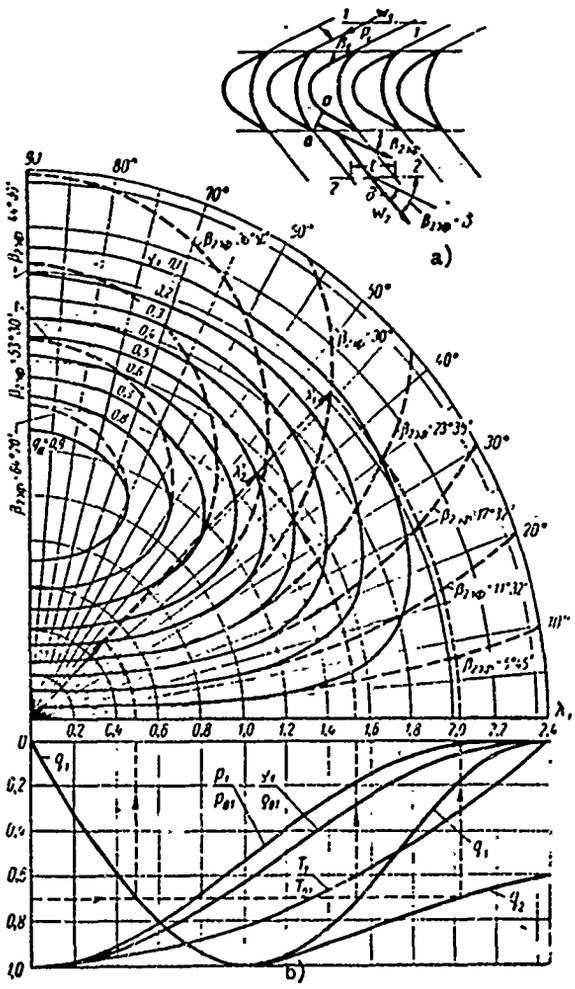

Fig. 187. Calculation of the flow area of a supersonic stage with help of a velocity hodograph: a) cross section of moving cascade; b) diagram of hodographs λ_w.

We shall use a continuity equation in relative motion, after writing it for the entrance and exit sections of the moving cascade (Fig. 187a):

$$q_{w1} \sin \beta_1 = q_{w2} \varepsilon_0 \sin \beta_2, \qquad (173)$$

where $\varepsilon_0 = p_{ow2}/p_{ow1}$; p_{ow}, and p_{ow2} are the stagnation pressures in relative motion at the entrance and behind the cascade;

$$q_w = \frac{\rho_w}{\rho_{*w} a_{*w}} = \left(\frac{k+1}{2}\right)^{\frac{1}{k-1}} \times$$

$$\times \lambda_w \left(1 - \frac{k-1}{k+1}\lambda_w^2\right)^{\frac{1}{k-1}} \qquad (174)$$

the given flow rate in relative motion (q_{w1} at the entrance and q_{w2} at the cascade exit); ρ_{*w} and a_{*w} are the critical density and velocity in relative motion.

Consequently, the axial projection of q_{w1} is equal to

$$q_{w1a} = q_{w1} \sin \beta_1 = q_{w2} \varepsilon_0 \sin \beta_2 = q_{w2a} \varepsilon_0. \tag{715}$$

With the help of formula (174) we obtain

$$q_{wa} = \left(\frac{k+1}{2}\right)^{\frac{1}{k-1}} \lambda_w \left(1 - \frac{k-1}{k+1} \lambda_w^2\right)^{\frac{1}{k-1}} \sin \beta. \tag{716}$$

It follows from expression (176) that various values of λ_w and β can correspond to a constant value of q_{wa}. Hence, we conclude that at q_{wa} = const the end of vector λ_w describes a certain transcendental curve, i.e., the hodograph of vector λ_w, in a polar coordinate system (λ_w, β). By assigning various, but constant values of q_{wa}, from $q_{wa} = 0$ to $q_{wa} = 1$ and β_1 from 0 to π, it is possible to construct a group of curves in the plant of the hodograph (Fig. 187b), which makes it possible to graphically calculate the flow in the moving cascades.

With supersonic velocities at the entrance, not all conditions that correspond to the velocity hodograph are practically accessible. Experiments show that in certain cases when $\lambda_{w1} > 1$, at the entrance to the cascade there appear systems of shocks that are not connected with the flow around the profiles; upon intersecting this system of shocks, the flow obtains subsonic velocities. Such conditions of the flow around impulse cascades are called "choking" conditions.

According to the condition of continuity, a certain other group of conditions with subsonic and supersonic velocities at the entrance also turns out to be unattainable.

Let us consider the methods of determining the unattainable conditions in an impluse cascade at supersonic velocities, and consequently, also in a stage.

We shall use the continuity equation written for the throat area of a nozzle cascade and the entrance and exit sections of a moving cascade:

$$F_{*c} \rho'_{*c} a'_{*c} = F_{w1} w_1 \rho_1 = F_{w2} w_2 \rho_2. \tag{177}$$

Here F_{*c} is the cross-sectional area of the nozzle cascade (throat areas); ρ'_{*c} and a'_{*c} are the density and velocity in the throat areas of the nozzle cascade under the given conditions; ρ_1, ρ_2, w_1, and w_2 are the densities and velocities at the entrance and behind the moving cascade (in relative motion).

We shall present equation (177) in the following form:

$$F_{*c}\frac{\rho'_{*c}a'_{*c}}{\rho_{*c}a_{*c}} = F_{w1}\frac{\rho_1 w_1}{\rho_{*w1}a_{*w1}}\frac{\rho_{*w1}a_{*w1}}{\rho_{*c}a_{*c}} =$$
$$= F_{w2}\frac{\rho_2 w_2}{\rho_{*w2}a_{*w2}}\frac{\rho_{*w2}a_{*w2}}{\rho_{*c}a_{*c}}, \qquad (178)$$

where ρ_{*c} and a_{*c} are the critical density and velocity in the throat areas of the nozzle cascade (absolute motion); ρ_{*w1}, ρ_{*w2}, a_{*w1}, and a_{*w2} are the critical densities and velocities at the entrance and behind the moving cascade (relative motion).

We shall introduce the given flow rate q into equation (178) and shall substitute:

$$\frac{\rho_{*w1}a_{*w1}}{\rho_{*c}a_{*c}} = \frac{p_{ow1}}{p_{oc}}\sqrt{\frac{T_{oc}}{T_{ow1}}};$$
$$\frac{\rho_{*w2}a_{*w2}}{\rho_{*c}a_{*c}} = \frac{p_{ow2}}{p_{oc}}\sqrt{\frac{T_{oc}}{T_{ow2}}},$$

where p_{oc}, T_{oc}, p_{ow1}, T_{ow1}, p_{ow2}, and T_{ow2} are the stagnation pressures and temperatures in absolute (in throat areas of nozzle cascade) and in relative motion.

If we consider for an axial stage that the stagnation temperature in relative motion is kept constant, then, after substitution and transformations, expression (178) obtains the following form:

$$q_{*c}\frac{AF_{*c}}{z_2 l_2 t_2} = q_{w1}\sin\beta_1 = q_{w1a} = \varepsilon_{ow}q_{w2}\sin\beta_2. \qquad (179)$$

Here q_{*c} is the given flow rate in the throat areas of the nozzle cascade;

z_2, l_2, and t_2 are the number, height, and pitch of the channels of the moving cascade;

$\varepsilon_{ow} = p_{ow2}/p_{ow1}$ is the stagnation pressure ratio on the moving cascade;

$$A = \frac{p_{oc}}{p_{ow1}}\sqrt{\frac{T_{ow1}}{T_{oc}}}.$$

This magnitude may be represented by dimensionless velocities:

$$M_{w1} = \frac{w_1}{a_1} \text{ and } M_{c1} = \frac{c_1}{a_1};$$

$$A = \left(\frac{T_{oc}}{T_{ow1}}\right)^{\frac{k+1}{2(k-1)}} = \left(\frac{1+\frac{k-1}{2}M_{w_1}^2}{1+\frac{k-1}{2}M_{c1}^2}\right)^{\frac{k+1}{2(k-1)}},$$

and the relationship between M_{w1} and M_{c1} is determined by the evident expression

$$\frac{M_{w1}}{M_{c1}} = \frac{\sin\alpha_1}{\sin\beta_1}.$$

Equation (179) may be presented in the following form;

$$\left.\begin{aligned} q_{*c}AB &= q_{w1}\sin\beta_1 = q_{w1a} \\ \text{and} \quad q_{w1a} &= \varepsilon_{ow}q_{w2}\sin\beta_2. \end{aligned}\right\} \tag{180}$$

where $B = \frac{F_{*c}}{z_2 l_2 t_2}$ is a geometric parameter of the stage.

We shall analyze these relationships for certain particular cases. Let us fing the condition for which there appear critical velocities at the entrance to or behind a moving cascade.

If $M_{w1} = 1$, then $q_{w1} = 1$, and from equation (180) we will obtain

$$\beta_{1*} = \arcsin(\varepsilon_{ow}q_{w2}\sin\beta_2) = \arcsin(\varepsilon_{ow}q_{w1a}) = \\ = \arcsin(q_{*c}A_1B), \tag{181}$$

where

$$A_1 = \left[\frac{2}{k+1}\left(1 + \frac{k-1}{2}M_{c1}^2\right)\right]^{\frac{k+1}{2(k-1)}}.$$

The critical velocity at a cascade exit is established when

$$\beta_{2*} = \arcsin\left(\frac{q_{w1a}}{\varepsilon_{ow}}\right) = \arcsin\left(\frac{q_{*c}}{q_{w1a}}AB\right). \tag{182}$$

The maximum flow rate through the stage corresponds to these conditions. It follows from this that conditions which corresponding to the condition of

$$q_{*c}AB = q_{w1a} > \sin\beta_{2*}, \tag{183}$$

are unrealizable in the stage.

It should be emphasized that the considered region of impossible conditions at the entrance to a cascade does not coincide with the region of "choking" conditions. In the last case, there appear shocks before the cascade and, consequently, "choking" conditions can form only when supersonic velocities are attained in the nozzle cascade.

As shown above, supersonic velocities before a moving cascade are possible when the continuity equation (173) is satisfied, with losses taken into account:

$$q_{w1}\sin\beta_1 = q_{w2}\frac{p_{ow2}}{p_{ow1}}\frac{p'_{ow2}}{p_{ow2}}\sin\beta_2.$$

Here $\frac{p_{ow2}}{p_{ow1}}$ is the change of stagnation pressure in a normal shock, depending only on M_1; $\frac{p'_{ow2}}{p_{ow2}}$ is the change of stagnation pressure in the cascade.

Since

$$\frac{p_{ow2}}{p_{ow1}} = \lambda_{w1}^2 \left(\frac{1 - \frac{k-1}{k+1}\lambda_{w1}^2}{1 - \frac{k-1}{k+1}\frac{1}{\lambda_{w1}^2}} \right)^{\frac{1}{k-1}},$$

then

$$\frac{q_{w1}p_{ow2}}{p_{ow1}} = \left(\frac{k+1}{2}\right)^{\frac{1}{k-1}} \frac{1}{\lambda_{w1}} \left(1 - \frac{k-1}{k+1}\frac{1}{\lambda_{w1}^2}\right)^{\frac{1}{k-1}}.$$

Consequently,

$$\left(\frac{k+1}{2}\right)^{\frac{1}{k-1}} \frac{1}{\varepsilon_{ow}\lambda_{w1}} \left(1 - \frac{k-1}{k+1}\frac{1}{\lambda_{w1}^2}\right)^{\frac{1}{k-1}} \sin\beta_1 = \sin\beta_{2\,эф}. \tag{184}$$

where $\beta_{2\ эф}$ is the exit angle of the moving cascade, if a normal shock is located before it and $\lambda_2 = 1$.

When $\lambda_{w1} = 1$, $\beta_1 = \beta_{2\ эф}$, i.e., the curves described by formula (174) coincide with the curves constructed according to the equation $\frac{q_{wa}}{\varepsilon_{ow}}$ = const or in accordance with expression (176) by the following formula

$$\left(\frac{k+1}{2}\right)^{\frac{1}{k-1}} \frac{\lambda_{w1}}{\varepsilon_{ow}} \left(1 - \frac{k-1}{k+1}\lambda_{w1}^2\right)^{\frac{1}{k-1}} \sin\beta_1 = \text{const}. \tag{185}$$

The curves that correspond to equations (184) and (185) are shown in Fig. 187b.

The hodograph of λ_w may also be used for an approximate calculation of the angles of deflection in the slanting shear of the moving cascades.

From the continuity equation, we shall express

$$q_{w2} = q_{w1}\frac{\sin\beta_1}{\sin\beta_2},$$

whence

$$\delta = \beta_2 - \beta_{2\,эф} = \arcsin\left(\frac{q_{w1}}{\varepsilon_{ow}q_{w2}}\sin\beta_1\right) - \beta_{2\,эф}.$$

For a zero reaction in the stage, $p_2 = p_1$ and $q_{w2} = \frac{q_{w1}}{\varepsilon_{ow}}$, and the deflection of flow $\delta = \beta_1 - \beta_{2\ эф}$, we arrive at the conclusion that $\beta_1 = \beta_2$.

When $\beta_1 = \beta_2$, the deflection is $\delta = 0$, and consequently, for any supersonic velocity of the incident flow, deflection does not occur in the slanting shear. When $\beta_1 < \beta_2$ - $\delta < 0$, i.e., contraction, not expansion of the flow, occurs in the slanting shear.

This behavior of the supersonic flow in impluse cascades is connected with the

fact that at supersonic velocities disturbances do not spread toward the flow and the pressure before the cascade p_1 can be selected arbitrarily. This condition is disturbed only in "choking" conditions, i.e., when vector λ'_{w1} lies in the region bounded by the dotted curve for $q_{aw2} = \sin \beta_{2\ эф}$ (Fig. 187b).

Thus, before the onset of choking conditions, the exit angle of flow from a cascade can be determined for the value of $\lambda_{w2}(p_2/p_{ow1})$ on the basic set of curves for q_{wa} = const, whereby β_2 does not depend on the geometric parameters of the cascade and the number of λ_{w2}.

In "choking" conditions, vector λ'_{w1} is inside the region bounded by the dotted curve for q_{wa} = const; the exit angle is determined with respect to λ_{w2} on the curve for $q_{wa} = \sin \beta_{2\ эф}$, i.e., it depends on the geometric parameters of the cascade.

We shall now consider some results of the calculation and experimental investigation of supersonic stages. Figure 188 shows the optimum flow areas of these stages, selected by calculation. All stages were calculated for one expansion ratio, $\varepsilon_2 = 0.08$ or $M_0 \approx 2.3$ (M_0 is the M number that is equivalent to the available heat drop in the stage).

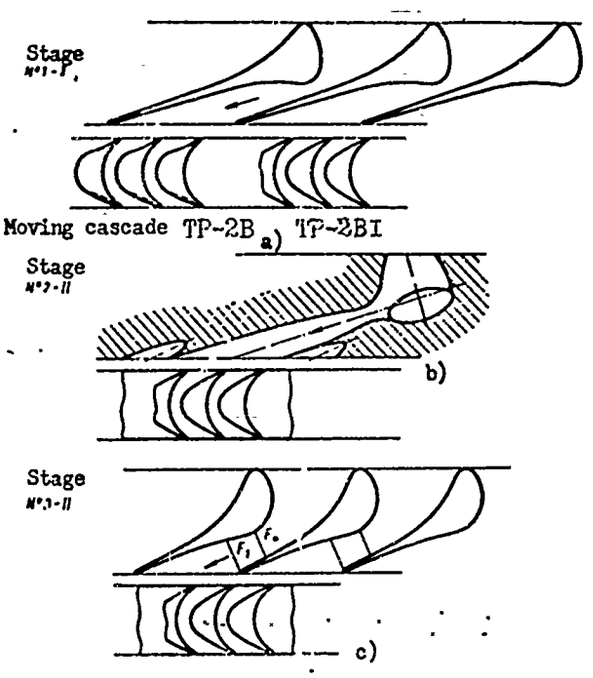

Fig. 188. Diagrams of supersonic single-wheel stages: a) stage No. 1-I, composed of a TC-1P nozzle cascade and three different moving cascades; b) stage No. 2-II, composed of a nozzle cascade with axially symmetric nozzles and a TP-2BI moving cascade; c) stage No. 3-II, composed of a TC-1BP nozzle cascade and a TP-2BI moving cascade.

Stage No. 1 includes a TC-1P nozzle cascade ($\alpha_1 = 16^\circ$); the ratio of the exit section of the channel F_1 to the throat section F_{*c} was $f = \frac{F_1}{F_{*c}} = 2.38$ (for k = 1.3); the cross sections of the channel are rectangular.

The nozzle cascade of stage No. 2 had axially symmetric channels with the same ratio, f = 2.3. The exit sections of the channel are made with a profile calculated by the analytic method. For decreasing the edge losses, the exit sections of the channels have mutual cutoff. Uniformity of flow at the cascade exit is ensured by cutting-off and trimming the trailing edges at the point of intersection of the adjacent channels. The drilled channels of this cascade are characterized by a

smoothly outlined subsonic portion; the profile of the supersonic section in the slanting shear is either conical or, for ensuring a uniform velocity field at the exit, curvilinear.

The nozzle cascades with axially symmetric channels are characterized by smaller end losses and therefore should have a higher efficiency with low heights. An essential advantage of nozzle cascades of this design is high productibility, which ensures a considerably high accuracy of dimensions of the channels and purity of their surfaces.

Stage No. 3 had a TC-1BP nozzle cascade (§ 7) with slight expansion of the vane channel (f = 1, 2) and a concave profile back in the slanting shear.

The moving cascades were of two types (see Chapter I) with stage deceleration at the entrance (TP-2B) and rectilinear backs (TP-2BI) with convergent-divergent channels. All cascades had approximately identical entrance and exit angles.

Consequently, the tests of stages with various nozzle and moving cascades were intended for finding the most rational cascade combination for a supersonic stage which would ensure a high efficiency in a wide range of conditions.

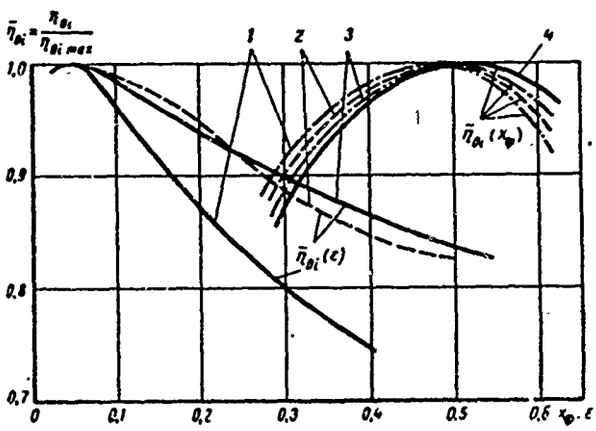

Fig. 189. Dependence of relative internal efficiency of supersonic single-wheel stages on $x_ф$ for a constant available pressure drop, ε = idem, and on a variable drop (ε_2), and for $x_ф$ = idem. Curves: 1 – stage No. 1-II; 2 – stage No. 2-II; 3 – stage No. 3-II; 4 – subsonic stage КД-1-2А (ε_2 = 0.7; Re_{c_1} = $4 \cdot 10^5$).

The results of the calculation, according to static investigations, and certain experimental data for three stages with different nozzle cascades and with one TP-2BI cascade, are shown in Fig. 189. Efficiency curves are given there, depending upon $u/c_ф$ for a constant available heat drop ($\varepsilon_2 \approx 0.08$) which corresponds to the design conditions of the TC-1P nozzle cascade (shown in Fig. 188a).

The experiments show that the efficiency of the three stages under design conditions are close. The particular advantage of the stage with the TC-1BP nozzle cascade is connected, apparently, with the fact that the profile chord in this case is less than in the two other variants. Let us note that the efficiency of stage No. 3 could be somewhat higher: however, in connection with the increased

angle α_1, the reaction in this stage, and consequently, the leakages, turned out to be higher (Fig. 189).

Stage No. 3 with the TC-1BP nozzle cascade has essential advantages in off-design conditions, especially with a decrease of the heat drop available on this stage. When comparing the efficiency curves, which were constructed depending upon the ε of various $u/c_{\text{ф}}$ (Fig. 189) it may be noted that stage No. 1 (Fig. 188a) is the most sensitive to the change of $\varepsilon > \varepsilon_p$. The intermediate position is occupied by stage No. 2 with axially symmetric channels of the nozzle cascade.

The experiments showed that for a design M_0 number equal to 2.3, the best results were exhibited by the TP-2B cascade, with stage deceleration at the entrance. For lower velocities, the TP-2B and TP-2BI cascades are equivalent.

The results of the investigation of supersonic stages distinctly show that the influence of certain geometric parameters, in particular the height of the nozzle cascade and the ratio of cross sections, is different than that for subsonic velocities. Actually, the graphs of the change of efficiency depending upon $\bar{l}_1$ and F_2/F_1, which are presented in Fig. 190, permit us to conclude that the influence of $\bar{l}_1$ weakens when $M_0 \gg 1$. This is explained by a certain lowering of end losses in the cascades at supersonic velocities. An especially weak sensitivity to changes in height is possessed by the stages in which we flow is supersonic both in absolute, and also in relative motion. With a mixed flow in a stage, the effect of height is more considerable. It should be noted that at low heights the advantages of stages with axially symmetric nozzle channels, which are calculated by the method of characteristics or analytically, are noticeable. These nozzle cascades, as shown by the KTZ laboratory, have minimum end losses, the relative magnitude of which, with the decrease of height, practically does not change.

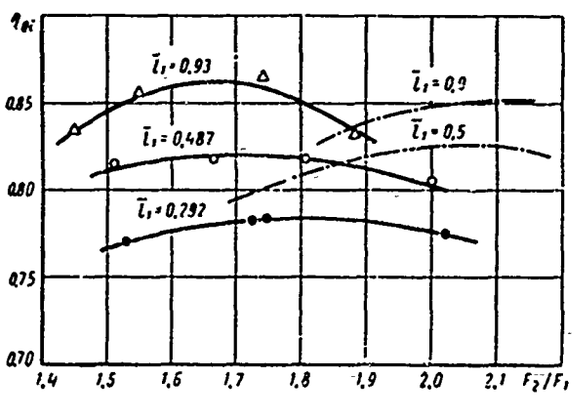

Fig. 190. Dependence of efficiency of single-wheel supersonic stages on height of nozzle cascade and area ratio: —— subsonic stages; — · — · — supersonic stages (calculation).

For supersonic stages, the optimum ratio of cross sections of the moving and nozzle cascades is larger with the same degree of reaction. As the M_0 number increases, the quantity $(F_2/F_1)_{\text{опт}}$ increases, which completely corresponds to the

peculiarity of a supersonic flow, the density of which decreases even more intensely than at subsonic velocities.

Considering the curves of relative efficiency, depending upon x_{Φ} (Fig. 189) for stage No. 1-II, one should note that when $x_{\Phi} > x_{\Phi_{опт}}$, the efficiency decreases more intensely than for subsonic stages and stages No. 2-II and No. 3-II. This result is explained by the phenomenon of choking in corresponding conditions, which are characterized by the increased angles of entrance to the moving cascade and deflection in the slanting shear of the rotor blades, which causes an increase of losses in the nozzle and moving cascades and losses with the outlet velocity.

The x_{Φ} ratio at which choking conditions occur may be determined by the diagram of the velocity hodograph of λ_w (Fig. 187b), with the help of which the region of unattainable conditions in the moving cascade is established.

As the experiments show, the losses during partial input without the application of special protective means in a supersonic stage are somewhat higher. In accordance with this, into the formulas for losses during partial input it is necessary to introduce a correction (see § 28).

In those cases when the calculated degree of partial admission is small, the application of turbines with repeated admission is expedient, in which several impulse pressure stages or velocity stage are placed on one disk.

Figure 191 gives a diagram of such a turbine: with consecutive gas input on one side of the disk and bypass channels (Fig. 191a) and with input on two sides of the disk without bypass channels (Fig. 191b). The first diagram has an advantage that is connected with the best organization of flow at the entrance to the moving cascade; its disadvantage consists in the necessity of bypass channels, which increase the losses somewhat. In the second diagram this disadvantage is not present; however, the conditions of entrance to the moving cascade will be less favorable.

Triple-stage, single-wheel stages can also be constructed on the basis of this diagram. The division of heat drops between stages during input from one direction is carried out in such a manner so that the absolute velocities at the nozzle cascade exit are identical, which leads to identical angles of entrance to the moving cascade. According to the second diagram (Fig. 191b), velocity triangles are constructed in such a way so that the condition of $\beta_1' = \beta_{2\,p}$ ($\beta_{2\,p}$ is the exit angle of the moving cascade) is ensured for the second stage.

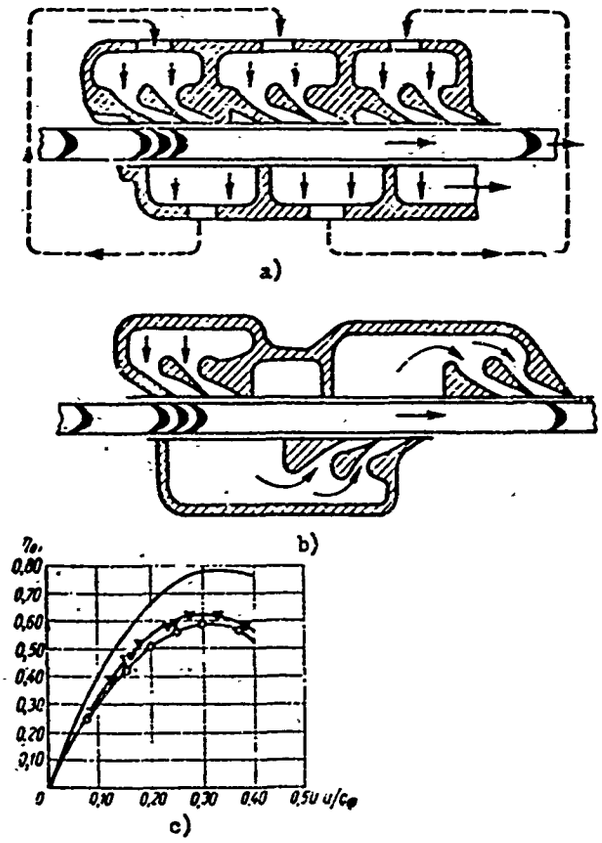

Fig. 191. Single-wheel double-stage superson turbine with partial admission: a) diagram of disk with single gas admission and bypass channels; b) the same, with double admission and without bypass channels; c) characteristic curves of turbine: — ▽ — ▽ — ▽ — experiments with axial clearance δ_a = 0.13 mm; — O — O — O — experiments with axial clearance δ_a = 0.43 mm; —— calculation.

The calculation of a single-wheel, multistage turbine consists in the construction of velocity triangles, the determination of the dimensions of the nozzle and moving cascades, and the determination of the additional losses due to partial input. It should be borne in mind that the losses due to partial input in this turbine will be greater than those in a single-wheel stage.

The results of tests of a single-wheel, double-stage turbine, conducted by G. D. Linkhardt and G. D. Silvern, are shown in Figure 191c. The tests were conducted at ε = = 0.058. Maximum efficiency was equal to 62% at x_ϕ = 0.3. This figure also contains a calculated curve for $\eta_{oi} = f(x_\phi)$; the experimental values of efficiency we considerably lower than those found by calculation. The indicated lowering of experimental efficiency is explained by increased losses in the nozzle and moving cascades and leakages over the shroud and in the root clearance, and also at the nozzle cascade exit of the first stage and through the seals of the nozzle box of the second stage. The design with the bypass channel (Fig. 191a) is more economical, since the leakages at the exit of the first stage are partially trapped by the nozzle box of the second stage.

For increasing efficiency at small x_ϕ, another method can also be used: the installation of a vaned diffuser behind the stage will make it possible to displace the region of maximum efficiency of single-wheel stages to the zone of x_ϕ – 0.3-0.4 with full input. With partial input, the optimum x_ϕ of a stage with a vaned diffuser will naturally be even lower.

§ 32. SUPERSONIC DOUBLE-WHEEL STAGES

In the practice of stationary and marine turbine construction, supersonic double-wheel stages have been employed for sometime. The first experimentally investigated double-wheel stages included the stages produced by the GE firm.

Figure 192 shows the flow area of one of the GE stages which consists of a supersonic nozzle cascade with divergent channels and old-type moving cascades (with rectilinear leading and trailing edges on the back and channels of almost constant width).

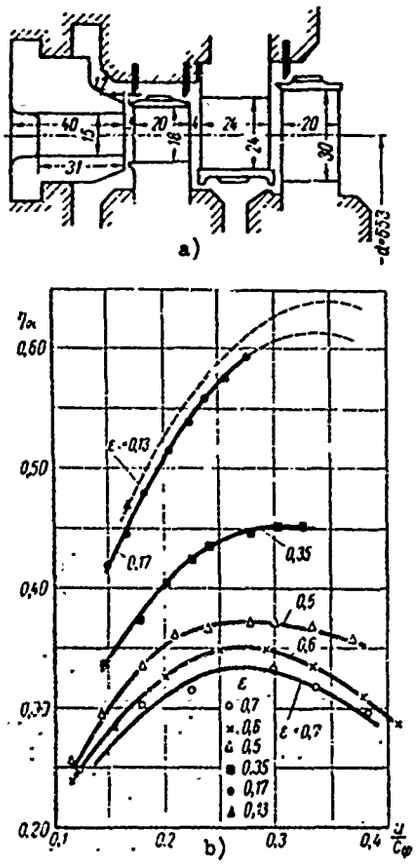

Fig. 192. Investigation of double-wheel stage No. 113: a) flow area of stage No. 113; b) internal efficiency of stage with full steam input at various $\varepsilon = p_2/p_0$.

Systematic tests of this stage were conducted at MEI. The basic geometric characteristics of the test stage are given in Fig. 192a.

Curves of the internal efficiency of the stage at various heat drops for full steam input are shown in Fig. 192b. Figure 151b illustrates curves of η_{oi} for the same stage, but with a subsonic nozzle cascade (with convergent channels). A comparison shows that the efficiency of the GE supersonic stage was considerably lower than that of the subsonic variant. Under design conditions, corresponding to the pressure ratio $\varepsilon \approx 0.13$ ($M_0 \approx 2.0$), the maximum efficiency of the supersonic variant amounts to 0.64, and the subsonic, at $\varepsilon \approx 0.55$ ($M_0 \approx 1.0$), is equal to 0.71. However, if a comparison is made of the two variants at $\varepsilon \approx 0.13$, the effectiveness of the supersonic stage turns out to be higher. Already these first experiments confirm the expediency of the special development of double-wheel stages for supersonic velocities.

At the same time, as may be seen from the graphs in Fig. 192b, the stage with the supersonic nozzle is very sensitive to changes of conditions (ε or M_0). As the heat drop available on the stage decreases (as ε increases), the efficiency of the stage is sharply lowered. Thus, at $\varepsilon = 0.13$, $\eta_{oi} = 0.64$, and at $\varepsilon = 0.7$, the efficiency drops twice, to 0.33.

Such an abrupt change of the efficiency of the supersonic stage under variable conditions is explained mainly by the corresponding behavior of the nozzle cascade

with divergent channels, which is very sensitive to changes in the pressure ratio $\varepsilon_1 = p_1/p_0$ (conditions). Actually, by comparing the curve of $\zeta = 1 - \varphi^2$ for the nozzle cascade (Fig. 25) with the curves of stage efficiency depending upon ε, one can be certain that they are practically equidistant. Consequently, the efficiency of the entire stage under variable conditions to a considerable extent is determined by the losses in the nozzle cascade. Hence, it may be concluded that improvement of the nozzle cascade may essentially increase the efficiency of a double-wheel stage, not only under design conditions, but also under variable conditions.

An illustration of these statements is the work of the Kaluga Turbine Plant on the improvement of the nozzle cascade of a double-wheel supersonic stage. The flow area of the investigated stage and its basic dimensions are shown in Fig. 193. The profiles of the first moving, rotating, and second moving wheels are reproductions of the well-known MEI combination of the KC-1A subsonic stage (see Chapter V). The nozzle cascade was manufactured in four variants (Fig. 194). The first variant (Fig. 194a) has cylindrical shrouds, and profiles of type TC-1P form divergent channels with an expansion ratio of $f = 1.5$. The design M_1 number is ≈ 2.01 ($\varepsilon_1 = 0.133$). The profile chord of the nozzle cascade was very large ($b_1 = 100$ mm) and the relative height was $\bar{l}_1 = 0.12$. In connection with the great length of the chord and the relatively small cascade diameter, the channel sections vary greatly with respect to length: the channels take on a complicated three-dimensionsl curvature. It

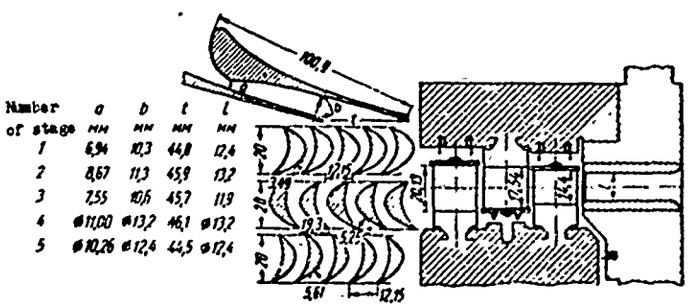

Fig. 193. Flow area part of KTZ double-wheel stage. Radial clearances in seals 0.4-0.7 mm; front open axial clearances 1.3-1.8 mm, rear — 2.5-3 mm.

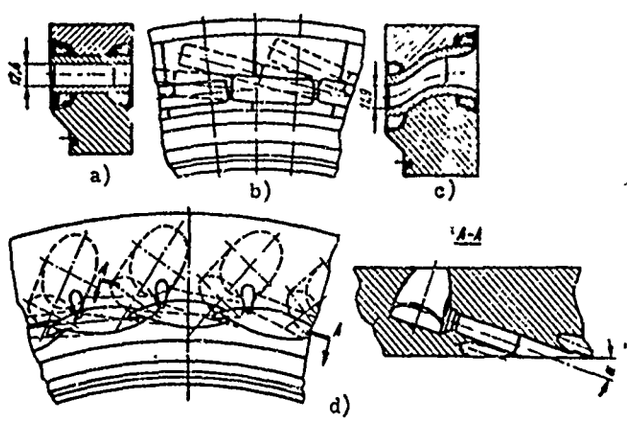

Fig. 194. Variants of nozzle cascades of double-wheel stages tested by KTZ: a) with cylindrical contours, welded; b) with two-dimensional channels; c) with profiled channels; d) with axially symmetric channels.

should be noted that for this variant, as also for all the others, the profile chord was selected so large without a proper basis.

The second variant of a nozzle cascade with the same profile was manufactured with two-dimensional vane channels (Fig. 194b). The three-dimensional curvature of the nozzle cascade is attained due to the fact that the profile generatrices, which belong to the adjacent channels, are inclined to one another at an angle equal to pitch angle of the cascade. The cross section of the channel is right-angled along the length. The end planes that bound the channel are oriented in space so that the axis of the stream is tangent to the mean circumference. This cascade has a somewhat smaller channel divergence, f = 1.31.

The third nozzle cascade is manufactured with the same profile, but it has specially profiled shrouds in the meridional plant (Fig. 194c) which ensures the location of the skeleton line of the profile in its end sections, in one plane.

The fourth and fifth variants, i.e., conical divergent nozzles (Fig. 194d), have a smoothly outlined subsonic section. Thus, as also for single-wheel stages (§ 31), for the purpose of decreasing edge losses here, the exit sections of the channels have a mutual cutoff. The velocity values in the cutoff region in the adjacent channels are practically identical. The axes of the channels are oriented approximately on a tangent to the mean circumference of blades of the first row. The cone angle is assumed to be small ($\gamma_c \approx 5^\circ$). Variants four and five differ only by the nozzle angle ($\alpha_{1c} = 15^\circ$ and $\alpha_{1c} = 17^\circ$).

The results of the tests of the five stages, under conditions close to design, are shown in Fig. 195. It follows from a comparison that the last three variants (nozzle cascade with profiled shroud, conical nozzles), the third, fourth, and fifth, have approximately identical efficiency and it is considerably higher than that of the first and second. The increase of efficiency amounts to 2-4% as compared to variants one and two.

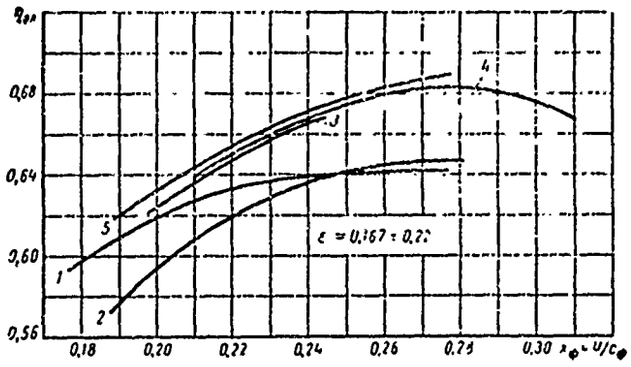

Fig. 195. Dependence of the efficiency of KTZ double-wheel supersonic stages on x_Φ with a constant heat drop on the stage: 1 – stage No. 1 (welded nozzle cascade with cylindrical contours); 2 – No. 2 (two dimensional channels); 3 – No. 3 (with profiled contours); 4 – No. 4 (drilled nozzles); 5 – No. 5 (drilled nozzles).

It should be emphasized that the KTZ double-wheel velocity stage with drilled conical nozzles turned out to be less

sensitive to changes in heat drop than stage No. 113 (Fig. 192), which is clear from the graphs in Fig. 196.

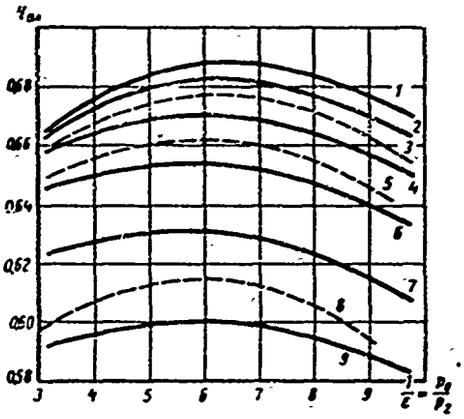

Fig. 196. Influence of the pressure ratio (M_0 number or heat drop) on the effectiveness of a stage whose nozzle cascade is designed with axially symmetric channels. Stages No. 5 — solid lines and 5a — dotted: 1 — stage No. 5 — x_Φ = = 0.28, No. 5a — x_Φ = 0.26; 2 — x_Φ = 0.26; 3 — x_Φ = 0.24; 4 — x_Φ = = 0.24; 5 — x_Φ = 0.22; 6 — x_Φ = = 0.22; 7 — x_Φ = 0.2; 8 — x_Φ = = 0.18; 9 — x_Φ = 0.18.

The efficiency obtained by the plant for double-wheel supersonic stages with low blade height (l_1 = 11.9-18.2 mm) are by far not limiting. It should be borne in mind that the moving and rotating blades of the test stages had subsonic contours. Replacement of the first moving cascade by TP-1Б profiles from MEI, which are designed for work at low supersonic inlet velocities ($M_{w1} \leq 1.25$), made it possible to increase the stage efficiency by 1-2% (relative). The increase in efficiency, as a result of the application of a new profile, continues to increase as x_Φ decreases, which is connected with the increase of velocity w_1 (and M_{w1}, correspondingly) in relative motion.

The KTZ also conducted other investigations of supersonic double-wheel stages, the geometric characteristics of which are given in Table 14, and a diagram of the flow area is shown in Fig. 197a. Transonic stages No. 1 and 2 are similar in their geometric parameters to the MEI KC-1A stage (§ 25), but differ from it by the ratio of flow areas. Stage No. 3 is equipped with new blading which was specially developed for the low heights (see Chapter I).

The efficiency of these stages, depending upon x_Φ, is presented in Fig. 197. The effectiveness of the KTZ-MEI supersonic double-wheel stages may be estimated by means of Fig. 198a. These experiments once again confirmed the expediency of the application of axially symmetric nozzle cascades with low heights. Expecially important in this case is the fact that a stage with axially symmetric nozzles, constructed on the condition of minimum wave losses and losses due to friction, behaves satisfactorily under variable conditions. Figure 198b gives curves of relative efficiency for these stages; the curves were constructed on the basis of tests of four stages with axially symmetric nozzle cascades which differ from each other by the expansion ratio of the supersonic portion of the channels. As can be seen from the graph,

nozzle cascades with axially symmetric channels perform satisfactorily under variable conditions.

Table 14. Geometric Characteristics of Experimental Stages

Designation of characteristic	Number of stages					
	1	2	3	4	5	6
Mid-diameter in mm	800	800	800	550	350	265
Height of nozzle cascade in mm	14.5	15.0	11.4	12.3	11.9	8.25
Area of throat sections in cm^2	45.2	38.2	24.8	7.41	14.8	1.08
Degree of partial admission	0.41	0.41	0.33	0.21	1.0	0.28
Profile of nozzle cascade	TC-2A	TC-2A	TC-2БМ	Axially symmetric		
Effective outlet angle	$17^\circ 40'$	$14^\circ 20'$	14°	17°	17°	16°
Profile of cascade of first wheel .	TP-1A	TP-1A	TP-1БК	TP-1Б	TP-1Б	TP-1B
Profile of cascade of rotating wheel	TP-3A	TP-3A	TP-3Ак	TP-3A	TP-3A	TP-3Б
Profile of cascade of second wheel	TP-5A	TP-5A	TP-5A	TP-4A	TP-4A	TP-4A
Expansion ratio of channels of nozzle cascade	1	1	1	1.48	2.24	3.97
Relative area of first wheel	1.56	1.6	1.76	1.51	1.7	1.55
Relative area of rotor apparatus ..	2.3	2.12	2.67	2.55	3.14	3.06
Relative area of second wheel	3.6	4.0	3.9	3.42	4.65	4.52
Profile chord of nozzle cascade in mm	43	43	45	45	41	42
Profile chords of moving and rotating cascades	25	25	25	20	20	15
Diameter of location of relief holes in mm	560	560	560	310	210	—
Diameter of relief hole	30	30	30	25	22	—
Number of relief holes	5	5	5	5	4	—

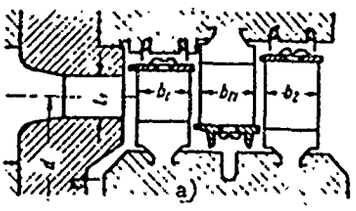

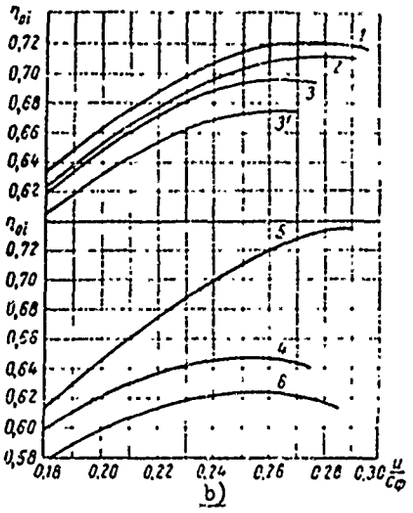

Fig. 197. Investigation of KTZ supersonic double-wheel stages: a) diagram of flow area with clearances in seals 0.5-1.0 mm and overlaps: root 0.5-1.5 mm and peripheral 1.5-2.5 mm; b) dependence of stage efficiency on x_Φ.

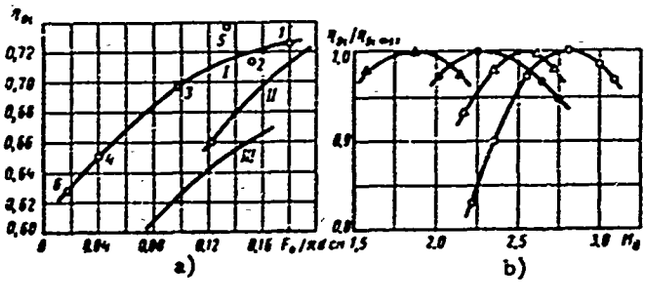

Fig. 198. Effectiveness of double-wheel subsonic and supersonic stages: a) dependence of efficiency of stages on parameter $F_*/\pi d$ (where F_* is the area of the throat sections of the nozzle cascade); b) the influence of M_0 numbers on the efficiency of stages with various nozzle expansion ratios: Curves: I — KTZ-MEI velocity stage: II — TsKTI stage; III — stage No. 113. ▲ — ▲ — ▲ — f = 1.48; ● — ● — ● — f = 2.24; Δ — Δ — Δ — f = 3.97; O — O — O — f = 4.17.

The sensitivity of a stage to a change of conditions increases as the design M_1 number increases at the calculated expansion ratio f. Thus, for instance, for a stage with a nozzle cascade, f = 1.48 (M_0 = 1.8), a 20% change as compared to optimum causes a 3% drop in economy. For a stage whose nozzle cascade has f = 4.17 (M_0 = 2.8), a corresponding change of the conditions causes a lowering in economy by 18%. This result is distinctly confirmed by graphs of the change of losses in a nozzle cascade with divergent channels (see Chapter I), and an even greater change of losses is observed under variable conditions, the higher f is.

In comparing the effectiveness of the three supersonic stages (No. 4, 5, and 6), let us note that by means of extrapolation for full input there can be obtained the following maximum values of efficiency (Table 15).

Table 15. Effectiveness of Certain Experimental Stages

Characteristic of stage	Transonic		Supersonic			
	number of stages					
	1	2	3	4	5	6
Maximum efficiency with full input, $\eta_{oi\ max}$	75.%	76%	75.5%	69.5%	73.7%	68%
Optimum velocity ratio, $x_{ф\,опт}$	0.29	0.28	0.27	0.26	0.28	0.26
Height of nozzle cascade, l_1, in mm	14.5	15.0	11.4	12.3	11.9	8.25

The data given in Table 15 distinctly show that supersonic stages can have an efficiency on a level with the best transonic and subsonic stages if the flow area is profiled correctly. The transition to considerable supersonic velocities

practically does not change the optimum velocity ratio $x_{\Phi_{опт}}$. This fact is indirectly confirmed also by the graph in Fig. 198b: the points characterizing the efficiency of the subsonic and supersonic stages lie on one curve, $\eta_{oi} = f(F_{*c}/\pi d)$.

It should be emphasized that the available experimental data confirm the effect of height on the efficiency of supersonic double-wheel stages, which turns out to be less considerable than that for subsonic ones (Table 15). This result is explained by the decrease of end losses in the cascades at $M > 1$ (in nozzle cascades with axially symmetric channels, these losses are extremely small).

The absence of normal regularity between efficiency and the basic geometric dimensions (height and diameters) for KTZ stages is explained by their particular design distinctions.

In the design of a supersonic double-wheel stage, an important role is played by the correct selection of the total degree of reaction and its division along the wheels.

The main geometric parameters that determine the degree of reaction are the cross-sectional ratios of the wheels. Numerous investigations showed that these ratios must be different, depending upon the type of nozzle cascade of the stage and its design conditions.

The experiments of KTZ and MEI also showed ways of further improving double-wheel supersonic stages. The solution of this problem requires: a) the application of nozzle cascades, which ensure stably high efficiency in a wide range of variation of conditions with respect to M_{c1} (or M_0); b) the selection of profiles for the first rotating wheel and second wheel of the stage, for which the selected M numbers and entrance angles are optimum; c) the guarantee of optimum reactions on the wheels by selecting the appropriate areas of flow sections of the wheels.

When solving this problem, MEI developed a new group of supersonic double-wheel stages. They considered that the possibility of employing large (supercritical) heat drops on a double-wheel stage with sufficiently high efficiency is very tempting not only for creating transport machines, but also steam turbine installations with super-high parameters.

As shown by the investigation of the influence of the M_0 number on the efficiency of double-wheel stages KC-0A and KC-1A, its increase in the beginning leads to a growth of efficiency, and the, with the transition to $M_0 > M_{0*}$ (M_{0*} is the critical M number for the stage), the efficiency starts to decrease, and especially intensely when $M_0 > 1$ (see Fig. 151).

Aerodynamic research on cascades shows that subsonic profiles with continuously variable camber which form convergent channels are characterized by increased losses at supersonic velocities.

Consequently, when designing a double-wheel stage for supersonic drops, it is necessary to apply special supersonic profiles for the nozzle, moving, and rotating cascades (profiles of group V).

These profiles are given in the atlas (see also Chapter I).

Furthermore, considering that for the given ratio of flow areas of the wheels, the reaction in the stage (and on separate wheels) increases as M_0 increases; therefore, it is necessary that such stages be designed with large area ratios.

Taking into account the results of the indicated investigations, MEI developed supersonic double-wheel stages that differ by the angles of the profiles and the heat drops used. Experiments conducted in certain laboratories made it possible to estimate the effectiveness of some of the new variants.

Depending upon the used heat drop and the angles of flow, the flow areas are composed of the profiles shown in Tables 16-18.

Table 16. Profiles of KC-0B Double-Wheel Stage

Cascade	Profile	Range of inlet angles	Range of outlet angles	Area ratio	Design M number at entrance	Design M number at exit
Nozzle	TC-0BP	—	11-14°	1.0	—	1.8-3.0
First wheel	TP-0BP	16-18°	15-17°	1.6	1.4-1.8	1.4-1.8
Rotating wheel	TP-2Б	22-26°	20-22°	2.7	0.9-1.4	1.1-1.2
Second wheel	TP-4A	30-32°	26-28°	4.5	0.7-0.9	0.5-0.6

Table 17. Profiles of KC-1B Double-Wheel Stage

Cascade	Profile	Range of inlet angles	Range of outlet angles	Area ratio	Design M number at entrance	Design M number at exit
Nozzle	TC-1BP	—	15-17°	—	—	1.8-3.0
First wheel	TP-1BP	19-22°	17-18°	1.55-1.65	1.4-1.8	1.4-1.8
Rotating wheel	TP-3Б	27-30°	23-25°	2.6-3.0	0.9-1.2	1.1-1.2
Second wheel	TP-5A	38-45°	29-31°	3.8-4.5	0.7-0.9	0.5-0.6

Table 18. Profiles of KC-2B Double-Wheel Stage

Cascade	Profile	Range of inlet angles	Range of outlet angles	Area ratio	Design M number at entrance	Design M number at exit
Nozzle	TC-2BP	—	16-19°	1.0	—	1.8-3.0
First wheel	TP-2B	25-27°	24-26°	1.56	1.4-1.8	1.4-1.8
Rotating wheel	TP-3Б	30-33°	30-33°	2.86	0.9-1.4	1.1-1.2
Second wheel	TP-5A	42-50°	38-45°	4.5	0.7-0.9	0.5-0.6

As can be seen from the tables, supersonic double-wheel stages are characterized by higher ratios of areas of flow sections; as already indicated, upon transition to supersonic velocities, the reaction of the wheels increases and therefore, for maintaining it on a low level, it is necessary to increase the cross-sectional areas of the wheels.

According to the tables, the profiles along the flow area consecutively vary from group B to group A in accordance with the change of the M number in absolute and relative motion.

The KTZ laboratory obtained the characteristics of a KC-1B stage with a diameter of d_1 = 700 mm and height of nozzle cascade l_1 = 15 mm for various M_0 numbers (heat drops). In connection with the fact that the given stage has new nozzle and moving cascades, the efficiency of the stage was high under design conditions and relatively weakly variable with deviations of the conditions from design.

These experiments also confirm the result noted in the preceding paragraph and in Chapter I (see § 7): the nozzle cascade for $M_{c1} > 1$ behaves better in variable conditions, if the outlet angle of flow α_1 is variable.

Of importance is the correct selection of the cascade profile of the first row, the pitch, and the angle of incidence of the profiles. Experiments show that an error in the angle of incidence of the profile of the first wheel (incorrect selection of inlet angle β_1) can lead to a lowering of economy of the stage not only in design conditions, but especially under conditions that differ from design.

§ 33. COMPARISON SINGLE-WHEEL STAGES AND VELOCITY STAGES

When designing a turbine, there sometimes arises the problem of selecting the type of stage, e.g., single-wheel or velocity stage. Quite frequently it is encountered when selecting the type of adjustable stage. In this case, not only the type of stage, but also its heat drop and diameter are variable. It is obvious that the selection of these characteristics is influenced by many factors:

1. The economy of the adjustable stage for the given d, h_0 and volume steam admission Gv_0.

2. Change of the economy of the subsequent, nonadjustable stages due to a change of the heat drop of the adjustable stage.

3. Change of steam temperature behind the adjustable stage and the problems of metals and strength that are connected with this.

4. Change of turbine dimensions (or the high-pressure portion for multicylinder machines) and the problems of maximum dimensions of forged pieces, critical rotor

speed, and others connected with this.

5. Change of steam leakages through forward end sealing.

6. The requirements of variable operating conditions of the turbine.

This entire set of questions goes beyond the scope of this book; however, for its solution the designer should have comparative data at his disposal for solving the problem with regard to points 1 and 6, i.e., he should be able to compare the economy of a single-wheel stage and a velocity stage under identical conditions. Inasmuch as in the majority of cases this problem arises in stages with partial input, the designer should use the material of the preceding paragraphs of this chapter for its solution. For a first estimate, comparative graphs of economy are presented below. These graphs are only comparative, i.e., they are not intended for determining the efficiency of any stage, but for comparing the economy of a single-wheel and double-wheel stage under specific operating conditions.

It should be pointed out that inasmuch as we are speaking of an adjustable stage, in the selection of the type and parameters of the stage it is necessary to consider that for a multistage turbine the losses (decrease in efficiency) in the first stage due to the phenomenon of heat return are less than in the subsequent stages and especially in the last stages.

If we consider a turbine with intermediate steam superheating, a decrease in the efficiency of the adjustable stage and a corresponding increase in the temperature of the steam proceeding to the secondary steam superheater require a smaller expenditure of heat for secondary superheating. This must also be considered when selecting the type and parameters of an adjustable stage.

Figure 199a and b, show comparative curves of the relative internal efficiency of single-wheel and double-wheel stages, considering all losses except leakages through the end sealing. The graphs were constructed for full input ($e = 1$) and three partial admissions ($e = 0.75$, 0.5, and 0.25). Stage diameter is 800 mm. Calculations were performed for КД-1-2А and КС-1А stages with identical angle α_1. The pressure ratio was $\varepsilon = 0.5$ for the velocity stage and $\varepsilon = 0.7$ for the single-wheel stage. The stages have no devices for lowering losses due to partial input. The number of nozzle arcs (pairs of ends) $i = 1$. The nozzle cascade does not have special meridional profiling, and the diaphragm is welded.

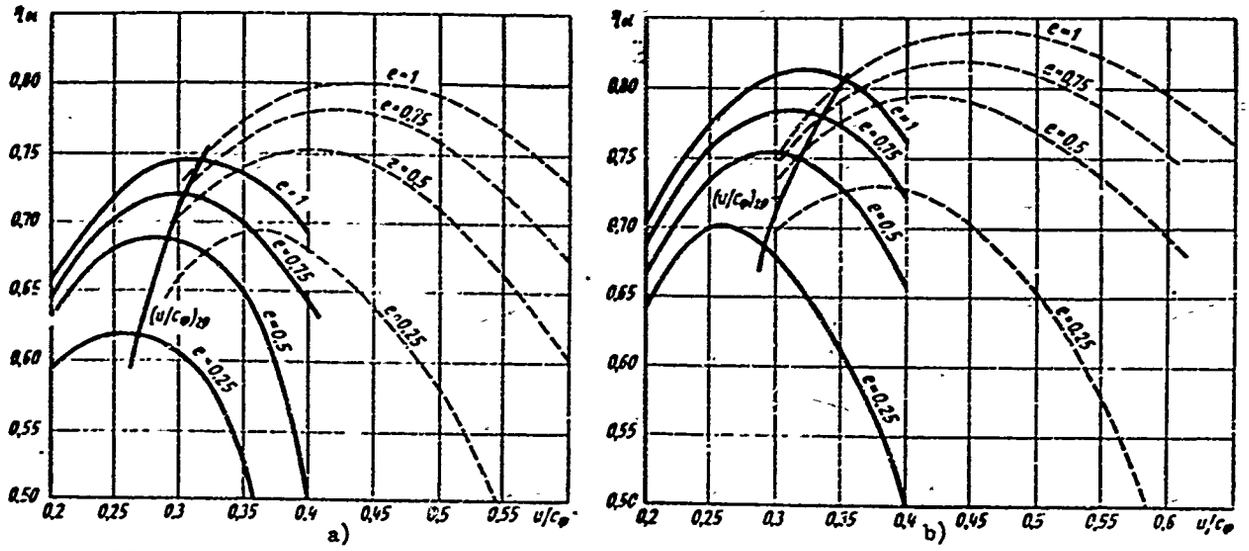

Fig. 199. Comparison of the economy of single-wheel (dotted lines) and double-wheel (solid lines) stages, depending upon $x_{ф}$ and partial admission e, for various heights of the nozzle cascade: a) l_1 = 15 mm; b) l_1 = 25 mm.

On the basis of these graphs it is possible to make the following conclusions:

1. For definite height l_1 and degree of partial admission e there is a bound of $u/c_{ф}$, below which the double-wheel stage has a higher efficiency η_{oi} than the single-wheel type.

2. Depending upon l_1 (when $15 \leq l_1 \leq 25$ mm) and e ($0.25 \leq e \leq 1$), the magnitude of this threshold velocity ratio, $x_{ф.гр}$ varies from 0.36 to 0.26.

As l_1 and e (volume steam admission) increase, $x_{ф.гр}$ increases.

Figure 200 presents graphs that were recalculated for various diameters from d = 700 mm to d = 1100 mm, and constant number speed, n = 3000 rpm. Calculation of the efficiency curves was performed under the same conditions as the previous graphs. The basic feature of the graph in Fig. 200 is the fact that it indicates efficiency for optimum partial admission of the stage, $e_{опт}$, and optimum velocity ratio, $x_{фопт}$.

This graph makes it possible to compare the maximum economy of stages under the given conditions, depending upon h_0 and F_1, and it is valuable in the selection of the main parameters of an adjustable stage. However, it cannot be used when there is a deviation of the stage characteristics from optimum.

It is obvious that under other conditions (other stage combinations, other speeds, increase of number of input arcs, meridional profiling of nozzle cascade, and so forth) it is possible to construct analogous graphs by using the material of this chapter.

§ 34. ADJUSTABLE STAGES OF EXTRACTING TURBINES

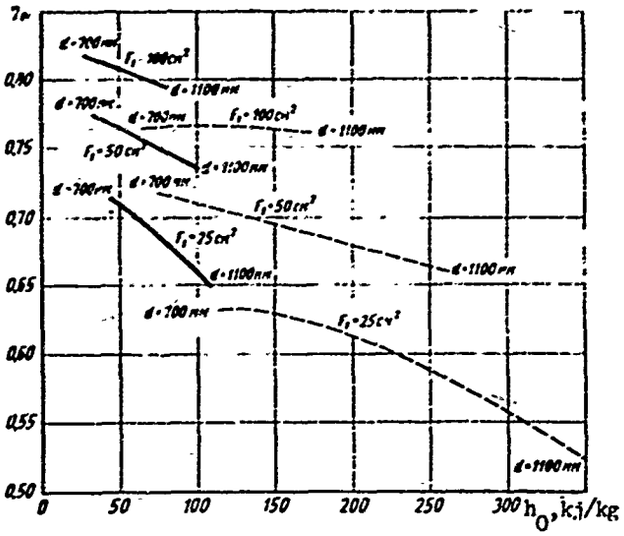

Fig. 200 Comparison of the economy of single-wheel (solid lines) and double-wheel (dotted lines) stages, depending upon the available heat drop of the stage h_0 and the outlet area of the nozzle cascade F_1.

In turbines with steam extraction, for production and heating, in distinction from condensing turbines, there are additional steam-distributing elements which make it possible to maintain a given pressure in the extraction chamber by means of regulating the steam admission through the subsequent stages of the turbine.

Most Soviet turbines use regulating rotary diaphragms for this purpose; they consist of a rotary ring and diaphragm body with blades. Rotary diaphragms essentially simplify the turbine design (they decrease the weight, length, and work capacity) as compared to turbines that have valve steam extraction distribution.

The presence of steam-distributing extraction elements leads to the appearance of regulating stages of medium and low pressure.

In turbine construction practice, various types of rotary diaphragms are employed for extracting turbines, which are equivalent to triple-valve, double-valve and single-valve (throttle) regulation.

A regulating stage with rotary diaphragm, both single-valve and multi-valve, consists of a rotary split ring 1, a stationary split diaphragm 2, and a rotor wheel 3 (see, for instance, Fig. 201b, and Fig. 202). The rotary ring has ports that are evenly arranged around the circumference. The number of ports in the ring can be equal to the number of nozzle channels in the diaphragm or less. In the last case, one channel of the throttle regulates the gas flow in two (or more) nozzle channels.

In distinction from valve-type steam distribution, the nozzle cascade in the stage with the rotary diaphragm is located directly behind the throttle channels. Some of the kinetic energy of the flow coming from the throttle slot, with partial opening of the nozzle channels, may be used on the rotor wheel.

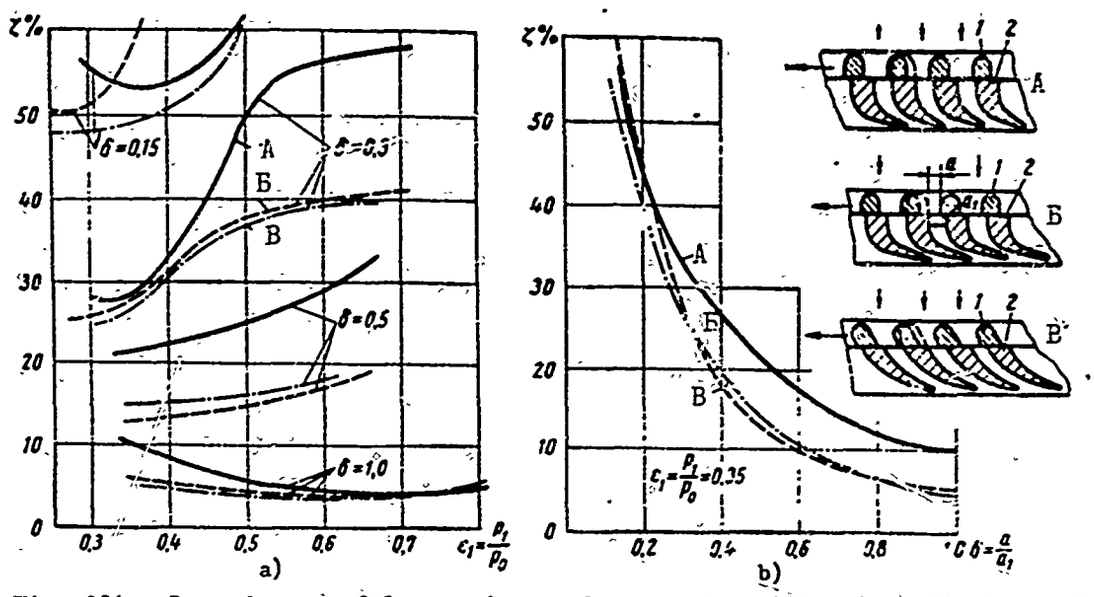

Fig. 201. Dependences of losses in nozzle cascades with rotary diaphragm for three profile variants A, Б, B: a) on the pressure ratio ε_1 for different degrees of opening δ; b) on the degree of opening δ for ε_1 = 0.35.

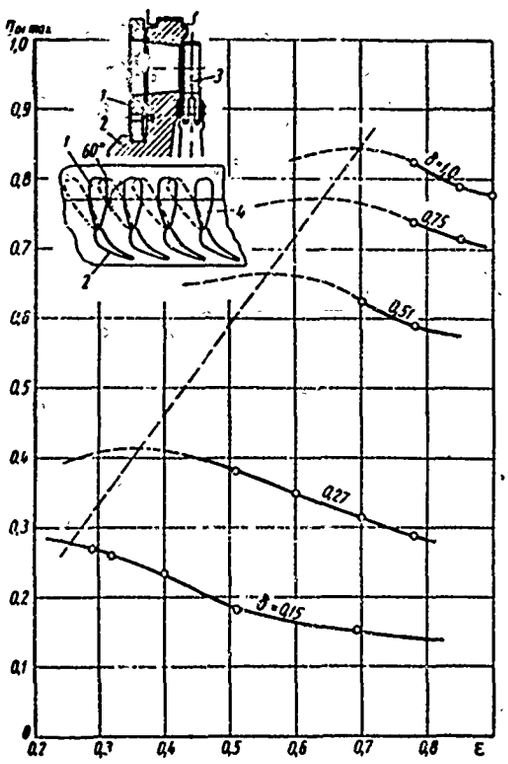

Fig. 202. Change of the efficiency of a regulating stage with rotary diaphragm (solid throttle), depending on the pressure ratio ε for various degrees of opening δ.

At the same time, the throttle channels can be designed as a direct continuation of the nozzle channels. The thickened profiles of this cascade are cut in a plane perpendicular to the axis of the stage, and their leading edges 1 form the throttle channels (Fig. 201b). This type of steam distribution may be called direct steam distribution with a one-piece throttle.

The throttle channels (rotary ring) are also designed separately from the nozzle cascade (Fig. 202). The one-piece nozzle blades are separated from the rotary ring by intermediate struts 4. The rotary ring and the struts may be inclined. This type of steam distribution may be called direct with a divided throttle.

A laboratory investigation was carried out on an НД rotary diaphragm of the 50-100 Mw turbine series of the Ural Turbine Plant (T-50-130, ПТ-50-130/7, T-100-130),

which is equivalent to single-valve steam distribution. It consists of a rotary ring and a stationary diaphragm with nozzle blades (Fig. 201b). In this diaphragm the nozzle cascade follows directly behind the rotary ring. As it was shown, with partial opening of the channel at the entrance, this makes it possible to most effectively use the kinetic energy of the flow coming from the throttle slot.

The investigation of the cascades of rotary diaphragms under static conditions and in an experimental steam turbine* made it possible to determine their aerodynamic characteristics and to work out recommendations for designing improved variants. Figure 201a and b, show diagrams of three cascade variants with a solid throttle, which were tested by TMZ under static conditions, and the energy loss coefficient, depending upon the degree of opening and the pressure ratio. With the decrease of the degree of opening, the cascade losses intensely increase. As the pressure drop in the cascade increases (as ε_1 decreases), when $\delta = 1$, the losses increase; with partial opening, they decrease. The character of curves of $\zeta(\varepsilon_1)$ for $\delta = 0.15-0.5$ is analogous to the loss curves for cascades with divergent channels (Fig. 25). It may be considered that the flow processes are qualitatively identical in the cascades of a rotary diaphragm with partial openings and in cascades with divergent channels under off-design conditions. Actually, the increase losses in divergent channels is connected with the formation of shocks and separations (§ 7). A detailed analysis of the flow structure in cascades of rotary diaphragms distinctly shows that behind the slot in the channel there appear shock waves, and the flow around the back and partially concave surface at the entrance is detached.

For decreasing the losses with partial openings it is necessary to design the channels in such a way that the zones of separation are of minimum length. As shown by experiments, the solution of this problem is attained by means of covering the channels in the direction of the concave surface (variant A, Fig. 201b), rounding the edges of the throttle strut (variant Б, Fig. 201b), the application of slanted entrance sections (at an angle of 60-70°, variant B, Fig. 201b), decrease of the convergence of the channels (variants Б and B), and design of the exit sections of the profile according to group Б profiles (Table 1).

In a number of cases, on the basis of technological considerations, the entrance in the channel of the rotary diaphragm is straight (variant Б). For increasing the mid-radius of curvature of the concave surface, it is necessary that the length of

*The work was carried out jointly by TMZ and MEI.

the nozzle channel along the center line be selected somewhat larger than in a cascade with slanted entrance.

The new profiles of rotary diaphragms that were designed according to these recommendations, with full opening ($M_1 = 0.9$) have small profile losses; the profile with the slanted entrance section has $\zeta_{пр} = 3.2\%$; the profile with the straight entrance section has $\zeta_{пр} = 3.7\%$.

A comparison of the losses in the initial variant (variant Б in Fig. 201) and in improved variants (Б and В) distinctly shows the essential advantages of the latter both under design conditions, and also with decreases pressure drops in the cascade (Fig. 201b).

An experiment also showed that rotary diaphragms with a solid throttle are characterized by significantly smaller losses as compared to the frequently applied diaphragms with a divided throttle. This result is obvious, since in the cascade with divided throttle a considerable part of the kinetic energy of the flow at the throttle outlet is annihilated before the nozzle cascade. In the cascade with solid throttle, annihilation of the energy of the flow occurs to a lesser degree.

Experiments in static conditions made it possible to determine the flow rate coefficients, $\mu = \mu(\delta)$. The results of the experiments confirm that in the zone of operating conditions ($\varepsilon_1 < 0.5$) the flow rate coefficient μ practically does not depend on the pressure ratio and the Reynolds number, and can be determined by the formula

$$\mu = f\delta \frac{F_0}{F_1} \text{ for } \delta < \frac{F_1}{F_0}$$

and

$$\mu = \mu_0 f \text{ for } \delta > \frac{F_1}{F_0}.$$

Here

$$\mu = \frac{G}{G_t} = \frac{G}{BF_1 q_0 \sqrt{\frac{p_0}{v_0}}},$$

where G, G_t are the actual and theoretical flow rates through the cascade;

$\mu_0 = 0.98$ is the flow rate coefficient with full opening;

F_0 and F_1 are the inlet area (with full opening) and the throat area of the nozzle channel;

f is the contraction ratio of the stream flowing from the throttle slot, which varies within the following limits:

δ	1.0	0.8	0.5	0.25	0.1
f	1.0	0.935	0.81	0.96	0.98

$B = 0.661$ is the discharge coefficient; q_0 is the given flow rate.

An important circumstance for the heat calculation of a stage is the established dependence of the outlet angle of flow from the cascade on the degree of opening. As δ decreases, the angle α_1, first weakly, and then, at small δ, very intensely, decreases [40].

For obtaining reliable experimental data on the effectiveness of a regulating stage with rotary diaphragm, a model of such a stage was tested in an experimental steam turbine. The basic characteristics of the model stage are given in Table 19.

Table 19. Characteristics of a Model Regulating Stage with Rotary Diaphragm

Mid-diameter, d mm	Axial clearance δ_a mm	Radial clearance, δ_p mm		Number of strips of radial sealing, z		Upper overlap, $\Delta l_п$ mm	Root overlap, $\Delta l_к$ mm	Area ratio, F_2/F_1
400	1.4	1.4		2		2	1.6	1.95
Nozzle cascade	Chord, b_1 mm	Width, B_1 mm	t_1 mm	a_2 mm	l_1 mm	$\alpha_{1\,эф}$	Thickness of edge, $\Delta_{кр}$ mm	Number of blades, z_1
Profile TC-P-БП-2, TMZ	55	26.93	2.26	5.57	47.75	$12^\circ 20'$	0.3	48 z_2
Moving cascade	b_2 mm	B_2 mm	t_2 mm	a_2 mm	l_2 mm	$\beta_{2\,эф}$	$\Delta_{кр}$ mm	
Profile TP-3A, MEI	25.5	25	16.5	6.41	51.3	$22^\circ 42'$	0.4	75

Experiments were conducted by MEI and TMZ for various diaphragm openings and pressure ratios, $\varepsilon_2 = p_2/p_0$. The corresponding results are shown in Fig. 202 and 203. The dependence of internal efficiency on $x_ф = u/c_ф$ and the degree of opening δ qualitatively coincide with the corresponding curves for stages with partial input. As δ decreases, the efficiency of the stage decreases, whereby the maximum values of η_{oi} are displaced in the direction of smaller $x_ф$. The efficiency of the stage essentially depends on ε (Fig. 202 and 203), whereby with the growth of the pressure drop to a definite ε, the efficiency sharply increases. The character of the change of stage losses, $1 - \eta_{oi}$, depending upon δ, is analogous to corresponding curves for a nozzle cascade (Fig. 201a). This circumstance gives us a basis to confidently use the data of static tests of rotary diaphragms for stage calculation.

It was experimentally established that with the decrease of the degree of opening, δ, the reaction in the stage increases. It may be considered that this

behavior of the reaction is explained by the sharp decrease in velocity behind the nozzle cascade, c_1, and consequently, the growth of the entrance angle of flow to the moving cascade, β_1.

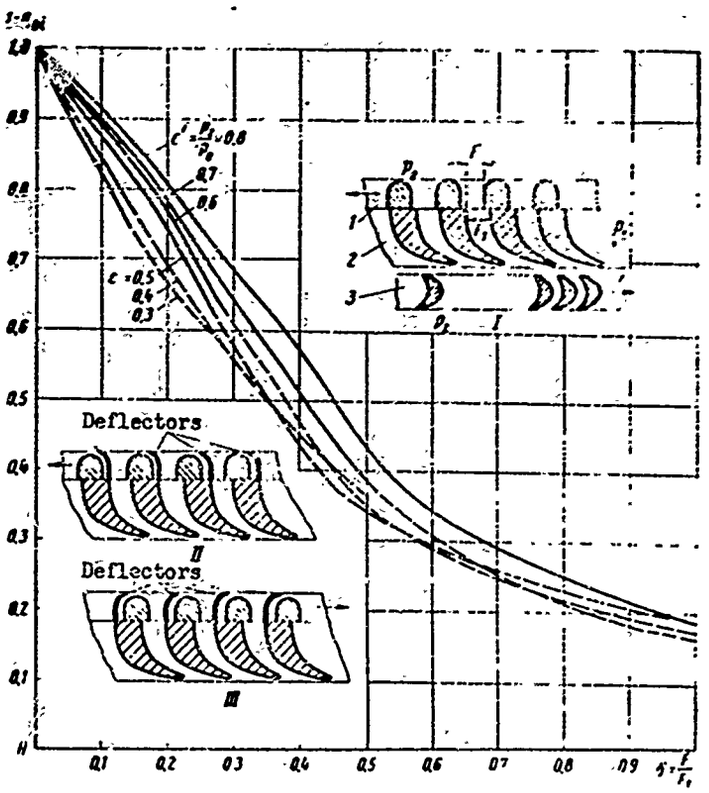

Fig. 203. Dependence of losses in a stage with rotary diaphragm ($1 - \eta_{oi}$) in the degree of opening δ and the pressure ratio ε, ($\theta = 8$ for variant I).

Of considerable interest is a comparison of the effectiveness of three types of regulating stages: I – with partial input; II – with rotary diaphragm and solid throttle; III – with divided throttle. The available experimental data show that the stage with rotary diaphragm and solid throttle occupies an intermediate position and has indubitable advantages upon comparison with purely throttle-type steam distribution.

A considerable increase in the efficiency of a regulating stage with rotary diaphragm and solid throttle may be attained by the application of deflectors which cover the angle on the back or concave surface with partial openings* (Fig. 203). Variant II in Fig. 203, in a wide range of variation of the degree of opening,

*The design for a rotary diaphragm was proposed by M. Ye. Deych and V. V. Frolov.

has an essentially higher efficiency than variant I. Physically, this result is explained by the fact that a decrease of the losses in the throttle with the application of deflectors leads to an increase of the kinetic energy behing the nozzle cascade, which is utilized on the moving cascade.

CHAPTER VII

STAGES WITH LARGE FLARE

§ 35. STRUCTURE OF FLOW IN ANNULAR CASCADES WITH LARGE FLARE AT SUBSONIC VELOCITIES

In annular cascades with small d/l ratio, the flow of gas has a three-dimensional-gradient character. Its essential features are: a) the presence of longitudinal, transverse, and radial pressure gradients in the channels and behind the cascade; b) intense variation of parameters and velocities mainly along the radius, and also in circumferential and axial directions; c) nonuniform spatial distribution of energy losses in channels and behind cascade.

The flow is formed in the vane channels of the nozzle cascade. Due to the rotation of flow inside the channel ("twisting") there will form transverse and radial pressure gradients,* while longitudinal gradients appear in connection with the pressure drop on the cascade. Consequently, before it leaves the cascade, the flow obtains a structure whose specific features are connected with the curvature of the vane channels, i.e., with the twisting of the flow.

Spatial nonuniformity of pressure fields in the channels causes complicated secondary motions in the boundary layers on the forming surfaces of the channels.

Let us consider the basic pattern of secondary flows which is represented in Fig. 204. The middle blade, which is depicted by the dotted line, and also the upper shroud, are thought to be transparent, which makes it possible to note the pattern of the flows on the concave surface and on the upper shroud.

---

*In examining the causes of the appearance of a radial gradient, it should be borne in mind that the flow at the exit moves in a field of centrifugal forces.

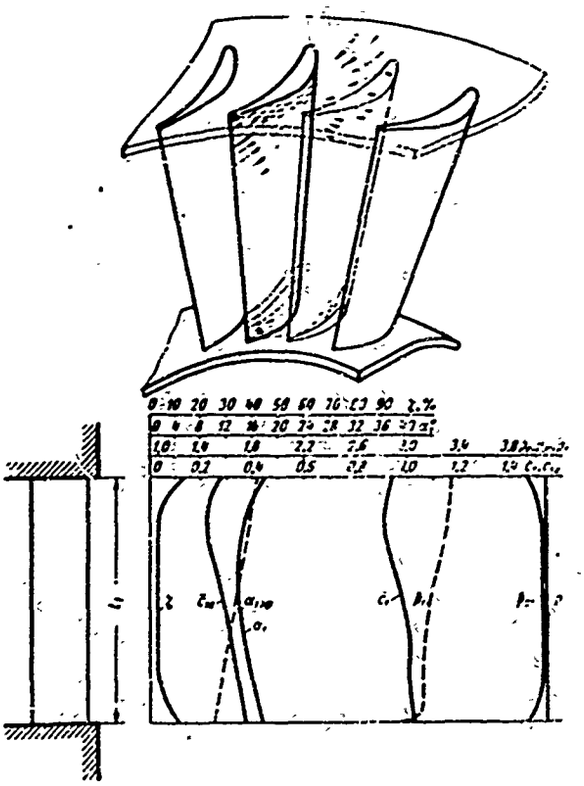

Fig. 204. Diagram of gas flow in boundary layers of blades, and distribution of parameters obtained by measurement at a distance of $0.16b_1$ behind a cascade with cylindrical contours at $M_1 = 0.7$ and $Re_1 = 4 \cdot 10^5$; $\theta = 2.88$ (experiments of L. Ye. Kiselev, MEI).

Under the action of excess pressure, on the concave surface there occur leakages in the boundary layers on the upper and lower shrouds to the back of the adjacent profile. Considering the direction of the radial pressure gradient (to the axis of the cascade), it is possible to affirm that the peripheral motion of the boundary layer on the concave surface at the blade vertex will be hampered: the transverse and radial pressure gradients excite motion in the boundary layer in different directions. In the root sections, the influence of these pressure gradients will be in one direction. Consequently, the radial gradient in the upper sections hampers the secondary flow of the layer on the concave surface, while in the root sections it intensifies this flow.

On the back of the blade, at the vertex and in the root section, the gradient promotes intensification of the secondary flows, since it displaces the boundary layer in a direction to the cascade axis. The region of secondary flows at the vertex is then displaced to sections of average height, and in the root part of the blade, to the shroud. The last circumstance leads to a sharp swelling of the layers in the root sections and, in certain cases, to separation.

These features essentially determine the structure of the flow behind the cascade. An example of the distribution of velocities, static and total pressures, angles, and losses along the radius behind an annular nozzle cascade with blades having constant chord along the height ($\theta = 2.88$, $\bar{t}_1 = 3.1$ mm), which are mounted with inclination toward the flow with a continuous flow at root, is shown in Fig. 204.

Here one may distinctly see the intense increase of losses in the root and

peripheral sections, whereby the zone of increases losses amounts to about 15% of the height.

In the peripheral sections, the radial extent of the zone of increases losses is approximately the same. This result is explained by the less intense secondary flows in the root sections in connection with the inclination of the blades toward the flow ($\gamma = +13^{\circ}$).

Theoretical and experimental investigations of annular nozzle cascades distinctly showed that at small θ in the root sections there can occur separation. According to the theoretical data of K. Bammert and H. Klaukens, separations in the root sections inside a cascade are sometimes observed when $\theta \leq 3$ to 3.5. Separations form behing a cascade at larger values of θ. Corresponding calculations showed [65] that the critical quantity, $\theta_{кр}$, depends on the outlet angle of flow α_1 and the M_1 number. Figure 205a gives a curve for $\theta_{кр}(\alpha_{1п})$ ($\alpha_{1п}$ is the outlet angle of flow at the vertex) which was obtained in reference [131]. According to these data, as $\alpha_{1п}$ increases, the value of $\theta_{кр}$ decreases; consequently, separation appears at smaller θ.

The cause of separation in an annular cascade, according to K. Bammert and H. Klavkens, consists in the following. With an increase of cascade flare (a decrease of $\theta = d/l$) and $r_п$ = const for a constant pressure drop $p_0 - p_{1к}$ in the root section and outlet angle at the vertex $\alpha_{1п}$, the pressure drop at the vertex will decrease. The velocity at the vertex c_1 then decreases, and together with it the axial component, $c_{a\,1п} = c_{1п} \sin \alpha_{1п}$. Considering a cascade with a uniform field of axial outlet velocities, it is simple to make the conclusion that the volume flow rate through the cascade, which is equal to

$$Q = Fc_{1a} = 2\pi r_к^2 \frac{4\theta}{(\theta - 1)^2} c_{1a},$$

where $r_к$ is the radius of the root section, will be an extreme function of $\theta = d/l$, since with the decrease of θ, the magnitude of $c_{1\,a}$ decreases, and $r_к$ increases.

As a characteristic of the change of the flow rate through the cascade, the authors of [131] took the dimensionless set

$$\Delta\bar{p} = \frac{p_0 - p_{1к}}{\frac{\rho}{2}\left(\frac{G}{\pi r_b^2}\right)^2}$$

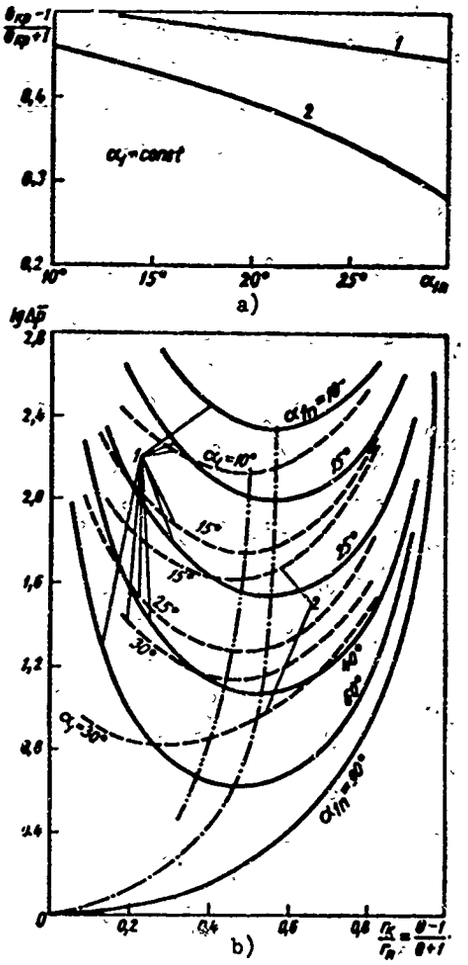

Fig. 205. Characteristics of separation of flow in an annular cascade: a) dependence of critical ratio $(\theta_{кр} - 1)/(\theta_{кр} + 1) = (r_к/r_п)_{кр}$ on outlet angle of flow $\alpha_{1п}$ at vertex; b) dependence of relative pressure drop, $\lg \Delta\bar{p}$, on hub-tip ratio $r_к/r_п = (\theta - 1)/(\theta + 1)$, with c_{u1} = const ——— (solid curve) and α_1 = const — — — — (dashed curve). Curves: 1 — for blades mounted radially along the flow; 2 — for inclined blades.

(or $1/\Delta\bar{p}$), the change of which, depending upon $r_к/r_п = \theta - 1/\theta + 1$, is shown in Fig. 205b for two methods of twisting the nozzle blades ($c_{1u}r$ = const and α_1 = const). The dot-dash line differentiates the region of continuous and separated flow in the cascade and makes it possible to establish the critical value of $\theta_{кр}$, which is shown in Fig. 205a.

A corresponding diagram of separation is illustrated in Fig. 206. In the opinion of the authors of [131], the lower branch of the flow rate curve corresponds to unstable motion and separation should occur when $\theta \leq \theta_{кр}$.

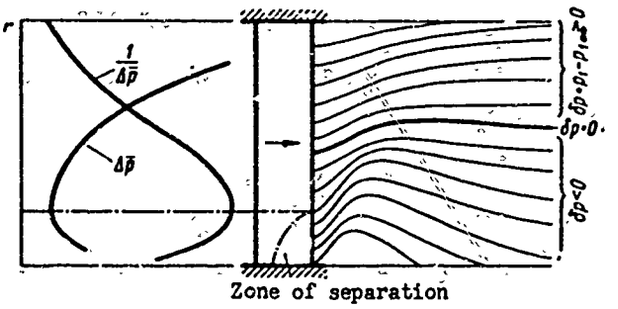

Fig. 206. Diagram of the appearance of separation of flow in the root sections of an annular cascade, according to K. Bammert and H. Klavkens, and the distribution of isobars behind the annular cascade.

This diagram of the formation of separation is not satisfactory because it is not connected with the physical causes that determine the appearance of separation.

First of all, it should be emphasized that the theoretical and experimental investigations of separation were conducted for an isolated nozzle cascade and the corresponding conclusions cannot be completely extended to a stage.

Turning back to the physical causes that explain the separation of flow in the root section, let us note that such separation is possible in the presence of

diffuser sections of flow in the slanting shear, or behind the cascade. Diffuser sections in the slanting shear can appear only as a result of incorrect meridional profiling of the cascade or due to secondary motions of the gas, which are caused by radial and transverse pressure gradients.

A diffuser section behind an isolated nozzle cascade always appears as a result of twisting of the flow. If the longitudinal pressure gradients are sufficiently great there, separation of flow will occur. Positive pressure gradients toward the flow increase with the decrease of θ and α_1, since the radial difference of pressures and, correspondingly, the difference of pressures between the external medium and the root section of the cascade, increase in this case.

In a real stage under design conditions, separation of the flow in the root section in many cases is not detected, since the moving cascade "removes" the twisting and balances the field of static pressures on a short section along the axis of the stage.

It should be emphasized once again that both in the quoted reference [131], and also in the investigations of M. Ye. Levina and P. A. Romanenko [65], the seperation detected is not related to the appearance of diffuser sections at the cascade hub. On the basis of a theoretical consideration of the problem, a statement can be made about the fact that the flow rate is an extreme function of the hub-tip ratio, $r_K/r_П$ (Fig. 206).

At the same time, the experiments of [65] and other investigations distinctly confirm the presence of diffuser sections behind a cascade (Fig. 206). The structure of the flow behind a cascade in the presence of separation in the root section is characterized by the graphs in Fig. 207, which are based on MEI experiments with TC-1A blades of constant profile. The characteristic distribution of static pressure should be noted: in a certain section p_1 reaches minimum and then increases toward the root (Fig. 207). In the presence of separation, the distribution of stagnation pressures, velocities, and angles becomes especially nonuniform.

It should be noted that the appearance of separation in the root sections leads to the appearance of considerable radial velocity components, since the flow is driven away to the periphery (Fig. 206). The outlet angles to the meridional plane, ν, essentially increase, and the nonuniformity of distribution of ν along the radius increases.

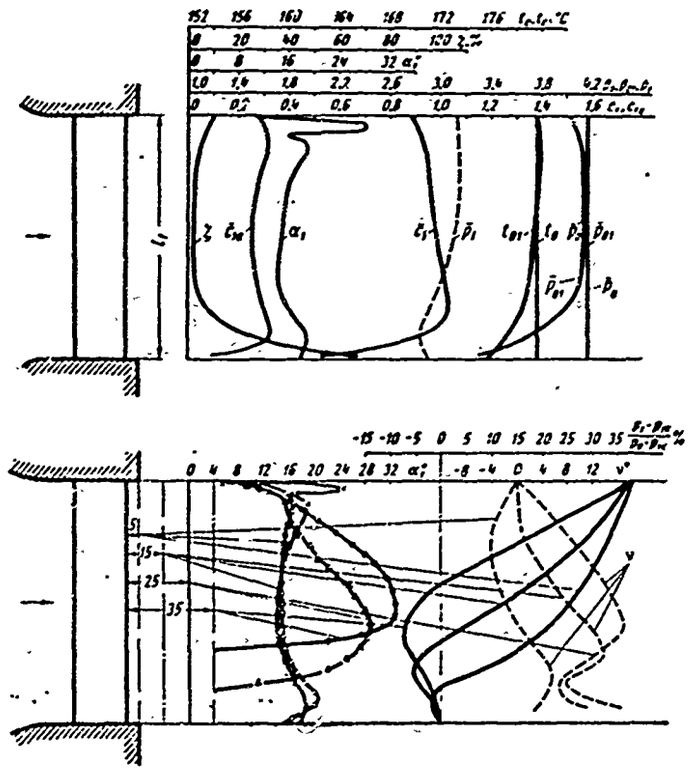

Fig. 207. Distribution of velocities, static and total pressures, angles, and stagnation temperatures in various sections behind a nozzle cascade with the appearance of a separation of flow in the root sections: $M_1 = 0.72$; $Re_1 = 4.5 \cdot 10^5$; $\theta = 2.88$; $\bar{t}_1 = 3.1$; $\alpha_{1\text{пэф}} = 13^\circ$; $\alpha_{1\text{пэф}} = 10^\circ$.

Both in the presence of separation, and also with a continuous flow, in the annular space behind a cascade there occurs spin-up of the flow, in the process of which the static pressure and velocities are balanced, and the angles of the velocity vectors increase. The region of separation noticeably increases in the radial direction.

The character and intensity of the spin-up essentially vary, depending upon the method of the experiment and, in particular, on the boundary conditions provided at the outlet behind the cascade. In connection with the reverse influence of disturbances in the subsonic flow, the structure of the flow in an investigated section, depending upon the outlet conditions of the cascade, will noticeably change.

Several diagrams of the organization of the flow behind an annular cascade are possible (Fig. 208). The most correct are diagrams d) and e) with a spin-up

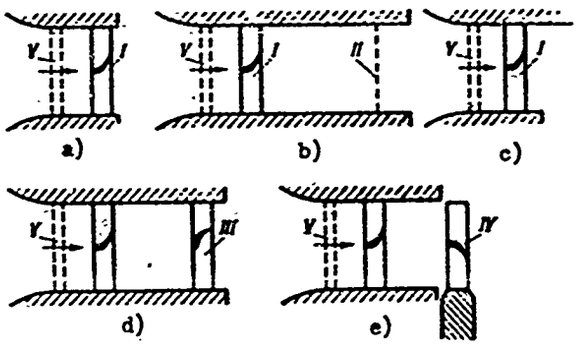

Fig. 208. Various diagrams of the organization of flow in the investigation of annular cascades.

compressor cascade III or with a rotor wheel IV. The last diagram corresponds to the natural conditions of flow in a stage with an enlarged axial clearance. Rotation of the moving cascade with various speeds makes it possible to change the degree of spin-up and create the necessary conditions behind the nozzle cascade, which correspond to its various operating conditions with the change of u/c_{Φ}. The installation of a rotor blade apparatus V in all diagrams on Fig. 208 may change the entrance of flow.

The rotor wheel essentially affects the structure of the flow behind the nozzle cascade, since it spins up the flow and changes the character of the flow rate distribution along the radius. The necessary law of flow rate distribution can be carried out by the application of screens II or washers. An analogous problem was solved by means of selecting cylindrical surfaces for the hub and outer contour of different length (variant c).

Unfavorable results are given by testing a cascade with a long annular offtake (variant b). With such organization of flow, developed separation zones and distortion of the fields of static pressures and velocities are observed, which is not characteristic for the cascade in the stage. Distorted results are also obtained with the use of diagram a) with short deflectors behind the cascade. In this case, the flow obtains the pressure of the external medium directly behind the cascade, which distorts the field of pressures and velocities in the investigated section.

The simplest to use, diagram c) (Fig. 208), requires careful preliminary adjustment, whereby the length of the boundary surfaces at the root and periphery should be varied with the change of the geometry of the cascade and the conditions of flow.

Special attention should be given to the nonuniformity of distribution of the stagnation temperatures along the radius behind a cascade; this nonuniformity was established in all experiments conducted at MEI with annular cascades. The indicated nonuniformity is confirmed by the graphs in Fig. 207.

An hypothesis on the temperature nonuniformity* in nozzle cascades was expressed by M. E. Deych in 1957; in 1961, it was confirmed experimentally at MEI.

As can be seen from Fig. 207, the stagnation temperature behind a cascade increases from the root to the periphery, whereby the most intense change t_{01} is revealed in the sections located at the hub. The change of the stagnation temperature Δt_{01} in percents of the heat drop expended in the cascade amounts to about 10-15% at $M_1 \approx 0.7$ and $Re_1 \approx 5 \cdot 10^5$ for a cascade with $\theta = 2.88$.

This important feature of the twisted flow behind a cascade should be considered both in cascade calculations, and also in the treatment of experimental** results.

It may be considered that the temperature nonuniformity*** behind a cascade is connected with the vortex effect of temperature separation of gas, which is analogous to the Rank effect. The basis of this effect is the turbulent transfer of energy by the vortex moles which are generated in a flow with nonuniform velocity distribution. By the action of centrifugal forces, the vortex particles are transferred to the periphery, whereby the total energy of moving gas is also increases.

A more detailed investigation of this effect is given in § 41.

§ 36. THE INFLUENCE OF CERTAIN GEOMETRIC AND PERFORMANCE PARAMETERS ON THE CHARACTERISTICS OF ANNULAR CASCADES AT SUBSONIC VELOCITIES

Let us consider the influence of certain geometric and performance parameters on the structure of flow and the losses in an annular cascade.

Let us turn first of all to the data which illustrate the possibility or removing separation in root sections in cascades with various flare (including those for $\theta < \theta_{кр}$).

For this purpose we shall consider the results obtained for a cascade with $\theta = 2.88$ (Fig. 209), which was tested with various blade inclination, and also other cascades of constant chord with variation of the angle of inclination. Separation in the considered cascade could be removed by means of changing the blade angle. Even radial blade mounting could decrease the separation zone. Inclination of the blades toward the flow at a small angle γ led to a sharp decrease of losses in the root sections (Fig. 209).

---

*With respect to stagnation temperatures.

**For calculation of the velocities behind a cascade, according to experimental data, the stagnation temperature at the entrance is usually used, which can lead to noticeable errors, especially in the root sections.

***With respect to stagnation temperatures.

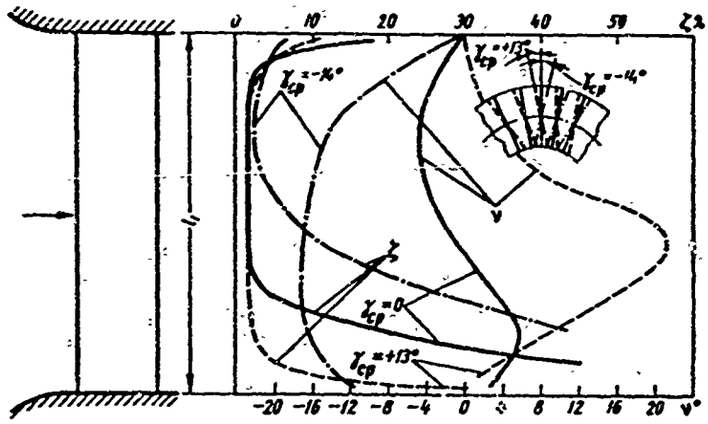

Fig. 209. Influence of blade inclination on distribution of losses behind a cascade. Blades of constant profile TC-1A; $\theta = 2.88$; $\bar{t}_1 = 3.1$; $\alpha_{1п} = 13^\circ$; $\alpha_{1к} = 10^\circ$; $M_1 = 0.72$; $Re_1 = 4.5 \cdot 10^5$ (MEI experiments).

The effect of blade inclination is also detected when determining the outlet angles of flow behind a cascade in the meridional plane ν. As can be seen from Fig. 209, inclination of blades toward the flow, $\gamma = -14^\circ$, leads to negative angles ν, i.e., to the appearance of radial velocity components directed toward the cascade axis.

Slight inclination of blades toward the flow makes it possible, due to contraction of the flow toward the axis of rotation, to lower the losses in the root sections in connection with a decrease of the intensity of the diffuser sections. In this case, the diagrams of static pressure behind the cascade turn out to be more sloping (the intensity of change of the reaction along the radius decreases), which leads to a decrease of twisting of the rotor blade.

However, it should be emphasized that full balancing of static pressure along the radius is inexpedient, since in this case it is practically impossible to attain an axial outlet of flow behind the stage ($\alpha_2 = 90^\circ$). Consequently, the losses with the outlet velocity will be increases. Furthermore, large angles of inclination of the nozzle blades lead to a considerable growth of profile losses and losses in the peripheral sections.

As an illustration we shall consider the results of tests of four annular cascades ($\theta \approx 8$) with various angles of inclination of trailing edges: $\gamma = -20^\circ$, -8°, 0°, and $+20^\circ$, which were conducted by G. A. Filippov (Fig. 210). Graphs of the losses distinctly show that within the limits of the change of $\gamma = -8^\circ$ to $+8^\circ$

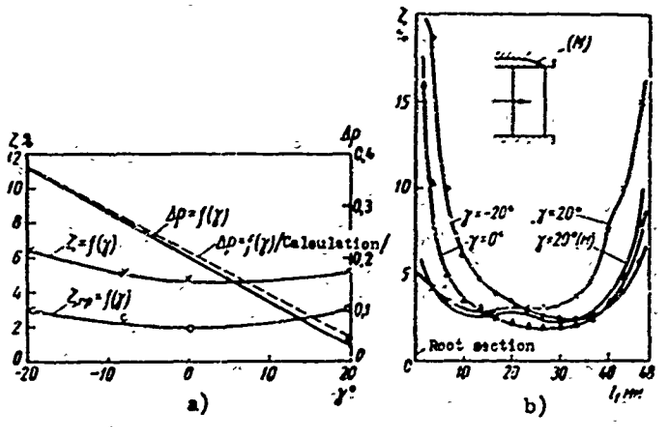

Fig. 210. Influence of blade inclination on the characteristics of a nozzle cascade: a) change of total losses and difference of reaction in nozzle cascade, depending upon angles of inclination, γ; b) distribution of losses along height of nozzle cascade TC-1A, for various values of blade angles: $\theta = 8.3$ and $\bar{t}_1 = 0.93$.

the profile losses in various sections practically do not change and they amount to 2-2.5%. When $\gamma = +20^\circ$ and $\gamma = -20^\circ$ the profile losses increase to 3%. This result is explained by the fact that flow goes around the profile along the slanted sections, whereby the shape of the streamlined profile depends on the shape of the initial profile and the blade angle γ. Total cascade losses remain practically constant within the limits of change of angle $\gamma = -6$ to $+14^\circ$.

Figure 210a also illustrates the dependence of the difference of reactions in the peripheral and root sections on the edge angle γ. When the blades are inclined toward the flow ($\gamma > 0$) this difference considerably decreases and, when $\gamma = 25$ to 30°, the reaction along the radius becomes constant (for a given stage with $\theta \approx 8$). In accordance with Fig. 210, let us note that the convergence of experimental and calculated [see formula (223)] values of $\Delta\rho$ is satisfactory.

Distribution of losses along the cascade height is shown in Fig. 210b. For negative edge angles, considerable losses are found in the root section, which is explained by the appearance of separation there. For cascades with positive edge angles, i.e., with contraction of flow toward the root, the losses in the peripheral sections increase.

The influence of the inclination of the trailing edges must be considered jointly with meridional profiling of the nozzle cascade. Thus, for instance, the design of the upper shroud of the nozzle cascade with contraction (Fig. 210) makes it possible to sharply decrease the losses in the peripheral sections and thereby balance the diagram of losses with respect to height. Total losses for $\gamma = +20^\circ$ decrease from 5.2 to 4.3%. In this case, both factors (meridional profiling and inclination of edges) promote a decrease of the gradient of static pressure in the clearance. The difference of the reactions, $\Delta\rho = \rho_П - \rho_К$, for a cascade with meridional contraction, decreases to $\Delta\rho = -2\%$ (instead of $\Delta\rho = 5\%$ for a cascade

only with inclination of edges $\gamma = +20^{\circ}$).

It should be considered, however, that for a different stage flare and other shapes of the meridional contour, the influence of the inclination of the edges can be quantitatively different.

By comparing the obtained results with the curves shown in Fig. 209, for a cascade with $\theta = 2.88$, having cylindrical generatrices, it is easy to note that for such a large flare, even an insignificant inclination of the blades leads to a sharp change of the distribution of losses and static pressure along the radius.

The distribution of losses along the height, with the change of the blade inclination, changes analogously to how this was noted for the cascade with $\theta = 8.0$ (Fig. 210). However, with the decrease of θ, the cascade becomes more sensitive to the inclination of the edges.

The graphs presented in Fig. 209 and 210 make it possible to estimate the influence of blade inclination of the distribution of losses, outlet angles, and reaction along the radius for nozzle cascades with various flare.

The logical development of a cascade diagram with inclined blades consists of the application of the curvilinear blades proposed by MEI. In these cascades it is possible to work out an arbitrary law of change of the reaction along the radius. The principle of construction of blades with curvilinear trailing edges is shown in Fig. 211, where the blade inclination toward the flow is variable along the height.

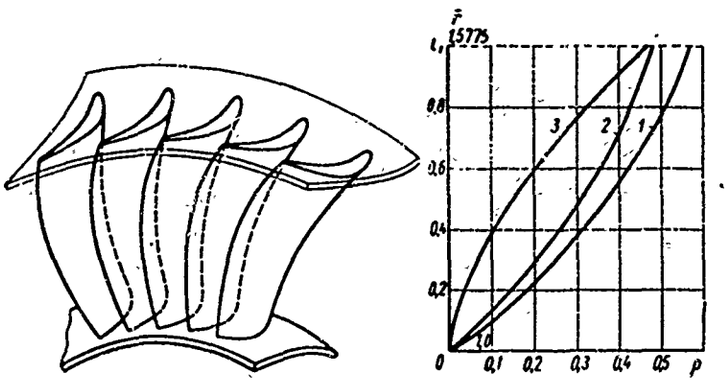

Fig. 211. Diagram of a nozzle cascade with large flare and curvilinear (saber-like) blades (MEI cascade), and distribution of the reaction along the radius behind nozzle cascades. Curves: 1 – radially mounted blades; 2 – blades inclined toward flow; 3 – curvilinear (saber-like) blades.

In accordance with this, such a change of the reaction along the radius is ensured, at which the radial pressure gradient in the root sections is minimum, increases in the mid-sections, and reaches maximum values in the peripheral sections. A decrease of the radial pressure gradient in the root sections lowers the intensity of leakages of the boundary layers, and thereby the losses in these sections. The contraction of the flow toward the hub also prevents separation on the internal cylindrical surface.

The blade camber in the peripheral sections and, correspondingly, the change of static pressure along radius in this zone of flow, depend on the shape of the meridional contour of the cascade. For cascades with a conical flow area, the blade camber is determined by the cone angle of the upper contour and is found experimentally.

Figure 211 shows the distribution of the reaction along the radius behind a nozzle cascade for three variants: radially mounted blades, blades with inclination toward the flow, and curvilinear blades. An experiment confirms the possibility of working out such a law of change of the reaction (static pressure) along the radius behind a nozzle cascade, which ensures minimum losses in the nozzle cascade and the most rational structure of flow in the stage.

The distribution of losses along the cascade height and the change of the total losses depending upon the M_1 number is shown in Fig. 212. Here for a comparison, corresponding curves are shown for a cascade with radially mounted blades. This series of experiments distinctly confirms the expediency of employing nozzle cascades with curvilinear blades. In the root sections (Fig. 212a) the losses are considerably less than in the cascade with rectilinear, radially mounted blades. A lowering of losses is also noted in the mid-sections, especially at large M_1 numbers. When $M_1 \approx 0.6$, in the peripheral sections there is observed a certain increase of losses in the cascade with curvilinear blades. However, with the growth of M_1 there occurs a redistribution of losses along the height: in the root sections ζ increases, and it decreases in the peripheral sections, whereby the total losses noteceably decrease (Fig. 212b). The advantage of curvilinear blades is especially great when $M_1 = 0.8$ to 0.9. In this zone of velocities the total cascade losses decrease by 2-2.5% as compared to the cascade with rectilinear blades.

An expecially considerable effect of curvilinear blades is found for annular cascades with a conical upper contour. In connection with the decrease of total convergence of the vane channels, the total losses in the two cascades being compared noticeably increase. However, in the cascade with curvilinear blades, this increase of ζ turns out to be less essential, and in the optimum zone of velocities the gain from the application of such blades amounts to 3-3.5% (Fig. 212b).

It should be noted that the two types of cascades that were compared had identical absolute values of angles $\alpha_{1\ эф}$ and an identical law of change of angles $\alpha_{1\ эф}$ with respect to height.

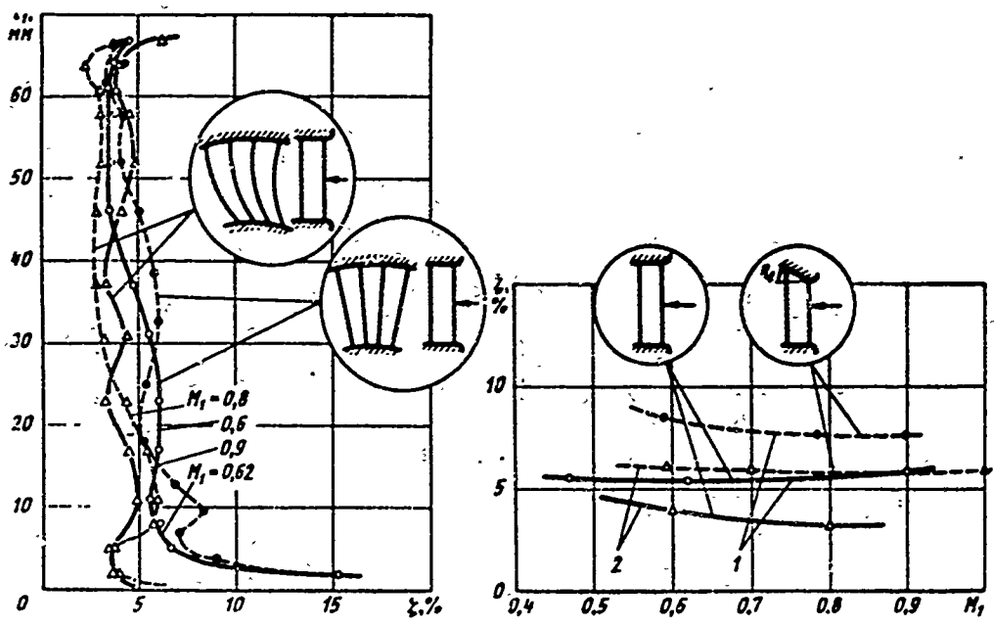

a) b)

Fig. 212. Experimental characteristics of annular cascades having curvilinear and rectilinear blades with cylindrical and conical generatrices (experiments of G. A. Filippov, MEI): a) distribution of losses along radius for various M_1 numbers (cylindrical contours); b) change of total losses: 1 — for rectilinear, and 2 — for curvilinear blades; $Re_1 = 6 \cdot 10^5$; $\theta = 4.3$; $\bar{t}_1 = 3.1$; $\alpha_{1\,п} = 16^\circ$; $\alpha_{1\,к} = 11^\circ$.

The results of the considered experiments distinctly confirm the expediency of employing curvilinear blades which make it possible to increase the efficiency of large-flare stages.

Returning to the results of the investigation of cascades with rectilinear blades (radially mounted), let us note that a considerable number of the conclusions made on the basis of the experiments may be also extended to cascades with curvilinear blades.

In this connection it should be emphasized that the application of blades that are inclined toward the flow or curvilinear ones makes it possible to essentially decrease the critical ratio $\theta_{кр}$ (see Fig. 205) which determines the continuous flow in a nozzle cascade. Thus, for instance, when $\alpha_1 = 15^\circ$, the quantity $\theta_{кр}$ decreases from $\theta_{кр} = 3$ to $\theta_{кр} = 2.5$. In another method of twisting the nozzle blades, the decrease of $\theta_{кр}$ is also considerable.

Important results were obtained at the LMZ laboratory* in an investigation of the influence of the entrance overlap in a nozzle cascade (Fig. 213). As the quantity

*The experiments were conducted by A. O. Lopatitskiy and M. A. Ozernov.

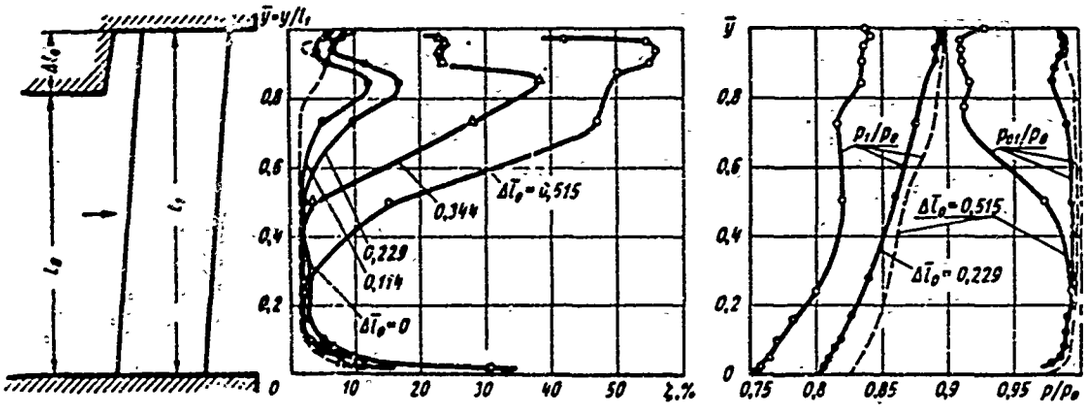

a) b)

Fig. 213. Influence of overlap at the entrance to an annular nozzle cascade on: a) distribution of losses, b) static and total pressures. When $\theta = 4.7$; $Re_1 = 5 \cdot 10^5$; $M_1 \approx 0.5$. LMZ experiments.

$\Delta l_0 = l_1 - l_0$ increases, the cascade losses intensely increase, especially at low velocities (M_1 numbers, Fig. 213a). It should be noted that with the increase of Δl_0 there is an especially intense increase of losses in the peripheral sections. The field of stagnation pressures behind the cascade takes on the characteristic nonuniformity (Fig. 213b). With the change of the overlap, the distribution of static pressure along the radius also changes. Due to the separation of flow and the formation of a vortex zone, the pressure in the peripheral sections decreases. As the M_1 number increases, the negative influence of overlap decreases.

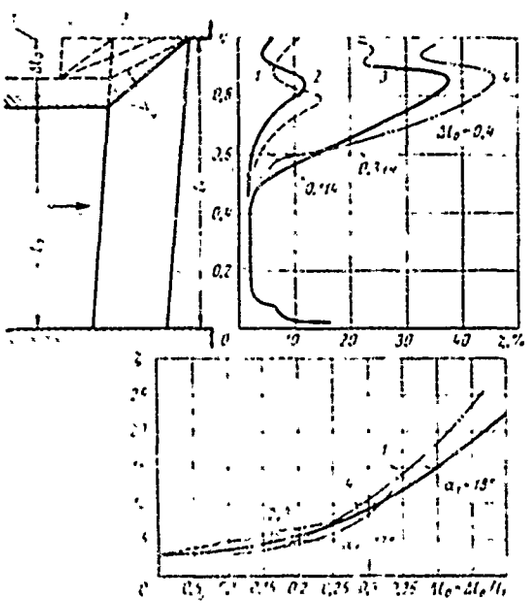

Fig. 214. Influence of the shape of the upper contour of a large-flare nozzle cascade: variants, 1, 2, 3 – LMZ experiments; variant 4 – MEI experiments: $M_1 = 0.5$; $Re_1 = (3$ to $6) \cdot 10^5$; $\theta = 4.7$.

As can be seen from Fig. 214, the conicity of the upper contour of a nozzle cascade also leads to a growth of losses in the peripheral sections. Experiments show that with the increase of conicity and, thereby, with the decrease of channel convergence, the losses in the upper sections increase the same as with an increase of overlap. According to the LMZ experiments, variants 2 and 3 gave poor results as compared to variant 1 (Fig. 214) for $\overline{\Delta l}_0 \leq 0.13$. Variant 4 of the upper contour, with small cone angles and low values of α_1, gives smaller cascade losses.

The design of a cascade with upper and lower conical contours and edge inclination toward the flow makes it possible to balance the diagram of losses at the ends with the same value of $\overline{\Delta l}_0$. The application of an intricate conical-cylindrical contour somewhat decreases the losses in the upper sections.

An investigation of the influence of twisting of flow at the entrance to a nozzle cascade with a conical contour, which was conducted at MEI, showed that a decrease of the entrance angle $\alpha < 90^\circ$ does not lead to a considerable growth of losses in these cascades.

The influence of flare on the distribution of losses along the height and the dependence of $\zeta(\theta)$ for an annular cascade composed of blades with constant profile, mounted radially, may be estimated according to Fig. 215. Here one may distinctly see the sharp growth of losses in the peripheral sections and especially in the root sections with the decrease of $\theta \leq 5$. Total losses vary slightly in the interval of $6 \leq \theta \leq 15$.

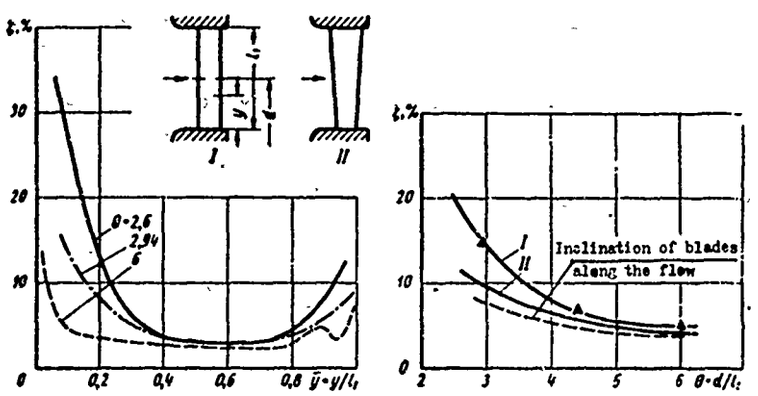

Fig. 215. Distribution of losses along blade height and their dependence on parameter θ in an annular cascade with various flare. Profile TC-1A; $M_1 = 0.72$; $Re_1 = 5 \cdot 10^5$ (MEI experiments).

The above-considered results of experiments pertain to cascades with cylindrical blades, whose relative pitch varies essentially with respect to height with large stage flare. A noticeable increase of the effectiveness of nozzle cascades is noted when the blades are designed with constant (optimum) relative pitch with respect to height (variant II). This condition can be maintained for various laws of twisting of blades, $\alpha_1(\overline{r})$, and also for rectilinear, inclined, and curvilinear blades.

A comparison of the results shows that when a cascade is designed with optimum pitch, and inclined blades (or curvilinear blades) the distribution of losses along

the height is considerably more uniform, and the total losses are intensely lowered.

However, these results were obtained for cascades with cylindrical generatrices and for comparatively high Reynolds numbers. A decrease of the Re_1 number can lead to a noticeable growth of losses. Actually, as may be seen from Fig. 216a, the total losses essentially change depending upon Re_1, especially at small $Re_1 \leq 1.5$ to $2.0 \cdot 10^5$.

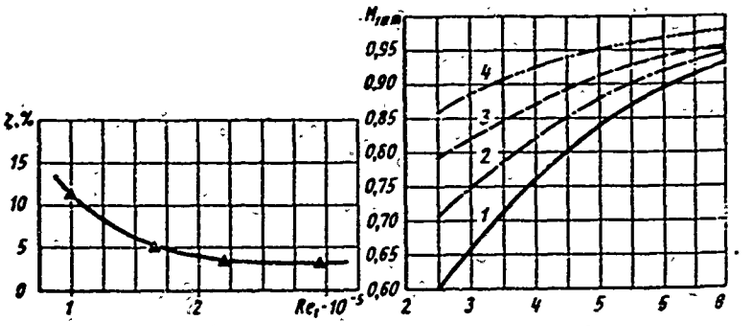

a) b)

Fig. 216. Characteristics of annular nozzle cascades: a) influence of Re_1 number on losses ζ in annular cascades with large flare; b) change of critical number, M_{1*m}, depending upon θ, for various cascades: 1 – radially mounted blades; 2 – inclined blades, $\gamma_m = +10^\circ$; 3 – inclined blades, $\gamma_m = +26^\circ$; 4 – curvinlinear blades.

Let us note that in annular cascades the region of Re_1 self-similarity is attained when there is a continuous flow for different values of Re_1 than in two-dimensional cascades.

It may be considered that the Re_1 that corresponds to the region of self-similarity will depend on the geometric parameters of the cascade and, in particular, on the flare (θ).

Cascades with constant relative pitch with respect to height are characterized by a more uniform distribution of Re_1 numbers along the radius; however, in the root sections the Re_1 numbers will be lower as compared to a cascade with constant chord. With a continuous flow in the root, the losses will increase with the decrease of Re_1. Consequently, the law of change of relative pitch (chord) along the radius at subsonic velocities must be selected on the assumption of minimum losses for the given distribution of velocities and angles along the radius. By no means does the constancy of relative pitch always lead to minimum losses, since the quantity $\bar{t}_{опт}$ depends on the Re_1 number (see p. 490).

Thus, the selection of a law of change of the chord of a nozzle cascade along the radius is carried out by means of variant calculations and on the basis of the experimental characteristics of the losses and angles obtained for various Re_1 numbers.

It is necessary also to consider the shape of the meridional contours of a cascade. For conical upper on lower contours, the flow at the entrance to a cascade can be divergent. In these cases it is also expedient to disregard the condition of constant relative pitch with respect to height, and to design the blades with increases width at the vertex, for which it is possible to ensure a more convergent flow.

The influence of compressibility on the characteristics of an annular cascade essentially depends on the flare θ. Depending upon this quantity, the distribution of velocities behind the cascade along the radius changes, whereby the smaller θ is, supersonic velocities are reached in the root sections at smaller drops in the mid-section. Consequently, for annular cascades it is expedient to introduce such a critical M_{1*m} number on the mid-section, at which $M_{1\,K} = 1$ is reached in the root section, M_{1*m} depends on the flare of the stage, the shape of the profile, and the geometric parameters of the cascade. It is obvious that with the decrease of the intensity of change of the reaction along the radius, M_{1*m} will increase (Fig. 216b).

In cascades with a decreased gradient of static pressure along the radius (inclined and curvilinear nozzle blades) the M_{1*m} number is increases.

At subcritical velocities and continuous flow, an increase of the M_1 number leads to a lowering of cascade losses, especially in the root sections. Total losses also are lowered, which is explained by the increase of the convergence of flow with the growth of M_1. In case of the appearance of separation in the root sections, an increase of M_1 leads to a growth of losses, in connection with the fact that the separation zone is displaced against the flow, since the pressure gradients are increased.

In connection with the considered question concerning the influence of flare on the characteristics of an annular nozzle cascade, let us note that with correct profiling it is fully possible to decrease the ratio $\theta = d/l$ in such cascades to 2.2-2.4. In comtemporary deisgn of last stages the optimum cascade flare reaches $\theta = 2.6$-2.8. A further lowering of θ to the indicated limits may be carried out by the application of curvilinear (saber-like) nozzle blades, and also combination inclined and curvilinear blades of variable chord and variable profile.

Corresponding experimental data on annular cascades with such flare (not yet obtained), and also new, more exact methods for calculating three-dimensionsl flow are necessary.

§ 37. APPROXIMATE METHOD OF CALCULATING THE FLOW IN A NOZZLE CASCADE WITH LARGE FLARE

As shown above in § 35 and 36, the structure of the flow in annular cascades is intricate. In attempts of an exact mathematical solution of the problem there appear practically insuperable difficulties. Therefore, all the available solutions are based on some simplification of the problem.

At present, two approaches to the calculation of three-dimensional flow in annular cascades and in a stage are possible.

The first method, the most popular one, is based on the application of equations of three-dimensional flow toward the sections at the entrance to a stage, in a clearance, and behind the stage where the flow in a circumferential direction may approximately be considered as uniform.

The second method can be used to calculate the three-dimensional flow in vane channels, by applying the channel theory for calculation of the potential flow, and then considering the three-dimensional boundary layer in the channels of the nozzle and moving cascades. Taking into account the specific boundary conditions, the flow is calculated in characteristic sections outside the channels (in clearances). Thi approach is more promising; however, the first method is being employed at the present time, since it is less complicated and tedious.

The solution of the problem by this method can be obtained with a various degree of approximation to actual conditions of three-dimensional flow in the flow area of a stage. At the present time several methods of calculation have been proposed, which are based on various assumptions concerning the rational structure of flow in the flow area. However, most of them do not consider the influence of certain essential design parameters of the stage and gas-dynamic factors, which distinguish the actual flow from an idealized diagram.

The exact theory of a stage should be based on the solution of equations for three-dimensional flow of a gas. For an ideal fluid and steady flow, the Euler equations in a cylindrical coordinate system have the following form (for an obsolute flow):

$$
\left.\begin{aligned}
&c_r\frac{\partial c_r}{\partial r}+\frac{c_u}{r}\frac{\partial c_r}{\partial\theta}+c_a\frac{\partial c_r}{\partial z}-\frac{c_u^2}{r}=F_r-\frac{1}{\varrho}\frac{\partial p}{\partial r}\\
&c_r\frac{\partial c_u}{\partial r}+\frac{c_u}{r}\frac{\partial c_u}{\partial\theta}+c_a\frac{\partial c_u}{\partial z}+\frac{c_rc_u}{r}=F_\theta-\frac{1}{\varrho r}\frac{\partial p}{\partial\theta}\\
&c_r\frac{\partial c_a}{\partial r}+\frac{c_u}{r}\frac{\partial c_a}{\partial\theta}+c_a\frac{\partial c_a}{\partial z}=F_z-\frac{1}{\varrho}\frac{\partial p}{\partial z}
\end{aligned}\right\}. \tag{186}
$$

Here c_r, c_u, and c_a are the radial, peripheral (tangential), and axial components of velocity;

r is the radius;

θ is the vectorial angle;

z is the distance along the axis of the stage;

F_r, F_θ, and F_z are the components of the external forces of influence of the flow.

Equations (186) can be written in Gromeko-Lamb form:

$$
\left.\begin{aligned}
&\frac{\partial}{\partial r}\left(\frac{c^2}{2}\right)-2\left(c_u\omega_z-c_a\omega_u\right)=F_r-\frac{1}{\varrho}\frac{\partial p}{\partial r}\\
&\frac{\partial}{\partial\theta}\left(\frac{c^2}{2}\right)-2\left(c_a\omega_r-c_r\omega_z\right)=F_\theta-\frac{1}{\varrho r}\frac{\partial p}{\partial\theta}\\
&\frac{\partial}{\partial z}\left(\frac{c^2}{2}\right)-2\left(c_r\omega_u-c_u\omega_r\right)=F_z-\frac{1}{\varrho}\frac{\partial p}{\partial z}
\end{aligned}\right\}, \tag{187}
$$

where

$$
\left.\begin{aligned}
&\omega_r=\frac{1}{2r}\left(\frac{\partial c_a}{\partial\theta}-\frac{\partial(c_ur)}{\partial z}\right)\\
&\omega_u=\frac{1}{2}\left(\frac{\partial c_r}{\partial z}-\frac{\partial c_a}{\partial r}\right)\\
&\omega_\theta=\frac{1}{2r}\left(\frac{\partial(c_ur)}{\partial r}-\frac{\partial c_r}{\partial\theta}\right)
\end{aligned}\right\}, \tag{188}
$$

are the components of the angular velocity of rotation of an element of gas.

Considering an axisymmetric problem, i.e., assuming that the parameters of the gas and velocities do not change ($\partial/\partial\theta = 0$) in a circumferential direction, the systems of equations (186) and (187) may be essentially simplified. This assumption is equivalent to the assumption concerning an infinite number of blades of a nozzle cascade and rotor wheel and it facilitates possibility of studying the influence of a number of important factors on the structure of flow in the clearances of a stage.

A second widely employed simplification consists in the fact that the radial velocity components are assumed to negligible ($c_r \approx 0$).

It is possible to show that for a steady flow of an incompressible, ideal fluid, the assumptions on axisymmetry ($\partial/\partial\theta = 0$) and the absence of radial velocity

components ($c_r = 0$) are equivalent to the assumption concerning the constancy of velocity circulation along the height of a nozzle blade.

Actually, in this case the equations (186) take on the following form ($F_r = F_\theta = F_z = 0$):

$$\left.\begin{aligned} &\frac{1}{\varrho}\frac{\partial p}{\partial r} = \frac{c_u^2}{r} \\ &\frac{\partial c_u}{\partial z} = 0; \quad c_a\frac{\partial c_a}{dz} = -\frac{1}{\varrho}\frac{\partial p}{\partial z} \end{aligned}\right\}. \tag{186a}$$

Considering the flow at the entrance to irrotational, from equations (188) we will obtain

$$\left.\begin{aligned} &\frac{\partial c_a}{r\partial\theta} - \frac{\partial c_u}{\partial z} = 0 \\ &\frac{\partial c_r}{\partial z} - \frac{\partial c_a}{\partial r} = 0 \\ &\frac{\partial c_u}{\partial_r} + \frac{c_u}{r} - \frac{\partial c_r}{r\partial\theta} = 0 \end{aligned}\right\}. \tag{188a}$$

Equations (186a), also for the assumptions (188a) made above, have a singular solution, i.e., $c_u r$ = const and c_a = const, which is a characteristic of potential (irrotational) motion with constant velocity circulation.

It should be emphasized that equations (187), which are Euler equations (186), also lead to the indicated solution, since for $\partial/\partial\theta = 0$, $c_r = 0$ and $F_r = F_z = 0$ give

$$\left.\begin{aligned} &\frac{1}{\varrho}\frac{\partial p}{\partial r} = \frac{c_u^2}{r} \\ &\frac{\partial}{\partial r}\left(\frac{c^2}{2} + \int\frac{\partial p}{\varrho}\right) = 0 \\ &\omega_z c_u - \omega_u c_a = 0 \end{aligned}\right\}. \tag{187a}$$

There directly follows an equation for the relationship between the axial and tangential velocity components:

$$\left(\frac{dc_u}{dr} + \frac{c_u}{r}\right)c_u + c_a\frac{dc_a}{dr} = 0$$

or

$$\frac{d}{dr}\left(\frac{c_a^2}{2}\right) = -\frac{1}{2r^2}\frac{d(c_u r)^2}{dr}. \tag{187b}$$

For the case when $\partial/\partial\theta \neq 0$ and $c_r \neq 0$, the relationship between c_u and c_a is expressed by the equation

$$\frac{c_u}{r}\frac{\partial c_r}{\partial\theta} + c_a\frac{\partial c_r}{\partial z} - \frac{1}{2r^2}\frac{\partial(c_u r)^2}{\partial r} = \frac{\partial}{\partial r}\left(\frac{c_u^2}{2}\right). \tag{187c}$$

Consequently, the error caused by the use of equation (187b) is estimated by the first two terms of equation (187c). It should be borne in mind that in this case the conditions of the constance of circulation ($c_u r$ = const) and axial velocity components (c_a = const) are not jointly satisfied.

A method for calculating the influence of the curvature of flow lines, the conicity of the flow area, and the forces of the influence of blades on the flow is given below; the method was formulated within the scope of assumption concerning axial symmetry of a steady flow.

We shall assume additionally that the flow in the nozzle cascade is continuous and that there is no energy exchange with the external medium.

In the considered case, equations (186) will be converted to the following form:*

$$\left.\begin{aligned} -\frac{dc_r}{dt}+\frac{c_u^2}{r}&=F_r+\frac{1}{\varrho}\frac{\partial p}{\partial r}\\ c_r\frac{\partial c_u}{\partial r}+c_a\frac{\partial c_u}{\partial z}+\frac{c_r c_u}{r}&=F_\theta \end{aligned}\right\}. \tag{189}$$

In the first equation of (189) the radial acceleration may be presented in the following form:

$$\frac{dc_r}{dt}=\frac{c_m^2}{R_m}\cos\nu+\frac{dc_m^2}{ds_m}\frac{\sin\nu}{2}, \tag{190}$$

where the terms entering the equation are shown in Fig. 217.

c_m is the velocity in the meridional plane;

R_m is the radius of curvature of a flow line in the meridional plane;

ν is the angle between the meridional and axial velocities;

s_m is the length of a flow line in the meridional plane;

F_r and F_θ are the radial and tangential force components of the influence of blades on the flow.

Forces F_r and F_θ are connected by the relationship

$$\operatorname{tg}\gamma=\frac{F_r}{F_\theta}; \tag{191}$$

γ is the blade angle (Fig. 217).

---

*It should be recalled that total radial acceleration $\partial c_r/\partial t$ does not contain local acceleration $\partial c_r/\partial t$, since the motion is considered to be steady.

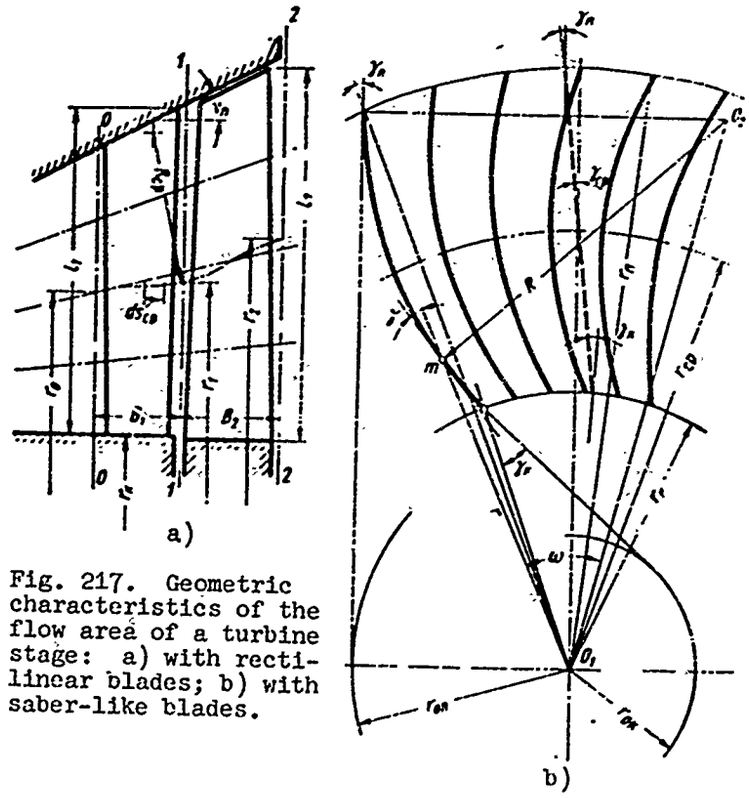

a)

Fig. 217. Geometric characteristics of the flow area of a turbine stage: a) with rectilinear blades; b) with saber-like blades.

b)

The tangential force component is determined by the formula

$$F_\theta = c_a \frac{\partial c_u}{\partial r}.$$

In equation (190) it is possible to disregard the quantity $dc_m^2/ds_m \sin \nu/2$ in connection with its smallness as compared to the first term $c_m^2/R_m \cos \nu$. Assuming that the terms $c_r \partial c_u/\partial r$ and $c_r c_u/r$ are small (radial velocity components are small), with the help of equations (189), (190), and (191) it is simple to obtain the following differential equation for radial equilibrium of the flow in a nozzle cascade:*

$$\frac{1}{\varrho}\frac{\partial p}{\partial r} = \frac{c_u^2}{r} - \frac{c_m^2}{R_m}\cos\nu - c_a \frac{\partial c_u}{\partial z}\operatorname{tg}\gamma. \qquad (192)$$

Radius R_m is considered to be positibe, if it is directed to the axis of the stage. In this case the curvature of the flow lines leads to a decrease of the radial pressure gradient.

Angle γ is determined from the triangle O_1O_2m (Fig. 217):

*The method, which will be discussed later, was developed by G. A. Gilippov.

$$\frac{R}{\sin\omega} = \frac{\overline{O_1O_2}}{\sin(90^\circ + \gamma)} \tag{193}$$

and

$$\frac{R}{\sin\omega} = \frac{r}{\cos(\gamma + \omega)}. \tag{194}$$

With the help of formulas (193) and (194), after simple transformations, it is easy to obtain

$$\sin\gamma = \frac{r_n^2 - r^2 - 2Rr_n \sin\gamma_n}{2rR}. \tag{195}$$

For the root section, formula (195) has the following form:

$$\sin\gamma_k = \frac{r_n^2 - r_k^2 - 2Rr_n}{2r_kR}.$$

It is clear from Fig. 217 that angles $\gamma_П$ and $\gamma_К$ for curvilinear blades have opposite signs. If we assume that the angle of inclination in the root section is positive, the angle at the periphery will be negative. The radius R is then expressed by the following formula:

$$R = \frac{r_n^2 - r_k^2}{2(r_k \sin\gamma_k - r_n \sin\gamma_n)}. \tag{196}$$

After substituting formula (196) into equation (195), and designating

$$A_1 = r_k \sin\gamma_k - r_n \sin\gamma_n,$$

and

$$A_2 = r_n \sin\gamma_n,$$

we find

$$\sin\gamma = \frac{r_n^2 - r^2}{r_n^2 - r_k^2}\frac{A_1}{r} + \frac{A_2}{r}. \tag{195a}$$

For a small blade angle, it is possible to stage approximately that

$$\operatorname{tg}\gamma \approx \sin\gamma. \tag{195b}$$

As shown earlier, the blade angle along the radius changes its sign. This means that on a certain radius the angle of inclination is equal to zero. For finding the radius which corresponds to the zero blade angle, we shall equate the expression for sin γ to zero. Then, by formula (195a), we will obtain

$$r_0 = \sqrt{(r_n^2 - r_k^2)\frac{A_2}{A_1} + r_n^2}. \tag{197}$$

Here r_0 is the radius which corresponds to the zero blade angle.

If the blade angles at the root and on the periphery are equal with respect to absolute value, then r_0 is determined by the formula

$$r_0 = \sqrt{2r_n^2 - r_n r_k}. \tag{197a}$$

Let us now express the velocity components:

$$c_r = \sqrt{\frac{c^2 \sin^2 \alpha \operatorname{tg} \nu}{1 + \sin^2 \alpha \operatorname{tg} \nu}}$$

and

$$c_a = \sqrt{\frac{c^2 \operatorname{tg}^2 \alpha}{1 + \frac{\operatorname{tg}^2 \alpha}{\cos^2 \nu}}}, \quad c_u = \sqrt{\frac{c^2}{1 + \frac{\operatorname{tg}^2 \alpha}{\cos^2 \nu}}}. \tag{198}$$

The velocity in the meridional plane, c_m, is determined by the following expression:

$$c_m = \sqrt{\frac{c^2 \operatorname{tg}^2 \alpha}{\cos^2 \nu + \operatorname{tg}^2 \alpha}}. \tag{199}$$

Let us assume an approximate law of change of the peripheral velocity components along the width of a nozzle cascade B in the following form:*

$$\frac{c_u}{c_{u1}} = \frac{1}{2}\left[\left(\frac{z}{B}\right)^3 + \left(\frac{z}{B}\right)^2\right], \tag{200}$$

where c_{u1} is the peripheral velocity at the nozzle cascade exit;

B is the width of the nozzle cascade profile.

After differentiating expression (200) with respect to z, and substituting equations (195), (198), (199) and $\partial c_u/\partial z$ into equation (192), we write the result for the outlet section, in which: $z = b$, $\alpha = \alpha_1$, $\nu = \nu_1$, $c = c_1$, etc. We then obtain

$$\frac{1}{\varrho_1}\frac{\partial p_1}{\partial r} = \frac{c_1^2 \cos^2 \nu_1}{\cos^2 \nu_1 + \operatorname{tg}^2 \alpha_1}\frac{1}{r} - \frac{c_1^2 \operatorname{tg}^2 \alpha_1 \cos \nu_1}{(\cos^2 \nu_1 + \operatorname{tg}^2 \alpha_1) K_{m1}} - \\ - \frac{1}{r}\frac{5}{2B}\left(\frac{r_n^2 - r^2}{r_n^2 - r_k^2} A_1 + A_2\right)\frac{c_1^2 \operatorname{tg} \alpha_1 \cos^2 \nu_1}{\cos^2 \nu_1 + \operatorname{tg}^2 \alpha_1}, \tag{201}$$

---

*This assumption means that into the calculation there is introduced a certain unreal blade surface, whereby on the trailing edge the force from the blades, $F_\theta = \pm c_a \partial c_u/\partial_r$, does not become equal to zero, as follows from formula (200). However, in accordance with the assumption on the axial symmetry of flow in the clearance, this force must be equal to zero. The contradiction contained in the considered method is corrected by an experiment, which clearly confirms that the indicated force does not disappear in the plane passing through the trailing edges and in the clearance; whereas on the edges it has a maximum value. Coordination of the flow lines in a channel and in a clearance is carried out by the introduction of experimental corrections (see below).

where c_1 and α_1 are the absolute velocity ang outlet angle of flow in the outlet section of the nozzle cascade;

ν_1 is the angle of inclination of the flow line in the outlet section of the nozzle cascade.

For practically applied angles α_1 with small changes of the angle of inclination of flow lines ν_1 it is possible to approximately consider that

$$\frac{\cos^2 \nu_1}{\cos^2 \nu_1 + \operatorname{tg}^2 \alpha_1} \approx \cos^2 \alpha_1.$$

Then

$$\frac{1}{\varrho_1}\frac{\partial p_1}{\partial r} = \frac{c_1^2 \cos^2 \alpha_1}{r} - \frac{c_1^2 \sin^2 \alpha_1}{R_{m1} \cos \nu_1} - \\ - \frac{5}{2B}\frac{c_1^2 \sin \alpha_1 \cos \alpha_1}{r}\left(\frac{r_a^2 - r^2}{r_a^2 - r_\kappa^2} A_1 + A_2\right). \tag{202}$$

We shall now use the energy equation for a stream of gas in the following form:

$$\frac{1}{\eta_1}\frac{c_1^2}{2} = \frac{c_{1t}^2}{2} = i_0 - i_{1t}, \tag{203}$$

where i_0 is the enthalpy of the stagnated flow;

i_{1t} is the enthalpy of flow at the end of isentropic expansion in a nozzle cascade;

c_1 and c_{1t} are the actual and theoretical flow rates at the nozzle exit;

η_1 is the efficiency of the nozzle cascade.

We shall differentiate the left and right sides of equation (203) with respect to the radius

$$\frac{1}{2\eta_1}\frac{\partial c_1^2}{\partial r} - \frac{1}{\eta_1^2}\frac{c_1^2}{2}\frac{\partial \eta_1}{\partial r} = \frac{\partial i_0}{\partial r} - \frac{\partial i_{1t}}{\partial r}. \tag{204}$$

Assuming the constancy of total energy along the radius ($\partial i_0/\partial r = 0$) and considering that

$$\frac{\partial i_{1t}}{\partial r} = \frac{1}{\varrho_{1t}}\frac{\partial p_1}{\partial r},$$

we shall present the energy equation in the following form:

$$\frac{1}{\varrho}\frac{\partial p_1}{\partial r} = \frac{c_1^2}{2\eta_1^2}\frac{\partial \eta_1}{\partial r} - \frac{1}{2\eta_1}\frac{\partial c_1^2}{\partial r}. \tag{205}$$

Here we assume that $\rho_{1t} \approx \rho_1$, i.e., that the density behind a cascade in actual and theoretical processes is identical. This assumption does not lead to a noticeable error in the case of subsonic velocities. For supersonic velocities the density ratio is determined by the following formula [22]

$$\frac{\varrho_1}{\varrho_{1t}} = \chi_c = \left(\frac{1 - \frac{k-1}{k+1}\lambda_{1t}^2 \eta_1}{1 - \frac{k-1}{k+1}\lambda_{1t}^2}\right)^{\frac{1}{k-1}},$$

where λ_{1t} is the dimensionless velocity behind the cascade for the theoretical process.

Equations (205) and (202) will be solved jointly. Then we will obtain

$$\frac{1}{c_1}\frac{\partial c_1}{\partial r} = \eta_1\left[-\frac{\cos^2\alpha_1}{r} + \frac{1}{2\eta_1^2}\frac{\partial\eta_1}{\partial r} + \frac{\sin^2\alpha_1}{R_{m1}\cos\nu} + \right.$$
$$\left. + \frac{5\sin\alpha_1\cos\alpha_1}{2Br}\left(\frac{r_n^2-r^2}{r_n^2-r_k^2}A_1 + A_2\right)\right]. \qquad (206)$$

Equation (206) reduces to quadratures. Integrating with respect to z = B, i.e., for a section at the trailing edges of the profiles, we obtain

$$\frac{c_1}{c_{1k}} = \sqrt{\frac{\eta_1}{\eta_{1k}}}\exp\left[-\int_{r_k}^{r}\frac{\eta_1\cos^2\alpha_1}{r}dr + \int_{r_k}^{r}\frac{\eta_1\sin^2\alpha_1}{R_{m1}\cos\nu_1}dr + \right.$$
$$\left. + \frac{5}{2B}\int_{r_k}^{r}\frac{\eta_1\sin\alpha_1\cos\alpha_1}{r}\left(\frac{r_n^2-r^2}{r_n^2-r_k^2}A_1 + A_2\right)dr\right]. \qquad (207)$$

Equation (207) serves for calculation of the velocity distribution along the radius at the nozzle cascade exit, taking into account the curvature of the flow lines and the influence of the blades on the flow.

The functions $R_{m1}(r)$ and $\nu_1(r)$ in equations (207) are determined with the help of a continuity equation:

$$G = 2\pi\rho_0' c_0(r_0^2 - r_k^2) = 2\pi\int_{r_k}^{r}\rho_1 c_{a1} r\,dr, \qquad (208)$$

where ρ_0' and c_0 are the density and velocity in the entrance section of the nozzle cascade.

Thus, for instance, for an incompressible fluid and α_1 = const, the radius of curvature of the flow lines is determined by the following formula:

$$\frac{1}{R_{m1}} = \frac{2(r-r_k)(r_n-r)\cos^2\alpha_1}{B^2(r_n+r_k)}. \qquad (209)$$

Taking compressibility into account we obtain

$$\frac{1}{R_{m1}} = \frac{1}{R_{cp}}\sin\pi\left(\frac{r-r_k}{r_n-r_k}\right). \qquad (210)$$

The quantity R_{cp} – the radius of curvature of a flow line on the mid-diameter – is determined by the method of successive approximations with the help of the continuity equation.

For a cascade with blades of constant profile and with cylindrical generatrices,

the radius R_{cp} can be determined by the formula*

$$\frac{1}{R_{cp}} = \frac{d^2r}{dz^2} = \pi^2 \frac{r_1 - r_0}{2B^2} \cos \pi \left(\frac{z}{B}\right) \tag{211}$$

or for $z/B = 1$,

$$\frac{1}{R_{cp1}} = -\pi^2 \frac{r_1 - r_0}{2B^2}.$$

For a conical flow area, the formula for R_{cp} has the following form:

$$\frac{1}{R_{cp1}} = \frac{\pi^2}{2B^2} \left(r_1 - \frac{r_0 + r_2}{2}\right). \tag{212}$$

Radii r_0, r_1, and r_2 are determined from the continuity equation written for the corresponding sections which are shown in Fig. 217.

$$\int_{r_K}^{r_{cp} - \Delta r_{max}} \rho_0 c_{a0} r \, dr = \int_{r_K}^{r_{cp} + \Delta r_{max}} \rho_1 c_{a1} r \, dr. \tag{213}$$

According to a preliminary heat calculation, in these sections the distribution of the axial components of velocity c_a and density ρ is known. According to equation (213) we determine the quantity Δr_{max}.

Then

$$r_0 = r_{cp} - \Delta r_{max};$$
$$r_1 = r_{cp} + \Delta r_{max}.$$

Considering that α_1 = const, we can obtain

$$\Delta r_{max} = \frac{(r_n - r_K)^2}{4(r_n + r_K)} \cos^2 \alpha_1. \tag{214}$$

We shall now convert equation (207), substituting R_{m1} in it according to formula (210), and stating that $\cos \nu_1 = 1$. Furthermore, assuming that η_1 = const and α_1 = const, we will obtain

$$\frac{c_1}{c_{1K}} = \left(\frac{r_K}{r}\right)^{\eta_1 \cos^2 \alpha_1} K_1 K_2. \tag{215}$$

Coefficients K_1 and K_2 consider the curvature of the flow lines (K_1) and the influence of the blades on the flow (K_2), respectively. Introducing the parameter $\theta = d/l$, the formulas for K_1 and K_2 can be obtained in the following form:

---

*A formula of the type (211) was used for the first time in reference [161]. It should be borne in mind that the rule expressed by this formula is hypothetical.

$$K_1 = \exp\left[\frac{2\eta_1 \sin^2\alpha_1}{\pi(\theta-1)\bar{R}_{cp}}\left(1-\cos\frac{\pi}{2}(\bar{r}-1)(\theta-1)\right)\right], \tag{216}$$

$$K_2 = \frac{\bar{r}\,\frac{5\eta_1 \sin 2\alpha_1}{4B}\left[\frac{(\theta+1)^2}{4\bar{B}}\left(\sin\gamma_K - \frac{\theta+1}{\theta-1}\sin\gamma_n\right) + \frac{\theta+1}{\theta-1}\sin\gamma_n\right]}{\exp\left[\frac{5\eta_1 \sin 2\alpha_1 (\theta-1)^2}{16\theta}\,\frac{\sin\gamma_K - \frac{\theta+1}{\theta-1}\sin\gamma_n}{\bar{B}}\,\frac{\bar{r}^2-1}{2}\right]}, \tag{217}$$

where

$$\bar{r} = \frac{r}{r_K}; \quad \bar{B} = \frac{B}{r_K}; \quad \bar{R}_{cp} = \frac{R_{cp}}{r_K}.$$

Formula (217) makes it possible to calculate the influence of blades on the flow for the general case of a saber-like (curvilinear)blade. For rectilinear blades ($R = \infty$) the coefficient K_2 is determined by the formula

$$K_2 = \bar{r}\,\frac{5\sin 2\alpha_1\, r_K \sin\gamma_K}{4B}. \tag{218}$$

With the help of equation (215) it is not difficult to find the change of the reaction along the radius for the assumptions that we made:

$$\varrho = 1 - (1-\varrho_K)\left(\frac{c_{1t}}{c_{1tK}}\right)^2, \tag{219}$$

where ρ_K is the reaction in the root section.

Substituting (215) into equation (219), we find

$$\varrho = 1 - (1-\varrho_K)\left(\frac{1}{\bar{r}}\right)^{2\eta_1\cos^2\alpha_1}(K_1K_2)^2. \tag{220}$$

The influence of certain parameters on coefficient K_1 may be estimated by means of the graphs in Fig. 218. The quantity K_1 intensely increases in the middle of the blade and reaches maximum values at the vertex. With the growth of angle α_1, the coefficient K_1 increases. The influence of flare θ is illustrated by the curves in Fig. 218.

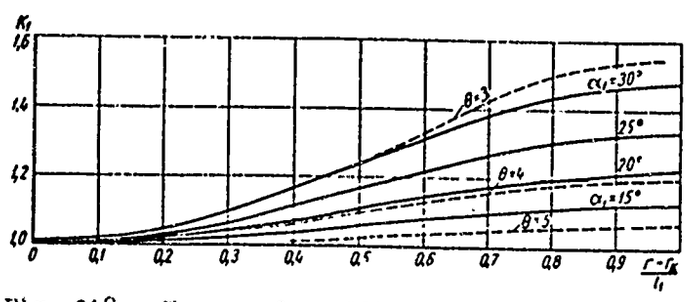

Fig. 218. Change of coefficient K_1, which consider the curvature of flow lines, along the blade height for various, but constant angles α_1 at $\theta = 3$ (solid lines), and for various θ at $\alpha_1 = 20^\circ$ (dotted lines).

Coefficient K_2 also depends on α_1, θ, and the character of change of α_1 along the radius (Fig. 219).

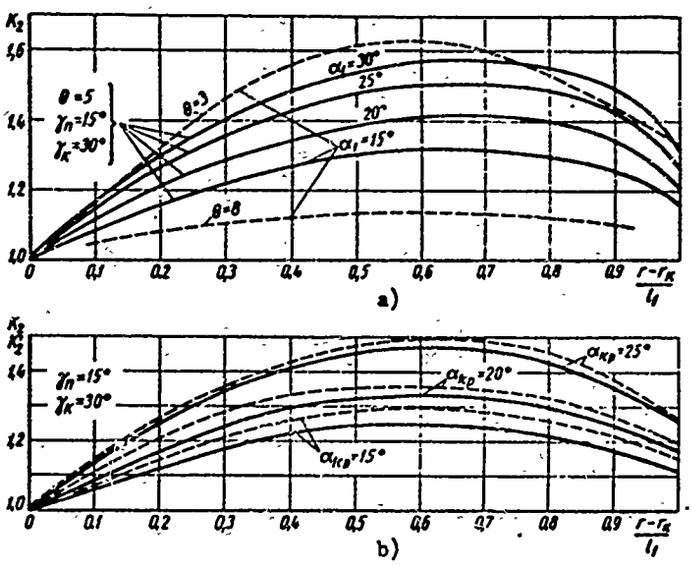

Fig. 219. Change of coefficients K_2 and K_2', which consider the inclination of nozzle blades, with respect to height: a) for various α_1 at $\theta = 5$ and for various θ at $\alpha_1 = 15^\circ$ ($\gamma_П = -15^\circ$, $\gamma_К = 30^\circ$; b) for various laws of change of angle α_1 along the height at $\theta = 5$ ($\gamma_П = -15^\circ$; $\gamma_К = 30^\circ$). Curves (solid) —— c_{u1} = const; – – – – α_1 = const.

Equation (215) and the other dependences do not reflect the influence of conicity of the flow area, since the term $dc_m^2/ds_m \sin \nu/2$, which enters the equation of radial equilibrium (190), was dropped.

A rough estimate of the influence of conicity on the distribution of velocities and the reaction along the radius can be obtained by means of solving the initial equations (189) and (190).

After tedious transformations it is not difficult to obtain an equation for velocity distribution in the following form:

$$\frac{c_1}{c_{1K}} = \left(\frac{1}{r}\right)^{\cos^2 \alpha_1} K_1 K_3, \tag{221}$$

which is valid for radially mounted blades.

Here

$$K_3 = \sqrt{\frac{\cos^2 \nu_1 + \operatorname{tg}^2 \alpha_1}{\cos \nu_1 \cos^2 \alpha_1 (1 + \operatorname{tg}^2 \alpha_1)}} \tag{222}$$

is a coefficient that considers the influence of conicity.

It should once again be emphasized that equation (206) and the others were obtained on the basis of a number of simplifying assumptions. We did not consider the important factors which distinguish an actual flow from an ideal one in this case, including the deviation of the flow from coaxial, radial gas leakages into the boundary layer, the presence of zones of separation of flow, the influence of the rotor wheel, and others. For this reason, into formula (220) we should introduce an experimental coefficient Q, writing it in the following form:

$$\varrho = 1 - (1 - \varrho_k)\left(\frac{r_{1k}}{r_1}\right)^{2Q\eta_1 \cos^2\alpha_1 (K_1 K_2 K_3)^2} \tag{223}$$

The experimental coefficient Q depends on many factors, mainly on the gradient of static pressure along the radius and height of the blades, or, in other words, on the intensity of radial leakages. For stage with high blade height, at small gradients of $\partial p/\partial r$ the coefficient Q is close to unity. In accordance with the results of experiments at $\theta \geq 8$, $2Q = 1.5 - 1.6$, and when $\theta < 8$, $2Q = 1.6 - 1.8$.

When estimating the influence of the other simplifications, one should note that an insignificant change of $\alpha_1 = \alpha_{1\,mn} \pm 3^\circ$ has a slight effect on the accuracy of the calculation, and the change of the radius R can be considered during the calculation of a stage with respect to streams (see § 45).

Of considerable interest is an estimate of the influence of the factors considered by coefficients K_1, K_2, and K_3. An increase of the cone angle of the upper contour, ν_π, leads to a decrease of the intensity of change of the reaction along the blade height, which coincides with the data from the experiments. An increase of the blade angle toward the flow also causes a decrease of the radial pressure gradient, i.e., a balancing of the reaction along the height, and this was shown in Fig. 211.

Distortion of the flow lines in the meridional plane in a clearance also affects the distribution of reactions and the difference of reactions in a section at the vertex and in the root section.

An estimate of the accuracy of the presented method of calculation, which is performed by comparison with experimental data, showed that for cascades with $\theta > 5$ the convergence of the results of the experiment and the calculation is satisfactory. At small $\theta < 4$ and large blade angles, a considerable divergence is noted between the experimental and calculated data. In these cases an essential influence is rendered by factors that are not considered by the calculation method: a) separation of flow around annular contours; b) radial leakages in the boundary layer; c) the influence of a finite number of blades.

§ 38. CALCULATION OF THE FLOW BEHIND A MOVING CASCADE

Calculation of the flow behind rotor blades is also performed with the help of conservation equations. However, this problem is more complicated than the preceding one, since the rotor blades are located on a revolving wheel, and consequently, the outlet angles of flow in absolute motion are not given.

As general equations of steady three-dimensional motion of an ideal fluid in moving cascades we may use equations (186), which can be written for a relative flow in the following form:

$$\left.\begin{aligned}
&w_r\frac{\partial w_r}{\partial r}+\frac{w_u}{r}\frac{\partial w_r}{\partial \theta}+w_a\frac{\partial w_r}{\partial z}-\frac{w_u^2}{r}-\omega^2 r+2\omega w_u=W_r-\frac{1}{\varrho}\frac{\partial p}{\partial r}\\
&w_r\frac{\partial w_u}{\partial r}+\frac{w_u}{r}\frac{\partial w_u}{\partial \theta}+w_a\frac{\partial w_a}{\partial z}+\frac{w_r w_u}{r}+2\omega w_r=W_\theta-\frac{1}{\varrho}\frac{\partial p}{\partial \theta}\\
&w_r\frac{\partial w_a}{\partial r}+\frac{w_u}{r}\frac{\partial w_a}{\partial \theta}+w_a\frac{\partial w_a}{\partial z}=W_z-\frac{1}{\varrho}\frac{\partial p}{\partial z}
\end{aligned}\right\} \qquad (224)$$

$$\frac{\partial(\varrho w_r)}{\partial r}+\frac{1}{r}\frac{\partial(\varrho w_u)}{\partial \theta}+\frac{\partial(\varrho w_a)}{\partial z}=0.$$

This system is obtained by substitution of the following evident relationships into (186)

$$w_a=c_a;\quad w_r=c_r;\quad w_u=c_u-u=c_u-\omega r,$$

where ω is the angular velocity of rotation of a moving cascade; W_r, W_θ, and W_z are the component forces of the influence of blades on the flow.

Besides the assumptions made above, in cross section 2-2 (see Fig. 217) it is possible to assume that the reconstruction of the flow in the radial direction, which occurs during passage through the moving cascade, is terminated mainly before the control cross section and the radial components of velocity are small there ($c_r \approx 0$). We also assume that the motion in this cross section 2-2 occurs along the cylindrical surfaces, i.e., the radii of curvature of the flow lines in the meridional plane are very great* ($R \approx \infty$).

Then the equation of radial equilibrium, i.e., the impulse equation (in projections on the direction of the radius), will have the following form:

$$\frac{1}{\varrho_2}\frac{dp_2}{dr}=\frac{c_2^2\cos^2\alpha_2}{r}. \qquad (224a)$$

---

*During the calculation of stages with conical flow areas, curvilinear contours, and other peculiarities, these assumptions can lead to considerable errors (see Chapter VIII).

Proceeding to the relative flow in this equation, we will use the relationship

$$c_2 \cos \alpha_2 = w_2 \cos \beta_2 - u,$$

where $u = \omega r$ is the peripheral velocity on the current radius r;

$\beta_2 = \beta_2(r)$ is the outlet angle, which is a given function of r.

Then (224a) is written in the following manner:

$$\frac{1}{\varrho} \frac{dp_2}{dr} = \frac{(w_2 \cos \beta_2 - u)^2}{r}. \tag{225}$$

Equation (225) directly follows also from the first equation of (224), after substitution

$$w_r = \frac{\partial w_r}{\partial r} = \frac{\partial w_r}{\partial z} = \frac{\partial w_r}{\partial \theta} = 0.$$

We shall now use the energy equation for a relative flow:

$$\frac{1}{\eta_2} \frac{w_2^2}{2} - \frac{w_1^2}{2} = i_1 - i_{2t}. \tag{226}$$

Here w_1 is the relative inlet velocity of gas to the rotor blades; i_1 and i_{2t} is the enthalpy of the gas before the rotor blades and at the end of isoentropic expansion in the moving cascade, respectively; $\eta_2 = \psi^2$ (ψ is the velocity coefficient of the moving cascade).

All quantities that enter equation (226) are functions of radius r.

Since

$$i_1 = i_0 - \frac{c_1^2}{2},$$

after substitution of this expression into equation (226), we will obtain

$$\frac{w_2}{\eta_2} \frac{dw_2}{dr} - \frac{w_2^2}{2\eta_2^2} \frac{d\eta_2}{dr} + \frac{d}{dr}\left(\frac{c_1^2 - w_1^2}{2}\right) = -\frac{di_{2t}}{dr}. \tag{227}$$

In the third term of equation (227) we shall perform the following substitution

$$c_1^2 - w_1^2 = 2uc_1 \cos \alpha_1 - u^2.$$

Furthermore, let us note that

$$\frac{di_{2t}}{dr} \approx \frac{1}{\varrho_2} \frac{dp_2}{dr}.$$

After substitution into (227), we finally obtain

$$w_2 \frac{dw_2}{dr} + \left(\frac{\eta_2 \cos^2 \beta_2}{r} - \frac{1}{2\eta_2} \frac{d\eta_2}{dr}\right) w_2^2 +$$
$$+ 2\eta_2 \omega \cos \beta_2 w_2 + \eta_2 \frac{d(c_{u1} r)}{dr} = 0. \tag{228}$$

As it is known, the obtained differential equation for the distribution of relative velocities behind a moving cascade is an Abel equation of the second kind.

When the velocity circulation around a nozzle blade is $c_{u1}r$ = const, the free term of equation (228) is equal to zero.

Equation (228) is integrated under certain simplifications. Thus, for instance, considering that* $\eta_2 = 1$ and $c_{u1}r$ = const, it is not difficult to obtain

$$\frac{dw_2}{dr} + \frac{\cos^2\beta_2}{r} w_2 + 2\omega\cos\beta_2 = 0. \tag{229}$$

The integral of equation (229) will be

$$w_2 = \left[w_{2m} + 2\omega\int_{r_m}^{r}\cos\beta_2\,dr\right]\exp\left(-\int_{r_m}^{r}\frac{\cos^2\beta_2}{r}\,dr\right), \tag{230}$$

where r_m is the mid-radius of the stage; w_{2m} is the relative outlet velocity on the mid-radius.

The gas flow through the nozzle and rotor blades should satisfy the continuity equation:

$$G = 2\pi\int_{r_k}^{r_n}\mu\varrho c_a r\,dr. \tag{231}$$

Depending upon the adopted law of change of angles along the radius in these sections, from (231) we can obtain the values of the velocities in the root or middle sections of the stage.

Coordination of the flow rate through the nozzle and moving cascade may be accomplished by dividing the flow into a number of elementary annular streams. Within the limits of each stream the problem may be considered as a one-dimensional one and the usual method of calculation may be employed. The transition from stream to stream should be accomplished in such a manner so that the equation of radial equilibrium in the control sections is satisfied.**

An increase (or decrease) of pressure Δp_1 upon transition to an adjacent stream in a clearance should be calculated by means of the approximate equation

$$\Delta p_1 = \frac{\varrho_1 c_{u1}^2}{r}\Delta r, \tag{232}$$

---

*Equation (228) is also integrated for $\eta_2 < 1$, if we consider that η_2 does not change along the radius.

**A more exact method of calculation for streams is given in Chapter VIII.

where Δr is the increase of the radius upon transition to the mid-section of an adjacent annular stream (if the radius decreases, then Δr is negative); c_{u1} and ρ_1 are the peripheral velocity component and the density of the gas in the considered elementary annular stream at mid-radius r, respectively.

An analogous equation for cross section 2-2 behind the rotor wheel is written in the following way:

$$\Delta p_2 = \frac{\rho_2 c_{u2}^2}{r} \Delta r. \tag{233}$$

The continuity equation for these sections may be presented in the following form:

$$\Delta G = \mu_1 \rho_{1t} c_{1t} f_1;$$
$$\Delta G = \mu_2 \rho_{2t} w_{2t} f_2.$$

Here ΔG is the flow rate of gas through the stream; ρ_{1t} and ρ_{2t} are the density at the end of isentropic expansion in the nozzle and moving cascades, correspondingly; c_{1t} and w_{2t} are the theoretical outlet velocities of flow from the cascades; f_1 and f_2 are the areas of the outlet sections within the bounds of one elementary stream; μ_1 and μ_2 are the flow rate coefficients in a given annular section of the nozzle and moving cascades.

The total flow rate through the stage G is equal to the sum of flow rates for all elementary streams. In a similar calculation the flow rate coefficients, μ_1, and μ_2, and the velocity coefficients, $\varphi = \sqrt{\eta_1}$ and $\psi = \sqrt{\eta_2}$, should be assumed to be variable and dependent upon the geometric parameters of the cascades and the performance parameters of the flow.

By using the method of calculation for streams when designing a stage, it is possible to select the degree of reaction and the outlet angles from the nozzle and moving cascades in the root or middle sections. In the last case it is not difficult to calculate the middle annular stream as that of an elementary turbine stage. Further, by means of formula (232) we can find the pressure behind the nozzle cascade for two adjacent streams.

The pressure behind the stage for two adjacent streams, in general, differs from the pressure behind the stage on the mid-diameter, and it can be found by means of formula (232). The pressure behind the stage in first approximation may be considered as being constant.

In the course of the calculation by means of the continuity equation, the distribution of angles α_1 and β_1 along the radius can be corrected.

§ 39. METHODS FOR TWISTING BLADES AND THE RATIONAL ORGANIZATION OF THE FLOW IN A STAGE

The existing methods for calculating the flow in a large-flare stage do not make it possible to solve the problem concerning the most rational organization of the flow in a stage, and consequently, the optimum methods for twisting blades.

This problem is solved with the aid of the results of an experimental investigation of nozzle and moving cascade and a stage on the whole (§§ 35, 36, 41, and 44).

The criteria for comparing the various methods for the organization of the flow in a stage are:

a) the effectiveness of the stage;

b) the discharge capacity;

c) the strength and vibration reliability of the blades;

d) the technological effectiveness of the cascades;

e) the peculiarities of the physical process.

The difficulty of constructing an optimum stage for given operating conditions consists in that the requirements of maximum effectiveness, reliability, and productivility are contradictory to a considerable degree. In a number of cases it is necessary to waive the considerations of economy for providing the necessary reliability and productibility of manufacture of the blades.

Questions concerning the twisting of blades only from the point of view of maximum effectiveness are considered below.

It is not possible to establish an optimum method for profiling long blades by means of a calculation since the appropriate methods of approximation make it possible to judge the comparative merits of the various twisting methods only with respect to indirect criteria.

The initial equation (206) is useful for calculating the parameters of flow in a clearance for an arbitrary law of change of α_1 along the radius or for α_1 = const.

However, the question of rational means for profiling the nozzle and rotor blades of a stage with considerable variation of parameters along the radius still remains unanswered. Within the confines of a one-dimensional flow diagram, the problem concerning rational methods for twisting blades is reduced to the correct selection of the variation of angles and velocities along the radius so that the efficiency of the stage is maximum. At the same time, with the selected field of angles and velocities, a high stage efficiency can be ensured only under the condition of the correct selection of blade profiles, and the shape of the contours in the

meridional plane, which ensure a flow structure in the stage which is close to that calculated.

The first part of problem — the selection of laws of distribution of flow parameters along the radius in a clearance and behind the stage — can be solved on the basis of various premises which are more or less equivalent. The most common ones are the following simplifying assumptions:

1. Constancy of velocity circulation along nozzle and moving cascades ($c_{u1}r$ = = const and $c_{u2}r$ = const) for a uniform field of axial velocities in the clearance and behind the stage.

2. Constancy of the outlet angle of flow from the nozzle cascade (α_1 = const) and axial outlet of flow from the stage.

3. A linear law of change of sin $\alpha_1(r)$ for cylindrical (constant profile) nozzle and rotor blades constructed under the condition of constant performance with respect to height.*

4. A law of change of $\alpha_1 = \alpha_1(r)$ which ensures a maximum discharge capacity for the stage and axial outlet from the stage.

The number of possible variants is very great (theoretically equal to infinity) in accordance with the fact that the differential equation (206) has an infinite number of solutions. It is obvious that the quantity of practically acceptable solutions, which correspond to the conditions of rational organization of the flow in a turbine stage, is limited. For this reason, and also considering that the equation of radial equilibrium (206) is approximate, one should use those methods for the organization of flow in stages, which are constructed on the basis of concise physical premises. In certain cases, when designing stages with vary long blades it is expedient to combine the various methods for organizing the flow, i.e., to select a complex law of change of angle α_1 along the radius.

It should be emphasized that, in accordance with the equation of radial equilibrium, the twisting of nozzle blades, i.e., the form of the function $\alpha_1(r)$, hardly affects the character of change of the reaction along the radius. Consequently, for any method of twisting $\alpha_1(r)$ with radially mounted blades, the distribution of pressures and velocities in the clearance remains about the same.

Thus, the selection of a rational method for twisting blades is reduced to the solution of two problems: a) the establishment of an optimum shape and twist

---

*Guarantee of condition L_u = const causes difficulties in connection with the sharp growth of losses in the root and peripheral sections.

$[\alpha_1(r)]$ of the nozzle blades to ensure minimum cascade losses; b) profiling of the moving cascade to ensure minimum losses in the channels and with the outlet velocity along the entire height.

As shown above, the question concerning the selection of a law of change of $\alpha_1(r)$ should be solved with the meridional shape of the nozzle cascade, and the shape and inclination of the blades taken into account.

Considering the results of an experimental investigation of annular nozzle cascades, it may be concluded that the most expedient method is to twist the blades according to the selected rational distribution of static pressures in the clearance.*

The $p_1(r)$ diagram can be influenced by: a) meridional profiling of the cascade contours; b) inclination of the blades; c) distortion of the blades (the application of saber-like blades). In certain cases it is necessary (or expedient) to employ combined methods, when inclined or curvilinear blades are designed with noncylindrical contours.

The application of curvilinear nozzle blades is promising; these blades provide a distribution of gradients in the vane channels and static pressures behind the cascade, at which the losses in the nozzle cascade will be minimum, and the rotor blades obtain a minimum twist. It is then possible to select a nozzle blade shape which ensures the given distribution of pressures in the clearance with few losses in the moving cascade.

In certain cases this problem is successfully solved by the application of blades that are inclined toward the flow. Both types of nozzle cascades increase the vibration reilability of the rotor blades: during rotation, the blade gradually enters (and emerges from) the edge wake of the nozzle blade, which decreases the inpulse of the disturbing force.

Above (see § 37) we obtained formulas for the calculation of stage with $\alpha_1 =$ $=$ const. With blade twisting under the condition of constant circulation ($c_{u1}r =$ $-$ const) the outlet angle of the flow from the nozzle cascade increases linearly from the root section to the peripheral section in accordance with the formula

$$\operatorname{tg}\alpha_1 = \bar{r}\operatorname{tg}\alpha_{1\kappa}. \tag{234}$$

Disregarding the small distortion of flow lines in the meridional plane ($K_1 = 1$) and considering that the efficiency of the nozzle cascad remains constant

*At supersonic velocities there appear peculiarities which impose additional conditions on the selection of blade twist (see Chapter VIII).

along the radius (η_1 = const), with the help of formula (234) it is not difficult to obtain the following equation for the distribution of absolute velocities in the clearance:

$$\frac{c_1}{c_{1\kappa}} = \left[\frac{1+\bar{r}^2 \operatorname{tg}^2 \alpha_{1\kappa}}{\bar{r}^2(1+\operatorname{tg}^2 \alpha_{1\kappa})}\right]^{\eta_1/2} K_2', \tag{235}$$

where

$$\left.\begin{aligned} K_2' &= \exp\left[q \operatorname{arc\,tg}(\operatorname{tg}\alpha_{1\kappa}\bar{r}) - q\alpha_{1\kappa} - p(\bar{r}^2 - 1)\right] \\ q &= \frac{5\eta_1}{2B}\left[\frac{\bar{A}_1}{\bar{r}_n^2 - 1}(\bar{r}_n^2 + \operatorname{ctg}^2\alpha_{1\kappa}) + \bar{A}_2\right] \\ p &= \frac{5\eta_1}{2B}\frac{\bar{A}_1}{\bar{r}_n^2 - 1}\operatorname{ctg}\alpha_{1\kappa} \\ \bar{A}_1 &= \frac{A_1}{r} = \frac{r_\kappa \sin\gamma_\kappa}{r} - \frac{r_n \sin\gamma_n}{r} \\ \bar{A}_2 &= \frac{r_n}{r}\sin\gamma_n. \end{aligned}\right\} \tag{236}$$

Here K_2' is a coefficient that considers influence of blade inclination on the velocity distribution behind the nozzle cascade with blade profiling according to the method of constant velocity circulation. The values of K_2' are shown in Fig. 219. It follows from this that for large angles α_1 the blade inclination has a practically equal effect on the distribution of velocity and reactions in the clearance for blades that are twisted under the condition of α_1 = const and according to the method of constant circulation.

Consequently, the effect from the application of inclined and curvilinear blades practically is not influenced by the change of the angle of flow with respect to height, expecially at large values of α_1.

Equations (215) or (235), and (236), which were obtained for the general case of a variable angle of inclination $\gamma(r)$, can be used for the calculation of curvilinear blades.

By assigning various laws of change of $\gamma(r)$ and finding the corresponding distribution diagrams of static pressure along the radius, it will not be difficult to find the optimum inclination or the camber of the nozzle blades by means of variant calculations.

As an example, Fig. 220 gives the distribution of angles, dimensionless velocities, and the reaction along the radius for a stage with θ = 2.8. Two variants are considered here: twisting of blades with α_1 = const (dotted line) and $\alpha_1 = \alpha_1(r)$. In the last case, the angle α_1 from the root to the vertex first increases, and

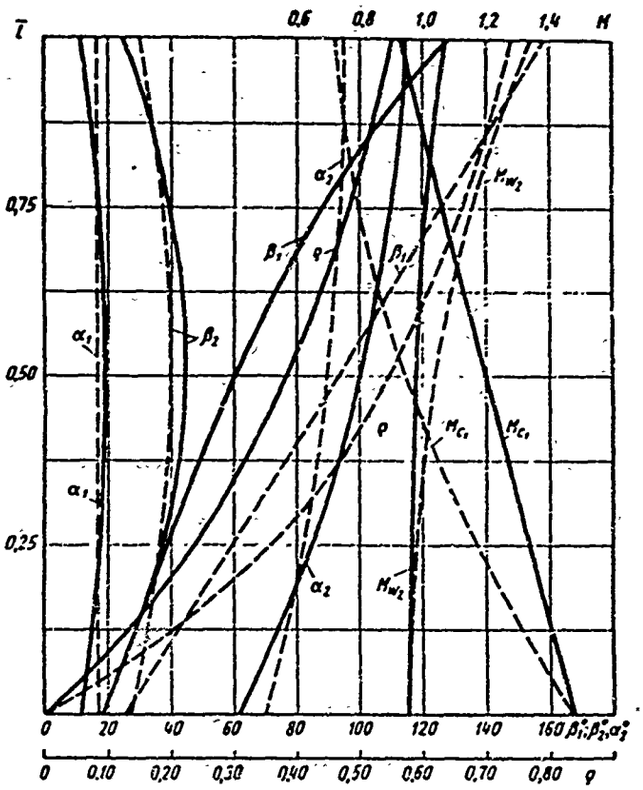

Fig. 220. Variation of stage parameters along the radius, with $\theta = 2.8$ and $x_{\text{ф}m} = 0.58$ (calculation). Curves: —— blades mounted with inclination; – – – – blades mounted radially.

then decreases, and the nozzle blades are curvilinear. The second variant has indubitable advantages: a) the reaction at the vertex was decreased by 19% ($\rho_{\text{п}} = 55\%$ instead of $\rho_{\text{п}} = 74\%$); b) the entrance angles to the moving cascade β_1 vary along the height within significant limits ($\Delta\beta_1 = 96^\circ$ and $\Delta\beta_1 = 129^\circ$); twisting of the rotor blades is then less intense; c) the velocities at the outlet from the moving cascade during relative motion in the peripheral sections are lowered; d) the absolute velocities at the outlet from the nozzle cascade vary along the height less intensely, which simplifies the profiling of the nozzle cascade. At the same time, as may be seen from Fig. 220, in a stage with saber-like blades the angle of absolute velocity behind the stage α_2 varies with respect to height more intensely, and the losses with the outlet velocity can appear larger than in a usual stage. These circumstances must be considered when selecting the "saber-like shape" of the inclination of the blades.

In considering the expediency of the application of inclined or saber-like blades, one should also bear in mind that the selection of R or the angle of inclination γ is carried out with the necessary change of $x_{\text{ф}}$ taken into account, since $x_{\text{фопт}}$ depends on ρ.

Let us consider as an example the calculation of the flow in a stage with nozzle blades of constant profile, assuming that the flow at the entrance to the stage has a uniform velocity field. We shall set up the following problem: find the distribution of parameters in the clearance and behind the moving cascade with respect to the radius. The solution of this problem permits the additional obtainment

of initial data for the calculation of a stage with blades of constant profile on the basis of the aerodynamic characteristics of the cascades, and it can be used for determining the optimum cascade flare at which it is possible to apply blades of constant profile.

The calculation of a stages with blades of constant profile may be performed if we consider that the angles α_1 and β_2 are constant along the radius. A more exact method of calculation, which will be given below, consists in the fact that the angles α_1 and β_2 are given in the form of functions of the radius r. This method is expedient to apply in those cases when the stage flare is considerable.

Numerous experiments show that the angle α_1 may be expressed, depending upon relative pitch, or radius, by the formula

$$\operatorname{tg}\alpha_1 = \operatorname{tg}\alpha_{1\text{к}} + \frac{\Delta \operatorname{tg}\alpha_1}{2}(\theta - 1)(\bar{r} - 1), \tag{237}$$

where

$$\Delta \operatorname{tg}\alpha_1 = \operatorname{tg}\alpha_{1\text{п}} - \operatorname{tg}\alpha_{1\text{к}}.$$

As before, $\alpha_{1\ \text{п}}$ and $\alpha_{1\ \text{к}}$ are the outlet angles of flow at the vertex and in the root sections, respectively; $\bar{r} = r/r_{\text{к}}$; $r_{\text{к}}$ is the radius of the root sections; r is the radius of a current section.

We shall now use the equation of radial equilibrium. Considering that the stage generatrices are cylindrical, we use the first equation of system (186a), representing it in the following form:

$$\frac{dp_1}{\varrho_1} = c_1^2 \cos^2\alpha_1 \frac{dr}{r}. \tag{186c}$$

Substituting (237) into equation (186c) and integrating it, we will obtain

$$\bar{c}_1 = \frac{c_1}{c_{1\text{к}}} \approx \frac{F(\bar{r})}{\bar{r}^{\varkappa}}. \tag{238}$$

Here

$$F(\bar{r}) = \left[1 + \frac{2n_1 b_1}{1 + n_1^2}(\theta - 1)(\bar{r} - 1) + \frac{b_1(\theta - 1)^2}{1 + n_1^2}(\bar{r} - 1)^2\right]^{1/2};$$

$$\varkappa = \frac{\eta_1}{1 + [n_1 - b_1(\theta - 1)]^2}; \quad n_1 = \operatorname{tg}\alpha_{1\text{к}};$$

$$b_1 = \frac{1}{2}(\operatorname{tg}\alpha_{1\text{п}} - \operatorname{tg}\alpha_{1\text{к}}).$$

For the determination of velocity c_1 it is necessary to know the value of $c_{1\ \text{к}}$ in the root section. For this purpose we shall use the continuity equation, writing it for cross section 0-0 and 1-1:

$$\frac{c_{0a}^2}{2}(\bar{r}_e^{-2} - 1) = \int_0^{\bar{r}_e} \bar{\varrho}_1 c_{1a} \bar{r}\, d\bar{r}, \tag{239}$$

where c_{0a} and c_{1a} are the axial velocity components in cross sections 0-0 and 1-1 (see Fig. 217);

$\bar{\rho}_1 = \rho_1/\rho_0'$ is the relative density in the clearance (ρ_0' is the current density in cross section 0-0).

The function c_{a1} in equation (239) can be found by the formula

$$c_{1a} = c_1 \sin \alpha_1 = \frac{c_1 \operatorname{tg} \alpha_1}{\sqrt{1 + \operatorname{tg}^2 \alpha_1}}$$

or approximately,

$$c_{1a} = c_{1\kappa} \bar{c}_1 \sin \alpha_1 = c_{1\kappa} \frac{F(\bar{r})}{\bar{r}^{\varkappa}} \sin \alpha_1, \tag{240}$$

where α_1 is found by means of formula (237).

The above-mentioned dependences are valid if the flow in the clearance is subsonic. For mixed flows in the clearance, when in the lower part of the stage (at the root sections) $c_1 > a_{*1}$, formula (237) is not applicable. In this case it is necessary to consider the deflection of the flow in the slanting shear of the nozzle cascade (see Chapter VIII).

Let us now turn to the calculation of the flow behind a stage. We shall use the fundamental equation (228) and integrate it for η_2 = const and $c_{u1} u \cdot r$ = const for the adopted law of change of angles along the radius, which was obtained from experiments

$$\sin \beta_2 = \sin \beta_{2\kappa} + \frac{\Delta \sin \beta_2}{2} (\theta - 1)(\bar{r} - 1). \tag{241}$$

As a result of integration, we find the approximate expression:

$$\bar{w}_2 = \frac{w_2}{w_{2\kappa}} = \bar{r}^{-q}. \tag{242}$$

here $w_{2\,\kappa}$ is the value of w_2 in the root section;

$\beta_{2\,\kappa}$ is the vector angle $w_{2\,\kappa}$;

$$q = 1 - [n_2 - b_2(\theta - 1)]^2; \quad n_2 = \sin \beta_{2\kappa};$$

$$b_2 = \frac{1}{2} \Delta \sin \beta_2 = \frac{1}{2} (\sin \beta_{2\text{п}} - \sin \beta_{2\kappa}).$$

With the known values of $\bar{w}_2$ it is easy to determine the available heat drop in the stage.

With the help of the derived formulas it is possible to calculate the distribution of parameters along the radius in a clearance and behind a stage with blades of constant profile.

The available heat drop in a nozzle cascade, according to (238), will be

$$\bar{h}_{01} = \frac{h_{01}}{h_{01\kappa}} = \bar{c}_1^2 = \frac{[F(\bar{r})]^2}{\bar{r}^{2\kappa}}. \tag{243}$$

It is also possible to use simplified formulas. Considering that $F(\bar{r}) \approx 1$, we find

$$\bar{h}_{01} = \frac{1}{\bar{r}^{2\kappa}}. \tag{243a}$$

We shall now find the change of the degree of reaction along the radius. Using formula (243), we obtain

$$\varrho = 1 - (1 - \varrho_\kappa)\frac{[F(\bar{r})]^2}{\bar{r}^{2\kappa}\bar{h}_0}, \tag{244}$$

where $\bar{h}_0 = h_0/h_{0\,\kappa}$.

Hence, we can obtain an approximate formula for determining the reaction on the mid-diameter of a stage with untwisted blades, proceeding from the given value of ρ_κ in the initial, i.e., root, section.

Considering that $b_1 \approx 0$, from formula (244) we will obtain

$$\varrho_{cp} = 1 - \frac{1 - \varrho_\kappa}{\bar{h}_{0m}}\left(\frac{\theta - 1}{\theta}\right)^{2\kappa}, \tag{245}$$

where

$$\bar{h}_{0m} = \frac{h_{0m}}{h_{0\kappa}}.$$

Formula (245) has a limited field of application. It is obvious that it is valid for relatively large θ, since only in this case is the difference of α_1 small at the vertex and at the root, and it is therefore possible to assume that $b_1 \approx 0$.

Of practical interest is the possibility of determining the minimum reaction on the mid-section, at which in the root section the reaction is $\rho_\kappa = 0$. Corresponding calculation formulas can be obtained for the adopted law of twisting. Thus, for instance, when α_1 = const, from equation (245) it is not difficult to obtain, for $\rho_\kappa = 0$,

$$\varrho_{cp\,\min} > 1 - \frac{1}{\bar{h}_0}\left(1 + \frac{2n_1 b_1}{1 + n_1^2}\right)^\kappa \left(\frac{\theta - 1}{\theta}\right)^{2\kappa} \tag{246}$$

or approximately, ($b_1 \approx 0$)

$$\varrho_{cp\,\min} \approx \left(\frac{\theta - 1}{\theta}\right)^{2\kappa}.$$

Considering a stage with inclined blades and conical generatrices, from equation (223) we find

$$\varrho_{cp\,min} = 1 - \left(\frac{\theta - 1}{\theta}\right)^{2Q\eta_1 \cos^2 \alpha_1} (K_1 K_2 K_3)^2 \tag{247}$$

where

$$\frac{r_m}{r_k} = \frac{\theta}{\theta - 1}.$$

Approximately,

$$\varrho_{cp\,min} \approx \frac{2\theta - 1}{\theta^2} \quad \text{and} \quad \varrho_{m\,min} \approx \frac{2}{\theta} \ (\text{for } \theta > 6).$$

The initial formula for the degree of reaction, (220), makes it possible to determine the difference of reactions in the peripheral and root sections. Since

$$\bar{r}_n = \frac{\theta + 1}{\theta - 1},$$

then, after substitution into (247), we will obtain

$$\frac{1 - \varrho_n}{1 - \varrho_k} = \left(\frac{\theta - 1}{\theta + 1}\right)^{2Q\eta_1 \cos^2 \alpha_1} (K_1 K_2)^2 \tag{248}$$

In first approximation,

$$\frac{1 - \varrho_n}{1 - \varrho_k} \approx \left(\frac{\theta - 1}{\theta + 1}\right)^2.$$

The change of performance on the wheel can be found in the following manner:

$$\bar{L}_u = \frac{L_u}{L_{uk}} = \bar{r} \frac{c_{u1} + c_{u2}}{c_{u1k} + c_{u2k}},$$

where

$$c_{u2} = w_{2k} \bar{w}_2 \cos \beta_2 - u.$$

The function $c_{u1}(r)$ also is known. Consequently, the quantity $\bar{L}_u(\bar{r})$ is determined.

The field of axial components of velocities behind the stage is calculated by the formula

$$c_{2a} = c_{u2} \operatorname{tg} \alpha_2 = w_{u2} \operatorname{tg} \beta_2 = (c_{u2} + u) \operatorname{tg} \beta_2.$$

By using the obtained relationships, it is possible to analyze the variation of parameters along the radius in a clearance and behind a stage, and to estimate the additional losses that appear in a stage with blades of constant profile.

The results of corresponding calculations show that the additional losses in a stage with untwisted blades (losses due to "nontwisting") are brought about by the increase of outlet losses, the change of the entrance angle of flow to the moving cascade, and also the change of the output work along the radius.

The flow is swirled behind the stage; balancing of the velocity field is accompanied by losses of kinetic energy which must be included in the overall

balance of stage losses.

The results of calculations perfomed with the proposed method for stages with cylindrical contours satisfactorily coincide with the experimental data. Additional losses due to "nontwisting" of blades can be determined by means of caluclation only when the aerodynamic characteristics of the nozzle and moving cascades are known from the data of static tests.

In conclusion, let us note that with large θ the change of the angles α_1 and β_2 is not great along the radius (see formulas (237) and (241)). The calculation of the velocities c_1 and w_2 in these stages may be performed by means of formulas which are easily obtained from the fundamental equations (238) and (242) under the following assumptions: η_1 = const, η_2 = const, α_1 = const, and β_2 = const.

Then

$$\bar{c}_1 = \bar{r}^{-2\eta_1 \cos^2 \alpha_1};$$

$$w_2 = \frac{(1 - \eta_2 \cos^2 \beta_2)\bar{r}^{-\eta_2 \cos^2 \beta_2} + 2\eta_2 \cos^2 \beta_2 \bar{r}}{1 + \eta_2 \cos^2 \beta_2}.$$

§ 40. RESULTS OF INVESTIGATIONS OF THE EFFECT OF INDIVIDUAL DESIGN ELEMENTS ON THE EFFECTIVENESS OF STAGES WITH LONG BLADES

Numerous experiments show that the transition to twisted blades in stages with $\theta < 10$ leads to a considerable growth of efficiency. The boundary of twisting, which is within the zone of $\theta \approx 8$-12 for certain stages, depends on the type of stage, and its geometric and performance parameters (M and Re numbers).

Therefore, the determination of the boundary of twisting is possible only experimentally or by means of calculation. In the last case, the method discussed in the preceding paragraph may be used. For each type of stage the problem is solved separately.

It should be noted that the boundary of twisting is not universal, and for some stage it lies beyond the indicated limits (θ = 8-12). The dependence of the boundary of twisting on the geometric and performance parameters of a stage explains the well-known experimental conclusion concerning the essential effect of losses due to "nontwisting," which are detected for various values of θ.

We shall consider certain results of an experimental investigation of stages with long blades.

The Influence of Blade Twisting

The influence of twisting the rotor blades on the efficiency of a stage with

$\theta = 4.18$ was investigated by P. Vesely and I. Camek [132]. They tested five stages with an identical nozzle cascade, but with differently twisted blades of the moving cascades, the shapes of which are shown in Fig. 221a. The twist of the rotor blades was changed by means of changing the angle of incidence of the profile at the vertex $\beta_{уп}$. The angle of incidence of the profile in the root section and the shape of the profiles for all sections were kept constant.

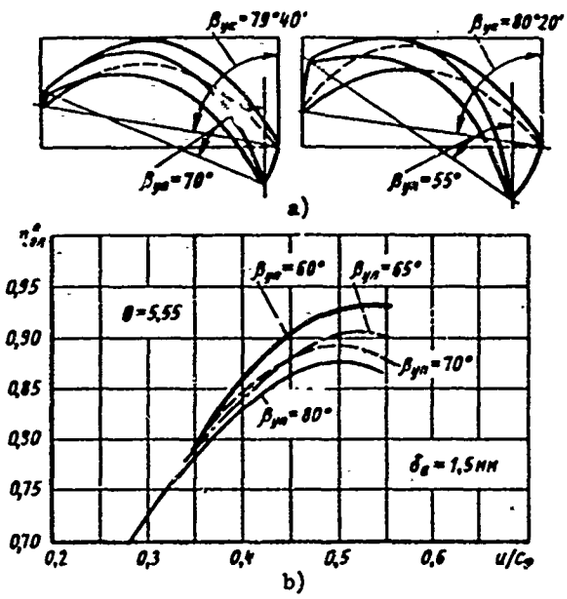

Fig. 221. Influence of twisting of a moving cascade on the efficiency of the stage: a) shapes of rotor blades; b) blade efficiency depending upon angle of incidence of profile in peripheral section. With $Re_{c1} = 1.5 \cdot 10^5$; $\theta = 4.18$. Experiments of P. Vesely and I. Camek.

The results of tests for one value of the axial clearance are shown in Fig. 221b. With the decrease of the angle of incidence of the profile in the peripheral section from $\beta_{уп} = 80°$ to $\beta_{уп} = 60°$, the maximum blade efficiency of the stage increased from 87 to 92.5% with an axial clearance of $\delta_a = 1.5$ mm. At small $u/c_ф$ the influence of twisting decreases. The influence of the axial clearance in the investigated range lies within the limits of the accuracy of the experiment.

A detailed investigation of the structure of flow, which was conducted by the authors, distinctly explains the influence of the twisting of rotor blades. Figure 222 shows the change of the reaction in the root and peripheral sections for differently twisted rotor blades. With the increase of $\beta_{уп}$, the reaction in the root and peripheral sections increases, and the difference in reactions also increases somewhat. This result was expected, since with the increase of $\beta_{уп}$, the cross-sectional area of a moving cascade decreases. Let us note that the investigated stage has a high reaction in the root section, the maximum value of which reaches $\rho_к \approx 20\%$ when $\beta_{уп} = 55°$.

However, the growth in efficiency is explained not so much by the increase of the reaction, but by the decrease of losses in the moving cascade in connection with the decrease of the angle of incidence, and also by the lowering of losses

with the outlet velocity.

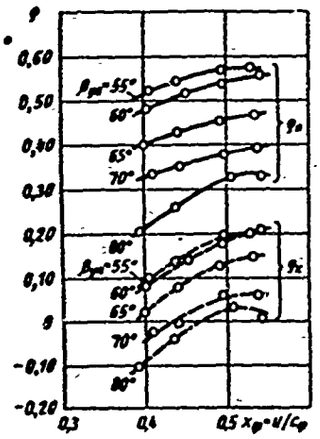

Fig. 222. Influence of twisting of rotor blades on the change of the reaction in the root section and at the vertex under different conditions for stages with the characteristics shown in Fig. 221.

Analogous experiments were performed by the authors on a stage with the ratio $\theta = 3.14$. The influence of twisting of rotor blades was investigated in a wider range of velocity ratios $u/c_{ф}$. Upon transition from blades of constant profile to the optimum version with twisting of the peripheral profile by 20°, the efficiency at optimum $u/c_{ф}$ was increased by 4.5-5%.

It should be emphasized that the influence of twisting in two of the investigated stages was so considerable mainly because the profile of the moving cascade is especially sensitive to changes of the entrance angle of flow.

Experiments with different nozzle cascades were conducted for a stage with $\theta = 3.92$. The moving cascade for all investigated variants was identical. The nozzle cascades had identical distribution of angles along the radius, but a different outlet area.

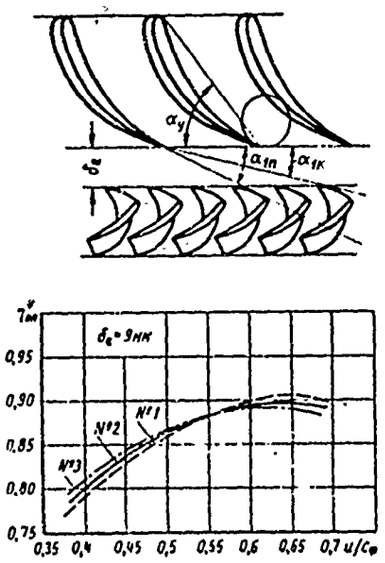

Fig. 223. Influence of the angle of incidence of the profile of a nozzle cascade on the efficiency of a stage. Values of cross-sectional ratios are equal to: curve No. 1 = 1.14; curve No. 2 = 1.01; curve No. 3 = = 0.914. With $Re_{c1} = 1.5 \cdot 10^5$; $\theta = 3.92$. Experiments of P. Vesely and I. Camek.

Variations in areas were attained by changing the angles of incidence of the nozzle blade (Fig. 223). The efficiency curves of these stages distinctly show that at optimum ratios $u/c_{ф}$ the best result is given by stage No. 1 with a maximum flow area of the nozzle cascade. For $u/c_{ф} < 0.55$, the best design is that of the stage with minimum angles α_1.

The obtained result has a simple physical explanation. With the decrease of the nozzle blade angle, the angles of entrance β_1 to the moving cascade decrease. With decreased $u/c_{ф} < (u/c_{ф})_{опт}$ in stage No. 3, the entrance angles β_1 are closer to optimum than in stages No. 1 and No. 2, which also leads to an increase in the efficiency of this stage. Under optimum conditions ($u/c_{ф} \approx 0.65$) the efficiency of stage No. 1 is higher, since the losses in the

nozzle cascade decrease with the growth of α_1, and the angles of entrance to the moving cascade are close to optimum. In the three compared stages, the reaction in the root and peripheral sections under all conditions was different. The maximum difference of the reaction and the maximum peripheral reaction corresponded to stage No. 3. It may be considered that this result to a small extent will reflect the influence of the reaction, since stage No. 1, with the large reaction in the root section, has a lower efficiency at small $u/c_ф$.

The considered projects on the study of the influence of twisting the blading of large-flare stages include the results of the earlier experiments of V. G. Tyryshkin [107] and N. N. Bykov [10]. The last work gives the results of the investigation of four stages that were designed according to the following specifications.

Stage No. 1 – $c_{u1}r$ = const; stage No. 2 – with decreasing angle α_1 to root section ($\Delta\alpha_1 = \alpha_{1\ к} - \alpha_{1\ ср} = -5^\circ$); stage No. 3 – with increasing angle α_1 to root section ($\Delta\alpha_1 = +6^\circ$); stage No. 4 – combined (rotor wheel of stage No. 3 and nozzle cascade designed according to the method of $c_{u1}r$ = const).

These experiments showed (Fig. 224) that stages No. 1, 2, and 3 in design conditions ($u/c_ф$ = 0.55) have about the same efficiency (approximately 90%). In conditions with lowered $u/c_ф$ ≈ ≈ 0.2, the efficiency of stage No. 2 was 4.5% higher, and the efficiency of stage No. 3 was 6.5% lower, as compared to stage No. 1. Stage No. 4 has maximum efficiency in a wide range of conditions. In design conditions, the increase of efficiency of this stage amounts to 3%; at $u/c_ф$ = 0.35, it is 6%, and at $u/c_ф$ = 0.2, it is ~3%, as compared to stage No. 1.

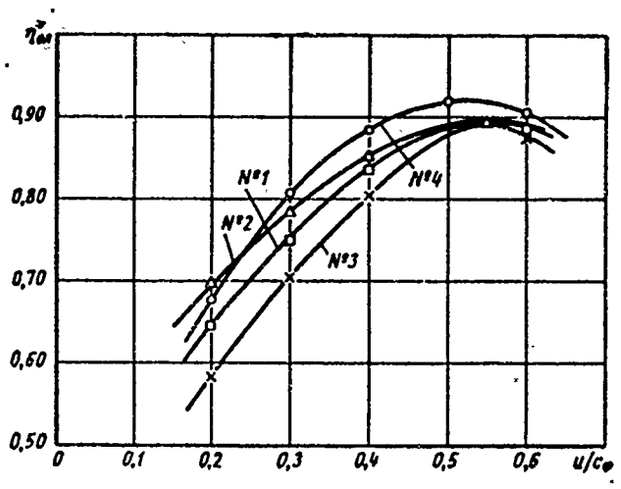

Fig. 224. Comparison of the effectiveness of four stages designed with various laws of twisting according to the experiments of N. A. Bykov [10]. Curves: No. 1 – □ – □ – $c_{u1}\cdot r$ = const; No. 2 – Δ – Δ – $\Delta\alpha_1 = -5^\circ$; No. 3 – x – x – $\Delta\alpha_1 = +6^\circ$; No. 4 – O – O – combined (nozzle cascade $c_u r$ = const, rotor wheel of stage $\Delta\alpha_1 = +6^\circ$).

The considered stages had identical data on the mid-diameter ($\alpha_{1\ ср} = 20^\circ$; $\rho_{ср} = 0.3$; $\varepsilon_2 = p_2/p_0$ = = 0.435) and an equal ratio of θ = = 6. It should be emphasized that at

the indicated pressure ratio the velocities in the flow area of the stage were transonic. Thus, the comparative estimates of the various methods of twisting that were obtained in this work are characteristic for transonic velocities. The advantages of stage in No. 4, in the opinion of the author, are explained by the lowering of losses in the root and peripheral sections of the moving cascade, since in this stage the reaction in the root is high; the losses at the periphery were lowered in connection with the increase of the entrance angles β_1. The sharp lowering of effectiveness of stage No. 3 in off-design conditions indicates that this twisting of the nozzle cascade, with an increasing outlet angle α_1 to the root, leads to an intense decrease of the angles of entrance to the moving cascade at lowered u/c_{Φ}. Furthermore, in this stage the specific flow rates of gas in the peripheral sections are decreased, while in the root sections, where the losses are essentially higher, they increase. The impractical distribution of flow rates is quite evident in off-design conditions. One should note the satisfactory characteristics of stage No. 2, which was designed with an untwisted nozzle cascade and a moving cascade that was profiled in accordance with the change of the angle $\alpha_1(\bar{r})$.

The results of a detailed investigation of the structure of the flow in the four stages show that the sharp divergence of the efficiency curves with decreased u/c_{Φ} is also explained by the different influence of compressibility (M number) on the characteristics of nozzle and moving cascades that were profiled by various methods.

When considering the comparative investigations of the laws of twisting, one should bear in mind that the above-described results, and also other investigations, [18], [47], and [132], are of particular value and cannot be generalized.

The influence of the method of profiling stages with large flare essentially depends on the geometric and performance parameters of the stage. In connection with the fact that systematic experiments with different θ, M, Re, etc. were not conducted, the recommendations that follow from the experiments of individual authors bear a random character. The results of work [10] should be considered in this light, which is also confirmed by V. M. Akimov's experiments.

Influence of the Degree of Reaction

In the experimental investigation of stages with twisted blades, significant attention is allotted to the influence of the reaction. Since with the radial arrangement of nozzle blades the change of the reaction along the radius hardly

depends on the law of twisting, the study of the influence of the reaction reduces to an estimate of the correctness of the selection of the root reaction.*

As a rule, the reaction in the root section is small and positive. It is known that if $\rho_к < 0$, then in the root sections there can appear a separation. In this case, through the root clearance there is developed an intense suction of gas. However, a considerable positive reaction in the root section can also negatively affect the economy of a stage due to the increase of leakages through the radial clearance, since this increases the reaction at the periphery. At the same time, an increase of the root reaction lowers the leakages through the sealing (or through an unsealed radial clearance) of the nozzle cascade. The root reaction should be selected with the design of the flow area taken into account, depending upon the magnitude and method of sealing the radial clearances of the nozzle and moving cascades, which are presented in § 41.

A number of works show that the root reaction essentially affects the efficiency of a stage whose cascades are aerodynamically improved.

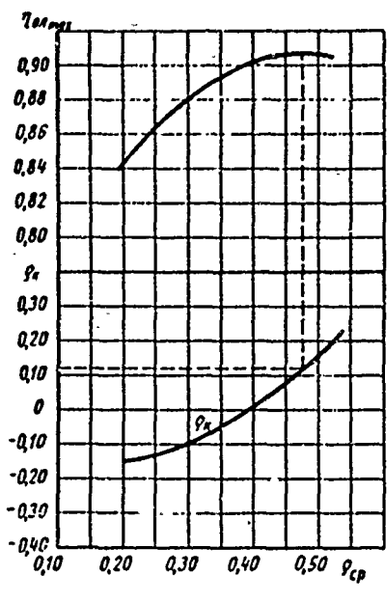

Fig. 225. Influence of the reaction in the root section $\rho_к$ on the maximum efficiency $\eta_{оп}$ of a stage, according to the experiments in [106].

The investigation of a stage with $\theta = 4.5$ [106], at low velocities, showed that for the given specific conditions the optimum degree of the reaction in the root section is on a level of about 10% (Fig. 225).

It should be emphasized that these experiments give only tentative values of the root reaction, which must be selected in every separate case, considering the specific peculiarities of performance of the given stage.

Experiments conducted at MEI did not indicate a clear dependence of stage efficiency on the reaction in the root section. Tests of a considerable quantity of stages with different variants of MEI cascades showed that a small positive reaction in the root section with good sealing of the nozzle cascade provides maximum stage efficiency (see Chapter IV).

---

*Selection of the root reaction for optimum-flare stages of steam turbines is substantiated in Chapter VIII.

Of interest are the results of an investigation of a group of stages with long blades at the NZL laboratory [18], [19]. For the purpose of studying the influence of the reaction on efficiency, tests were conducted with three stages having a different number of rotor blades. On the basis of these data, a decrease of the reaction in the root section to -6% does not lead to a noticeable lowering in efficiency, which coincides with the MEI results.

Influence of Nozzle Blade Twisting

Above, in § 39, it was indicated that a number of stages (with not too small θ) may be manufactured with cylindrical (untwisted) blades. Appropriate experiments were conducted by LMZ, MEI, TsKTI, and NZL (see Chapter VIII). The experiments indicated that the application of untwisted nozzle cascades, even with large stage flare, provides a high stage economy.

As shown in § 39, the distribution of angles α_1 along the radius in such cascades is linear, and the change of the velocity circulation is relatively small. Consequently, a cascade of constant profile comparatively little differs from a nozzle cascade that is twisted under the condition of $c_{u1}r$ = const.

The TsKTI investigation [7] was conducted with two stages, $\theta = 2.95$, the nozzle blades of which were untwisted. The variation of cos α_1 along the radius for the nozzle cascade was close to linear. The rotor blades were twisted under the condition of a constant heat drop along the radius. TsKTI profiles TH-2 and T-3 were used for the stage. The moving cascades were designed in two variants: in stage No. 1 the blade chord did not vary with respect to height, while in stage No. 2 it decreased toward the tip. The relative pitch of the rotor blades in the peripheral section for stage No. 1 amounted to $\bar{t}_п = 1.062$, and for stage No. 2 it was $\bar{t}_п = 1.416$.

The experiments were conducted at low velocities ($M_{c1} \approx 0.25$) and Re_{c1} numbers equal to $1.9\text{-}3.8 \cdot 10^5$. The efficiency curves of the two stages are shown in Fig. 226. The maximum values of efficiency of the two stages were approximately identical and equal to $\eta_{оп} \approx 91\%$ (including the losses due to leakages in the peripheral section). This result shows* that at low velocities it is quite permissible

*Somewhat overestimated values of efficiency and optimum $x_ф$ were obtained in these experiments, and the independence of efficiency from the Reynolds number was found in the range of $Re_{c1} = (1.9\text{-}3.88) \cdot 10^5$, whereas the experimental points of $\eta_{оп}$ which refer to smaller Re_{c1}, are higher as a rule. [FOOTNOTE CONT'D ON NEXT PAGE]

to employ of large relative pitches in the peripheral sections. Furthermore, the described experiments confirm that the application of nozzle blades of constant profile is permissible also for large-flare stages ($\theta = 2.95$).

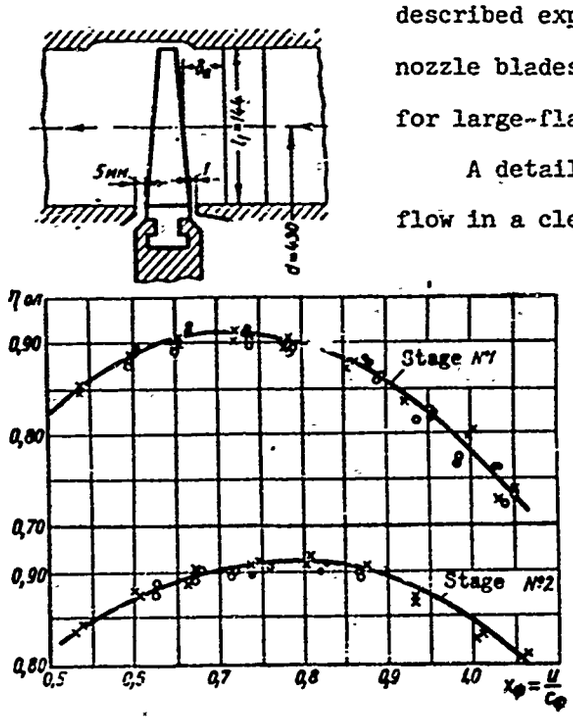

Fig. 226. Dependence of the value of blade efficiency on x_φ for two stages with nozzle blades of constant profile. With $\theta = 2.95$ $M_{c1} = 0.13$ to 0.25. Stage No. 1 with constant blade chord; stage No. 2 with variable blade chord. According to TsKTI data: points: O – O for $Re_{c1} = 1.9 \cdot 10^5$; x – x $Re_{c1} = 2.5 \cdot 10^5$; O – O $Re_{c1} = 3.8 \cdot 10^5$.

A detailed investigation of the structure of the flow in a clearance and behind a stage was conducted by Kh. L. Babenko. The distribution of the reaction in the clearance (Fig. 227) was close to the calculated value whereby a change of the distance of the measuring section from the trailing edges of the nozzle cascade practically did not lead to a change of the curves for $\rho(r)$. This result is not confirmed by the data on the investigation of annular cascades in §§ 35 and 36.

Figure 227 also shows the distribution of pressure and angles in a clearance and behind a stage. One should note the uniformity of the fields of static and total pressures behind the moving cascade. The diagram of total pressures in the clearance also is characterized by satisfactory uniformity.

At the same time, the outlet angles of the nozzle cascade differ essentially from the computed values, whereby in the root sections and at the periphery there is noted a sharp growth of angles α_1, which may be explained by the increase of losses in these zones.

The results obtained at the NZL laboratory for three stages with $\theta = 5$, which are shown in Fig. 228, somewhat contradict the TsKTI data. The values of the angles in different sections are the following:

[FOOTNOTE CONT'D FROM PRECEDING PAGE]

It may be assumed that these deviations are connected with a certain error in the calibration tests for determining the losses due to disk friction and the bearing losses.

Stage	№ 1	№ 2	№ 3
Ratio θ . .	5	5	5
Angle $\alpha_{1эф}$ . . .	17°; 20° 50'; 24° 50'	19°; 21° 20'; 24° 18'	17° 43'; 19° 20'; 23°
Angle $\beta_{2эф}$	30°; 26° 26'; 22° 25'	30°; 26° 26'; 22° 25'	30°; 26° 26'; 22° 25'

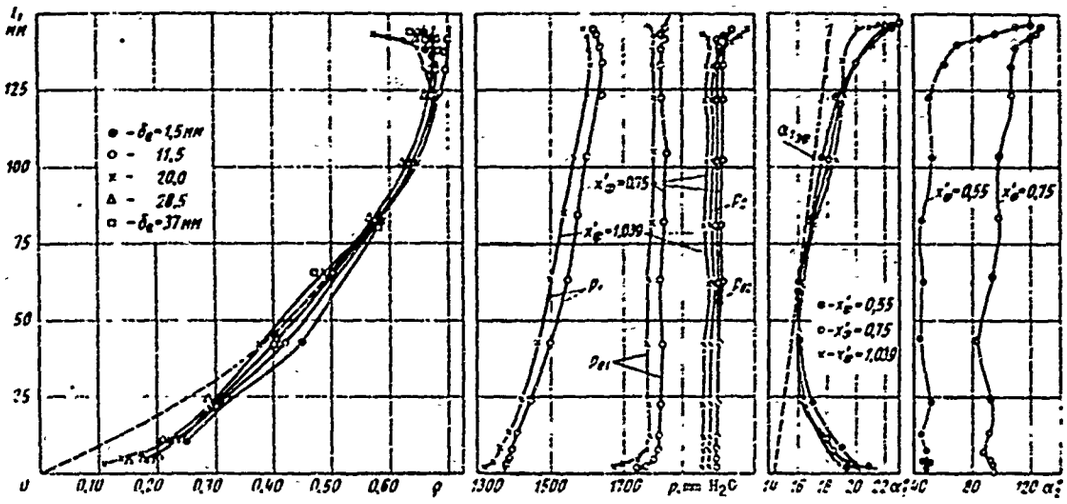

Fig. 227. Distribution of reaction, static and total pressures along radius, and distribution of angles in clearance and behind stage No. 1 (see Fig. 226). Curves: —— (solid) experiment; – – – – (dotted line) – calculation.

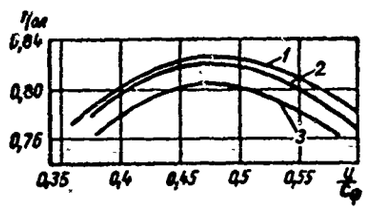

Fig. 228. Results of the investigation of three stages with nozzle blades twisted under the condition of c_{u1} r = const (stage No. 1) and blades of constant profile (stages No. 2 and No. 3). NZL experiments.

Stage No. 1 was designed with twisted nozzle blades; stages No. 2 and No. 3 had cylindrical nozzle blades. The efficiency curves of stages No. 1 and No. 2 practically coincide, and the efficiency of stage No. 3 was 1.8-2.0% lower. The decrease in efficiency of this stage is explained not so much by the appearance of flare losses, as noted by the author of [19], but by the decrease of the outlet angle α_1, which led to a lowering of the reaction and the entrance angles of flow to the rotor blades.

These experiments were also conducted at low velocities (M_{c1} = 0.4 to 0.45) and Re_{c1} numbers (2.5 to 3.0)10^5. The obtained results, on the whole, confirm the MEI conclusions concerning the practicality of employing stages with untwisted nozzle blades in stages with $\theta \geq 4$ to 5 at subsonic velocities along the entire height of the nozzle cadcade (see Chapter IX).

Influence of Individual Design Elements

The efficiency of a stage does not only depend on the way the blades are twisted. An essential influence on its effectiveness is rendered by a number of design elements:

a) the axial clearances between cascades;

b) the radial clearances between the stator (or rotor) and the blade tips, and the way they are sealed;

c) the amount of overlap;

d) the wire connections,* and also the methods of organizing the flow before and after the stage.

In connection with the evident difficulties of theoretical research, the influence of the enumerated elements was studied experimentally by different authors [5], [7], [47], [66], [106].

Influence of Axial Clearances

Detailed investigations of the influence of open and closed axial clearances on the efficiency of a large-flare stage were performed at the laboratories of BITM, LMZ, TsKTI, and MEI.

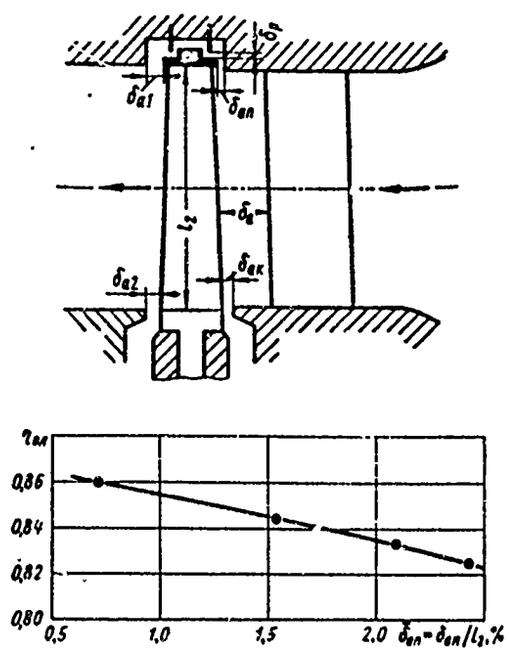

Fig. 229. Influence of a peripheral open axial clearance on the efficiency of a stage with twisted blades. According to LMZ experiments at $Re_{c1} = 4.5 \cdot 10^5$; $\theta = 4.6$; $\bar{\delta}_a = 3.4\%$; $\bar{\delta}_p = 8.1\%$.

Stage efficiency varies noticeably, depending upon the size of the open axial clearance at the tip δ_{an} (Fig. 229) for sufficiently large relative radial clearances δ_p. Actually, as may be seen from Fig. 229, the change of blade efficiency as a function of an open peripheral clearance, according to LMZ experiments, follows a linear law.

It is known that when $\bar{\delta}_{an} > \bar{\delta}_p$ the efficiency of a stage depends slightly on $\bar{\delta}_a$, since in this case the losses due to leakage over the shroud are already determined by the radial clearance.

Experiments conducted at LMZ by

*The influence of wire connections is not considered here.

A. O. Lopatitskiy and M. A. Ozernov confirmed the essential influence of an open axial clearance on the reaction at the tip $\rho_п$ and in the root section $\rho_к$ (Fig. 230). With the increase of $\bar{\delta}_{ап}$ the peripheral reaction $\rho_п$ drops. The reaction in the root section $\rho_к$ as a function of $\bar{\delta}_{ап}$ varies irregularly: in the beginning, with the growth of $\bar{\delta}_{ап}$ the reaction $\rho_к$ increases somewhat, and then decreases. If the root reaction depends upon the given clearance,*

$$\bar{\delta}_{экв} = \frac{1}{l_2}\sqrt{\frac{1}{\frac{1}{\delta_р^2}+\frac{1}{\delta_{ап}^2}+\frac{1}{\delta_{ак}^2}}},$$

in accordance with the LMZ experiments, in a wide range of variation of $\bar{\delta}_{пр}$, $\rho_к$ remains constant.

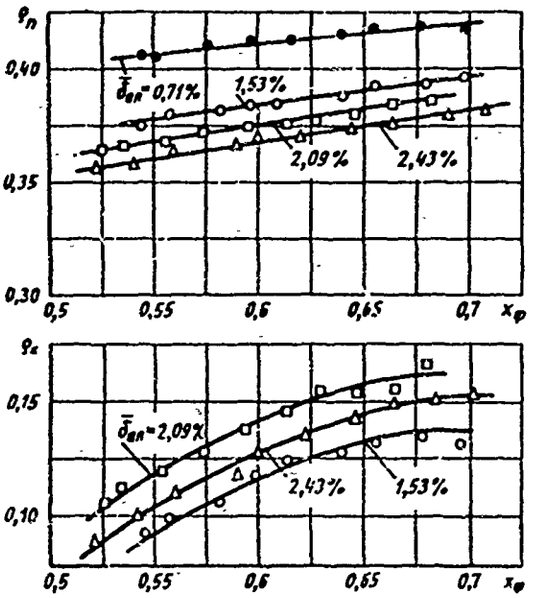

Fig. 230. Influence of a peripheral open axial clearance $\bar{\delta}_{а\,п}$ on the reaction in the root and peripheral sections, depending upon $x_ф$. LMZ experiments with $Re_{c1} = 5\cdot10^5$; $M_{c1} = 0.5$; $\theta = 4.6$.

In the TsKTI project quoted above [7], the influence of the total axial clearance δ_a (Fig. 226) which varied from 12 to 37 mm was investigated. The relative axial clearance $\bar{\delta}_a = \frac{\delta_a}{l_2}$ varied correspondingly from $\bar{\delta}_a$ = 8.3 to 25.5%. In this range of variation of $\bar{\delta}_a$, the efficiency continuously decreased, and at $\bar{\delta}_a$ = 25.5% it decreases by 1-1.5%. It should be borne in mind that the TsKTI stage was designed with a high reaction in the root section.

The experiments of LMZ, BITM and MEI confirm the existence of an optimum closed axial clearance in large-flare stages.

Thus, for instance, for a stage with $\theta = 4.6$, maximum efficiency was obtained when $\bar{\delta}_a$ = 15% (Fig. 231). It was determined that the total axial clearance essentially affects the degree of reaction in the peripheral sections and especially in the root sections (Fig. 232).

*The formula for $\bar{\delta}_{экв}$ is approximate here. See Chapter II.

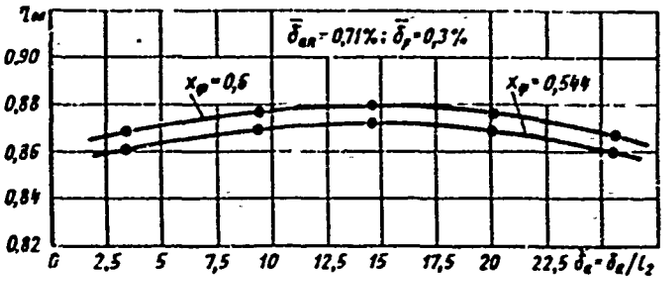

Fig. 231. Change of blade efficiency, $\eta_{ол}$, depending upon total axial clearance, δ_a. According to LMZ experiments with $Re_{c1} = 5 \cdot 10^5$; $M_{c1} = 0.5$; $\theta = 4.6$; $\bar{\delta}_{a\,л} = 0.71\%$; $\bar{\delta}_p = 0.3\%$.

A change of the total axial clearance also affects the efficiency of a stage for several reasons: a) in connection with the change of the peripheral nonuniformity of the velocity field at the entrance to the moving cascade; b) due to twisting of the flow and the corresponding change of the angles of entrance to the moving cascade, the reaction, and the mean velocities in absolute and relative motion; c) in connection with the change of losses due to friction in the clearance and, in certain cases, with the appearance of separation; c) in connection with the eddy effect of the stage (see § 41), which appears in the nonuniform distribution of total energy along the radius, whereby the degree of this nonuniformity increases as the clearance increases. The overall influence of all these factors predetermines the shape of the curve for $\eta_{ол} = f(\bar{\delta}_a)$, which has a different character, depending on the geometric and performance parameters of the stage.

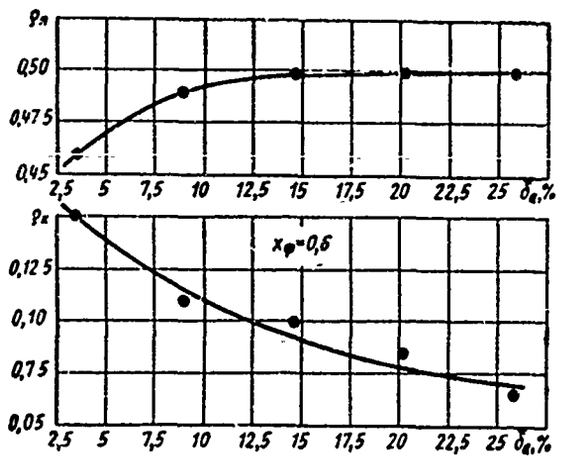

Fig. 232. Change of the root and peripheral reaction of a stage, depending upon $\bar{\delta}_a$. According to LMZ experiments with $\theta = 4.6$; $x_ф = 0.6$; $Re_{c1} = 5 \cdot 10^5$; $M_{c1} = 0.5$.

Thus, with the increase of δ_a, the losses in the clearance increase; these losses are connected with the balancing of pitch nonuniformity, the losses due to friction, and losses caused by the eddy effect. However, the losses in the moving cascade, which are caused by the nonuniformity of the velocity fields and angles at entrance, and also the profile and end losses in connection with the growth of the entrance angles β_1, decrease in this case.

In certain experiments it was revealed that with a negative reaction in the root section the optimum axial clearance increases.

The qualitatively different influence of the axial clearance, depending upon the reaction, is physically explained by the fact that when $\rho_K < 0$ the balancing of the flow behind the nozzle cascade, which occurs at considerable distances behind it, promotes an increase of efficiency. Moreover, into the moving cascade there enters an equalized flow with large angles β_1, and the losses in it are lowered. However, in this case the losses due to friction in the clearance increase.

With a high reaction, the balancing of the flow in the clearance plays a smaller role, since the moving cascade is convergent and turns out to be less sensitive to nonuniformity and changes of angle β_1 at the entrance. In this case the additional losses due to friction in the clearance are decisive.

An increase of the axial clearance has a favorable effect on the vibration reliability of the moving cascade. Consequently, increased axial clearances should be applied if it does not lead to a lowering of stage efficiency.

The experiments of MEI and BITM, just as the LMZ experiments, pointed out the existence of an optimum axial clearance which, obviously, is physically more justified than a continuous change of efficiency as a function of the clearance.

Influence of Radial Clearance

The stage efficiency of a gas and steam turbine is considerably influenced by the radial clearance. The long rotor blades in many cases are designed without shrouding, and leakage is decreased in them by decreasing and sealing of the radial clearance between the stator and the tips of the rotor blades. Sealing of the radial clearances between the nozzle cascade and rotor is also an important problem.

The influence of the radial clearance on the efficiency of an unshrouded stage was investigated by BITM, LMZ, NZL, KAI, TsKTI, and MEI. In addition, the TsKTI conducted investigations of the influence of the radial clearance of nozzle cascades. The losses in the radial clearance of a moving cascade besides the size of the clearance, are influenced also by a number of geometric and performance parameters of the stage, which determine the structure of the flow in the peripheral sections. These parameters include the pitch, chord, and shape of the profile in the peripheral section, the flare of the moving cascade and its relative height, the angles of inlet and outlet of flow, and the Re and M numbers in the peripheral section. Thus, of decisive value are the parameters which determine the intensity of the secondary flows and the reaction at the tip.

The physical structure of the three-dimensional flow in the radial clearance of unshrouded cascades has been studied insufficiently, and the existing methods

of calculation mainly use a continuity equation with experimental correcting factors, or purely empirical dependences whose field of application is limited.

The use of the continuity equation calculation is based on the assumption that the losses caused by a radial clearance are determined mainly by the leakage of gas. This assumption is a considerable simplification of the problem, in the solution of which it is necessary to consider the influence of leakage of the stagnant layer from the concave surface to the convex surface over the stator and through the open end of the blade.

The existence of the dependence of losses in the radial clearance of rotor blades on the above-mentioned parameters is confirmed by experiments. Figure 233a gives corresponding results that were obtained by LMZ and TsKTI. The figure shows the relative decrease in stage efficiency, $\Delta\eta_{ол} = \Delta\eta_{ол}/\Delta\eta_{ол0}$ ($\eta_{ол0}$ is the stage efficiency with $\bar{\delta}_p = 0$), depending upon the relative radial clearance for different stages with negative (TsKTI experiments) and positive (LMZ experiments) overlap. One should note the stratification of the experimental points that refer to stages with different flare θ and with a different reaction on the mid-section.

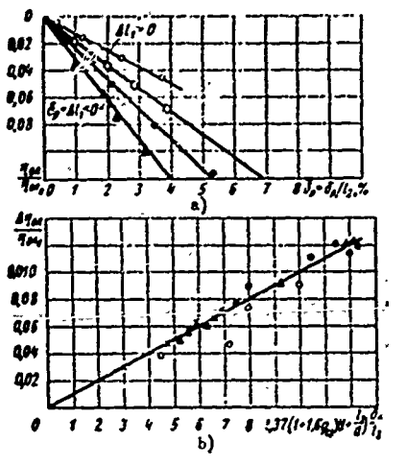

Fig. 233. Influence of radial clearance on the efficiency of a stage with twisted, unshrouded blades: a) change of efficiency, depending upon $\bar{\delta}_p$; TsKTI experimental points: □ – □ – ρ_{cp} = 16%; θ = 12.4; ● – ● – ρ_{cp} = 22%; θ = 7.7; Δ – Δ – ρ_{cp} = 50%; θ = 4.5; LMZ experimental points: O – O – ρ_{cp} = 60%; θ = 6.8; b) generalized curve of losses in radial clearance, according to A. Ye. Zaryankin; experimental points: O – O – θ = 12.4; x – x – θ = 11; ● – ● – θ = = 7.7; ▲ – ▲ – – 4.5.

The influence of flare is physically explained by the fact that with the change of θ the reaction in the peripheral section changes (for the given values of ρ_K in the root section), and the transverse and radial pressure gradients, which determine the structure of the secondary flows, also change in the channel at the tip. An increase of the reaction on the mid-section leads to an increase of the reaction on the periphery and consequently, to an increase of leakage.

Of interest is an estimate of the influence of blade twisting on the losses in a radial clearance. A comparison shows that for small relative clearances the efficiency of a stage with twisted blades is higher; with the increase of the clearance, the advantage of twisted blades decreases and it disappears when the

clearances become large.

The results of the experiments make it possible to conclude that in a wide range of variation of $\bar{\delta}_p$ the dependence $\overline{\Delta\eta}_u(\bar{\delta}_p)$ can be assumed to be linear.

The losses due to the radial clearance depend on the performance parameters: $u/c_{ф}$, Re, and M. The influence of $u/c_{ф}$ is explained by the fact that when this parameter changes, the reaction in all sections of the stage changes, including the reaction at the periphery; the intensity of the secondary flows, which depends on the entrance angle β_1, also changes. The Re and M numbers render an influence on the intensity of the secondary flows in the peripheral sections of the channel and in the clearance. However, the influence of the last two factors has not yet been studied.

The losses due to the radial clearance are decreased by applying the various methods for aerodynamic sealing of the clearance which are shown in Fig. 234. An investigation of the influence of tapering blade ends (variants I and Ia) made at the NZL laboratory proved that this method for lowering of leakage did not give the expected results. However, the application of tapered blades in an unshrouded stage design is practical in certain cases, since it makes it possible to apply smaller radial clearances in real machines. It should also be borne in mind that tapering that is done on the back provides a certain increase of stage efficiency. The experiments performed at NZL confirmed that the optimum value of undercutting amounts to 2-3.0 mm, depending upon the radial clearance.

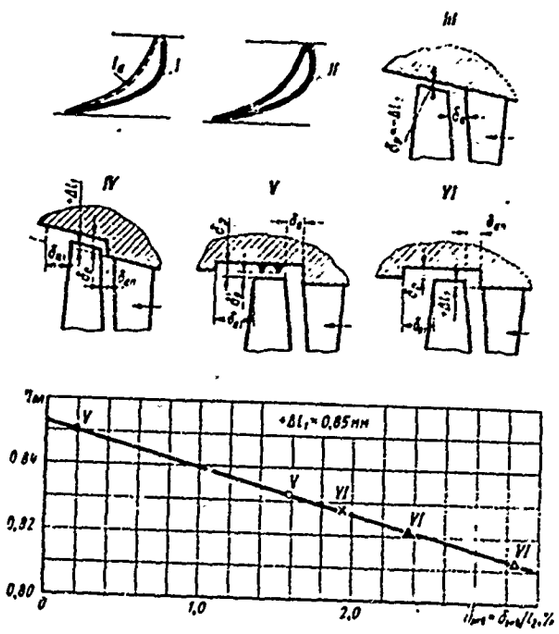

Fig. 234. Methods for sealing the radial clearance of unshrouded rotor blades and their influence on efficiency, depending on the given clearance, $\bar{\delta}_{окв}$. LMZ experiments. For variant V: point O – δ_p = 5.7 mm; δ_{a1} = = 18 mm; $\delta_a = \delta_p$ = 3 mm; ● – δ_p' = 0.275 mm; δ_p = 2.7 mm. For variant VI: point x – δ_a = = $\delta_p = \delta_{a1}$ = 3 mm; ▲ – $\delta_a = \delta_p$ = 3 mm; δ_{a1} = = 18 mm; Δ – δ_a = 3 mm; δ_p = 1.0 mm; δ_{a1} = = 18 mm. Height of rotor blade, l_2 = 89 mm.

The best results are provided by tapering that is accomplished along the entire periphery of a blade at the tip (see variant II

2

in Fig. 234). The end of the blade has a recess (chamber) which creates an aerodynamic clearance sealing without distortion of the profile at the tip.

The radial clearance can be organized differently by making a negative (variant III) or positive (variant IV, Fig. 234) overlap. In the first case the stator has a smooth cylindrical or conical surface. In the second case the surface has grooves of steps. An intermediate variant of V is possible with zero overlap at the entrance to the moving cascade. An experimental check in a turbine showed that the positive overlap (variant IV together with the circular taper according to variant II) gives the best results. This method of setting up a radial clearance is especially expedient to apply in stages with relatively low blade heights. A check of the other variants confirms this conclusion.

The experimental data shown in Fig. 234 were obtained at the LMZ laboratory. The illustration represents the dependence of stage efficiency on the given clearance, which is determined by the formula

$$\bar{\delta}_{\text{экв}} = \frac{1}{l_2}\sqrt{\frac{1}{\delta_{an}^2} + \frac{1}{\delta_p^2} + \frac{1}{\delta_{al}^2}}.$$

Thus, for example, sealing according to variant V for large clearances δ_p has an essential advantage, while for small clearances it yields to variant III. An investigation of variant V indicated the dependence of its dependence on the axial clearance.

Considering that the losses in a radial clearance depend essentially on the reaction at the tip in stages with unshrouded rotor blades, nozzle blades inclined toward the flow or curved blades should be employed (see §§ 37-39). For a selected reaction in the root section, the reaction at the tip can thus be considerably decreased.

Several empirical formulas are proposed for calculating the losses in a radial clearance. An attempt to generalize some of the available data, which was undertaken by A. Ye. Zaryankin, indicated that many of the points lie on a straight line which corresponds to the following equation (Fig. 233b)

$$\overline{\Delta\eta}_{oi} = \frac{\Delta\eta_{oi}}{\eta_{oi\,0}} = a(1 + b\rho_{cp})\left(1 + \frac{l_2}{d}\right)\frac{\delta_p}{l_2},$$

where ρ_{cp} is the reaction on the mean section; a, and b are experimental coefficients that depend on the method of organization of the radial clearance (Fig. 234). For

stages with negative overlap overlap and smooth casing surface (Fig. 234, III), it may be assumed that a = 1.37 and b = 1.6. For positive overlap and with aerodynamic sealing of the clearance, and also with inclined nozzle blades, the coefficients a and b are lowered.

Influence of Overlap and Shroud

I. I. Kirillov investigated the influence of positive and negative overlap on the performance of a stage. The curves of the decrease in efficiency which are illustrated in Fig. 235 depending upon the radial clearance, graphically depict the especially sharp lowering in efficiency with the growth of δ_p for negative overlap (see variant III in Fig. 235). These data once again prove that unshrouded rotor blades should be designed with positive overlap and an aerodynamically sealed minimum radial clearance.

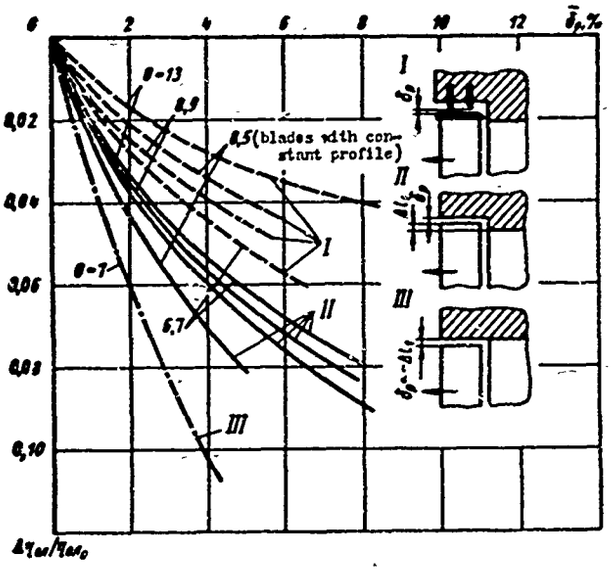

Fig. 235. Influence of radial clearance for shrouded and unshrouded moving cascades on the efficiency of stages with different flare, according to experiments of I. I. Kirillov. For $Re_{c1} = (3 \text{ to } 4)\cdot 10^5$; M_{c1} = 0.3 to 0.5. Variant 1 – with shroud and positive overlap; II – without shroud and with positive overlap; III – without shroud and negative overlap.

The application of shrouds with well-developed sealing on rotor blades makes it possible to essentially increase the efficiency of a stage. Thus, for instance, according to the experiments of I. I. Kirillov, the application of a shroud in a stage with θ = 4.5 provided a 3 to 3.5% increase in efficiency for an optimum velocity ratio of x_{Φ} = 0.56.

For other stages, the influence of a shroud may be estimated by means of Fig. 235 (variants I and II). Even with small radial clearances, the installation of a shroud considerably increases the stage efficiency. The experiments of A. M. Zavadovskiy also confirm an essential increase in stage efficiency resulting from the application of shrouds with shroud seals. For small relative radial clearances, a shroud increases the efficiency by 2-2.5%, and for large ones, by 3-3.5%.

A shroud does not only lead to a decrease of leakage; a shroud removes the

additional end losses that appear in the flow around the open ends of a blade. This conclusion is confirmed by LMZ experiments: an unshrouded stage with a small radial clearance, δ_p = 0.27 mm, has an efficiency that is 2% lower than a stage with a shroud.*

The influence of the radial clearance and shroud for a nozzle cascade was investigated at TsKTI. Three diagrams of the test variants are shown in Fig. 236 (I, II, III). The results of stage tests showed (Fig. 236a) that a shrouded nozzle cascade with two sealing chambers has a higher efficiency in a wide range of variation of the relative radial clearance, $\delta_{p\,1} = \frac{\delta_{p\,1}}{l_1} \cdot \frac{d_y}{d}$ (Fig. 236a). A study of the influence of the reaction in the root section showed (Fig. 236b) that an increase $\rho_к$ from 0 to 14% noticeably increases the stage efficiency, since this decreases the pressure drop in the radial clearance.** The application of a developed shroud seal with number of chambers z > 2 considerably increases stage efficiency. It is natural that the maximum permissible decrease of the diameter of the shroud seal (variant IV), which is done in the KTZ designs, promotes an increase in efficiency.

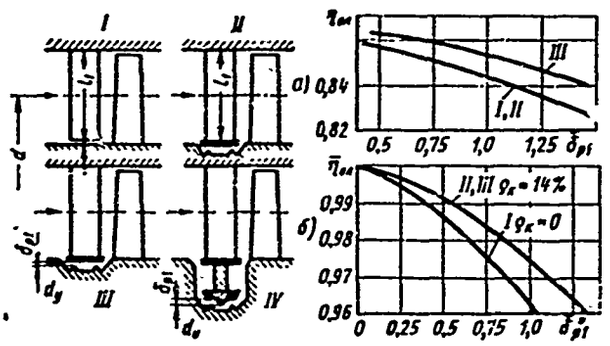

Fig. 236. Various methods for sealing the radial clearance of a nozzle cascade: a) influence of given radial clearance, $\delta_{p\,1} = \delta_{p\,1}/l_1 \cdot d_y/d$, on stage efficiency; b) influence of given radial clearance, $\bar{\delta}^*_{p\,1} = \delta_{p\,1}/\sqrt{z}$ (z is the number of sealing chambers), on relative stage efficiency. According to experiments of V. G. Tyryshkin and B. A. Shirkov (TsKTI), with θ = 4.5, Re_{c1} = (3 to 4)·10^5, and M_{c1} = 0.3 to 0.35.

In connection with the noted influence of the root reaction, we should once again emphasize the expediency of the application of nozzle blades inclined toward the flow, which ensure a minimum reaction in the upper sections.

---

*The model of turbine stage ПВК-200 that was tested in the LMZ laboratory, which was designed with an MEI untwisted nozzle cascade TC-2A, has a high efficiency ($\eta^*_{ол}$ = 0.93 to 0.92, without taking into account the losses with the outlet velocity) with θ = 4.6.

**In Fig. 236b, the relative stage efficiency $\bar{\eta}_{ол} = \eta_{ол}/\eta_{ол_0}$ is represented depending upon the relative radial clearance, $\bar{\delta}^*_{p\,1}$; the magnitude of efficiency $\eta_{ол_0}$ characterized the stage when δ_p = 0.

The effectiveness of a stage also depends on the correct selection of the upper and lower overlap, which, as indicated, can vary from negative to positive values in an unshrouded stage.

Investigations showed that the upper overlap in unshrouded stages can vary in certain limits from $\overline{\Delta l}_1 = \frac{\Delta l_1}{l_2} = +0.01$ to $+0.02$, whereby the stage efficiency in range of variation of Δl_1 practically does not change.

The lower overlap should also be always positive, especially for large axial clearances ($\overline{\Delta l}_K > 0$); the limits of its variation for certain types of stages were established experimentally and amount to $\overline{\Delta l}_K = 0.005$-$0.015$ [6], [16].

The influence of the upper overlap in stage with shrouded blades was subjected to an experimental study [5], [47]. This problem was also solved theoretically [39], [47] (see also § 22).

For a stage that has no shroud seals, A. M. Zavadovskoy recommends that the upper overlap be determined by the following formula:

$$\overline{\Delta l}_1 = (0{,}7 \div 0{,}8)\, k_{мд} \bar{\delta}_{ан}^{1,3},$$

where

$$\overline{\Delta l}_1 = \frac{\Delta l_1}{l_1};\ \bar{\delta}_{ан} = \frac{\delta_{ан}}{l_2}\left(1 + \frac{1}{\theta}\right)\frac{1}{\sin\beta_2}$$

is the relative open axial clearance; $k_{МД}$ is a coefficient that characterizes the flow swirl in the clearance, which is determined by the formula

$$k_{мд} = \frac{\theta \operatorname{ctg} \alpha_1}{1 + \theta}.$$

Influence of the Inlet Conditions and the Shape of the Meridional Contour of a Nozzle Cascade

In conclusion, we shall consider the influence of the conditions of inlet to a nozzle cascade and, in particular, the shape of the diffuser. The indicated investigations were conducted at the LMZ and BITM laboratories, the LMZ experiments involved the study of the influence of overlap at the entrance to the nozzle cascade shown in Fig. 237. With the increase of distance δ_2 and the decrease of overlap $\Delta\bar{l}_0$, the stage efficiency increases (Fig. 237) with a corresponding decrease of losses in the nozzle cascade (see § 35, Fig. 213).

It should be noted that the reactions in the peripheral and root sections essentially depend on the magnitude of overlap Δl_0 and the distance (clearance) δ_L.

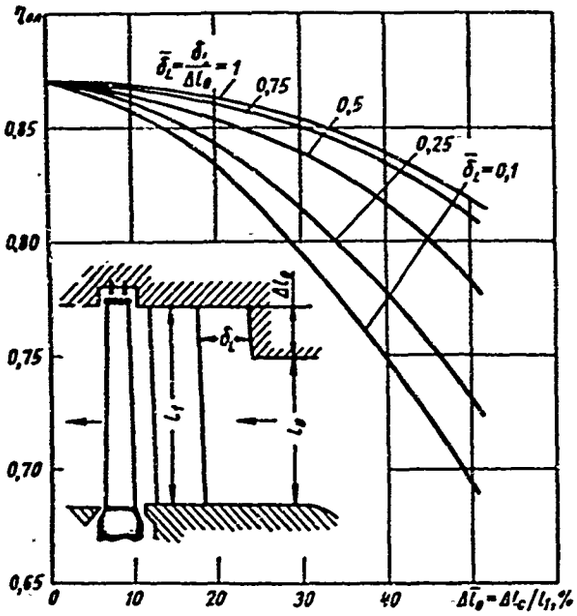

Fig. 237. Influence of overlap at the entrance to a nozzle cascade on the efficiency of a stage with various clearances $\bar{\delta}_L$. LMZ experiments with $Re_{c1} = (5 \text{ to } 6)\cdot 10^5$, $M_{c1} \approx 0.5$, and $\theta = 4.6$.

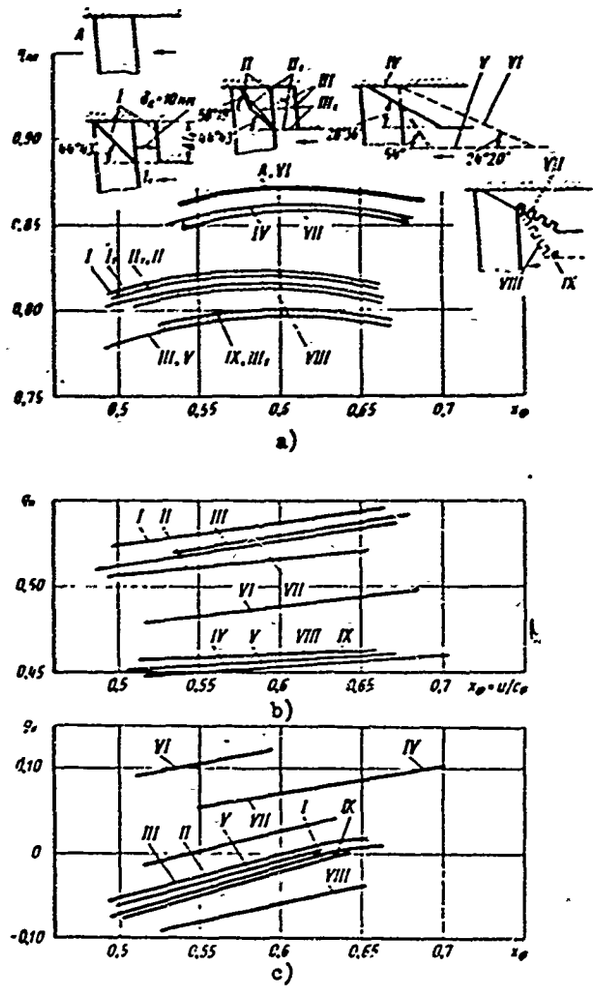

Fig. 238. Influence of the shape of the upper contour of a nozzle cascade on the stage characteristics: a) on stage efficiency; b) on degree of reaction at tip; c) on degree of reaction in root section. LMZ experiments. $Re_{c1} = (5 \text{ to } 6)\cdot 10^5$; $M_{c1} \approx 0.5$; $\theta = 4.6$.

Actually, an increase of the clearance δ_L with constant overlap leads to an increase of the reaction at the tip and in the root section. An increase of overlap lowers $\rho_п$ and $\rho_к$ at the given value of the clearance δ_L. An expecially intense growth of the reaction occurs with the growth of δ_L for small clearances, $\bar{\delta}_L \leq 40\text{-}60\%$.

A further development of this investigation is the detailed study of the influence of the shape of the meridional contour of a nozzle cascade on efficiency and the reaction, which was performed by LMZ. Diagrams of the test variants and results of the investigation are shown in Fig. 238. Maximum stage efficiency is attained with a cylindrical stage contour (variant A). In the presence of overlap at the entrance ($\Delta l_0 > 0$), the best results were exhibited by the variant of contour VI with a small cone angle of the diffuser before the nozzle cascade. Variants A and VI have practically identical efficiency.

The least economic and practically identical variants were III, III_1, V, and

IX, which are characterized by large cone angles of the upper contour either before the nozzle cascade (variants V and IX), or inside the cascade (variants III and III_1). A certain increase in stage efficiency at large cone angles was attained by making annular grooves on the generatrices of the diffuser (variants VIII and IX). However, at moderate cones angles, less than 50°, the application of the annular grooves proposed by V. K. Migay results in a negative effect (see variants IV and VII).

A comparison of variants II_1 and III_1 makes it possible to establish the expediency of increasing the cone angle of the upper contour toward the nozzle cascade exit; variant II_1 showed an increase in efficiency by approximately 1.5% (Fig. 238a).

The presence of an axial clearance at the entrance to a nozzle cascade, δ_L, has an essential effect only with small cone angles of the upper contour. With large angles, a small axial clearance hardly affects the efficiency of a stage (see variants I and I_1, II and II_1, III and III_1).

The considered experiments distinctly show the very considerable influence of the cone angle of the diffuser before a cascade and the upper contour of the cascade itself.

The results of the experiments also convince us of the fact that when the relative overlap at the entrance is $\overline{\Delta l}_0 = 0.344$, a change of the clearance from $\overline{\delta}_L = 0$ to $\overline{\delta}_L = 0.33$ practically does not change the characteristics of the stage, if the channel has meridional profiling, which ensures a smooth transition from the height l_0 to the outlet height l_1 (see Fig. 237).

The change of the reaction in the peripheral and root sections clearly confirmed that the shape of the upper contour essentially affects the quantities $\rho_п$ and $\rho_к$ (Fig. 238b and c). The maximum values of the reaction at the tip $\rho_п$ and the minimum values in the root section were obtained for variants I, II, and III, which have conical-cylindrical upper contours with moderate overlap at the entrance, $\overline{\Delta l}_0 = 0.344$. For a large overlap, $\overline{\Delta l}_0 = 0.515$ (variants V, VI, VII, and IX), the reaction at the tip and in the root section is sharply lowered. Variants IV and VI are the exception.

The value of the described experiments consists in the fact that they indicated the essential influence of the shape of the upper contour not only on the efficiency of the stage, but also on the distribution of the reaction, and consequently, the velocities and angles along the radius in a clearance. It may be concluded from this that when profiling the blades of stages with noncylindrical contours or with overlaps at the entrance, it is necessary to consider the essential deflection of

the flow from the cylindrical type.

The considered group of investigations also includes the experiments of I. I. Kirillov [56].

Such a sharp influence of the overlap and organized diffuser inlet in the investigated stage was revealed at small pressure drops. With supercritical drops in the stage, the influence of the inlet decreases (see Chapter VIII). One should also consider that with the increase of the outlet angle of the nozzle cascade, α_1, the influence of the inlet condition in the stage increases.

Organization of the Flow Behind the Last Stage of a Turbine

The kinetic energy of the flow behind the last stage can be partially converted into potential energy which, as indicated in § 24, essentially increases the efficiency of the stage and the turbine. This conversion is carried out in the diffuser outlet ducts.*

Experimental investigations showed that with the correct selection of the basic geometric parameters in an outlet duct, up to 40-50% of the kinetic energy behind the last stage $c_{a2}^2/2$ can be restored.

The basic elements of an outlet duct are the diffuser (axial, radial, or diagonal) and the housing (shell), which extracts the gas behind the diffuser in a direction dictated by the design of the machine.

The structural types of outlet ducts that are encountered in practice are very diverse and cannot be considered within the scope of this book. We shall mention only certain results of investigations where were obtained at MEI.

The basic geometric parameters of a duct with axial and radial diffusers are shown in Fig. 239. The geometric divergence of the duct is characterized by the ratios of the areas of the outlet and inlet sections:

$$f_\partial = F_3/F_2 \text{ and } f_\kappa = F_4/F_3,$$

where F_2 and F_3 are the areas of the inlet and outlet sections of the diffuser;

F_4 is the area of the outlet section of the duct.

Other important geometric parameters are:

1. The relative length of the diffuser $\bar{l}_Д = l_Д/l_2$ ($l_2 = \frac{1}{2}(D_2 - D_{20})$ is the width of the ring at the inlet; D_2 and D_{20} are the external diameters of the diffuser at the entrance).

---

*Section 24 gives the results of the calculation and investigation of vaned diffusers for stages with a low velocity ratio x_∂.

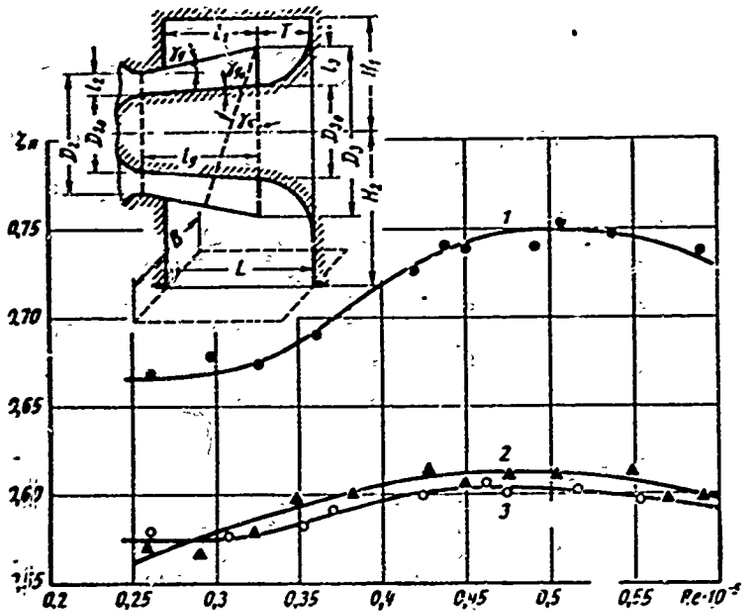

Fig. 239. Diagram of an outlet duct and the dependence of its coefficient on the Reynolds number for various diffusers: 1 – diffuser with straight cutoff; 2 – diffuser with slanted cutoff; 3 – diffuser without housing. MEI experiments: $F_3/F_2 = 2.6$; $F_4/F_2 = 5.4$.

2. The cone angles of the inner and outer contours of the diffuser, $\gamma_д$ and $\gamma_{д\,0}$.

3. The distance between the outlet section of the diffuser and the wall of the duct, $\overline{T} = T/l_3$ ($l_3 = \frac{1}{2}(D_3 - D_{30})$ is the width of the ring at the outlet; D_3 and D_{30} are the external and internal diameters of the diffuser at the outlet).

4. The dimensions of the duct housing: H_1 – the height of the upper portion; H_2 – the height of the lower portion; L and B – the length and the width of the outlet section F_4.

The enumerated geometric parameters are interconnected. Depending upon the permissible building dimensions of the duct, various optimum combinations of the indicated parameters are possible.*

Essential features of the performance of a duct are the nonuniformity of distribution of static pressures and flow rates along the height l_2 and along the circumference at the entrance, and the high degree of turbulence. An important feature is the asymmetry of the exhaust, which is prompted by the necessity of extracting the gas flow at a right angle to the axis of the machine. The negative

*For optimum combinations, the degree of pressure recovery in a duct will be different.

influence of rotation may be distinctly seen in Fig. 239, which represents the curves of the coefficients $\zeta_п$ for a duct that consists of a diffuser and a shell (curve 1) and for a diffuser without a sheel (curve 3). Let us recall that the duct coefficient $\zeta_п$ is the ratio of heat drops:

$$\zeta_п = \frac{H_{02}}{H_{01}},$$

where H_{02} is the isentropic drop, which corresponds to the expansion from the stagnation pressure before the diffuser to the static pressure behind the duct p_4; H_{01} is the isentropic drop, which is equivalent to the kinetic energy of the flow behind a stage ($H_{01} = c_2^2/2$).

It is not difficult to see that if $\zeta_п > 1 (H_{02} > c_2^2/2)$, then $p_4 < p_2$, and the outlet duct is not of the diffuser type; if $\zeta_п < 1$, then $p_4 > p_2$ and the duct restores part of the kinetic energy behind the last stage, which is equal to $1 - \zeta_п$ (in relative quantities).

The duct coefficient is connected to its efficiency by the evident relationship

$$\zeta_п = 1 - \eta_п + \bar{h}_{2к},$$

where $h_{2к} = c_4^2/2H_{01}$ is the kinetic energy of the flow at the outlet from the duct (referred to the quantity $H_{01} = c_2^2/2$).

The curves illustrated in Fig. 239 show that if the degree of restoration of kinetic energy in a diffuser amounts to $1 - \zeta_п = 40\text{-}45\%$ (curve 3), then, with a shell, the restoration is lowered to $1 - \zeta_п = 25\text{-}30\%$ (curve 1).

The experiments confirmed the possibility of a considerable increase in the degree of restoration. Thus, for instance, the design of a diffuser with slanted cutoff (cutoff angle $\gamma_к = 16^\circ$) makes it possible to increase the restoration to a quantity that is very similar to a single diffuser without a shell (curve 2).

This result has an important practical value. In accordance with the physical features of the motion in a diffuser, a duct with an asymmetric outlet should also have an asymmetric diffuser. The outlet conditions then sharply improve for the upper and lower halves of the diffuser, the uniformity of distribution of parameters around the circumference at the entrance to the diffuser increases, the efficiency of the duct increases, and the reliability of the blades of the last stage, which in this case experience a smaller vibration load, also increases.

The design advantage of such a duct with a diffuser having a slanted cutoff consists in that the height of the upper part of the housing H_1 (or $H_1 - D_3/2$) can be considerably decreased. Experiments confirm that a diffuser with a slanted

cutoff has more favorable characteristics than a diffuser with rotary blades.

The curves in Fig. 239 show that with the growth of the Reynolds number, when $Re^* < 5 \cdot 10^4$, restoration in the duct decreases, and then increases. This is explained, obviously, by the fact that with the increase of Re the region of the transition of laminar conditions to turbulent conditions moves in the direction opposite the flow.

Systematic investigations of the influence of the most important geometric parameters of a duct make it possible to determine the optimum ratios which are presented in Table 20. As the initial (independent) parameters we selected:

1 — the flare of the last stage, which is determined by the ratio $\theta = d/l$;

2 — the relative dimensions of the duct outlet;

3 — the M_2 number at the inlet.

Table 20. Optimum Geometric Parameters of an Outlet Duct with an Axial Diffuser*

Initial data.			Optimum ratios							
$\theta = d/l$	L/B	M_2 number	F_0/F_1	F_0/F_2	T/l_0	l_0/l_2	γ_0	$\gamma_{\partial 0}$	L_1/D_0	γ_K
5—7	0,6—0,8	0,3—0,5	2,5—3	4—5,5	1,0	5—6	10—15°	5—8°	0,4—0,6	12—16°
3—4	0,6—0,8	0,3—0,5	2,2—2,5	5—6	1,2	4	10°	2—3°	0,6—0,8	16°
2,5	0,6—0,8	0,3—0,5	2,0—2,2	5—6	1,4	3	10°	0	1,0	18—20°

*The data given for $\theta = 3 - 4$ and $\theta = 2.5$ are tentative and were not checked experimentally.

§ 41. SOME SPECIAL PROBLEMS OF THE THEORY OF LARGE-FLARE STAGES

With small ratios $\theta = d/l$ behind an annular nozzle cascade, nonuniformity of the field of stagnation temperatures is detected along the radius (eddy effect of the stage, see § 35). In connection with the necessity of calculating this nonuniformity, there arise two interconnected problems:

1. Finding a calculation method that would make it possible to approximately estimate the magnitude of the indicated nonuniformity, depending upon the basic performance and geometric parameters of the stage.

2. Introducing the appropriate correction into the aerodynamic calculation stage twisting.

The physical causes that provoke the nonuniform distribution of stagnation temperature in a section of an adiabatically moving flow of a compressible, viscous, and heat-conducting liquid consist in the following. In such a flow, part of the

kinetic energy is converted into heat, which is propagated in the flow by means of thermal conduction and as a result of turbulent transfer.

Depending upon the structure of the flow, the character of the velocity distribution along the flow through the section, and the degree of turbulence, the intensity of the internal heat exchange can vary considerably. The heat given off is distributed nonuniformly in the flow, so that some gas streams can possess a higher, and some, a lower, reserve of total energy than that which corresponds to an integral-adiabatic flow. The condition of i_0 = const for each stream separately cannot serve as a characteristic of the flow and an integral of the energy equation in this case.

The considered phenomenon of nonuniform distribution of total energy in an adiabatic flow especially distinctly appears in a Rank vortex tube.

In a turbine stage with axial gas flow, the vortex effect is considerably weaker. However, at small θ and large M numbers, the nonuniformity of the field of stagnation temperatures behind a nozzle cascade can be considerable; therefore, it should be considered in the thermal calculation of the stage and in the experimental study of annular cascades and stages.

If, in distinction from the preceding, we consider the influence of not only viscosity, but also thermal conduction, then the fundamental equations, i.e., for radial equilibrium and energy, will take on the following form:

$$\frac{dp_1}{\varrho_1} = c_{u1}^2 \frac{dr}{r}; \tag{249}$$

$$\frac{d}{dr}\left\{\mu r\left[\frac{d}{\mathrm{Pr}}\left(\frac{i}{\mu r} + \frac{c_{u1}^2}{2}\right) + c_{u1}\frac{dc_{u1}}{dr} - \frac{c_{u1}^2}{r}\right]\right\} = 0. \tag{250}$$

Here $\mathrm{Pr} = \frac{\mu c_p}{\lambda}$ is the Prandtl number; μ is the coefficient of dynamic viscosity; c_p is the heat capacity at constant pressure; λ is the coefficient of thermal conduction.

The system of equations (249) and (250) should be augmented by the equation for the swirling of the flow, which determines the profile of the peripheral velocity components:

$$c_{u1} r^m = \text{const}, \tag{251}$$

and also the equation of state

$$\varrho = \frac{p}{RT} = \frac{kp}{(k-1)i}. \tag{252}$$

The four fundamental equations contain five unknowns: c_{u1}, c_{a1}, i, p, and ρ. The fifth equation necessary for the solution of the problem can be obtained in the form of a relationship between the velocity components c_{u1} and c_{a1}. Since

$$c_1^2 = c_{u1}^2 + c_{a1}^2,$$

from the momentum equation for a mass of gas moving between sections at the entrance and behind the cascade, taking losses into account, we can obtain

$$\frac{\varphi^2 c_{u1}^2}{r} + c_{u1}\frac{dc_{u1}}{dr} + c_{a1}\frac{dc_{a1}}{dr} = 0 \tag{253}$$

In the derivation of this equation we used the equation radial equilibrium (249). We shall now use the swirl equation (251). After differentiating it, we find

$$\frac{dr}{r} = -\frac{1}{m}\cdot\frac{dc_{u1}}{c_{u1}}. \tag{254}$$

After substitution into equation (253), we will obtain

$$c_{a1}\,dc_{a1} + \frac{m-\varphi^2}{m}\,c_{u1}\,dc_{u1} = 0. \tag{255}$$

We shall convert equation (250) with the help of (254) and (255), and obtain

$$\frac{\partial}{\partial r}\left\{\mu r\left[\frac{\partial}{\partial r}\left(\frac{i_1}{\Pr} + \frac{c_{u1}^2}{2}\right) + \frac{c_{u1}^2}{2}\left(\frac{\varphi}{m} - \varphi^2 - 1\right)\right]\right\} = 0.$$

Considering that μ = const, φ = const, and Pr = const,* we shall integrate this equation twice, taking the swirling into account (251); then we will obtain

$$i_1 + \Pr\frac{c_{u1}^2}{2}\left(\frac{1+\varphi^2}{m}\right) = \text{const}. \tag{256}$$

The enthalpy of absolute stagnation of flow is determined by the formula

$$i_{01} = i_1 + \frac{c_{u1}^2 + c_{a1}^2}{2}. \tag{257}$$

After integrating** (255) and substituting the obtained result and equation (256) into (257), we finally find***

$$i_{01} = \frac{c_{u1}^2}{2}\left[\frac{\varphi^2}{m} - \Pr\left(\frac{1+\varphi^2}{m}\right)\right] + \text{const}. \tag{257a}$$

We find the constant, writing (257a) for the root section.

---

*The Pr number it may be considered as a physical constant only for an ideal gas.

**For simplification of the problem, in all conversions we assume that φ does not change along the radius.

***The energy equation (250) for one-dimensional circular motion of a viscous gas at c_{a1} = 0 was integrated by L. A. Vulis on the assumption that μ = const and Pr = const.

Let us designate r_K as the radius of the root section; $c_{u1\,K}$ is the peripheral velocity component in the root section; then

$$\text{const} = i_{01\,K} - R_\varphi \frac{c_{u1\,K}^2}{2},$$

where

$$R_\varphi = \frac{1}{m}[\varphi^2 - \Pr(1+\varphi^2)];$$

$i_{01\,K}$ is the enthalpy of stagnation in the root section of the nozzle cascade. After substitution into equation (257a), we finally obtain

$$\frac{i_{01}}{i_{01\,K}} = 1 + R_\varphi \frac{c_{u1\,K}^2}{2i_{01\,K}}(\bar{r}^{-2m} - 1). \tag{258}$$

Since $2i_{01\,K} = \frac{k+1}{k-1}a_{*K}^2$, where $a_{*\,K}$ is the critical velocity in the root section, then

$$\frac{c_{u1\,K}^2}{2i_{01\,K}} = \frac{k-1}{k+1}\lambda_{1K}^2 \cos^2\alpha_{1K}.$$

Consequently:

$$\frac{i_{01}}{i_{01\,K}} = 1 + \frac{k-1}{k+1} R_\varphi \lambda_{1K}^2 \cos^2\alpha_{1K}(\bar{r}^{-2m} - 1), \tag{259}$$

where $\alpha_{1\,K}$ is the outlet angle; $\lambda_{1\,K} = \frac{c_{1K}}{a_{*K}}$ is the dimensionless velocity in the root section.

The total change of the stagnation enthalpy along the height of the nozzle cascade can be determined by the formula

$$\frac{i_{01\,\text{п}}}{i_{01\,K}} = 1 + \frac{k-1}{k+1} R_\varphi \lambda_{1K}^2 \cos^2\alpha_{1\,K}(\bar{r}^{-2m} - 1),$$

where $\bar{r}_\text{п} = r_\text{п}/r_K$ is the relative radius of the section at the tip. Considering that

$$\bar{r}_\text{п} = \frac{\theta+1}{\theta-1},$$

we finally obtain

$$\frac{i_{01\,\text{п}}}{i_{01\,K}} = 1 + \frac{k-1}{k+1} R_\varphi \lambda_{1K}^2 \cos^2\alpha_{1\,K}\left[\left(\frac{\theta-1}{\theta+1}\right)^{2m} - 1\right]. \tag{260}$$

From equations (258) and (260) it follows that the stagnation enthalpy increases toward the cascade tip, if $R_\varphi < 0$, i.e., if the Prandtl number $\Pr > \frac{\varphi^2}{1+\varphi^2}$.

An analysis of formula (260) also shows that the cascade losses increase the stratification of total energy behind the outlet section. The nonuniformity of the field of axial velocities, which is characterized by a decrease of c_{a1} towards the tip, lowers the nonuniformity of the field of stagnation temperatures behind the

cascade. The influence of the method of twisting the nozzle blades may be estimated, considering the limiting values of the index $m = \pm 1$. The minimum change of i_{01} corresponds to the condition of constant velocity circulation, $c_{u1} = \text{const}$. The most intense change of i_{01} is revealed with twisting $c_{u1}/r = \text{const}$ for equal distribution of axial velocities behind the cascade.

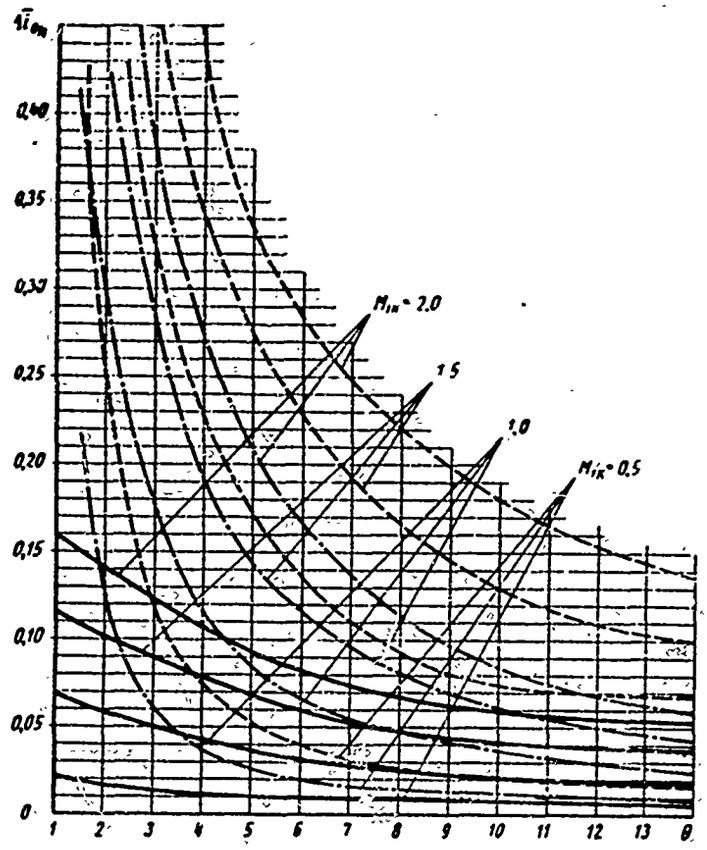

Fig. 240. Analytic curves of the change of enthalpy of absolute stagnation along the radius in a clearance, $\Delta i_{0\,n}$, depending upon θ and $M_{1\,K}$ with $k = 1.4$ and $Pr = 0.72$. Curves for various laws of twisting of nozzle blades: —— (solid) $m = 1 (c_{u1}\ r = \text{const})$; – – – – (dotted line) $m = -1 (\frac{c_{u1}}{r} = \text{const})\ \frac{\partial c_{a1}}{\partial r} = 0$; – · – · – (dot and dash) $m = -1 (\frac{c_{u1}}{r} = \text{const})\ \frac{\partial c_{a1}}{\partial r} \neq 0$.

The corresponding results of the calculations are shown in Fig. 240. Curves are given there for the relative difference of stagnation enthalpies (temperatures)

$$\Delta\bar{i}_{01\,n} = \frac{i_{01\,n} - i_{01\,K}}{i_{01\,n}} = \frac{\bar{\theta} R_{\eta} \lambda_{1\,K}^2 \cos^2 \alpha_{1\,K}}{1 + \bar{\theta} R_{\eta} \lambda_{1\,K}^2 \cos^2 \alpha_{1\,K}}, \qquad (2.1)$$

where

$$\bar{\theta} = \frac{k-1}{k+1} \left[\left(\frac{\theta - 1}{\theta + 1} \right)^{2m} - 1 \right]$$

depending upon θ and the $M_{1\,к}$ number. Calculations were performed for $k = 1.4$, $Pr = 0.72$, $\alpha_{1\,к} = 11^{\circ}$, $m = \pm 1$.

It should be noted that at small values of θ the change of stagnation enthalpy is essential, whereby with the growth of $M_{1\,к}$ the quantity $\overline{\Delta i}_{01\,п}$ intensely increases. Consequently, the effect of vortex stratification of total energy behind a cascade actively appears in large-flare stage at high velocities, $M_{1\,к} \geq 1$.

Analogous calculations may also be performed for steam. Sufficiently accurate determination of the Pr number is important. For turbulent gas motion it is necessary to introduce the effective value of the Prandtl number, $Pr_{турб}$, which may be considered constant in first approximation.

Experiments* confirm the existence of vortex effect in stages of axial and radial turbines. Figure 241 illustrates the experimental values of t_{01} for certain cascades with axial gas flow whose results were given above (see § 37). It may be distinctly seen there that the field of stagnation temperatures is nonuniform at sufficiently great distances behind the cascade.

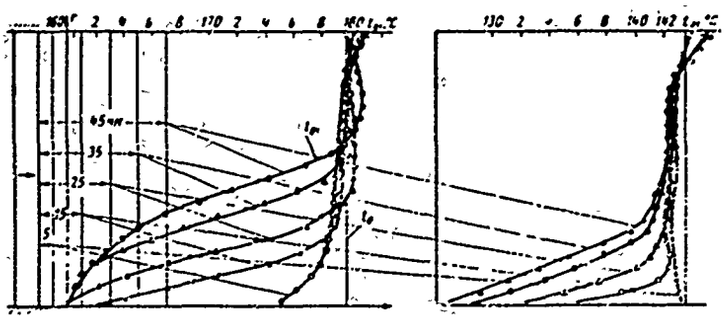

Fig. 241. Change of the stagnation temperature along the radius behind a nozzle cascade with continuous and separated flow. According to MEI experiments: $\theta = 2.88$; $M_{c1} = 0.72$.

With the increase of distance from the trailing edges, the nonuniformity of the field of stagnation temperatures increases, and especially intensely when there appears separation on the hub.

In the last case, the physical nature of the nonuniformity, $t_{01}(i_{01})$, which is especially intense in the zone of separation, cannot be described by the above-given equations.*

With continuous motion in the root sections, the temperature nonuniformity turns out to be weaker. However, in all cases the stagnation temperature at the tip is higher than at the root.

---

*Performed at MEI by L. Ye. Kislev and M. F. Zatsepin.

**The nonuniform distribution of stagnation temperature which accompanies the separations in the root sections behind the trailing edges of blades and is detected in the boundary layers also pertains to the "vortex effects" in the stage.

Especially significant is the nonuniformity of the distribution of stagnation temperatures in a radial stage. Studies of this type of stage, even at moderate M numbers, confirmed the existence of nonuniformity not only behind the nozzle cascade, but also behind the rotor wheel (Fig. 242).

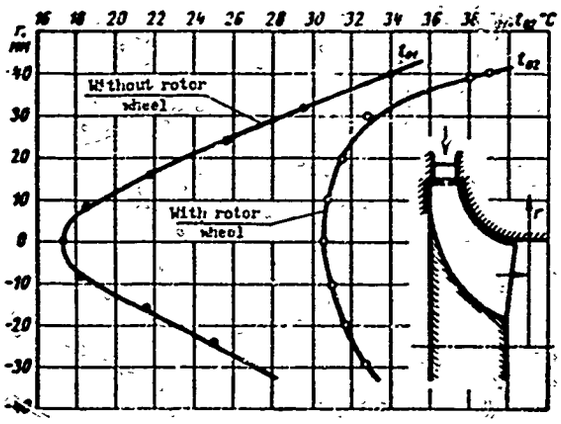

Fig. 242. Change of stagnation temperature along the radius at the outlet from a centripetal stage with a rotor wheel and without a rotor wheel. MEI experiments.

The influence of the vortex effect that we detected must be considered in the calculations of the distributions of velocities, pressures, temperatures, and reactions along the radius.

It is obvious that when this effect is perceptible, twisting of blades should be performed with the change of $T_{01}(i_{01})$ along the radius taken into account.

This problem may be solved approximately within the confines of the simplified flow diagram that was considered above (see § 37).

The energy equation for an absolute flow in a clearance may be solved in differential form (204) together with the equation of radial equilibrium (202), not assuming that $i_{01} = \text{const}$ $\left(\frac{\partial i_{01}}{\partial r} \neq 0\right)$.

The differential equation of distribution of absolute velocities in the clearance in this case will have the following form [see equation (206)]:

$$\frac{1}{c_1}\cdot\frac{\partial c_1}{\partial r} = \eta_1\left[-\frac{\cos^2\alpha_1}{r} + \frac{1}{2\eta_1^2}\cdot\frac{\partial\eta_1}{\partial r} + \frac{\eta_1}{2h_{01}}\cdot\frac{\partial i_{01}}{\partial r} + \right.$$
$$\left. + \frac{5\sin\alpha_1\cos\alpha_1}{2B_1 r}\left(\frac{r_n^2 - r^2}{r_n^2 - r_k^2}A_1 + A_2\right)\right], \qquad (262)$$

where h_{01} is the current value of the available heat drop in the nozzle cascade;

$\eta_1 \approx \varphi^2$ is the efficiency of the nozzle cascade.

By using formula (258), it is not difficult to obtain

$$\frac{\partial i_{01}}{\partial r} = [Pr(\varphi^2 + 1) - \varphi^2]\,\frac{c_{1k}\cos^2\alpha_{1k}}{r^{2n+1}}. \qquad (263)$$

Formula (263) considers the change of total energy in the clearance along the radius, which is caused by the vortex effect only. In reality, nonuniformity

of the field i_{01} can also be brought about by other causes.* In this case it is necessary to assign the function $i_{01}(r)$ on the basis of physical considerations and introduce the appropriate term into equation (262), which may be integrated by the numerical method.

It is of interest to estimate the change of stagnation enthalpy along the radius in fractions of the available heat drop in the root section of a stage by the formula

$$\overline{\Delta i_{01}} = \overline{\Delta T_{01}} = \frac{i_{01} - i_{0\kappa}}{i_{01\kappa} - i_{2t\kappa}} = R_\varphi \cos^2 \alpha_{1\kappa} (\bar{r}^{-2m} - 1)(1 - \varrho_\kappa). \tag{264}$$

Formula (264) is obtained with the help of the following evident relationships:

$$i_{01\kappa} - i_{2t\kappa} = h_{0\kappa} = \frac{h_{01\kappa}}{1 - \varrho_\kappa}; \quad h_{01\kappa} = \frac{c_{1\kappa}^2}{2},$$

where $h_{0\,\kappa}$ is the available heat drop in the root section of the stage; $h_{01\,\kappa}$ is the available heat drop in the nozzle cascade in the root section; ρ_κ is the degree of reaction in the root section; $i_{2t\,\kappa}$ is the enthalpy of the flow behind the stage in an ideal process for the root section.

The above-stated method makes it possible to approximately estimate the change of static parameters behind the cascade. Thus, for instance, with the help of formula (256) we can find the enthalpy distribution of the flow behind the cascade

$$i_1 = i_{01\kappa} - \frac{c_{a1\kappa}^2}{2}\left[1 + \Pr\left(\frac{1 - \varphi^2}{m}\right)(\bar{r}^{-2m} - 1) - \frac{c_{a1\kappa}^2}{2}\right]$$

and the distribution of static pressure

$$\frac{p_1}{p_{1\kappa}} = \left[1 + \frac{\Pr(1 + \varphi^2)(1 - \bar{r}^{-2m})}{m\left(\frac{k+1}{k-1} - \frac{1}{\lambda_{m\kappa}^2} - \sec^2 \alpha_{1\kappa}\right)}\right]^{\frac{k}{\Pr(k-1)(1+\varphi^2)}}.$$

In conclusion, it should be stressed that the proposed method** of estimating the nonuniformity of stagnation temperatures in the nozzle cascade is quite approximate, and its error should be thoroughly tested by experiments, the quantity of which is still insufficient. At the same time, when carrying out experimental investigations of cascades and stages with large flare, at large M numbers it is

---

*Taken into account are the nonuniformity of the temperature field at the combustion chamber outlet, the influence of the preceding stage, at whose outlet i_{02} is not constant, the influence of cooling, and other factors.

**Developed jointly with Ye. He. Likherzak.

necessary to measure the stagnation temperatures in a clearance and behind the stage.

CHAPTER VIII

LAST STAGES OF CONDENSING STEAM TURBINES

§ 42. DESIGNS OF LAST STAGES

In domestic and foreign turbuine construction there are various designs of the last stages of condensing machines. This distinction of stages may include the following:

Meridional Configuration of Stage

The meridional configuration of a stage is determined by the transition from the preceding stage and by the selected law of variation of stage diameters. In the low-pressure portion of steam turbines we find three laws of variation of diameter:

a) constancy of root diameter, see [137] for example;

b) decrease of root diameter, see [138] for example;

c) increase of root diameter, as, for example, the low-pressure flow area of the LMZ K-300-240.

It is obvious that the most favorable external configuration of the flow area is attained in case "b." However, sometimes because of the conditions of disk strength and the reluctance to obtain low blade heights in the first stages of a low-pressure cylinder, and also for decreasing the number of stages, designers reject this type of flow area. The least useful variant is "c," since it causes a very sharp increase of the diameters on the periphery of the stages, where it is difficult to attain a smooth transition from one stage to the other.

The angle of incidence of the upper configuration of a diaphragm is sometimes

decreased by considerably increasing its width. An example of this is the diaphragm of the last stage of the LMZ turbine ПВК-200.

This method is feasible only in very rare cases, since the overall design requirements, including the forging dimensions and the requirements of rotor reliability, do not make it possible to essentially increase the width of the diaphragm. Furthermore, a large diaphragm width requires such a large nozzle cascade chord that l/b turns out to be very small and the influence of end losses becomes considerable. If, however, the blades in a wide diaphragm are narrow, then the long entrance section which is formed will undoubtedly create additional losses (see Chapter VII).

The external meridional configuration of a diaphragm also will be different. Two fundamentally different solutions are possible: a purely conical configuration and a configuration with a smooth transition to a cylindrical surface. The results of tests performed on stages with various forms of external meridional configuration are given in §§ 40 and 44. It should be borne in mind that for a flow of moist steam the first type may possibly be better for removing moisture and may appear to be more expedient. In certain turbuines, the desire to remove more moisture renders an influence on the configuration of the external contour; in particular, this requires the lowering of the initial entrance point of the external contour of the stage.

Technology of State Manufacture

Nozzle blades can be manufactured by various methods. Recently, blades manufactured from a sheet of constant thickness have been widely employed (see diaphram of last stage of LMZ turbine ПВК-200, shown in Fig. 243). These blades made it difficult to obtain the necessary profile shape and its desired variation with respect to height. The thin leading edges created large sensitivity to the variation of the leakage angle. In the last stages of turbines, due to the inaccuracy of calculation of the preceding stages, noticeable deviations of the entrance angle α_0 from the calculated value are possible. Because of strength conditions these blades usually were very wide or they required additional partitions, which cause a lowering of economy (for instance, the last stage of the turbines ВКТ-100 KhTGZ and ПВК-200 LMZ).

The transition from sheet blades to solid ones makes it possible to increase stage economy.

NZL experiments showed that for a stage with blades l_1 = 22.5 mm the replacement of stamped sheet blades by TC-2A MEI milled blades led to a 4.2% growth of efficiency [41]. MEI experiments with the last stage of a 25-Mw turbine with d/l = 3.7 and l_1 = 160 mm (in a model) and two diaphragms, i.e., with blades stamped from a sheet of constant thickness and with milled blades, in the last case showed a gain in efficiency of $\Delta\eta_{oi}$ = 4 to 6%.

Solid nozzle blades can be welded and stampled. These blades are applied in the latest KhTGZ turbines [122]. These blades, undoubtedly, are better than the sheet type, but, due to conditions of technology, it is difficult to arbitrarily change their shape with respect to height. The latter is necessary for limiting stage, where the M number changes so much with respect to height that the various sections, in accordance with the flow rate, must be designed differently in principle.

For rotor blades, just as for the nozzle blades of limiting stages, where there is a large difference with respect to height in the configuration of the profiles and the conditions of flow, manufacture of blades by means of a three-dimensional master form is more preferable than angular milling.

Stage Heat Drop

For stages that are designed for large heat drops, and consequently, for high exhaust velocities, the M numbers in the nozzle cascades, as well as in the moving cascades in a number of sections — especially in the root sections of the nozzle cascade and in the upper sections of the moving cascade are so much greater than unity that special profiling is required.

The Ratio $\theta = d/l$

There are presently stages with the ratio $\theta < 2.5$. In these stages there is a very large difference in the entrance angles of steam into the moving cascade (angle β_1), which reaches a peak value of 160-165°. This requires special moving cascades with a very low rate of flow. For small d/l the velocities change very significantly along the height. An important design feature of stages with small d/l ratios is the considerable increase of the absolute cascade pitch from root to tip.

Thus, if at $\theta = 5$ the pitch t from root to tip increases 1.5 times, then at $\theta = 3$ it increases 2 times, and at $\theta = 2.5$, 2.33 times. It is obvious that, by maintaining the blade chord approximately identical with respect to height on all

radii, it is not possible to obtain cascades with optimum relative pitch $\bar{t} = t/b$. Therefore, the nozzle blades in stages with small d/l frequently are designed with an increase of chord from the root to the peak value of chord.

Reliability Conditions

The requirement of ensuring the reliability of rotor blades limits the designer in the process of making profiles and channels optimum from the point of view of aerodynamics. The last rotor blades, especially limiting ones, require thick profiles in the root section, an decrease in area with respect to height, and very thin profiles at the tip (see profiles in § 43). The sometimes desirable decrease of pitch in the upper sections of the rotor blades leads to an increase of their number, which usually is limited by the strength of the disks. There are possible cases when the increase of pitch is limited by the strength of the wire connections of the cascade.

Vibration reliability of blades requires the installation of connective or damper wires which not only noticeably lower the economy of these sections, but sometimes block the flow so much that it significantly disturbs the process of flow also in the adjacent sections. All this leads, as compared to the calculation, to a redistribution of flow rates, angles, and reactions along the height, and in a considerable part of the stage it affects the flow. In a number of cases when drilling a blade under a wire, the profile is thickened in this spot, which results in a change of the flow process. An especially unfavorable effect is brought about by the installation of several rows of wires in direct proximity to one another. A disturbance of the flow can appear in this case even at a large distance from the place of installation of the wires.

From these positions, it is favorable to replace the connective wires by an external shroud, which decreases steam leakage over the blades. Such blades are applied by certain foreign firms [147]. Unfortunately, we do not have any experimental data which characterizes the influence of a blade shroud on the removal of moisture.

Anti-erosion protection of blades is carried out in last stages either in the form of stellite inserts, or by means of special treatment of the blade surface. Both these, and other methods can lower the effectiveness of given sections. Stellite inserts (that are correctly made), according to the results of MEI

experiments, do not render a perceptible influence on cascade losses.

Selection of Law of Twisting

At present, all stages with small d/l are calculated by means of the equation of radial equilibrium in a clearance. However, as a rule, such a calculation is performed only with simplified formulas, without considering a number of additional factors (for details see §§ 37, 38, 45, and 46). But also in this case it is possible to select a law of twisting that determines the change of angles α_1 and β_2 with respect to height, and consequently also the geometric characteristics of the stage. The mean values of the angles depend on the dimensions of the stage and the volume steam admission. Usually the next-to-the-last stages of condensing turbines it is necessary to design the cascade with very small angles α_1 and small angles β_2, accordingly, in order to provide a smooth transition to the last stage.

In the practice of designing last stages we encounter laws of twisting with cylindrical nozzle blades, with a nozzle cascade that ensures the constancy of angle α_1 along the radius; cascades with angle α_1 increasing from root to tip, and finally, we may find nozzle blades with a decrease of angle α_1 from root to tip (see Chapter VII).

The outlet angle the moving cascade β_2 either remains constant (cases of helical blading are rarely encountered) or usually decreases somewhat from root to tip.

A special case is a two-level stage that preceeds the last stage (the so-called Bauman stage). An example of this stage is shown in Fig. 243. Two-level stages are applied by the Metro-Vickers firm and by our LMZ. In particular, a two-level stage is included in the LMZ turbines СВК-150 and ПВК-200.

It is sometimes considered that a two-level step is hardly economical and therefore it is not expedient for use in high-power turbines. This opinion is based mainly on the results of testing the turbine СВК-150, the low-pressure cylinder of which indicated an unsatisfactory economy. The low economy of the two-level stage of the existing turbines, in our opinion, is caused not by the specific peculiarity of this stage, but by its incorrect designing. This was indicated in the following:

1. Sections of cascades of last stages, and especially the upper level of the next-to-the-last stage, were constructed without taking into account the peculiarities of supersonic flow, although it is known that in many sections of these stages the

steam rates are considerably higher than critical. Stamped nozzle blades, for a variable M number with respect to the height of the entire stage, were not generally designed. Moreover, manufacture of nozzle blades of the lower and upper level from one sheet inevitably connected the configuration of these cascades with a high supersonic velocity for upper, and with a velocity close to M = 1 for the lower one.

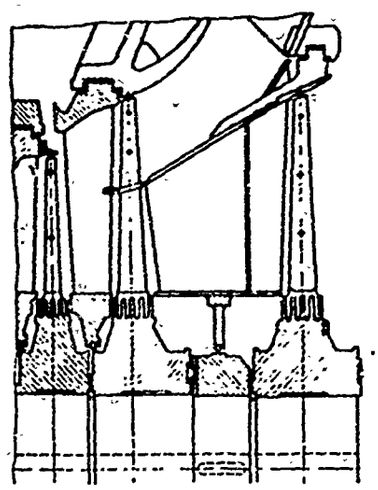

Fig. 243. Two-level next-to-last stage and last stage of a large steam turbine.

2. A partition between levels in the nozzle blade was made only in the outlet section. In a large part of the channel there occurred free movement of stage from one level to the other; this disturbed the flow, but was not at all considered in the calculation.

3. The chords of the nozzle cascades of the upper and lower levels, and also the last stage, are so large that the relative height of these cascades $l_1/b_{1\ cp}$ is commensurable with the first stages.

Turbine	Last stage	Next-to-last stage	
		lower level	upper level
СВК-150 ПВК-200	1.25 4/0.9	1.8 1.34	1.10 1.00

It is obvious that in these stages the end losses considerably lower the economy.

4. The stage sealing is not satisfactory. The clearances are very great, and consequently, the leakages between levels also; they are also large over the rotor blades.

The economy of the low-pressure part of a turbine with a two-level stage can be of the same order as without it.

Actually, inasmuch as every level has a low height, and consequently, a d/l ratio at which the reaction varies insignificantly with respect to height, it is not difficult to profile the cascades of the next-to-the-last stage. As it is known, when designing last stages, large difficulties arise when making the root

sections; the angles β_1 and β_2 are very small in them. For a two-level stage, where $d/l > 5$ in each level, this difficulty is eliminated. The upper section of the moving cascade is very complicated; the β_1 angles reach 150-160° there. The angle β_1 for the upper level does not exceed 120-130°. Inasmuch as the reaction on the level does not vary much, at the top of the upper level it will be considerably less than at the top of the last stage, which lowers the losses due to leakage. However, leakages of steam from the lower to the upper level through the clearance between the diaphragm and rotor blade remain. For eliminating this, one might install a good sealing here.

For sections of the nozzle and moving cascades of the upper level, where the velocities are maximum, it is possible to select cascades with moderate losses (see § 43).

In particular, apparently, one should apply nozzle cascades with divergent channels, i.e., Laval nozzles. Since the exhaust in the moving cascades of the upper level occurs with velocities exceeding critical, the velocities in the nozzle cascade will vary only with a considerable impairment of the vacuum, which makes it possible to apply Laval nozzles.

In our opinion, this type of stage has several shortcomings:

First, a considerable amount of moisture will be concentrated in the upper level, that will significantly lower its efficiency. In this case it may be assumed that some success in removing the moisture and, in particular, the location of the last steam extraction in front of a two-level stage for regeneration of input water, will make it possible to decrease the influence of moisture.

Secondly, some difficulty is brought about behind a two-level stage by the diaphragm of the last stage, which must either have a large inclination of the meridional contour or a very great width. The solution of this problem requires special investigations which make it possible to find an optimum answer.

Thirdly, the outlet duct behind the upper level should be developed specially by experimental means. The LMZ, together with MEI, has already conducted such research work for making such outlet ducts for the ПВК-200 turbine.

Certainly, only special investigations in a twin-shaft experimental turbine will make it possible to exactly compare the economy of the flow area with a two-level stage and without it; however, even now it is possible to speak of the competitive value of the model with a two-level stage. It should be borne in mind

that this model makes it possible to essentially simplify the turbine design, reduce its cost, employ a deeper vacuum in a number of cases, and, in the final result, to increase the economy of the unit.

§ 43. PROFILING AND THE RESULTS OF STATIC INVESTIGATION OF CASCADES OF LAST STAGES

As a result of a detailed* calculation of three-dimensional flow in a stage with a small d/l ratio for each radius, and consequently, for each cascade section, all performance parameters are known. Thus, for profiling a given cascade section, the initial parameters are: dimensionless inlet velocity, M_0 (for a moving cascade, M_{w_1}, calculated with respect to relative velocity), on outlet velocity, M_{c_1} (or M_{w_2}), inlet angle, $\alpha_0(\beta_1)$, outlet angle, $\alpha_1(\beta_2)$, and also the viscosity coefficient, ν, which is necessary for determining the Reynolds number. When profiling cascades of last stages, especially limiting stages, it is necessary to consider sometimes the very stringent requirements of strength and vibration reliability (including the reliability of the disk and the rotor blade). Although the use of profile machines for treating blade surfaces considerably facilitated optimum cascade profiling, with this type of profiling it is nevertheless impossible not to consider the technology of manufacture.

The requirements of reliability limit the selection of the dimensions of thickness of the trailing edge, the magnitude of absolute pitch (i.e., the number blades, and consequently, the stresses in the disk), the width and thickness of the rotor blade profile, and sometimes the value of the area of the profile, the moments of inertia, and resistance.

Selection of cascades for a stage cannot be performed without having data on the variation of its operating conditions. For condensing steam turbines, as it is known, the conditions of only one last stage vary; for low-power turblines, the conditions of the next-to-the-last stage also vary.

In a last stage of limited power the velocities of steam outlet from the moving cascade, w_2, are noticeably greater than the critical values almost along the entire blade height; therefore, the conditions of flow in the nozzle cascade will

*This detailed calculation can be performed only for given values of the loss coefficient and therefore, strictly speaking, it should be conducted, based on the results of static cascade investigations (see § 45).

vary only at very high temperatures of the cooling water: namely the velocities c_1 and w_1, and the angle β_1. For these stages only M_{w_2} will be practically variable. For stages with computed values of $M_{w_2} \leq 1$, M_{c_1}, M_{w_1}, and angle β_1 will vary. For all last stages of steam turbines, depending upon the pressure in the condenser, the Reynolds number will vary.

For turbines with variable speed, besides the above-indicated changes, M_{c_1}, M_{w_1}, angle β_1, and angle α_0 will vary in all cases. Expecially essential is the change of conditions in stages of extracting machines.

It should be noted also that certain errors, which are permitted for several reasons in the complicated calculation of three-dimensional flow, and also certain manufacture deviations from drawings, require the selection of cascades which, independently of variable stage conditions, would not be very sensitive to some variation of the angles α_0 and β_1 and the inlet and outlet velocities.

The main criterion in the selection of cascade type is the M_{c_1} (or M_{w_2}) number.

Three cases are possible: 1) completely subsonic flow in stage, 2) mixed flow; supersonic in root sections of nozzle cascade and in upper sections of moving cascade, and subsonic in upper sections of nozzle cascade and in root sections of moving cascade; 3) completely supersonic flow in clearance and in relative motion behind stage.

Let us first consider the structure of the profiles for a stage with subcritical velocities. In this case, for the majority of sections, we should be guided by the atlas or the profile standards, whereby it is the most expedient to select standard profiles for the mid-sections. If we select effective profiles and correspondingly optimum geometric parameters (pitch and angle of incidence) for the mid-sections, then even in the most remote sections, i.e., the root and peripheral sections, the losses will be moderate.

In accordance with the selected law of twisting of the nozzle cascade, the form of the function $\alpha_1(r)$ is known. For a guarantee of the given change of $\alpha_1(r)$ it is possible to change the profile angle α_y and the relative pitch. It is obvious that the geometric parameter which has the weakest effect on cascade losses should be subjected to maximum changes. By using the results of cascade tests in static conditions, it is not difficult to establish which of the two parameters (α_y or $\bar{t}$) should be subjected to variation for guarantee of the selected law of $\alpha_1(r)$. With

a not very large change of α_1 from root to top, it is more expedient that the relative pitch with respect to height be maintained approximately constant and the change of α_1 be ensured by turning the profile, i.e., increase the profile chord from root to top. In certain cases, depending upon the type of profile twisting of the nozzle cascade is rationally accomplished by simultaneously changing α_y and $\bar{t}$.

Thus, for the solution of the problem on hand, it is necessary to rely on the characteristics $\alpha_1 = f(\alpha_y, \bar{t})$ and $\zeta_{пр} = f'(\alpha_y, \bar{t})$ (see Chapter I).

In attempting to reduce the number of stages in a low-pressure cylinder, small nonoptimal ratios u/c_Φ are sometimes selected for them. In this case the angle of entrance to the nozzle cascade can be considerably less than 90°. These cascades cannot be constructed from the usual profiles that are intended for $\alpha_0 \approx 90^\circ$. It is especially bad to use these profiles in extreme sections, where the influence of end phenomena is perceptible. In this case it is possible to use the profiles recommended in § 24 or to specially design them for the calculated angle α_0.

Profiles for subsonic velocities should respond to the condition of continuously varying curvature (profiles of group "A"): the diffuser sections should be as short as possible, and the pressures gradients in them should be minimum.

In the root sections of a moving cascade, where the reaction is small, in a number of cases it is expedient to design the divergent-convergent channels as recommended for cascades of group "K" (Chapter I).

Of importance is the question concerning the selection of the inlet angles of the moving cascades. In accordance with experimental data, with the increase of reactance, the influence of the inlet angle of flow on cascade losses decreases (see Chapter I). Minimum losses are detected in impulse cascades at inlet angles that are somewhat greater than the geometric angle of the leading edge. In reaction cascades with small angles of rotation ($\beta_1 > 90^\circ$) a reverse picture is observed, i.e., minimum losses correspond to inlet angles of flow that are somewhat less than the geometric angles. For an illustration of this, Fig. 244 [98] and [99] gives the loss coefficients, depending upon β_1 for the root and peripheral sections of a moving cascade of the limiting stage of a large steam turbine. Therefore for a moving cascade, the geometric angles of the leading edges of the blades may be noncoincident with the angles of flow: $\beta_1 \neq \beta_{1л}$. In the root sections, $\beta_1 > \beta_{1л}$. The difference of angles decreases toward the tip and $\beta_1 < \beta_{1л}$ in the peripheral sections. In accordance with the experimental data, this law of change of $\beta_{1л}$

ensures minimum losses in the moving cascade.

With a mixed flow in a clearance, the velocities in the root sections of a nozzle cascade are supersonic, and subsonic in the peripheral sections. In this case the shape of profiles varies with respect to blade height not only as a result of twisting, but also in connection with the change of the M number (at the outlet).

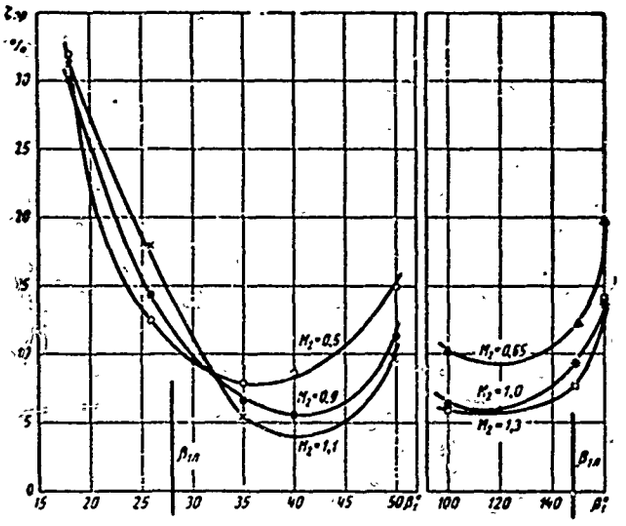

Fig. 244. Influence of the angle of leakage on profile losses of the moving cascade of a stage with d/l = 265 in the following sections: root (on the left) M_2 = 1.1; inlet angle $\beta_{1л}$ = 28°; minimum losses at β_1 = 35-40°; upper section (on the right): inlet angle $\beta_{1л}$ = 148°, minimum losses at β_1 = 115-125°.

In those sections where the velocities are subsonic, $M_{c1} < 0.9$ (upper sections of nozzle cascade), the profiles have the usual subsonic shape (profiles of group "A").* In sections where the flow is transonic, profiles of group "Б" are applied (mid-section of nozzle cascade). In the root sections the M_{c1} number is considerably greater than unity and profiles of group "B" or specially profiled divergent nozzles must be used here. The inlet conditions vary essentially in a moving cascade. In the root sections the profiles are similar to impulse profiles and the inlet and outlet velocities in them are transonic or low supersonic at the outlet.

In accordance with this, impulse profiles of group "Б" or "B" must be placed in these sections.

Only in very rare cases, under calculated conditions, are moving cascades design designed with supersonic inlet velocities. However, in this case the M_{w1} is not much greater than the critical value.

Frequently, especially for the limiting stages of both steam, and also gas turbines, the geometric characteristics of the root sections of the rotor blades differ essentially from the standard profiles. This is connected with the reliability

*This is one of the most important specific features of the nozzle cascade of a last stage, which requires a new and different approach to their investigation and design.

of blades and disks. Usually the root sections have relative pitch $\bar{t}$ and thickened profiles, in consequence of which very narrow channels are formed. Sometimes thick profile edges are necessary. Furthermore, one should consider that the root sections of blades of last stages must operate stably during changes of angle β_1 and velocities w_1 and w_2. Specific features of the root sections of rotor blades of last stages are small design Reynolds numbers.

Under design conditions they reach up to 1 to $2 \cdot 10^5$, decreasing with the deepening of the vacuum.

Toward the middle and upper sections of a moving cascade the profiles become reaction type. The mid-sections of a moving cascade are like the usual supersonic nozzle cascades which have, because of strength conditions, thinner profiles and thinner leading edges. The upper sections of a moving cascade differ by very small angles of rotation, thin (almost constant thickness) profiles, and large pitch.

Optimum blade shape is the most difficult for a mixed section in a stage. Due to technological conditions, it is not always possible to completely work out this shape. In this case the permissible deviations must be checked experimentally.

With a completely supersonic flow in a stage, the blades of the nozzle and moving cascades correspond to group "Б" and "В" or, depending upon the M numbers in absolute and relative motion, only to group "В." It is characteristic that the outlet areas of many sections of the nozzle and moving cascades of such a stage must be carried out with a slight expansion of the vane channel and concave back in the slanting shear.

The relationship between geometric angles and angles of flow should be different as compared to subsonic stages. In the considered case $\beta_1 < \beta_{1л}$ in the upper sections; in the root sections of a moving cascade, when $\beta_1 < \beta_{1л}$, there can appear choking conditions that are connected with the impracticability of such flows when $M_{w_1} > 1$.

A similar remark can be made with respect to stages having a mixed flow, in the root sections of which the flow at the entrance to the moving cascade is supersonic.

In an actual stage, where M_{w_1} decreases from root to periphery, this "choking" at the entrance to the root sections will lead to a redistribution of flow rates with respect to height, and consequently, to a decrease in economy.

An example of profiling blades for a mixed flow is shown in Fig. 245, a and b. Here, in the root sections of the nozzle cascade, reaction profiles are employed for supersonic velocities, with a slightly divergent section at the vane channel outlet and concave back in the slanting shear. Impulse profiles are used in the root sections of the moving cascade. The upper sections of the nozzle cascade, for low supersonic are made from the usual profiles of group "Б."

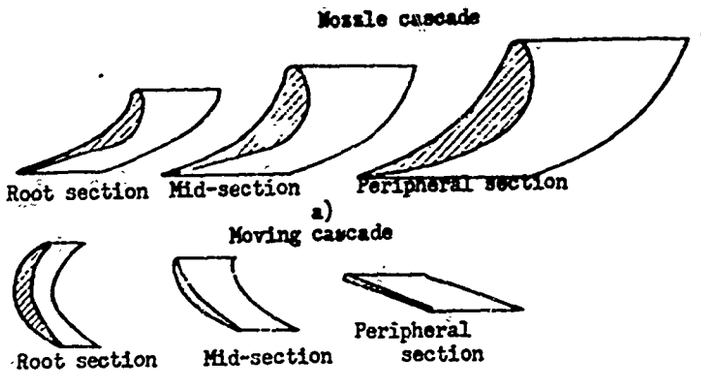

Fig. 245. Blade profiling for a stage with mixed flow: a) nozzle cascade — root section (M_{c1} = 1.57) of special cascade with divergent channels and concave back in slanting shear; mid-section (M_{c1} = 0.98) of standard cascade TC-2A; peripheral section (M_{c1} = 0.74) of same cascade TC-2A; b) moving cascade — root section M_{w1} = 0.92; M_{w2} = 1.22; mid-section M_{w1} = 0.25; M_{w2} = 1.46; peripheral section M_{w1} = 0.68; M_{w2} = 1.72.

Let us consider some results of an investigation (in static conditions) of sections of nozzle and moving cascades of limiting stages of large turbines.

The distribution of velocities, angles, and reactions for the calculation of a limiting stage is shown in Fig. 246. This stage was designed under the condition of $\alpha_{1\ эф} \approx$ const.

Figures 247 and 249 give graphs of losses for three types of nozzle cascades whose blades are milled (Fig. 248). For profiles with a convergent channel, minimum losses are found at $M_{c_{1t}}$ = 0.7 to 1.0. In design conditions for the root section, the $M_{c_{1t}}$ number equals 1.57; the profile losses have larger values. It is obvious that the transition to cascades with divergent channels at high velocities (see Chapter I) should lead to an essential lowering of losses. The curves on Figs. 247 and 249 distinctly show that the design of the channel in the root section with slight divergence at the outlet makes it possible to decrease the profile losses a few times under design conditions, and the deflection of flow in the slanting shear also essentially decreases. It should be emphasized that the modern form has the best results for the range of conditions that are practically encountered in normal operation.

For a section of the nozzle cascade that is at a distance of 0.1l from the root, the design M_{c_1} number amounts to 1.38. The advantage of the group "B" cascade, with smaller divergence of the vane channel (f = 1.11) in design conditions, is obvious: the losses are lowered by 4.5% in this section upon transition to the A-A shape of the back (see Fig. 248). For a section, that is at a distance of 0.35l from the root, the usual shape of the back, which is applied for profiles of group "Б," has indubitable advantages; when M_{c_1} = 1.1, the profile losses in this section amount to 3 to 3.5%.

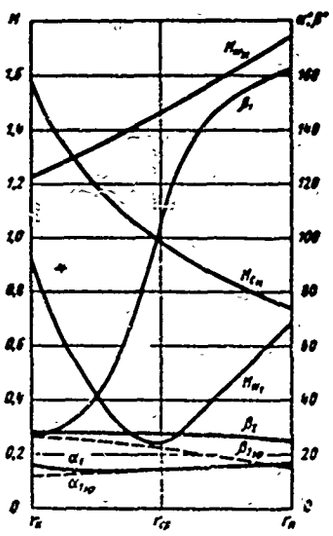

Fig. 246. Distribution of velocities and angles with respect to height for the limiting stage of a large condensing turbine (calculation performed by means of a simplified equation for radial equilibrium in a clearance).

The given results distinctly show that for obtaining maximum efficiency, the profile of a nozzle cascade should vary in height in accordance with the change of the M_{c_1} number. This method of profiling ensures not only minimum losses in a nozzle cascade, but makes it possible to better organize the flow in an annular cascade. Actually, the application of profiles of group "B" for the root sections leads to a decrease of the angle of deflection of flow in the slanting shear. Since deflection in the slanting shear in a real annular cascade occurs also in a radial direction, a decrease of the expansion ratio of the flow in the slanting shear by means of the application of cascades of group "B" makes it possible to decrease the radial velocity components and the radial leakages, respectively.

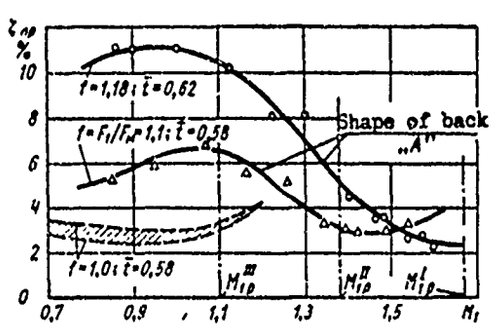

Fig. 247. Influence of the channel shape of a nozzle cascade on profile losses (see Fig. 248).

The sections of a nozzle cascade that are calculated for a large M_{c_1} number may be designed according to the method of characteristics. Let us mention some of the features of this kind of profiling for given conditions of flow in a specific section. Calculation of the channel is performed, starting from the minimum throat area, where it is assumed

that $M_{c_1} = 1$.

The expansion ratio of the channel should always be assumed as less than that found by stage calculation. Appropriate recommendations for the selection of $f_{опт}$ are given in Chapter I. However, taking into account the peculiarities of steam flow in last stages, certain deviations are possible.

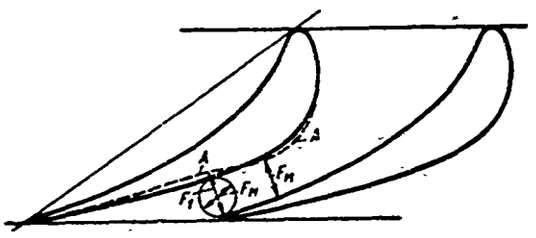

Fig. 248. Different shapes of a nozzle cascade.

First of all it is necessary to consider that supersonic cascades noticeably react to a change of Reynolds number at small Re numbers and with decreases of M_{c_1} numbers as compared to the design values. Furthermore, one should consider the inevitable additional expansion of the flow beyond its limits, which is caused, in particular, by the finite thickness of the trailing edges.

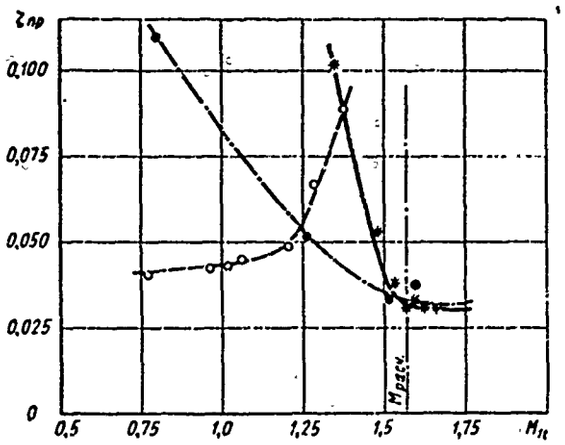

Fig. 249. Influence of change of cascade on profile losses in the root section of a nozzle cascade at $\alpha_0 = 90^\circ$ and b = 60.5 mm. (MEI experiments); curves: ——— (solid) — cascade with divergent channels; — — — — (dotted line) — cascade with convergent channels. Experiments in air, $Re_{max} = (5 \text{ to } 8) \cdot 10^5$. In both of these cascades the geometric parameters $\bar{t}$, b, a, $\delta_{кр}$, and α_0 are identical; — . — . — . — (dot and dash) — cascade from the same profiles, but with larger pitch (with smaller f > 1). Experiments were conducted in steam, $Re_{max} = 2.3 \cdot 10^5$.

Given experiments for special shapes of profiles of last stages showed that the parameter f should be selected according to the M_1 number $\approx$ $\approx 0.9 M_{расч}$.

Figure 250 shows an example of the calculation of the channel of the root section of a nozzle cascade by the method of characteristics, and Fig. 249 gives the results of investigations of a straight cascade in this section.

Dependences of profile losses on the M_{c_1} number (experiments were conducted by engineer Ye. V. Mayorskiy in an air wind tunnel of the MEI) are shown here for this cascade and for a usual cascade without a divergent section. From a comparison of the curves, and also

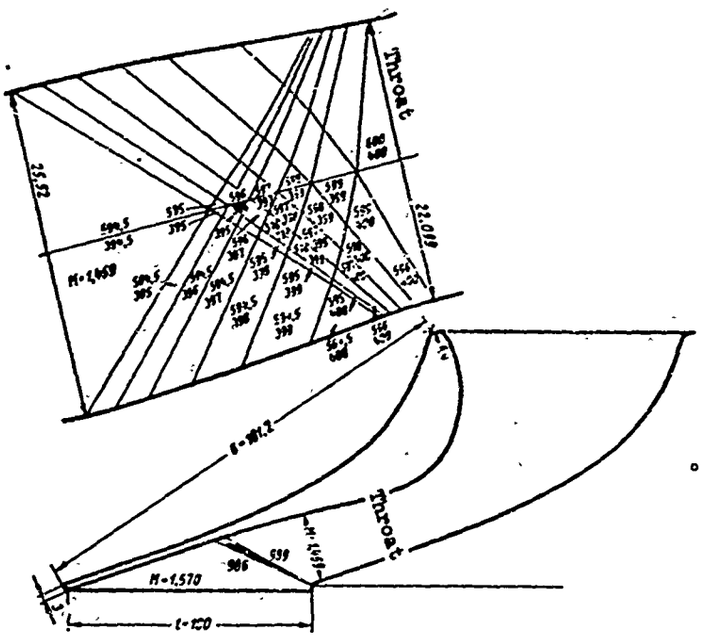

Fig. 250. Calculation of a channel of the root section of a nozzle cascade by the method of characteristics.

from an analysis of the distribution of curves of stage losses, it is clear that in a convergent channel, in spite of the favorable straightening of the back of the profile in the trailing section, starting with M > 1.25, there is a sharp increase in losses which is caused mainly by separation of the boundary layer in the shock wave zone.

Although the given experiments were not reduced to the design number $M_{c_1} = 1.57$, nevertheless it is obvious that the losses in an ordinary cascade with this M number will be even greater; these statements are confirmed by other, similar investigations.

A specially profiled divergent channel has very small losses at M number > 1.5; at the same time, at low velocities the profile losses are essentially increased.

It is obvious that for high stability of the given cascade, it should be designed for a smaller M_{c_1} number, i.e., with smaller expansion, f < 1.15. However, inasmuch as the given cascade is intended for steam operation in a region of little moisture, then for k = 1.135 the cascade will have more sloping characteristic with minimum losses at smaller M numbers (experiments were conducted in air).

Figure 249 shows the dependence of profile losses for a cascade composed of the same profiles, but with a somewhat larger pitch, and consequently, a smaller expansion

f. The experiments were conducted in steam (final moisture content (1 - x) = 0.02 to 0.03) at a constant Reynolds number (for the influence of the Re number on losses in divergent cascades, see below on p. 430).

For the root sections it is impossible to disregard the end phenomena. The above-considered cascade (see Fig. 250) was investigated in different sections with respect to height both in a straight, and also in an annular cascade. The results of this investigation are shown in Fig. 251. Inasmuch as the experiments were conducted under different conditions, we will not compare the total losses, but only the end ones. For a straight cascade, the influence of the ends is perceptible for l/b = 0.2 to 0.25, whereby the mean value of losses in this zone is greater than that of the profile losses by $\Delta\zeta \doteq 3\%$. In an annular cascade, the zone of end losses extends to l/b = 0.4 to 0.55, which in an actual stage corresponds to a distance of 100 mm from the root. In this zone the losses increase by $\Delta\zeta \approx 3.8\%$.

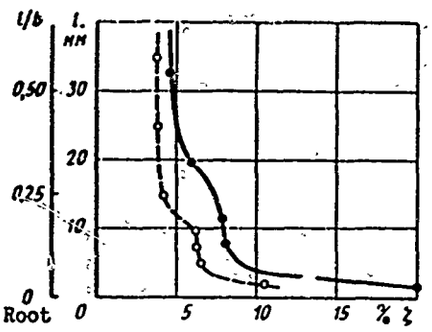

Fig. 251. Losses in the nozzle cascade shown in Fig. 250 (MEI experiments). Curves: ——— (solid) – steam experiments in an annular cascade, M_{c1t} = = 1.60; $Re_{max} = 3.3 \cdot 10^5$; – – – (dash) – air experiments in a straight cascade, M_{c1t} = 1.57; $Re_{max} = 8.8 \cdot 10^5$.

If these losses are referred to half of the height of a limiting stage with $l \approx 1000$ mm (taking into account the end phenomena in the upper contour of the diaphragm), then total cascade losses will be increased by 0.8%.

Let us consider in detail the results of profiling and the investigation of the upper sections of rotor blades. It should be noted that in connection with the very large reaction at the top and the highest specific flow rate, the influence of the economy of these cascades is greater than for all other sections of both nozzle, and also moving cascades.

The configurations for these cascades are specific, e.g., small thickness and camber of profiles, large pitch, small deflection of flow in channel, and components sometimes consisting of several degrees. A change of chord and thickness of a profile is possible only within very narrow limits, since it is limited by blade strength. These cascades, even in design operating conditions of a turbine, have high supersonic exhaust velocities that reach $M_{w_{2t}}$ = 1.7 to 1.8; upon deepening the vacuum, the velocities increase to $M_{w_{2t}} \approx 2$. The MEI laboratory conducted an investigation of

several cascades on the upper sections of the rotor blades of the limiting stage of a 300 thousand kilowatt turbine [99].

The results of an investigation of one of the upper sections are given below. This section of the turbine is at distance of 930 mm from the blade root. One of forms of this section I is shown in Fig. 252. The same figure shows a diagram of pressure distribution along the profile, depending upon the M_{2t} number at the outlet (design value of M_{2t} = 1.72). The inlet angle is $\beta_1 = 161^\circ$. In all investigated conditions the inlet convergent portion of the channel is streamlined on the back approximately identically with a sufficiently smooth change of velocity. At the same time, at the inlet on the concave side of the profile we see a diffuser section, the presence of which confirmed the calculation of the flow that was performed according to the channel method [93].

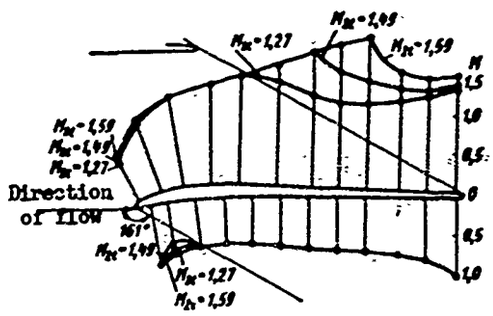

Fig. 252. Diagram of velocity distribution along a profile of the upper section of a moving cascade (form I) of a limiting stage (MEI experiments) at Re = (7 to 9)·10^5, b = 62.3 mm, and $\bar{t}$ = 0.907.

In general, at the entrance section of the concave wall the pressure gradient is very small.

The diagram of velocities around the contour of profile I allows us to make the following very interesting conclusions. If the velocities on the concave side of the profile are continuously variable and the diffuser sections, apparently, are small, then on the back in the slanting shear there occurs a sharp change of pressure which is caused by a system of shocks. With the increase of velocity, this intermittant, shock-like character of flow is evident to a large extent.

At higher velocities the system of shocks leads to a separation, and consequently to essential losses.

The dependence of profile losses on the M_{2t} number, which is represented in Fig. 253, shows that in the range of M_{2t} numbers from 1 to 1.45 the losses amount to 6 to 7%, and at high velocities, beginning with M_{2t} = 1.45, they grow sharply and attain a magnitude of 10.5% at M_{2t} = 1.66. Upon transition to design conditions and, all the more so, to conditions of deep vacuum, the losses will strongly increase. Calculation of the upper section of the entire stage shows that at M_{2t} = 1.8 the losses in the moving cascade (in kJ/kg) exceed the sum of losses in the nozzle cascade and

with the outlet velocity. Then, 20% of the length of the blades, in which the sections are essentially similar, admits as much steam as 40% of the height computed from the root.

Another cascade, form II (Fig. 253), has a straight-sided profile at the inlet and a smaller, in comparison with form I, angle of incidence (for the cascade of form I, the angle of incidence is equal to 16°, and for form II, it amounts to 8°).

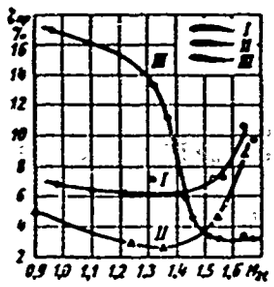

Fig. 253. Profile losses in a moving cascade of the upper section of a limiting stage at Re = 7 to 9)·10^5 (MEI experiments).

The dependence of profile losses on the M_2 number is also analogous for cascade II. It is true that the improvement of the conditions of flow at the inlet led to a decrease of losses here. At M_{2t} = 1.35 they attain a minimum magnitude, i.e., a total of 2.5%. However, starting with M_{2t} = 1.45, they grow steeply and attain 10% at M_{2t} = 1.67; at higher velocities, they tend to grow, which is even more favorable than for cascade I.

In order to increase the effectiveness of a cascade in zone zone of design velocities, i.e., high supersonic velocities, a new cascade was constructed. This design retained not only the performance parameters (inlet and outlet angles and velocities, size of throat), but also the strength requirements profile area, thickness, trailing edge, and others). The new cascade, which was profiled and checked experimentally, is shown in Fig. 254. After the short inlet section, which is calculated for optimum conditions of flow at a given inlet angle of β_1 = 161°, the profile does not have a concave part. Behind the inlet section there follows a divergent channel.

The expansion ratio of the channel is less than that calculated for the given value of M_{2t}, and it amounts to f = 1.104. The slanting shear of the channel has a so-called reverse concavity which makes it possible to essentially reduce the losses in the slanting shear, i.e., the main losses in cascades of forms I and II. Such a profile configuration, even with pre-expansion in the slanting shear, should lead to a stabler dependence of $\zeta_{пр} = f(M)$ (see Fig. 253) in a sufficiently wide range of high supersonic velocities. The new cascade of form III was investigated on a 1 : 2 scale under the same conditions as cascades I and II. A qualitative picture of the velocity distribution along the profile, which was obtained by draining it, is represented in Fig. 254. It is obvious that the velocity diagrams are

more favorable than for cascade I. For the back of the profile here, under all conditions there is observed a continuous change of velocities from the inlet right up to the outlet, including the velocity in the expanded portion of the channel. In the inlet section, which was designed with two convex sides, there is no diffuser region. The other side of the profile has a less successful pressure distribution, but in the expanded part of the channel there is observed a continuous change of velocity under all supersonic conditions.

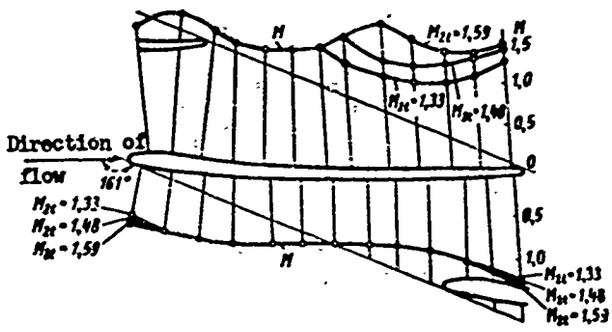

Fig. 254. Diagrams of velocity distribution around a profile of the upper section of a moving cascade (form III) of a limiting stage (MEI experiments) at Re = 7 to $9 \cdot 10^5$; $f = F_1/F_{1\,min}$ = = 1.1.04; b = 62.3 mm; $\bar{t}$ = 0.907.

It should be pointed out that, in distinction from cascade I, critical pressure in this cascade is attained in the minimum design section. This coincidence is very important for an exact determination of the flow rate characteristics, the calculated cascade areas, and the entire stage. It is obvious that an inaccurate knowledge of the minimum sections and there parameters in them will lead to a redistribution of the flow rates, reaction, and velocities with respect to height, and to a noticeable lowering of efficiency (see § 44). The flow in the expanded part of the channel is accelerated to $M_{2t} \approx 1.35$, which corresponds to the calculation.

The integral characteristics of cascade III (see Fig. 253) are the following: under conditions of subsonic and low supersonic velocities (to $M_{2t} = 1.35$) the profile losses are great and exceed 13%. In the zone from $M_{2t} = 1.35$ to $M_{2t} = 1.45$ there is observe a sharp decrease in losses to $\zeta_{пр} = 5\%$, and at $M_{2t} = 1.5$ to 1.7 the losses attain a minimum magnitude of $\zeta_{пр} = 3\%$. Cascade III can still be further improved. As shown by an analysis of velocity distribution along the profile, the configuration of the profile in the slanting shear should be changed somewhat, in order to smooth out the diagrams and decrease the negative influence of shocks. Depending upon the requirements of variable operating conditions of a stage, it is possible to transfer the zone of minimum losses both in the direction of smaller, and also larger M_{2t} numbers.

For the same relative pitch, $\bar{t}$ = 0.907, cascade III was investigated at various inlet angles (Fig. 255). The experiments showed that even with a decrease of angle

β_1 by 30° (this is possible by decreasing the actual reaction in the given section as compared to the proposed design reaction) both the character and the magnitude of the losses are practically unchanged. With the decrease of angle β_1 in the zone of high velocities, the profile losses tend to decrease. At the same time, at lower velocities ($M_2 < 1.4$), a decrease of angle β_1 leads to a growth of losses. This is explained the large influence of the inlet section, where a separation is formed on the back of the blade.

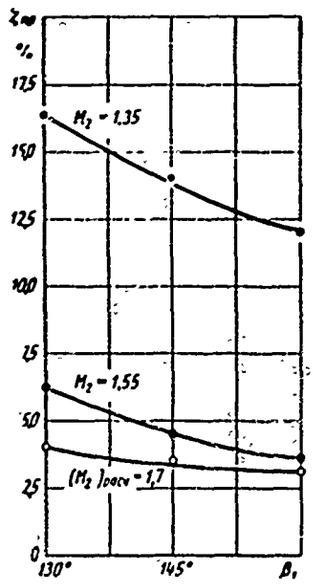

Fig. 255. Influence of inlet angle of flow on profile losses in the moving cascade of the upper section of a limiting stage (form III) (MEI experiments).

Of much interest are the investigations of the influence of pitch of this type of cascade. A change of pitch, and consequently, also the number of blades, affects the strength characteristics of the disk and the conditions of flow in the root sections of the blades, where the pitch is usually small and the channel is very narrow. A section of cascade III was investigated with a calculated pitch of $\bar{t} = 0.907$, and with a 10 and 20% decrease in pitch, i.e., to $\bar{t} = 0.726$, and with an increased pitch to $\bar{t} = 1.12$. Simultaneously for two values of $\bar{t}$ ($0.9\bar{t}_{расч}$ and $1.1\bar{t}_{расч}$) the angle of incidence changed by $\pm 5^\circ$. Thus, seven different expansion ratios from $f = F_1/F_{min} = 1$ to $f = 1.28$ were investigated for the given cascade. The results of these experiments (with inlet angle $\beta_1 = 161^\circ$) are presented in Fig. 256. The following conclusions can be made from them:

a) even the biggest possible deviations with respect to $\bar{t}$ and $\beta_{уст}$ did not lead to a very large increase of losses in the calculated zone of M_{2t} and ($M_{2t} = 1.55$ to 1.7). The losses in the worst case are lower than for other cascade types (see [99]).

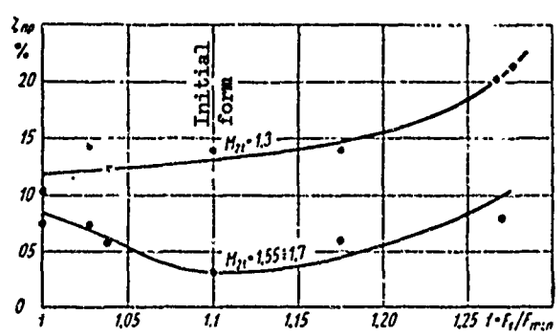

Fig. 256. Influence of relative channel expansion f on profile losses in a stage cascade (form III) (see Fig. 254).

b) minimum losses at high velocities are not attained at any arbitrary value of $\bar{t}$, but at the pitch for which the given cascade was specially profiled;

c) at M_{2t} numbers essentially smaller than the design values, the losses

naturally increase; the smaller f is, the smaller the magnitude of losses $\zeta_{пр}$.

With the increase of pitch and high velocities it is very difficult to obtain a cascade with small losses. However, in this case, it seems to us, the difficulty of an exact determination of the design outlet area is more essential.

Simultaneously with the measurement of losses, the outlet angle was also determined. As can be seen from Fig. 257, for the selected cascade III ($\bar{t}$ = 0.907) the angle β_2 from M_{2t} = 0.9 to M_{2t} = 1.67 practically did not change and amounted to 19.5°, which is 3° less than the effective angle. With a smaller pitch ($\bar{t}$ = 0.726), when the divergent section of the channel was retained, the angle β_2 also changed very little. However, for $\bar{t}$ = 1.12, just as for cascades of types I and II, when there is not divergent part, the influence of the M_{2t} number on angle β_2 turns out to be very noticeable, i.e., there occurs a deflection of the flow in the slanting shear.

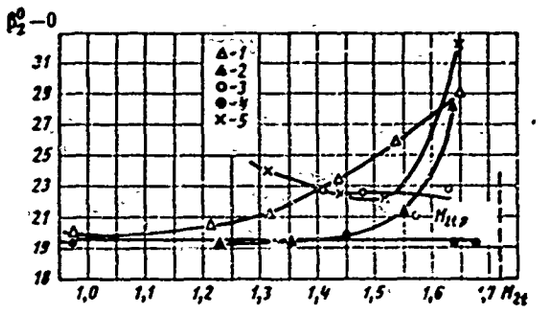

Fig. 257. Outlet angle of flow at the upper section of a moving cascade, depending upon exhaust velocity (β_1 = = 161°) (MEI experiments). Experimental points of various types of cascades: 1) cascade of type I; $\bar{t}$ = 0.907; 2) cascade II; $\bar{t}$ – 0.908; 3) cascade III; $\bar{t}$ = 0.726; 4) cascade III; $\bar{t}$ = 0.907; 5) cascade III, $\bar{t}$ = 1.120.

The total effect obtained from the application of profiles of optimum shape for the selected laws of change of $M_{c_{1t}}$ and $M_{w_{2t}}$ with respect to radius may be estimated by the curves in Fig. 258. In the nozzle cascade, modernization of the profiles in the root sections, where $M_{c_{1t}} \gg 1$, makes it possible to lower the total losses by 2%, whereupon the diagram of losses is essentially balanced along the blade length. In the moving cascade the profile losses decrease by 4.5% under design conditions.

By using the graphs of cascade losses, it is possible to estimate the magnitude of stage efficiency. Correct aerodynamic profiling of cascades of the considered stage with limiting dimensions makes it possible to increase the relative blade efficiency by approximately 3 to 5%.

The last stages of condensing turbines operate at low values of Reynolds numbers.

If in many cases, stages of high and intermediate pressure have Re numbers

that are so high that the influence of this criterion may be disregarded, although for last stages this disregard is not permissible. Investigations of cascades (see Chapter I), stages (see Chapter IV and § 44), and theoretical calculations show that the influence of the Re number is perceptible when Re < 3 to $6 \cdot 10^5$. In last stages the Re numbers are considerably lower. Thus, in a last step of limiting dimensions with p_K = 0.035 bar, the Re numbers for the rotor blade vary from $1.5 \cdot 10^5$ to $2 \cdot 10^5$ (at the root, where w_2 is less and Re, correspondingly, is lower). In small steam turbines, where both the velocities and chords are less, the Re number with the same vacuum can reach up to $0.5 \cdot 10^5$.

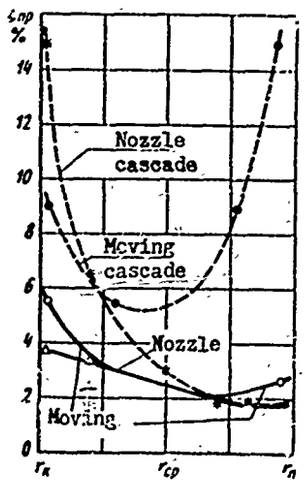

Fig. 258. Change of profile losses in nozzle and moving cascades of last stages (without taking into account the influence of Re number). Experimental points: ×—×— and ·—·— for initial profiles; —— Δ and ○ — for new profiles.

It is obvious that the investigations of these cascades and stages should be conducted at actual Re numbers. Moreover, cascade profiling in a number of cases should be performed with their flow taken into account at low Re numbers. Unfortunately, the investigation of the influence of low Re numbers on the characteristics of cascades is allotted little attention; this especially concerns cascades that operate at supersonic velocities; this is explained mainly by experimental difficulties.

For last stages, the investigation of cascades at actual Re and M numbers may be practically conducted in steam wind tunnels with steam outlet into a condenser.

Figure 259 presents the results of such an investigation for the upper section of the moving cascade of a limiting stage (see Fig. 254, form III) for three values of M_{2t} numbers: design M_{2t} = 1.72 and lowered M_{2t} = 1.5 and M_{2t} = 1.0 in a wide range of variation of the Re number from $9 \cdot 10^5$ to $1 \cdot 10^5$. The dimensions of this cascade corresponded to those of the one investigated earlier in an air wind tunnel (b = 62.2 mm, $\bar{t}$ = 0.907).

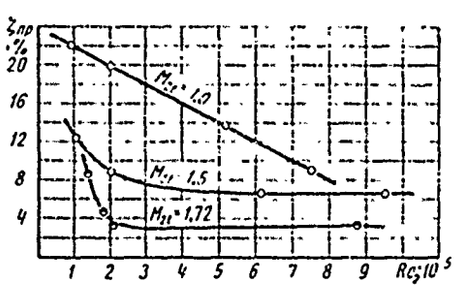

Fig. 259. Variation of profile losses in the upper section of the moving cascade of a limiting stage with expanded channels, depending upon Re and M_{2t} (MEI experiments) in a steam medium.

At the design M_{2t} number of 1.72, the cascade losses at Re ≈ $8 \cdot 10^5$ are small and amount to 3%. These losses are composed of the losses in the boundary layer and on the profile, which,

judging by the magnitude of total losses and the diagram of losses with respect to pitch, are small; they are also composed of edge losses and wave losses. The wave losses at such a large M number are concentrated in the outlet part of the slanting shear and behind the cascade.

A decrease of the Re number somewhat increased the losses in the boundary layer; the losses in the edge wake for a wide range of variation of Re number also do not change. Only at very small Re numbers less than $2 \cdot 10^5$, and with a subsequent decrease of the Re number, the losses noticeably increase. The character of the interaction of shocks with the boundary layer depends on the Re number.

For a smaller, off-design, M_{2t} number, in the slanting shear of a cascade there are observed shock waves, in the zone of which there occurs separation of the boundary layer, and consequently, an increase of losses. For such conditions, a decrease of the Re number, which leads to less stability of the boundary layer, makes separation of the layer more probable, and this leads to a growth of losses. This phenomenon had a slight effect on the magnitude of losses at $M_{2t} = 1.5$, when shock waves appeared in the slanting shear, and at the same time it rendered an essential influence on $\zeta_{пр}$ with a considerable decrease in velocity, when a shock wave appeared in the expanded part of the channel, near the throat.

These experiments showed that also when $M > 1$ the Re number affects cascade losses; however, at low Re, supersonic turbine cascades remain highly effective at design M numbers; with deviations from design velocities, the cascade losses increase considerably with the decrease of the Re number. In this case, specially profiled cascades with divergent channels should be employed. The difference in profile losses at M_{2t} numbers from 1.5 to 1.7, which is obtained by a comparison of convergent and divergent cascades in experiments with Re = 8 to $10 \cdot 10^5$, will increase considerably upon transition to Re = 2 to $3 \cdot 10^5$. Thus, if at Re = 8 to $10 \cdot 10^5$ the losses for this type of profile in a divergent cascade amount to $\zeta_{пр}^{расш} = 3\text{-}4\%$, and in a convergent cascade $\zeta_{пр}^{сужк} = 12\text{-}15\%$, then with a 3-4-fold decrease of the Re number the magnitude of losses $\zeta_{пр}^{расш}$ remains approximately the same, while $\zeta_{пр}^{сужк}$ will increase to 18-20%.

Experiments in a steam tunnel for sufficiently large cascade dimensions (b = = 62.2 mm, l = 70 mm, six channels) made it possible to perform investigations at high M numbers, keeping Re = const. The results of these experiments for Re = = $2.5 \cdot 10^5$ = const are shown in Fig. 260.

It is necessary to specially stipulate the procedure of the measurements. At

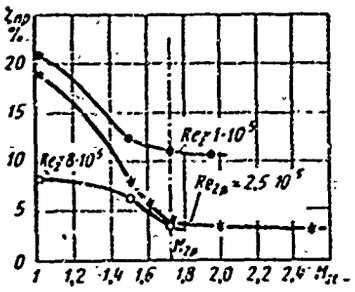

Fig. 260. Influence of M_{2t} on profile losses in the upper section of a moving cascade at Re_2 = const; Re_{2p} is the design number.

high M numbers greater than 2.0, steam expansion already occurs beyond the bounds of the slanting shear; as the distance to the plane of measurement from the cascade increases, the static pressure behind the cascade noticeably changes. Therefore, the M number was determined with respect to the pressure in the chamber behind the cascade, and the losses were calculated for static and total pressures at distance of 6 mm from the cascade. In connection with this, the wave losses were mainly concentrated outside the zone of measurement. In accordance with this, with the increase of the M number greater than 1.8-2.0 (see curve on Fig. 260), the cascade losses do not change.

Inasmuch as the given cascade is the last cascade of the turbine, and the velocity at its outlet is greater than critical, the losses that appear behind it almost do not influence the conditions of flow in the cascade itself, or the force, created by the steam on the blades. The picture of flow beyond the edges of the last blades will affect practically only the conditions of flow in the outlet duct of the machine. The influence of the losses that arise directly behind the last cascade on the losses and pressure recovery in the outlet duct of condensing steam turbines is insignificant.

From this there follows the conclusion that the moving cascades of last stages can be quite effectively designed not only for the design M_{w_2} number ($M_{w_2} > 1$), but can also have small losses even with an essential increase of velocity. In this case the upper sections of this cascade should be designed for velocities somewhat lower than the calculated ones, which will lead to expansion of the zone of their stable operation.

§ 44. RESULTS OF INVESTIGATION OF LAST STAGE IN EXPERIMENTAL STEAM TURBINES

If we understand last stages to be stages with small d/l, then many combinations of such stages were investigated in experimental turbines. Some of these experiments were described above in § 38. However, the results of such investigations, as a rule, cannot be used and, all the more so, they cannot be directly extended to the last stage of steam condensing turbines. This is caused by the following factors:

1. The stage tests are conducted in experimental air turbines at low subsonic velocities, whereas the last stages of steam turbines usually operate with high supercritical velocities, and only the first stages of the low-pressure cylinder of a large turbine and the last stages of a small turbine are calculated for transonic velocities.

2. Stage tests in experimental air turbines are conducted without taking into account the separate influence of the M and Re numbers and, as a rule, with Reynolds numbers that are considerably higher than in the actual stages of steam turbines, where they are usually lower than Re_{ABTOM}.

3. The peculiarities of the behavior of steam moisture are not considered.

4. The stages investigated in air-driv turbines are usually experimental (made in the laboratory) with cylindrical meridional contours. At the same time, the low-pressure stages of steam turbines have an intricate, usually noncylindrical, meridional diaphragm contour and special technology.

In connection with this, a number of laboratories are conducting investigations of last stages in experimental steam turbines. At present, we know the results of such tests for single stages that we conducted in the laboratory of the MEI Department of Steam and Gas Turbines [100]. Several organizations investigated a group of last stages. Although such tests do not make it possible to estimate the peculiarities of performance of an individual stage, they are of much interest. These tests were conducted for model stages in the KhTGZ laboratories and at the Westinghouse Company (United States), for actual low-pressure stages in a General Electric experimental turbine (United States); tests of low-pressure cylinders of permanent turbines are being conducted at electric power plants by ORGRES.

Tests of a Series of Stages with d/l = 3.7 to 4.4 in an MEI Experimental Steam Turbine

The same MEI experimental steam turbine was used for testing four stages.*

As a result of the experiments the relative internal efficiency η_{oi} of the stage was obtained; it was calculated for the inlet stagnation parameters and took into account the following losses:

1) losses in the nozzle cascade, including those at the entrance to it; 2) losses

*See Chapter III for testing procedure. Experiments were conducted by engineer F. V. Kazintsev and L. Ye. Kiselev.

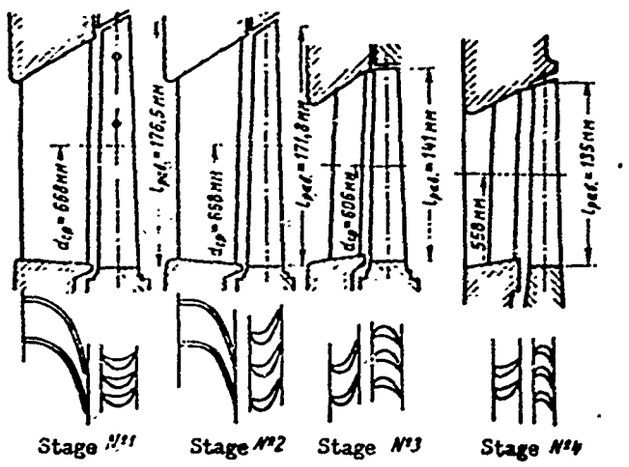

Fig. 261. How areas of stages with $d/l = 3.7$ to 4.4, investigation in the MEI experimental steam turbine.

in the moving cascade, including those at the entrance to it; 3) losses with the outlet velocity; 4) losses due to friction of the disk against steam, which are very small in all experiments since the steam density was low (final pressure varied from 0.12 to 0.035 bar); 4) losses due to leakage into the clearance over the rotor blade. There were no diaphragm seals (diaphragm was solid), the disk had no drillings, and consequently, there were no leakages in the root clearance of the stage.

Treatment of the test results was also conducted for the value of efficiency η^*_{oi} with the use of the kinetic energy of the outlet velocity

$$\eta^*_{oi} = \eta_{oi} \cdot \frac{1}{1 - h_{вс}/h_0}.$$

Here h_0 is the available stage drop from p_0 and t_0 to p_2; $h_{вс}$ was calculated by means of a continuity equation and for the mean stage angle β_2.

The flow areas of the investigated steps are shown in Fig. 261, and their geometric characteristics are given in Table 21.

Comparison of Economy of Investigated Stages

In Fig. 262, for approximately identical performance characteristics, $\varepsilon = p_2/p_0$ and $Re_{c_1} = b_1 c_1 t/\nu_1$, the dependences of relative internal efficiency η^*_{oi} on $u/c_ф$ are given for all investigated stages with the use of the outlet velocity. As can be seen from the curves, the highest efficiency η^*_{oi} is attained in stage No. 3, which is explained by the following factors:

1. The stage has contemporary, aerodynamically developed cascades with optimum pitch. The profile losses are small in this stage along the entire optimum pitch. The profile losses are small in this stage along the entire height at subsonic velocities and even low supersonic velocities. Angle α_1, which is greater than in

Table 21. Geometric Characteristics of Investigated Stages

Stage No.	1	2a	2b	3	4
Model of actual turbine stage	Next-to-last stage of turbine BK-50-1	Projected last stage of turbine BПT-25-4		Last stage of turbine AП-6	Last stage of turbine AK-12
Manufacturer's model	UTMZ	UTMZ	UTMZ	KTZ	KTZ
Scale model	1:2.5	1:2.5	1:2.5	1:2	1:3
d/l_2	3.88	3.7		4.4	4.15
Blade height in mm:					
nozzle	163	160.2		130.5	124
moving	176.5	171.8		137	134.2
Type of diaphragm	Cast	Cast	Welded	Cast	Cast
Law of twisting:					
nozzle cascade	Constant profile	α_1 = const		Constant profile	Constant profile
moving cascade	Hydraulic: with respect to velocity triangles	Simplified radial equilibrium in clearance; performance constancy (at $\varphi = \psi$ = const)		Simplified radial equilibrium in clearance; performance constancy	Simplified radial equilibrium in clearance; performance constancy
Area ratio F_2/F_1	2.15	1.58	1.48	1.51	1.38
Nozzle cascade:	Stamped	Stamped	Milled	TC-3A MEI	TC-2A MEI
pitch $\bar{t} = t/b$	0.34-0.42	0.37-0.52	0.55-0.71	0.47-0.71	0.55-0.87
height $\bar{l} = l/b_{cp}$	2.3	2.42		3.28	4.9
effective angle $\alpha_{1эф}$	14°20'-15°30'	16°-14.7°		20°-24.5°	16°45'-21°24'
Moving cascade:	Old type	New		New	New
pitch $\bar{t} = t/b$	0.38-0.64	0.56-0.97		0.61-1.01	0.58-0.84
height $\bar{l} = l/b_{cp}$	6.43	5.9		5.5	5.8
Effective angle $\beta_{2эф}$	25°25'-32°30'	23.3°-22.9°		38°-27°	28°25'-20°10'
Radial clearance in mm	1.5	1.5	1.5	1.5	4.5
Wire connections	2 wires Ø 3 mm	None*	None	None	None

*Stage No. 2a was also tested with two rows of wires 3.4 mm in diameter. Difference in efficiency amounted to 0.5-0.8%.

the remaining stages, although it leads to a consdierable output loss, it nevertheless improves the conditions of entrance to the moving cascade, since the latter operates with a smaller deflection of flow.

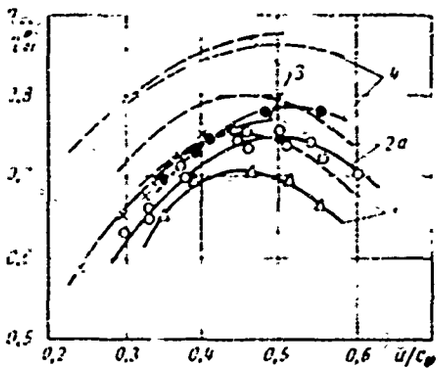

Fig. 262. Measured relative internal efficiency η_{oi} (solid lines) and efficiency with the use of the outlet velocity η^{*}_{oi} (dotted lines) for four stages, depending upon $u/c_{\text{ф}}$. For a stage pressure ratio of ε = = 0.6 to 0.67; Re number equals $b_1 c_{1t}/\nu$ = (0.5 to 0.8)·10^5 (MEI experiments) (the numbers on the curves refer to the stages in Fig. 261).

2. The high relative blade height, in combination with large angles α_1, β_1, and β_2, led to minimum end losses. The meridional contour of the diaphragm with small conicity on the periphery did not cause considerable additional losses, which take place in certain other stages.

3. Correct selection of the combination and ratio of areas gave an optimum reaction for stage No. 3, while good sealing of the peripheral clearance resulted in very little steam leakage.

The highest stage efficiency with the use of the outlet velocity at optimum ε and the highest Re number, amounts to η^{*}_{oi} = 92 to 94%. For such a stage, a further increase of economy is possible as a result of a more exact calculation of the three dimensional flow and a corresponding change of the profiles of the moving cascade, a better quality of manufacture, and better sealing of the peripheral clearance. It is interesting to note that the experiments in the LMZ laboratory for the investigation of stage No. 21 of turbine ПВК-200, which has practically the same dimensions and is similar with respect to cascade characteristics, made it possible to obtain an efficiency of η^{*}_{oi} = 92 to 94% [13]. The LMZ stages investigated in the air-driven turbine had a better laboratory quality of manufacture and a cylindrical meridional contour.

Under the same conditions, stage No. 4 has an efficiency η_{oi} 1.5 - 3% lower in spite of the good selection of cascades. This is explained by the smaller angle α_1, the larger radial peripheral clearance, and the considerable conicity (cone angle equals 40°) of the upper meridional contour of the diaphragm.

Stage No. 2a has an efficiency η_{oi} that is approximately 8% lower than stage No.3; this is explained mainly by the significant losses in the nozzle cascade. The old stamped profiles, even with small nonoptimum pitch $\bar{t}$, have large profile losses,

$\zeta_{пр} \approx 4$ to 5%. On the other hand, even for such long blades ($l_1 \approx 160$ mm) other end losses are perceptible (including frictional losses on the bounding walls of a cast diaphragm).

Figure 263 present a graph of the distribution of losses in the nozzle cascade of stage No. 2a. The diaphragm was tested in the same experimental turbine with the rotor removed. In spite of the fact that $\bar{l} = l/b = 2.42$, such a noticeable influence of end phenomena is explained, first, by the high surface roughness of the cast diaphragm. Furthermore, the influence of the contours — cylindrical at the root and conical on the periphery — should be considered.

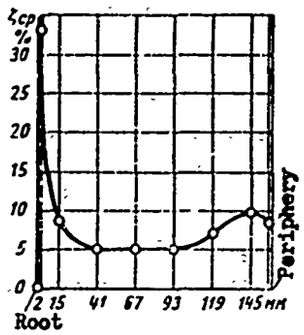

Fig. 263. Graph of the distribution of losses with respect to height in the nozzle cascade of stage No. 2a (MEI experiments).

As can be seen from Fig. 263, the losses increase a great deal particularly in the root portion of an annular cascade (see Chapter VI). This all indicates that even for stages with long blades we cannot disregard the end phenomena, which usually are not considered when designing these stages.

The cascade combination in stage No. 2a is not optimum; even under design conditions, in the root sections the stage has a severe negative reaction which will be especially unfavorably reflected in an actual turbine stage with steam suction in the root clearance.

It is interesting to note that the stage calculations that were performed taking into account the nozzle opening and the distortion of the meridional flow lines (see § 45) showed a very good approximation to the experimental data. Figure 264 presents the experimental and calculated distribution of the reaction for stage No. 2a. It should be noted that the stage calculation was performed for constant (with respect to height) velocity and flow rate coefficients.

Stage No. 1 has an even lower efficiency. Its losses are of the same order as for stage No. 2a, but an incorrect calculation of swirling (without taking into account the change of pressure along radius) caused large flare losses. It should be added to this that in this stage the profiles of the rotor blades are of the old type with straight inlet and outlet sections and sharp variations in camber. Such cascades, as it is known, not only have large losses, but are also very

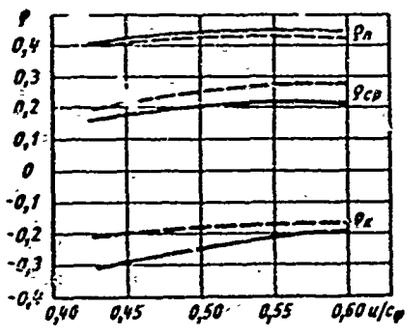

Fig. 264. Experimental and calculated (dotted line) distribution of reaction in stage No. 2a: $\varepsilon = 0.75$; $Re = 0.8 \cdot 10^5$.

sensitive to changes of the inlet angle, which is bad for all long blades, and all the more so for blades designed without taking into account the change of the reaction with respect to height.

Influence of Operating Conditions on Stage Characteristics

Let us consider the influence of the three basic parameters of a stage: $u/c_{\text{ф}}$, ε, and Re.

The influence of $u/c_{\text{ф}}$ was the usual, as for the other stages that were tested. In all five stages the value of the mean reaction is not especially great. In connection with this, the optimum value of the velocity ratio also is not great:

$$(u/c_{\text{ф}})_{\text{опт}} \approx 0{,}5 - 0{,}6.$$

As shown by experiments, the stage reaction in a wide range of variation of $u/c_{\text{ф}}$ changes insignificantly. This circumstance is explained by the fact that in the upper part of the blades β_1 is close to a right angle; therefore, the influence of the redistribution of drops between cascades is not great, and also the losses due to steam leakage do not change very much. The influence of $u/c_{\text{ф}}$ (at ε = const) on stage efficiency is determined mainly by two factors: the losses with the outlet velocity and the changes that occur in the moving cascade at β_1 = var.

The influence of the pressure ratios in the stage, $\varepsilon = p_2/p_0$, affects efficiency by the variation of the M numbers which are calculated for velocities c_1 and w_2. For stage No. 2a with a small reaction, the efficiency η^*_{oi} is determined mainly by the losses in the nozzle cascade. This is graphically illustrated in Fig. 265, where, depending upon $\varepsilon = p_2/p_0$, curves are given for η^*_{oi} and φ^2 (φ is the velocity coefficient obtained on the basis of the results of static diaphragm investigations. The curve for φ^2 was constructed depending $\varepsilon = p_2/p_0$ by means of recalculation of the stage reaction. Inasmuch as the experiments with the diaphragm, which are represented here in the form $\varphi^2 = f(\varepsilon)$, and the experiments with the stage, were conducted at different Re numbers, these curves can be compared only qualitatively.

For stage No. 3, the curve of $\eta^*_{oi} = f(\varepsilon)$ has a completely different character, which is very similar to the results of experiments with cylindrical blading and a

similar nozzle cascade (see Fig. 90). Inasmuch as in stage No. 3 both the nozzle and the moving cascades are designed for subsonic velocities, the highest stage efficiency also corresponds to subsonic conditions of flow (the losses were especially increased at high velocities and small Re).

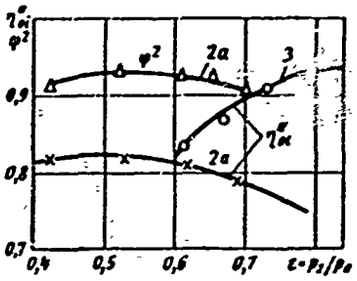

Fig. 265. Change of relative internal efficiency with the use of the outlet velocity η^*_{oi} and the value of φ^2, depending upon $\varepsilon = p_2/p_0$, for stages No. 2a and No. 3 (MEI experiments).

All investigated stages were tested at different Re numbers. The Reynolds number was changed at a constant ε ratio, i.e., constant numbers, by M number simultaneously changing the initial and final pressure. Final pressure was changed in a number of conditions more than three times. For stage No. 4, interesting experiments were also conducted on the influence of the Reynolds number for a constant stage heat drop and variable initial temperature. As expected, the influence of the Re number, which was detected at variable p_2 and variable t_0, turned out to be identical. In analyzing the results of the experiments, one should consider that in the experiments with a single stage there is no turbulence of the inlet flow. Furthermore, the relative roughness of the channel walls in a model is naturally greater than in an actual stage.

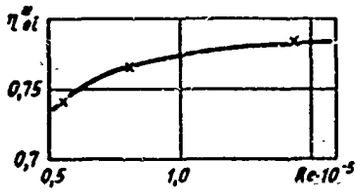

Fig. 266. Dependence of relative internal efficiency with the use of the outlet velocity on the Reynolds number for stage No. 2a. MEI experiments with $u/c_\Phi = 0.5$ and $\varepsilon = 0.6665$.

Figure 266 shows a curve of the dependence of maximum efficiency η^*_{oi} (at $\varepsilon = 0.65$) on the Re number for stage No. 2a. The influence of the Reynolds number is especially perceptible when Re is less than $1 \cdot 10^5$. This is confirmed by experiments with other stages of this series, and also by the experiments considered in § 18.

The change of efficiency from the Re number is explained mainly by the influence of this number on the cascade losses. Inasmuch as the dependence of losses (profile and end) on the Re number is determined by many geometric and performance parameters, then also for different stages the dependence of $\eta_{oi} = f(Re)$ can be essentially different.

These statements are distinctly confirmed by the experiments with stage No. 4, when the influence of the Re number was investigated for various values of ε. The

results of these experiments are shown in Fig. 267. As can be seen from the graph, the influence of the Re number is especially perceptible under subsonic conditions.

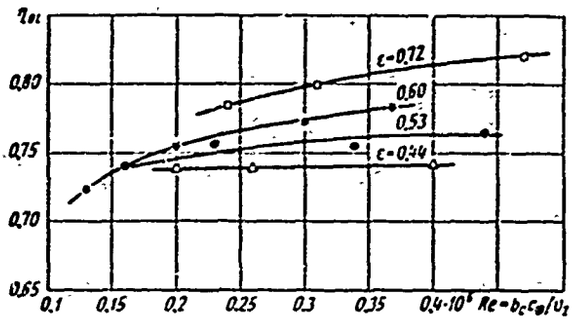

Fig. 267. Separate influence of Re and M numbers on the efficiency of stage No. 4. MEI experiments with $d/l_2 = 4.15$, $F_2/F_2 = 1.38$, and $u/c_\Phi = 0.5$.

As the M number increases, the influence of Re decreases, and at minimum ε it is insignificant. This is confirmed by certain experiments with cascades; however, this picture of the separate influence of Re and ε is not universal. In the light of these experiments, we discovered the errors of a number of researchers, who analyzed the influence of the Reynolds number at variable M numbers, and sometimes even with only the M numbers taken into account.

Simultaneously with the determination of stage economy, the stage reaction in root and peripheral sections and the steam flow were measured.

Figure 268 represents the dependence of the mean reaction of stage No. 2a on on u/c_Φ and ε. After examining it, we can easily see that, as usual, with the increase of u/c_Φ and the decrease of $\varepsilon = p_2/p_0$, the reaction increase.

However, as was noted above (on p. 438), the influence of u/c_Φ on the reaction ρ is less than in stages with large d/l ratios.

The influence of Reynolds number on the stage reaction is analogous to stages with large d/l and is determined by the dependence of the flow rate coefficients on the Re number.

As the Reynolds number of the stage decrease, the reaction increases; this is confirmed by experiments, the results of which are shown in Fig. 269. It should, however, be pointed out that in certain stages the difference in Re numbers for nozzle and moving cascades can be small, and in this case a decisive value can be obtained by such factors as the non-uniformity of flow at the inlet and roughness of the channel walls. Furthermore, each cascade can be in a mode of continuous flow or can be streamlined with separation; in this case the influence of the Re number is different. Therefore, it is possible that in certain cases a decrease of the Reynolds number

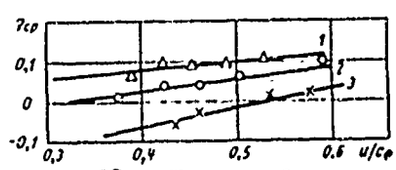

Fig. 268. Change of mean reaction depending upon ε and u/c_Φ for stage No. 2a at Re = const (MEI experiments). Curves: 1) ε = 0.57; 2) ε = 0.67; 3) ε = 0.73.

may not lead to an increase of the reaction, but just the opposite, i.e., a decrease of it.

The dependences of the relative steam flow rate, $\mu q = G_{нзк}/G_{1t}$, on $u/c_{ф}$ and ε are analogous to those obtained for other stages (see § 20). The flow rate coefficient of the nozzle cascade only (even with plant manufacture of the diaphragm), both in experiments with a separate diaphragm, and also in experiments in an experimental turbine, amounts to μ_1 = 0.97-0.99 (with an accuracy of the determination of area). The flow rate was measured in all experiments by means of weighing the condensed steam.

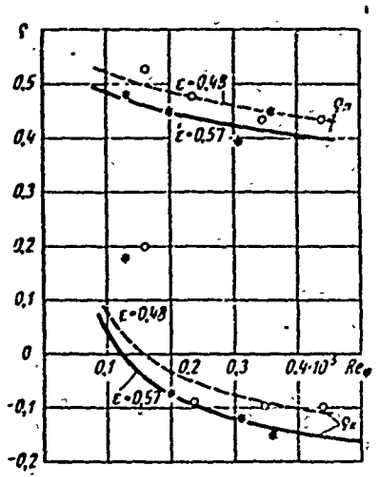

Fig. 269. Change of reaction at the periphery $\rho_п$ and at the root $\rho_к$ of stage No. 4 depending on $Re_{ф}$ for $u/c_{ф}$ = = 0.5 and ε = const.

The flow rate coefficient μ_1 of the nozzle cascade of stage No. 2a, which has a cast diaphragm and stamped blades, is shown in Fig. 270.

The experiments conducted with stages of this series showed that for long blades, during discharge of superheated steam, with a large degree of accuracy we may assume that $\mu_1 \approx 0.975$.

Fig. 270. Flow rate coefficient μ_1 of nozzle cascade (cast diaphragm with stamped blades) of stage No. 2a.

Investigation of a Stage with the Ratio d/l = 2.75

In the same MEI experimental turbine, F. V. Kazintsev investigated a model (in a scale of 1:3.6) of the last stage of a large turbine. The basic stage characteristics: l_1 = 207 mm, $l_1/b_{ср}$ = 3.45, $\alpha_{1\ эф} = 18^{\circ}$, l_2 = 212.5 mm, $\beta_{2\ эф} = 35^{\circ}$ to 24°, and F_2/F_1 = 1.68. Nozzle blades were stamped from a sheet of constant thickness with a small increase of angle $\alpha_{1\ эф}$ from root to periphery. The moving cascade was designed according to a simplified equation of radial equilibrium.

The influence of ε and $u/c_{ф}$ on the efficiency of the stage is the same as for stage No. 2a; maximum efficiency is attained at $\varepsilon \approx 0.52$. The influence of Re on

the efficiency of the stage is shown in Fig. 271.

Of much interest is the dependence of the reaction on $u/c_{ф}$, which is shown in Fig. 272. If, for the root section, the reaction $\rho_{к}$ grows with the increase of $u/c_{ф}$, then for the peripheral section, conversely, it decreases. This is explained by the fact that when $\beta_1 > 90^{\circ}$, a growth of $u/c_{ф}$ leads to an increase of w_1. As a result, the mean reaction of the stage almost does not depend on $u/c_{ф}$ and is equal to $\rho_{cp} = 0.26$-0.24. The difference of the reaction at the periphery and the root, $\Delta\rho$, was noticeably less than according to the plant calculation. This may be explained by a number of factors: by disregarding the inclination of the meridional contour (angle of opening 26°), by leakage over the blades (blade not shrouded, radial clearance 3 mm), and by a high reaction at the root. For investigated conditions it may be assumed that in the root zone of the nozzle cascade there is a separation of flow, when measurements usually show a raised static pressure. According to experiments, the reaction at the root was approximately equal to zero, whereas in a detailed calculation it should be negative.

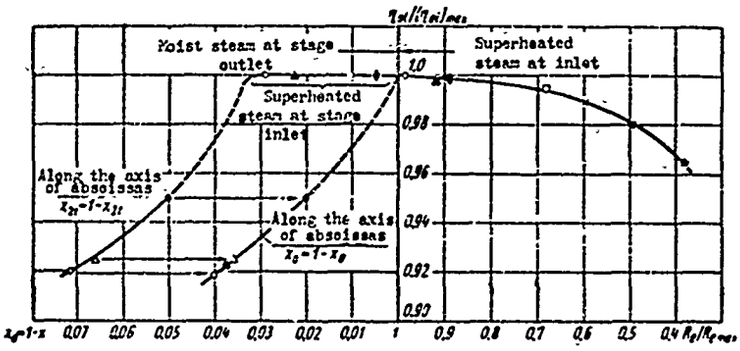

Fig. 271. Influence of Reynolds number and moisture on the efficiency of a stage with $d/l = 2.75$ (MEI experiments) at $\varepsilon = 0.49$ to 0.65 $(Re_{c1})_{max} = 1.2 \cdot 10^5$.

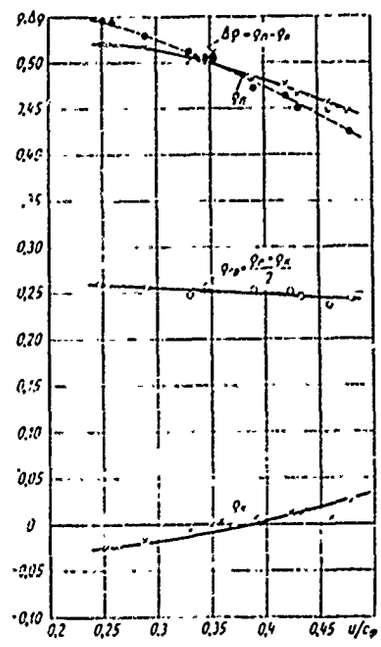

Fig. 272. Influence of $u/c_{ф}$ on the reaction of a stage with $d/l = 2.75$ (MEI experiments) at $\varepsilon = 0.54$ and $Re_{c1} = 5.2 \cdot 10^4$.

The influence of moisture is illustrated in Fig. 271. If the beginning of the process of steam expansion is above the saturation line, the efficiency of the stage does not change, even when almost the whole process of expansion occurs in moist steam. This may be explained by the fact that the process of condensation does not occur in this stage. If, however, the beginning of the process is in a region of moist steam, the efficiency essentially drops, whereby its lowering is approximately proportional to the final moisture x_{2t} (see Chapter X).

Influence of Certain Design Factors on Stage Economy

In tests of a series of stages with $d/l \approx 4$ the influence of various design factors was investigated. Thus, for instance, stage No. 4 was tested with two diaphragms that were manufactured according to the same drawings. One of diaphragms had a somewhat increased (as compared to the drawing) lower overlap and the upper overlap was increased 3.5 mm. Thus, the height of a nozzle blade, instead of 124 mm, was equal to 118.6 mm, and the mean angle $\alpha_{1\ эф}$ was decreased by $1^{\circ}10'$.

Consequently, the area of the nozzle cascade turned out to be almost 10% less than that calculated. The other diaphragm had a somewhat better quality of blade filling, but, due to metal shrinkage around the diaphragm contour, almost half of the blades had thickened trailing edges. In the first diaphragm, almost near every blade there were metal shrinkage cavities.

Therefore, the difference in the economy of a stage with two diaphragms can be attributed mainly to the change of area and increased overlaps.

Under the same conditions of flow the lowering of efficiency $\Delta\eta_{oi}/\eta_{oi}$, which was obtained with the first diaphragm, amounted to 4-6%.

Stage No. 4 was investigated in an MEI experimental turbine with two alternate arrangements of the inner contour of the duct. With the location of the duct close to the blades, the efficiency of the stage decreased by $\frac{\Delta\eta^*_{oi}}{\eta^*_{oi}} = 4$ to 8%.

Stage No. 2a was investigated with two overlaps. The overlap was changed by varying the height of the rotor blade. An increase of blade length from 168.8 to 171.8 mm, and an increase of the external overlap from 3 to 16 mm, lowered the efficiency of the stage (with the use of the outlet velocity) by 2%. Stage No. 2b differs from stage No. 2a by its diaphragm: the stamped nozzle blades were replaced by contemporary milled ones. The efficiency of the stage was then increased by 4 to 6%.

Investigation of a Group of Stages

From the number of experimental turbines intended for the investigation of a group of stages in [61] we shall consider the KhTGZ multistage experimental turbine. The experimental turbine of the GE Company (United States) [136] makes it possible to perform such investigations with actual dimensions and parameters of the low-pressure portion of turbines of practically any capacity. The turbine has two water brakes, a maximum power of 15 thousand kilowatts, and each one has a speed

from 1800 to 4000 rpm. The maximum steam flow rate is 135 t/hr. From a small number of published results of measurements [136], two graphs are of interest.

Figure 273 shows the measurement of the deflection of flow in a radial direction behind the moving cascade of the next-to-the-last stage of a turbine.

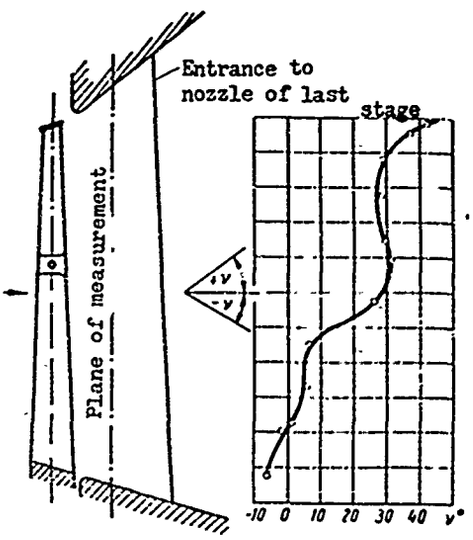

Fig. 273. Change of radial angle of direction of outlet velocity with respect to height behind the next-to-the-last stage of a group of low-pressure stages (GE experiments).

The velocity is directed downwards only in the lower part (the largest measured angle is 6°), the velocity on the mid-radius is directed upwards at an angle of 27°, and at an angle of more than 42° at the top.

These experiments show that even with a moderate inclination of the external meridional contour for the last stages of steam turbines it is impossible to assume that the flow surfaces are cylindrical in a calculation. This (see § 44), first of all, leads to an oversized discharge capacity of the stage. If we assume in Fig. 273 that the weighted mean angle of the radial direction of velocity is 30°, then the discharge capacity of the moving cascade will be 15% lower.

Figure 274 shows the influence of steam moisture on the economy of a group of stages. An increase of the initial moisture by 10% leads to a lowering in efficiency of the section by 10% (relatively).

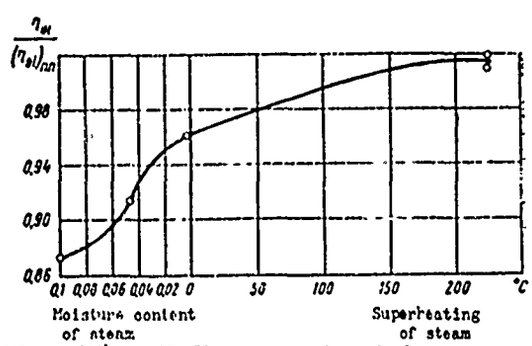

Fig. 274. Influence of moisture on the economy of a group of last stages; $(\eta_{oi})_{пп}$ is the calculated efficiency for superheated steam; along the axis of abscissas — state of steam in front of stage (GE experiments).

When comparing the influence of moisture according to the GE and MEI experiments, one should pay attention to the different conditions of entry to the stage. In the GE experiments, which were conducted in a multistage turbine, the average moisture at the entrance to the stage, undoubtedly, did not correspond to the moisture for the entire height. In [136], neither ε, nor x_2 is indicated for these experiments. In these experiments

the stagnation temperature behind the stage in the root and peripheral zone was 35°C higher than in the middle of the stage. This indicates large end losses that accumulated in the three preceding stages. If we judge these losses with respect to stagnation temperature, the zone of end losses covers 30% of the height at the root, and 12% at the periphery.

In an experimental turbine of the Westinghouse Company (United States) [148] a group of last stages was tested in a scale of 1:2, and three low-pressure stages of a 100 thousand-kilowatt turbine were tested at 3600 rpm. In a model, the speed was n = 8280 rpm and the maximum power was 11 thousand kilowatts. From the data given in the article [148], interest is aroused by the change of the flow rate components and outlet angle with respect to height behind the last stage (Figs. 275 and 276). In the first conventional version of blading, in the lower third of the blade height the flow rate is less than that calculated. Thus, in a section at a distance of 0.2l from the root, it is 2.5 times less than that calculated. But then, the flow rate at the top exceeds the calculated value by more than 60%. The outlet angle of flow also deviates considerably from the calculated value.

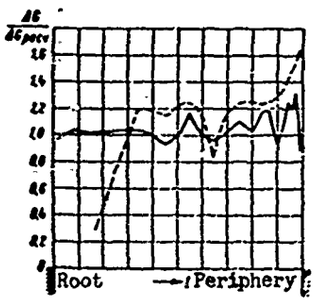

Fig. 275. Comparison (data of Westinghouse experiments with calculation) of flow rate components with respect to height behind a last stage. Curves: – – – – ordinary blading; ——— – improved blading.

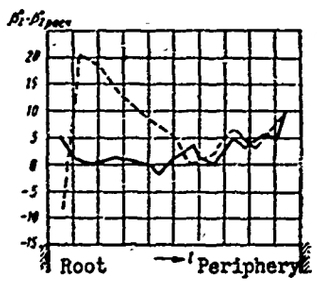

Fig. 276. Deviation of outlet angle of flow behind a last stage (Westinghouse experiments from calculation). Curves: – – – – (dotted line) – ordinary blading; ——— (solid) – improved blading.

In some sections this deviation amounts to 20°. In our opinion, the noncoincidence of the flow rate and vector characteristics of the blading is explained by the very large relative pitch in the upper part of the blades, where the cascade is "translucent." For these sections, neither by means of calculation, nor by static investigations, it is almost impossible to sufficiently exactly find the minimum section and the parameters of flow in it. In a cascade with a modified profile, in the first place, due to the increase of chord at the top, it turned out to be possible to more exactly calculate the steam flow rate with respect to height and the angle of flow. The new blading has small deviations in the flow rate and the out

the outlet angle from the values taken in the calculation. Simultaneously with the impr ement of rotor blades, the firm also midified the nozzle blades. With the transition to more favorable nozzle profiles, the efficiency of the last two stages was increased by a total of 2.5-5% (depending upon the flow rate through the stages). At the same time, the transition to new blading for the nozzle and moving cascades increased the efficiency of the last two stages at the design steam flow rate by 17.5%. It is doubtful whether such an increase (15%) in stage economy could be attained by decreasing the losses in the moving cascade. Undoubtedly, this improvement in efficiency is mainly connected with the correct calculation of three-dimensional flow, which is possible, in particular, only after a sufficiently accurate determination of the flow rate characteristics of separate sections.

§ 45. METHOD FOR CALCULATION OF THE LAST STAGES OF CONDENSING TURBINES

The complete calculation of the three-dimensional flow of steam in the last stage of a turbine is very complicated and tedious, and it usually requires a knowledge of certain characteristics which the calculator does not have at his disposal when designing a new stage. Therefore, it is natural that in most cases it is limited to a simplified calculation. Moreover, it is frequently possible to simplify the fundamental equations of flow without a noticeable error in the final results. At the same time, we cannot disregard such factors as the change (with respect to radius) of the velocity and flow rate coefficients, and we also cannot extend the formulas derived on the basis of equations of an ideal gas to moist steam.

Here we shall consider the procedure for calculating last stages by the method of successive approximation.

During the calculation, in each specific case we must decide the approximations to which we should be limited. This decision will depend on the purpose of the calculation, the time which can be spent for the calculation, and a knowledge of a number of auxiliary quantities which are needed for a more exact solution.

Although the errors obtained when using simplifying assumptions essentially depend on the specific problem, the numerical example given in this paragraph should be of assistance in this estimation.

In the numerical example we shall consider the limiting stage of a large steam turbine. The calculation of all remaining stages, i.e., the preceding stages of such

a turbine of the last stages of smaller turbines, and the stages of gas turbines in particular, as a rule, will be simpler.

The calculation of stages with small d/l can be performed by originating from the middle, as well as the root sections. The calculation that begins from the root section usually is less exact than the calculation from the middle, since the calculation errors increase from blade root to tip and a noticeable error can appear in the integral characteristics of a stage and especially in the steam (gas) flow through a stage. However, this method of calculation is convenient in a number of cases and, in particular, when model stages are used, where we applied it (see § 49).

For such individual stages as the last stages of condensing turbines (where for several reasons — the difference in velocities, the specific requirements of reliability, the individual shape of the meridional contour, etc. — model stages are rarely applied), it is usually more expedient to begin the calculation from the middle, which provides sufficiently accurate integral stage characteristics even with rough assumptions.

The initial data for the calculations are:

1. Diameter d_1, m, and height l_1, m, of nozzle cascade (in outlet section). 2. Diameter d_2, m, and height l_2, m, of moving cascade (in outlet section.). 3. Rotor speed n, rpm. 4. Steam flow rate G, kg/sec. 5. Parameters of steam before stage, p_0, bar, t_0°C (dryness x_0 or enthalpy i_0, kJ/kg), and velocity vector c_0, m/sec. All these parameters can be variable with respect to radius at the entrance to a stage.* 6. Final pressure behind stage p_2, bar. Usually p_2 is given for the mid-radius. 7. Meridional contour of stage, and consequently, cascades diameters and heights at the entrance, which are denoted by a "prime," d_1', l_1', d_2', l_2'. 8. Other design elements of a stage: clearances, dimensions, and location of connecting and damping wires, and so forth.

I. Stage Calculation for Mid-Section

This part of the calculation does not differ from the simplified calculation which is conducted for all turbine stages.

---

*The above-considered (see p. 444) results of experiments in a multistage turbine clearly show how necessary it is to introduce variable inlet parameters into the stage calculation.

1. The parameters of the stagnated flow before the stage (for mid-diameter d_1') are calculated and the total available heat drop of the stage is determined from the stagnation parameters ($\bar{i}_0$, $\bar{p}_0$):

$$h_0 = \bar{i}_0 - i_{2t}. \tag{265}$$

2. The reaction on the mid-diameter of the stage is given.

In first approximation, ρ_{cp} is selected so as to ensure a small positive reaction at the root, i.e., by means of the following approximate formula:

$$\rho_{cp} \geqslant \frac{1.8}{1.8 + d_2/l_2}, \tag{266}$$

[cp = mn = mean]

(this reaction pertains to the total available heat drop h_0).

3. The available heat drop of the nozzle cascade, the pressure behind the nozzle cascade $p_{1\ cp}$, the quantity $\varepsilon = p_1/\bar{p}_0$, and the angle of direction of flow are determined:

$$\sin \alpha_1 = \frac{G v_{1t}}{\pi d_1 l_1 \mu_1 c_{1t}}. \tag{267}$$

Here μ_1 is selected to Chapters I and X.

4. If $\varepsilon_1 < \varepsilon_*$, then in a nozzle cascade with convergent channels (on the mid-radius) there takes place a deflection of flow in the slanting shear.

Then the effective angle should be found by the following formula:

$$\frac{\sin \alpha_{1\phi}}{\sin \alpha_1} = m_1 = \left(\frac{\varepsilon_1}{\varepsilon_*}\right)^{1/\kappa} \cdot \sqrt{\frac{k+1}{k-1}\left(1 - \varepsilon_1^{\frac{\kappa-1}{\kappa}}\right)} \tag{268}$$

or by means of Fig. 277.

If the flow process terminates in a region of moist steam, the use of formula (268) or the graph in Fig. 277 gives a certain error. In this case it is better to use the following formula:

$$\frac{\sin \alpha_{1\phi}}{\sin \alpha_1} = m_1 = \frac{v_*}{v_{1t}} \cdot \frac{c_{1t}}{c_*}, \tag{268a}$$

where v_* and c_* pertain to the critical (minimum) section.

5. Knowing the velocity coefficients, which in first approximation may be assumed to be $\varphi = 0.96$ and $\psi = 0.93$, we construct velocity triangles with them.

The angle of direction of flow at the moving cascade outlet is found by the following formula:

$$\sin\beta_2 = \frac{G v_{2t}}{\pi d_2 l_2 \mu_2 w_{2t}}. \qquad (269)$$

[here μ_2 is selected on the basis of the data in § 9 or (more correctly) by means of formula (56a).].

6. Somewhat like we did for the nozzle cascade, we find $\varepsilon = p_2/\overline{p}_1$ for the moving cascade and for $\varepsilon_2 < \varepsilon_*$, by formula (268) or Fig. 277, we determine

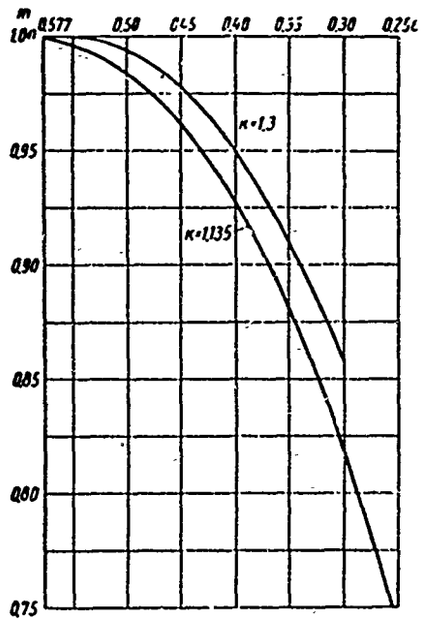

Fig. 277. Calculation of the deflection of flow in the slanting shear of a cascade (for superheated steam at k = = 1.3 and dry saturated steam at k = 1.135),

$$m = \frac{\sin(\alpha_1 + \delta)}{\sin\alpha_1}.$$

$$m_2 = \frac{\sin\beta_{2эф}}{\sin\beta_2}.$$

7. For the performed calculation we find, by usual means, the efficiency $\eta_{oл}$, the additional losses, including losses due to moisture (see Chapter X), and efficiency η_{oi}.

II. Stage Calculation for Three Sections

The calculation for the mid-section is not only a rough estimate, but it does not make it possible to form the stage, since this requires a knowledge of at least the change along the radius of angles α_1, β_1, and β_2. At first this may be done after constructing velocity triangles not only for the middle, but for two more sections, i.e., the root and peripheral sections, using the equation of radial equilibrium in the clearance. For this calculation it is necessary to select a law of twisting for the nozzle cascade.

1. The law of twisting for the nozzle cascade is usually given by one of three functions:

a) the dependence of angle α_1 (or $\alpha_{1\,эф}$) on the radius;

b) the dependence of the tangential velocity component c_{1u} (or c_{1tu});

c) the dependence of the axial velocity component c_{1a} (or c_{1ta}) on the radius.

2. By the formulas in Chapter VII for any of these functions we can find the

change of the reaction with respect to the radius:

For the calculation it is more convenient to give the change of the angle with respect to the radius, $\alpha_1 = \alpha(r)$.

Then we will have approximately:

$$\frac{c_1}{c_{1cp}} = \exp\left(-\int_{r_{cp}}^{r} \varphi^2 \frac{\cos^2 \alpha_1}{r}\, dr\right). \qquad (270)$$

Assuming that $\varphi = \varphi(r)$, we determine the values of c_1 and ρ for the root and peripheral sections, and we find the pressure p_1, angle β_1, and velocity w_1.

For $\varphi = \varphi_{cp} = \text{const}$ and $\alpha_1 = \alpha_{1cp} = \text{const}$,

$$c_{1t}/c_{1tcp} = (r/r_{cp})^{-\varphi^2 \cos^2 \alpha_1}.$$

3. In all cases the angle β_2 for the moving cascade in the root and peripheral sections is found by means of continuity equations:

for the root section

$$\frac{\sin \beta_{2\kappa}}{\sin \beta_{1\kappa}} = \frac{w_{1\kappa}}{w_{2t\kappa}} \cdot \frac{v_{2t\kappa}}{v_{1t\kappa}} \cdot \frac{(d_1 - l_1)\, l_1}{(d_2 - l_2)\, l_2}; \qquad (271)$$

for the peripheral section

$$\frac{\sin \beta_{2n}}{\sin \beta_{1n}} = \frac{w_{1n}}{w_{2tn}} \frac{v_{2tn}}{v_{1tn}} \frac{(d_1 + l_1)\, l_1}{(d_2 + l_2)\, l_2}; \qquad (271a)$$

in these formulas the specific volumes correspond to each section.

4. It is necessary to analyze the obtained results. In the first place one should pay attention to the reaction in the root section. It is very undersirable that ρ_K be negative. Therefore, if it turns out that $\rho_K < 0$, one should return to the first calculation and select another, larger value of the mean reaction of the stage.

With an increase of the reaction in the root section by $\Delta\rho_K$, one should increase the reaction on the mid-section by approximately the following quantity:

$$\Delta\varrho_{cp} = \Delta\varrho_\kappa \left(1 + \frac{l}{d}\right)^{-2\varphi^2 \cos^2 \alpha_1} \approx \Delta\varrho_\kappa \left(1 + \frac{l}{d}\right)^{-1,8}. \qquad (272)$$

It should be pointed out that an increase of the root reaction due to a corresponding increase of the reaction on the periphery, and consequently, due to an increase of leakage on the periphery, is insignificant for stages with small d/l. For stages with small d/l ($d/l < 3$) the reaction on the periphery depends very little on the root reaction.

Thus, for instance, for a stage with $\alpha_1 = \text{const}$, the value of ρ_n, upon

transition from $\rho_K = 0$ to ρ_K, is determined by the following formula:

$$\Delta\rho_K = \Delta\rho_C \left(\frac{\theta+1}{\theta-1}\right)^{-2\varphi^2 \cos^2 \alpha_1}. \qquad (273)$$

Thus, for instance, when $\theta = 2.65$ and $2\varphi^2 \cos^2 \alpha_1 = 1.8 \approx$ const, we obtain:

$$\Delta\rho_K = 0.24\Delta\rho_C.$$

i.e., if at $\rho_K = 0$ we obtain $\rho_\Pi = 0.76$, when $\rho_K = 0.1$ (i.e., when $\Delta\rho_K = 0.1$) we will obtain $\rho_\Pi = 0.784$. However, for large or even moderate values of θ the change of the root reaction already has a noticeable effect on ρ_Π. Thus, for instance, when $\theta = 10$ and $2\varphi^2 \cos^2 \alpha_1 = 1.8$, we correspondingly obtain: when $\rho_K = 0$ on the periphery, $\rho_\Pi = 0.309$, and when $\rho_K = 0.1$ on the periphery, $\rho_\Pi = 0.373$.

5. After the final calculation of the three sections, one should give special attention to the angle of direction of the absolute outlet velocity, i.e., angle α_2.

If the last stage of the turbine is not being calculated, the value of angle α_2 is not decisive, since it is assumed that the flow area of the turbine is designed in such a way that all the kinetic energy of the outlet velocity can be used. This, of course, requires that the nozzle cascade of the following stage be profiled in accordance with angle α_2.

If conventional nozzle cascades are employed in the following stage (designed for an inlet angle $\alpha_0 \approx 90^\circ$), then one should try to make $\alpha_2 \approx 90^\circ$. Deviation of α_2 from a right angle within the limits of $\pm(15$ to $20^\circ)$ is practically permissible.

The direction of the outlet velocity is very important for the last stage, where the quantity

$$h_{sc} = \frac{c_2^2}{2}$$

is not only the main loss for the given stage, but it determines the economy of the whole turbine to a large extent.

If the last stage is not a limited one, i.e., the dimensions of the last rotor blade (l_2 and d_2) can be increased, and the outlet velocities in the stage are subsonic, the minimum value of c_2 will appear when $\alpha_2 = 90^\circ + \beta_2$ (see p. 100).

For a limited stage, i.e., a stage with a maximum permissible annular area,

$F_a = \pi d_2 l_2$; if the angle noticeably differs from 90°, the losses with the outlet velocity increase at the given value of F_a; recovery in the contemporary outlet ducts of large steam turbines is very difficult, and sometimes it is even impossible. Therefore, for these stages one should try to make α_2 come as close as possible to 90°. Practically the only method is to change the drop in the stage, i.e., change $u/c_{\bar{\varphi}}$. Selection of the stage drop is considered in the following paragraph.

6. After calculating the three sections, it is possible to select the profiles of the nozzle and moving cascades of the stage in these sections. For this we must know the inlet and outlet angles, and also the flow rates.

The profiles should be selected with reliability and technology of manufacture taken into account. By having cascades only for these three sections, and selecting intermediate sections, it is possible to form a stage, which will approximately correspond to the boundary conditions and will be satisfactory from the point of view of economy. When forming cascades and changing profiles with respect to the radius, it is necessary to use the conclusions made in § 43. If the stage does not have limiting small values of d/l, is calculated for subsonic velocities in all sections, and has a cylindrical meridional contour, then even this roughly approximate method of designing gives fully satisfactory results.

III. Detailed Stage Calculation by Means of the Simplified Equation of Radial Equilibrium in a Clearance

For this part of the approximate calculation we shall use the simplified equation of radial equilibrium in a clearance:

$$\frac{dp_1}{dr} = \frac{c_{1u}^2}{r}\frac{1}{v_1}. \tag{274}$$

With the help of this equation we can determine all the characteristics of flow in each section (if the laws of variation with respect to the radius of one of three quantities are given α_1, c_{1u}, or c_{1a}) either by means of integral equations (see § 36) or by changing from one elementary stream to an adjacent one by the following formula (see Chapter VII):

$$\Delta p_1 = \frac{1}{v_1}\frac{c_{1u}^2}{r}\Delta r, \tag{275}$$

$$\Delta h_{01} = \frac{c_{1u}^2}{r}\Delta r. \tag{275a}$$

The analytic method requires less time, but it is not always possible equation

(274) is not integrated for all laws of variation of the angle or c_{1u}. In a number of cases this method gives an error when using the equations for an ideal gas (for stages that operate in a region of moist steam), and it does not make it possible to perform the calculation for an arbitrary law of variation of the velocity coefficient $\varphi = \varphi(r)$.

1. The law of twisting of the nozzle cascade is selected: either $\alpha_1 = f(r)$, or $c_{1u} = f'(r)$ or $c_{1a} = f''(r)$.

2. The law of variation of the velocity coefficient, $\varphi = \varphi(r)$, is selected. It is better that this law be based on the results of specific investigations of various sections for given M and Re. If it is possible to get at least approximate geometric characteristics of the cascades for the three sections from the second calculation, then, using the data in Chapter I and § 43 and the atlas of profiles, it is not difficult to at least roughly express the dependences $\varphi = \varphi(r)$ and $\psi = \psi(r)$. It should be pointed out that φ and ψ will depend not only on the cascade parameters (angles, M and Re numbers), but also to a considerable extent on how the cascade is designed or selected. Thus, for instance, if a conventional cascade for subsonic velocities is selected for the root section of the nozzle cascade, then at large M numbers only the profile losses it can amount to more than 10%. If, however, this section is specially designed for the given M, then these losses can be decreased by 2 to 3 times.

Inasmuch as this portion of the calculation usually does not contain sufficiently complete data on the cascades, Fig. 278 gives a graph of the velocity coefficient (taking into account all end phenomena) for a steam turbine with cast diaphragm and solid (not stampled from a sheet) blades.

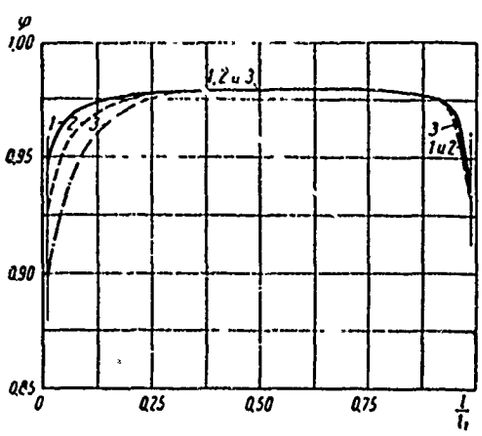

Fig. 278. Change of velocity coefficient with respect to the height of a nozzle cascade for milled nozzles cast into a cast-iron diaphragm.

The graph in Fig. 278 can serve only for a preliminary estimate; it assumes the cylindrical flow of superheated steam, and the Reynolds number

$$Re_{c_1} = \frac{b_1 c_1}{\nu_1} \approx 4 \div 10 \cdot 10^5.$$

This graph is constructed for three cases: 1) $d/l = 2.65$; $(M_{c_1})_K = 1.65$, cascades with divergent channels of the type

shown in Fig. 250 are used in the root sections; 2) $d/l = 2.65$, $(M_{c_1})_K = 1.65$, cascades of group "b" are employed in the root sections; 3) $d/l = 3$, $(M_{c_1})_K = 1.3$, the usual standard cascades are applied in all sections.

3. The law of variation of the flow rate coefficient, $\mu_1 = \mu(r)$, is selected. Figure 279 shows an approximate graph of this function, constructed for a cast nozzle diaphragm for superheated steam (or gas). For moist steam, this graph should be reconstructed in accordance with the data in Chapter X.

4. Using the selected law of twisting, for instance, angle $\alpha_1 = \alpha_1(r)$, the graphs for $\varphi = \varphi(r)$ and $\mu_1 = \mu(r)$, and going from the central stream to adjacent streams, we find all the necessary quantities, i.e., p_1, h_{01}, ρ, c_1, c_{1u}, w_1, β_1, and ΔG.

For this calculation it is necessary to select the number of streams into which the blade is divided with respect to height. Obviously, the greater the number of streams, the more accurate the calculation. At the same time, an increase of the number of streams increases the time necessary for this calculation. The minimum number of streams depends on d/l and ε. For $\varepsilon = 0.5$ and $d/l = 2.65$, no less than 21 streams are required. For larger ε, and especially for large d/l, it is possible to limit oneself to a smaller number of streams. For a zone of moist steam, the minimum number of streams may be estimated for the calculation by the following formula:

$$i \approx 50\, l/d + 3.$$

It should be pointed out that the stream calculation can be essentially simplified without a loss in accuracy because only Δp_1, Δh_{01}, and p_1 is found for all streams. The remaining quantities may be found for a smaller number of sections after dividing the blade with respect to height, let us say, not into 21, but into 7 sections. In the zone of the root and peripheral sections, however, it is recommended to select the sections frequently, since in these zones there is a sharp change in the basic characteristics, including φ, μ_1, and sometimes angle α_1.

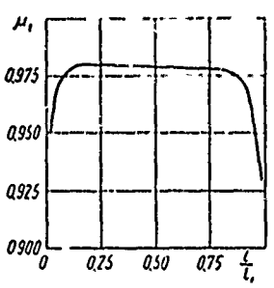

Fig. 279. Change of the flow rate coefficient with respect to the height of a nozzle cascade for a cast diaphragm; steam is superheated.

5. If there are no divergent channels in the nozzle cascade, then, by means of formulas (268) and (268a) or the graph in Fig. 277, the effective angles, $\alpha_{1\,эф}$, should

be found.

6. The steam flow through the streams is summarized:

$$G = \Sigma \Delta G.$$

If $\Sigma\Delta G$ noticeably differs from the given flow rate, it is necessary to make a recalculation. The following forms of recalculation are possible:

a) change of the initial pressure before the stage, which may be considered as proportional to the flow rate (in the majority of sections the flow rates are either critical or near-critical); this naturally requires a redistribution of the drops between stages;

b) change of the height of the nozzle cascade, l_1; in this case it is necessary to conitor the continuity of the flow area and the overlap of the stage;

c) change of angle α_1 (and consequently, angle $\alpha_{1\,эф}$). It should be noted that if the flow rate $\Sigma\Delta G$ turned out to be somewhat greater than the given value (not more than by 5 to 10%), it is meaningless to recalculate the stages, since in following step of the approximation, as a rule, the flow rate through the nozzle cascade turns out to be decreased in comparison with the given step of the approximation. If recalculation is performed, this circumstance must be taken into account and $\Sigma\Delta G$ for the recalculated version should be approximately 5% greater than the given value.

7. After recalculation of the stage, all the initial parameters of the moving cascade, i.e., p_1, w_1, β_1, $\overline{p}_1$, and $\overline{i}_1$ (stagnation parameters in relative motion) are variable with respect to radius. The moving cascade is divided into <u>the same quantity of streams</u> as the nozzle cascade, but the stream height corresponds to the outlet height of the moving cascade, i.e,

$$\Delta r_2 = \Delta r_1 \frac{l_2}{l_1}.$$

The velocity w_{2t} is calculated for each section.

8. Angles β_2 are determined for all sections by the following formula:

$$(\sin \beta_2)_i = (\sin \beta_1)_i \frac{v_{2t_i}}{v_{1i}} \frac{d_{1i}}{d_{2i}} \frac{\Delta r_1}{\Delta r_2} \frac{w_{1i}}{w_{2ti}}. \qquad (276)$$

If the places of installation of wires are approximately known beforehand, they must be taken into account when using formula (276).

For the streams where the wires will be located, $\sin \beta_{2\,эф}$ should be greater, and if the profile is assumed to be thickened, then it is necessary to increase

further. If this cannot be done, then in an actual stage, not only in the streams where the thickened profiles and wires are, but also sufficiently far from them, the flow rates ΔG will change as compared to the calculated values, ρ_1 (the reactions) and angles β_1 will change, and there will occur a noticeable distortion of the meridional flow lines. As a result of this, the economy of the stage will drop, not to mention the direct influence of the wires on the cascade losses.

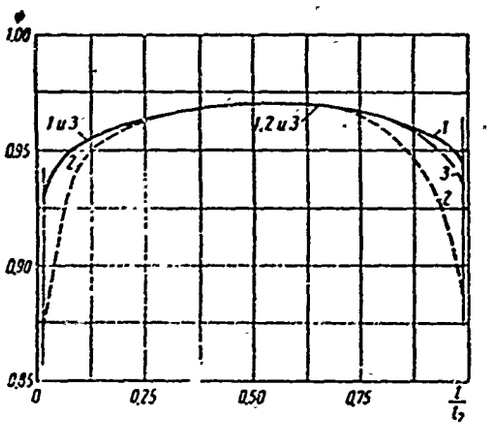

Fig. 280. Change of the velocity coefficient ψ with respect to the height of the moving cascade for the last stages of large condensing steam turbines.

9. The law of variation of the velocity coefficient, $\psi = \psi(r)$ is selected. The principle of construction of the graph for $\psi = \psi(r)$ is the same as for the graph of $\varphi = \varphi(r)$. This graph can be most reliably constructed on the basis of the results of static investigations of separate sections at actual M and Re numbers (see § 43). But also for a preliminary calculation it is possible to construct a tentative graph for ψ. Such a graph is presented in Fig. 280 for three types of cascades. This graph, which was constructed for a preliminary estimate, assumes the flow of superheated steam, and Reynolds number $Re_{w_2} = \frac{b_2 w_2}{\nu_2} = 5$ to $10 \cdot 10^5$. Here, the change of the profile and pitch takes into account the requirements of strength. An estimate of coefficient ψ is also made, taking into account the cascade entry losses that occur due to periodic instability of the flow. The end phenomena are considered in the root sections of the blades:

a) $d/l = 2.65(M_{w_2})_{\text{п}} = 1.7$, in the root section $\beta_1 + \beta_2 \approx 70^\circ$, and the peripheral sections have the type of cascade shown in Fig. 254;

b) $d/l = 2.65(M_{w_2})_{\text{п}} = 1.7$, in root section $\beta_1 + \beta_2 \approx 45^\circ$, and the peripheral sections have the type of cascade shown in Fig. 252;

c) $d/l = 3$, $(M_{w_2})_{\text{п}} = 1.45$, in the root section $\beta_1 + \beta_2 \approx 70^\circ$, and the peripheral section has the type of cascade shown in Fig. 252;

10. All the stage characteristics, i.e., angle α_2, c_2, c_{2u}, and $\eta_{\text{ол}}$, are determined depending upon the radius.

11. The deviation of p_2 along the radius from p_2 on the mid-section is calculated by the following formula:

$$p_{2i} - p_{2cp} = \frac{(c_{2u})_i^2}{r_{2i}v_{2i}} - \frac{(c_{2u})_{cp}^2}{r_{2cp}v_{2cp}}. \tag{277}$$

In case of a noticeable deviation of p_{2i} from $p_{2\,cp}$, the moving cascade is recalculated for more exact values of v_{2t} and h_{02}.

12. If divergent channels are not employed, the effective angle $\beta_{2\,эф}$ is calculated by formulas (268) and (268a) or by means of the graph in Fig. 277.

The results of a more exact stage calculation are given in a graph, an example of which is shown in Figs. 287 and 288, where the dependences of the following quantities on stage height (or radius) are given: angles α_1, $\alpha_{1\,эф}$, β_1, $\beta_{2\,эф}$; ρ; M_{c_1} and M_{w_2}

$$\eta_{oi} = \frac{u_1c_{1u} + u_2c_{2u}}{(i_0 - i_{2t})}, \tag{278}$$

$$\eta^*_{oi} = \frac{\eta_{oi}}{1 - \zeta_{oc}}. \tag{279}$$

13. The weighted mean efficiency of the stage is calculated:

$$\eta_{oi} = \frac{\sum \eta_{oi}\Delta G}{\sum \Delta G}; \tag{280}$$

and

$$\eta^*_{oi} = \frac{\sum \eta^*_{oi}\Delta G}{\sum \Delta G}. \tag{281}$$

14. The losses due to moisture and leakage are considered and the total relative internal efficiency of the stage η_{oi} and η^*_{oi}.

IV. Calculation of a Stage with Flow Lines on Conical Surfaces

Up to this point, the calculation of a stage began with the assumption that the flow lines lie on coaxial cylindrical surfaces. In reality, the flow lines in the meridional plane were complex curves. In this step of the calculation we shall assume that the flow lines lie on conical surfaces, i.e., they are straight lines in the meridional plane.

The calculation will be performed for three sections: at the entrance to the nozzle cascade, in the clearance between cascades, and at the stage exit. Thus, each flow line will generally be a broken line (see Fig. 281).

To do this, we shall divide the inlet height l_1' of the nozzle cascade into the same number of portions as l_1 and l_2.

1. Assuming that all flow lines in the meridional plane pass through the lines connecting the centers of the portions at the entrance to the nozzle cascade, in the clearance, and at the stage exit, for each portion we shall determine the angle of inclination of the flow line (see Fig. 281)*, i.e.,

for the nozzle cascade, ν_1,

and for the moving cascade, ν_2.

2. The steam (gas) flow through each stream for the nozzle cascade is found by the following formula:

$$\Delta G_{IV} = \Delta G_{III} \cos \nu_1. \tag{282}$$

Here the subscripts III and IV pertain to the step of the calculation.

The flow rate for all streams is summarized and the flow rate through the whole nozzle cascade is calculated.

This flow rate will always be less than the flow rate, obtained by analogous summation in step III of the calculation, i.e., in the calculation with flow lines lying on coaxial cylindrical surfaces.

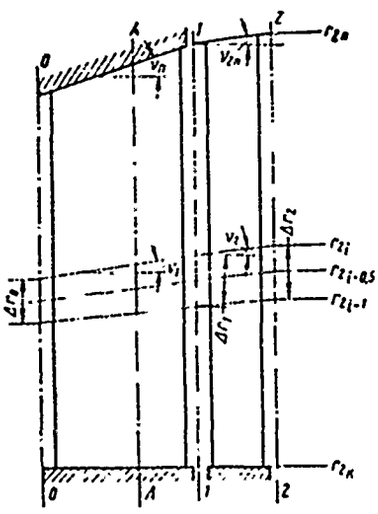

Fig. 281. Calculation of stage with flow lines on conical surfaces; streams on radius $r_{i-0.5}$.

The change of G_{IV}, as compared to G_{III} depends on two factors – the inclination of the external generatrices (in the meridional plane) and the nozzle cascade and distribution of specific flow rates through the streams. It is natural that angle ν_1 will mainly be at the periphery of the cascade (in the root sections, angle ν_1 usually is small). If we select the law of constancy of angle $\alpha_{1\ эф}$ along the cascade height, for a supersonic flow (and practically, for a transonic flow) the flow rate through the streams will be proportional to the radius of the stream. If angle $\alpha_{1\ эф}$, and consequently, also the specific flow rate, increases

*Here and subsequently the angle α_1 implies the angle of direction of velocity c in the plane of this velocity, and not on the cylindrical surface of the flow (see Fig. 282).

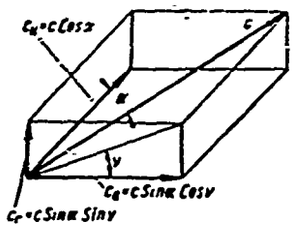

Fig. 282. Velocity parallelogram.

from root to top, the influence of the inclination of the flow lines on the total flow rate (a decrease as compared to G_{III}) will be great. With the decrease of the cascade drop, i.e., upon transition to subsonic velocities, the influence of angle ν_1 turns out to be smaller, since the specific flow rates through the upper sections (where the reaction is greater) will correspondingly decrease.

The change of the flow rate, as compared to that obtained in step III of the calculation, is determined by the following formula:

$$\frac{\Delta G}{G} = \frac{\Delta G_{IV} - G_{III}}{G_{III}} = -\frac{(\operatorname{tg}\nu_n)^2}{2}\left(\frac{r_K}{l_1}\right)^2 \frac{\int\limits_{r_K}^{r_n} q\sin\alpha_{1\text{эф}}\left(\frac{r}{r_K}-1\right)^2 r\,dr}{\int\limits_{r_K}^{r_n} q\sin\alpha_{1\text{эф}} r\,dr}, \qquad (283)$$

where $\nu_{\text{п}}$ is the angle of inclination of the peripheral flow line, i.e., practically the line of the meridional external contour of the diaphragm.

Formula (283) can be expanded for certain particular cases.

In general, for an estimate of $\frac{\Delta G}{G}$ it is possible to use the following formula:

$$\frac{\Delta G}{G} = -K(\operatorname{tg}\nu_n)^2, \qquad (284)$$

where K can be found on the graph in Fig. 283. The graph was constructed for two cases:

$$\sin\alpha_{1\text{эф}} = \text{const}$$

and

$$\sin\alpha_{1\text{эф}} = (\sin\alpha_{1\text{эф}})_{\text{ср}}\frac{r}{r_{\text{ср}}}.$$

It is clear from the graph that the greatest deviation will be observed when d/l is minimum and the angle increases toward the top. For $r_{\text{п}}/r_{\text{к}} = 2.5$ and $q = 1$,

$$\frac{\Delta G}{G} = -0{,}235(\operatorname{tg}\nu_n)^2.$$

When $\nu_{\text{п}} = 30^\circ$ this deviation amounts to $\frac{\Delta G}{G} = -7.9\%$. If the flow in the cascade is subcritical, then, inasmuch as the reaction toward the top is increased, which means that the specific flow rate decreases (as compared to the cascade having $q = 1 = \text{const}$), the influence on the inclination of the flow lines the steam (gas) flow rate will be smaller.

Thus, having the diagram of the meridional contour of the diaphragm, and

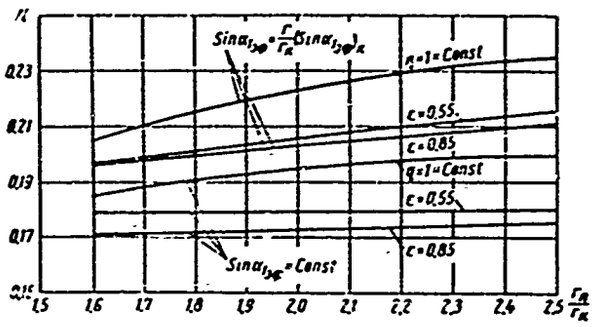

Fig. 283. Coefficient K for calculating the change of the steam flow through a nozzle cascade in comparison with the calculation for flow lines lying on coaxial cylindrical surfaces.

consequently, the angle $\nu_п$, it is possible in first approximation, without a detailed calculation, to estimate the influence of the inclination of the meridional flow lines on the steam flow rate and to consider this when determining the stage dimensions. In particular, when calculating the angles β_2 of the moving cascade, in formula (276) it is necessary to add the factor $\frac{\cos \nu_1}{\cos \nu_2}$, where ν_2 is determined analogous to ν_1, on the basis of the inclination of the lines of the corresponding streams in the moving cascade.

V. Stage Calculation for More Accurate Flow Lines

It is obvious that flow lines in general, even if they are straight in the meridional plane, will not exactly correspond to the lines directed to the vertex of the triangle formed by the bounding walls of the diaphragm.

For construction of these lines it is first necessary to find the parameters of flow before the nozzle cascade. If the width of the meridional contour of the diaphragm is bounded by a nozzle blade, it is possible to consider that these parameters will be the parameters at the entrance to the stage, i.e., at the exit of the preceding stage. In this case we have the dependence of the following necessary parameters on the radius $c_0 = c(r)$ and $v_0 = v(r)$: specific volume v_0 and velocity c_0.

If the width of the diaphragm is considerably larger than the width of the nozzle blade, one should conduct at least an elementary calculation of the annular diffuser which precceds the nozzle cascade and is formed by the entrance section of the diaphragm. It is best to use the results of the investigation of this diffuser or a similar one. However, it is usually necessary to be limited to an estimate of the effectiveness of this diffuser. We shall perform this estimate for two coefficients, i.e., the utilization factor $\lambda_д$ and the flow coefficient $\eta_д$, which takes into account the flow losses in the diffuser (Fig. 284):

$$\lambda_д = \frac{2h_д}{c_0^2}, \qquad (285)$$

$$\eta_д = (c_{01}/c_{01t})^2. \tag{286}$$

After obtaining $\lambda_д$ and $\eta_д$ by means of experiments or by making an estimate, it is easy to calculate the values of p_{01}, v_{01}, and c_{01}, which are necessary for further calculation of the stage.

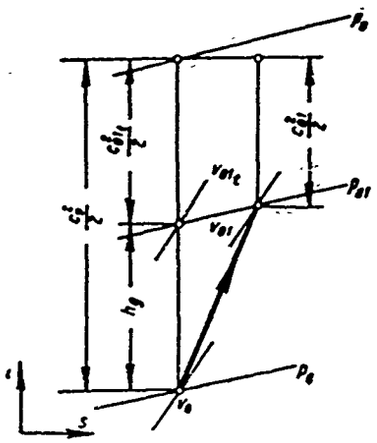

Fig. 284. Determination of the characteristics of the entrance section of a diaphragm (diffuser).

For this we use the continuity equation

$$\frac{c_{01t}}{c_0} = \frac{F_0}{F_{01}} \cdot \frac{v_{01t}}{v_0}. \tag{287}$$

Disregarding the influence of the change of temperature, we write:

$$v_0/v_{01t} = p_{01}/p_0 = \frac{p_0 + \Delta p_д}{p_0} = 1 + \frac{\Delta p_д}{p_0}.$$

For small $h_д$ it is possible to use the following formula:

$$h_д = v_0 \Delta p_д.$$

Then

$$\frac{\Delta p_д}{p_0} = \frac{h_д}{p_0 v_0} = \frac{\frac{c_0^2}{2}\lambda_д}{p_0 v_0} = \frac{\lambda_д}{2} M_0^2, \tag{288}$$

where M_0 is calculated with respect to velocity c_0.

As a result, we obtain the following dependence:

$$\frac{c_{01}}{c_0} = \sqrt{\eta_д}\,\frac{F_0}{F_{01}}\,\frac{1}{1 + \frac{1}{2}\lambda_д M_0^2}. \tag{289}$$

Coefficients $\lambda_д$ and $\eta_д$ depend on the shape and dimensions of the diffuser, in particular on angle $\nu_п$, the degree of nonuniformity of the velocity field at the entrance, the M and Re numbers, and also on the roughness of the walls. The various types of diffusers and their influence on the efficiency of an entire stage are considered in Chapter VII and in § 46. It is usually assumed that $\lambda_д$ = 0.4 to 0.8 and $\eta_д$ = 0.8 to 0.95.

After the values of c_{01} and v_{01} are found at the entrance to the nozzle cascade, for each value of the flow rate determined for the first stream from the root behind the nozzle cascade (preceding step IV of the calculation) we determine the area of stream at the entrance:

$$(F_{01})_1 = \frac{\Delta G v_{01}}{c_{01}}, \tag{290}$$

where $F_{01} = \pi(d_{01_K} + \Delta l_{01})\Delta l_{01}$; d_{01_K} is the root diameter of the stream at the entrance to the cascade, and Δl_{01} is the height of this stream.

After determining Δl_{01}, we go on to the next stream, etc. It is obvious that $\Sigma\Delta l_{01} = l_{01}$. In case of divergence, it is necessary to check the calculation, and in particular, to check the determination of the parameters c_{01} and v_{01}.

For simplification of the calculation it is possible to perform detailed calculations immediately for a group of streams, and then carry out interpolation. In certain cases the calculation is essentially simplified. Thus, for instance, for a cascade with constant specific flow rate, i.e., with

$$\frac{c_{1t}\sin\alpha_1\cos\nu_1}{v_{1t}}\mu_1 = \text{const}$$

and with a uniform field of velocities and inlet pressures, i.e., with $\frac{c_{01}}{v_{01}} = \text{const}$, the flow lines in the meridional plane coincide with the lines determined in the preceding step IV of the calculation. In this case the present step V of the calculation is not needed.

It is possible that the condition of constant specific flow rate is retained only in a portion of the cascade. This case is discussed later in an example. If a stage is designed with a nozzle cascade having $\alpha_{1\,\text{эф}} = \text{const}$, it is obvious that the portion of the cascade where the flow is critical, i.e., where $c_{1t} \geq \alpha$, may be <u>approximately</u> calculated for $\frac{c_{1t}\sin\alpha_1}{v_{1t}} = \text{const}$ (in reality, $\cos\nu_1\mu_1 \neq \text{const}$). In the subcritical portion there will be a change of the inclination of the flow lines as compared to the calculation of step IV, but it is small. In this case it is important to determine the flow line for the stream, where $M_{c_1} = 1$, and a more exact determination should be made only for streams higher than the given one. Then, after designating this boundary stream by the superscript *, we will obtain:

$$\pi\left(d_{01k} + l_{01}^{*}\right) l_{01}^{*}\frac{v_{01}}{c_{01}} = \sum_{1}^{*}\Delta G. \qquad (291)$$

After determining all Δl_{01}, new, more exact, straight flow lines are made, and angle ν_1' is determined more accurately for all streams.

After that, the steam flow rates for all streams are determined with greater accuracy:

$$\Delta G_V = \Delta G_{III}\cos\nu_1' \qquad (292)$$

The value of the total flow rate, $\Sigma\Delta G_V$, is also made more exact.

If we are limited to this calculation, we should compare $\Sigma\Delta G_V$ with the given flow rate and determine the value of angle β_2 more accurately:

$$\sin\beta_2 = (\sin\beta_2)_{III}\frac{\cos v_1'}{\cos v_2}. \qquad (293)$$

In reality, the flow lines in the meridional plane are not straight. If a more detailed calculation is necessary, the flow lines can be found more exactly. It should be borne in mind, however, that such a calculation is extremely tedious and time-consuming, and rather conditional at the same time. For construction of a low line it is necessary to find the stream height that corresponds to the given flow rate inside the blade cascade. For this we take the control plane normal to the axis of the turbine, i.e., in the meridional plane we draw a line normal to the axis (Fig. 285). We trace channels (sections) of the cascade for several radii. For all these sections we find the position of the sought control plane, and we determine τ, the coefficient of constraint, which considers the profile thickness in a given section (see Fig. 285). Using the drawing of the channel we find in the given section the angle of direction of flow α, which is determined in the following way. We draw circles in the channel, tangent to the walls of the profile; the line connecting the centers of these circles is considered as the middle flow line. At the point of intersection of the sought section from this middle flow line we determine the tangent to it and the angle α (see Fig. 285). We perform this construction for several sections, including the root, peripheral, and middle sections. Obviously, this requires that the cascades for these sections be selected or profiled after step IV of the calculation. Further, for the found values we construct a graph for $\tau = f(r)$ and $\alpha = \alpha(r)$, which makes it possible to find τ and α in the control plane for any radius.

For the mid-radius, by the channel method (see Chapter I), we calculated the velocity and pressure distribution in the channel and find the values of c_t and p in the sought section.

Now we have all the data for calculating the radial equilibrium with the simplified formulas in the control plane that we selected. The calculation is performed in absolutely the same manner as it was done for the clearance between cascades, i.e., for streams.

As a result of this calculation, the values for all streams are found for the sought control plane:

$$\Delta G = 2\pi r_i \Delta r_i \tau \frac{r_i}{v_i} \mu. \qquad (294)$$

After that, each ΔG is multiplied by ν_1', which was obtained for each stream earlier. Having a graph of the flow rate for three control sections (in front of cascade, in cascade, and behind it), which increases from root to tip, and following Traupel [96], it is possible to construct flow lines for three points.

If the sum of flow rates $\Sigma\Delta G$ in the control section does not noticeably coincide with the $\Sigma\Delta G$ that was obtained in the preceding calculation, strictly speaking, the calculation should be performed either with an exact equation of radial equilibrium or, at least, a new angle α_1 should be given on the mid-radius. Practically, in view of a certain conditionality of the calculation, this cannot be done; it is sufficient to change all ΔG in proportional to the quantity $G/\Sigma\Delta G$.

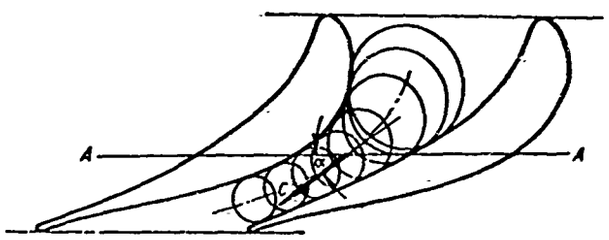

Fig. 285. Calculation of the cross section intersecting a cascade.

Now, for the three points it is necessary to construct a flow line, giving this curve an analytic character. A literature reference [96] proposes that this curve be considered as part of a circle. It is possible to think of it as part of a sinusoid [161] and another form [159]. After that, it is not difficult to determine the radius of curvature and find a more accurate value of angle ν_1'.

It is obvious that for confidence in the determination of ν it is necessary to have on a flow line not three, but a larger number of points, especially near the trailing edges. Unfortunately, such a calculation is not only very tedious, but also very unreliable, especially in the region of supersonic flow. For a slanting shear with a supersonic flow it is necessary to use the method of characteristics. However, the presence losses in the slanting shear of a cascade does not permit us to perform an exact calculation.

VI. Stage Calculation with the Complete Equation of Radial Equilibrium*

By means of the preceding calculations it is possible to find more exact (than for calculation of step III) values of the velocity coefficients, φ and ψ, for cascades depending upon radius. Calculations of steps III, IV, and V permit us to find the values of the angles, velocities, and also the Re number in all sections, i.e., to form a stage with high accuracy. By means of these characteristics (M, Re, and the angles) it is possible, on the basis of results of static investigations taking into account experiments with annular cascades and with stages, to quite reliably have the dependences $\varphi = \varphi(r)$ and $\psi = \psi(r)$.

Performing the calculation of the nozzle cascade, we will write the complete equation of radial equilibrium in a plane normal to the axis (see § 35), in the following manner:

$$v\frac{\partial p}{\partial r} = \frac{c_u^2}{r} - c_a\frac{\partial c_r}{\partial z} - c_r\frac{\partial c_r}{\partial r} + F_r. \tag{295}$$

Here (see Fig. 282)

$$\left.\begin{aligned} c_u &= c\cos\alpha \\ c_a &= c\sin\alpha\cos\nu \\ c_r &= c\sin\alpha\sin\nu. \end{aligned}\right\} \tag{296}$$

The influence of F_r – the radial component of the force of influence of a blade on the flowing medium – is not considered by us, although in certain cases it is of value to create this force by a special inclination of the blades (see § 37).

After dividing the blade into a large number of streams, we, as before, replace the differential changes of parameters by finite differences. The change of the radial velocity component in the direction of axis z may be roughly found for the quantity c_r in two control planes (for instance, in front of and behind the cascade). In view of the small influence of this term, such an approximation will not render a noticeable influence on the concluding calculation:

$$\frac{\partial c_r}{\partial a} = \frac{c_{r1} - c_{r0}}{z}. \tag{297}$$

*Later, in an example of the last stage of a large turbine, the difference in the results of the simplified and complete calculation is shown.

Here z is the distance between the control planes, 0 and 1, along the axis (Fig. 281).

In final form, for the transition from the i-th stream to the following one, we obtain:

$$\Delta p_i = \frac{1}{v_{1i}}\left[\frac{(c_{1i}\cos\alpha_{1i})^2}{r_{i+0.5}} - c_{1i}\sin\alpha_{1i}\times\right.$$

$$\times\frac{c_{1i}\sin\alpha_{1i} - c_{0i}\sin\alpha_{0i}}{z}\sin\nu_{1i}\cos\nu_{1i} - c_{1i}\sin\alpha_{1i}\times$$

$$\left.\times\frac{(c_{1r})_i - (c_{1r})_{i-1}}{\Delta r}\sin\nu_{1i}\right]\Delta r_i = \Delta r_i\,\frac{K_{\mathrm{I}} + K_{\mathrm{II}} + K_{\mathrm{III}}}{v_{1i}}; \qquad (298)$$

$$\Delta h_{0i} = (K_{\mathrm{I}} + K_{\mathrm{II}} + K_{\mathrm{III}})\,\Delta r_i. \qquad (299)$$

In these formulas $r_i + 0.5$ is the radius between streams

$$r_{i+0.5} = \frac{r_i + r_{i+1}}{2}.$$

As indicated by analysis and examples of calculation for a nozzle cascade, the component of equation (298) $c_r(\partial c_r/\partial r$ is usually extremely small and is disregarded. Thus, in the example of the limiting stage with $d/l = 2.65$ and $\nu_{1\text{п}} = 30^\circ$ which is considered below, with a complete change of the drop in the nozzle cascade from root to tip by more than 110 kj/kg, this term gives only 1.3 kj/kg, i.e., a little more than 1%.

For a moving cascade with a conventional design, angle $\alpha_2 \approx 90^\circ$, and it is possible to disregard the term K_1. However, in certain stages when $\alpha_2 \neq 90^\circ$, and especially under variable operating conditions, the term K_1 can be essential and therefore cannot be disregarded.

It is usually considered that when $\alpha_2 = 90^\circ$ the pressure behind a moving cascade is practically constant along the radius and the stage is calculated for a constant available heat drop on all radii. This is valid for the calculation with the simplified equation of radial equilibrium and for stages of gas turbines with low velocities of flow and a slight change of specific volume, when the error in disregarding the term

$$c_a\frac{\partial c_r}{\partial z} \approx c_{a_2}\frac{c_{a_2} - c_{a_1}}{z_1}\operatorname{tg}\nu_2 \qquad (300)$$

will be small due to the fact that $c_{a2} \approx c_{a1}$.

However, in the last stages of steam turbines, in the mid-section at $\rho \approx 0.5$ to

0.6, the difference $c_{a2}-c_{a1}$ is usually on the order of 100 m/sec. Then, for instance, at $c_{ar} = 250$ m/sec, $c_{a1} = 150$ m/sec, $z_2 = 0.07$ m, and $\nu_2 = 10^{\circ}$, the change of the heat drop due to this term, when $\Delta r = 0.05$ m ($\frac{1}{20}$ of the blade is 1 m long), will be

$$\Delta h_a = c_{a2} \cdot \frac{c_{a2}}{z_2} \cdot \frac{c_{a1}}{z_2} \operatorname{tg} \nu_2 \Delta r = 3{,}1 \text{ кдж/кг}.$$

It is obvious that in the root sections, due to the smaller reaction and, consequently, the smaller difference of $c_{a2}-c_{a1}$, and also because of the decrease of angle ν_2, the influence of this term will decrease; in the direction towards the blade tip the opposite picture is observed.

Due to the large absolute values of the velocities c_a, and consequently, the velocities c_r also, the influence of the term $c_r(\partial c_r/\partial r)$ behind the rotor blade also becomes noticeable.

After the calculation of the moving cascade, it is necessary to consider the influence of it on the flow behind the nozzle cascade, i.e., on the angle ν_1, and to recalculate the nozzle cascade. With a supersonic flow in the nozzle cascade, such a calculation is not needed.

It is obvious that the more exact calculation, as compared to step III of the calculation by means of the simplified equation of radial equilibrium, changed the angles α_1, the flow rate, the reaction of the stage, its efficiency, and the angles β_1 and β_2.

The change of the M numbers is very important and essential, especially $M_{w_{2t}}$ at the tip.

In an example of calculation, this quantity for a detailed calculation amounted to $M_{w_{2t}} = 1.78$, and for a simplified calculation, $M_{w_{2t}} = 1.58$. With such a considerable difference it is necessary to design the cascade in a somewhat different manner.

As a result of calculating the stage, we obtain the pressure distribution p_2 with respect to the radius. This distribution, as also the quantity p_2 itself, is determined by resistances following the given stage, i.e., for the last stage — the outlet duct, and for the next-to-the-last stage — the last stage and the outlet duct, etc.

It is obvious that impossible to be limited to a stage calculation without considering these resistances. The stage calculation should be performed in the

following way.

After a detailed calculation, analogous to the one described above, at the entrance to the duct we obtain the velocity field. On the basis of the characteristics of the duct, which can now be obtained as a result of an experimental investigation, we obtain the pressure distribution along the radius (in the ducts of steam turbines the pressure will change not only along the radius, but also along the circumference at the duct inlet, which, of course, must be disregarded in the calculations). Having this pressure distribution, again for the streams, we determine the characteristics of the flow behind the blade cascade, which must satisfy the equations of equilibrium and continuity. In general, this will be possible only with variation of the parameters in the clearance before the moving cascade. The continuity and equilibrium equations are further checked for this clearance, which leads to a change of the parameters before the stage, etc. In essence, it is necessary to perform the calculation as if for variable turbine performance from the final stage, which differs from the usual calculation [83] by the fact that it is performed not for the mid-radius, but for the streams, taking into account the equation of radial equilibrium.

This calculation is not only difficult and very tedious, but for the last stages of condensing turbines it is almost practically impossible now. This is explained by the fact that for the outlet ducts of steam turbines there are almost no complete characteristics that consider variable velocities and, all the more, the swirling at the entrance.

Analytic Dependences for Calculation of Last Stages

Sometimes in variant and preliminary calculations of stages, the use of methods of detailed calculation for streams requires very much time, and the analytic dependences obtained from the simplified equation of radial equilibrium give large errors. In this case it is possible to use the analytic dependences obtained from the complete equation of radial equilibrium with certain simplifying assumptions.

Assuming that $F_r = 0$, and taking into account

$$di_1 = d\bar{i}_0 - c_1\,dc_1 = \varphi^2 v_1 d\bar{p}_1, \tag{301}$$

from equation (295) we obtain:

$$\frac{1}{\varphi_1} c_1 \frac{\partial c_1}{\partial \bar{r}} = -\frac{c_{1u}^2}{\bar{r}} + c_{a1}\frac{\partial c_{r1}}{\partial \bar{z}} + c_{r1}\frac{\partial c_{r1}}{\partial \bar{z}} + \frac{1}{\varphi^2}\frac{\partial \bar{i}_0}{\partial \bar{r}}, \tag{302}$$

where $\bar{r} = r/r_{rt}$ and $\bar{z} = z/r_{rt}$.

For conical flow surfaces, $\frac{\partial \nu}{\partial \bar{z}} = 0$. For the term $\frac{\partial \bar{c}_a}{\partial \bar{z}}$ (and not in general for the change of the axial velocity component) we shall assume that

$$c_{a1} = c_{a1\kappa}\bar{r}^{\gamma} \tag{303}$$

and consequently:

$$\frac{\partial c_{a1}}{\partial \bar{z}} = \frac{c_{a1\kappa}(\bar{r}^{\gamma} - A)}{\bar{z}_{01}}, \tag{304}$$

where A is obtained from the boundary conditions, while the index γ depends on the law of twisting, $\alpha = \alpha(r)$, and can be of any sign.

Then equation (301) will be converted to the following form:

$$\frac{dc_1}{d\bar{r}} = F_1(\bar{r})c_1 + F_2(\bar{r}) + F_3(\bar{r})\frac{1}{r_1}. \tag{305}$$

where

$$F_1(r) = \frac{\sin^2\alpha_1 \sin\nu \frac{d\sin\nu}{d\bar{r}} + \sin\alpha_1 \frac{d\sin\alpha_1}{d\bar{r}}\sin^2\nu - \frac{\cos^2\alpha_1}{\bar{r}}}{1/\varphi^2 - \sin^2\alpha_1\sin^2\nu}; \tag{305a}$$

$$F_2(r) = \frac{\frac{c_{a1\kappa}(\bar{r}^{\gamma} - A)}{\bar{z}_{01}}\sin\alpha_1\sin\nu}{1/\varphi^2 - \sin^2\alpha_1\sin^2\nu}; \tag{305b}$$

$$F_3(r) = \frac{\frac{1}{\varphi^2}d\bar{i}_0/d\bar{r}}{1/\varphi^2 - \sin^2\alpha_1\sin^2\nu}. \tag{305c}$$

It is obvious that for the solution of this equation it is necessary to know: $d\bar{i}_0/d\bar{r}$, which is known from the calculation of the preceding stage, $\varphi = \varphi(\bar{r})$, $\alpha_1 = \alpha(\bar{r})$, and the index γ, which can be found for adopted law of twisting by means of the simplified equation of radial equilibrium, and the dependence $\nu = \nu(\bar{r})$.

For obtaining the last term, we shall write the continuity equation for the plane in front of the cascade and behind it*

$$2\pi\int_1^{\bar{r}_0}\frac{c_{a0}}{v_0}\bar{r}\,d\bar{r} = 2\pi\int_0^{\bar{r}_1}\frac{c_{a1}}{v_1}\bar{r}\,d\bar{r}.$$

Usually (this will hardly show up in the final results of the calculation) it is possible to use the formula obtained for the particular case of c_a/v = const

---

*Here, for simplicity of notation, it is assumed that

$$\mu_1\frac{c_{1n_1}}{v_{1_1}} = \frac{c_{1n}}{v_1}.$$

$$\frac{\bar{r}_0^2-1}{\bar{r}_{\kappa 0}^2-1}=\frac{\bar{r}_1^2-1}{\bar{r}_{\kappa}^2-1}. \tag{306}$$

In many cases it is possible to assume conical coaxial flow surfaces. Then

$$\lg v=\frac{\bar{r}-1}{\bar{r}_{\kappa}-1}(\lg v_{\kappa}-\lg v_{K})+\lg v_{K}. \tag{307}$$

The use of formula (307) is convenient only for an analytic solution of equation (305). In general, the solution of this equation is possible only by means of numerical methods and it is not very difficult. Thus we obtain the radius distribution of velocity c_1 and all the other parameters.

If we consider that $\bar{i}_0$ does not depend on the radius, equation (305) will take on the following form:

$$\frac{dc_1}{d\bar{r}}=F_1(\bar{r})c_1+F_2(\bar{r}) \tag{308}$$

and the following solution:

$$\frac{c_1}{c_{1\kappa}}=\exp\left[\int_1^{\bar{r}}F_1(\bar{r})\,d\bar{r}\right]\left\{1+\int_1^{\bar{r}}\Phi(\bar{r})\exp\left[-\int_1^{\bar{r}}F_1(\bar{r})\,d\bar{r}\right]d\bar{r}\right\}, \tag{309}$$

where $F_1(\bar{r})$ is according to expression (305a), and

$$\Phi(\bar{r})=\frac{\dfrac{\bar{r}^{\gamma}-A}{\bar{z}_{01}}\sin\alpha_{1K}\cos v_K\sin\alpha_1\sin v}{1/\varphi^2-\sin^2 v\sin^2\alpha_1}. \tag{310}$$

It is obvious that equation (309) is easy to convert for the case when $c_{1\,cp}$ is given, and not $c_{1\,K}$.

Equation (309) is essentially simplified for certain wide-spread particular cases of twisting. Thus, at α_1 = const we obtain $\frac{d\sin\alpha_1}{d\bar{r}}=0$ and $\gamma=-\varphi^2\cos^2\alpha_1$. At $\sin\alpha_1=\bar{r}\sin\alpha_{1\,K}$ the expressions $F_1(\bar{r})$ and $\Phi(\bar{r})$ also are simplified, since

$$\frac{d\sin\alpha_1}{d\bar{r}}=\sin\alpha_{1K}\ \text{and}\ \frac{c_{1u}}{c_{1\alpha_K}}\approx\bar{r}^{1-\varphi^2\cos^2\alpha_{1K}}.$$

The steam parameters behind the moving cascade are calculated in the following way:

We write the equation for the plane behind the moving cascade

$$v_2\frac{\partial p_2}{\partial\bar{r}}=\frac{c_{2u}^2}{\bar{r}}-c_{2u}\frac{\partial c_{2r}}{\partial\bar{z}}-c_{2r}\frac{\partial c_{2r}}{\partial\bar{r}}. \tag{311}$$

If the outlet angles of the moving cascade are found from the condition of equality of flow rates in similar cascade streams, then

$$\sin\beta_2 \approx \sin\alpha_1 \frac{c_1}{w_2}\frac{v_2}{v_1}\frac{r_1}{r_2}\frac{l_1}{l_2}$$

and

$$c_{2a} = c_{1a}\frac{v_2}{v_1}\frac{r_1}{r_2}\frac{l_1}{l_2} = Q(\bar{r})\,v_2. \tag{312}$$

Then

$$v_2\frac{\partial p_2}{\partial \bar{r}} = \frac{c_{2a}^2}{\bar{r}}\frac{\operatorname{ctg}^2\alpha_2}{\cos^2\nu} - c_{2a}\frac{\partial c_a}{\partial \bar{z}}\operatorname{tg}\nu - c_{2a}\operatorname{tg}\nu\times\left[c_{2a}\frac{\partial\operatorname{tg}\nu}{\partial\bar{r}} + \frac{\partial c_{2a}}{\partial\bar{r}}\operatorname{tg}\nu\right]. \tag{313}$$

We make a number of simplifications:

inasmuch as the influence of the term $\frac{c_{2a}^2}{\bar{r}}$ is small, and usually $\alpha_2 > 70^\circ$, then for this term we shall assume that

$$\operatorname{ctg}^2\alpha_2 \approx \operatorname{ctg}^2\alpha_{2k}.$$

As also for the nozzle cascade, we shall assume that for the given flow line

$$\frac{\partial c_a}{\partial \bar{z}} = \text{const}, \text{ i.e., } \frac{\partial c_a}{\partial \bar{z}} = \frac{c_{2a}}{z_{1,2}}(1 - B\bar{r}^\nu).$$

The influence of the term $c_r\frac{\partial c_r}{\partial \bar{r}}$ also is not very great; therefore, it is possible to simplify the expression:

$$\left[c_{2a}\frac{\partial\operatorname{tg}\nu}{\partial\bar{r}} + \frac{\partial c_{2a}}{\partial\bar{r}}\operatorname{tg}\nu\right] \quad c_{2a}\frac{\partial\operatorname{tg}\nu}{\partial\bar{r}}\times\left[1 + \frac{\operatorname{tg}\nu}{\frac{\partial\operatorname{tg}\nu}{\partial\bar{r}}}\frac{\frac{\partial c_{2a}}{\partial\bar{r}}}{c_{2a}}\right].$$

The second term in the bracket is essentially less than unity; therefore,

$$c_{2r}\frac{\partial c_{2r}}{\partial\bar{r}} \approx c_{2a}\frac{\partial\operatorname{tg}\nu}{\partial\bar{r}}.$$

We shall assume that $p_2v_2 = RT_2$ for the zone of change of parameters with respect to the radius behind the moving cascade. Then equation (313) is converted to the following form:

$$v_2\frac{\partial p_2}{\partial\bar{r}} = \frac{v_2^2}{\bar{r}}Q^2(\bar{r})\frac{\operatorname{ctg}^2\alpha_2}{\cos^2\nu} -$$

$$-\frac{v_2^2}{z_{1,2}}Q^2(\bar{r})\operatorname{tg}\nu(1 - B\bar{r}^\nu) - Q^2(\bar{r})\,v_2^2\operatorname{tg}\nu\frac{\partial\operatorname{tg}\nu}{\partial\bar{r}}$$

and

$$\frac{dp_2}{d\bar{r}} = Q^2(\bar{r})\left\{\frac{\frac{\operatorname{ctg}^2\alpha_2}{\cos^2\nu}}{\bar{r}} - \operatorname{tg}\nu\left[\frac{1 - B\bar{r}^\nu}{z_{1,2}} + \frac{d(\operatorname{tg}\nu)}{d\bar{r}}\right]\frac{RT_2}{p_2}\right.. \tag{314}$$

The solution of this equation:

$$p_2^2 = p_{2k}^2 + 2\int_1^{\bar{r}} \Psi(\bar{r})\, d\bar{r}, \tag{315}$$

where

$$\Psi(\bar{r}) = Q^2(\bar{r})\left\{\frac{\operatorname{ctg}^2\alpha_2}{\bar{r}} - \operatorname{tg}\nu\left[\frac{1-B\bar{r}^{\nu}}{\bar{z}_{1,2}} + \frac{d(\operatorname{tg}\nu)}{d\bar{r}}\right]RT_2.\right. \tag{316}$$

For the solution it is necessary to know $Q(\bar{r})$, which is given by the calculation of the nozzle cascade.

At a very large deviation of α_2 from 90°, and a considerable error of the equation of state of an ideal gas, a second approximation should be made.

The calculations with the formulas given above showed a good approximation to the results of the calculations for streams that were performed in this paragraph.

Example of the Calculation of the Last Stage of a Large Condensing Turbine

Given: steam flow rate G = 52.0 kg/sec, rotor speed n = 3000 rpm; steam parameters: at entrance to stage p_0 = 0.130 bar, i_0 = 2488 kj/kg, $\frac{c_0^2}{2}$ = 7 kj/kg; behind stage: pressure on mid-diameter p_2 = 0.0342 bar.

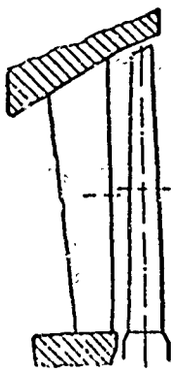

Fig. 286. Flow area of stage (example of the calculation of the last stage of a large condensing turbine).

Dimensions of stage: nozzle cascade: mid-diameter d_1 = = 2430 mm, height l_1 = 900 mm; moving cascade: mid-diameter d_2 = = 2480 mm, height l_2 = 960 mm.

Flow area of stage is represented in Fig. 286.

I. Calculation for Mid-Radius

On an is-diagram we find the parameters of the stagnated flow: i_0 = 2495 kj/kg, $\bar{p}_0$ = 0.138 bar, $\bar{x}_0$ = 0.958, and the available heat drop of the stage

$$h_0 = \bar{i}_0 - i_{2t} = 185 \text{ кдж/кг}.$$

The velocity ratio on the mid-diameter

$$\frac{u_1}{c_{1t}} = \frac{u_1}{\sqrt{2h_0}} = 0{,}627.$$

The minimum reaction on the mid-radius

$$(\rho_{cp})_{min} = \frac{1{,}3}{1{,}3 + d_1/l_1} = 0{,}41.$$

For a preliminary estimate we select $\rho_{cp} = 0.60$; then $p_1/p_0 = 0.587 > \varepsilon_*$. We shall assume that $\varphi = 0.96$, $\varphi = 0.93$, $\mu_1 = 1.01$; $\mu_2 = 1.0$.

$$\sin\alpha_1 = \frac{Gv_{1t}}{\mu_1 \pi d_1 l_1 c_{1t}} = 0{,}325;\quad \alpha_1 = 18°58'.$$

From the velocity triangles we obtain $w_1 = 125$ m/sec, $\beta_1 = 106°30'$, and $w_{2t} = 487$ m/sec.

$$\sin\beta_2 = \frac{w_1}{w_{2t}}\frac{v_{2t}}{v_1}\frac{d_1}{d_2}\frac{l_1}{l_2}\sin\beta_1 = 0{,}493,\quad \beta_2 = 29°33',$$
$$\alpha_2 = 88°50';\quad c_2 = 223{,}5\ \text{м/сек};\quad \eta_{ol} = 0{,}747.$$

Since $w_{2t} > w_*$, it is necessary to determine the angle $\beta_{2\,эф}$:

$$\sin\beta_{2эф} = \frac{v_1}{v_{2t}}\frac{w_{2t}}{w_*}\sin\beta_2 = 0{,}453;$$
$$\beta_{2эф} = 26°56'.$$

II. Calculation of Stage for Three Sections

For this calculation we must select law of twisting for the nozzle cascade. We shall assume that the nozzle cascade should have:

$$\alpha_{1эф} = \text{const} = 18°58'.$$

Then we can roughly find the reaction by the following formula:

$$\frac{1-\rho_r}{1-\rho_{cp}} = \left(\frac{r}{r_{cp}}\right)^{-2\varphi^2\cos^2\alpha_1}.$$

For the root section:

$$\rho_к = 0{,}142;\quad h_{01к} = 159\ \text{kj/kg};\quad p_{1к} = 0{,}0426\ \text{bar};$$
$$\alpha_{1к} = 22°40';\quad \beta_1 = 39°20';\quad w_1 = 314{,}5\ \text{m/sec};$$
$$w_{2t} = 389\ \text{m/sec};\ \beta_2 = 36°14';\quad \alpha_2 = 78°10';\quad c_2 = 211{,}5\ \text{m/sec}.$$

For the peripheral section:

$$\rho_п = 0{,}762;\quad h_{01} = 44\ \text{kj/kg};\quad p_1 = 0{,}1025;\quad \alpha_{1п} = \alpha_{1эф};$$
$$\beta_1 = 160°23';\quad w_1 = 273{,}5\ \text{m/sec};\ w_{2t} = 594{,}4\ \text{m/sec};$$
$$\beta_2 = 20°51';\quad \alpha_2 = 95°09';\quad c_2 = 198{,}5\ \text{m/sec};\ \beta_{2эф} = 17°59'.$$

III. Detailed Calculation of Stage by Means of the Simplified Equation of Radial Equilibrium in a Clearance

The calculation is shown in Table 22.

Note on the calculation: For the mid-section we selected the reaction $\rho_{cp} = 0.56$; angle $\alpha_{1\,эф} = 20°$ = const. The velocity coefficients, φ and ψ, were taken

from Figs. 278 and 280 (curves 1); the flow rate coefficients were taken from Fig. 279.

The blades are divided into 21 sections with respect to height: for the nozzle cascade we assumed that $\Delta r_1 = 0.043$ mm, and for the moving cascade, $\Delta r_2 = 0.046$ mm. The root section rt and the peripheral section per, which are 0.020 mm from the nearest radii of the streams, are calculated separately.

Sequence of calculation.

First the middle section of No. 11 is calculated. Then for the transition to the adjacent stream (for instance, No. 10) we determine:

$$\Delta h_0 = \frac{c_{1u}^2}{r} \Delta r_1$$

and

$$\Delta p_1 = \frac{1}{v_1} \frac{c_{1u}^2}{r} \Delta r_1.$$

Here c_{1u} and v_1 are selected for stream No. 11, and r on the boundary of streams No. 11 and 10 i.e., $r = \frac{r_{10} + r_{11}}{2}$.

We find $(h_{01})_{10} = (h_{01})_{11} + \Delta h_{01}$ for stream No. 10 and calculate the nozzle cascade for stream No. 10.

All remaining streams are calculated analogously. Upon transition to the root and peripheral section, $\Delta r_1 = 0.020$ m is substituted.

Angle α_1 is determined for all sections where $M_{c_{1t}} > 1$:

$$\sin \alpha_1 = \sin \alpha_{1эф} \frac{v_{1t}}{v_0} \frac{c_0}{c_{1t}} = q \frac{v_{1t}}{c_{1t}},$$

where

$$q = \sin \alpha_{1эф} \frac{c_0}{v_0} = \text{const}.$$

For sections where $M_{c_{1t}} < 1$, angle $\alpha_1 = \alpha_{1эф} = \text{const}$. In the calculation of the moving cascade it is assumed that $p_2 = \text{const}$.

Angle β_2 is found by the following formula:

$$\sin \beta_2 = \frac{w_1}{w_{2t}} \frac{v_{2t}}{v_1} \frac{d_1 \Delta r_1}{d_2 \Delta r_2} \sin \beta_1.$$

For determination of v_{2t} it is necessary to know x_{2t}, for which the losses in the nozzle cascade should be estimated:

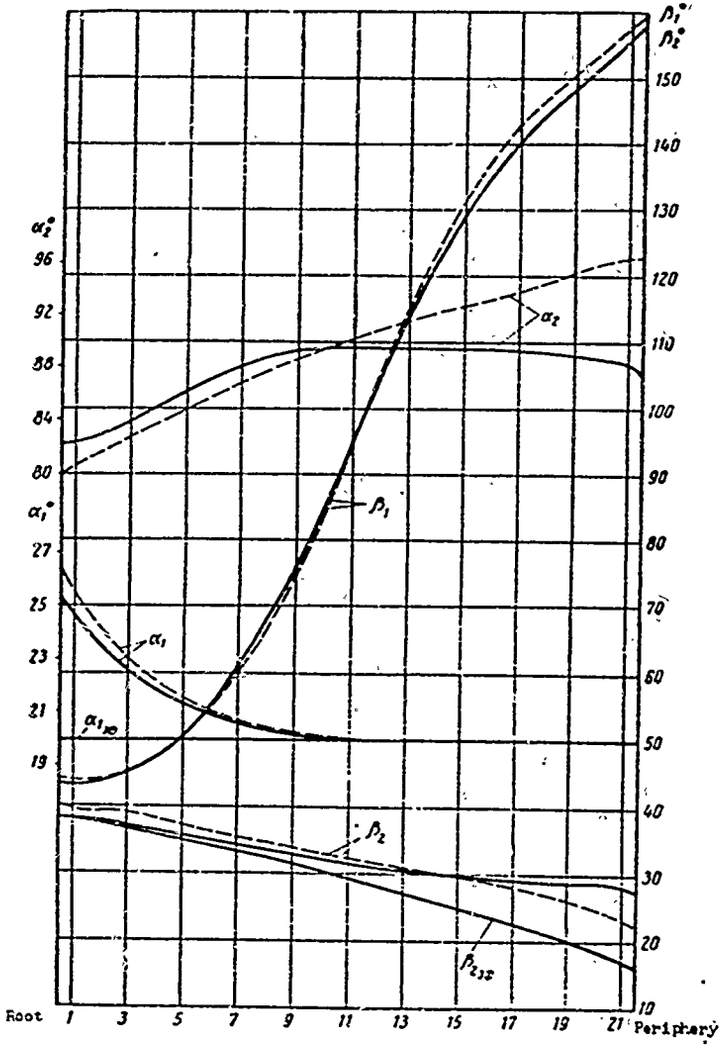

Fig. 287. Results of calculation of last stage (example); angles of flow, α_1, β_1, β_2, α_2; curves: — — — (dotted) step III of calculation by means of simplified equation of radial equilibrium with cylindrical flow surfaces; ——— (solid) — by more accurate calculation.

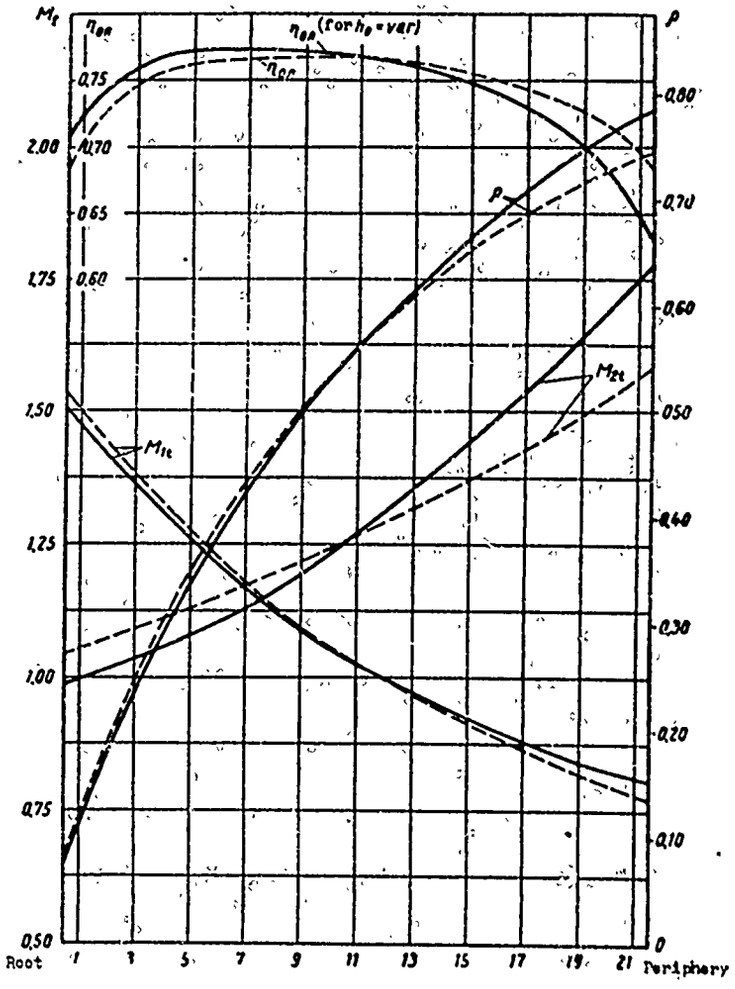

Fig. 288. Results of calculation of last stage (example); flow velocities, M_{1t} and M_{2t}; reaction ρ and efficiency η_{OII}, curves: — — — (dotted) step III of calculation by means of simplified equation of radial equilibrium with cylindrical flow surfaces; ——— (solid) by more accurate calculation.

$$h_c = h_{01}(1 - \varphi^2).$$

After calculating the flow rate for the streams, ΔG, the steam flow through the whole cascade should be determined:

$$G = 0{,}043 \sum_{2}^{20} \Delta G + 0{,}0415\,(\Delta G_1 + \Delta G_{21}) = 53{,}75 \text{ кг/сек}.$$

It is interesting to note that the steam flow, which ic calculated for the middle section, amounts to 53.58 kg/sec, i.e., it differs by a total of 0.32%. The obtained flow rate is greater than the given one, G = 5.20 kg/sec, by 3.4%. However, in connection with the decrease of the flow rate due to the conical meridional contour of the stage, a more precise determination of the dimensions of the stage should not be made.

Let us compare the results of step III of the calculation with the calculation for three sections; in step III of the calculation the mean reaction was decreased and angle $\alpha_{1\ эф}$ was somewhat increased.

The reaction at the root was decreased and it amounts to 8.2%; in the root section the angle β_2 was increased by 4°; angle β_2 changed at the periphery: it increased by 1.5°. The discharge velocity at the root and at the periphery was practically unchanged. This all shows that even a rough estimate of a stage for three sections is close to the detailed calculation by means of the simplified equation of radial equilibrium.

The weighted mean relative blade efficiency of a stage with full loss of outlet velocity amounts to $\eta_{0л} = 0.746$.

The stage calculation is shown in the graphs on Figs. 287 and 288, where it is indicated by the dotted lines.

IV. Calculation of Stage with Flow Lines on Conical Surfaces

In the diaphragm, the conicity of the external meridional configuration amounts to $\nu_{1\ п} = 30^\circ$. It is not difficult to find angle ν_1 for each stream (see line 1 in Table 23). Then the steam flow in each stream will be found by the following formula:

$$\Delta G' = \Delta G \cos \nu_1.$$

The flow through the whole stage, which is found as the sum $\Sigma\Delta G'$, is equal to G' = 50.77 kg/sec, i.e., 5.6% less than for the preceding step III of the calculation.

Table 23. Results of Stage Calculation with Flow Lines on Conical Surfaces.

№	Designation	Symbols	Root	Number of streams 1	2	3	4	5	6	7	8	9	10	11	12
1	Angle of inclination of flow line in nozzle cascade, degrees	ν_1	0	0°45′	2°20′	3°55′	5°30′	7°00′	8°35′	10°05′	11°40′	13°05′	14°40′	16°05′	17°30′
2	Steam flow per unit height, kg/sec/m	$\Delta G' = \Delta G \cos \nu_1$	37,3	38,5	41,4	43,5	45,45	47,5	49,45	51,4	53,2	55,0	56,65	58,4	60,0
3	Angle of inclination of flow line in moving cascade, degrees	ν_2	0	0°20′	1°20′	2°20′	3°20′	4°20′	5°20′	6°19′	7°19′	8°19′	9°17′	10°16′	11°14′
4	More accurate value of angle β_2, degrees	β_2'	40°23′	39°58′	39°21′	38°20′	37°53′	37°13′	36°14′	35°20′	34°20′	33°33′	32°33′	31°37′	30°44′
5	More accurate value of angle ν_1, degrees	ν_1'	0	0°45′	2°20′	3°55′	5°30′	7°00′	8°35′	10°05′	11°40′	13°05′	14°40′	16°05′	17°30′
6	Steam flow per unit height, kg/sec/m	$\Delta G'' = \Delta G \cos \nu_1'$	37,3	38,5	41,4	43,5	45,45	47,5	49,45	51,4	53,2	55,0	56,65	58,4	60,0

№	Designation	Symbols	Number of streams 13	14	15	16	17	18	19	20	21	Periphery	Remarks
1	Angle of inclination of flow line in nozzle cascade, degrees	ν_1	18°55′	20°20′	21°45′	23°05′	24°25′	26°00′	27°00′	28°15′	29°40′	30°	
2	Steam flow per unit height, kg/sec/m	$\Delta G' = \Delta G \cos \nu_1$	61,6	63,05	63,65	65,0	65,65	66,1	67,0	67,05	64,6	64,3	$G = 50,77$ kg/sec
3	Angle of inclination of flow line in moving cascade, degrees	ν_2	12°05′	13°08′	14°05′	15°02′	16°00′	16°54′	17°49′	18°14′	19°37′	20°	
4	More accurate value of angle β_2, degrees	β_2'	29°47′	28°59′	28°17′	26°56′	26°17′	25°20′	23°46′	23°06′	21°24′	20°21′	
5	More accurate value of angle ν_1, degrees	ν_1'	18°55′	20°25′	21°30′	22°45′	24°00′	25°25′	26°45′	28°15′	30°00′	30°	
6	Steam flow per unit height, kg/sec/m	$\Delta G'' = \Delta G \cos \nu_1'$	61,6	63,05	63,7	65,1	65,8	66,35	67,15	67,05	64,25	64,3	$G = 50,75$ kg/sec

Let us compare this change with the calculation performed by means of formula (284):

$$\frac{\Delta G}{G_{III}} = -K (\operatorname{tg} \nu_n)^2,$$

where K is taken from the graph on Fig. 283.

For the case of $\sin \alpha_{1\,эф}$ = const, q = 1, and $r_п/r_к = 2.18$, coefficient K = 1.97. Then $\frac{\Delta G}{G} = -0.065$. A detailed calculation gave a smaller absolute value of $\frac{\Delta G}{G}$, since q < 1 in the stage.

Proceeding from the overlap, we will find angles of inclination of the flow lines for the moving cascade, ν_2. They are given in Table 23.

If we limit ourselves in the stage calculation only to the introduction of angles ν_1 and ν_2 into the flow rate and dimensions of the cascades, then only angle β_2 and the outlet velocity triangles for all streams should be recalculated. It is obvious that this change will be small for the angles $\nu_{1п}$ and $\nu_{2п}$, adopted in the given example. The biggest deviation will be for the periphery, where instead of $\beta_{2п} = 22^\circ 16'$, we obtain $\beta_{2п} = 20^\circ 21'$. For the middle section, correspondingly, instead of $\beta_2 = 32^\circ 29'$, we obtain $\beta_2 = 31^\circ 37'$. All accurate values of β_2 are presented in Table 23.

V. More Accurate Determination of Flow Lines in the Meridional Plane

First, we evaluate the inlet diffuser section of the diaphragm. For this we use formula (289). The ratio of areas at the entrance to the diaphragm and in front of the nozzle cascade is $F_0/F_{01}=0.815$; the M_0 number is equal to 0.31. Let us assume that $\lambda_д = 0.5$ and $\eta_д = 0.90$. Then at $c_0 = 123$ m/sec, we obtain $p_{01} = 0.137$ bar and $c_{01} = 92.5$ m/sec.

From Table 21 it is clear that $M_{c1} = 1.00$ is attained in the 12th stream. We shall unite all streams from the root to the 12th one and find the corresponding value of l^*_{01} by means of formula (291); further, for every $\Delta G'$ we determine Δl_{01}. Thus, more accurate values are found in the beginning (at entrance to nozzle cascade) for the flow line and angles ν'_1.

Practically, $\cos \nu'_1$, as compared to $\cos \nu_1$, was changed only in the streams starting with the 15th and proceeding through the 21st. The variation of the flow rate is also calculated for these streams:

$$\Delta G'' = \Delta G \frac{\cos \nu'_1}{\cos \nu_1}.$$

It should be emphasized that such a small zone along the length of the blade, where the influence of the change of the position of the flow lines is noticeable as compared to that step IV of the calculation, is characteristic only for stages with approximately constant specific flow rate. An analogous recalculation of the value of ν_2 should have been made for the rotor blade. However, in the method that we adopted for twisting the rotor blade, when angle β_2 is found from the constancy of the flow rate in identical streams of the nozzle and moving cascades, this is not necessary.

Inasmuch as angles ν'_1 scarcely differ from angles ν_1 in our example, it is not necessary to perform a more accurate determination of the calculation of β_2 and the outlet triangles. The change of the steam flow, as compared to step IV of the calculation, is very small and amounts to a total of 0.02 kg/sec, i.e., a total of 0.04%.

VI. Calculation of Stage by Means of Complete Equation of Radial Equilibrium

The calculation is shown in Table 24. It is practically necessary to recalculate all the data in Table 22. From it there remain: lines 1, 2, 10, 15, 21, 22, 24, and also the condition of $\alpha_{1\ эф} = 20^\circ = \text{const}$ (strictly speaking, since in Step V

of the calculation we obtained $G' = 50.75$ kg/sec, which is less than the given value of $G = 52.0$ kg/sec, since $\alpha_{1\,эф}$ should be increased in proportion to the flow rate, i.e., instead of $\alpha_{1\,эф} = 20.0^{\circ}$ it is necessary to take $\alpha_{1\,эф} = 20^{\circ}30'$. In our example we will not perform this recalculation for the sake of simplicity.

Lines 5 and 3 are used from Table 23.

Sequence of calculation.

For the nozzle cascade, as compared to step III, the following change is introduced:

$$\Delta h_{01} = \Delta r_1 \left(\frac{c_{1u}^2}{r} - c_{1a} \frac{c_1 \sin \alpha_1 - c_{01}}{a} \sin \nu_1 \right)$$

and

$$\Delta p_1 = \frac{\Delta r_1}{v_1} \left(\frac{c_{1u}^2}{r} - c_{1a} \frac{c_1 \sin \alpha_1 - c_{01}}{a} \sin \nu_1 \right),$$

where $c_{1a} = c_1 \sin \alpha_1 \cos \nu_1$, $c_{01} = 92.5$ m/sec, $a \approx 0.1$ const (width of nozzle blade or more exact distance on axis between two control planes), ν_1 is taken from line 2 of Table 23.

Analogously to step III of the calculation, for every stream we construct an inlet velocity triangle. However, if in the preceding calculations it was assumed that the available heat drop of the stage does not change with respect to height, then velocity w_{2t} was also calculated as usual, i.e.,

$$\frac{w_{2t}}{2} = \frac{w_1^2}{2} + (h_0 - h_{01}),$$

then in the calculation of the section behind the rotor blade, by means of the equation of complete radial equilibrium h_0 of the stage, it will be constant.

Therefore, for the section behind the rotor blade, we find

$$\Delta h_0 = \Delta r_2 \left(\frac{c_{2u}^2}{r} - c_{2a} \frac{c_{2a} - c_{1a}}{a_2} \sin \nu_2 - c_{2a} \frac{(c_{2r})_i - (c_{2r})_{i-1}}{a_2} \right.,$$

and, analogous to this, we find Δp_2.

Here c_{2u}, c_{2a}, c_{1a}, and ν_2 are selected for the given stream, while the term $(c_{2r})_{i-1}$ is selected for the preceding stream, which is located at a distance of Δr_2 from the i-th stream.

The available heat drop of the moving cascade is calculated with Δh_0 taken into account, i.e.,

$$h_{02} = h_0 + \Delta h_0 - h_{01}.$$

Angle β_2 is found by the following formula:

$$\sin\beta_2 = \frac{w_1}{w_{2t}}\,\frac{v_{2t}}{v_1}\,\frac{r_1\Delta r_1}{r_2\Delta r_2}\sin\beta_1\cdot\frac{\cos v_1}{\cos v_2}.$$

It should be borne in mind that the reaction, $u/c_{\text{ф}}$, and $\eta_{0\text{л}}$ of each stream are determined for the changed value of h_0.

The results of the calculation are shown on the graphs in Figs. 287 and 288, where they are represented by solid lines. These graphs permit us to compare the results of the calculation for steps III and VI. From this comparison we note the following important features:

1. The pressure behind the stage, and consequently also the available heat drop, essentially change with respect to height.

2. Angle β_2 was decreased in the root part of the blade. In the root section, instead of $\beta_1 - \beta_2 = 44^\circ16' - 40^\circ23' = 3^\circ43'$, it became $\beta_1 - \beta_2 = 43^\circ21' - 38^\circ22' = 5^\circ$; angle β_2 is increased in the upper part, and on the periphery, instead of $20^\circ16'$, it amounts to $27^\circ23'$;

3. The relative outlet velocities of steam from the moving cascade were noticeably changed. In step III of the calculation they changed from root to tip from $M_{w_2} = 1.04$ to 1.58, in the more exact step VI of the calculation, $M_{w_2} = 0.98$ to 1.78, correspondingly.

4. The efficiency of stage was increased; it was calculated for an available heat drop of $h_0 = h_{0cp} = 185.0$ kj/kg.

One should note the low value of the efficiency $\eta_{0\text{л}}$ of the upper sections in step VI of the calculation. Although in steps III and VI of calculation it is assumed that φ and ψ are identical, and for the upper sections in step VI of the calculation we obtained angles α_2 that were closer to 90° than in step III of the calculation, the more exact calculation gave a lower value of efficiency.

This is explained by the small effectiveness of stages at very high velocities, when expansion beyond the limits of the slanting shear does not create effective performance in the stage.

If we select cascades with divergent channels, for the upper sections, as this is proposed in § 43, then there will be no deflection of the flow in the slanting shear or it will at least decrease, and the efficiency of the stage in this section will increase.

5. The change of the stage reaction with respect to height in both methods

of calculation was not very noticeable.

As a result of the more accurate calculation, the steam flow through the stage amounted to $G = 50.99$ kg/sec, and the efficiency on the blades (without taking into account the peculiarities of flow of moist steam) was $\eta_{\text{сл}} \doteq 0.779$.

§ 46. FUNDAMENTALS OF DESIGNING THE LAST STAGES OF CONDENSING TURBINES

Selection of the Law of Twisting for the Nozzle Cascade (see § 3.9)

For a subcritical flow and $d/l > 5$, practically without lowering economy, it is possible to apply nozzle blades of constant profile (cylindrical). In this case it is necessary to monitor the selection of the number of blades, i.e., the cascade pitch. It is necessary to select the cascade pitch in such a way, so that there would be no noticeable deviation from the optimum value of relative pitch, $\bar{t} = t/b$, in the root or peripheral sections. For this method of twisting it is possible to apply the model stages that were considered in § 49. These stages have an angle α_1 that increases from root to periphery.

For a subcritical flow and $3 < d/l < 5$, with cylindrical bladdng, it is difficult to ensure optimum pitch $\bar{t}$ for the entire height, therefore it is desirable to twist the nozzle cascade. Inasmuch as the stage efficiency is greatly influenced by the cascade economy, especially that of the nozzle cascade, it is best of all to base our methods on well developed and checked cascades. Therefore, for such a stage it is perferable to have the nozzle cascade made from the same profile.

Consequently, it is necessary to increase the profile chord from root to periphery. Then, if this chord changes in proportion to the radius, while the profile and its angle of incidence remain constant for the entire cascade, every section will have a constant relative pitch $\bar{t}$. It is obvious that it is not necessary to strictly maintain the constancy of $\bar{t}$; it is necessary only that along the entire height $\bar{t}$ be in the optimum zone for the given profile. This makes it possible to change the chord with respect to height not in proportion to the radius, but to a somewhat smaller degree. Thinning of the trailing edge is favorable and, if the requirements of technology and reliability permit, it is necessary to select the edge thickness as small as possible. For a nozzle cascade with variable chord it is not necessary to proportionally increase the edge thickness to the periphery; it is possible to change it, retaining the allowed minimum $\Delta_{\text{кр}}$. There

stages will have an angle α_1, that changes little with respect to height.

For a stage with supersonic flow, in the lower root sections it is necessary to twist the nozzle cascade, since the requirement of ensuring small losses can be carried out only by selecting special profiles that are different for the upper subsonic and the lower supersonic sections. For such stages, in particular, the law of constant specific flow rate may be used.* If the M number for a stage in the middle section amounts to $M_{c_1} = c_{1t}/a = 0.8$ to 0.9, then the angle α_1 along the cascade height (without taking into account the deflection in the slanting shear) will remain approximately constant. The advantage of the law of twisting, i.e., constant specific flow rate, as compared to the many other laws, consists in the more uniform distribution of the flow rate along the height, and also in the fact that in first approximation it is possible to assume that the meridional flow lines (for rectilinear restriction of the flow area) are straight. This essentially facilitates the calculation of the stage and brings the calculation closer to the true character of a three-dimensional flow.

For limiting stages with very large heat drops and small d/l in the middle section $M_{c_1} > 1$, and the constancy of the specific flow rate signifies a decrease of the angle of flow α_1 from root to tip. Actually, with the constancy of angle $\alpha_{1\,эф}$, due to an increase of the heat drop of the nozzle cascade, the angle of flow α_1 will increase toward the root. Thus, from the root, where M_{c_1} is maximum, angle α_1 will increase with respect to height, while $M_{c_1} > 1$, and at $M_{c_1} = 1$ angle $\alpha_1 = \alpha_{1\,эф}$; further, with the decrease of velocity, the constancy of the specific flow rate requires a decrease of angle α_1.

In this case it is possible to use formulas [96]:

$$\frac{r}{r_{cp}} = \exp\left\{-\int_{\lambda_{1cp}}^{\lambda_1} \frac{q^2\lambda_1 d\lambda_1}{\lambda_1^2 - q^2\left[\frac{k+1}{2} - \frac{k-1}{2}\lambda^2\right]^{-\frac{2}{k-1}}}\right\} \tag{317}$$

$$\sin\alpha_1 = \frac{q}{\lambda_1\left[\frac{k+1}{2} - \frac{k-1}{2}\lambda_1^2\right]^{\frac{-1}{k-1}}}, \tag{318}$$

*This law of twisting was first proposed by V. G. Tyryshkin.

where

$$\lambda_1 = \frac{c_1}{a_*}; \qquad q = \frac{c_1 \sin \alpha_1}{a_*} \cdot \frac{v_*}{v_1} = \text{const.} \tag{319}$$

Equation (317) can be solved only by numerical integration; if the stage is calculation in a region where it is impossible to apply the equation of an ideal gas, the solution of equation (317) should be performed with the help of finite differences, as done in the preceding paragraph.

Figure 288 shows the results of the calculation of a stage with q = const. The stage is calculated for operation in a region of slightly moist steam; $d/l_1 = 2.7$; $(\lambda_{c1})_{cp} = 1.03$; $\varphi = \varphi(r)$; $\mu = \mu(\rho, x)$.

With constancy of angle $\alpha_1^{горл} = 20^\circ$ in the entire zone of supercritical flow, at the root $\alpha_{1\,к} = 20^\circ 45'$ and at the periphery $\alpha_{1\,п} = \alpha_{1\,п.эф} = 22^\circ 35'$. Thus, in spite of the large change of the radius, $\alpha_{1\,эф}$ changes by a total of $2^\circ 35'$, which makes it relatively easy to select the effective profiles, changing the magnitude of the chord, of course, in order to preserve the optimum relative pitch $\bar{t}$.

The same graph represents the curves of change of angle α_1 for a stage with $d/l = 5$ [96] at values of $\lambda_{1\,cp} = 1.5$, 1.0, 0.5, and 0. Calculation is performed for k = 1.135 and without taking into account the losses.

For twisting according to the law of constant specific flow rate for a supersonic flow, in the lower half of the blade the angle of flow α_1 will be the biggest at the root. Owing to this, angle β_1 increases at the root and profiling of the root sections of the rotor blades is facilitated. As already indicated in § 43, at small angles β_1 it is difficult to profile a cascade with small losses; in this case not only the profile losses, but also the end losses will be great. In connection with this, an increase of β_1 at the root has a favorable effect on the flow around the root profile of the moving cascade.*

Let us compare, for instance, the frequently encountered law of twisting, $c_{1u}r$ = const, with the law q = const. The comparison will be made for a limiting stage, where the M_{c1} numbers equal to 1 are attained approximately on the mid-diameter. The requirement of $c_{1u}r$ = const for such a stage cannot simultaneously ensure the condition of c_a = const, i.e., the main advantage of this law of twisting

*Here, indeed, the moment of resistance of the profile, W_x, decreases.

for stages where it is possible to disregard the influence of compressibility. At the same time, according to this law, angle α_1 will be minimum at the root, and maximum at the tip. As a result of this, the losses will increase (both profile and end losses) at the root sections of the nozzle and moving cascade; the losses in the peripheral section of the nozzle cascade will decrease somewhat (due to the larger angle α_1), profiling will be complicated, and the losses in the upper section of the moving cascade will increase (where angle β_1, which increases as α_1 increases, is very great). It is possible to assume that the cascade losses in a stage that is designed according to the law of q = const will be less than in one designed according to the law when α_1 increases from root to tip.

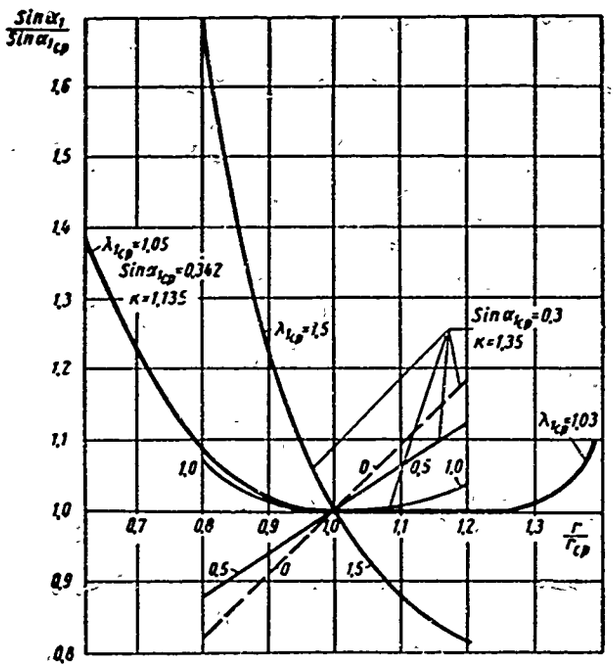

Fig. 289. Change of outlet angle of nozzle cascade, depending on radius, with twisting according to constant specific rate, q = = const.

However, if the flow in the nozzle cascade occurs with velocities below critical, then at q = const the angle α_1 will increase from root to tip, and at $\lambda_1 \approx 0$ we will obtain the known case of $c_u r$ = const, For a subsonic flow it may be preferable to perform twisting at α_1 = const (with variable chord); if, however, the angle in such a stage is very small (for instance, the next-to-the-last stage of a large turbine, where the last stage is a limiting one), then it is of value to change the angle α_1, decreasing it toward the tip, or maintain angle α_1 = = const almost along the entire height, increasing it in the root sections and decreasing it in the peripheral sections.

When selecting the law of twisting for the nozzle cascade, i.e., the dependence $\alpha_1 = \alpha(r)$, one should consider the possibility of separation of flow. The works K. Bammert and H. Kläukens [131], which were developed at KhPI by M. Ye. Levina and P. A. Romanenko [64], and the investigations conducted at MEI, proved that separation of flow is possible in the root sections of annular cascades (see Chapter VII). This

separation of flow may occur in the cascade itself, as well as behind it. The possibility of this separation and the place of separation depend on a number of factors: on the law of twisting, i.e., the dependence $\alpha_1 = \alpha(r)$, the flare d/l, the angle α_1 itself, and the M number; the meridional curvature of the flow line, the clearance between cascades, the character of the flow, the cascade losses, and so forth. A detailed analysis of the influence of these factors is given in the works of KhPI and in the preceding chapter. The presence of separation of flow is confirmed by many experiments, including the experiments of N. Scholz [152] and D. Shepherd, the experiments conducted by M. A. Romanenko at KhPI [65], and MEI experiments (see § 35). Very interesting experiments in a test turbine were conducted by A. O. Lopatitskiy and M. A. Ozernov at the LMZ laboratory. In the root sections of the rotor blade of a stage with $d/l = 6.8$ darkened zones of deposition of particles are detected, which are connected with the separation of flow behind the nozzle cascade, and also in the moving cascade.

Calculations of a cascade with distortion of the meridional flow lines showed that the data of Bammert and others require considerable correction; the same also pertains to the calculation of the influence of friction, the influence of the next cascade, and so forth.

The KhPI [65] conducted investigations in an experimental air turbine with $d_{cp} = 248$-418 mm at $\theta = 3.31$, 4.33, and 5.13, angle $\alpha_1 = 12$-14°, and very small flow rates.

For a cascade with $\theta = 5.13$ and $\alpha_1 = 12^\circ$, with cylindrical blading, the experiments showed that at a large distance behind the cascade there nevertheless occurs separation of flow. If behind the nozzle cascade there was mounted a disk with rotor blades, separation of flow was not observed; however in the moving cascade there occurs an essential distortion of the flow lines which is especially noticeable when there is a large axial clearance between cascades. At the stage outlet almost half of the height (from the root) admits a total of 20% of the flow. It is necessary, indeed, to consider that the moving cascade was not twisted in accordance with the variation of the parameters of flow behind the nozzle cascade, which naturally influenced the distribution of parameters and flow rates behind the stage.

For a stage with high supersonic velocities ($M_{c_{1\,K}} \approx 1.5$), selection of the law of twisting, $\alpha_1 = \alpha(r)$, should be performed in such a way, so as to ensure minimum losses along the entire cascade height, taking into account the requirements of reliability.

In this case, just as for moderate velocities ($M_{c_{1\,к}} \approx 1$) and $d/l > 3.5$-4.5, in the form of a first approximation we can recommend the law of $\alpha_1 \approx$ const or $q \approx$ const, which results in an analogous change of angle $\alpha_1 = \alpha(r)$. In this case, the interblade clearance should be reduced as much as possible.

For ensuring reliability it is sometimes necessary to decrease α_1 in the root zone.

Blading with a noticeable increase of angle α_1 from root to tip (cylindrical, and also designed according to the law of $c_u \cdot r$ = const) should be recommended only for sufficiently large angles $\alpha_1 (\alpha_{1u} > 30^\circ)$, large $d/l > 4$-5, and small interblade clearances.

Angle $\beta_{1\,л}$ for the moving cascade should be selected, taking into account the angle β_1, which is obtained from the inlet velocity triangle. As indicated in § 43, for cascades where $\beta_1 < 90^\circ$, it is necessary that the design inlet angle be somewhat less than the calculated β_1, and for cascades where $\beta_1 > 90^\circ$, conversely, $\beta_{1\,л} > \beta_1$.

Angle $\beta_{2\,ф}$ for the moving cascade should be selected from the conditions of uniform (corresponding to the flow in the nozzle cascade) distribution of flow rates with respect to height. One should consider the change (with respect to height) of the flow rate coefficients here. This is especially important for the root sections, where the coefficients μ are lower than in the middle sections. In the calculation of angle $\beta_{2\,ф}$ one should also consider the possible obstructions of flow, e.g., wire, thickening of profile, stellite linings.

Selection of Meridional Contour of Diaphragm

For the last stage of condensing steam turbines, this question obtains a large value. The conditions of designing a low-pressure flow area, in distinction from areas of high and intermediate pressure, do not make it possible to pass from stage to stage with a slight increase in height. The height of the blades increases es especially sharply in the transition from the next-to-the-last stage to the limiting last stage, and also after the lower level of Bauman's stage.

Turbine plants in this case employ various solutions (see § 42). A detailed investigation of the influence of the meridional contour on the efficien of a stage for actual stage parameters has not been conducted by us and is not described in the literature. The LMZ and BITM laboratories conducted investigations of the

influence of overlap at the inlet and the meridional contour in air-driven turbines (see Chapter VII).

At BITM, Prof. I. I. Kiriilov investigated a stage with $d/l_1 = 7.4$ and cylindrical meridional restriction of the flow area. He investigated different versions of an inlet conical diffuser having a cylindrical contour 110 and 190 mm in length on the root diameter (mid-diameter of stage was 560 mm); the external contour of the diffuser had conicity from 0° to 60°. The diffuser ended at a distance of 15 mm from the entrance to the nozzle cascade (this entrance section was cylindrical). The author indicates that since the experiments were conducted for a small heat drop ($M_{c1} = 0.25$), the influence of losses at the entrance to the stage was considerably greater than in actual stages of steam turbines. Thus, even for conicity with an angle of 20°, the kinetic energy at the entrance amounted to 17% of the total heat drop. Let us recall that in the last stage of the K-300-240 turbine it is less than 4%.

Interesting experiments also were conducted in the LMZ laboratory by engineers A. O. Lopatitskiy and M. A. Ozernov. They investigated a model of stage No. 21 of the LMZ turbine ПВК-200. The experiments were conducted in an air-driven turbine at $d/l_2 = 4.6$ with nozzle blades of constant profile of the type TC-2A MEI and with twisted rotor blades (§ 40). The stage was tested with a cylindrical meridional contour, with overlap at the entrance, and with different forms of meridional contour. The stage was investigated in two versions: with shrouded and unshrouded rotor blades.

In the LMZ experiments, the variants with the conical contour, starting without a clearance directly from the entrance to the stage, improved the stage's economy. In particular, the variant with the very large overlap ($\Delta l_0/l_1 = 0.52$) and conicity 24° had the same efficiency as in the initial cylindrical stage (Fig. 298). This is indirectly confirmed by the MEI experiments with the last stage of the KTZ turbine АП-6 [100]. Unfortunately, this variant was not investigated in detail, and it is possible only to assume that in this case the flow at the entrance to the nozzle cascade is more uniform.

When extending the results of the LMZ experiments to the last stages of condensing turbines and the last stages of large gas turbines, one should consider that the LMZ experiments were conducted with moderate heat drops ($M_{c1} \approx 0.5$), when the kinetic energy of the inlet velocity amounted to 2.5-5%.

In spite of the fact that there are few experiments, especially with actual M and Re numbers, on the influence of the meridional contour and overlap at the inlet. it is possible to make certain preliminary recommendations.

1. An abrupt transition from the preceding stage to the diaphragm of the next stage has an unfavorable effect. The external diameter of the entrance to the diaphragm should not be essentially higher than the external dimaeter of the rotor blade of the preceding stage.

2. The diaphragm should have a conical, or close to conical, diffuser at the entrance to the nozzle cascade, which can end in front of the nozzle cascade and should smoothly pass into the cylindrical contour or continue inside the channel of the nozzle cascade itself. The conicity of the diffuser and the meridional contour of the nozzle cascade should not be large, e.g., up to 20-30°.

A conical contour of the cascade itself, especially at a large angle of opening, can lead to the fact that the channel of the nozzle cascade will appear divergent in the upper part and the losses in the end will increase; therefore, it is best of all at the end of the channel to have a smooth transition from a cone to a cylindrical configuration or to a cone with a smaller angle.

It should be noted that the presence of a conical diffuser, and, all the more so, a conical meridional configuration of the nozzle cascade when designing a stage, requires the calculation of the influence of distortion of the meridional flow lines. The procedure for this calculation was outlined in the preceding paragraph. It is especially important to consider the change of the steam flow rate, which is confirmed not only by calculation, but also by experiments.

3. The inlet diffuser of the stage should not have large losses, i.e., $\eta_Д$ should be sufficiently high. Practically, $\eta_Д$ corresponds to the utilization factor of the outlet velocity from the preceding stage (but it is not equal to it, since the velocity at the entrance to the cascade is less than the outlet velocity of the preceding stage).

Of great importance is the uniformity of the flow at the diffuser outlet, i.e., in front of the nozzle cascade, since the effectiveness of the cascade itself depends on this.

At MEI, A. Ye. Zaryankin conducted some interesting investigations in conical and annular diffusers, the results of which can be used when designing and calculating the diaphragms of steam turbines.

The experiments showed that in the zone of angle γ from 8 to 20° the influence of the M number is not great.

The change of the loss coefficient here is practically linear and it is caused only by the increase of length of the diffuser, i.e., it is not connected with the cone angle. This obviously is also confirmed by the experiments where separation of the boundary layer is not observed. With the increase of angle γ to more than 20°, the losses already essentially increase. Apparently, separation of the boundary layer is indicated here.

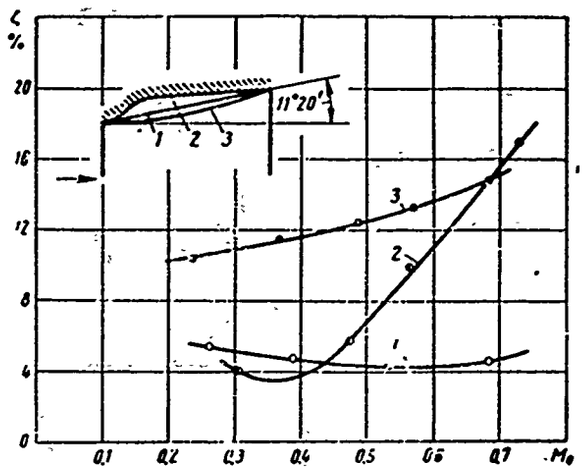

Fig. 290. Influence of diffuser shape and M_0 number on losses. MEI experiments at $f = F_1/F_0 = 2.33$.

It is obvious from what was said that conicity of the diffuser preceding the nozzle cascade is permissible to 20-30°.

Tests of a diffuser with various configuration at identical f and L, i.e., diffuser length, the results of which are represented in Fig. 290, showed that the losses in a conical diffuser (angle $\gamma = 11°20'$) in a wide range of M numbers almost do not depend on velocity. The so-called isogradient diffuser (curve 3 on Fig. 290) has its main expansion in the outlet portion. Diffuser 2, conversely, has a sharp increase of area immediately after the inlet. This diffuser is preferable for low (to M = 0.4) velocities. With the increase of the M number, in this diffuser there appear considerable positive pressure, gradients at which the losses due to separation increase.

Thus, at low M numbers less than 0.4, a diffuser with a sharp change of area in the inlet section is somewhat more preferable than a conical diffuser, which is better for high velocities.

Selection of Other Design Characteristics of a Stage

Above we considered the question of such geometric characteristics of a stage as the change of angles $\alpha_{1\ эф}$, β_1, $\beta_{2\ эф}$, and the meridional configuration of the diaphragm. However, this is not sufficient for forming a stage. It is necessary to know how to select the profile chord, trailing edge, blade incidence, overlap, etc.

First we shall discuss the geometric characteristics of profiles. The pitch of the nozzle cascade must be selected on the basis of the characteristics of separate sections. As a rule, this leads to an increase of chord from root to tip. Inasmuch as the dependence of losses on pitch is very linear with the increase of $\bar{t}$, in most cases it is not necessary to increase the chord in proportion to the radius; it is quite permissible to increase the chord to a smaller degree. Selection of the absolute value of chord b of the nozzle cascade also should be decided from the position of minimum losses, if, of course, it is not limited by strength. On the one hand, a decrease of chord is favorable, since this lowers the end losses; on the other hand, it may be unfavorable, since the Reynolds number decreases.

In general, the problem concerning the determination of optimum chord can not be solved at this time. For the end losses it is possible to use the dependences that are known in literature [22]. It is true that these formulas do not consider the peculiarities of supersonic flow and they pertain to straight cascades, not annular ones. Earlier (see § 35 and 43) it was shown that the end losses will be greater in annular cascades. If for stream turbines in stages of high and intermediate pressure, just as in gas turbines, the Reynolds numbers are so high that their influence is usually disregarded, then for the last stages of condensing turbines this is impermissible.

For cascades at subsonic flow rates there is rather limited material concerning the influence of the Re number on losses. For supersonic flows and, in particular, for cascades with expanded channels, these data are still insufficient for obtaining generalized characteristics; therefore, the solution of the problem concerning the optimum value of chord is possible only for a specific case, if there are the following dependences for it:

$$\left.\begin{aligned} \zeta_{\kappa} &= f(l/b,\ \mathrm{Re},\ b/r_{\kappa}) = f'(b); \\ \zeta_{\kappa p} &= f(\mathrm{Re}) = f'(b); \\ \zeta_{\kappa p} &= f\left(\frac{\Delta_{\kappa p}}{b},\ \mathrm{Re}\right) = f'(b), \end{aligned}\right\} \qquad (320)$$

where $\mathrm{Re} = bc_{1t}/\nu_1$.

Inasmuch as in this chapter we are concerned with relatively long blades, for which the chord changes along the radius, it is of value to refer all losses not to the entire length, but only to a certain section of the blade, starting from the

root, and thus select the chord for this root section. In this case, naturally, by l we imply not the entire blade height, but only the height of a section. The height l of the root section should be at least no less than the zone of propagation of end phenomena on the order of 100 mm.

The sum of the losses in the root section of the blade will be equal to

$$\zeta = \zeta_{к} + \zeta_{пр} + \zeta_{кр} = f(b).$$

We shall consider an examp e of the root section of the nozzle cascade of a limiting stage, which was investigated in detail at MEI (see § 43).

Let us assume that all sections of the root portion are under approximately equal performance conditions (Re, M). Here the M number is 1.5.

The profile losses in this cascade will be estimated by means of the following empirical formula (for Re > $3 \cdot 10^5$):

$$\zeta_{пр} = \frac{0{,}16}{\mathrm{Re}^{0{,}2}} = \left(0{,}76 \frac{\nu^{0{,}2}}{c_{1t}^{0{,}2}}\right) b^{-0{,}2}.$$

The end losses on a 100-mm section for an annular cascade ($\frac{t}{r_к} \approx 0.13$, $\alpha_1^{горл} = 13^\circ$):

$$\zeta_{к} = 0{,}28 \frac{b}{l} \mathrm{Re}^{-0{,}2} = \left(\frac{0{,}28}{l} \frac{\nu^{0{,}2}}{c_{1t}^{0{,}2}}\right) b^{0{,}8}.$$

The edge losses (see § 4) at $\Delta_{кр} = 1.5$ mm and $\bar{t} \approx 0.56$:

$$\zeta_{кр} = \frac{0{,}004}{b}.$$

Then for $l = 0.1$ m, $c_{1t} = 570$ m/sec, and $\nu_1 = 8.5 \cdot 10^{-2}$ m^2/sec, we obtain the total losses:

$$\zeta = 0{,}0326 b^{-0{,}2} + 0{,}116 b^{0{,}8} + 0{,}0024 b^{-1}.$$

Minimum total losses are attained at b ≈ 180 mm; however, in the optimum zone the dependence $\zeta = f(b)$ is very linear. Thus, at b = 150 mm the losses increase by a total of 0.02%, i.e., by a disregardable quantity that is essentially less than the accuracy which the formulas for ζ give.

For the middle of the nozzle cascade it is possible also to find the optimum value of chord. Here one should consider the influence of the Re number on the profile losses, the influence of chord on the edge losses, the influence of chord on relative pitch, and consequently, on the profile losses. The influence of chord on the end losses in this zone, naturally, is not considered.

For the upper section of a blade it is necessary also to consider the influence of the meridional configuration of the diaphragm.

It is obvious that the selection of optimum chord of the nozzle cascade is possible only in the presence of a large number of experimental data obtained for different cascades investigated in a wide range of variation of M and Re numbers. Our statements concern not only straight cascades, but also annular ones with different types of meridional configurations.

The trailing edge of a nozzle blade should be minimum, as much as the requirements of reliability and technology of manufacture permit; in root supersonic sections, a rounded edge may be expedient.

Selection of the chord of a rotor blade is determined by the same factors as for a nozzle blade. If it is a question of blades that are not limited with respect to their strength characteristics, for instance the next-to-the-last stages or last stages of small and imtermediate turbines, the chord should be selected by proceeding from minimum losses. In distinction from the nozzle cascade, the Re number is less here (especially in the root sections) and, at the same time, the end losses are greater due to the large deflection of flow and the lower velocities in the root sections.

For last blades of limited dimensions, the selection of chord is almost completely determined by the strength characteristics. However, in this case it is also necessary to know and, if necessary, to numerically estimate, how the cascade effectiveness will change when the chord is changed.

Selection of the thickness of the trailing edge of the rotor blade profile of all stages except last ones, is determined by the conditions of reliability and technology. From the point of view of the possibility of using the outlet velocity in the following stage, the edge should be minimum.

For the last rotor blade of a turbine, the question concerning the selection of the thickness of the trailing edge is specific. In limiting stages the flow past the entire blade or, forthe most part, past its length at the cascade outlet, is supersonic. Consequently, the edge losses, including the mixing losses, as well as processes taking place behind a cascade in a supersonic flow, practically will not affect the character of flow inside the cascade or the distribution of pressure and velocities along the profile. Thus, there will practically be no change in the magnitude of the force P_u created by the steam in the stage, which also means the

effectiveness of the stage.

The flow process occurring outside the last cascade will affect the losses in the outlet duct of the machine; however, for real ducts of condensing turbines, the influence of the thickness of the trailing edge on the duct losses is practically imperceptible.

Consequently, for the last cascade with supersonic velocities, the thickness of the trailing edge within limits up to $\Delta_{кр}$ = 2-3 mm, in itself, almost does not influence the effectiveness of the stage, and it should be selected (taking into account reliability) in such a way as to ensure an optimum channel shape in a cross section. In this case, for certain supersonic sections, where it is preferable to have reverse concavity of the profile back in the outlet area, it may sometimes be expedient to employ edges that are thicker than required by the conditions of technology of manufacture and reliability.

It is obvious that also for a subsonic flow, the process occurring outside the cascade practically will not determine the magnitude of P_u; therefore, in this case also, the edge losses should not enter as components into the balance of the stage losses. However, for a subsonic flow, a change of the thickness of the trailing edge leads to a change of the flow in the edge wake and in the pressure distribution behind the edge, which affects the character of flow inside the channel, and as a result, the effectiveness of the cascade. Here the question about the selection of trailing edge thickness should be solved concretely, depending upon the configuration of the cascade and the behavior of the flow. However, it is obvious that the influence of the thickness of the trailing edge is different for a last stage; it is less than for other cascades, and its increase in a number of cases may be expedient.

Selection of the axial clearance between cascades, as already noted earlier (see § 22), is determined, on the one hand, by the increase of mixing losses with the increase of this clearance and with another smaller nonuniformity at the entrance to the moving cascade. Experiments on the study of the influence of the axial clearance on the economy of a stage were conducted at very low subsonic velocities and without taking into account the specific peculiarities of last stages; therefore, they cannot be used for selecting the optimum value of the clearance.

It should also be stressed that in a number of stages (depending upon the law

of twisting, the flare, angle α_1, etc.) separation of flow is possible in the root sections at a certain distance behind an annular cascade. For such stages (see § 35) it is desirable to maintain an axial clearance, especially in the root area of the blades; this clearance should be as small as the requirements of reliability permit (see Chapter VII).

The influence of overlap for the last stages of condensing turbines almost was not investigated. With the flow of moist steam, for decreasing blade erosion and large suction of moisture, frequently zero overlap or even a small negative one is employed on the periphery. Bowing of the nozzle blades, which makes it possible to somewhat decrease the change of the reaction along the radius, is expedient (see § 39); however, it still has not undergone an experimental check in a test turbine that simulates the flow in the last stages of condensing turbines. After these experiments are performed, it will be possible to make concrete quantitative recommendations on the selection of blade angle and curvature.

CHAPTER IX

GENERALIZED ECONOMY GRAPHS AND CALCULATION OF MODEL STAGES

When designing a turbine, practically for all stages with the exception of limiting stages of large condensing steam turbines and certain special turbines, it is possible to use cascade combinations of model stages that have been tried out and checked beforehand in experimental turbines. In this case it is best to use generalized graphs that are constructed on the basis of numerous investigations which have been discussed in the preceding chapters.

We shall discuss the procedure for calculating model stages for three types of stages: a single-wheel stage with cylindrical blading, a single-wheel stage with variable blading, and a double-wheel velocity stage.

§ 47. SINGLE-WHEEL STAGES WITH CYLINDRICAL BLADING

We shall first determine the basic dimensions of the nozzle cascade. The area of its outlet section is found by the following formula:

$$F_1 = \frac{G}{B_t \mu_1 q \sqrt{p_0/v_0}}, \tag{321}$$

where p_0[N/m^2] and v_0[m^3/kg] are the parameters of the stagnant flow before the stage.

Here q is the relative flow rate, which is determined by means of gas-dynamic tables depending upon the pressure ratio in the cascade, $\varepsilon_1 = p_1/p_0$; B_t is a numerical coefficient that is determined by the isentropic exponent k.

For k = 1.3, B_t = 0.661; for k = 1.4, B_t = 0.674.

Inasmuch as all stages must be designed with a small positive reaction in the root section, the reacton ρ on the mid-diameter d may be assumed to be greater than

$\frac{1.8}{1.8+d/l}$, and the pressure ratio ε_1 in the nozzle cascade is found by the following formula:

$$\varepsilon_1 \approx \varepsilon + q(1-\varepsilon). \tag{322}$$

If $\varepsilon_1 \leq \varepsilon_*$, then $q = 1$.

Instead of formula (321), frequently for a subcritical flow it is more convenient to use the continuity equation:

$$F_1 = \frac{Gv_{1t}}{\mu_1 c_{1t}}. \tag{323}$$

Here v_{1t} is the specific volume behind the nozzle cascade; it is determined for an isentropic flow process; c_{1t} is the theoretical discharge velocity of the nozzle cascade; it is calculated on the basis of the parameters of the stagnant flow before the cascade.

Various initial conditions are possible when designing a stage. Let us first consider the case of full input of the working medium. If a single stage is being calculated, usually the mid-diameter d of the nozzle cascade is known from a preliminary calculation and, thus, the following product is determined:

$$l_1 \sin\alpha_{1\,эф} = \frac{F_1}{\pi d}. \tag{324}$$

Then for a selected cascade we will know $\alpha_{1\,эф}$, and l_1 is then calculated.

The dimensions of the moving cascade are found for a given combination according to the optimum ratio $(F_2/F_1)_{опт}$ (see Chapter IV) and the angle $\beta_{2\,эф}$, i.e.,

$$\left.\begin{aligned} F_2 &= F_1\left(\frac{F_2}{F_1}\right)_{опт}; \\ l_2 &= \frac{F_2}{\pi d \sin\beta_{2\,эф}}. \end{aligned}\right| \tag{325}$$

For stages with cylindrical blading, as a rule, the diameters of the nozzle and moving cascades are practically equal. In another case, into formulas (323) and (325) we substitute different values of d.

After determining l_2 by formula (325), it is necessary to check the overlap. If it exceeds the limits that were recommended earlier (see Chapter IV), either the ratio $(F_2/F_1)_{опт}$ or the angle $\beta_{2\,эф}$ should be changed; small deviations of these quantities from the optimum value practically do not affect economy, but can somewhat change the magnitude of ρ, and consequently, the flow rate through the stage.

A decrease of F_2/F_1 leads to an increase of the reaction. The reaction is then increased by $\Delta\rho$:

$$\Delta\rho = 0{,}7\left[1 - \frac{(F_2/F_1)}{(F_2/F_1)_{опт}}\right]. \qquad (326)$$

Then the area of the nozzle cascade F_1' should be changed as compared to F_1, which is found by formula (321). This ratio F_1'/F_1 is determined by either a detailed calculation, or by means of the graph in Fig. 291.

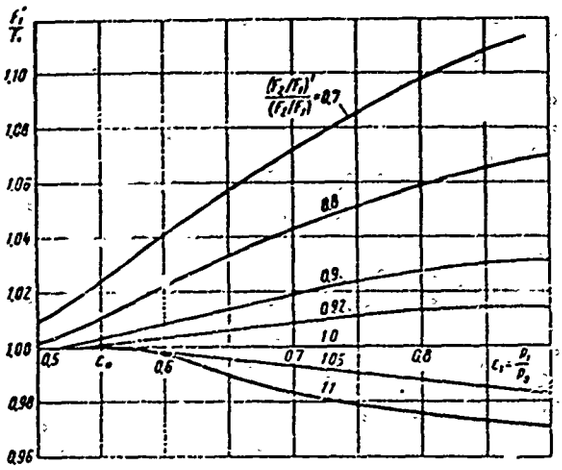

Fig. 291. Change of area of nozzle cascade, calculated by formula (321) for a deviation of the area ratio (F_2/F_1) from the optimum value, $(F_2/F_1)_{опт}$ (for calculating the dimensions of a stage with cylindrical blading).

A deviation of $\beta_{2\ эф}$ from the recommended value renders an insignificant influence on the area F_1 (at the same F_2/F_1), and it is usually disregarded.

In general, the accepted value of F_2/F_1 cannot correspond to the selected value of ρ. For a subcritical flow, this will lead to an error in the determination of F_1.

It is necessary to check the actual reaction ρ, determining it first by means of Fig. 50, and then determine the exact value of F_1 by formula (321) or (323). In most cases this exact determination will be insignificant.

If a group of stages is being calculated, then for all the blading of the group it is desirable to retain blades that have identical profiles and the same pitch t in the root section. Inasmuch as such a group of stages usually is designed with a constant root diameter, the relative cascade pitch on the mid-diameter will increase from stage to stage.

Area F_1, which is determined by formula (321), is found for each stage of the group not only for different parameters of the stagnant flow (p_0, v_0), but also for different ε_1, inasmuch as d/l, and consequently, the reaction on the mid-diameter, will be different for each stage.

For any stage of the group, the root diameter $d_к = d - l$ and all cascade dimensions in the root section will be given, i.e., angle $(\alpha_{1\ эф})_к$:

$$F_1 = \pi l_1^2 \left(\frac{d_к}{l_1} - 1\right) \sin\left[\operatorname{arc\,tg}\left(\frac{\frac{d_к}{l_1}+1}{d_к/l_1} \operatorname{tg} \alpha_{1к}\right)\right]. \qquad (327)$$

Here, for determining F_1, it is assumed that in a cascade of constant profile

$$\operatorname{tg} \alpha_{1ф} \approx \frac{r}{r_к} \operatorname{tg} (\alpha_{1ф})_к.$$

After calculating F_1 beforehand by formula (321), for which it is necessary to first know the ratio d/l, it is possible, knowing $d_к$ and $\alpha_{1к}$, to solve equation (327) with respect to l_1. After that, a more accurate value of d/l and F_1 should be found. For convenience of calculation, Fig. 292 graphically represents formula (327).

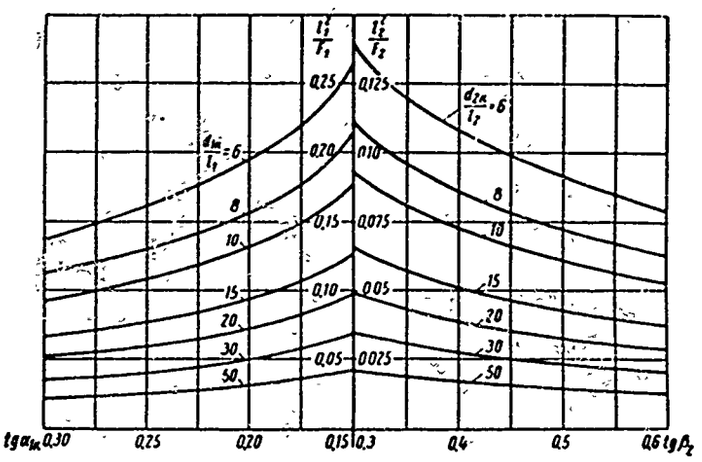

Fig. 292. Determination of cascade height according to diameter and outlet angle in root section.

After taking the optimum value of $(F_2/F_1)_{опт}$ and determining the area of the moving cascade F_2, we calculate the height of the moving cascade l_2 by the following formula:

$$F_2 = \pi l_2^2 \left(\frac{d_к}{l_2} + 1\right) \sin\left[\operatorname{arc\,tg}\left(\frac{\frac{d_к}{l_2}+1}{d_к/l_2} \operatorname{tg} \beta_{2к}\right)\right] \qquad (328)$$

This procedure is similar to the one followed above for the nozzle cascade in Fig. 292.

The blade efficiency $\eta_{оп}$ of a stage with cylindrical blading composed on MEI cascades may be determined by generalized graphs [103] that have been constructed on the basis of experimental data and theoretical calculations given in the preceding chapters of this book.

Efficiency is calculated as the product of the primary value of efficiency $\eta'_{оп}$ times a number of correction factors. Figure 293 presents a graph* of primary

*The graph in Fig. 293 was constructed on the basis of the results of stage tests that were not conducted under simulated conditions, but with the real plant technology of manufacture. In all doubtful cases, in case of divergence of the results of experiments, and so forth, the lowest value of economy was taken; therefore, the efficiency calculated according to Fig. 293 is taken with a certain reserve.

efficiency $\eta'_{оп}$ depending upon $u/c_{ф}$ and nozzle cascade height l_1

$$\eta'_{оп} = f\left(\frac{u}{c_ф}, l_1\right).$$

Here u is determined for the mid-diameter of the nozzle cascade, while $c_ф$ is calculated for the entire stage drop, starting from the stagnation parameters before the nozzle cascade to the static pressure behind the moving cascade.

$$c_ф = \sqrt{2h_0 + c_0^2}.$$

The graph of Fig. 293 was constructed for the following geometric and physical parameters:

1. MEI cascade combinations: КД-1-2А; КД-2-2А; КД-2-3А (see Table 8).
2. Welded diaphragm with unprofiled cylindrical shrouds.
3. Ratio of stage diameter to height of nozzle cascade, $d/l_1 = 20$.
4. The ratio of outlet (throat) areas of the moving and nozzle cascades, $F_2/F_1 = 1.50$-1.75.
5. Chords of cascade profiles: nozzle, $b_1 = 52$ mm; moving, $b_2 = 26$ mm.
6. Thicknesses of trailing edges of profiles:

$$\Delta_{кр1} = 0{,}6 \text{ мм and } \Delta_{кр2} = 0{,}5 \text{ мм}.$$

7. Overlap, 2.5-3.5 mm.
8. Shroud of moving cascade can be cylindrical, as well as conical, with an increase of cascade height in the direction of steam flow. In last case, an obligatory condition is the preservation of channel convergence.
9. The total axial clearance – the distance between the trailing edges of the nozzle cascade and the leading edges of the moving cascade – 5-7 mm. Peripheral stage sealing, i.e., the axial clearance between blade shroud and diaphragm (open clearance), $\delta_a = 1$ mm; two radial seals above the shroud with clearance $\delta_p = 1$ mm. In this case there is no steam leakage through the root clearance.

In all deviations from the enumerated geometric characteristics the efficiency can change, in consequence of which it is necessary to introduce corrections.

The correction $k_{мер}$ is introduced for meridional profiling of the nozzles. It is assumed that the meridional configuration is executed according to the MEI method and the recommendations given in this book. The area rate here changes

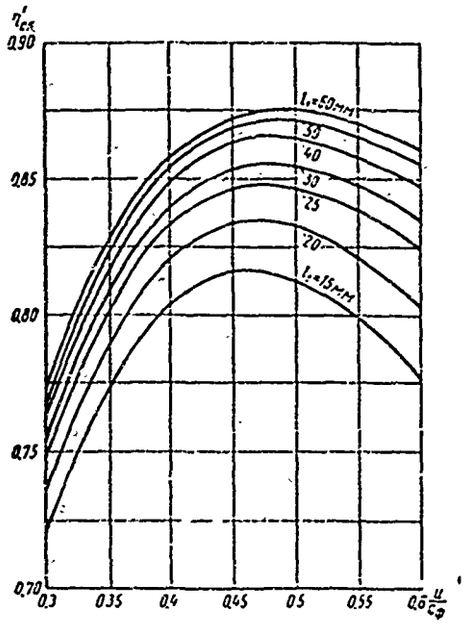

Fig. 293. Primary efficiency of MEI single-wheel stages with cylindrical blading.

somewhat, since with the recommended minimum permissible root reaction it is possible to lower the reaction on the mid-diameter.

When introducing meridional profiling, one should certainly consider the shift of the minimum section into the region of the cross section, as a result of which there will occur a certain increase of the outlet area (see § 10).

The correction for meridional profiling $k_{мер}$ is given depending upon the cascade height l_1 and is represented in Fig. 294a. A correction is given there for flare $k_{d/l}$, which indicates the dependence of efficiency on the d/l ratio.

A correction for deviation of the area ratio is not introduced, since it is assumed that the optimum ratio F_2/F_1 has been taken. However, the further change of F_2/F_1 is considered when calculating the reaction at the root and tip, and also its influence on economy, in corrections for the pressure ratio in the stage and, finally, when computing the losses with the outlet velocity.

Figure 294b gives corrections k_b for the profile chord of the nozzle cascade b_1 and the moving cascade b_2, which are also given depending upon height. A correction for the chord of the nozzle cascade is introduced only for a cylindrical meridional configuration. For special meridional profiling, it is assumed that the chord b is selected in accordance with our recommendations.

Corrections $k_{\Delta\,кр}$ for the thickness of the trailing edge of the nozzle $\Delta_{кр\,1}$ and the moving $\Delta_{кр\,2}$ cascades are given in Fig. 294a.

The performance parameters, for which the graph of the primary efficiency $\eta_{ол}$ was constructed in Fig. 293 have the following values:

1. Angle of entrance into nozzle cascade, $\alpha_0 = 70\text{-}110^\circ$.

2. Pressure ratio in stage (with respect to stagnation parameters at entrance), $\varepsilon = \frac{p_2}{p_0} = 0.65\text{-}0.75$.

3. Fictitious Reynolds number, $Re_ф = b_1 c_ф/\nu_2 \approx 5\cdot10^5$, where $c_ф = \sqrt{2h_0}$ is calculated for the entire stage drop depending on the stagnation parameters; ν_2 is

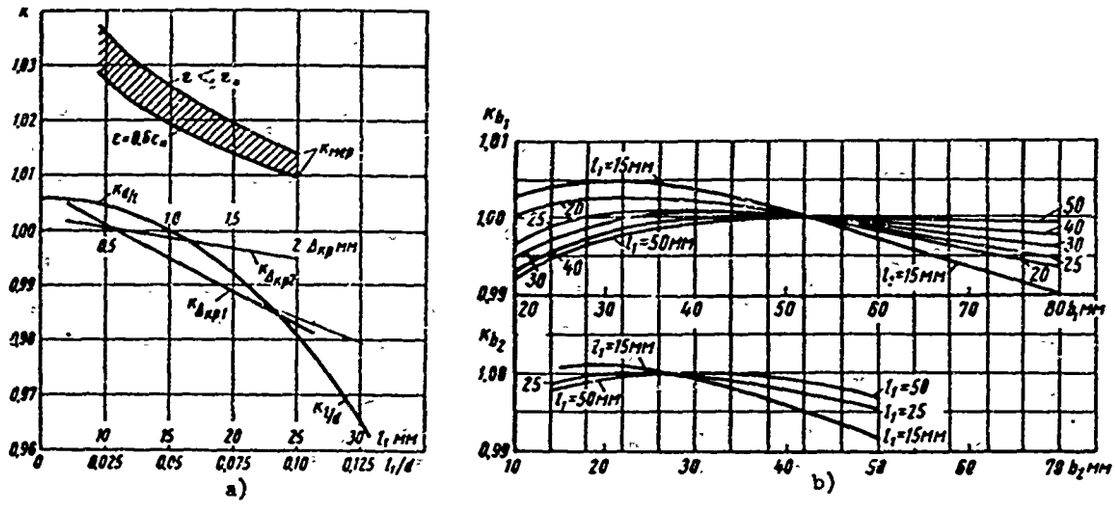

Fig. 294. Correction factors are calculating the efficiency of a single-wheel stage with cylindrical blading: a) corrections for meridional profiling $k_{мер}$ of nozzle cascade, depending upon height l_1; for flare $k_{d/l}$, depending upon d/l, and corrections for thickness of trailing edge of nozzle $k_{\Delta\ кр\ 1}$ and moving $k_{\Delta\ кр\ 2}$ cascades; b) corrections for chord of nozzle k_{b1} and moving k_{b2} cascade, depending upon height. For cascades of group "K," the increase in efficiency is considered by the upper curve of $k_{мер}$.

the kinematic viscosity of steam behind the stage; it is calculated for an isentropic process of expansion.

4. Gas or superheated steam.

5. The kinetic energy of the outlet velocity $\frac{c_2^2}{2}$ is completely lost. In case of deviations of the performance parameters from the above-indicated, correction factors are introduced.

If there occurs a change of the inlet angle of flow in the stage with a possible off-design ratio $u/c_ф$ of the preceding stage, the correction k_{α_0} is introduced, which depends upon angle α_0 and the relative height of the nozzle cascade l_1/b, as shown in Fig. 295.

It should be recalled that it is possible to avoid a decrease of stage economy in this case by applying special profiles developed at MEI (see Chapter IV). Then $k_{\alpha_0} = 1$ also at small angles α_0.

In case of a change of $\varepsilon = p_2/p_0$, the correction k_ε is introduced, which also depends on the area ratio F_2/F_1 and the ratio d/l, as shown in Fig. 296. Here p_2 is the static pressure behind the moving cascade, while p_0 is the stagnation pressure before the nozzle cascade.

At low $Re_{ф}$ numbers less than $5 \cdot 10^5$, one should also introduce a correction which will depend on l_1/b (see Fig. 295).

The following series of corrections is connected with the stage sealing. Over both leakage and suction are possible the blade shroud. The direction of flow may be judged by means of the nomograph represented in Fig. 297, where, depending upon $u/c_{ф}$, F_2/F_1, and d/l_1, the auxiliary quantity A is determined.

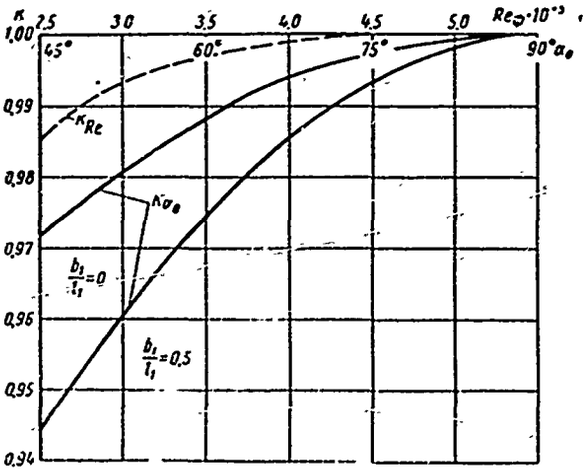

Fig. 295. Corrections for deviation of inlet conditions of nozzle cascade and for Reynolds number $Re_{ф} = b_1 c_{ф}/\nu_2$.

For stages with single meridional profiling, the quantity $A_м$ is determined by the following formula: $A_м = A - 2$.

Further, Fig. 298 presents graphs that show the magnitude of correction for efficiency, $k_{у.п}$, for suction and leakage, depending upon the equivalent clearance, $\delta_{экв}$,

$$\delta_{экв} = \frac{1}{\sqrt{4/\delta_a^2 + 1{,}5z/\delta_p^2}},$$

where δ_a and δ_p are open axial and radial clearances, respectively; z is the number of radial strips above the shroud.

Stage economy, in the event of leakage or suction in the root axial clearance, is also lowered. If suction takes place, then Fig. 299 is used to determine the correction $k_{у.к}$ depending upon the relative percent of absorbed substance and the root reaction $\rho_к$. If $\rho_к$ is not known from a preliminary calculation of the stage, then for cylindrical blading it can be found by the following formula:

$$\rho_к = \rho_p - \frac{1{,}8}{1{,}8 + d/l}.$$

The quantity of absorbed steam (gas) should be determined according to the leakage balance in the stage, which was covered in § 12.

The correction for leakage in the root clearance is calculated by the following formula:

$$k_{у.к} = 1 - 0{,}7\,\frac{G_к}{G}.$$

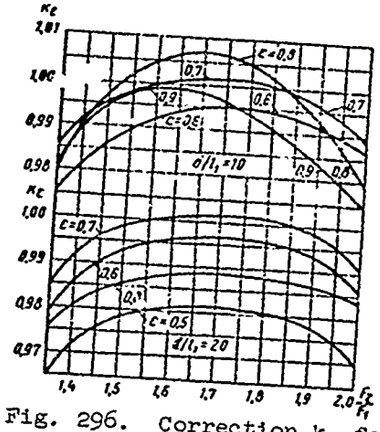

Fig. 296. Correction k_ε for pressure ratio in stage, $\varepsilon = p_2/p_0$, depending upon ratios F_2/F_1 and d/l.

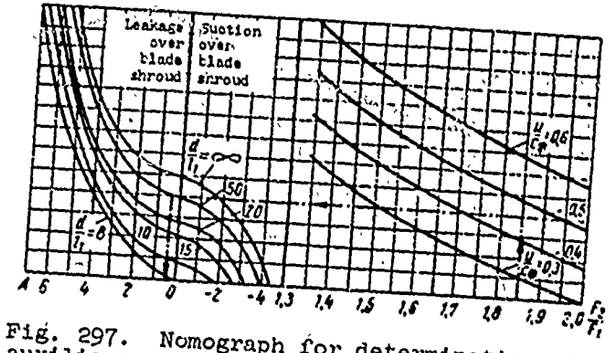

Fig. 297. Nomograph for determination of the auxiliary quantity that is necessary for calculating the correction for leakage over a blade shroud (for a stage without meridional profiling).

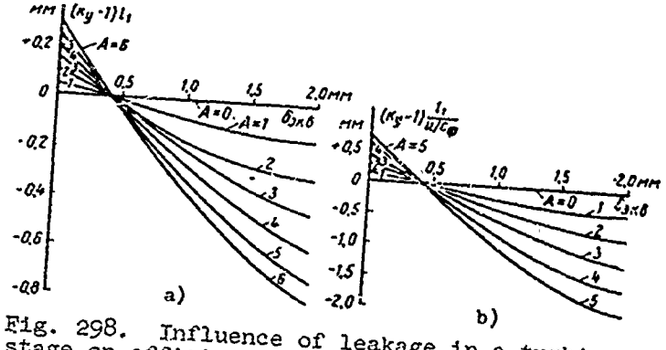

Fig. 298. Influence of leakage in a turbine stage on efficiency η_{OM} : a) correction for leakage over blade shroud; b) correction for suction over blade shroud.

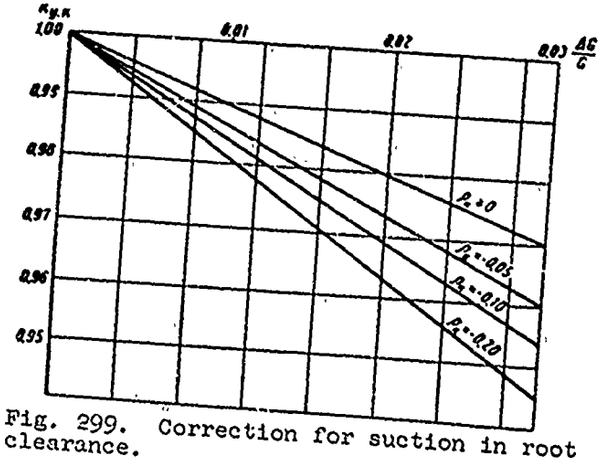

Fig. 299. Correction for suction in root clearance.

Then, taking into account all corrections, the relative blade efficiency of the stage with complete loss of outlet velocity is calculated by the following formula:

$$\eta_{oл} = \eta^{*}_{oл} k_{кер} k_{d/l} k_{e_1} k_{\varepsilon_2} k_{\Delta_{кр}} k_{u_0} k_{\varepsilon} k_{Re} k_{y.n} k_{y.к}.$$

The order of substitution of the correction factors into this formula is not of importance. If the following stage uses the axial component of the outlet velocity, the efficiency of the given stage, taking this utilization into account, is determined by the following formula:

$$\eta^{*}_{oл} = \eta_{oл} = k_{в.с},$$

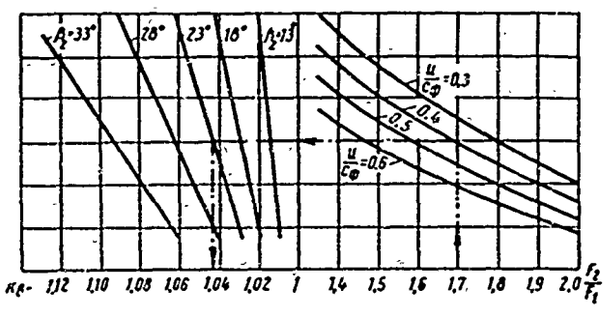

Fig. 300. Correction $k_{B.C}$ with the use of the axial component of the outlet velocity.

$k_{B.C}$ is found from Fig. 300.

For a determination of the relative internal efficiency, which includes all losses in the stage, it is necessary to consider the losses due to disk and shroud friction and the losses caused by leakage through the diaphragm seal:

$$\eta_{oi} = \eta_{oл} - \zeta_{т} - \zeta_{д.у}; \quad \eta^{*}_{oi} = \eta^{*}_{oл} - \zeta_{т} - \zeta_{д.у}.$$

These losses are calculated according to the material presented in § 12. For stages that operate in a region of moist stage, one should consider the losses due to moisture, which are determined according to the data in Chapter X.

A partial stage has the following features:

1. The optimum area ratio $(F_2/F_1)_{опт}$ is found according to the data in § 28. A more exact value of $(F_2/F_1)_{опт}$ should be found only for small degrees of partial admission.

2. The area F_1 is calculated for the reaction ρ = 3-8%. Recommendations on the selection of ρ are presented in § 28.

3. The optimum velocity ratio $u/c_ф$ is determined according to the data in § 30.

4. Selection of blade height, depending on degree of partial admission, is performed according to the data in § 30.

5. When calculating the economy of a stage, it is necessary to add the additional losses that are determined according to the data in § 28.

Example. We shall determine the dimensions of an intermediate stage and its economy. The stage is combined with the other stages of the group. Given: nozzle cascade TC-2A, $d_K = 0.928$, $\alpha_{1\,K} = 14^\circ$; moving cascade TP-3A, $d_K = 0.925$ m, $\beta_{2\,K} = 22^\circ 30'$.

Steam flow rate, G = 102.8 kg/sec; stagnation parameters before nozzle cascade: $p_0 = 44.6$ bar; $v_0 = 0.0661$ m^3/kg; pressure behind stage, $p_2 = 37.3$ bar. Available heat drop of stage, depending on stagnation parameters, $h_0 = 52.2$ kj/kg. Turbine speed n = 3000 rpm.

By means of formula (321) we find the outlet area of the nozzle cascade:

$$F_1 = \frac{G}{0.661\mu_1\sqrt{p_0/v_0}} \cdot \frac{1}{q} = 251 \text{ см}^2.$$

Here it is assumed that $\mu_1 = 0.97$.

For calculating ε_1 it is necessary to know ρ. After assuming approximately that $\theta = d/l = 27$, we find $\rho_K > \frac{2}{2+\theta} = 0.06$.

Let us say that $\rho_K = 0.10$. Then, by formula (322),

$$\varepsilon_1 = \varepsilon + \varrho(1-\varepsilon) = 0.851,$$

where $\varepsilon = p_2/p_0 = 0.835$; $q = 0.940$ (for $\varepsilon = 0.851$).

By means of formula (327) or Fig. 292, we find $l_1 = 33.2$ mm, d = 928.2 mm, and $\alpha_1 = 14^\circ 25'$ after a more accurate determination.

Analogously, by means of formula (328) we calculate the area $F_2 = 430$ cm^2, after assigning on overlap of $\Delta l = 3$ mm, and consequently, assuming that $l_2 = 36.2$ mm.

The area ratio $\frac{F_2}{F_1} = \frac{430}{251} = 1.71$ corresponds to the optimum value for stage КД-2-3А (see Table II). We check the selected reaction on Fig. 50. It turns out to be approximately equal to the value found earlier; therefore, it is not necessary to find a more accurate value of area F_1.

Characteristics of moving cascade: $d_2 = 963.2$ mm, $\beta_2 = 23^\circ 15'$.

Efficiency $\eta_{ол}$ is determined by means of the graphs of this paragraph. For $u/c_ф = 0.465$ and $l_1 = 33.2$ mm, we find $\eta'_{ол} = 0.859$ on Fig. 293. Corrections for chords and trailing edges can be determined if the dimensions of the profiles are known. Let us assume that $k_b \approx 1$ and $k_{\Delta кр} = 1$. The correction for flare is found in Fig. 294a, where $k_{d/l} = 1.003$. The correction for the pressure ratio $k_\varepsilon = f(\varepsilon, F_2/F_1, d/l)$ is found in Fig. 296, where $k_\varepsilon = 0.989$. Since the Reynolds

number is great,

$$Re_{\phi} = \frac{b_1 c_{\phi}}{\nu_s} = \frac{0{,}045 \cdot 324{,}5}{1{,}77 \cdot 10^{-6}} = 8 \cdot 10^{4}$$

and lies in a self-similar region, then $k_{Re} = 1$.

Taking the magnitude of the equivalent clearance as $\delta_{экв} = 0.64$ mm, in Fig. 297 we find $\Lambda = 3$, and in Fig. 298a, $k_{у.п} = 0.997$.

According to the leakage balance in the stage, we calculate the quantity of steam, absorbed through the root clearance, $\frac{\Delta G_к}{G} = 0.2\%$ (the procedure for this calculation is given in § 12), and in Fig. 299 we find $k_{у.к} = 0.998$.

Thus, the relative blade efficiency of the stage with complete loss of the outlet velocity amounts to:

$$\eta_{oл} = 0{,}859 \cdot 1{,}003 \cdot 0{,}989 \cdot 0{,}997 \cdot 0{,}998 = 0{,}847.$$

With the use of the axial component of the outlet velocity, in Fig. 300 we find $k_{вс} = 1.041$ and the efficiency

$$\eta^{*}_{oл} = 1{,}041 \cdot 0{,}847 = 0{,}882.$$

The losses due to disk friction are calculated by formula (83):

$$\zeta_{тр} = B \frac{d_k^2}{F_1} \left(\frac{u}{c_{\phi}}\right)^3 = 0{,}014,$$

where B is found in Fig. 65 at $Re_u = \frac{ud_к}{\nu} = 8 \cdot 10^7$; the losses due to shroud friction, $\zeta_{тр.б} = 0.001$ [by means of formula (86)]. The losses due to leakage through the diaphragm seal amount to [see formula (88)]:

$$\zeta_y = \frac{\mu_y F_y \eta^{*}_{oл}}{\mu_1 F_1 \sqrt{z_y}} = \frac{2{,}55}{0{,}97 \cdot 251} 0{,}882 = 0{,}009.$$

The equivalent area of the diaphragm seal clearance here will be:

$$\frac{\mu_y F_y}{\sqrt{z_y}} = 2{,}55 \text{ см}^2.$$

The total relative internal efficiency of the stage:

$$\eta^{*}_{oi} = \eta^{*}_{oл} - \zeta_{тр} - \zeta_{тр.б} - \zeta_{д.у} = 0{,}858.$$

§ 48. DOUBLE-WHEEL VELOCITY STAGES

The area of the outlet section of the nozzle cascade is found by the following formula (for superheated steam):

$$F_1 = \frac{G}{0{,}66 l \mu_1 q \sqrt{p_0/v_0}}, \qquad (329)$$

where p_0 and v_0 are the parameters in front of the stage; q is the relative flow rate, which is determined from gas-dynamic tables, depending upon the pressure ratio in the cascade, $\varepsilon_1 = p_1/p_0$. For critical flow, q = 1.

The reaction of an MEI velocity stage, when selecting the area ratio, according to the data presented in Chapter V, for subcritical flow, can be estimated on the graph in Fig. 301 for determination of F_1, depending upon u/c_Φ, ε_u, and partial admission e:

$$\sum \rho = f\left(\frac{u}{c_\Phi}, \varepsilon, e\right).$$

Then $\varepsilon_1 = \varepsilon + \Sigma\rho(1 - \varepsilon)$, where $\varepsilon = p_2/p_0$ is the pressure ratio of the entire stage.

For the selected type of stage at the known magnitude of angle α_1, we find:

$$el_1 = \frac{F_1}{\pi d \sin \alpha_{1эф}}. \qquad (330)$$

We select the degree of partial admission e, and consequently, the height l_1, according to the data in § 30, taking into account the requirements of reliability, design, and unification.

The dimensions of the separate cascades are determined according to the data in Chapter V.

The blade efficiency $\eta_{0л}$ of an MEI velocity stage can be determined by means of generalized graphs [104] constructed on the basis of experimental data and theoretical calculations presented in the preceding chapters of this book. These graphs are constructed for three combinations of velocity stages developed at MEI: KC-0A, KC-1A, and KC-1Б. The basic geometric characteristics of these stages are given in Chapter V.

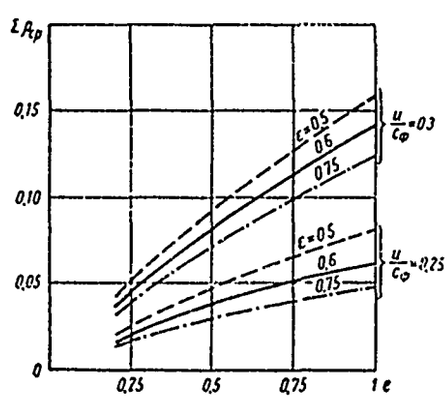

Fig. 301. Graph for estimating the total reaction of an MEI double-wheel velocity stage (for calculating the area F_1).

The relative blade efficiency $\eta_{0л}$ is the stage efficiency with full input and it considers the following losses:

1. Losses in all cascades, including those at the entrance to the cascades.

2. Losses in clearances between cascades.

3. Losses due to leakages past the cascade channels into the clearances above the shrouds of the rotor blades and under the shroud of the rotor cascade.

4. Losses with the outlet velocity.

Thus, not considered here are the losses due to disk and shroud friction, losses due to leakage through relief holes and end seals, and losses connected with partial input.

The stage efficiency $\eta_{ол}$ is found as the product of the primary efficiency $\eta'_{ол}$ times a series of correction factors:

$$\eta_{ол} = \eta'_{ол} k_{хср} k_{в} k_{\Delta_{пр}} k_{г} k_{у} k_{ук} k_{d}. \qquad (331)$$

The order of substitution of the correction factors into formula (331) is of no importance.

The primary efficiency $\eta'_{ол}$ is determined in Fig. 302,* depending upon $u/c_{ф}$ and the height of the nozzle cascade l_1. Here $c_{ф} = \sqrt{2h_0}$ is the fictitious velocity calculated for the entire available heat drop of the stage.

The graph in Fig. 302 was constructed for the following conditions: 1. Pressure ratio in stage, $\varepsilon = p_2/p_0 = 0.55\text{-}0.65$.

2. Reynolds number, $Re = b_1 c_{ф}/\nu_2 > 5 \cdot 10^5$, where ν_2 is the kinematic viscosity with respect to the stage behind the stage.

3. Welded diaphragm nozzle cascade without special meridional profiling.

4. Diameter of stage, d = 600 mm.

5. Chords of profiles:

$$b_1 = 52 \text{ мм}; \quad b_{1р} = b_п = b_{2р} = 26 \text{ мм}.$$

6. Trailing edge thicknesses:

$$\Delta^{с}_{кр} = 0{,}6 \text{ мм}; \quad \Delta^{р}_{кр} = \Delta^{п}_{кр} = 0{,}5 \text{ мм}.$$

7. Total axial clearance, i.e., the distance between the trailing edges of the blades and the leading edges of the following cascade, is 4-7 mm. The peripheral stage sealing, i.e., the open axial clearance between the blade shroud and diaphragm, is $b_{а п}$ = 1 mm, and special seals above the blade shroud (see Fig. 147). There is no leakage through the root clearance between the diaphragm and the wheel.

For all deviations from the indicated stage characteristics, the efficiency

*See footnote on p. 498.

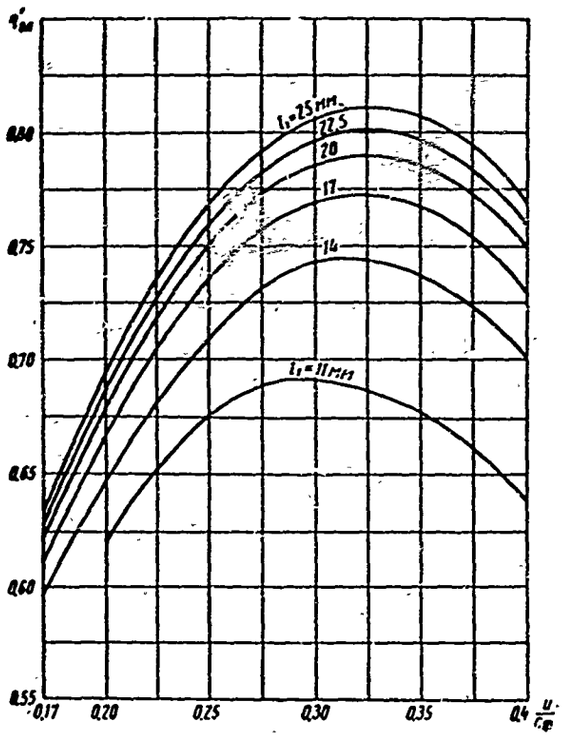

Fig. 302. Primary efficiency $\eta'_{ол}$ of double-wheel velocity stages, depending upon $u/c_ф$ and different nozzle cascade heights l_1.

can change; then corrections should be introduced.

The correction $k_{мер}$ is introduced for meridional profiling of the nozzles. It is assumed that the meridional configuration is executed according to the MEI method and the recommendations given above. When introducing meridional profiling, one should certainly consider the shift of the minimum section into the region of the cross section and, as a result of this, the certain increase of the outlet area of the nozzle cascade (see p. 111).

The correction for meridional profiling $k_{мер}$ is shown in Fig. 294; in this case, $k_{мер}^{double\text{-}wheel} = 0.9k_{мер}^{single\text{-}wheel}$. (For cascades of group "K" the upper curve should be used.)

Figure 303 gives the correction for the stage diameter, $k_д$, depending upon height l_1. Here the dotted line indicates the curves of $k_д$ for ganged nozzles with straight bounding walls.

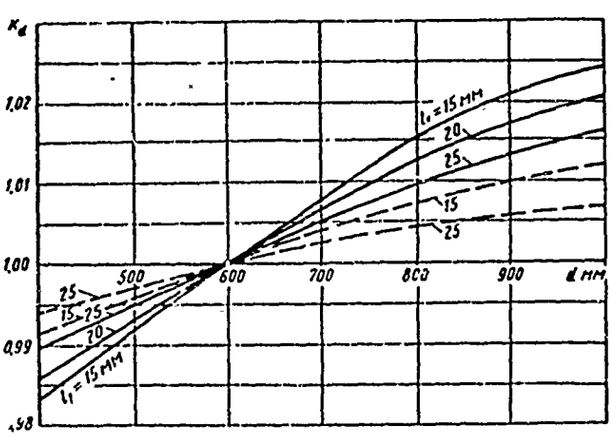

Fig. 303. Correction for diameter $k_д$ (for calculating the efficiency of a double-wheel velocity stage). Curves: —— (solid) – for nozzle cascades with cylindrical bounding walls; – – – (dotted) – for ganged nozzles with straight bounding walls.

The correction for profile chord, k_b, is found as the product of the corrections referred to all cascades:

$$k_b = k_{b1}k_{b1p}k_{b2}k_{b2p},$$

each of which depends upon the magnitude of chord of the given cascade and the height of the nozzle cascade l_1 according to Fig. 304. For meridional profiling, within

the limits of the chord value,

$$7\sqrt{l_1} < b_1 < 15\sqrt{l_1} \; (l_1 \text{ in mm})$$

the correction $kb_1 = 1$.

The correction for thickness of the trailing edge of the profile, which is shown in Fig. 304, is found in a similar manner.

$$k_{\Delta_{кр}} = k_{\Delta^c_{кр}} k_{\Delta^p_{кр}} k_{\Delta^к_{кр}}.$$

Inasmuch as each of the recommended velocity-stage combinations is designed for a definite pressure ratio, $\varepsilon_{расч}$, a noticeable deviation from $\varepsilon_{расч}$ brings about a corresponding change of stage efficiency; therefore, Fig. 305 represents a graph for the correction factor k_ε.

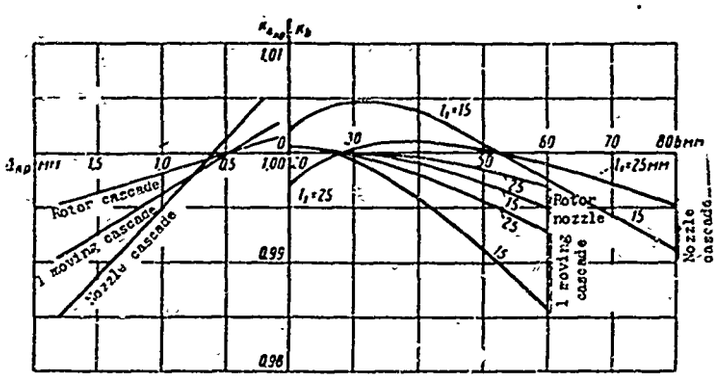

Fig. 304. Corrections for cascade chord k_b and thickness of trailing edge of profile $k_{\Delta_{кр}}$.

For deviation of the open axial and radial shroud clearances, one should introduce a correction that considers the change of parasitic leakages. Since the influence of leakages over the blades of the second wheel is small, and upon observance of one of the requirements — minimum open clearance to 2 mm or radial seal with clearance to 1 mm — the stage efficiency practically does not change, the influence of leakages only past the first moving and rotor cascades is considered:

$$k_y = k_{y1} k_{yn}.$$

For determination of the coefficient $k_{y\,1}$, in Fig. 306 we preliminarily find the auxiliary quantity Λ, which is connected with the reaction of the stage at the tip. Depending upon the sign of Λ, a further determination of $k_{y\,1}$ is performed by means of Fig. 307 or 308.

The coefficient $k_{y\,1}$ is found in Fig. 307 for leakage, and in Fig. 308 for suction, depending upon the equivalent clearance:

$$\delta_{экв} = \frac{1}{\sqrt{4/\delta_a^2 + 1{,}5\,z/\delta_r^2}},$$

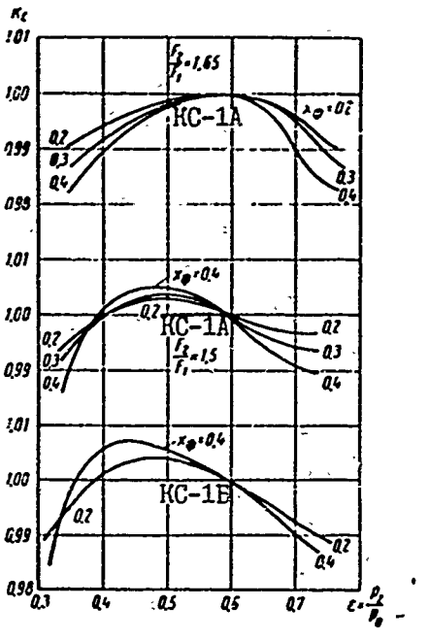

Fig. 305. Correction for pressure ratio k_ε.

(where δ_a is the open axial clearance; δ_p is the radial shroud clearance; z is the number of sealing bands above the shroud), and also depending upon the height of the nozzle cascade l_1.

If the nozzle cascade has single meridional profiling, the value of $A_м = A - 2$, should be used, where A is found by means of the nomograph in Fig. 306. For milled and ganged nozzles without meridional profiling, but with straight bonding walls,

$$A_{фр} = A - 1.$$

The loss due to leakage past the rotor blades is considered by the coefficient $k_{y_п}$, which is found by the following formula:

$$k_{y_п} = 1{,}003 - 0{,}003\,\delta_{уп}\,(\delta \text{ in mm}).$$

For leakage or suction in the root clearance between the nozzle and first moving cascades we calculate the correction $k_{yк}$. First, according to the leakage balance, we determine the direction of flow in this clearance. If leakage takes place, the correction factor is found by the following formula:

$$k_{yк} = 1 - 0{,}7\,G_к/G,$$

where $G_к$ is the amount of leakage through the root clearance;

G is the total flow rate through the stage.

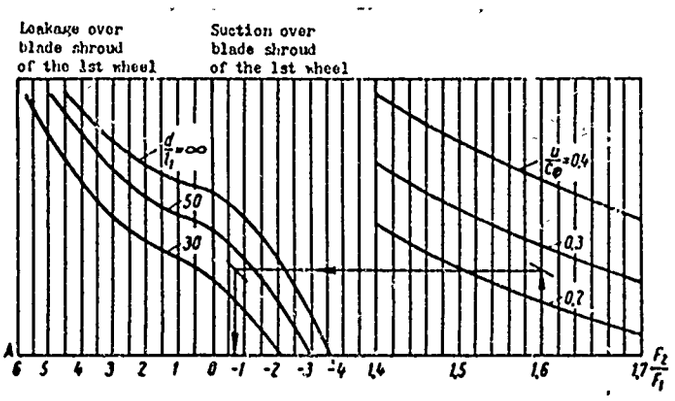

Fig. 306. Auxiliary graph for determining corrections for steam leakage or suction over the shroud of the 1st wheel.

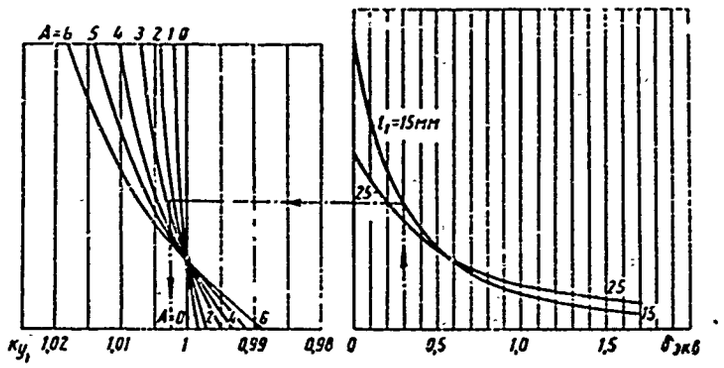

Fig. 307. Correction for steam leakage over blade shroud of 1st wheel.

In the case of suction, for want of special experiments with velocity stages, it is necessary to use an analogous graph, which was obtained for a single-wheel stage and is shown in Fig. 299.

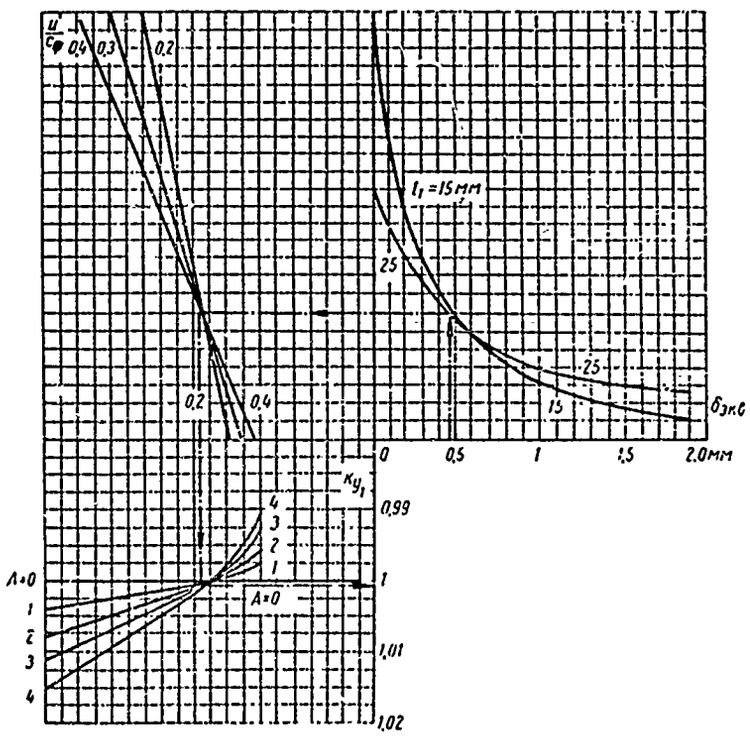

Fig. 308. Correction for steam suction over blade shroud of 1st wheel.

The root reaction ρ_K, which is necessary for calculation of G_K, can be estimated by the following formula:

$$\varrho_K = \varrho_{cp} - \chi \frac{2}{2+0}.$$

Here $\chi = 1$ is for conventional blading; $\chi = 0.5$ is for single meridional profiling; $\chi = 0.75$ is for ganged and milled nozzles with straight bounding walls, $\theta = d/l_1$.

Then, taking all corrections into account, the relative blade efficiency of the stage with complete loss of the kinetic energy of the outlet velocity is calculated by means of formula (331).

For a determination of the relative internal efficiency, which includes all losses in a velocity stage with full input, it is necessary to consider the losses due to disk and shroud friction:

$$\eta_{oi} = \eta_{oa} - \zeta_{тр}.$$

These losses are calculated according to the data in § 12.

For a partial stage, one should use the materials in § 30, which make it possible to select optimum stage characteristics. The additional losses connected with partial input are calculated according to the data in § 29.

§ 49. MODEL STAGES WITH VARIABLE BLADING

For small d/l ratios, cylindrical blading cannot ensure a high stage efficiency; therefore, variable blading is employed. In practice, it is frequently necessary to reject cylindrical blading when $d/l < 10$-6. For stages where the velocities no not exceed critical in none of the sections of both the nozzle and moving cascades, it is possible to employ combinations that have been tried out beforehand and are suitable for use in a wide range of variation of geometric characteristics. For stages where in separate sections there appear high supersonic velocities, it is difficult to provide universal combinations, and here, as a rule, it is necessary to use the recommendations made in Chapter VIII.

We shall consider the recommended combinations, their calculation, and graphs for determining their economy.

Stages with a Cylindrical Nozzle Cascade and Variable Rotor Blade (see Chapter VII)

These stages can perform quite effectively when $d/l > 5$; in an extreme case, the velocities should not essentially exceed the critical values (to $M_{1t} < 1.1$).

However, with a certain lowering of economy, it is permissible to employ such stages to $d/l \approx 4$. These stages have MEI nozzle cascades: TC-1A, TC-2A, and TC-3A.

If angles* $\alpha_{1\,K}$ and relative pitch $\bar{t}_K$ are in the root section of the nozzle cascade, then in the current section it is possible to approximately consider that

$$\alpha_1 = \operatorname{arc\,tg}\left(\frac{r}{r_K}\operatorname{tg}\alpha_{1K}\right);$$
$$\bar{t} = \frac{r}{r_K}\bar{t}_K.$$

and in the middle section

$$\alpha_{1cp} = \operatorname{arc\,tg}\left(\frac{\theta}{\theta-1}\operatorname{tg}\alpha_{1K}\right);$$
$$\bar{t}_{cp} = \frac{\theta}{\theta-1}\bar{t}_K.$$

where $\theta = d_1/l_1$.

The twisted rotor blade is formed from standard profiles.

In this case the considered combinations will have the designations K3-1-A, K3-2-A, and K3-3-A.

The stages were designed under the following conditions:

1. The conditions of entrance to the moving cascade were determined by the simplified equation of radial equilibrium in the interblade clearance.

2. The ratio areas of the moving and nozzle cascades ensures a positive reaction in the root section at $\varepsilon = \frac{p_2}{p_0} \leq 0.75$ and $u_K/c_{\Phi} \geq 0.45$, i.e., when $(u/c_{\Phi})_{cp} \geq$ $\geq 0.45\frac{\theta}{\theta-1}$.

3. Approximate constancy of the flow rate between similar sections (streams) of the nozzle and moving cascades.

The flow area of stages K3-1-A, K3-2-A, and K3-1-A is shown in Fig. 309.

The results of the calculation of stages of group K3 are given on the graphs in Figs. 310-315. These graphs were constructed in the following way. The reaction was determined by the following formula:

$$\frac{1-\varrho}{1-\varrho_K} = \exp\left(-\int_{r_K}^{r}\frac{2\varphi^2\cos^2\alpha_1}{r}dr\right).$$

For the calculation of ρ and F_2/F_1 we used velocity and flow rate coefficients with a variable value of height.

---

*Here and subsequently in the calculations for subsonic velocities, α_1 and β_2 imply the effective angles.

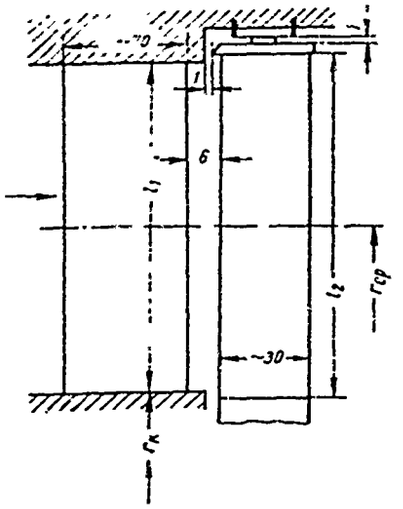

Fig. 309. Flow area of model stages having cylindrical nozzle and helical moving cascade.

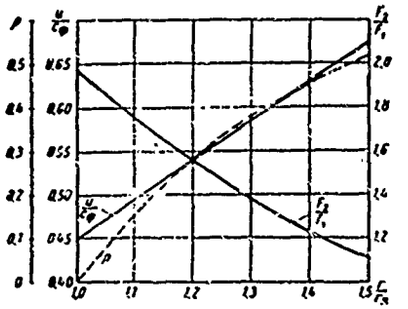

Fig. 310. Characteristics of stage K3-1A (ρ, u/c_Φ, and F_2/F_1) depending upon relative radius r/r_K.

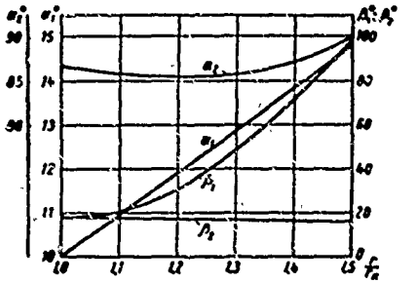

Fig. 311. Dependence of flow angles of stage K3-1A (α_1, β_1, and α_2, β_2) on relative radius r/r_K.

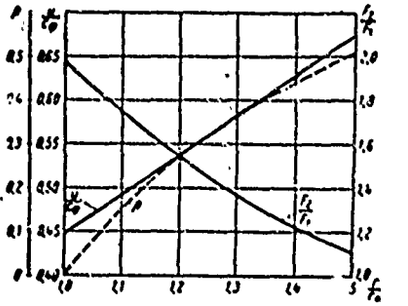

Fig. 312. Dependence of characteristics of stage K3-2A (ρ, u/c_Φ, and F_2/F_1) on relative radius r/r_K.

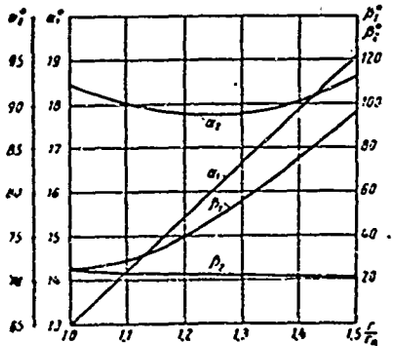

Fig. 313. Dependence of flow angles in stage K3-2A (α_1, β_1, and α_2, β_2) on relative radius r/r_K.

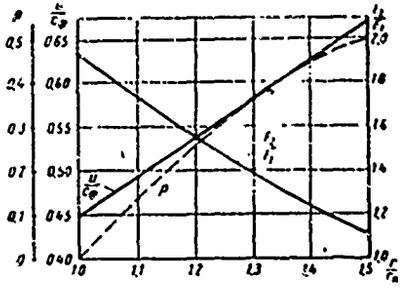

Fig. 314. Dependence of characteristics of stage K3-3A (F_2/F_1, u/c_Φ, and ρ) on relative radius r/r_K.

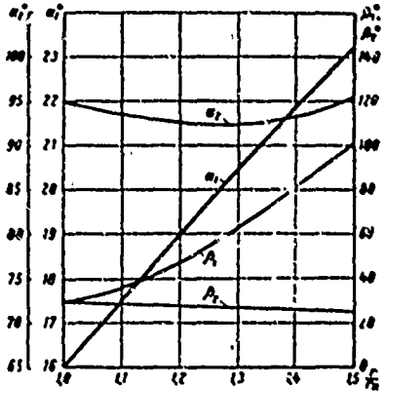

Fig. 315. Dependence of flow angles in stage K3-3A (α_1, β_1, and α_2, β_2) on relative radius r/r_K.

The dependence $F_2/F_1 = f(r/r_K)$, which is represented in these graphs, characterizes the ratio of areas of the elementary sections. If it is necessary to determine the F_2/F_1 ratio of the entire stage, the calculations should be performed by means of the following formula:

$$(F_2/F_1)_{cm} = \frac{\int_{r_K}^{r_R} (F_2/F_1)\, dr}{r_R - r_K}.$$

The results of the given calculation are shown in the graphs of Figs. 310, 312, and 314. The dependences of angles α_1, β_1, β_2, and α_2 for all these combinations are shown on the graphs of Figs. 311, 313, and 315. For performing the calculations of angles β_2 it was assumed that $l_2/l_1 = 1.06$.

The results of the calculation show that only at the tip of the nozzle cascades with the maximum ratio for these stages, $d/l \approx 5$, angle α_1 somewhat exceeds the optimum values obtained in static tests. Inasmuch as practically along the entire height it is possible to ensure optimum values of relative pitch, it is obvious that the flow around the entire cascade will occur with small profile losses.

The calculated angle β_1 corresponds to optimum conditions of entrance to the moving cascade and in the direction towards the blade tip it increases at $\theta = 5$ to $\beta_1 \approx 90^\circ$.

Angle β_2 changes very little, and decreases from root to tip. In the root section, at zero reaction $\rho_K = 0$, angles β_1 and β_2 will be practically equal.

During the designing, a large value was given to the observance of an approximately axial outlet along the entire height of the stage. As can be seen from the graphs, in all three combinations the deviations of angle α_2 from 90° in an extreme case does not exceed 5°. The change of angle α_2 with respect to height and, in particular, the certain increase of it at the root, is connected with the larger losses in the root sections.

The axial outlet shows that there is no swirling of the flow behind the stage, and it permits a better use of the outlet energy in the next stage.

Everything said above permits us to make a conclusion concerning the high economy of the developed combinations, which (within limits to $\theta \geq 5$) almost does not depend on d/l.

The calculated graphs of Figs. 310-315 were constructed for a stage pressure

ratio of $\varepsilon \simeq 0.75$ and $(u/c_{ф})_{к} = 0.45$.

For other values of ε and $u/c_{ф}$ there will be a different reaction and other angles β_1 and α_2.

Figure 316 shows the dependence of the root reaction on ε and $(u/c_{ф})_{к}$.

When $u/c_{ф}$ is not equal to the calculated value that is shown in Figs. 310, 312, 313, 314, and 315, the change of the mean reaction is found by means of formulas of variable conditions. It should be borne in mind that in formula (73) for the periphery when $\theta < 3$, the coefficient $A < 0$, and $(\rho_{п} - \rho_{к})$ in all cases decreases with the increase of $u/c_{ф}$.

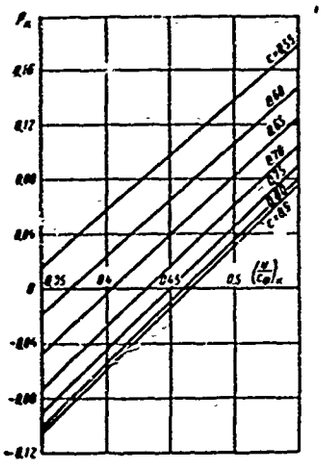

Fig. 316. Root reaction $\rho_{к}$ in type K3-A stages, depending upon $\varepsilon = p_2/p_0$ and $(u/c_{ф})_{u}$.

The flow rate can be determined in first approximation by means of the continuity equation for the mid-radius.

Detailed calculations show that for an incompressible fluid ($\varepsilon \to 1$), the flow rate determined for the middle section G_{cp} practically coincides with the flow rate determined for the sum of the flow rates of separate streams. It is true that this is valid only for a calculation that is performed as in this chapter, i.e., by means of the simplified equation of radial equilibrium and the hypothesis of coaxial cylindrical flow surfaces.

Furthermore, the certain decrease of the actual flow rate due to the lowered flow rate coefficients on the bounding walls of the channels is not considered. Disregard of this last factor gives an error of less than 1%, and it is usually permissible. If, as done for the construction of the calculated graphs of this paragraph, we take a somewhat decreased mean value of μ, the error will be insignificant.

With the increase of the heat drop of the stage, i.e., with the decrease of $\varepsilon = p_2/p_0$, the flow rate calculated for the middle section will be somewhat less than the flow rate obtained by integration with respect to the radius.

This deviation can always be taken into account by using the data for $\varepsilon = 0.55$ and $\theta = 5$, in which the integral flow rate will exceed the mean value by 4%; for the same value of ε and $\theta = 8$ this difference amounts to a total of 1%.

If the parameters and dimensions of the root section are given, for an approximate calculation of the flow rate it is possible to use the following formula:

$$G = \mu_1 \frac{2\pi \sin \alpha_{1\text{к}}^{*\phi} c_\phi}{v_{1\text{к}}} \Phi, \qquad (332)$$

where

$$\Phi = 2x^{2-n}(x-1)\frac{1}{\varepsilon}\left[1 - x^{-2n}(1-\varepsilon)\right], \quad x = \frac{r_{cp}}{r_\text{к}};$$
$$n = \varphi^2 \cos^2 \alpha_1.$$

Formula (332) is useful for $\varepsilon \geq \varepsilon_*$.

Figure 317 illustrates the dependence $\Phi = \Phi(r_{cp}/r_\text{к}, \varepsilon)$ for $n = 0.9$.

The efficiency of a model stage with complete loss of the outlet velocity is determined by means of generalized graphs. The relative efficiency of stage КЗ-1А, $\eta'_{\text{ол}} = f(u/c_\phi; l_1)$, is shown in Fig. 318. Here the stage dimensions are taken from Fig. 309, and the nozzle cascade is of type ТС-1А.

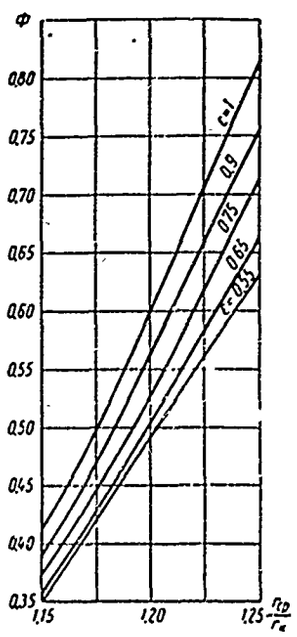

Fig. 317. Coefficient Φ for determining the flow rate through type КЗ-А stages (at $\rho_\text{к} \approx 0$).

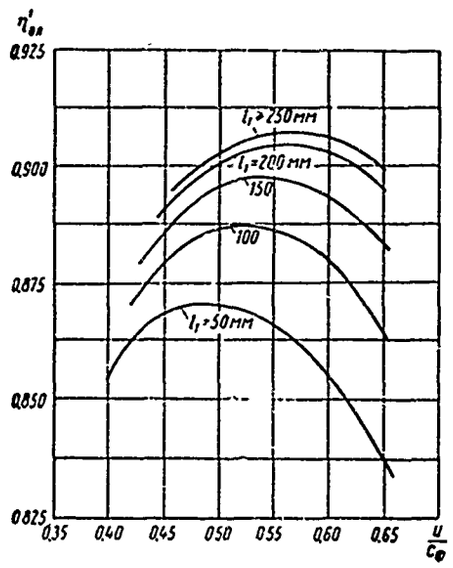

Fig. 318. Relative blade efficiency of stage КЗ-1А with cylindrical nozzle cascade and helical moving blades, depending upon u/c_ϕ and l_1; for the ratio $d/l = 8$, $l_2/l_1 = 1.06$, $\varepsilon = p_2/p_0 = 0.75$, and $Re_\phi = b_1 c_\phi/\nu_2 > 5 \cdot 10^5$.

We further introduce a series of corrections.

1. Calculation of the applied blading — coefficient $k_{\text{ст}}$. For a stage with a ТС-1А cascade, coefficient $k_{\text{ст}} = 1$, and for stages with ТС-2А and ТС-3А cascades, coefficient $k_{\text{ст}}$ is given in Fig. 319 depending on d/l_1.

A decrease in efficiency upon transition to stages No. 2 and No. 3 does not mean that these stages are less effective. Conversely, with the use of the outlet velocity, the most effective stage is No. 3, and the least economic is stage No. 1. A decrease of $\eta_{ол}$ upon transition to larger angles α_1 is connected with the corresponding increase of losses with the outlet velocity.

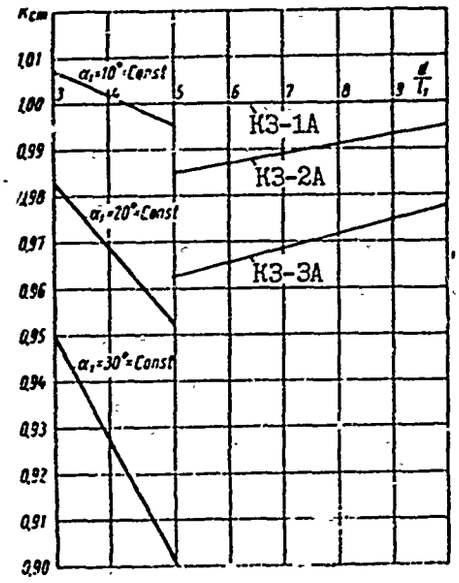

Fig. 319. Correction for calculation of relative blade efficiency of a stage (with complete loss of outlet velocity) $\eta_{ол}$ for various forms of blading.

2. The influence of d/l shows up on the stage efficiency in connection with the increase of ρ at the tip and the increase of leakages over the rotor blades. Furthermore, for small d/l, the nozzle cascade in the upper sections has angles α_1 and relative pitch $\bar{t}$ which go beyond the optimum zone; therefore, the correction factor $k_{d/l}$ is introduced.

With the decrease of d/l the mean reaction of the stage increases, and consequently, the optimum value of the velocity ratio $u/c_ф$ also increases. The dependence of $(u/c_ф)_{опт}$ on d/l_1 and l_1 is represented in Fig. 320. A graph of the correction $k_{d/l}$, depending upon $u/c_ф$, is given in Fig. 321, whereby in this case the base is $(u/c_ф)_{опт}$ for $\theta \geq 8$, which is represented on the graphs of Figs. 318 and 320. Here the height l_1 affects $(u/c_ф)_{опт}$ due to change of end losses and leakages. It should be borne in mind that with the decrease of d/l for the given geometric characteristics of the root section, the middle angle α_1 increases, which leads to an increase of outlet losses and to a decrease of $\eta_{ол}$, correspondingly.

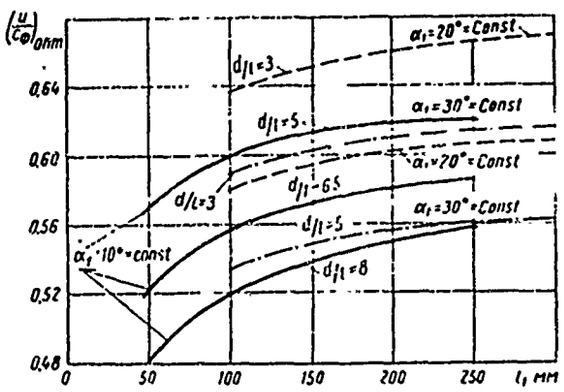

Fig. 320. Optimum velocity ratio (for $\eta_{ол}$ – efficiency with complete loss of outlet velocity) depending upon the ratio d/l_1 and l_1 (for $\rho_к \approx 0$-0.05).

3. The correction factor k_ε for the pressure ratio, $\varepsilon = p_2/p_0$, is found from Fig. 322.

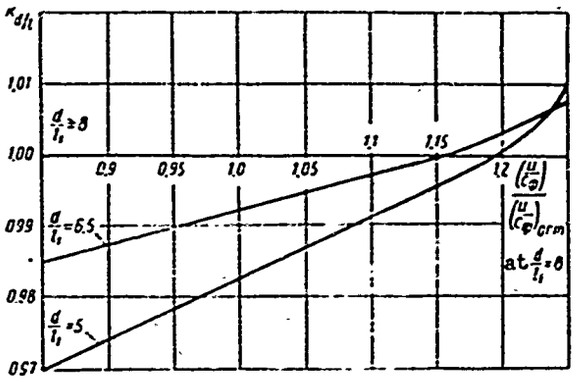

Fig. 321. Correction $k_{d/l}$ (with complete loss of outlet velocity) depending upon d/l_1 and the change of the u/c_{Φ} ratios to $(u/c_{\Phi})_{опт}$ at $d/l_1 = 8$.

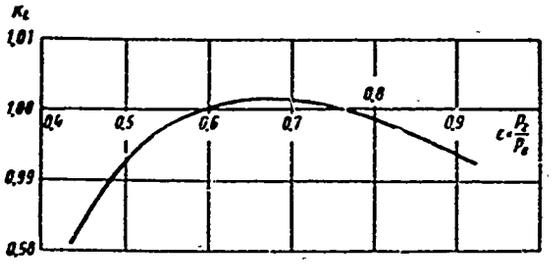

Fig. 322. Correction factor k_ε that considers the influence of pressure ratio $\varepsilon = p_2/p_0$ on efficiency $\eta_{ол}$ (at $\rho_к \approx 0$) and $(u/c_{\Phi})_{опт}$.

4. The correction factor k_{Re}, which considers the influence of the fictitious Reynolds number, $Re_{\Phi} = b_1 c_{\Phi}/\nu_2$, is shown in Fig. 295.

5. The correction for leakage over the rotor blades is introduced by the coefficient k_y; for the case of a shrouded moving cascade, the correction is found on the graphs of Figs. 291-300, and for unshrouded rotor blades, in Fig. 323.

For simplification of the calculation we do not introduce corrections for suction (or leakage) in the root clearance (which is found on the graphs of Figs. 293-300), for the change of chords and trailing edges determined by the data in Chapter IV, and others. Furthermore, the interdependence of a number of corrections is not considered here. As a result, the relative blade efficiency of a stage with complete loss of kinetic energy of the outlet velocity, $\eta_{ол}$, is found as the product

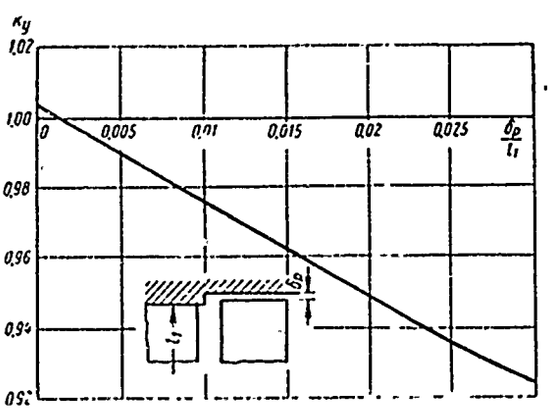

Fig. 323. Correction for leakage k_y depending upon δ_r/l_1 for an unshrouded stage (at $\rho_к \approx 0$ and $(u/c_{\Phi})_{опт}$.

$$\eta_{ол} = \eta'_{ол} k_{cm} k_{d/l} k_\varepsilon k_{Re} k_y.$$

It should be noted that the efficiency calculated in this way gives the mean value, since in reality the efficiency depends on such unaccounted for factors as the meridional configuration, the quality and technology of manufacture, etc.

Construction of the economy graphs in the given paragraph was based on the

experimental and theoretical works of a number of organizations and on literary sources.

Example of the selection and calculation of a model stage.

We shall calculate an intermediate-pressure stage of a large steam turbine.

The stagnation pressure before the stage is $p_0 = 5.85$ bar, the pressure behind the stage is $p_2 = 4.36$ bar, and the specific volume of steam behind the stage (for an isentropic process of expansion) is $v_{2t} = 0.465$ m^3/kg. The steam flow rate is $G = 138.7$ kg/sec; $n = 3000$ rpm. The stage is one of the stages of a group, where the combination K3-2A is selected with $\alpha_{1\,K} = 13^\circ$ and $d_K = 1.010$ m.

We find the ratio $r_П/r_K$ by the following formula:

$$G = \mu_1 \frac{2\pi \sin \alpha_{1K} c_\Phi}{v_{1K}} r_K^2 \Phi$$

for

$$\varepsilon = \frac{p_2}{p_0} = 0.744; \quad \left(\frac{u}{c_\Phi}\right)_K = 0.15.$$

According to Fig. 316, $\rho_K \approx 0$. Consequently, $v_{1\,K} \approx v_2$.

By means of the formula for G, assuming that $\mu_1 = 0.97$, we find $\Phi = 0.522$, and according to Fig. 317 we determine $r_{cp}/r_K = 1.2$. Consequently, $d/l_1 = 6$, $d_{cp} = 1.212$ m, and $l_1 = 202$ mm.

From Fig. 313 we determine the basic characteristics of the stage.

For r_K $\varrho = 0$; $\alpha_1 = 13°$; $\beta_1 = 25°$; $\beta_2 = 25°$; $\alpha_2 = 92{,}5°$;

for r_{cp} $\varrho = 0{,}27$; $\alpha_1 = 15{,}4°$; $\beta_1 = 40°$; $\beta_2 = 23°$; $\alpha_2 = 89°$;

for r_n $\varrho = 0{,}44$; $\alpha_1 = 17{,}9°$; $\beta_1 = 75°$; $\beta_2 = 21°\,5'$; $\alpha_2 = 90{,}5°$.

We shall determine the economy of the stage.

Knowing $l_1 = 202$ mm and $(u/c_\Phi)_{cp}$, from Fig. 318 we first find $\eta'_{OЛ} = 0.905$.

Inasmuch as the stage K3-2A is applied, from Fig. 319 for $\theta = 6$ we find $k_{CT} = 0.987$.

The optimum ratio $(u/c_\Phi)_{OПТ}$ for $\theta = 8$ and $l_1 = 202$ mm, according to Fig. 320, amounts to $(u/c_\Phi)_{OПТ} = 0.55$.

Then for $\dfrac{u/c_\Phi}{(u/c_\Phi)_{OПТ}} = 0.985$ and $\theta = 6$, from Fig. 321, the correction $k_{d/l} = 0.988$, the correction $k_\varepsilon = 1$, and also $k_{Re} = 1$.

We find the correction for leakage over the shroud:

On the basis of design considerations, we assume that $\delta_a = 3$ mm, $\delta_p = 2$ mm, and $z_y = 2$. Then

$$\delta_{экв} = \frac{1}{\sqrt{\frac{4}{3^2} + \frac{1.5 \cdot 2}{2^2}}} = 1.1 \text{ мм}.$$

For $\left(\frac{F_2}{F_1}\right)_{cp} = 1.55$ (Fig. 312) and $u/c_ф = 0.541$ and $\theta = 6$ (Fig. 297), we find A = = 6.5, and for $(k_y - 1)l_1 = -0.45$ mm (Fig. 298a). Then $k_y \approx 1$.

Thus:

$$\eta_{oл} = \eta^*_{oл} k_{cm} k_{d/l} k_z k_{ke} k_y = 0.905 \cdot 0.987 \cdot 0.988 \cdot 1 \cdot 1 \cdot 1 = 0.883.$$

If necessary, one should consider the losses due to friction of the disk and shroud, the leakage through the diaphragm seals, the leakage or suction in the root clearance, and also the change in efficiency caused by other dimensions of the chords, edges, meridional contour of the flow area, wire connections, etc.

If the given stage is an intermediate one, it is possible to calculate efficiency with the use of the outlet velocity taken into account. For this we find the velocity w_2, using the continuity equation

$$w_2 \approx \frac{Gv_2}{F_2} = 182 \text{ m/sec},$$

where

$$F_2 = \pi d_{cp} \cdot l_1 \cdot l_2 / l_1 \sin \beta_{2cp}.$$

Inasmuch as $\alpha_2 \approx 90^\circ$, $c_2 = c_{2a} = w_2 \sin \beta_2 = 71$ m/sec.

We shall obtain the efficiency with the use of the outlet velocity:

$$\eta^*_{oл} = \eta_{oл} \Big/ \left(1 - \frac{h_{вс}}{h_0}\right) = 0.920.$$

It should be noted that the obtained value of $\eta^*_{oл}$ is not the maximum accessible one, since the economy graphs were constructed with a reserve that considers the actual conditions of manufacture and assembly of the blades.

Stages with Constant Angle α_1

Stages with constant angle α_1 require twisting of the nozzle cascade, i.e., nozzle blades of variable profile. The condition of α_1 = const may be ensured by

various methods of profiling; however, as a rule, it is preferable that all sections have the same profile and the same cascade, differing only by their absolute dimensions. For this it is necessary that the profile chord, and consequently, also all the remaining dimensions, be increased from root to tip in proportion to the radius. This method of nozzle blade profiling makes it possible to have a constant optimum value of relative pitch in all sections, i.e., the main advantage of a stage with α_1 = const, as compared to a stage having constant profiles of the nozzle blade.

Another advantage of a cascade with α_1 = const and $\bar{t}$ = const is the possibility of using cascades that have been tried out in static conditions in all sections.

For creation of a stage with α_1 = const and $\bar{t}$ = const, any nozzle cascade can be used. This chapter presents calculations of a stage with three nozzle cascades: $\alpha_1 = 10^\circ$, $\alpha_1 = 20^\circ$, and $\alpha_1 = 30^\circ$. The cascade with $\alpha_1 = 10^\circ$ can be recommended only in exceptional cases, since small angles α_1 are not only unfavorable for the nozzle cascade itself, but also lead to very small angles β_2. The moving cascade of such a stage should have a very large deflection of flow in the root section and unfavorable characteristics in the upper section (thus, for $\theta = 3$, $\beta_2 = 9^\circ$ in the upper section).

It follows from this that detailed calculations are conducted for cases only at $\alpha_1 = 20^\circ$ and $\alpha_1 = 30^\circ$. The results of these calculations are represented in Fig. 324.

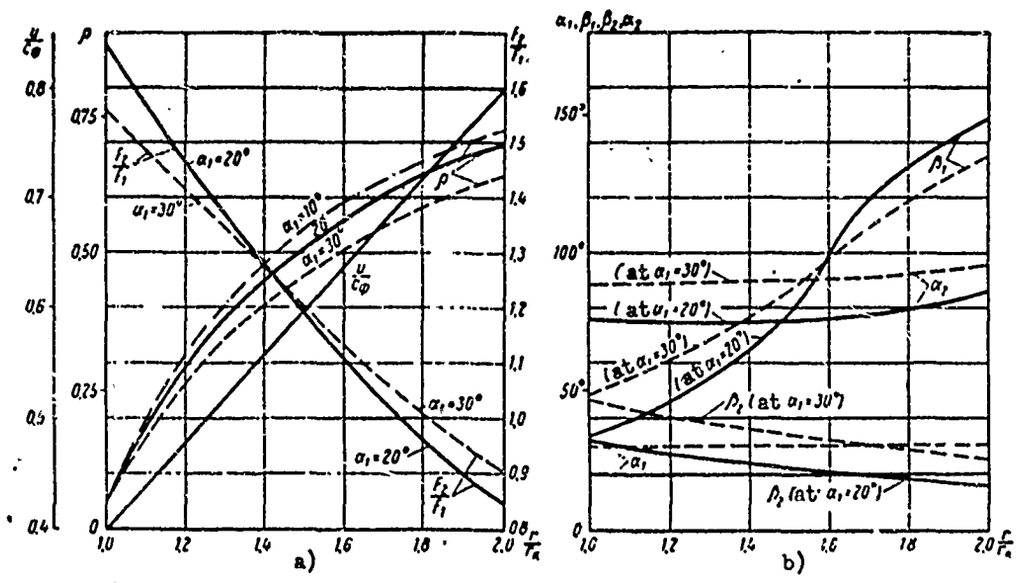

Fig. 324. Behavior of a stage with α_1 = const, depending upon relative radius: a) velocity ratio u/c_ϕ, area ratio F_2/F_1, and reaction ρ; b) angles of flow α_1, β_1, α_2, and β_2.

The principle of the calculation of stages with α_1 = const is the same as for stages with cylindrical nozzle blades.

The stages were calculated for up to $\theta = 3$. Calculation data of the stage: pressure ratio $\varepsilon = p_2/p_0 = 0.65$; $(u/c_ф)_к = 0.4$; $\rho_к = 0.05$. Conversion to other conditions is performed just as for stages with cylindrical nozzle blades.

The reaction of the stage is calculated by the following formula:

$$1 - \varrho = (1 - \varrho_к)(r/r_к)^{-2\varphi^2 \cos^2 \alpha_1}.$$

Although the stage calculation assumed different values of φ with respect to blade height, the reaction can be determined by using the averaged value of φ.

With regard to design characteristics, both stages have $\beta_1 > \beta_2$ and angle α_2 in the root section, and the blades are almost constantly straight along the entire height.

For an estimate of the economy of stages with α_1 = const it is possible to use the graphs in Figs. 318 and 322. For the transition from Fig. 318 to stages with α_1 = const, curves are constructed in Fig. 319. These curves consider the magnitude of losses with the outlet velocity, which depends on α_1 and $\rho_{ср}$, and also the decrease of the profile and end losses upon transition to a larger angle α_1.

The selection of optimum $(u/c_ф)_{опт}$ can be performed by using the curves on Fig. 320. It should be taken into account that for the given $(u/c_ф)_{опт}$ the stage will have the highest efficiency with a complete loss of the outlet velocity. If the outlet velocity is used in the following stage or in a specially installed diffuser, the magnitude of the optimum velocity ratio increases, especially at large angles α_1. However, the curve of the dependence $\eta^*_{ол} = f(u/c_ф)$ is very linear in a wide range of variation of $u/c_ф$.

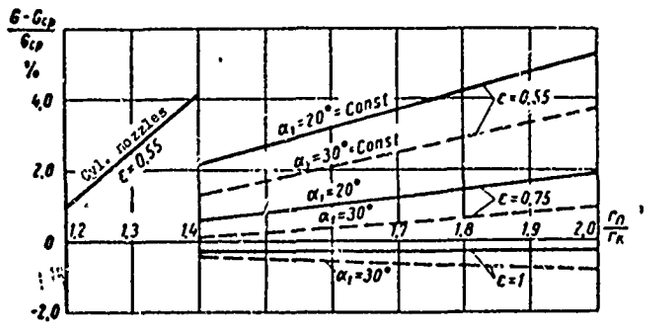

Fig. 325. Flow rate through stage, as compared to the flow rate calculated for the middle section for stages with α_1 = const.

The steam (gas) flow through the stage can be calculated for the middle section with high accuracy. If it is necessary to find a more accurate value of the flow rate, the curves in Fig. 325 should be used; they were obtained by integration of the flow rate with respect to the radius. As can be seen from the graph, the biggest error

at $\alpha_1 = 20^\circ$, $\varepsilon = 0.55$, and $r_\Pi/r_K = 2$ ($\theta = 3$) amounts to a total of 5.2%. However, it should be stressed that this pertains only to a stage that is calculated by means of the simplified equation of radial equilibrium with coaxial cylindrical flow surfaces. For the changes of the flow rate for an actual three-dimensional flow, see § 45.

CHAPTER X

INFLUENCE OF MOISTURE ON THE CHARACTERISTICS OF TURBINE STAGES

§ 50. SOME PROPERTIES OF THE FLOW OF MOIST STEAM IN THE FLOW AREA OF A STAGE

As it is known, moisture has a negative effect on the performance of a turbine stage; it causes a lowering of efficiency and erosion of the blading. Additional losses of energy in a stage that is operating with moist steam appear due to:

a) the shock braking influence of water drops on the rotor blades;

b) the decrease of the mass of steam (due to condensation) which develops effective performance on the wheel;

c) the change in shape of the nozzle and rotor blades under the influence of erosion, i.e., mechanical destruction of the blades;

d) the appearance of condensing (thermal) shocks which provoke additional wave losses ("irreversibility" losses of the process);

e) the redistribution of parameters (velocities, pressures, and others) in the vane channels in the clearance and behind the stage, as compared to the calculation for dry steam;

f) the different direction of the velocity vectors of the water and steam in absolute and relative motion, which leads to swirling of the main flow;

g) the expenditure of part of the steam energy for acceleration of water drops, whose velocity, as a rule, is less than the steam velocity.

The difficulties of investigating the enumerated factors are caused by the fact that during motion of moist steam with high velocities, the steam is supercooled, the dispersive ability of the moisture changes, the thermodynamic interaction of steam and moisture and nonuniformity of the distribution of moisture is observed in the

section of the flow, which is increased by the various degrees of dispersion.

Such an analysis should be based essentially on the results of a detailed investigation of the thermo- and gas-dynamic regularities of flow of moist steam, which are nonexistant at the present time. Corresponding experimental investigations are hampered by the absence of reliable meters of local moisture and other measuring equipment, and also the procedure employed in the experiments.

Below we shall consider some theoretical results that are based on simplified flow diagrams of moist steam, and the results of an experimental investigation of the elements of a flow area and turbine stages which were obtained in a number of laboratories.

The elimination of moisture in a flow of partially condensed steam can occur in two ways:

a) as a result of continuous and uniform condensation of steam due to a constant increase of the dimensions of the drops;

b) due to condensing shocks.

Both mechanisms of condensation are carried out depending upon moisture, velocity, (M number), and velocity gradient along the flow.

In a sufficiently prolonged process (low speeds and velocity gradients) we find the first, and in a short process, chiefly the second form of condensation. As experiments show, both forms of condensation can exist jointly at high velocities.

The formation of drops in the flow, their development, and intensification is a complicated thermo- and gas-dynamic process which has been little studied up to now. The kinetics of the phase transitions in a steam flow in the minimum necessary volume is not considered, which naturally hampers an analysis of the basic properties of the flow of moist steam in the flow area of a turbine.

The essential features of the process of condensation in moving steam* are:

1) supercooling of steam, which is expressed in the fact that its temperature in the process of expansion (acceleration) from the saturation state or slight overheating, and also at the initial moisture content, attains values that are lower than the saturation temperature which corresponds to the pressure at the end of expansion;

2) Polydispersity of the liquid phase after the beginning condensation, which

*In a metastable system.

can exist in the form of small and large drops, and also in the form of a film on the channel boundaries.

Let us first consider the motion of moist steam in a turbine stage with a small degree of moisture content, assuming that steam expansion starts in a zone of slight overheating near the upper boundary curve. The process of expansion for this case is depicted in Fig. 326. The stage of absolute stagnation before the nozzle cascade is depicted by point 0; the process of actual expansion in a nozzle cascade corresponds to line 0-1, and in a moving cascade, line 1-2. The stagnation parameters in relative motion at the entrance to the moving cascade can be found at point 0'.

The actual picture of expansion in a stage essentially differs from that depicted in Fig. 326. The steam, expanding in the nozzle cascade, intersects the boundary curve without condensation, since a drop in the steam volume cannot appear without an essential disturbance of the equilibrium between the liquid and vapor phases. Consequently, the steam will be supercooled at the nozzle cascade exit. The magnitude of supercooling, $\Delta T = T_H - T$ (T_H is the saturation temperature at the given pressure p_1, T is the actual temperature behind the nozzle cascade), depends on a large number of factors. Theoretical analysis and experimental data show that ΔT can be determined by the following formula:

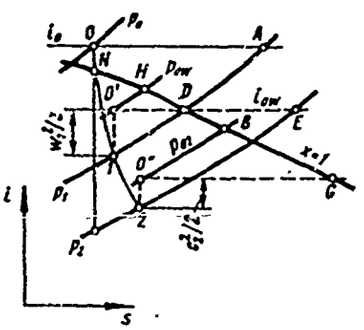

Fig. 326. Thermal process of a turbine stage in an i-s diagram with steam expansion from a region of slight overheating.

$$(\Delta T)^4 = \frac{K}{\tau}, \qquad (333)$$

where τ is the time necessary for passage of a vapor particle from the saturation state (see point N on Fig. 326) to the beginning of condensation;

K is a constant that is equal to K = 9360 sec $(^\circ K)^4$ for air.

Figure 327 shows the dependence of ΔT on τ, which is calculated according to formula (333). Experimental points are plotted there for moist air; they were obtained by Wegener and Smelt.

It should be emphasized that τ depends on the flow rate and the longitudinal gradient of velocity (or pressure), i.e.,

$$\tau = \tau\left(c, \frac{dc}{dx}\right).$$

It is obvious that the magnitude of supercooling also depends on the velocity and the longitudinal velocity gradient. Consequently, from equation (333) we can disregard τ and express supercooling in the following manner:

$$\Delta T = \varphi\left(c, \frac{dc}{dx}\right).$$

The existence of the dependence of ΔT on the velocity gradient is confirmed by numerous experiments that reveal considerable supercooling of steam in nozzles. Experiments have established a connection between the steam rate and the rate of condensation and supercooling. It is obvious that the lower the rate of condensation as compared to the change of the flow rate, the greater the supercooling.

The theory of phase transitions considers processes of condensation that occur in a stationary medium. Let us consider certain relationships that characterize the condensation of stationary steam. In this case the magnitude of supercooling can be determined by Ya. I. Frenkel's formula [116]:

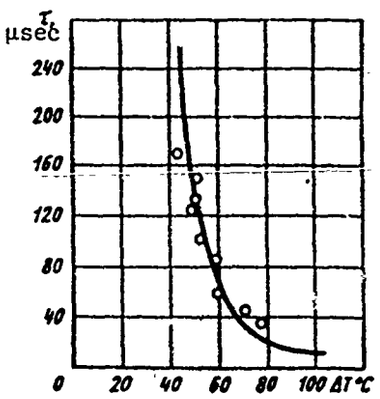

Fig. 327. Dependence of steam supercooling ΔT on expansion time in nozzle τ according to V. Kantorovich; experimental points were obtained by Wegener and Smelt.

$$\Delta T = \frac{4\sigma T_{\text{н}} v_{\text{м}}}{r d_{\text{к}}^*}, \qquad (334)$$

where σ is the surface tension; $v_{\text{м}}$ is the molecular volume of the liquid phase; r is the latent heat of vaporization; $d_{\text{к}}^*$ is the critical diameter of a droplet.

The quantity $d_{\text{к}}^*$ determines the size of these droplets, which are in thermodynamic equilibrium with the vapor phase. If $d_{\text{к}} < d_{\text{к}}^*$, the droplets will evaporate, since the vapor will not be saturated with respect to such small droplets. When $d_{\text{к}} > d_{\text{к}}^*$, the droplets will develop due to vapor condensation on their surfaces.

The critical diameter of a stably behaving (not evaporating) droplet is determined from the condition of equilibrium of the forces acting on the droplet (forces of static vapor pressure, gravitational forces, and forces of surface tension).

In accordance with L. I. Degtyarev's data [21], the critical diameter of a droplet will be:

$$d_{\text{к}}^* = \frac{4\sigma v'}{v' v'' (p'' - p_{\text{н}})},$$

where v' and v" are the specific volumes in the beginning and at the end of expansion;

p" and p_H are the pressures at the end of expansion and saturation.

Consequently, d_K^* depends on the pressure of the medium and the magnitude of supercooling. With the increase of pressure and the decrease of supercooling ΔT, d_K^* increases.

In the initial period of condensation, when the droplets have small dimensions ($d_K \geq d_K^*$), the relation between the length of the free path of the molecules and the droplet diameter has an important value [116]:

$$L/d_K = \frac{3\mu}{d_K p}\sqrt{\frac{\pi RT}{8}},$$

where L is the length of the free path; R is the gas constant; μ is the coefficient of dynamic viscosity.

When $L/d_K \gg 1$, the rate of condensation is determined by Ya. I. Frenkel's formula [116]:

$$V = \frac{z}{j}\left[\exp\left(-\frac{\pi\sigma d_K^{*2}}{3kT}\right)\right]\frac{d_K^{*2}p}{2kT}\sqrt{\frac{kT\ln p/p_H}{3m_z}}\,j. \qquad (335)$$

Here V is the number of droplets in a mass of vapor containing z molecules per unit time; j is the number of molecules in incipient form; m_z is the mass of a molecule; k is the Boltzmann constant; p_H is the saturation pressure.

It follows from formula (335) that the rate of condensation depends very strongly on the magnitude of supercooling; with the increase of ΔT, the rate V sharply increases.*

When considering the process of condensation in a vapor flow, it is necessary to consider the aerodynamic features of the flow spectrum. In the initial period of condensation, when the droplets have small dimensions (finely-dispersed moisture structure), the velocities of the vapor and the droplets are close. In this case the droplets are centers of condensation, which leads a gradual increase of their mass and dimensions.

The increase of the droplet diameter in this stage of condensation ($L/d_K \gg 1$)

---

*In connection with the difficulty of an exact determination of surface tension σ, the accuracy of formula (335) and the others is low.

can be determined by the following formula:*

$$\frac{d}{dt}(d_k) = \frac{c_p}{r}\frac{\varrho_n}{\varrho_e}\sqrt{\frac{RT}{2\pi}}\frac{T_k - T}{1 - \frac{4\sigma}{d_k \varrho_e r}} \tag{336}$$

or by Oswatitsch's formula for rarefied gases [149]:

$$\frac{d}{dt}(d_k) = \frac{3}{4}\cdot\frac{p}{r\varrho_e}\sqrt{3\frac{R}{T}}(T_k - T). \tag{337}$$

Here T_K is the surface temperature of a droplet.

Gradually, as the mass and dimensions increase, the droplets start to lag behind the vapor phase and are enveloped by the steam flow; therefore, the mechanism of condensation essentially changes. Further enlargement of separately considered droplets occurs under the influence of the peculiarities of the spectrum of the aerodynamic flow around the droplets.

The difference in the vapor and droplet velocities leads to a flow around the droplets, which are then deformed, taking on the shape of a streamlined body (body of minimum resistance).

Along the surface of a droplet there takes place a nonuniform distribution of velocities, pressures, and temperatures. On the lateral surface, where the pressure and temperature of the steam will be lower than in the main flow of steam due to the considerable local supercooling of the steam, there occurs additional condensation. Consequently, enlargement of a droplet occurs mainly due to local condensation on the lateral surface. On the front portion of the droplets, the pressure will be close to the stagnation pressure of relative motion. The average pressure inside a droplet can be higher than the pressure of the steam flowing around the droplet.

In the considered case, the condition of a stably behaving droplet (critical diameter d_K^*) is determined with the dynamic influence of the steam flow taken into account.

An increase of the dimensions of the droplets can occur due to different causes: a) due to the merging of small droplets during continuous condensation;

---

*I. I. Kirillov and R. M. Yablonik.

b) due to nonuniformity of the velocity and pressure fields; c) in connection with the geometric and aerodynamic peculiarities of the duct in which the two-phase liquid is moving. A well-known role is played in this process by supercooling. As a rule, all the enumerated factors act jointly.

The moisture droplets formed on the first stage have extremely small dimensions (fractions of a micron). The velocity of these particles is very close to the steam velocity. The wave length of any small disturbance in this uniform liquid-steam mixture should be considerably larger than the size of a droplet (diameter of suspended particles). Only in this case, in accordance with the data of L. D. Landau and E. M. Lifshitz, the velocity of small disturbances can be calculated by means of a Laplace equation.

Consequently, if

$$d_k \ll \Omega,$$

where Ω is the wave length of the disturbance, i.e., when

$$d_k \ll \frac{a}{\omega}$$

($\omega = a/\Omega$ is the frequency of the disturbance and a is the velocity of propagation of the disturbance), the determination of the velocity of small disturbances can be performed with the use of the Laplace equation:

$$a = \sqrt{\left(\frac{\partial p}{\partial \varrho}\right)_s},$$

which can be converted to the following form:

$$a = \sqrt{-v^2\left(\frac{\partial p}{\partial v}\right)_s}. \qquad (338)$$

Here v is the specific volume of steam; the subscript s indicates the isentropic character of the process of propagation of the disturbance; k is the index of the isentropic process, which is equal to

$$k = -\frac{v}{p}\left(\frac{\partial p}{\partial v}\right)_s. \qquad (339)$$

After substitution of (339) into equation (338), it is easy to obtain:

$$a = \sqrt{kpv}.$$

Thus, with the decrease of the frequency of disturbances, the permissible

diameter of a droplet in moist steam increases, at which equation (338) will ensure a satisfactory accuracy.

For various gas-dynamic calculations of flows of moist steam, it is necessary to know the velocity of sound and the index k. This problem was solved by a number of authors with the assumption of an equilibrium change of the stage of the moist steam. In particular, V. V. Sychev, for a determination of a and k in a two-phase region, obtained the following formulas:

$$a = v\frac{dp}{dT}\sqrt{\frac{T}{c_v'(1-x)+c_v''\cdot x}} \tag{340}$$

and

$$k = -\frac{v'(1-x)+v''x}{\left[p\left(\frac{\partial v}{\partial p}\right)_s'(1-x)+\left(\frac{\partial v}{\partial p}\right)_s''x\right]}. \tag{341}$$

Here v' and v" is the specific volume on the lower and upper boundary curves; x is the degree of dryness; c_v' and c_v'' are the heat capacities for constant volume on the boundary curves in the area of the two-phase region.

The derivatives $(\frac{\partial v}{\partial p})_s'$ and $(\frac{\partial v}{\partial p})_s''$, and also dp/dl, were calculated with high accuracy and presented in appropriate tables [92].

For simplification of the calculations, V. V. Sychev constructed a nomograph a (T, x) for steam, which is presented in the appendix.

Formulas (340) and (341), and also the indicated nomograph, give a satisfactory accuracy of calculation only when the two-phase medium is finely-dispersed and monodispersed, and contains very small droplets of approximately identical dimensions.

In reality, as shown earlier, the structure of the flow of moist steam can essentially differ from this ideal picture.

Let us assume that the change of the vapor state in the two-phase region will be quasi-static and equilibrium, i.e., the vapor state in each point of the process will correspond to the diagram parameters (in the i-s diagram).

In this case, with a low moisture content of the steam flow, the structure of the two-phase system is the simplest. The liquid phase exists mainly in the form of extremely small suspended particles. Under these conditions there cannot be large droplet and films. As a result, the actual enthalpy of the gas on a wall will

be equal to

$$i_{ocm} = i + r\frac{c^2}{2},$$

where $r = \sqrt[3]{Pr}$ is the recovery factor for a turbulent flow. Since $Pr \approx 1$ for steam, it is obvious that $i_{0CT} \approx i_0$, i.e., the enthalpy of the flow at the wall will be rather close to the enthalpy of absolute stagnation.

When considering Fig. 326, let us note that the line O-A, on the assumption of complete recovery of enthalpy in the boundary layer, characterizes the state of the steam on the surfaces of the nozzle channels.

Since, in relative inlet motion, point O' characterizes the state of absolute stagnation, under the same assumption concerning complete recovery of enthalpy in the boundary layer, the line O'DE depicts the change of the steam stage on the surfaces of a moving cascade. It is not difficult to see that moist steam flows over only an insignificant part of the blade surface (on section O'D). Consequently, with a small degree of moisture, the steam at the walls turns out to be overheated. The channel walls in this case do not play a role in the process of condensation.

As the moisture increases during vapor expansion in the flow area, conditions appear which favor the formation of enlarged droplets. The droplets will lag in their motion from the steam flow, which also promotes the formation of films.

Finely-dispersed moisture weakly affects the structure of the steam flow and, with the degree of moisture $\chi = 1 - x \leq 0.05$, it does not cause blade erosion. The effect of condensation can only show up in the reaction and the efficiency of a stage.

The process of increasing the dimensions of the droplets is connected with the peculiarities of motion in the flow area of the stage. During steam expansion in the nozzle cascade there occurs a concentration of moisture on the concave surface, which is caused by the curvature of the flow lines in the channel (Fig. 328a), i.e., by the influence of centrifugal forces on curvilinear trajectories. Due to ejection of droplets of moisture towards the concave surface, on it there occurs the primary concentration of droplets. Droplets can fall onto the back of a blade during secondary motion of steam and as a result reflection from the concave surface.

A further increase of the size of the droplets occurs on the rotor blades. Here the droplets, falling into the boundary layer, move under the influence of centrifugal

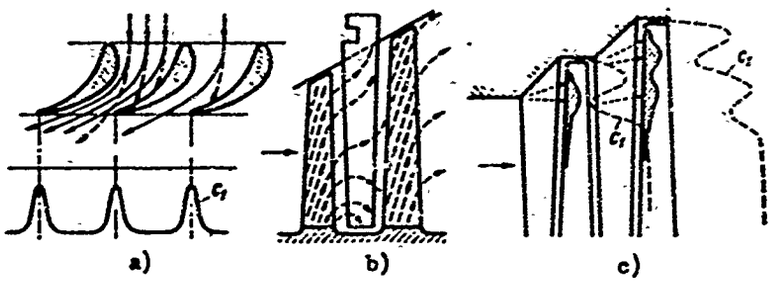

Fig. 328. Diagrams of the motion of moisture droplets in the flow area of a stage: a) motion of droplets in a nozzle cascade with velocity distribution behind the cascade; b) motion of liquid in boundary layers on blades; c) influence of secondary flows on erosional damages to blades.

forces in a radial direction and, merging with one other, are increased. It should be emphasized that the concentration of mo sture in the peripheral sections of a stage is explained not only by the swirling of the flow at the nozzle cascade outlet (in the clearance), but also by the influence of the centrifugal forces acting on the droplets that are moving in the boundary layer of the rotor blades.

The condition at which there occurs movement of particles in the boundary layer of the rotor blades in a direction to the periphery is given in reference [163]:

$$\frac{R}{d_K x_1^2}\frac{\rho_п}{\rho_в} > 1,$$

where $x_1 = u/c_1$; R is the radius of the location of the droplet; d_K is the diameter of the droplet; $\rho_п$ and $\rho_в$ is the vapor and water density.

This condition always is fulfilled for stages of steam turbines, since $R/d_K >> >> 1$.

A diagram of the motion of the droplets in a cross-sectional view is shown in Fig. 328b. The moisture droplets in the boundary layer of the rotor blades have large radial velocity components and move in a direction to the periphery; the droplets in the peripheral sections are ejected from the blades. Some of these droplets go into the main flow of steam and are pulverized under the action of the velocity head $(c_п^2-c_в^2)/2$. New formations of large droplets begin in the following nozzle cascade.

It should be emphasized that an especially intense accumulation of condensed steam on the nozzle blade occurs at the tip and in the root sections, in the zone of secondary flows (Fig. 328b). Numerous experiments confirm that precisely in these zones the erosional damages turn out to be maximum.

It follows from this that the process of increasing the dimensions of droplets

is essentially influenced by the structure of flow in the cascades, which is determined by the geometric parameters of the cascades (flare θ, angle of deflection of flow, shape of blades, shape of flow area in meridional plane, and also by the gas-dynamic and performance parameters (M and Reynolds numbers, inlet angle). It is necessary to consider the influence of the radial and transverse pressure gradients in the nozzle channels, which depend on the above-mentioned geometric and performance parameters. These gradients determine the flow in the boundary layers on the blades. Experiments confirm that an essential influence on the process of interaction of the droplets with the moving cascade is rendered by the size and shape of the edge wakes behind the nozzle blades, depending on the structure of the boundary layers on the trailing edge and its thickness. Large drops of water are concentrated in the edge wakes; the drops enter the rotor blade with maximum angles of incidence. If the axial clearance is increased, then, under the influence of the core of the flow, the moisture droplets in the edge wake will be accelerated and pulverized, which will have a favorable effect on the flow in the moving cascade and will decrease erosional wear. Enlarged axial clearances improve the separation of moisture from the stage.

Of interest is a rough estimate of the thickness of the film on the surfaces of the nozzle and moving channels. This estimate is given in W. Traupel's work [158]. It may be assumed that the film thickness is determined by the heat exchange between the film and the supercooled steam-water mixture in the core of the flow. On the basis of this assumption we determine the amount of heat given off by the film to the core of the flow, and consequently, the quantity of moisture precipitated on the wall. According to the author's data, the flow rate ratio of moisture in the film and the steam in the core of the flow amounts to $j = (0.25\text{-}0.5)\cdot 10^{-3}$; the quantity $\frac{j}{1-x}$, which characterizes the ratio of the flow rate of film moisture to the total flow rate of the liquid phase in the channel, amounts to ~2%. An estimate of the film dimensions at the trailing edges of the blades shows that its thickness lies within the limits of $\delta_B \approx (2 \text{ to } 4)\cdot 10^{-3}$ mm.

It should be emphasized that the thickness of liquid films on the back and concave surface of a profile will be unequal. In accordance with the mechanism of motion of the droplets in the channel, the thickness of the film on the concave surface turns out to be larger.

Thus, moisture can occur in the flow area of a stage simultaneously in three

forms: in the form of small suspended droplets, in the form of a film covering a blade, and in the form of enlarged droplets. The numerical ratio of the various forms of moisture depends on the above-mentioned factors, and also on the intensity of steam expansion, and consequently, on the primary condensation. It should be borne in mind that, besides the droplets proceeding to the considered stage during steam expansion in the given stage (secondary droplets), new (primary) droplets can be separated in the flow.

The influence of moisture on profile and end losses in turbine cascades has been insufficiently studied. This investigation must be conducted in a wide range of variation of Reynolds and M numbers for various degrees of moisture, separating the conditions with the transition through the saturation line ($\chi_0 = 0$) from the stage of weak overheating and the conditions with high initial moisture.

Available experimental data show that when the initial humidity is $\chi_0 > 0$, the losses in reaction and impulse cascades increase as compared to superheated steam.

Some data that illustrate the change of profile losses are shown in Fig. 329. These experiments show that in a reaction cascade an increase of losses in noted at large values of initial moisture. Thus, for instance, the transition from the state of overheating to the boundary curve (moisture $\chi_0 \approx 0$) practically did not change the level of profile losses in this cascade. However, at $\chi_0 = 4\%$, the profile losses noticeably increased.

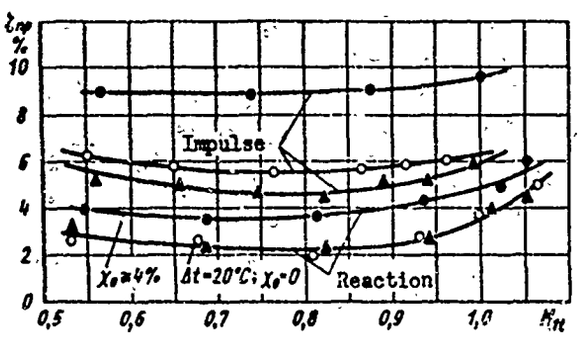

Fig. 329. Influence of steam moisture on profile losses in impulse and reaction cascades. [пр = pr = profile]

A characteristic fact is that the increase of losses is noted mainly in the edge wakes behind the cascade, i.e., in the zone where detachment of the films occurred and small and larger droplets were formed, which are again carried away by the flow. The more intense influence of moisture on losses in an impulse cascade is explained by the fact that the velocities at the entrance to this cascade are considerable and the droplets lag even before the cascade. Furthermore, in an impulse cascade the flow accomplishes a more significant circulation. Experiments showed that even at a low initial moisture, $\chi_0 = 0$-1%, the profile losses in an

impulse cascade increased. Especially noticeable is the increase of losses with the increase of moisture to $\chi_0 > 5\%$.

§ 51. EQUATIONS OF ONE-DIMENSIONAL MOTION OF MOIST STEAM AND THE SLIP FACTOR

We shall apply general conservation equations to a flow of moist steam, considering the motion to be steady and one-dimensional; the distribution of the liquid phase in a cross section is assumed to be uniform. The existence of an internal heat exchange between phases, caused by condensation, is assumed.

The continuity equation may be written in the following form:

$$m = m_n + m_e = (F - \Delta F)\varrho_n c_n + \Delta F \varrho_e c_e,$$

where F is the cross-sectional area of a channel; ΔF is the portion of the cross-sectional area occupied by the liquid phase; m_Π and m_B are the mass flow rates of the steam and liquid phases; m is the total mass flow rate; ρ_B and ρ_Π are the densities of the liquid and steam phases.

This equation is not difficult to convert to the following form:

$$1 - \Delta\bar{F} + \Delta\bar{F}\bar{\varrho}_e v = \frac{m}{m_n}.$$

Here $\overline{\Delta F} = \frac{\Delta F}{F}$; $\bar{\rho}_B = \rho_B / \rho_\Pi$ is the density ratio of the liquid and steam phases; $v = c_B / c_\Pi$ is the slip factor.

In the initial (entrance) and intermediate sections, the continuity equation for the steam phase takes on the following form:

$$m_n' = F\varrho_n c_n = \frac{1 - \Delta\bar{F}_1}{1 - \Delta\bar{F}} F_1 \varrho_{n1} c_{n1}$$

(subscript 1 pertains to the initial section).

Substituting the quantity m_Π', we finally obtain:

$$\Delta\bar{F} = \frac{1}{1 + \left(\frac{1}{\chi} - 1\right)\bar{\varrho}_n v}. \tag{342}$$

Here $\chi = m_\Pi/m$ is the degree of moisture of the flow in a given section.

The momentum equation in differential form will be presented in the following manner:

$$d(m_n c_n + Fp + m_e c_e) + \xi \frac{\varrho_n c_n^2}{2} d\bar{S} + dJ_x = 0. \tag{343}$$

Here ξ is the coefficient of steam friction against the walls, $d\bar{S} = dS/D$ is an

element of the length of a wall (D is the diameter of a channel); dJ_x is the impulse of the resisting forces of the droplets in the flow.

Disregarding the influence of friction against the walls ($\xi = 0$) and considering that $dJ_x = 0$, we shall integrate equation (343) on an area between the entrance and intermediate sections:

$$m_n c_n + Fp + m_e c_e = m_{n1} c_{n1} + F_1 p_1 + m_{e1} c_{e1}.$$

For the steam phase we will use the B. M. Kiselev transform:

$$m_n c_n + Fp = \frac{k+1}{2k} m_n a_{*n} \psi(\lambda_n),$$

where $\psi(\lambda_\Pi) = \lambda_\Pi + \frac{1}{\lambda_\Pi}$; $\lambda_\Pi = c_\Pi/a_*$ and a_* are the dimensionless and critical velocities of the steam phase. After simple transformations, we can obtain:

$$\bar{a}_* \left[(1 - \chi)\psi(\lambda_n) + \frac{2k}{k+1}\chi\lambda_e\right] = (1 - \chi_1)\psi(\lambda_{n1}) + \frac{2k}{k+1}\chi_1\lambda_{e_1}. \tag{343a}$$

Here $\lambda_B = c_B/a_{*1}$; $\bar{a}_* = a_*/a_{*1}$; χ_1 is the initial degree of moisture.

The energy equation, taking into account the internal heat exchange, is presented in the following form:

$$d(m_n i_{0n}) + m_e c dT_e + m_e \frac{d(c_e^2)}{2} = 0, \tag{344}$$

where $i_{0\Pi}$ is the stagnation enthalpy of the steam phase; c and T_B is the heat capacity and the temperature of the liquid phase.

If cooling of the droplets can be disregarded, equation (344) is integrated:

$$m_n i_{0n} + m_e \frac{c_e^2}{2} = m_{n1} i_{01} + m_{e_1} \frac{c_{e_1}^2}{2}.$$

Since*

$$2i_{0n} = \frac{k+1}{k-1} a_*^2,$$

the energy equation takes on the following form:

$$\frac{1-\chi}{1-\chi_1}\bar{a}_*^2\left(1 + \frac{k-1}{k+1}\frac{\chi\lambda_e^2}{1-\chi}\right) = 1 + \frac{k-1}{k+1}\frac{\chi_1\lambda_{e_1}^2}{1-\chi_1}. \tag{344a}$$

*It is assumed that for the steam phase it is possible to take the average, but constant, value of index k.

Considering a droplet as a moving material point (sphere), we can write the impulse equation (equation of droplet motion) in the following form:

$$\Delta m_в dc_в = P_x dt.$$

Here P_x is the drag of a droplet; Δm_B is the mass of a droplet, whose shape is assumed to be spherical.

The drag of the sphere can be determined by the following formula:

$$P_x = c_x F_м \varrho_п (c_п - c_в)^2,$$

where c_x is the drag coefficient; $F_м$ is the cross-sectional area of the sphere.

Noting that

$$\Delta m_в = \varrho_в \frac{\pi d_к^3}{6}; \quad F_м = \frac{\pi d_к^2}{4}; \quad \bar{x} = \frac{x}{d_к},$$

we shall convert the motion equation to the following form:

$$\frac{c_в dc_в}{(c_п - c_в)^2} = \frac{3}{4} \cdot \frac{c_x}{\varrho_в} d\bar{x}, \tag{345}$$

since $dt = dx/c_B$; dx is an element of the droplet's trajectory.

For low degrees of moisture, equation (345) may be presented in the following form:

$$\frac{\varphi(\lambda_п)\bar{a}_в}{\left(\frac{\lambda_п}{\lambda_в}\bar{a}_в - 1\right)^2} \frac{d\lambda_в}{\lambda_в} = \frac{3}{4} \cdot \frac{c_x}{\varrho_в} d\bar{x}, \tag{346}$$

where

$$\varphi(\lambda_п) = \left(\frac{1 - \frac{k-1}{k+1}\lambda_п^2}{1 - \frac{k-1}{k+1}\lambda_{п1}^2}\right)^{\frac{1}{k-1}}.$$

Equation (346) is integrated:

$$\bar{x} = \frac{4}{3} \int_{\lambda_{в_1}}^{\lambda_в} \frac{\bar{\varrho}_в}{c_x} \frac{\varphi(\lambda_п)\bar{a}_в}{\left(\frac{\lambda_п}{\lambda_в}\bar{a}_в - 1\right)^2} \frac{d\lambda_в}{\lambda_в}. \tag{347}$$

The equations of conservation and motion are supplemented by the equation of state for the steam phase:

$$p = f(\varrho_п, T_п)$$

(for an ideal gas $\frac{1}{T_n}\frac{dT_n}{dx}=\frac{1}{p}\frac{dp}{dx}-\frac{1}{\varrho_n}\frac{d\varrho_n}{dx}$), the equation of droplet resistance:

$$c_x=\varphi(\mathrm{Re}_n)$$

and the equation of heat exchange between the droplets and the steam; the latter may be presented in the following form:

$$-\alpha(T_e-T_n)\frac{\pi}{4}d_k^2dt=c\varrho_e\frac{\pi d_k^3}{6}dT_e.$$

Here α is the coefficient of heat radiation, which depends on the Reynolds number, the slip factor, and the droplet radius; c is the heat capacity of water.

Hence we obtain a linear differential equation with respect to T_B

$$\frac{dT_e}{dt}=-\frac{6\alpha}{c\varrho_e d_k}(T_e-T_n), \qquad (348)$$

where T_n is taken as a function of time.

The equations obtained above form a closed system, the solution of which is carried out by a numerical method* or on an electronic computer.

One of the main problems in the investigation of the structural form of the two-phase system reduced to finding the dimensions of the droplets and the relation between the velocities of the two phases (slip factor).

The establishment of this relation makes it possible to quite easily determine the change of the effectiveness of a stage and its flow rate characteristics, depending upon moisture within the confines of a one-dimensional flow diagram by means of velocity triangles). For this reason, attempts have been made for some time to establish an appropriate connection between the velocities of steam and moisture. One of the first works in this direction is that of L. I. Degtyarev [21].

It is obvious that the sought relationship of the velocities of steam and water depends on the quantitative distribution of the various dimensions of the droplets and films of moisture in the flow and consequently, this relationship cannot be exactly determined. The above-mentioned system of equations permits an approximate solution of this problem within the confines of a one-dimensional diagram.

Let us consider a simpler method of determining the slip factor, which was

*Because of the limited volume of this book, the solution of the indicated equations is not given.

developed by Yu. Ya. Kachurirer [54]. Using the experimental Nukiyama-Tanazava dependence for the maximum diameter of a stably behaving droplet (taking into account the dynamic pressure of the steam flow),

$$d_{\text{макс}} = \frac{0{,}519}{c_e - c_n}\sqrt{\frac{\sigma}{\varrho_e}}$$

and assuming that

$$c_x = 5{,}35\mathrm{Re}_x^{-\frac{1}{2}},$$

the author reduces equation (345) to the following form:

$$c_e dc_e = S(c_n - c_e)^2 dx, \tag{349}$$

where

$$S = 18\frac{\sqrt{\mu_n \varrho_n}}{\sqrt[4]{\varrho_e \sigma^3}}.$$

Equation (349) is integrated for c_Π = const.

Since at x = 0 (in an initial section) $c_{B_1} = \nu_1 c_\Pi$, then

$$\nu = \frac{c_e}{c_n} = \frac{(1-\nu_1)\alpha + \nu_1^2 - \sqrt{(1-\nu_1)\alpha + \nu_1^2(1-\nu_1)^2}}{(1-\nu_1)^2\alpha - 1 + 2\nu_1}. \tag{350}$$

In formula (350) we designate:

$$\alpha = 2Sc_n x.$$

For the particular case of $\nu_1 = 0$ ($c_{B_1} = 0$ when x = 0), we obtain:

$$\nu' = \frac{c_e}{c_n} = \frac{\alpha - \sqrt{\alpha}}{\alpha - 1}. \tag{351}$$

Equations (350) and (351) are valid for a constant velocity of the steam phase. For the linear law of change

$$c_n = kx.$$

Yu. Ya. Kachuriner obtained the following formula:

$$\nu = \frac{1}{2}\sqrt{\alpha}\left[1 - 0{,}6\sqrt{\alpha} + 0{,}47\alpha - 0{,}23\alpha\sqrt{\alpha} + \right.$$
$$\left. + 0{,}142\alpha^2 - 0{,}081\alpha^2\sqrt{\alpha} + 0{,}0549\alpha^3 + \cdots\right]. \tag{352}$$

Equations (350) and (352) are convenient to represent graphically. Figure 330a shows the curves of change of ν, depending upon α for different ν_1. The curves on Fig. 330b characterize the influence of the parameters of the medium on the value of α.

Calculations according to equation (352) show that for small droplet dimensions, $d_K = (1\text{-}3)\cdot 10^{-3}$, the velocity ratio ν is close to unity. In this case the lag of moisture particles from the steam flow is small, and the losses in the stage, which are caused by the braking effect of moisture, also will be small.

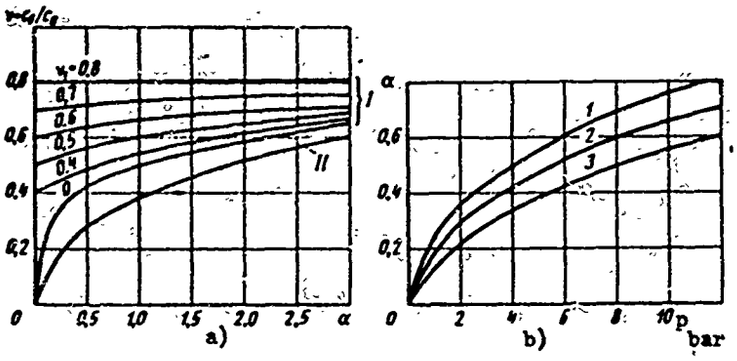

Fig. 330. Graphs for determining the slip factor according to Yu. Ya. Kachuriner's method: a) dependence of slip factor on α for different ν_1; b) influence of pressure on α for different temperatures; curves: 1 and 2) for air, T = 373° and T = 273°; 3) for steam, $c_П$ = 100 m/sec.

For nonlinear velocity distribution of the steam flow along x, the initial equation (349) can be solved by integration with respect to separate sections.

Let us emphasize that Yu. Ya. Kachuriner's solution leads to an intense dependence of the slip factor ν on the Reynolds number, since

$$\alpha = 2Sc_n x = 20{,}3\mathrm{Re}_x \frac{\mu_n \sqrt{c_n x}}{\sqrt[4]{\mu_e \sigma^3}},$$

where $\mathrm{Re}_x = c_П x \rho_П / \mu_П$ is the Reynolds number referred to the length of a flow line.

§ 52. CONDENSING SHOCKS IN A FLOW OF MOIST STEAM

The available experimental data distinctly show that condensation can be carried out in condensing shocks at high velocities. In this case, an intense release of moisture occurs on a short length of the flow. Consequently, in the section where a condensing shock is located there occurs an intense release of the heat of vaporization; as a result, the shock changes the pressure, density, temperature, and velocity of the flow.

An analytic investigation of condensing shocks is carried out by means of the joint solution of conservation equations under the following assumptions: a) condensation occurs instantly, so that a clear-cut line that separates the steam from the mixture is formed; b) the effect of condensation reduces to the liberation of the latent heat of vaporization; c) the change of the physical properties of the

steam phase and its parameters occurs only in a shock; d) the influence of viscosity, heat conduction, and diffusion may be disregarded; e) after the shock, the moisture and steam have identical velocities.

The enumerated assumptions make it possible to obtain calculation equations for condensing shocks by means of the joint solution of three conservation equations: continuity, energy, and momentum [22], [150].

In the form of a connection between the vertical and longitudinal components of velocity, the fundamental equation of a condensing shock has the following appearance [22]:

$$\bar{v}_2^2 = (\bar{\lambda}_1 - u_2)^2 \cdot \frac{\frac{\lambda_1}{\lambda_1 - \bar{u}_2}\left[\bar{u}_2(\lambda_1 - \bar{u}_2) - \bar{\Delta i}_0\right]}{\frac{2}{k+1}\lambda_1^2 - \lambda_1 \bar{u}_2 + 1}. \tag{353}$$

Here $\lambda_1 = c_1/a_{*1}$ is the dimensionless velocity before the shock;

$\bar{u}_2 = u_2/a_{*1}$ is the dimensionless longitudinal velocity component behind the shock;

$\bar{v}_2 = v_2/a_{*1}$ is the dimensionless vertical velocity component behind the shock;

$\bar{\Delta i}_0 = \Delta i_0/i_{01}$ is the relative change of stagnation enthalpy due to the release of heat during condensation;

a_{*1}, i_{01} are the critical velocity and stagnation enthalpy before the shock.

Equation (353) represents the shock polar of a condensing shock. As it is known [22], condensing shocks can appear only in definite quantities of condensing liquid. The maximum increase of stagnation enthalpy in a shock is calculated by the following formula:

$$\bar{\Delta i}_{0\,max} = \frac{1 - \bar{a}_{*\,min}^2}{\bar{a}_{*\,min}^2}, \tag{354}$$

where

$$\bar{a}_{*\,min} = \left(\frac{a_{*1}}{a_{*2}}\right)_{min},$$

a_{*2} is the critical velocity behind the shock.

The quantity $\bar{a}_{*\,min}$ determines the maximum increase of critical velocity in a condensing shock. The increase of stagnation enthalpy in the shock is connected with the degree of moisture before the shock by the following relationship:

$$\overline{\Delta i_0} = \frac{\chi_1}{1-\chi_1}. \tag{355}$$

Formulas (354) and (355) jointly give:

$$\chi_{max} = 1 - \alpha_{min}^{-2}. \tag{356}$$

Consequently, with relative moisture $\chi > \chi_{max}$, condensing shocks are not able to exist. In this case, at any velocities there occurs continuous and uniform condensation of the steam portion.

The theory of shocks shows that condensing shocks can be of two types: a) subsonic shocks, which corresponding to the condition of $c_{n1} < a_1$ and $c_{n2} < a_2$; b) supersonic shocks, in which $c_{n1} > a_1$ and $c_{n2} < a_2$ (c_{n1} and c_{n2} are the normal velocity components before and after the shock).

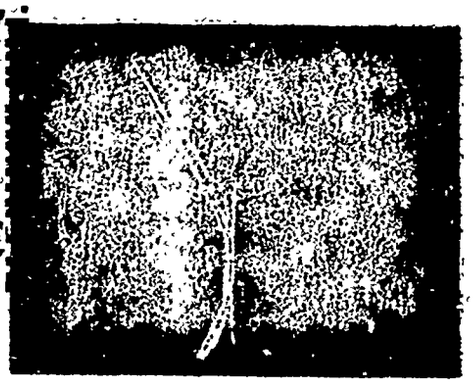

Fig. 331. Condensing shock in a flow of moist air at M = 1.7 and degree of moisture χ = 0.33.

An experiment confirms the possibility of the formation of the two types of shocks. Figure 331 shows the spectrum of moist flow of air in a convergent-divergent nozzle. Here we can distinctly see the system of intersection oblique shock waves, the appearance of which is not connected with the shape of the nozzle walls or the conditions of flow.

In accordance with a theory, the position of a shock, its shape, and intensity are decisively influenced by the air moisture content and the flow rate. Figure 332 gives curves of relative pressure and number M_1 before a condensing shock, depending upon the absolute air moisture content χ, according to the experiments of A. A. Stepchkov which were conducted in a convergent-divergent nozzle. With the increase of moisture, the condensing shock moves into a region of lower M_1 numbers. With the increase of moisture, the supersaturation of the air flow by steam decreases, which is determined by the ratio of partial steam pressure to the saturation pressure, $p_{1п}/p_{1н}$, and there also occurs supercooling, ΔT (Fig. 332).

The movement of a condensing shock, depending upon moisture, is explained, apparently, by the fact that as the quantity of steam decreases, its condensation occurs at a lower temperature which corresponds to a higher M_1 number.

The shock also changes shape when it moves: at a high moisture content, the

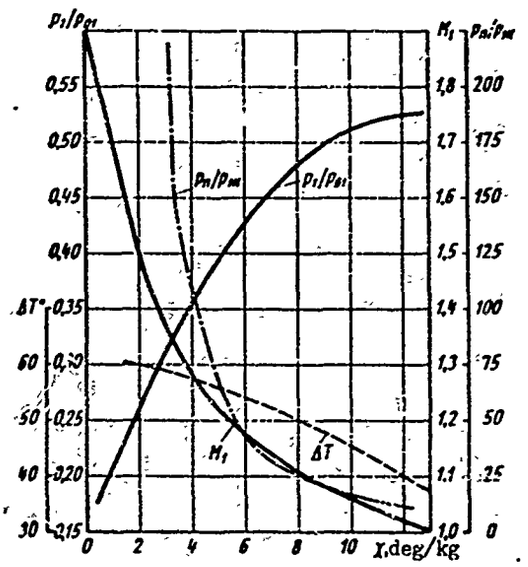

Fig. 3-2. Influence of absolute moisture χ in a convergent-divergent nozzle on supercooling ΔT, M_1 number, pressure ratio p_1/p_0, and the ratio of partial pressure to saturation pressure $p_{1п}/p_{1н}$, according to A. A. Stepchkov's experiments.

shock becomes bridge-like and is almost straight; with the decrease of moisture, as a rule, a system of two intersecting shocks is observed.

In this case one can determine the variation of parameters in a condensing shock according to the following formulas:

pressure ratio

$$\frac{p_2}{p_1} = \frac{1 + kM_1^2 \sin^2 \beta_K}{1 + \frac{kM_2^2}{\bar{u}_2^2 + \bar{v}_2^2} (\bar{u}_2 \sin \beta_K - \bar{v}_2 \cos \beta_K)^2},$$

where the velocity behind the shock is

$$M_2 = \left[(k-1) \left(\frac{k+1}{2(k-1)} \frac{1 + \overline{\Delta i}_0}{\bar{u}_2^2 + \bar{v}_2^2} - \frac{1}{2} \right) \right]^{-\frac{1}{2}},$$

β_K is the angle of the condensing shock;

density ratio:

$$\frac{\varrho_2}{\varrho_1} = \frac{p_2}{p_1} \left(\frac{M_2}{M_1} \right)^2 \frac{\lambda_1^2}{\bar{u}_2^2 + \bar{v}_2^2};$$

stagnation pressure ratio:

$$\frac{p_{02}}{p_{01}} = \frac{p_2}{p_1}\left(\frac{1+\frac{k-1}{2}M_2^2}{1+\frac{k-1}{2}M_1^2}\right)^{\frac{k}{k-1}}.$$

Increase of entropy:

$$\Delta S = R \ln\left[(1+\overline{\Delta i_0})^{\frac{k}{k-1}}\frac{p_{01}}{p_{02}}\right].$$

The very limited quantity of available experimental data shows that condensing shocks form in the nozzle cascades of turbines in an oblique cross section, and at $M_1 > 1$ they are located near the main shocks which appear during steam expansion in this section.

With the increase of moisture, just as in a convergent-divergent nozzle (Fig. 331), the shocks move in a direction to the narrow section of the vane channel and, with the increase of velocity, the condensing shocks move toward the flow.

It may be assumed that supercooling attains maximum values in the transonic zone that is characterized by maximum longitudinal velocity gradients. This peculiarity of transonic flows gives us a basis to consider that at $M_1 \approx 1$ condensation does not generally occur in a flow of steam. This assumption is indirectly confirmed by experiments with Laval nozzles, in the minimum section in which $M \approx 1$, and the observed supercooling attains very large magnitudes. Condensation in a Laval nozzle is found in the divergent (supersonic) portion.

In conclusion, let us note that from the aerodynamic point of view the process of condensation, which causes a local decrease of pressure at the points where the condensation centers are located, apparently leads to turbulization of the flow, since condensation is accompanied by an intense exchange of impulses in a trancverse direction.

§ 53. FLOW RATE CHARACTERISTICS OF NOZZLES OPERATING WITH MOIST STEAM

For ideal gases that are governed by an equation of stage, the theoretical mass flow density in any given section may be determined by the following known relationship [22]:

$$j_t = \frac{m_t}{F_*} = \sqrt{k\left(\frac{2}{k+1}\right)^{\frac{k+1}{k-1}}}\, q_t \sqrt{\frac{p_0}{v_0}} = B_t \sqrt{\frac{p_0}{v_0}}, \qquad (357)$$

where m_i is the theoretical mass flow of gas per second;

F_* is the area of the nozzle outlet section;

p_0, v_0 are the pressure and specific volume of the stagnated flow;

$q_t = \frac{\rho_t c_t}{\rho_* a_*} = \left(\frac{k+1}{2}\right)^{\frac{1}{k-1}} \lambda_t \left(1 - \frac{k-1}{k+1}\lambda_t^2\right)^{\frac{1}{k-1}}$ is the given theoretical flow rate;

ρ_t, c_t are the density and velocity in the nozzle outlet section for an isentropic flow;

ρ_*, a_* are the critical density and velocity in the outlet section;

$\lambda_t = c_t/a_*$ is the dimensionless velocity;

$B_t = q_t \sqrt{k\left(\frac{2}{k+1}\right)^{\frac{k+1}{k-1}}}$ is the theoretical discharge coefficient.

The actual mass flow density will differ from the theoretical one, and it can be found by the following formula:

$$j = B\sqrt{\frac{p_0}{v_0}}, \tag{358}$$

where B is the actual discharge coefficient.

The flow rate coefficient of the nozzle is equal to

$$\mu = \frac{B}{B_t}.$$

For superheated steam, the flow rate coefficient μ characterizes the decrease of the outlet section of the nozzle by the boundary layer. This decrease quantitatively is expressed by the depth of displacement, δ^*. It is obvious that the discharge coefficient B and the flow rate coefficient μ depend on the basic parameters that determine the development of the boundary layer in the nozzle, i.e.,

$$B = f\left(\mathrm{Re}_1, \mathrm{M}_1, k, \frac{d\bar{p}}{d\bar{x}}\right)$$

and

$$\mu = \psi\left(\mathrm{Re}_1, \mathrm{M}_1, k, \frac{d\bar{p}}{d\bar{x}}\right).$$

Here Re_1 is the Reynolds number in the outlet section of the nozzle;

M_1 is the M number calculated with respect to the pressure ratio in the nozzle, $\varepsilon = p_2/p_{01}$;

p_2 is the static pressure in the external medium;

$d\bar{p}/d\bar{x}$ is the dimensionless pressure gradient.

As indicated earlier, convergent flows of saturated and moist steam differ by a number of peculiarities: a) the change of state cannot be expressed by the equation of state of an ideal gas, and the isentropic exponent k ceases to be a constant that characterizes the process on the whole; b) the steam in the critical section of the nozzle is in a supercooled state, whereby the equation of state of this steam is unknown; c) the phase homogeneity of the flow is disturbed in any section of the nozzle; in the region of flow near the wall, a film will form, the velocities of the liquid and steam phases will be unequal, and the velocities proceeding to the nozzle will also be different due to the initial moisture and the droplets formed during motion; d) the flow process is unbalanced and metastable; therefore, the thermodynamic method of investigating the equilibrium processes turns out to be unacceptable.

Consequently, the discharge coefficient B for moist steam should depend on, besides Re_1, M_1, and the longitudinal pressure gradient, the initial degree of moisture, $\chi_0 = 1 - x_0$ (x_0 is the initial degree of dryness), on the magnitude of supercooling $\Delta\bar{T}$, on the area of the nozzle section occupied by film $\frac{F_{пл}}{F_1}$, and on the slip factor. Thus:

$$B = f\left(Re_1, M_1, \frac{d\bar{p}}{d\bar{x}}, \chi_0, \Delta\bar{T}, \nu, \frac{F_{пл}}{F_1}\right).$$

We shall first consider the results of an investigation of the flow rate characteristics of a nozzle operating with superheated steam (MEI experiments). Figure 333 presents curves of the discharge coefficient B depending upon Re_1 and ε. The discharge coefficient B ceases to depend on Re_1 when $Re_1 \geq 4.5 \cdot 10^6$.

With the decrease of ε, the discharge coefficient increases from B = 2.015 at $\varepsilon = 0.52$ to B = 2.07 at $\varepsilon \approx 0.1$. The increase of the coefficient occurs with the increase of the pressure drop on the nozzle at supercritical pressure drops, which is explained by the structure on the boundary layer in the outlet section of the nozzle. As shown in reference [22], under such conditions the actual minimum section of flow does not coincide with the outlet section of the nozzle.

At subcritical drops the boundary layer continuously increases along the nozzle generatrices and the depth of displacement in the outlet section has a maximum value.

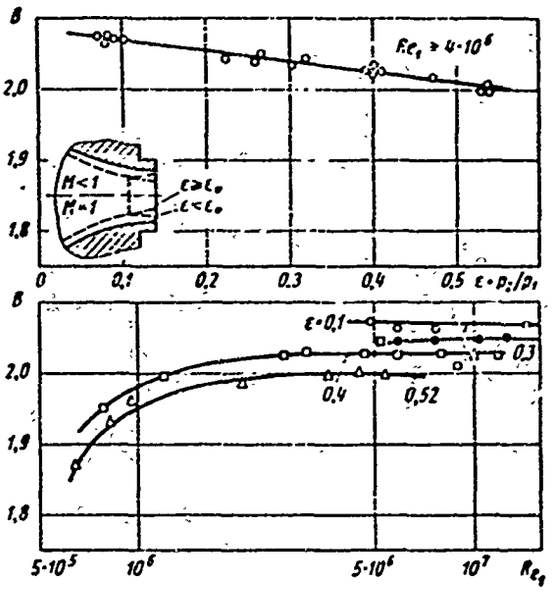

Fig. 333. Dependence of the discharge coefficient of an axially symmetric convergent nozzle on the Reynolds number and pressure ratio (M number); experiments of G. V. Tsiklauri (MEI) with superheated steam.

With supercritical drops, the pressure near the outlet section is equal to critical, and it is less than critical behind the nozzle. Under the action of the pressure difference on the outlet section of the nozzle there occurs a sharp decrease in the depth of displacement ("blow-out" of the boundary layer), whereupon reconstruction of the layer starts inside the nozzle, since the disturbances through the subsonic part of the layer are propagated against the flow. This reconstruction of the boundary layer at the outlet section involves an increase of the actual ("effective") critical section of flow (as compared to subcritical conditions), and the steam flow rate increases.

With the decrease of ε, there occurs a more intense "blowing-out" of the boundary layer at the nozzle section; the actual critical section is then even more displaced against the flow (Fig. 333). The area of the critical section continues to increase, and the flow rate through the nozzle increases. The discharge coefficient B then increases.

For a confirmation of this hypothesis, we measured the pressure distribution along a nozzle wall. Graphs of the pressure distribution show that when $\varepsilon \approx 0.25$, inside the nozzle at a distance of 4 to 5 mm from the edge, the steam flow is supersonic, i.e., the critical section of the nozzle, which corresponds to $\varepsilon_* = 0.546$, is located inside the nozzle (see Fig. 334).

Calculation of the depth of displacement by the method presented in [22] gives the value of δ^* in the nozzle throat as equal to 0.3 mm. An increase of the discharge coefficient from 2.02 to 2.07 for the tested nozzle should correspond to a decrease of δ^* by 0.25 mm. Consequently, it is possible to expect that at $\varepsilon \approx 0.1$ there occurs almost complete "blowing-off" of the boundary layer.

Thus, experiments on the determination of discharge coefficients for superheated steam showed that, in distinction from foregone conclusions, in supercritical pressure

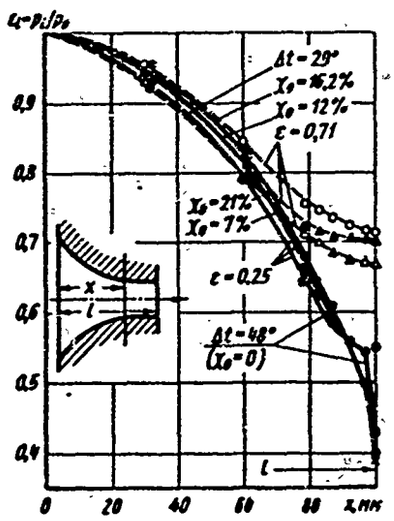

Fig. 334. Influence of moisture on pressure distribution along a nozzle wall under subcritical and supercritical conditions: experiments of G. V. Tsiklauri (MEI).

drops the discharge coefficient for convergent nozzles depends on the Reynolds number and the pressure drop on the nozzle. This means that the flow rate coefficient μ also under supercritical conditions depends on Re_1 and M_1.

The results of an investigation of the flow rate characteristics of a nozzle with saturated and moist steam at supercritical pressure drops are presented in Fig. 335. These experiments show that with the approximation of the initial steam parameters to the boundary curve of the phase transition, the coefficient B starts to increase. Upon transition to the two-phase region, the discharge coefficient continues to increase, but more intensely, whereupon where all four curves gradually converge. This approximation, with a high initial moisture content, may be explained by the formation of a liquid film in the throat area of the nozzle, which is stabler, and consequently, the depth of displacement of the mixed boundary layer (liquid film and steam) decreases less intensely with the decrease of ε.

As can be seen from Fig. 333, the experiments revealed the influence of the Re_1 number on the discharge coefficient, whereby the influence of R_1 is noticeable at higher Re_1 than in the case of superheated steam ($Re_{1\text{автом}} = 6.3 \cdot 10^6$ for moist steam, instead of $Re_{1\text{автом}} = 4.5 \times 10^6$ for superheated steam. This fact confirms the more intense mechanism of viscosity in a flow of moist steam.

Thus, the flow rate characteristics of nozzles in supercritical conditions for moist steam qualitatively change depending upon ε (or M_1) and Re_1 just as for superheated steam.

The above-considered results of the investigations distinctly showed that the value of the discharge coefficient with supercritical pressure drops for moist steam, B = 2.035, which was recommended by Bendeman in 1907 and is widely used in calculations of the flow areas of steam turbines, lies below the given experimental data.

The dotted line in Fig. 335 shows the change of the theoretical discharge coefficient B_t depending upon the initial moisture content and superheating for

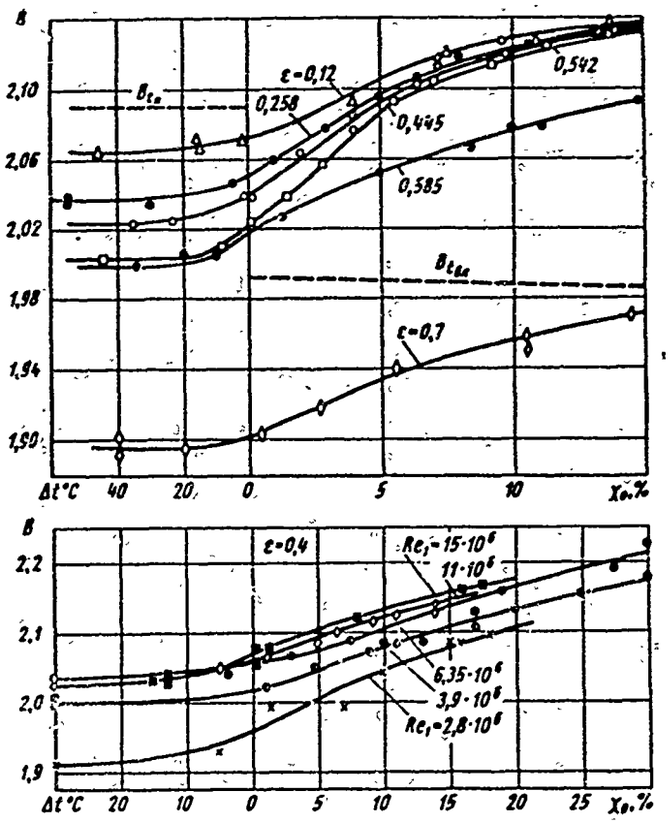

Fig. 335. Dependence of discharge coefficient B on moisture content at different Reynolds numbers and pressure ratios (MEI experiments).

supercritical conditions. It is obvious that upon transition from superheated steam to moist, the exponent k, and consequently also B_t, change abruptly. The isentropic exponent changes from 1.3 for superheated steam to 1.135 for dry saturated steam, which corresponds to a change of B_t from 2.09 to 1.99. With the increase of the degree of moisture, the discharge coefficient B_t, which is calculated according to V. V. Sychev, continues to drop slightly, while, according to an experiment conducted at MEI, B_t increases. This divergence of theory and experiment can be explained by the circumstance that a thermodynamic analysis does not consider the above-mentioned peculiarities of the flow of saturated and moist steam in a nozzle.

The character of the influence of moisture on the discharge coefficient in subcritical conditions remains the same as in supercritical conditions; however, this influence turns out to be weaker quantitatively. With the increase of the initial moisture, the discharge coefficient B increases less intensely than in supercritical drops.

The qualitatively identical influence of moisture is also confirmed by graphs of the pressure distribution. Along a nozzle wall (see Fig. 334); with the increase of moisture, the pressure in all sections increases. This increase of pressure is a result of the simultaneous heat and flow rate influence on the flow. However, the graphs in Fig. 334 also lead to another conclusion. Thus, for example, for the case of superheated steam and dry saturated steam, the pressure curves shown on the graph completely coincide. This indicates that during expansion from the saturation

line, the steam behaves in the same way as superheated steam; there does not occur a noticeable release of moisture, which would lead to deformation of the pressure curve (due to the internal heat input and change of the flow rate) during condensation.

The increase of the steam flow through a nozzle with the increase of moisture is explained by the joint influence of several factors: supercooling of the steam phase, increased cross-sectional area of the steam phase, and supply of heat to it from the liquid phase (even in the absence of phase transitions), and also stagnation of the steam flow by droplets of moisture. A decrease of the flow rate promotes the formation of a liquid film on the nozzle walls and expenditure of energy for accelerating the motion of liquid particles.

An evaluation of the significance of separate factors shows that their influence essentially depends on the degree of moisture. Thus, for instance, the increase of the cross-sectional area of the steam phase, which is caused by the increase of the velocity of the droplets as they pass through the nozzle, turns out to be insignificant with degrees of moisture $\chi \leq 10\text{-}20\%$ and slip factors ν close to unity [see formula (342)]. In those cases when the slip factors $\nu \ll 1$, the influence of this factor can be perceptible.

Small values of ν are characteristic of the liquid film on the nozzle walls. Consequently, as one may see from equation (342), its influence on the steam flow rate can be essential. A decisive value is obtained by supercooling when the supply of heat to the steam phase is the most intense, when the dimensions of the droplets are small and the steam is decelerated by the droplets, which causes an increase of its density.

The influence of the enumerated factors leads to an intricate redistribution of the parameters of flow, as a result of which the pressure on the nozzle walls is increased (Fig. 334).

As the moisture content increases, the film blockage of the minimum section increases and the slip factor changes in the core of the flow, which leads to a less intense increase of the flow rate.

On the basis of experimental data for supercritical and subcritical pressure drops, we constructed the dependence of the discharge coefficient B on the pressure ratio ε for different degrees of moisture at the inlet (Fig. 336). For a comparison, Fig. 336 shows Bendeman's experimental points and an analytic curve of B_t for

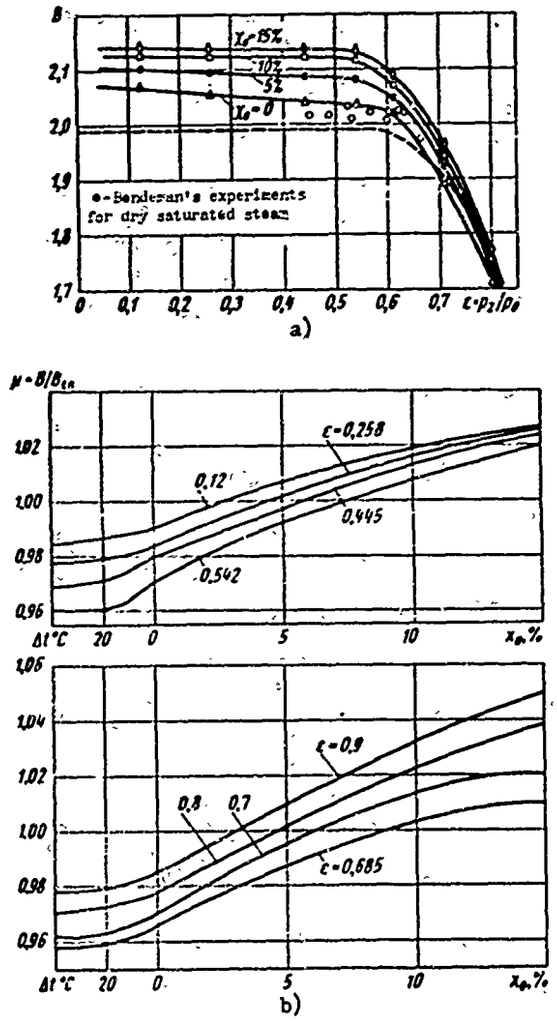

Fig. 336. Flow rate characteristics of convergent nozzles with moist steam: a) dependence of discharge coefficient on ε for different moisture contents; b) dependence of flow rate coefficient on moisture content for different ε (MEI experiments).

k = 1.135 (dotted line).

The calculation of the flow areas of turbine cascades usually employs the flow rate coefficient $\mu = B/B_t$, whose value for moist steam depends on the method of determining the theoretical discharge coefficient B_t. If B_t is determined with respect to exponent k, depending on the degree of moisture [see formula (357)], the flow rate coefficient upon transition through the saturation line changes abruptly. This creates evident inconveniences for practical calculations.

In an area of small superheating and small degrees of moisture, the flow rate coefficient can be determined by referring the actual discharge coefficient to the theoretical one that was calculated for k = 1.3. The corresponding curves that are shown in Fig. 336b can be used for the calculations. It should be borne in mind, however, that the graphs in Fig. 336 were obtained for an axially symmetric nozzle. At small degrees of moisture ($\chi_0 \leq 10\%$) the values of μ for nozzle cascades closely coincide with those shown in Fig. 336. For impulse cascades (and for nozzle cascades with high moisture content) there is nonuniformity of the liquid phase (small and large droplets, films of different thickness on the back and concave surface), and the flow rate coefficients can noticeably differ.

§ 54. INFLUENCE OF MOISTURE ON THE CHARACTERISTICS OF A TURBINE STAGE

Systematic investigations of the effect of moisture on the efficiency, reaction, and flow rate coefficient of turbine stages are being conducted at

MEI, NZL, BITM, KTZ, and TsKTI. The material accumulated is not yet sufficiently complete; however, it permits us to make a number of essential conclusions concerning the performance of a stage in a region of moist steam.

The KTZ laboratory studied the influence of moisture on the efficiency of a double-wheel regulating stage. The corresponding data are given in Fig. 337. The influence of moisture turns out to be quantitatively different, depending upon the heat drop in the stage, i.e., on the M_0 number. At subsonic velocities, moisture causes a more intense lowering of efficiency than at supersonic velocities for a double-wheel stage. It may be assumed that this result is explained by the considerably great supercooling of steam at $M_0 > 1$. The main process of condensation then occurs either on the second wheel, or behind the stage. Furthermore, at high velocities, the size of the droplets decreases and the relative velocity of their motion increases (see § 50).

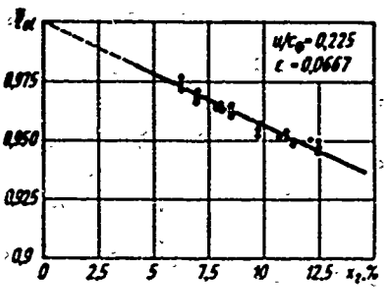

Fig. 337. Change of the relative internal efficiency of a double-wheel stage, depending upon final moisture content at supersonic velocities; $X_\phi = 0.225$; $\varepsilon = 0.0667$ (KTZ experiments).

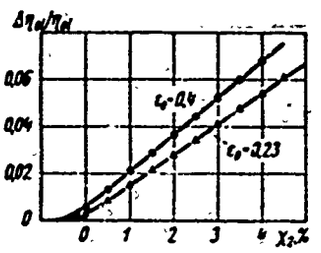

Fig. 338. Relative decrease in efficiency of a group of three stages, according to KTZ experiments, depending upon the moisture behind the turbine.

These considerations are also confirmed by KTZ experiments with a group of stages [128]. The magnitude of the decrease in efficiency, depending upon the degree of moisture, is shown in Fig. 338. It should be noted that when the pressure ratio in a group of three stages is $\varepsilon_0 = 0.4$, the drops along all stages are subcritical, and on the last stage, when $\varepsilon_0 = 0.23$, the drop is supercritical.

An investigation of the influence of moisture on the performance of intermediate stages was carried out by Yu. Ya. Kachuriner and A. P. Fadeyev [110].

These experiments were conducted at subsonic velocities $M_0 \approx 0.5$ ($\varepsilon_0 = 0.82$-0.935) and low Reynolds numbers $Re \approx 2 \cdot 10^5$ in one stage with a diameter of d = 730 mm nozzle grid height $l_1 = 43.9$ mm at $\alpha_1 = 13^\circ$ and $\beta_2 = 21^\circ$.

Figure 339 gives efficiency curves, depending upon x_ϕ, for different degrees of moisture. As the moisture increases, the graphs show a noticeable lowering in efficiency, and the flow rate coefficients also increase.

By the location of η_{oi} curves 1 and 3 it is clear that the influence of moisture increases as $x_ф$ increases. Obviously, this result can be explained by the sharp increase of the angle of entry of water droplets β_{1B} onto the rotor blades; the increase of β_{1B} turns out to be intense in connection with the fact that the velocity of the droplets decreases as $x_ф$ (since the steam velocity $c_{1п}$ then drops).

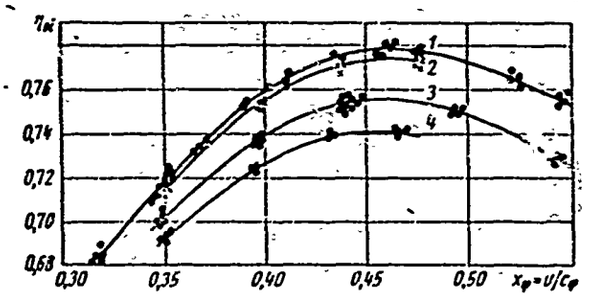

Fig. 339. Influence of moisture on the internal efficiency of a stage, according to the experiments of Yu. Ya. Kachurinner and I. P. Fadeyev (NZL) with $\theta = 14.6$, $\alpha_1 = 13°$, and $\beta_2 = 21°$; curves: 1 — superheated steam; 2 — $\chi_0 = 0.9$; $\chi_2 = 1.4\%$; 3 — $\chi_0 = 2.8\%$; $\chi_2 = 3.3\%$; 4 — $\chi_0 = 3.9\%$; $\chi_2 = 4.5\%$.

As can be seen from the curves on Fig. 340b, for the given $x_ф$ the decrease in efficiency $\Delta\eta_{oi}$ linearly increases from the initial degree of moisture, while at χ_0 = const it increases linearly, depending on $x_ф$. Let us note that the linear character of the curves for $\Delta\eta_{oi} = f(\chi_0)$ is confirmed also for a group of stages (see Fig. 338).

The experiments of the authors can be described by a formula of the following form:

$$\overline{\Delta\eta}_{oi} = \frac{\Delta\eta_{oi}}{\eta_{oi_{x=1}}} = k\chi_0 x_ф, \qquad (359)$$

where coefficient k varies within comparatively small limits. In accordance with the graphs on Fig. 340, it may be assumed that

$$k = 2{,}0-2{,}4;$$

χ_0 is the initial moisture in the stage.

It should be emphasized that formula (359) is valid for subsonic velocities. Considering, however, that the linear character of the dependence $\Delta\eta_{oi}(\chi_0)$ remains also for supersonic velocities, it is possible, assuming that k = 1.7-1.8, to also use it for this region.

Investigations of single-wheel stages for different degrees of moisture were conducted at MEI. Some results of these experiments, which are shown in Fig. 340a, partially confirmed the data obtained at NZL. Thus, for instance, it is confirmed that the lowering of stage efficiency linearly depends on $x_ф$. The data in § 53 concerning the influence of an increase in the degree of moisture on the increase

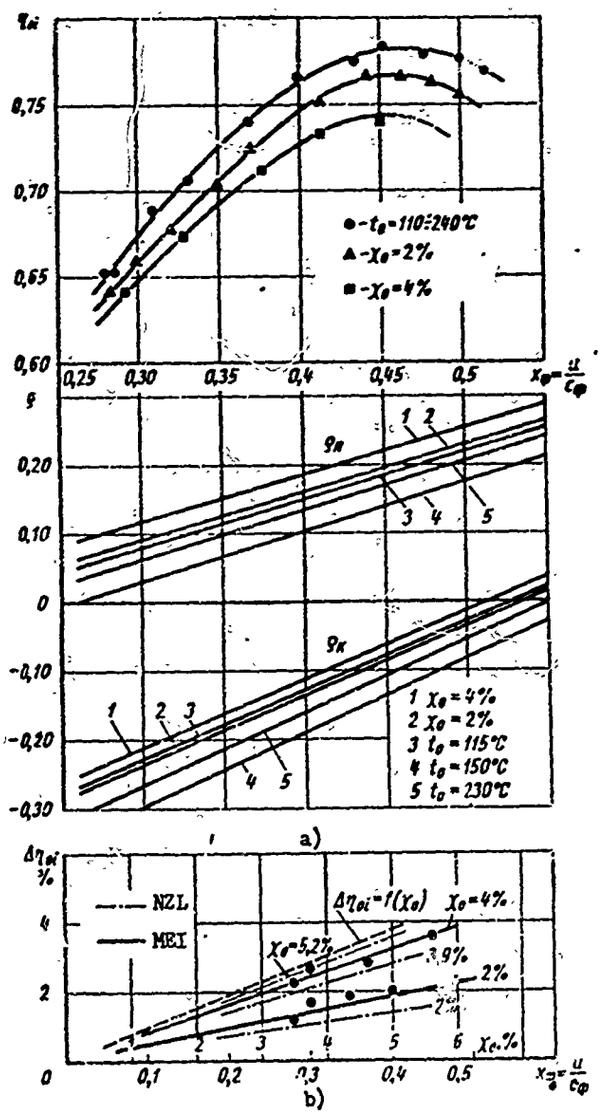

Fig. 340. Influence of steam moisture on stage performance: a – internal efficiency and reaction in root and peripheral sections, depending upon x_Φ and χ_0 (MEI experiments); b – lowering in efficiency, depending upon x_Φ for various χ_0; according to NZL experiments, curves – · – · –; for θ = 14.6, $\alpha_1 \approx 13^\circ$, and $\beta_2 = 22^\circ$; MEI experiments, —— (solid lines).

of the flow rate coefficient of a stage are also confirmed. The linear dependence of $\Delta\eta_{oi}$ on the initial degree of moisture is proved in the same way (Fig. 340b).

The obtainment of different absolute values $\Delta\eta_{oi}$ at MEI and NZL is explained by the design peculiarities of the test stages. Thus, for instance, the MEI stage was tested in an unshrouded model.

The experiments conducted at MEI also showed that the degree of moisture renders a noticeable influence on the stage reaction. With the increase of moisture, the reaction at the tip and in the root section increases, especially at large x_Φ (see Fig. 340). It may be assumed that the increase of the reaction is caused by the fact that the flow rate coefficients for a nozzle cascade increase more intensely than for a moving one (due to the larger convergence of channels). The decrease in steam velocity at the nozzle cascade outlet, in connection with additional losses due to moisture, has a well-known value. The angles of entry to the moving cascade β_1 increases then, and the reaction also increases. An analogous change of the angle β_1 and the reaction causes a decrease of the slip factor ν.

In the last stages of condensing turbines with large flare, the influence of

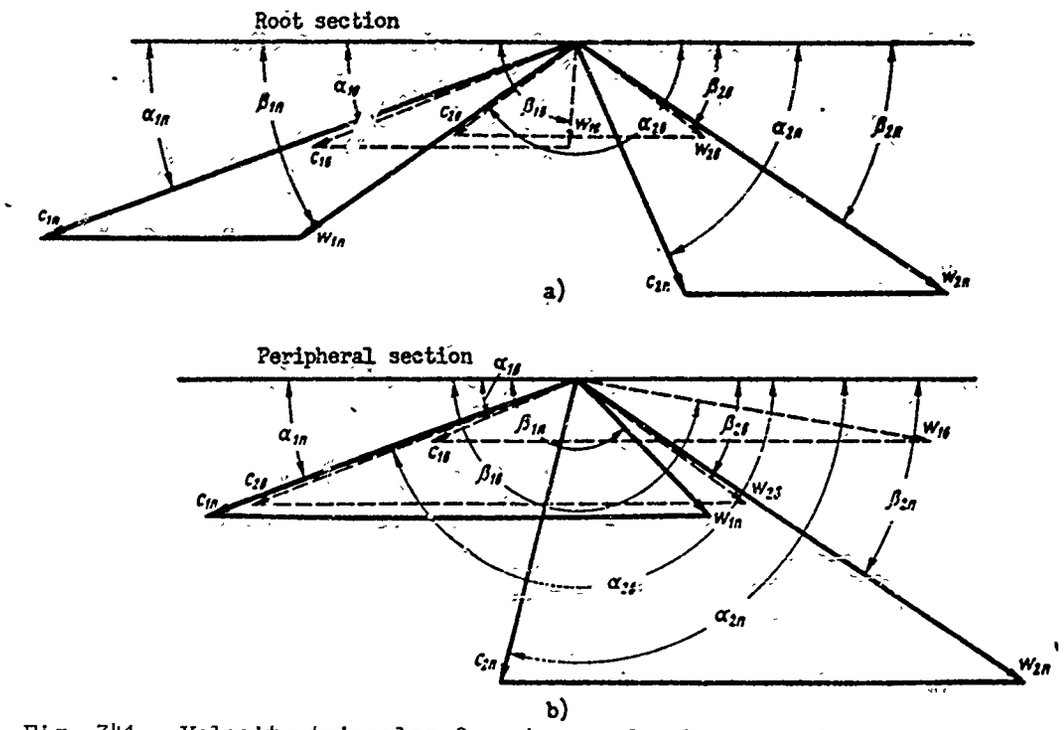

Fig. 341. Velocity triangles for steam and water: a – in root sections of large-flare stage; b – in peripheral; ——— (solid lines) for steam; – – – – (dotted line) – for moisture.

moisture will be different in the various sections along the blade height. Let us consider the velocity triangles in the peripheral and root sections of a stage (Fig. 341). The absolute steam velocity in a clearance $c_{1\,п}$ at the periphery will be considerably lower than in the root section. In accordance with this, the velocities of the moisture droplets $c_{1\,в}$ will be lower at the periphery (the ratio $c_{1\,в}/c_{1\,п}$ also decreases from root to periphery, since this quantity depends on the M number). In connection with the fact that the peripheral velocity increases toward the tip, the absolute value and the angles of the relative velocity of the droplets, $w_{1\,в}$ and $\beta_{1\,в}$, sharply increase toward the tip (see Fig. 341a). As a result, the braking action of the moisture droplets and the losses due to moisture intensely increase toward the peripheral sections, where, naturally, there is concentrated a larger quantity of moisture (the droplets of moisture are rejected to the periphery by centrifugal forces).

The stage outlet, in absolute motion, the moisture droplets have significantly greater swirling ($\alpha_{2\,в} \gg \alpha_{2\,п}$), which also leads to additional losses of energy.

From a consideration of the velocity triangles, it may be concluded that in the

the root sections the liquid phase, which causes losses, also develops some effective work and, in the peripheral sections, this work is a negative quantity. Consequently, the losses due to moisture in a stage with long blades are variable along the radius.

Investigations of large-flare stages in a region of moist steam are being conducted at this time on a very limited scale.

Of considerable interest are the results obtained by F. V. Kazintsev (MEI) in the investigation of a stage with $\theta = 2.74$. The experiments were conducted at low supersonic velocities ($M_0 = 1.04$, $\varepsilon = 0.52$) in a zone of low Reynolds numbers ($Re_{c_1} = (0.4\text{-}1.2)\cdot 10^5$) in superheated and moist steam. An increase of the Re_{c_1} number, which is carried out by lowering the initial superheating and increasing the final pressure, leads to an increase of stage efficiency (Fig. 342, curves 1 and 2). A further lowering of superheating to $\Delta t_0 = 1.4^\circ$ (curve 3) leads to an increase of the Re_{c_1} number ($Re_{c_1} = 1.2\cdot 10^5$) and to the appearance of moisture behind the stage, $\chi_2 = 1.6\%$.* However, the efficiency of the stage practically did not change. Only with the increase of moisture to $\chi_2 = 5.6\%$ (initial moisture $\chi_0 = 3\%$) an intense decrease in efficiency of the stage is noted.

Thus, the transition through the boundary curve during expansion in a stage, and the appearance of final moisture at low Reynolds numbers, when the influence of this parameter is considerable (conditions outside the zone of self-similarity), does not lead to a decrease in efficiency. In comparison with a zone of superheated steam (curve 1), the efficiency of a stage with little moisture (curve 3) is increased.

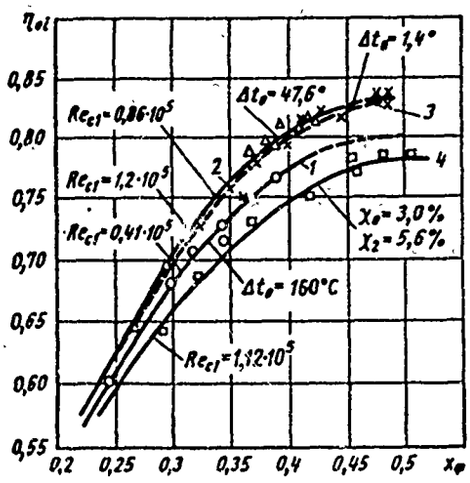

Fig. 342. Change of the efficiency of a stage with long blades at different Reynolds numbers, depending upon steam moisture; F. V. Kazintsev's experiments (MEI) with $\theta = 2.74$ and $\varepsilon = 0.52$ ($M_0 \approx 1.04$).

Consequently, in a zone of low Re_{c1} numbers and small amounts of steam moisture, the influence of the Re numbers is more essential.

Above we gave empirical formulas that made it possible to estimate the influence of moisture on the efficiency of turbine stages. This problem may be considered within the framework of the usual equations of one-dimensional

*Separation of moisture was not considered in the MEI experiments.

flow in a stage under certain simplifying assumptions. This problem was first solved by Tserkovits, who established the influence of stage parameters on the losses due to moisture.

We shall first determine the energy expended by a steam flow for accelerating the water droplets. The differential equation of impulses has the following form [110]:

$$m\chi_0 c_n dc_e - m\chi_0 c_e dc_e - dE = 0, \tag{360}$$

where dE is the impulse of dissipative forces, which is equivalent to the loss of kinetic energy during acceleration.

Considering that the steam velocity in the acceleration phase can be assumed as constant ($c_{1\ п}$), and the droplet velocities increase from zero to $c_{1\ в}$, and integrating expression (360), we will obtain:

$$\Delta E = m\chi_0 c_{1n} c_{1e}.$$

When the steam velocity in the acceleration phase is increased, the magnitude of the loss is determined by the following formula:

$$\Delta E = 0{,}65\, m\chi_0 c_{1n} c_{1e}.$$

The relative loss will be:

$$\overline{\Delta E} = \frac{\Delta E}{(1-\chi_2) m \frac{c_\phi^2}{2}} = 1{,}3 \frac{\chi_0}{1-\chi_2}\left(\frac{c_{1n}}{c_\phi}\right)^2 \frac{c_{1e}}{c_{1n}} =$$

$$= 1{,}3 \frac{\chi_0}{1-\chi_2} \varphi^2 (1-\varrho) \frac{c''_{1e}}{c_{1n}}, \tag{361}$$

Here χ_0 and χ_2 is the degree of moisture before and after a stage;

φ is the velocity coefficient;;

$c''_{1\ в}$ is the velocity of secondary droplets at the nozzle cascade exit.

We shall now determine the power developed by a stage in moist steam, considering the steam and water phases separately.

The power of the steam phase will be:

$$N_{in} = (1-\chi_2) m (H_0 - \overline{\Delta E})\, \eta_{oi}, \tag{362}$$

where $1 - \chi_2 = x_2$ is the degree of dryness behind the stage.

The power developed by the primary droplets that have formed in the given stage is equal to

$$N'_{ie} = (\chi_2 - \chi_0) m H_0 \eta'_e. \tag{363}$$

The quantity $1 - \chi_0 = x_0$ is the degree of dryness at the entrance to the stage;

η'_B is the efficiency of the primary water phase.

The power developed by the secondary droplets will be:

$$N''_{ie} = \chi_0 m H_0 \eta''_e \tag{364}$$

where η''_B is the efficiency of the secondary water phase, which proceeds from the preceding stage.

The stage efficiency in a region of moist steam is determined by the following formula:

$$\eta_{oi\,x} = \frac{N_{in} + N'_{ie} + N''_{ie}}{N_0},$$

where N_0 is the available power of the stage.

After substituting expressions (362), (363), and (364) into the last formula, we will obtain:

$$\eta_{oi\,x} = \frac{1}{mH_0}\left[(1-\chi_0)(H_0 - \Delta E)\eta_{oi} + (\chi_2 - \chi_0) \times \right.$$
$$\left. \times mH_0\eta'_e + \chi_0 mH_0\eta''_e\right]. \tag{365}$$

The relative decrease in efficiency is equal to

$$\overline{\Delta\eta_{oi}} = \frac{\eta_{oi} - \eta_{oi\,x}}{\eta_{oi}} = \chi_2\left(1 - \frac{\eta''_e}{\eta_{oi}}\right) - (\chi_2 - \chi_0) \times$$
$$\times \left(\frac{\eta'_e}{\eta_{oi}} - \frac{\eta''_e}{\eta_{oi}}\right) + (1 - \chi_2)\overline{\Delta E}. \tag{366}$$

Formula (366) can be simplified on the assumption that the primary droplets have the same efficiency as the steam phase.

Substituting the value of $\overline{\Delta E}$ into (366) according to formula (361), and using the condition of $\eta'_B \approx \eta_{oi}$, we can find the relative decrease in efficiency in the following form:

$$\overline{\Delta\eta_{oi\,min}} = \chi_0\left(1 - \frac{c''_{1e}}{c_{1\kappa}}\right)\left[1 + \frac{2}{\eta_{oi}}\left(\frac{u}{c_\phi}\right)^2\right] +$$
$$+ 1{,}3\chi_0 q^2 (1 - \varrho)\frac{c''_{1e}}{c_{1n}}, \tag{367}$$

and

$$\overline{\Delta\eta}_{oi\,max} = \chi_0 \left[1 - \frac{2}{\eta_{oi}} \frac{u}{c_\phi} \left(\varphi \sqrt{1 - \varrho} \cos\alpha_1 \times \right.\right.$$

$$\left.\left. \times \frac{c_{1a}}{c_{1n}} - \frac{u}{c_\phi}\right)\right] + 1{,}3\, \chi_0 \varrho^{3/2} (1 - \varrho) \frac{c_{1a}}{c_{1n}}. \qquad (368)$$

Formulas (367) and (368), which were obtained by Yu. Ya. Kachuriner, give the minimum and maximum decrease in the efficiency of a stage that is operating in a region of moist steam. The minimum values of $\Delta\eta_{oi\ min}$ correspond to case when the work accomplished by the droplets on the blades is maximum, and the maximum values ($\Delta\overline{\eta}_{oi\ max}$), when the work of the liquid phase is minimum.

It directly follows from formulas (367) and (368) that the dependence of $\overline{\Delta\eta}_{oi}$ on u/c_ϕ and the other stage parameters turns out to be considerably more complicated than shown by the empirical formulas.

It should be noted that for calculation of $\overline{\Delta\eta}_{oi}$ it is necessary to know the slip factor in a clearance ν, the procedure for whose calculation was presented in § 51.

A simpler formula can also be used for calculation of $\overline{\Delta\eta}_{oi}$ [110]:

$$\overline{\Delta\eta}_{oi} = \chi_0 \left[1 - \frac{2}{\eta_{oi}} \frac{u}{c_\phi} \left(\varphi \sqrt{1 - \varrho} \cos\alpha_1 \frac{c_{1a}}{c_{1n}} - \frac{u}{c_\phi}\right)\right], \qquad (369)$$

which satisfactorily coincides with the experimental data.

Tserkovits obtained formulas for the efficiency of a stage in moist steam in the following form:

$$\eta_{oi\,x} = \xi \eta_{oi}, \qquad (370)$$

where the coefficient ξ is determined separately for an impulse stage

$$\xi_a = \frac{\sqrt{x} \cos\alpha_1 - \frac{u}{c_1}}{\cos\alpha_1 - \frac{u}{c_1}} \qquad (371)$$

and a reaction stage

$$\xi_p = \frac{2\sqrt{x} \cos\alpha_1 - \frac{u}{c_1}}{2\cos\alpha_1 - \frac{u}{c_1}} \qquad (372)$$

the quantity $\chi = 1 - 1/2(\chi_0 + \chi_2)$ is the mean degree of dryness of a stage.

Formulas (369), (371), and (372) distinctly show that the influence of moisture at constant u/c_1 will be more essential at larger u/c_1, which is well confirmed qualitatively by experiments. As α_1 increases, the influence of moisture also increases.

The obtained theoretical and experimental results that show the influence of α_1 and x_Φ are physically explained quite simply: as α_1 and x_Φ increase, the stagnation effect of moisture increases in a stage, which may be seen from the velocity triangles.

Let us note that calculation by means of the Tserkovits formulas, (371) and (372), shows that with an increase of moisture by 1%, the efficiency of a stage decreases by 1 to 1.1%, which closely coincides with Bauman's data in which he proposed that $\xi = x$ in formula (370). It should be stressed that the theoretical considerations of Tserkovits concerning the decrease of the influence of moisture in a reaction stage [formula (372)] are not confirmed by experiments.

The presented method of determining the decrease in efficiency can also be extended to a large-flare stage. Two ways of solving the problem are possible.

1. The distribution of parameters of the steam phase is established with respect to the radius in a clearance with the additional losses due to moisture taken into account, and the quantity $\Delta\eta_{oi}$, which is variable along the radius, is calculated. A preliminary estimate of the moisture distribution with respect to the radius in a clearance is performed.

2. The field of velocities and pressures of the liquid and steam phases is calculated in a clearance and behind a stage and, on this basis, the additional stage losses are determined.

The first method, before obtaining reliable experimental data, is simpler and more reliable. The initial data are those from the stage calculation carried out for dry steam according to the equations of radial equilibrium, energy, and continuity (Chapters VII and VIII).

For estimating the moisture distribution with respect to the radius behind a nozzle cascade, it is possible in first approximation to take the linear law of $\chi(\bar{r})$. If, in the absence of moisture (see Chapter VIII), the distribution c_{1n} with respect to the radius is known, it is not difficult to find the slip factor ν_1 in the various sections. In this case, it is determined on graphs in Fig. 330 or analytically by means of formula (350) or (352).

After estimating the moisture χ_1 in an initial (root or middle) section, and assuming a linear law of increase of moisture toward the periphery, by means of formula (369) we find the decrease of efficiency in the various sections with respect to the radius, $\Delta\overline{\eta_{oi}} = f(\overline{r})$.

The mean value of the decrease in efficiency due to moisture for a stage is determined by the following formula:

$$\Delta\eta_{oi\,cp} = \int_0^G \Delta\eta_{oi}\,dG.$$

It is further necessary to find a more exact value of the distribution of the reaction with respect to the radius with moisture taken into account. For this purpose we shall use the continuity equation, after writing it for a separate stream in control sections in a clearance and behind the stage:

$$(1-\chi_1)\,\Delta G\cdot v_{1t} = \mu_1 c_{1t} f_1,$$
$$(1-\chi_2)\,\Delta G v_{2t} = \mu_2 w_{2t} f_2,$$

where ΔG is the flow rate of dry steam through an elementary stream;

v_{1t} and v_{2t} are the specific volumes at the end of isentropic expansion in the nozzle and moving cascades;

f_1 and f_2 are the areas of the outlet sections within the limits of one elementary stream;

μ_1 and μ_2 are the flow rate coefficients in a given annular section of the nozzle and moving cascades.

Hence we find the corrected values of c_{1t} and w_{2t}, and consequently, the values of the reaction for separate streams.

After determining the efficiency of a single stage, it is possible to estimate the change of the effectiveness of an entire group that is operating in a region of moist steam by the following formula:

$$\Delta\eta_{oi} = \frac{\chi_2}{2},$$

where χ_2 is the degree of moisture at the end of the actual process of expansion in a group of stages.

An essential influence on the efficiency of an entire turbine is rendered by the distribution of the available heat drop between the zones of superheated and moist steam. After designating

$$h_1 = \frac{H_{oH}}{H_0}; \quad h_2 = \frac{H_{oB}}{H_0},$$

where H_{OH} and H_{OB} are the available heat drops in the region of superheated and moist steam; $H_0 = H_{OH} + H_{OB}$; we can then obtain:

$$\eta_{oi\,x} = \eta_{oi}\left(h_1 + h_2 \frac{\chi_2}{2}\right), \tag{373}$$

where η_{oi} is the efficiency of a group of stages without moisture taken into account.

The Tserkovits method [formula (373)] was extended to a multistage turbine by L. I. Degtyarev. He obtained an expression similar to the following:

$$\eta_{oi\,x} = \eta_{oi}(h_1 + h_2 h_m), \tag{374}$$

where

$$h_m = \frac{\frac{1+\sqrt{1-\chi_2 T}}{2}\cos\alpha_{1\,cp} - \left(\frac{u}{c_1}\right)_{cp}}{\cos\alpha_{1\,cp} - \left(\frac{u}{c_1}\right)_{cp}},$$

$\alpha_{1\,cp}$ and $(u/c_1)_{cp}$ are the mean values of α_1 and u/c_1 for stages operating in a region of moist steam.

In conclusion, we shall give Forner's rather simple formula:

$$\eta_{oi\,x} = k\eta_{oi}, \tag{375}$$

where

$$k = 1 - h\frac{\chi_2 T}{2};$$

$$h = \frac{H_{oB}}{H_0},$$

$\chi_2 T$ is the degree of humidity at the end of the process of expansion in the turbine.

In comparing the various methods of estimating the effect of moisture on the efficiency of a stage and a turbine on the whole, let us note that the formulas which were derived theoretically (Tserkovits, Forner, Yu. Ya. Kachuriner, and others) and obtained experimentally (Melank, Pake, and others) give different results. The difference in the correction factors for moisture amounts to 2-4%. Elementary calculations by means of the given formulas show that with a change of moisture by 1%, the efficiency of a turbine on the whole varies in wide limits, depending upon the distribution of the heat drop between regions of superheated and moist steam.

Experiments on the study of the influence of moisture on the characteristics of a turbine stage, which were conducted in a number of laboratories with moist steam, are confirmed qualitatively by investigations in moist air.

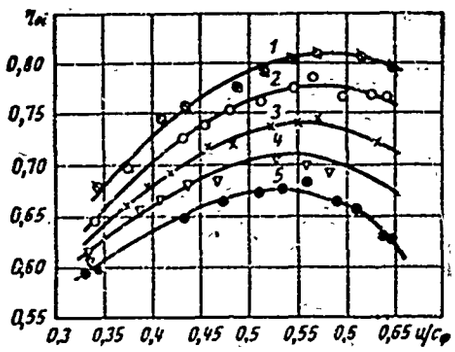

Fig. 343. Dependence of the efficiency of a stage on x_Φ and the degree of moisture during tests in moist air, according to R. M. Yablonik's data; $\theta = 10.45$ $M_{c1} \approx 0.3$; $Re_{c1} = 5 \times 10^5$; rotor blades are twisted according to the law c_{u1r} = const. Curves: 1) $\chi_0 = 0$; 2) $\chi_0 = 4.1\%$; 3) $\chi_0 = 7.0\%$; 4) $\chi_0 = 9.6\%$; 5) $\chi_0 = 12.9\%$.

Thus, Fig. 343 gives the efficiency curves of a stage with long blades, depending upon x_Φ and the degree of moisture, which were obtained by R. M. Yablonik in air experiments. The character of the location of the efficiency curves confirms the results obtained with moist steam for analogous values of M and Re numbers. The linear character of the change of losses due to moisture, depending upon x_Φ is also confirmed.

At the same time, the given results do not provide a basis for a generalization of the conclusions concerning the possibility of replacing moist steam by moist air in model investigations of stages. In spite of the fact that the quantitative coincidence of losses due to moisture in steam and air is satisfactory, extrapolation of these results to other M and Re numbers would be invalid.

§ 55. SOME RESULTS OF AN INVESTIGATION OF BLADE EROSION

As a static investigation shows, erosion of blade cascades at a given moisture content essentially depends on the length of operation, a number of design factors of the flow area, the technology of manufacture and the material of the blades, and also the thermo-and gas-dynamic stage parameters.

Of much interest are the results that indicate the influence of droplet size and the slip factor ν on the erosional damages to blades.

Available experimental data illustrate the influence of some of the enumerated factors on the intensity of erosional damage to blades. Table 25 and Fig. 344, which are borrowed from the work of G. Preiskorn [163], give the erosion characteristics for two types of turbine blades manufactured from various materials and placed in use for different lengths of time at various peripheral velocities and degrees of moisture.

Table 25. Influence of Certain Design and Performance Characteristics of Turbines on Erosional Damages to Blade Cascades

Type of turbine	Impulse	Relative	Impulse	Relative	Impulse	Reaction							Impulse			Reaction			Impulse, reaction					
Blade material	5% Ni																VSM						VIM	M5M
Operating time in hours, $\tau \cdot 10^{-3}$	3	3,5	8,5	2,5	10	4	20	35	15	10	30	30	40	50	28	23	30	2,4	7,5	5,0	7,5	11	15	7,5
Peripheral velocity on external diameter in m/sec	310	291	311	300	314	275	276	285	275	265	212	188	235	319	306	294	291	332	310	340	340	322	278	340
Degree of moisture X in %	11	10,12	8,5	8/9	8,5	12,5	8,5	9,5	8,5	8,5	7/9	8,5	7/8	8,5	8,5	10	9/10	10/12	13	13	13	9,10	10	13
Relative decrease of blade surface F/F_H in %	35	28	39	46	36	32	42	43	50	40	35	34	32	34	41	49	41	33	0	0,51	0,77	37	44	0,77
Designation in Fig. 344	a	m	f	i	g	q	o	n	r	s	t	v	u	e	h	l	k	b	w	x	y	j	p	y

First of all, it should be noted that the type of flow area slightly affects the intensity and character of erosional damages. As can be seen from Table 25 and Fig. 344, under identical operating conditions the erosional damages to blades of impulse and reaction flow areas remain approximately identical.

The development of the erosional process is nonuniform in time. Blades erode most intensely in the initial period of operation, which continues for 3000 to 5000 hours. During longer operation, erosional damages increase insignificantly. It should be emphasized that, depending on the quality of the material, the period of the most severe erosion is displaced in time: for high-alloy durable steel, intense erosion is detected at $\tau \geq 5$ to 8000 hours, and for blades made from low alloys, from the moment of the beginning of operation.

The bibliography presents data that indicate the features of the process of erosion which is caused by moisture droplets with high velocity and large angles of incidence that enter an operating channel, and consequently, strike against the surface of a blade. The degree of blade damage in this instance depends on one size and number of the droplets, the difference in the velocities of steam and moisture, and also on the crumpling resistance of the blade material.

The mechanism of erosion to the present time has not yet been sufficiently studied; however, the available results of observations distinctly show that the purely mechanical influence of droplets cannot explain the phenomenon of erosion [163]. As calculations show, the kinetic energy of the droplets is not sufficient enough to cause any considerable blade wear. In order to cause such wear during the interaction of the

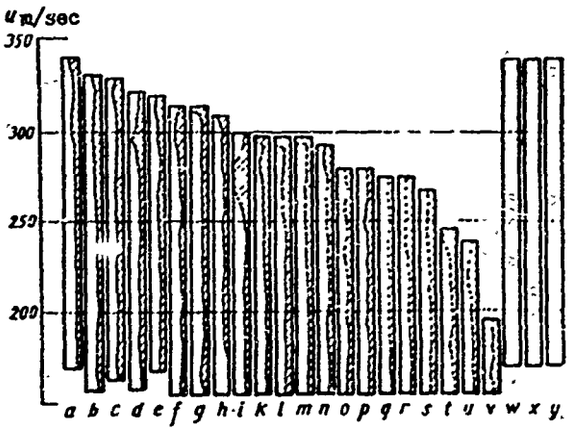

Fig. 344. Diagrams of erosional damage to blades of condensing steam turbines of various design (see Table 25).

droplets with the surface of a blade, very large forces must be developed; the local increases of pressure in this case must attain magnitudes of the order of 10,000 kg/cm^2. Such high pressures can appear only as a result of vapor separation. Consequently, it is possible to consider that erosion of blades working in a region of moist steam is caused mainly by vapor separation phenomena. A definite role is played here by both the mechanical and electrical influence of moisture on the blade surface.

During vapor separation there appear not only very high pressures, but also correspondingly high local temperatures, which cause chemical reactions on the blade surface. It should be emphasized that the available data indicate the possibility of the appearance of resonance, at which the frequency of pulsations in the bubbles is multiple to the frequency.

The complex role of the various factors that determine erosional wear indirectly is confirmed by experiments oriented on the study of the influence of the mechanical properties of the blade material: hardness, viscosity, and others.

From the conducted experiments, the influence of those properties of materials was not detected. However, nonmetallic inclusions have a negative effect on erosional wear, just as does the quality of treatment of the blade surface: roughness and unsatisfactory connection of the filler metal with the base material promotes erosional wear.

It should be noted that the protection of blades from erosional wear, besides the use of stellite filler plates, requires the application of other methods, such as electrolytic chrome-plating or electric-spark machinery of working surfaces.

Returning to the evaluation of the influence of external factors (size and velocity of droplets), let us note that experiments [163] confirmed the theoretically predicted influence of these factors. Erosional wear increases approximately in proportion to the absolute size of the droplets and in proportion to the square of the difference of the velocities of steam and water. Figure 345, which was

taken from the article by G. Preiskorn, represents the most important results of these experiments. It appears from them that the decrease of blade weight sharply increases with the increase of the peripheral velocity (the difference in velocities of steam and droplets increases in this case) for an identical duration of operation.* With the increase of the number of droplet impacts, the erosional wear at first increases sharply, and then decreases (Fig. 346).

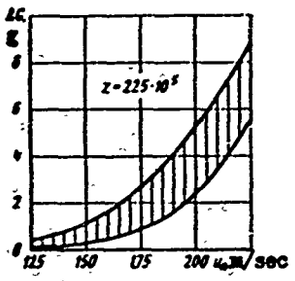

Fig. 345. Decrease in the weight of a rotor blade due to erosional wear, depending upon the peripheral velocity at the tip.

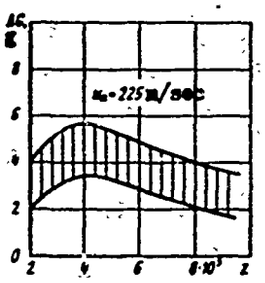

Fig. 346. Decrease in the weight of a rotor blade due to erosional wear, depending upon the number of droplet impacts.

On the basis of operational observations, and also the physical and theoretical considerations given above, it may be concluded that the erosional wear of turbine blade cascades can be essentially decreased if certain constructive measures are taken.

Thus, for instance, a decrease in number and extent of edge wakes behind a nozzle cascade, which are attained by increasing the relative pitch, careful profiling of the nozzle cascades, which ensure minimum losses, and thinning of the edges, makes it possible to decrease erosional wear, since in this case the formation of large droplets in a clearance is hampered.

A decrease of the transverse pressure gradients is also favorable in the peripheral channel sections, which leads to a lowered intensity of secondary leakages and erosional wear correspondingly. This is attained by decreasing the angle of rotation in the nozzle cascade and by selecting appropriate increased angles of entrance into the nozzle cascade. In moving cascades, if there are moisture collectors, it is expedient to apply large angles of rotation of the flow. Conversely, if there are no moisture collectors, the angles of rotation in the moving cascade should be decreased.

It is expedient to employ enlarged axial clearances between the edges of nozzle and rotor blades, which promotes a balancing of the flow in the clearance and dispersion of the droplets. Selection of enlarged clearances also ensures better

*The number of droplet impacts z is taken to be equal to the blade speed in a period of operation.

moisture separation.

The external configurations of cascades in the meridional plane should be smooth (conical ones are desirable) in order to ensure good separation of moisture.

It should be stressed that the application of protective coverings and fillers, stellite for instance, which are widely used in the turbine-construction industry, gives a noticeable effect only if the blade surface remains smooth and large temperature strains do not appear in the blade material.

§ 56. TUBINE MOISTURE COLLECTORS

An effective method of decreasing losses due to moisture in turbine stages and as a result of blade erosion is separation of moisture from the flow area by means of moisture collectors.

At present, various designs of separators are being employed; there are no reliable data that characterize the comparative advantages of the designs in use.

In turbine-construction practice, two basic types of moisture collectors are applied. The first type includes devices which use the effect of separation of water droplets under the action centrifugal forces; the second type includes devices in which moisture suction on the periphery of a stage is additionally utilized.

We shall consider some of the most popular designs of moisture collectors. Figure 347 shows diagrams of the first type which is employed by domestic and and foreign turbine-construction firms. The moisture collector (see Fig. 347a) consists of moisture-collecting channel 3 and a moisture-retaining chamber 2 with projections 4 and drain channels 1. A shortcoming of this design is the relatively narrow and long moisture-collecting channel.

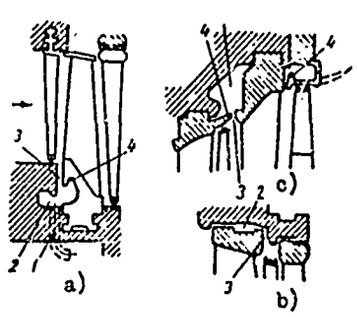

Fig. 347. Diagrams of moisture collectors without vapor suction for low-pressure steam turbine stages: 1 — drainage of moisture; 2 — moisture-retaining chamber; 3 — moisture-outlet ducts; 4 — moisture-retaining projection.

A characteristic feature of the moisture-collecting system of the GE Company (see Fig. 347b) is the shorter and wider inlet channel. Furthermore, moisture is collected behind the nozzle cascade of the last stage in this case, which decreases the intensity of erosion. The design shown in Fig. 347c permits separation behind the nozzle and moving cascades through one moisture-outlet channel 3 into a common chamber 2.

Domestic turbine designs have also worked out certain progressive solutions and, in particular, individual separation of moisture behind the nozzle and moving cascades is performed (KTZ, LMZ, and KhTGZ designs). The most promising designs are those with repelling projections which are being applied in the latest models of large turbines of KhTGZ.

Figure 348 gives diagrams of moisture collectors with vapor suction. The design illustrated in Fig. 348a employs suction into a condenser by one channel which is connected to the outlet channels of the last two stages. The outlet channels are very long, and consequently, they have increased resistance. Since there is no collecting chamber, the suction system must provide for considerable velocities which would stop the moisture from falling back into the flow area.

Another type moisture collector with suction is shown in Fig. 348b. Here, besides the very well-developed system of moisture collectors, separating sheets are employed, the purpose of which reduces to separating the wettest peripheral layer of steam and draining it into a condenser (past the rotor blades).

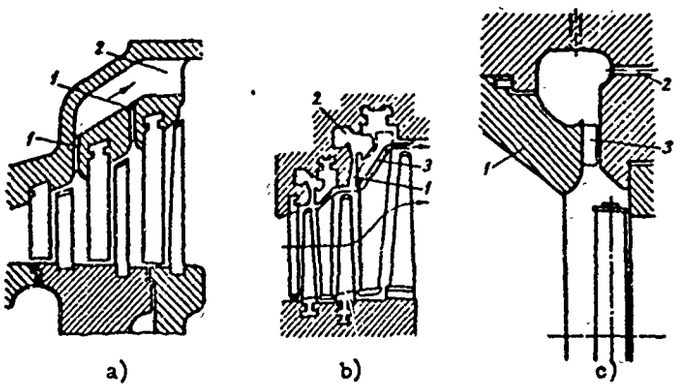

Fig. 348. Diagrams of moisture collectors with vapor suction for low-pressure steam turbine stages: a — 1 — moisture-outlet channels; 2 — suction chamber; b — 1 — moisture-outlet channel 2 — moisture-retaining chamber; 3 — moisture-separating sheets, c — 1 — diaphragm; 2 — parts for suction of steam-water mixture; 3 — guide inserts.

Another promising device is the one with guide inserts in the moisture-outlet channel (see Fig. 348c). The guide inserts prevent the return of condensed steam from the upper part of the chamber and guide it into the lower part of chamber, and from there the moisture is absorbed into the condenser.

This brief survey of the types of moisture collectors shows the large variety of designs employed by various firms. The operational experience of various machines confirms that the design of moisture collectors, their location with respect to the rotor wheel and nozzle cascade, the size of the clearances, the width of the blades, the presence or absence of a shroud on the rotor blades, etc. all have an influence on the effectiveness of separation.

However, there are still no complete experimental data concerning the comparative merits of the various designs moisture collects and the influence of the most important performance and geometric stage parameters on the effect of separation.

At the same time, certain investigations of moisture separation in moist steam and air are presently being conducted; these studies make it possible to evaluate the individual designs of such devices. The expediency of moisture separation behind a nozzle cascade was shown in the BITM projects. Partial removal of moisture before the rotor wheel decreases the erosion of rotor blades and reduces additional stage losses.

R. M. Yablonik investigated the effectiveness of the three types of moisture collectors that are shown in Fig. 349. These designs differed in dimensions and shape of the outlet channel, and also in the size of the closed axial clearance at the periphery. A result of these experiments was the obtainment of a dependence of the moisture-removal factor:

$$\bar{q}' = \frac{q}{q_n},$$

where q is the quantity of outgoing moisture;

q_n is the quantity of moisture supplied to a stage, depending on the degree of moisture in the presence of open axial clearances δ_a (see Fig. 349).

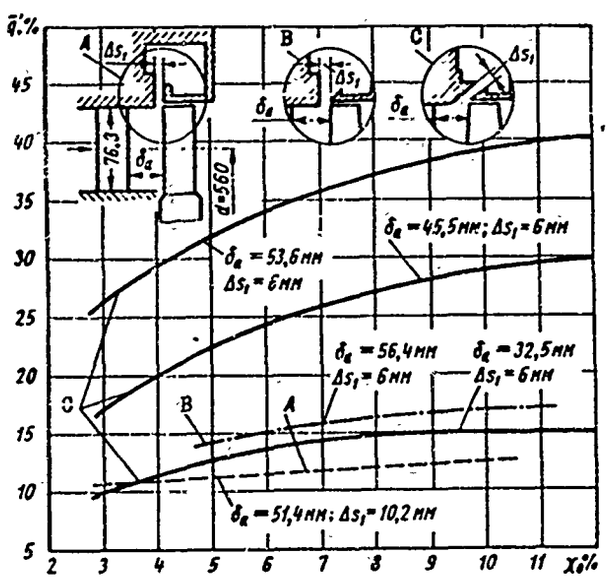

Fig. 349. Dependence of the moisture-removal factor $\bar{q}'$ on the degree of moisture for three types of moisture collectors; according to R. M. Yablonik (BITM); stage $\theta = 7.35$; $\alpha_1 \approx 13^\circ$; $M_{c1} \approx 0.3$; $Re_{c1} \approx 5 \cdot 10^5$; for different values of Δs_1 – the width of the moisture-outlet channel and the dimensions of the axial clearance δ_a.

With a practically identical width of the outlet channel ($\Delta s_1 \approx 6$ mm), the best results are obtained with a moisture collector that has a channel inclined at an angle of 40° and a smooth, rounded entrance (model C). With the increase of the clearance,* the effectiveness of all models increases, and

*The distance between the trailing edges of the nozzle cascade and the back edge of the channel.

especially intensely in the case of model C. Considerable better results were exhibited by model B with a straight, short channel. Model A, with the long, straight moisture-outlet channel, is the least effective.

The moisture-removal factor increases as the degree of moisture increases, whereby the intensity of the increase of $\bar{q}$ burns out to be greater for model C.

Model C was tested with positive, zero, and negative overlaps, whereby the introduction of the zero, and all the more so, the negative overlap, promoted a noticeable increase in the moisture-removal factor. An increase of the channel width increases the effectiveness of models A and B.

Investigations of several types of moisture collectors placed behind rotor blades are conducted at TsKTI by A. N. Astaf'yev [4].

Four models are shown in Fig. 350. Model I was made with guide inserts 5 which prevent the moisture from falling into the flow area. Model II, III, and IV differ only in the shape of the moisture-retaining ring 7.

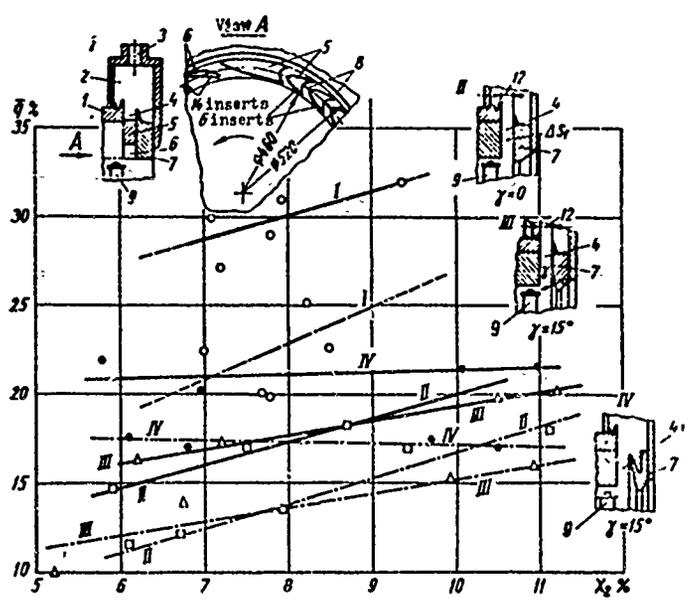

Fig. 350. Effectiveness of four types of designs of moisture collectors placed behind moving cascades (TsKTI data [4]): 1 – with guide inserts; II, III, IV – with different moisture-retaining ducts and no guide inserts; 1 – casing of device; 2 – moisture-collecting chamber; 3 – port for steam suction; 4 – annular moisture-outlet channel; 5 and 6 – guide inserts; 7 – moisture-retaining ring; 8 – radial moisture-outlet channels; 9 – rotor blade.

The effectiveness of the device was characterized by the following quantity:

$$\bar{q} = \frac{q}{q_{cm}},$$

where q_{CT} is the quantity of moisture behind a stage.

The results of the tests show that model I is more effective under all conditions. The quantity of separated moisture here reaches 24% with the degree of moisture behind the stage $X_2 = 8.5\%$.

Models II and III have practically identical effectiveness ($\bar{q}_{II,\ III} = 14\%$); model IV, with the indicated moisture content, separates the moisture somewhat better ($\bar{q}_{IV} = 17\%$).

The advantages of model I become especially noticeable in the organization of the suction. In this case, when $\chi_2 = 8.5\%$, $\bar{q}_I = 30\%$, $\bar{q}_{II,III} = 18\%$, and $\bar{q}_{IV} = 21\%$.

Interesting data concerning the influence of certain design parameters of a moisture collector behind rotor blades and a stage of the effectiveness of separation were obtained in the works of R. M. Yablonik with moist air [129]. Diagrams of models of the tested device are shown in Fig. 351.

A stage ($\theta \approx 10$) with twisted rotor blades and no shroud was tested. Models I, III, IV, and V differ by the presence and location of the moisture-retaining projections. Model II is similar to model I, but it has a partially open end surface of unshroud rotor blades. Model V has a long moisture-outlet channel.

Figure 351 gives the dependences of the moisture-removal factor on the degree of moisture. The distance between the trailing edges of the rotor blade and the back wall of the moisture-outlet channel Δs_2 was selected as identical ($\Delta s_2 = 15$ mm). The opening of the end surface of the rotor blades amounted to $\Delta B = 5$ mm ($\bar{\Delta B} = \frac{\bar{\Delta B}}{B_2} \approx 14\%$).

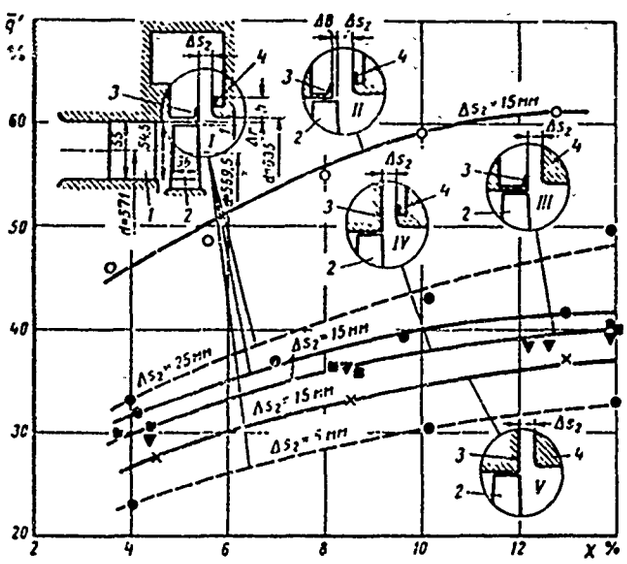

Fig. 351. Diagrams of models of a moisture collector and their characteristics, $\bar{q}'$, depending upon moisture content and design parameters; according to BITM experiments: 1 — nozzle cascade; 2 — moving cascade; 3 — front wall of moisture-outlet channel; 4 — back wall of moisture-outlet channel.

The experiments showed that the effectiveness of separation increases with the increase of the degree of moisture, especially for small values of χ. This result is obvious, since the dimensions and the mass of the droplets, and consequently, the centrifugal forces acting on the droplets, increase as the moisture increases.

The experiments confirmed that partial opening of the end surface of a blade (model II) essentially increases the effectiveness of separation, since in this design a considerably greater quantity of moisture goes into the moisture-outlet channel. An increase of the opening ΔB (see Fig. 351) will lead an increase of the effectiveness of moisture removal; however, the stage efficiency will then decrease.

The experiments conducted by the author showed that a relative opening of $\overline{\Delta B} \approx 20$ to 25% does not cause a noticeable lowering of efficiency. In this connection, let us note the efficiency of a stage only slightly depends on the quantity of moisture separated. This result indicates that the stagnation influence of the moisture droplets does not render as large an influence on efficiency as was assumed earlier.

These experiments resulted in an evaluation of the influence of the width of the moisture-outlet channel Δs_2 on the effectiveness of separation. The corresponding results, which are shown in Fig. 351, confirm the expediency of employing wide moisture-outlet channels. With the application of narrow channels, just as with complete closure of the end surface of the blades, some of the moisture falls back into the steam flow and goes into the following stage.

The author also estimated the influence of overlap Δr (see Fig. 351). With the decrease of Δr from 4.5 mm to 0, the coefficient $\overline{q}'$ increased by 15 to 20% with the degree of moisture $\chi = 4$ to 14%. These experiments confirmed the expediency of employing "moisture-repelling" projections.

Of importance are the number and location of the moisture-retaining projections that prevent the return of moisture and ensure the best conditions of moisture outlet into the chamber and the drain. The results of comparative tests of models I, III, IV, and V show that designs III and IV have approximately identical effectiveness, and model I has a maximum coefficient $\overline{q}'$. Moisture is removed in model V in the poorest manner.

An investigation of the effect of projection height h showed that a decrease of this parameter improves the work of the separating device. Inclination of the back wall of the channel impairs the separation conditions, since the entrance to the moisture-retaining chamber is then closed.

The separating ability of a stage is influenced by some of its geometric parameters, in particular, the outlet angles of the nozzle (α_1) and moving (β_2) cascades, and also the ratio $\theta = d/l$ and the axial clearance δ_a.

Between the quantities θ, α_1, and δ_a there exists a dependence which is approximately established from the condition that the moisture droplets which leave the nozzle cascade fall into the area of the peripheral section. This condition determines the size of the necessary axial clearance, δ_0, depending on α_1 and θ.

Assuming that only part of the moisture proceeding from the upper portion of the nozzle cascade should be separated in the clearance, this dependence can be

obtained in the following form [5]:

$$\frac{\delta_{a\,min}}{l_1} = \frac{\operatorname{tg} \alpha_1}{2} \sqrt{2\theta + 1}.$$

It follows from this that the minimum axial clearance that is necessary for separation of moisture decreases as θ, c_1, and the height of the nozzle cascade l_1 decrease. However, even under the assumed condition of separation of moisture only from the upper half of the nozzle cascade, the necessary axial clearances are very large.

Final selection of the axial clearance should be performed taking into account the influence of the clearance on the aerodynamic losses in the stage (see § 40). In particular, it is necessary to consider the additional losses due to friction, swirling of the flow, the vortex effect in the stage, and also the influence of nonuniformity at the entrance to the moving cascade.

With the increase of the clearance, the additional losses due to friction and losses due to expansion of the flow in the clearance increase. Furthermore, the degree of moisture increases in the root sections, which is caused by the vortex effect (see § 35 and 41) and leads to more intense supercooling of steam in these sections.

For these reasons, in spite of the favorable influence of the decreasing nonuniformity at the entrance to the moving cascade, the size of the axial clearance $\delta_{a\,min}$ should be selected on the basis of an experiment that takes into account the influence of all the ennumerated factors.

APPENDIX

I/1 and I/2. Aerodynamic characteristics of a nozzle cascade for subsonic velocities (MEI profile TC-2A).

C-9015A
(TC-2A)

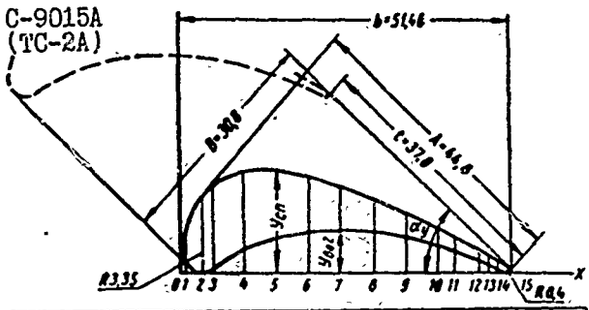

№№	0	1	2	3	4	5	6	7	8	9	10	11	12	13	14	15
x мм	0,00	0,88	3,35	5,33	10,24	15,28	20,33	25,37	30,57	35,46	40,50	43,07	46,80	48,37	49,80	51,46
$y_{сп}$ мм	3,35	7,69	11,72	13,30	14,87	14,67	13,64	12,25	10,36	8,36	6,04	4,85	2,97	2,12	1,39	0,40
$y_{вл}$ мм	3,35	1,15	0,00	0,60	3,32	4,91	5,65	5,85	5,45	4,68	3,52	2,83	1,60	1,02	0,43	0,40

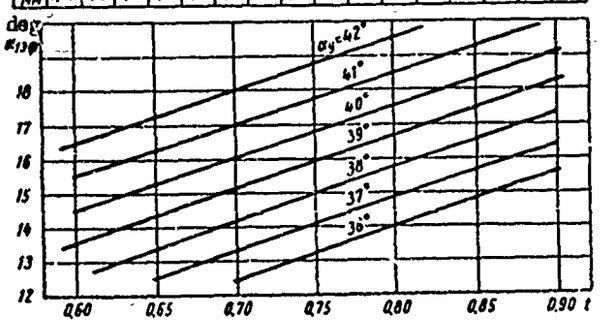

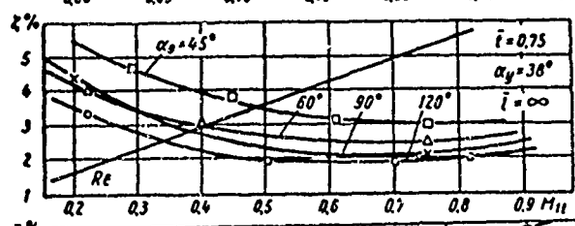

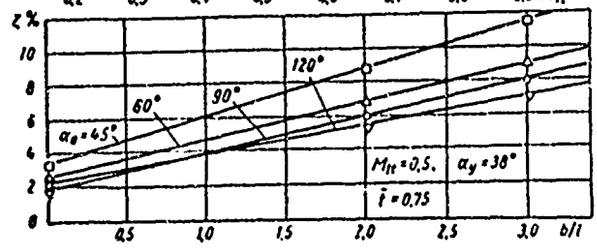

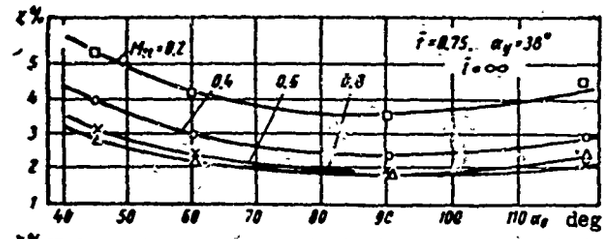

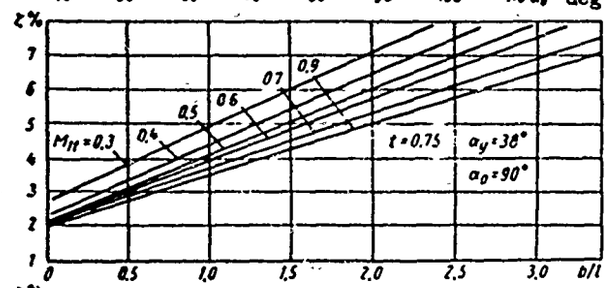

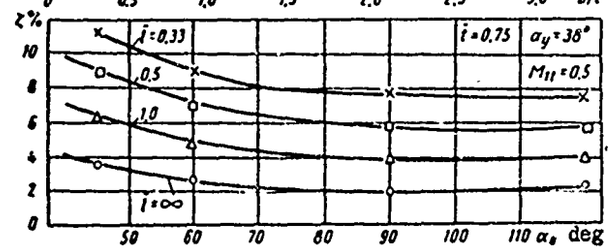

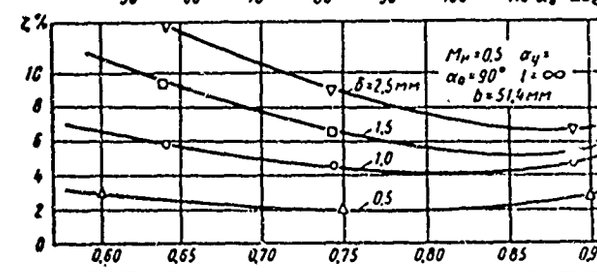

f см²	X_0 мм	Y_0 мм	J_{xx} см⁴	$W_{xx}^{сп}$ см³	$W_{xx}^{пр}$ см³	J_{yy} см⁴	$W_{yy}^{вл}$ см³	$W_{yy}^{вых}$ см³
3,3	17,47	2,96	0,36	0,45	0,51	4,63	2,58	1,39

II. Aerodynamic characteristics of a moving impulse cascade for subsonic velocities (MEI profile TP-2A)

P-3525A

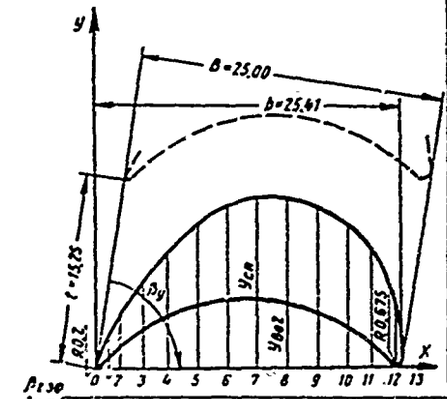

№	X мм	y_{cn} мм	$y_{вн}$ мм
0	0,00	0,20	0,20
1	1,06	2,20	0,97
2	2,80	3,90	1,87
3	4,80	6,87	3,27
4	6,80	9,34	4,29
5	8,50	11,63	5,11
6	11,00	13,15	5,52
7	13,50	13,87	5,54
8	16,06	14	5,18
9	18,50	12,83	4,41
10	21,00	11,43	3,17
11	23,50	9,20	1,75
12	25,00	4,90	0,00
13	25,41	0,68	0,68

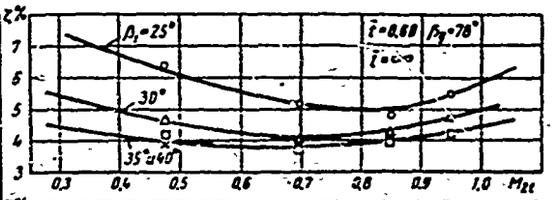

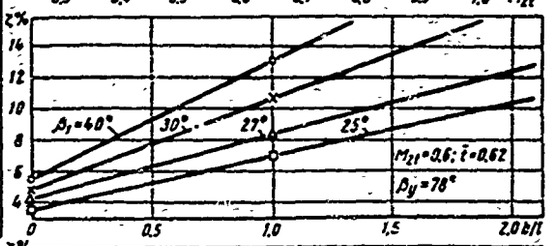

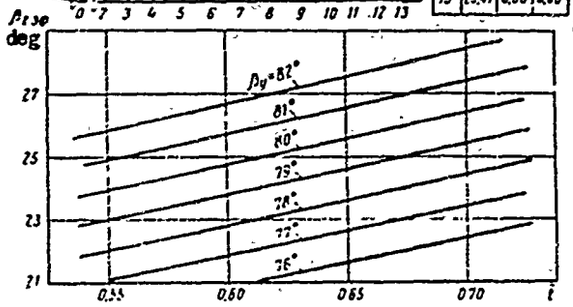

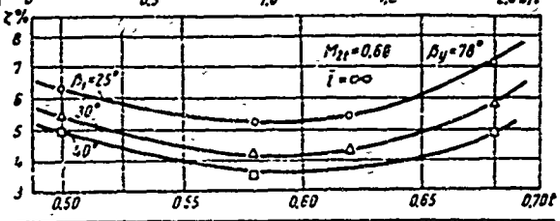

f см²	X_0 мм	Y_0 мм	J_{zz} см⁴	W_{zz}^{cn} см³	$W_{zz}^{вн}$ см³	J_{yy} см⁴	W_{yy}^{cn} см³	$W_{yy}^{вн}$ см³
1,65	14,49	6,97	0,1415	0,227	0,150	0,664	0,616	0,473

III. Graph of the dependence of function δ on $\bar{n}_{зог}$ and n for calculation of curvilinear channels according to the method of A. N. Sherstyuk

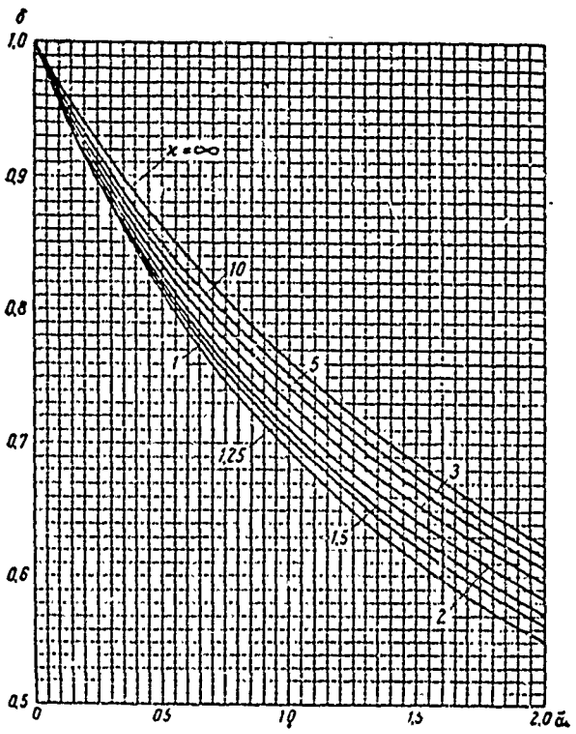

IV. Graphs of functions for calculating the depth of impulse losses of a turbulent boundary layer at moderate and large longitudinal pressure gradients

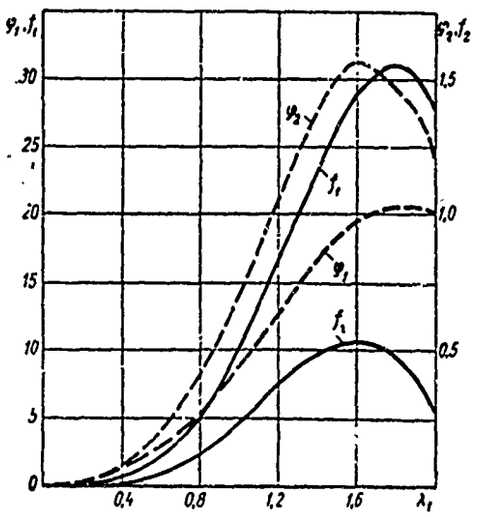

V. Graphs of functions for calculating the depth of impulse losses of a turbulent boundary layer at moderate and large longitudinal pressure gradients

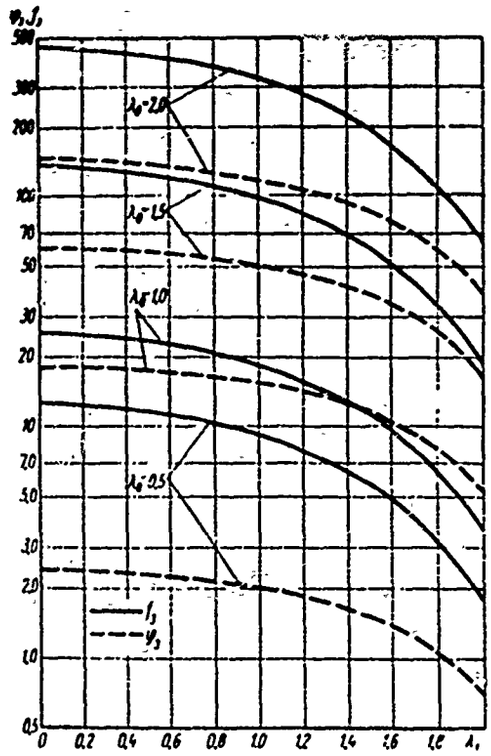

VI. Velocity of propagation of small disturbances (velocity of sound) depending on the degree of dryness and the saturation temperature for steam, according to V. V. Sychev (MEI)

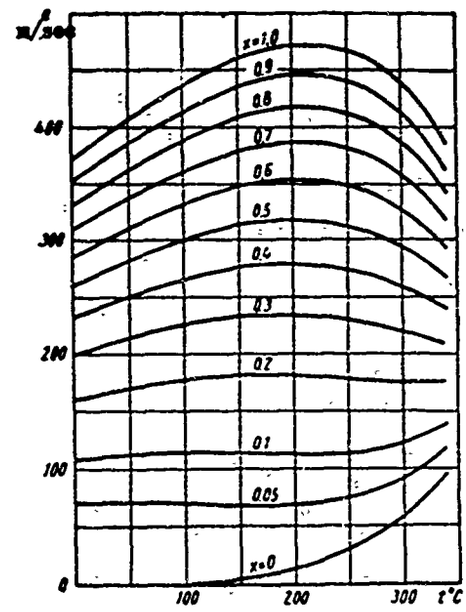

LITERATURE

1. V. D. Abiants. Theory of aviation gas turbines. Oborongiz, 1953.

2. V. I. Abramov and B. M. Troyanovskiy. Selection of optimum characteristics for a partial stage. "Heat power engineering," 1962, No. 6.

3. R. N. Alekseyeva, I. D. Lyakhovitskiy, and Yu. V. Rzhenznikov. Test procedure for short turbine blades and their profiling. "Heat power engineering," 1956, No. 6.

4. A. N. Astaf'yev. Some results of an experimental investigation of moisture collectors of steam turbines. "Power equipment construction," 1960, No. 2.

5. Aerodynamics of the flow area of steam and gas turbines, edited by I. I. Kirillov. Mashgiz, 1958.

6. Kh. L. Babenko. Axial forces in steam turbines. "Electric power plants," 1959, No. 2.

7. Kh. L. Babenko. Investigation of gas turbine stage with a small D_{mn}/l ratio. "Heat power engineering," 1961, No. 2.

8. L. B. Belik. Application of theoretical and experimental methods for designing impulse turbine cascades. "Heat power engineering," 1958, No. 8.

9. Ye. I. Benenson. Performance of the last stage of a condensing turbine with small volume steam admissions. "Power equipment construction," 1960, No. 12.

10. N. N. Bykov. Turbine investigations with various laws of profiling. News of higher education institutions. "Aeronautical engineering," 1961, No. 1.

11. E. G. Bratuta. Concerning the problem of determining the flow rate coefficient when subjecting a two-dimensional cascade to a blast of superheated steam. KhPI Transactions, Volume XXXVI, 1961.

12. I. M. Vol'fson. A rough estimate of the influence of sinking the trailing edges of blades on end losses of energy in straight profile cascades. LMZ Collection. No. 6, Mashgiz, 1960.

13. I. M. Vol'fson, V. S. Yelizarov, A. O. Lopatitskiy, et al. Aerodynamic research on plane and annular cascades with TS-2A MEI profiles. MEI Transactions, 1963.

14. V. A. Vrublevskaya. The influence of initial turbulence of flow on the performance of guide and moving cascades of turbines. "Heat power engineering," 1960, No. 6.

15. V. A. Vrublevskaya. Concerning the problem of the influence of turbulence of an external flow on a turbulent boundary layer. News of higher educational institutions. "Power engineering," No. 7, 1960.

16. A. K. Garkusha and M. F. Fedorov. Investigation of the influence of overlap on the efficiency of a turbine stage. KhPI Transactions, Volume XL, 1962.

17. I. L. Gazheman. The influence of technological deviations on end losses in the guide vanes of welded diaphragms. Collection of transactions of the Institute of heat power engineering of the Academy of Sciences USSR, 1958, No. 14.

18. S. V. Grishchuk. Aerodynamic research on NZL turbine stages with twisted blades. "Power equipment construction," 1957, No. 4.

19. S. V. Grishchuk. An investigation of T-1H blading. "Power equipment construction," 1961 No. 7.

20. Ye. A. Gukasov, M. I. Zhukovskiy, A. M. Zavadovskiy, et al. Aerodynamic improvement of blade cascades of turbines. State power engineering publishing house, 1960.

21. L. I. Degtyarev. The influence of steam moisture on the efficiency of a steam turbine. "Heat and Power," 1933, No. 12.

22. M. Ye. Deych. Technical gas dynamics. Stage power engineering publishing house, 1961.

23. M. Ye. Deych, V. A. Baranov, V. V. Frolov, et al. The effect of blade height on certain characteristics of single-wheel turbine stages. "Power equipment construction," 1961, No. 1.

24. M. Ye. Deych and A. V. Gubarev. Investigation of impulse cascades at high velocities. "Heat power engineering," 1958, No. 12.

25. M. Ye. Deych and A. V. Gubarev. Concerning the problem of "choking" of the delivery nozzle of a moving cascade of profiles in a supersonic flow. "Heat power engineering," 1960, No. 12.

26. M. Ye. Deych, A. V. Gubarev, and V. V. Frolov. Investigation of new profiles for cascades of regulating stages and pressure stages. "Heat power engineering," 1956, No. 5.

27. M. Ye. Deych and A. Ye. Zaryankin. An experimental investigation of a turbulent boundary layer. "Heat power engineering," 1958, No. 3.

28. M. Ye. Deych, A. A. Zaryankin, G. A. Filippov, et al. Increase of efficiency of impulse turbine cascades of low height. "Heat power engineering," 1960, No. 8.

29. M. Ye. Deych, F. V. Kazintsev, L. K. Kiselev, et al. Investigation of variable conditions of stages with long blades of constant profile. "Heat power engineering," 1959, No. 6.

30. M. Ye. Deych, L. Ya. Lazarev, A. V. Gubarev, et al. Investigation of new MEI cascades for supersonic velocities. "Heat power engineering," 1962, No. 10.

31. M. Ye. Deych, K. A. Rozanov, and V. V. Frolov. Investigation and improvement of the profiles of a double-wheel regulating stage. MEI Transactions, No. 23, 1955.

32. M. Ye. Deych, G. S. Samoylovich, B. M. Troyanovskiy, et al. Investigation of double-wheel regulating stages in an experimental steam turbine. "Heat power engineering," No. 5, 1957.

33. M. Ye. Deych and G. S. Samoylovich. Fundamentals of the aerodynamics of axial turbomachines. Mashgiz, 1959.

34. M. Ye. Deych, B. M. Troyanovskiy, F. V. Kazintsev, et al. Comparative studies of double-wheel velocity stages. "Heat power engineering," 1958, No. 5.

35. M. Ye. Deych, B. M. Troyanovskiy, F. V. Kazintsev, et al. Investigation of a series of single-wheel stages. "Heat power engineering," 1959, No. 4.

36. M. Ye. Deych, B. M. Troyanovskiy, V. I. Abramov, et al. Investigations of partial input of double-wheel velocity stages. "Power equipment construction," 1961, No. 3.

37. M. Ye. Deych and G. A. Filippov. Calculation of turbine stages with long blades of variable profile. "Heat power engineering," 1961, No. 9.

38. M. Ye. Deych, A. Ye. Zoryankin, G. A. Filippov, et al. A method for increasing the efficiency of turbine stages with low blade heights. "Heat power engineering," 1960, No. 2.

39. M. A. Deych and A. G. Sheynkman. Determination of the optimum size of the upper overlap of a shrouded turbine stage. "Heat power engineering," 1962, No. 1.

40. M. Ye. Deych and A. G. Sheynkman. Investigation of the cascades of rotor diaphragms. "Heat power engineering," 1963, No. 1.

41. A. A. Dorfman and S. V. Grishchuk. A study of turbine stages with sheet guide vanes. "Power equipment construction," 1958, No. 12.

42. G. S. Zhiritskiy. Aviation gas turbines. Oborongiz, 1950.

43. M. I. Zhukovskiy. Calculation of the flow around cascades of profiles of turbomachines. Mashgiz, 1960.

44. M. I. Zhukovskiy, N. I. Durakov, and O. I. Novikova. Calculation of the potential flow of an incompressible fluid past arbitrary cascades of blade profiles on an electronic computer. "Heat power engineering," 1963, No. 6.

45. M. I. Zhukovskiy and N. A. Sknar'. New cascades of turbine profiles. "Heat power engineering," 1955, No. 1.

46. M. I. Zhukoskiy, N. A. Mikhaylov, et al. Investigation and aerodynamic improvement of cascades of blades of the last stage of the K-300-240 turbine produced by the S. M. Kirov KhTGZ. "Heat power engineering," 1962, No. 4.

47. V. M. Zavadovskiy. Design fundamentals of the flow area of steam and gas turbines. Mashgiz, 1960.

48. G. A. Zal'f and V. V. Zvyagintsev. Heat calculation of steam turbines. Mashgiz, 1961.

49. A. N. Zanadvorova. Calculation of losses due to the radial clearance of rotor blades. "Power equipment construction," 1960, No. 10.

50. A. S. Zil'berman. Experimental research in the field of steam and gas turbine construction. Collection: "The development of technology at LMZ." Mashgiz, 1957.

51. L. N. Zysina-Molozhen. An approximate method for calculating losses in cascades of blades of turbomachines. "Heat power engineering," 1955, No. 9.

52. Yu. Ya. Kachuriner. Investigation of double-wheel velocity stages of steam turbines. "Power equipment construction," 1959, No. 7.

53. Yu. Ya. Kachuriner. Test of a KB-16 double-wheel velocity stage. "Power equipment construction," 1960, No. 9.

54. Yu. Ya. Kachuriner. Determination of the velocity of water droplets, attracted by the flow of a gas. "Journal of engineering physics," Volume III, No. 10, 1960.

55. I. I. Kirillov. Gas turbines and gas turbine power plants. Mashgiz, 1956.

56. I. I. Kirillov. The influence of the shape of the low-pressure flow area of steam turbines on efficiency. "Power equipment construction," 1961, No. 12.

57. I. I. Kirillov and R. M. Yablonik. The influence of a closed axial clearance on the efficiency of impulse stages with cylindrical blades. "Power equipment construction," 1957, No. 5.

58. I. I. Kirillov and R. M. Yablonik. Characteristics of turbine stages at various angles of rotation of guide blades. "Power equipment construction," 1961, No. 6.

59. G. M. Konovalov, A. K. Kirsh, and V. P. Markin. The economy of the VKT-100 steam turbine of the Kharkov plant. "Heat power engineering," 1960, No. 3.

60. Yu. F. Kosyak. An experiment in moisture removal in turbine stages operating in a region of moist steam. "Power equipment construction," 1958, No. 9.

61. I. A. Lavrov, T. M. Zil'ber, and A. M. Zavadovskiy. Test facility of the EPT-2 experimental turbine at the Kirov KhTGZ, "Power equipment construction," 1960, No. 11.

62. Z. L. Lapteva and A. O. Lopatitskiy. "The ETV-1 experimental air turbine and its test facility. LMZ Collection, No. 6, Mashgiz, 1960.

63. A. V. Levin. The selection of optimum unit capacities of single-shaft steam turbines. "Heat power engineering," 1960, No. 2.

64. M. Ye. Levina and P. A. Romanenko. A theoretical study of separation phenomena in annular cascades. "Steam and gas turbines." Collection of KhPI transactions, Volume XXIX, No. 2, 1960.

65. M. Ye. Levina and P. A. Romanenko. An experimental investigation of separation phenomena behind an annular cascade. "Steam and gas turbines." Collection of KhPI transactions, Volume XXIX, No. 2, 1960.

66. A. D. Lopatitskiy. Investigation of a typical high-pressure stage of LMZ in an experimental air turbine. LMZ Collection, No. 6. Mashgiz, 1960.

67. I. D. Lyakhovitskiy. Turbulence of the flow in a turbine stage an profile losses of impulse blades. "VTI News," 1950, No. 5.

68. N. M. Markov. Investigation of the flow area of turbines. Mashgiz, 1958.

69. N. M. Markov. The influence of Re numbers on the performance of turbine stages with different degrees of reaction. "Power equipment construction," 1961, No. 4.

70. G. A. Matveyev, G. F. Kamnev, N. M. Markov, et al. Aerodynamics of the flow area of marine turbines. Sudpromgiz, 1961.

71. A. D. Mezheritskiy. Some methods of decreasing steam moisture. "Power equipment construction," 1960, No. 3.

72. Yu. I. Mityushkin. Some results of an experimental investigation of turbine stages and annular cascades. News of higher educational institutions. "Power engineering," 1959, No. 11.

73. I. I. Novikov. Calculation of the flow of saturated and moist steam from nozzles. "Heat power engineering," 1961, No. 6.

74. M. V. Polikovskiy and A. A. Tamarchin. Tests of a KTZ transonic regulating stage with partial steam input. "Heat power engineering," 1958, No. 5.

75. M. V. Polikovskiy and A. V. Shchekoldin. The selection of a nozzle cascade design for a supersonic regulating stage. "Heat power engineering," 1958, No. 11.

76. I. L. Povkh. An aerodynamic experiment in machine building. Mashgiz, 1959.

77. L. Prandtl. Hydroaeromechanics. IIL, 1949.

78. V. D. Pshenichnyy. Investigation of a double-wheel stage with divergent-convergent channels. "Heat power engineering," 1962, No. 9.

79. Ya. M. Rubinshteyn, N. M. Gribkov, and N. F. Komarov. Results of the modernization of the LMZ turbine SVK-150-1. "Heat power engineering," 1958, No. 5.

80. G. S. Samoylovich. Calculation of the potential flow of a gas in a curvilinear channel. "Heat power engineering," 1954, No. 7.

81. G. S. Samoylovich and B. I. Morozov. Flow rate coefficients through the relief holes of turbine disks. "Heat power engineering," 1957, No. 8.

82. G. S. Samoylovich and B. M. Troyanovskiy. Steam turbines (collection of problems). State power engineering publishing house, 1957.

83. G. S. Samoylovich and B. M. Troyanovskiy. Variable performance of steam turbines. Gosenergoizdat, 1955.

84. G. S. Samoylovich and A. N. Sherstyuk. An approximate calculation of axially symmetric channels. News of the Academy of Sciences of the USSR, No. 4, 1958.

85. Ya. A. Sirotkin. Calculation of an axially symmetric vortex flow of an inviscid compressible fluid in axial turbomachines. News of the Academy of Sciences of the USSR. "Mechanics and machine building," 1961, No. 2.

86. N. A. Sknar'. Investigation of the separate influence of M and Re numbers on the aerodynamic characteristics of turbine cascades with "TN" profiles. "Power equipment construction," 1959, No. 8.

87. L. I. Slobodyanyuk. Concerning the problem of the influence of certain design parameters on the performance of a turbine stage. News of higher educational institutions. "Power enginerring," 1959, No. 4.

88. S. P. Sobolev and V. Ye. Granov. Modernization of the VR-25-1 turbine of the Kharkov turbine plant and an analysis of the results obtained. "Heat power engineering," 1958, No. 8.

89. G. Yu. Stepanov. Fundamentals of the theory of bladed machines, combined and gas-turbine engines. Mashgiz, 1958.

90. G. Yu. Stepenov. Hydrodynamics of turbomachine cascades. GIFML, 1962.

91. V. S. Stechkin, I. K. Kazandzhan, L. P. Alekseyev, et al. Theory of jet engines (bladed machines). Oborongiz, 1956.

92. V. V. Sychev. A new equation for the adiabatic exponent of moist stezm. "Heat power engineering," 1961, No. 3.

93. V. B. Taushkanova. Calculation of the flow around blade cascades with high subsonic velocities. LMZ Collection, No. 6. Mashgiz, 1960.

94. I. K. Terent'yev. Losses due to friction and windage of the rotor wheels of turbines. News of higher educational institutions of the Ministry of Higher Education. "Power engineering," 1959, No. 7.

95. A. M. Topunov. Concerning the problem of a procedure for testing annular blade cascades. News of higher educational institutions. "Power engineering," 1959, No. 1.

96. V. Traupel. Thermal turbomachines. State power engineering publishing house, 1961.

97. B. M. Troyanovskiy. Steam flow through labyrinth seals of steam turbines. VTI News, 1950, No. 1.

98. B. M. Troyanovskiy and Ye. V. Mayorskiy. Investigation of sections of limiting rotor blades of steam turbines. News of higher educational institutions, "Power engineering,"1962, No. 5.

99. B. M. Troyanovskiy and Ye. V. Mayorskiy. Profiling and investigation of the upper sections of rotor blades of the last stages of large steam turbines. "Heat power engineering," 1962, No. 7.

100. B. M. Troyanovskiy, F. V. Kazintsev, L. Ye. Kiselev, et al. Investigation of the last stages of condensing turbines. "Power equipment construction," 1962, No. 3.

101. B. M. Troyanovskiy. Some questions on the calculation of the last stages of condensing steam turbines. MEI Transactions, No. XXIII, 1963.

102. B. M. Troyanovskiy. Some questions on the design and operation of steam turbines. State power engineering publishing house, 1957.

103. B. M. Troyanovskiy. Generalized graphs of the economy of MEI single-wheel turbine stages. "Heat power engineering," 1959, No. 6.

104. B. M. Troyanosvkiy, L. Ye. Kiselev, and V. G. Fillipova. A method for calculating double-wheel velocity stages. "Power equipment construction," 1960, No. 5.

105. L. I. Tubyanskiy and L. D. Frenkel'. LMZ high-pressure turbines. State power engineering publishing house, 1959.

106. V. G. Tyryshkin. The selection of a design value for the degree of reaction in a turbine stage with long blades. "Heat power engineering," 1957, No. 2.

107. V. G. Tyryshkin. Concerning the problem of selecting a method of designing long blades of a turbine stage. News of the Academy of Sciences USSR, Department of Technical Sciences, No. 6, 1954.

108. V. V. Uvarov. Profiling of long blades of gas and steam turbines. TsIAM Transactions, No. 99, 1945.

109. Improvement of designs and operation of turbine power plants, edited by Ya. M. Rubinshteyn and A. V. Shcheglyayev. State powere engineering publishing house, 1959.

110. A. P. Fadeyev and Yu. Ya. Kachuriner. The influence of steam moisture on turbine stage performance. "Power equipment construction," 1961, No. 8.

111. N. Ya. Fabrikant. Aerodynamics, Gostekhizdat, 1955.

112. M. F. Fedorov and V. A. Garkusha. Investigation of the structure of flow in an interwheel clearance and energy losses in the nozzles of a turbine stage with different chords. KhPI Transactions, Volume XXXVI, 1961.

113. M. F. Fedorov, Yu. I. Pogorelov, and A. I. Kusenkov. Experimental investigations of end losses in convergent cascades and nozzle sections of diaphragms of a steam turbine. KhPI Transactions, Vol. XXIV, 1957.

114. M. F. Fedorov. Improved integral method for an experimental flow rate coefficient of nozzle blades. "Heat power engineering," 1958, No. 8.

115. G. Flyugel'. Steam turbines, GEI, 1939.

116. Ya. I. Frenkel'. Kinetic theory of fluids. Soviet Academy of Sciences Publishing House, 1945.

117. D. A. Chuprirev. Design and thermal calculations of stationary steam turbines. Mashgiz, 1953.

118. A. N. Sherstyuk. An approximate method for calculating curved channels. "Heat power engineering," 1955, No. 8.

119. H. Schlic .ting. Boundary layer theory. Foreign literature publishing house, 1956.

120. Ya. I. Shnee. Gas turbines. Mashgiz, 1960.

121. Ya. I. Shnee and A. V. Garkusha. The influence of the method of twisting on the magnitude of outlet losses. KhPI Transactions, Volume XXIX, 1960.

122. L. A. Shshubenko-Shubin. An experiment on the improvement of the flow area of steam turbines. "Power equipment construction," 1958, No. 7.

123. L. A. Shubenko-Shubin. Moving blades of the last stages of Soviet large steam turbines. "Power equipment construction," 1959, No. 1.

124. R. Sheval'skiy, B. Verchorek. A new design for low-pressure diaphragms of steam turbines. "Power equipment construction," 1960, No. 3.

125. A. V. Shcheglyayev, M. Ye. Deych, and G. A. Filipov. Calculation of steam turbine stages according to the results of static cascade scavenging. "Heat power engineering," 1962, No. 3.

126. A. V. Shcheglyayev. Steam turbines, 3rd edition. State power engineering publishing house, 1955.

127. A. V. Shchekoldin and V. I. Kiryukhin. Regulating velocity stages of small and intermediate turbines. "Heat power engineering," 1961, No. 3.

128. A. V. Shchekoldin and V. N. Sapozhnikov. Investigation of the perform of a group of last stages of the AR-4-3 turbine. "Heat power engineering," 1961, No. 8.

129. R. M. Yablonik. Model tests of turbine stages in moist air. "Heat power engineering," 1962, No. 5.

130. Amboz I., Bem K., Budlovsky I., Malek B., Lajik V. Parni Turbiny, I, Praha, 1956.

131. Bammert K. und Kläukens H. Nabenlotwasser hinter Leiträdern von axialen Strömungsmaschinen, Ing. Archiv, Bd. XVII, 1949.

132. Bilek I., Čamek I. a Veselý P. Sonstvaný výzkum lopatkove účinnosti na modelovych turbinách, Proudeni v lopatkovych strojch, Sbornik ústavu pro výzkum stroju čsav, 1958.

133. Carl Č., Holmquist O. and Rannie W. An Approximate Method of Calculating Three Dimensional Compressible Flow in Axial Turbomachines, Journal of the Aeronautical Sciences 1956, № 6.

134. Daily I. W., Nece R. E. Chamber Dimension Effects on Induced Flow and Frictional Resistance of Enclosed Rotating Disks. Journal of Basic Engineering, 1960, № 2.

135. Dettmering W. Experimentalle Untersuchungen an einer axialen Turbinenstufe, Forschung Berichte des Landes Nordrhein Westfallen, 1960, № 908.

136. Downs I. E., Coffon K. C. Low-pressure turbine testing, Mechanical Engineering, 1958, N 8.

137. «Electrical World», 1960, V. 153, N 9.

138. «Electrical World», 1960, V. 154, N 1/2.

139. «Electrical World», 1960, V. 154, N 9.

140. Fredenreich W. Der schädliche Einfluss der Dampfnässe in Dampfturbinen, «BBC Mitteilungen», 1927, H. 5.

141. Comi M. On the deviation of outlet flow angles caused by secondary flows in turbine cascades, Bulletin of ISME, Tokyo, 1959, N 8.

142. Hagetschweiler H., Bartlett R., Predicating Performance of Large Steam Turbines-generator Units for Central Stations, Transactions of the ASME, 1957, N 5.

143. Hartmann W. Versuche an einer Dampfturbinenstufe, Archiv fur Wärmewirtschaft und Dampfkesselwesen, 1941, N 4.

144. Heffner F. E., A practical solution of a three-dimensional flow problem of turbomachinery. Journal of Basic Engineering, 1960, N 2.

145. Kantrowits A. Nucleation in very rapid vapor expansions, Journal of Chem. Physic, 1951, N 19.

146. Karman T. Supersonic Aerodynamic, N. I. 1959.

147. Kearton A. Steam Turbines, London, 1961.

148. Meyer C., Seglem C. and Wagner I. A turbine-testing Facility, Mechanical Engineering, 1960, N 7.

149. Oswatitsch K. Kondensationserscheinungen in überschalldüsen, ZAMM. 1942, N 22.
150. Ross F. The propagation in a compressible fluid of finite oblique disturbances with energy exchange and change of state, Journal of Applied Physics, 1951, N 12.

151. Schlichting H. Application of Boundary-Layer Theory in Turbomachinery, Journal of Basic Engineering, 1959, N 4.
152. Scholz N. Strömungsuntersuchengen an Schaufelgittern, VDI Forschungsheft, 1954, Bd. 20.
153. Schulz-Grunow F. Der Reibungswiderstand rotierender Scheiben in Gehäusen, ZAMM, 1935.
154. Soo S. Z. Laminar flow over an enclosed rotating disk, Paper ASME, 1957, SA—28.
155. Shepherd D. Principles of turbomachinery, N. 1. 1959.
156. Suter P., Traupel W. Untersuchengen über den Ventilationsverlust von Turbinen rädern., Zürich, 1960.
157. Stodola A. Dampf- und Gasturbinen, Berlin, 1924.
158. Traupel W. Zur Theorie der Nassdampfturbine, Schweizerische Bauzeitung, 1959, H. 20.
159. Vavra M. N. Aero-thermodynamics and Flow in Turbomachines, N. Y. 1960.
160. Wu Chung Hua The aero dynamic problem of radially long blades in turbomachines, Chinese Journal of Mechanics, 1957, N 3.
161. Wu Chung Hua and Wolfenstein L. Applications of Radial Equlibrium Condicions to Axial-Flow Compressors and Turbine Design, NACA Report, 1955, N 955.
162. Wull W., Christ A. Dampffeuchtigkeits-messungen am Niederdruckteil einer 50-MW-Dampfturbine, Escher-Wyss Mitteilungen, 1960, n. 1.
163. Preiskorn G. Erosionsschaden an Endstufen von Kondensation-Dampfturbinen und Massnahmen zuihrer Minderung, «Maschinenbautechnik», Heft 11, 1958.